CR-180867

NASA

National Aeronautics and
Space Administration

FULL SCALE TECHNOLOGY DEMONSTRATION OF A MODERN COUNTERROTATING UNDUCTED FAN ENGINE CONCEPT

DESIGN REPORT

December 1987

by
GE Aircraft Engines
GE36 Project Department
Cincinnati, Ohio 45215

Prepared for

National Aeronautics and Space Administration

NASA-Lewis Research Center
Contract NAS3-24210

NASA

National Aeronautics and
Space Administration

FULL SCALE TECHNOLOGY DEMONSTRATION OF A MODERN COUNTERROTATING UNDUCTED FAN ENGINE CONCEPT

DESIGN REPORT

FOREWORD

The design discussed in this report was conducted by the Aircraft Engine Business Group of the General Electric Company, Cincinnati, OH for the NASA Lewis Research Center, Cleveland, OH under Contract NAS3-24210. The program was carried out under the technical cognizance of Mr. R.D. Hager of the Advanced Turboprop Project Office. The contract effort was performed by the GE36 Project Department at the Evendale Plant of General Electric.

TABLE OF CONTENTS

TABLE OF CONTENTS (Continued)

TABLE OF CONTENTS (Continued)

TABLE OF CONTENTS (Continued)

TABLE OF CONTENTS (Concluded)

LIST OF ILLUSTRATIONS

LIST OF ILLUSTRATIONS (Continued)

LIST OF ILLUSTRATIONS (Continued)

LIST OF ILLUSTRATIONS (Continued)

LIST OF TABLES

LIST OF TABLES (Concluded)

1.0 SUMMARY

Design and development of the Unducted Fan (UDF™) counterrotating turbo-fan engine has been completed based on the requirements of NASA Contract NAS3-24210 and additional General Electric requirements. The program objective was to design a high thrust to weight engine with exceptional fuel economy as a technology base for future commercial and military transport, subsonic aircraft. This report documents the final component design and analysis.

The engine system consists of a modified F404 gas generator engine and counterrotating propulsor system, mechanically decoupled, and aerodynamically integrated through a mixing frame structure. Utilization of the existing F404 engine minimized engine hardware, cost, and timing requirements and provided an engine within the desired thrust class. The power turbine provides direct conversion of the gas generator horsepower into propulsive thrust without the requirement for a gearbox and associated hardware. Counterrotation utilizes the full propulsive efficiency by recovering the exit swirl between blade stages and converting it into thrust.

Cross sections of the UDF™ engine are shown in Figures 1-1 and 1-2. The evolution of design improvements made during the ground test and test-related experience will be covered in detail in the engine test and component test reports.
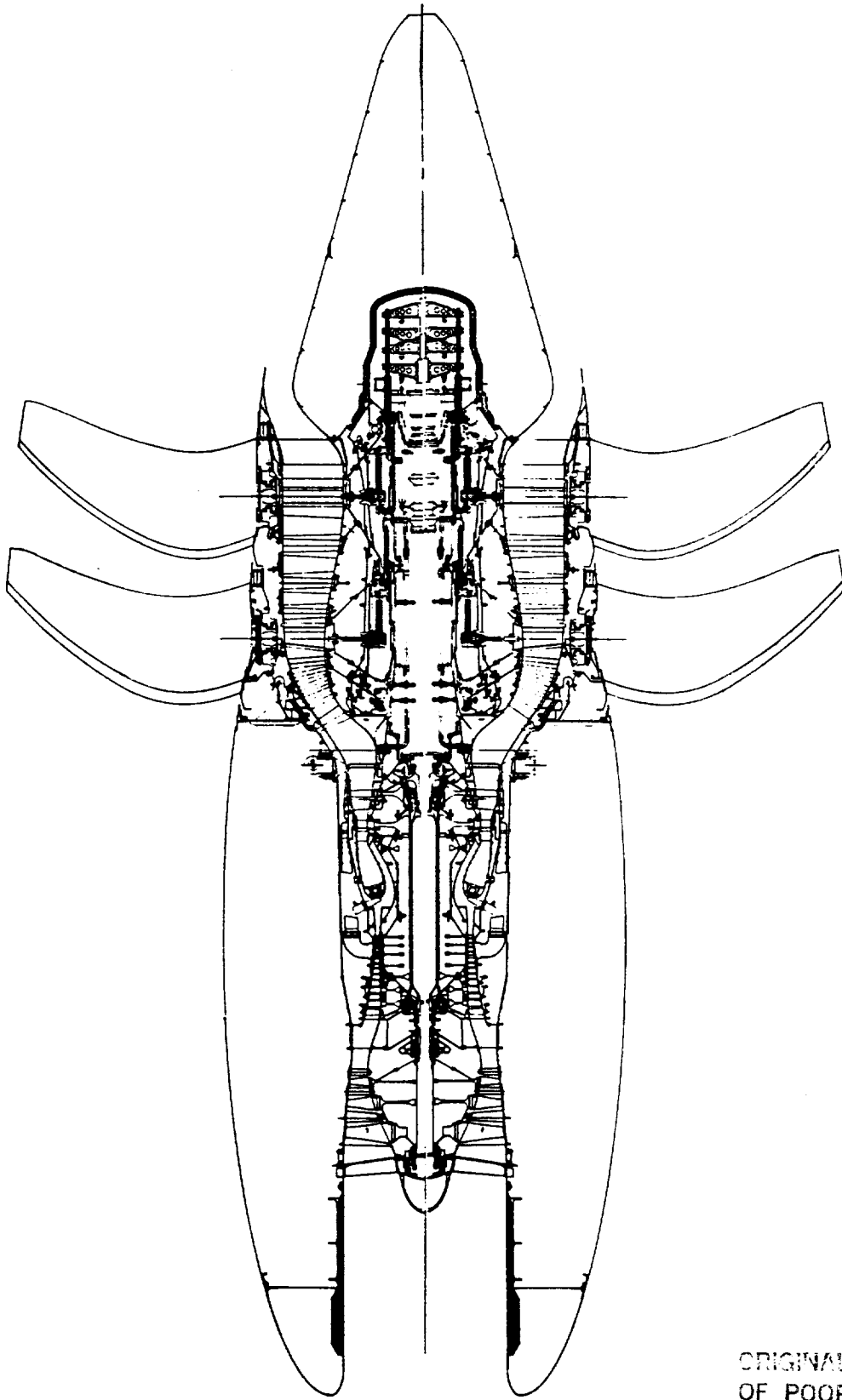
Figure 1-1. Cross Section of Unducted Fan Engine.

2
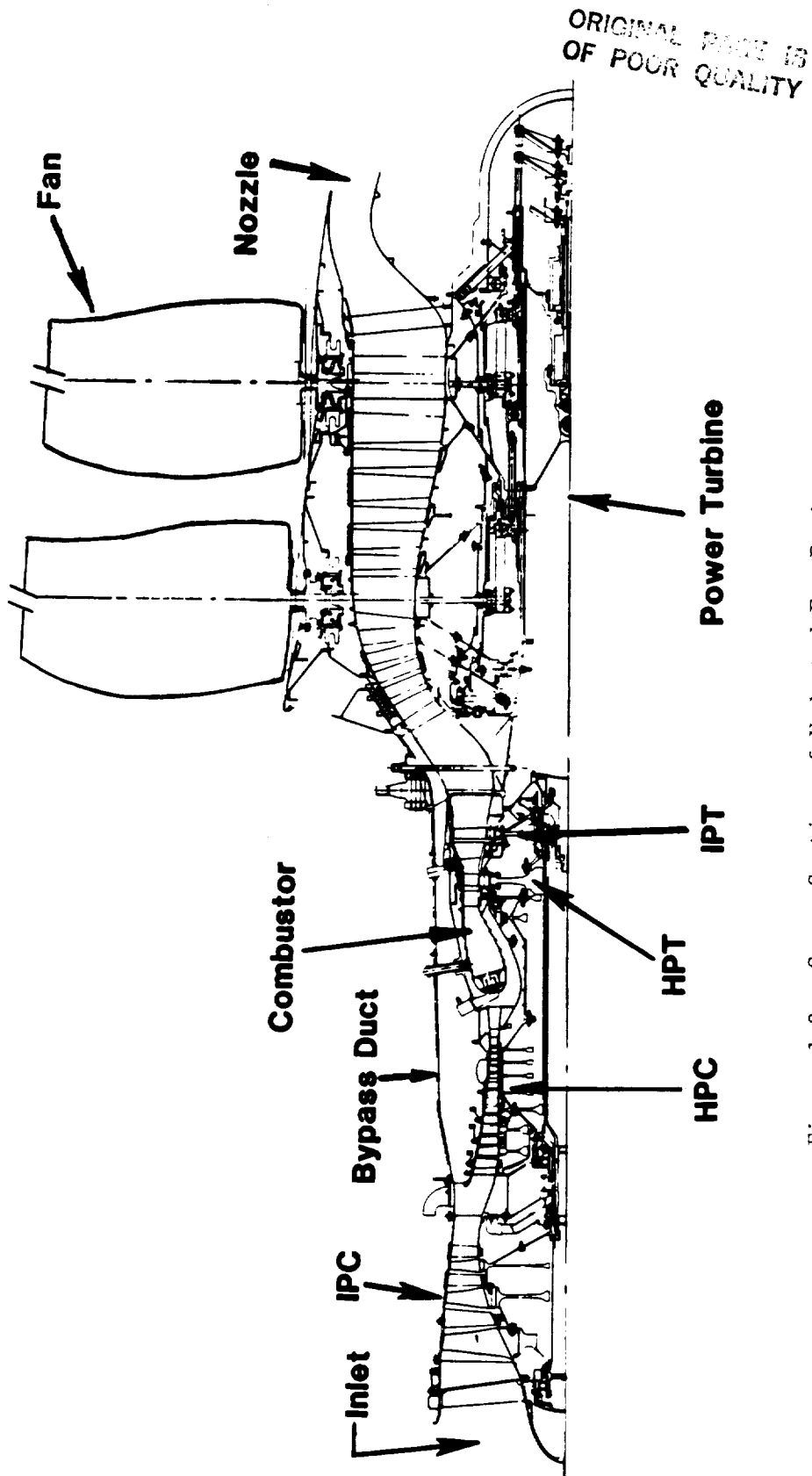
Figure 1-2. Cross Section of Unducted Fan Engine.

2.0 INTRODUCTION AND DESIGN OVERVIEW

This report covers the major areas of the UDF™ design including the counterrotating propulsor and the refurbishment of an F404 for use as the gas generator.

The following section presents an introduction and overview to each of the design sections, starting with Cycle Design and Performance (Section 2.4 corresponds with Section 4.0; Section 2.5 corresponds with Section 5.0, etc.).

2.4 CYCLE DESIGN AND PERFORMANCE

The updated D4A and D5A cycles were developed for the UDF™ by upgrading the earlier D3 cycle. Improved modeling techniques, scale model program data (NAS3-24080), and the F404 green run were utilized. Pretest predictions for the Peebles ground test were created at various operating conditions utilizing the D5A cycle. Ground test thrust accounting methodology and specific fuel consumption (sfc) uncertainty analysis were also defined.

2.5 AERODYNAMIC DESIGN

Aerodynamic design is separated into three distinct classifications: (1) nacelle, (2) fan, and (3) turbine. The fan hub flowpath portion of the nacelle extends from the nacelle maximum diameter to the nozzle trailing edge.

2.5.1 Nacelle Aerodynamic Design

The nacelle design provides low inlet spillage drag and consequently low distortion into the unducted fan at all operating conditions within the flight envelope. Redesign of the exit nozzle was required after early ground testing indicated a potential flight, high altitude, maximum climb, nozzle aerodynamic separation problem. The new part is longer, having a less severe radius of curvature at the crown.

2.5.2 Fan Aerodynamic Design

The UDF™ fan blades, designated F7-A7, were designed to run at 780 feet per second tip speed with a disk loading of 85. The flowpath shape allows

4

flow diffusing upstream of the blades to lower blade inlet Mach numbers, and area rule scalloping of the blade platforms compensates for blade thickness, thus reducing through-flow Mach numbers. An additional fan aerodynamic design requirement was the maximization of aero sweep within the aeromechanical blade stability constraints.

2.5.3 Turbine Aerodynamic Design

The power turbine aerodynamic design features a 10-stage unshrouded configuration with flowpath air introduced through a high slope transition mixer frame. The overall predicted design point efficiency was approximately 91% prior to incorporation of opened tip clearance and power turbine airfoil damper pins. Predicted efficiency loss for the modified turbine was 3.24 points.

2.6 F404 REFURBISHMENT AND MODIFICATIONS

A Navy QT F404 engine, on loan through NASA, was refurbished to new engine quality and modified for the UDF™ application. Major modifications included structural enhancement of the outer bypass ducts, new low pressure turbine (LPT) support structure, and interface with the UDF™ mixer frame and revised inlet to accommodate the nacelle structure.

2.7 HEAT TRANSFER AND SECONDARY FLOW ANALYSIS

The UDF™ transition mixer frame and sump system design utilizes the F404 bypass air to pressurize and cool the UDF™ static structure. The bypass air is introduced to the system through the mixer, which is then film-cooled by approximately 41,000 laser-drilled holes. The remaining air enters the internal sump secondary air circuit and packs labyrinth seals and the sump system. Failed seal criteria were utilized to avoid backflow problems associated with large labyrinth seal clearances.

2.8 PROPULSOR MECHANICAL DESIGN SUMMARY

2.8.1 Static Structure

The mixer frame is the main structural support for the propulsor, it provides the aft engine mount and serves as a transition duct from the F404 exit to the larger propulsor inlet. Film cooling keeps the structure temperatures uniform, thus reducing thermal gradients and assuring low cycle fatigue (LCF) life requirements are met. Results of stiffness trade studies set the strut hub configuration and strut quantity (20).

The power turbine support, attached to the aft flange of the mixer frame, provides support for the power turbine bearings, seals, lube jets, and actuation system components. The support was sized to have blade-out load capability and to prevent rotor whirl and plug nozzle instability.

The 60 inlet guide vanes (IGV), attached in groups of 3 on a 360° inner band, turn the mixer exit flow into the power turbine rotors. The vane assembly is bolted to the mixer frame at the inner band and has a radial slip joint at the outer band. Airfoil frequencies were tuned to avoid excitation from turbine blading at steady-state operating points of the engine.

The outlet guide vane (OGV) assembly turns the gas flow exiting the Stage 12 rotating frame. Cost and weight trade studies on the assembly substantiated the use of a lightweight sheet metal construction. Both two-dimensional (2D) and three-dimensional (3D) finite element models were used to determine critical frequencies and stress levels on both the vanes and the supporting structure.

2.8.2 Turbine Blades, Spools, Shafts, and Seals

The turbine blades are a sheet metal fabrication designed to reduce unit cost and weight with the primary emphasis on dynamic design criteria. Due to the large number of blades designed, early analyses were generic in nature. Conventional design practice for frequency and aeroelastic stability set the requirements. Fundamental mode beam analyses were conducted to establish constraints for final aero design consistent with dynamics requirements; 3D finite element analyses were used to design the blades for initial drawing release, and follow-on changes were defined through detailed dynamic analyses

on each stage. Upon receipt of engine hardware, component bench tests were conducted to confirm analytical predictions.

Initial engine test experience confirmed all intended design criteria were met, except that the first flexural mode of all stages was highly responsive, indicating lack of damping expected from the dovetail. The design was modified for Build 2 by the addition of coulomb dampers in the form of pins which span between airfoils.

The power turbine spools are 360° turned parts with circumferential dovetails and a minimum number of flanges. A rock and twist-in blade assembly technique was developed to accomplish this.

Trade studies also revealed thermal response characteristics of the inner and outer spools would have to be matched to meet clearance objectives and that frequency tuning of the spools would be necessary during detail design to meet dynamics requirements. Structural shell models of both rotors were created and used for stress, clearance, and dynamics analysis. Preliminary analyses were conducted in all three areas to size parts for initial drawing release. Follow-on detailed design analyses were conducted, and designs were modified as required to meet objectives. Major follow-on design changes were the addition of a removable stiffening disk to the aft outer spool to meet dynamics criteria and modifications to the forward outer spool-to-seal bolted joint to improve LCF life.

Six labyrinth seals were designed for the power turbine. Three of these seals were counterrotating, and the dynamics criteria developed for counterrotating spools were utilized in their design. All seals incorporated dampers of some form to minimize the potential for vibratory response. Heat transfer, stress, and clearance analyses were conducted to match the thermal growth characteristics of the seals and size stability rings.

2.8.3 Fan Blade Design

The propulsor fan blades were designed to meet the design objectives of: high cycle fatigue (HCF) and LCF life, stability, frequency margin, overspeed, foreign object damage (FOD), and on-wing maintainability.

The engine uses two counterrotating stages of eight fan blades each. The blade tip diameter is 11.67 feet when mounted in the engine. The maximum operating speed is 1395 rpm, with a 140% overspeed capacity. The blades were designed for high disk loadings and a high hub-to-blade-tip-radius ratio. Two blade configurations have been developed for this program, one for 0.72 M, and the other for 0.8 M, although only the 0.72 M configuration has been designed and fabricated. This 0.72 M configuration has been optimized for 0.72 M, but has the capability for enduring aircraft speeds in excess of 0.8 M. The 0.8 M design has been analytically studied, but no detailed design has been issued.

The blades were designed to be of composite construction, consisting of a composite shell with a titanium spar. The feasibility study predicted that this type of design would have good aerodynamic performance, an adequate frequency margin, satisfactory stress margin in all structural components, and be aeroelastically stable. The titanium spar extends out from the bottom of the composite to form a dovetail. This dovetail slides into the fan blade retention and actuation system for attachment to the engine. The dovetail provides the fan blades on-wing maintainability feature.

2.8.4 Sump and Carbon Seal Design

The UDF™ sump (lube) system is completely separate from the F404 gas generator lube system. This additional lube system supplies oil for the propulsor, the starter adaptor gearbox, and the lube pump adaptor gearbox. The main components of the lube system are proven accessories "borrowed" from more mature engine programs. These components were modified both in size and flow, as required. The lube system is a dry sump, pressure supply design vented to ambient pressure. A unique feature of this system is that the sump walls are rotating.

The primary seals of the propulsor sump are carbon seals which are used to seal off the area between the two rotors, between the stationary frame and the aft rotor, and around the radial fan blade actuation rods. The types of carbon seals employed are: air-bearing piston ring intershaft seals, circumferential bore-rubbing seals, and magnetic face seals. A unique feature of the seals is the large diameter of the intershaft and circumferential seals and the high gravity field of the magnetic seal.

2.9 ENGINE DYNAMICS

An engine dynamics analysis was conducted to predict the dynamic behavior of the UDF™ engine. A model of the UDF™ engine was built for this analysis utilizing VAST (an in-house engine dynamics program). The flexibilities used to develop this mount-system model were based on predictions from the NASTRAN finite element (3D) model of the pylon/aircraft structure.

Four separate analyses are presented in this report:

- Nominal unbalance (1000 gm-in) in the forward and aft UDF™ P/T rotors
- Single blade-out in each of the P/T rotors simultaneously
- Nominal unbalance (20 gm-in) in various stages of the gas generator
- Maneuver loads and deflections.

2.10 POWER CONTROL AND CONFIGURATION DESIGN

2.10.1 Power Control System

The power control system for the UDF™ controls the engine's forward and reverse thrust by means of mechanical linkages and cabling. The system includes a pylon-mounted throttle converter assembly, a push/pull cable arrangement to actuate the engine hydromechanical control power lever, an electric power circuit to actuate the engine mounted shut-off solenoid valve, and instrumentation to indicate throttle lever position. The engine portion of the control system interfaces with the aircraft mechanical throttle control system on the pylon's forward mount beam structure.

2.10.2 Configuration Design

Configurations is the provision of pipes and hoses which transfer fluids between the engine and the controls and accessory hardware. The major design objectives are sufficient fluid flow, proper routing, and adequate support. Other design requirements include keeping the natural frequency of the piping out of the operating range of the engine and to have adequate pressure capacity margin in the piping.

2.11 CONTROL SYSTEM DESIGN

The control system for the GE36 demonstrator engine provides control of the following:

- Fuel flow
- Gas generator HP compressor variable geometry
- Gas generator IP compressor variable geometry
- Bypass duct bleed
- Fan pitch.

By controlling each of these functions, the system provides steady-state and transient control of engine thrust in response to power lever demand and does not exceed any operating limits or require any special crew attention.

The control system incorporates the following features:

- Integrates unducted fan blade pitch and gas generator schedules

- Provides thrust/power level management

- Provides the capability to synchronize and synchrophase counterrotating blade rows to minimize noise

- Provides the capability to run in both off-design and alternate modes for investigation of performance and noise sensitivities

- Controls fan speeds through adjustment of blade pitch angle to secure maximum fan operating efficiency

- Controls fan speed and/or blade pitch angle and gas generator power level to set reverse thrust.

2.12 NACELLE STRUCTURES DESIGN

The nacelle structures hardware consists of cowling assemblies, strut (pylon), mount beam, strut fairings, vibration isolators, and fuse pin assembly. The cowling assemblies consist of the inlet, core cowling, apron cowling, and aft bulkhead. These structures provide an aerodynamic flowpath, nacelle ventilation and fire protection. The centerbody (along with the rotating exhaust nozzle) provides the power turbine exit flowpath. The strut attaches to the aircraft or test stand and acts as the load path between the aircraft and the engine mount beam. The mount beam acts as the load path

between the isolators and the strut. The strut fairings provide an aerodynamic flowpath around the strut. The isolators provide the structural link between the engine and the mount beam. These isolators provide controlled flexibility and damping to the connection. The fuse pin assembly provides a known failure point in the mount system to allow a clean break between the engine and the mount beam in the event of a catastrophic engine failure (as in the loss of more than one fan blade per rotor). This is to protect the aircraft from any damage.

3.0 ENGINE TECHNICAL REQUIREMENTS

Minimum life objectives for all hardware were set at ___ cycles and ___ hours per current engine manual limits. Generic 95/99 material properties were utilized for all life calculations, unless same part data were available.

Engine maneuver and blade-out conditions imposed additional design constraints on the propulsor hardware. During normal operation, all clearances were set to meet a combined 2g plus 0.25 radians/second load. Under ultimate load conditions, the static structure meets a 9g maneuver load requirement. Stringent blade-out capability was set for all propulsor hardware. Ultimate load capability was required for a complete simultaneous airfoil loss for both stages in conjunction with a 1g maneuver. Additional design capability for various components is covered in the mechanical design section of this report.

To meet UDF™ blade-out requirements, enhancement of the F404 structure was necessary. However, the normal operating cycle for UDF™ application was reduced from the typical F404 cycle. The maximum operating environment for each application is summarized in Table 3-1.

Table 3-1. Maximum Operating Cycle Comparison:
Takeoff Conditions.

Speed (rpm)	UDF™ Application	F404 Cycle
HP	15,844	16,435
LP	11,941	13,382
Temperature (° F)		
T2 (Inlet)	86	89
T3	906	1,010
T41	2,318	2,516
T46	1,435	1,506
T15	392	423
Pressure (psi)		
P2 (Inlet)	14.7	14.7
P3	257.5	332.6
P41	241.8	312.6
P46	44.9	48.3
P15	45.3	50.5

4.0 CYCLE DESIGN AND PERFORMANCE

4.1 CYCLE DESIGN

4.1.1 Preliminary Cycle Design

Performance definition for the GE36/UDF™1 Study D3 was established before the start of NASA Contract NAS3-24210. The engine cycle model represents the F404 gas generator driving a counterrotating, low pressure turbine attached to a counterrotating (eight blades per row), unducted fan. The power turbine flow function was sized to maximize the power output consistent with the available stall margin. The F404 consists of a three-stage, axial low pressure compressor (IP spool); a seven-stage high pressure compressor; an annular combustor; a single-stage, axial flow high pressure turbine; a single-stage IP turbine; and an IPC bypass duct.

4.1.2 Definition of Status D4A Cycle

Definition for the GE36/UDF™1 Status D4A cycle had the following upgrades from the GE36/UDF™1 Study D3 cycle:

- Addition of the variable IPC Stator 1 model
- Fuel heating by the LPT sump oil
- Revised mixing plane logic
- Redefined LPT secondary flows
- Redefined mixer frame and LPT exit frame losses
- Addition of LPT parasitic power and heat losses
- Revised LPT exit swirl angle definition
- Revised nozzle coefficients
- Revised UDF™ and LPT maps.

Effects of the variable IPC Stator 1 on the IPC stall line are shown in Figure 4-1. The parasitic flow schematic is shown in Figure 4-2. Comparison of overall performance (sfc versus thrust) between Study D3 and Status D4A is illustrated in Figure 4-3.
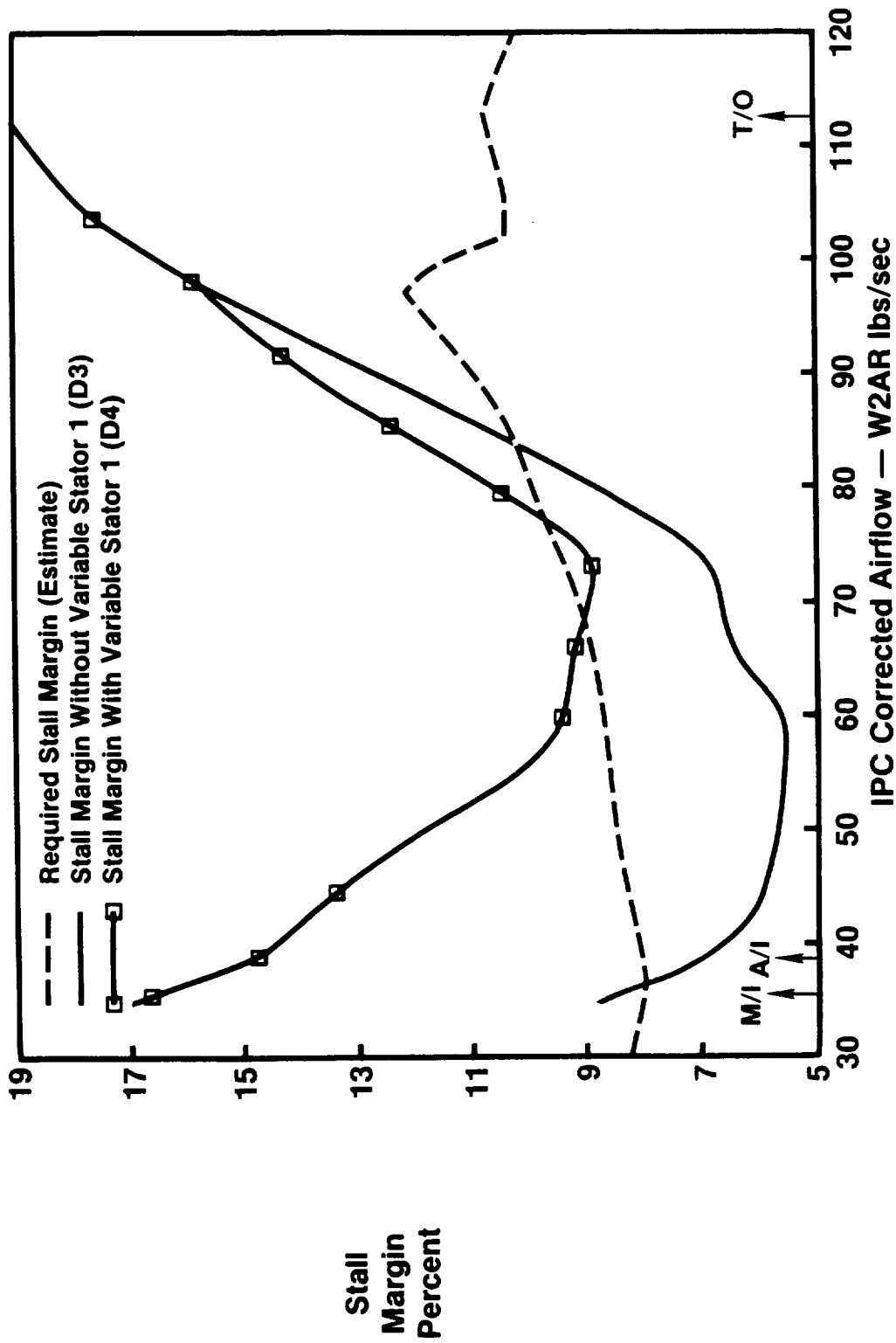
Figure 4-1. Effects of Variable Stator 1 - Required and Available Stall Margins (SLS/STD).
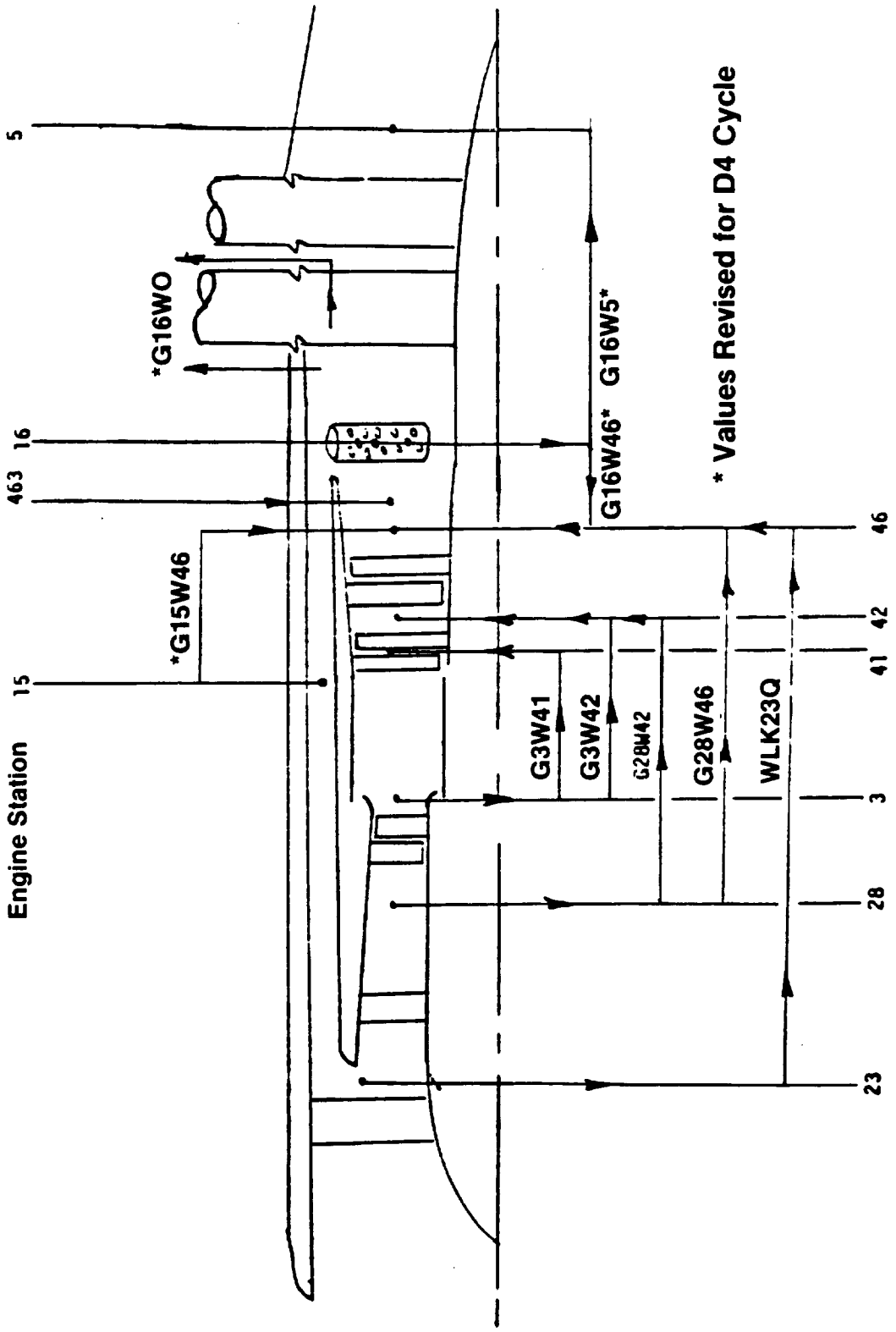
Figure 4-2. Parasitic Flow Schematic.

15
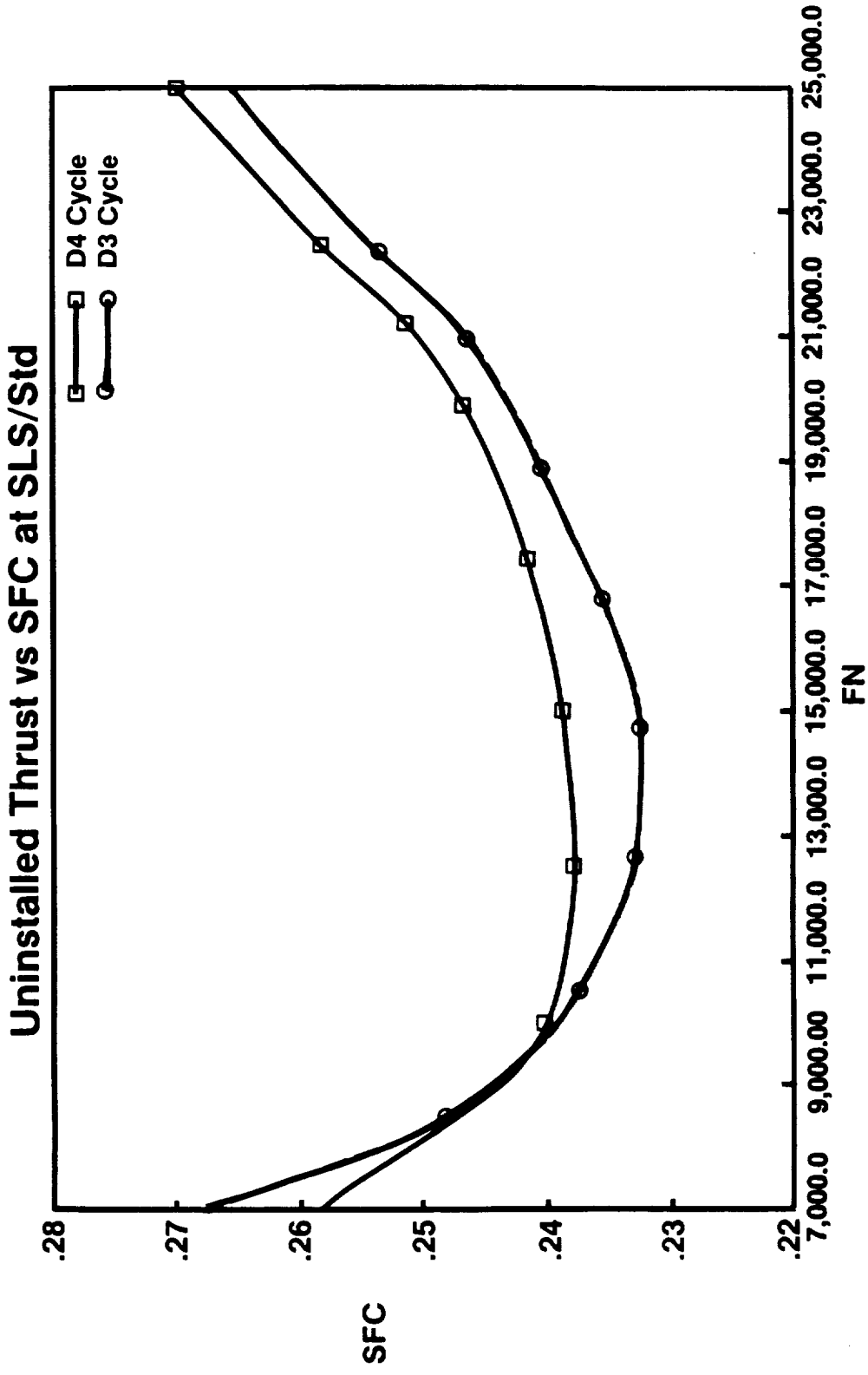
Figure 4-3. SFC Versus Thrust Comparison Between Study D3 and Status D4A.

16

4.1.3 Ground Test Thrust Accounting

Thrust accounting for the ground tests at Peebles Site IV-A were defined as follows:

- FN   - Engine Uninstalled Net Thrust
- FNIN1   - Engine Installed Net Thrust
- FGE   - Core Engine Gross Thrust
- FRAME   - Core Engine Ram Drag
- FNAV91 - Unducted Fan Average Thrust
- FDCPS   - Core Plug Scrubbing Drag
- FDNACS - Nacelle Pressure and Friction Drag
- FDPYL   - Pylon Pressure and Friction Drag
- FDSTND - Drag Due to Facility Structure on the Link Side of the Stand
- FNINM   - Measured Installed Thrust on the Stand.

The following parameters are measured or defined analytically:

- FNINM is the thrust measured by facility measurement devices

- FGE is defined using the exhaust nozzle exit properties (P_8, T_8, W_8, A_8, Pamb, nozzle coefficients)

- FDSTND is the stand drag defined as a function of stand geometry and freestream Mach number

- FRAME is defined as a function of freestream Mach number and IPC flow

- FDCPS is defined plug geometry and exhaust nozzle exit properties (P_8, T_8, and W_8)

- FDNACS is defined as a function of nacelle geometry and freestream Mach number

- FDPYL is defined as a function of pylon geometry and freestream Mach number.

The following parameters are defined as functions of measured or analytically defined parameters:

- FNIN1 = FNINM + FDSTND
- FNAV91 = FNINM + FDSTND - FGE + FRAME + FDCPS + FDNACS + FDPYL
- FN   = FNAV91 + FGE - FRAME.

A schematic of the thrust parameters is illustrated in Figure 4-4.

4.1.4 Specific Fuel Consumption Uncertainty Analysis

The object of the uncertainty analysis undertaken was to evaluate the accuracy to which specific fuel consumption can be determined from the ground test. The approach taken for the study was as follows:

- Ground tests would be conducted with a headwind from facility fans

- Determine appropriate means of stating performance

- Identify elemental measurements and assumptions which determine performance

- Define uncertainties for each element

- Determine the sensitivity of performance calculation to each element

- Statistically combine elemental uncertainties and sensitivities to determine overall uncertainty.

The defined performance parameter of interest for the uncertainty analysis was the corrected, installed specific fuel consumption at constant thrust. The sfc was corrected for an 86° F standard day, sea level, at a freestream Mach number of 0.10.

Figure 4-5 shows the model diagram of all the error elements considered and their relationships with the performance parameter of interest. Figure 4-6 defines the terminology used in the statistical methods employed for the study. The overall result of the study was that the corrected, installed sfc, at the Peebles test site, could be defined within ± 1.9%, given a confidence level of 99.1%, and ± 1.4%, given a confidence level of 95.0%.

4.1.5 F404 Green Run Test

The F404 used for the GE36/UDF™1 demonstrator engine was tested at the GE Lynn, MA facility. The scope of the test was to run the break-in, mechanical check-out, baseline performance calibration, conduct IPC mapping and low speed stall line evaluation, examine starting characteristics with various exhaust nozzle areas, and evaluate IPC variable geometry schedules.

18
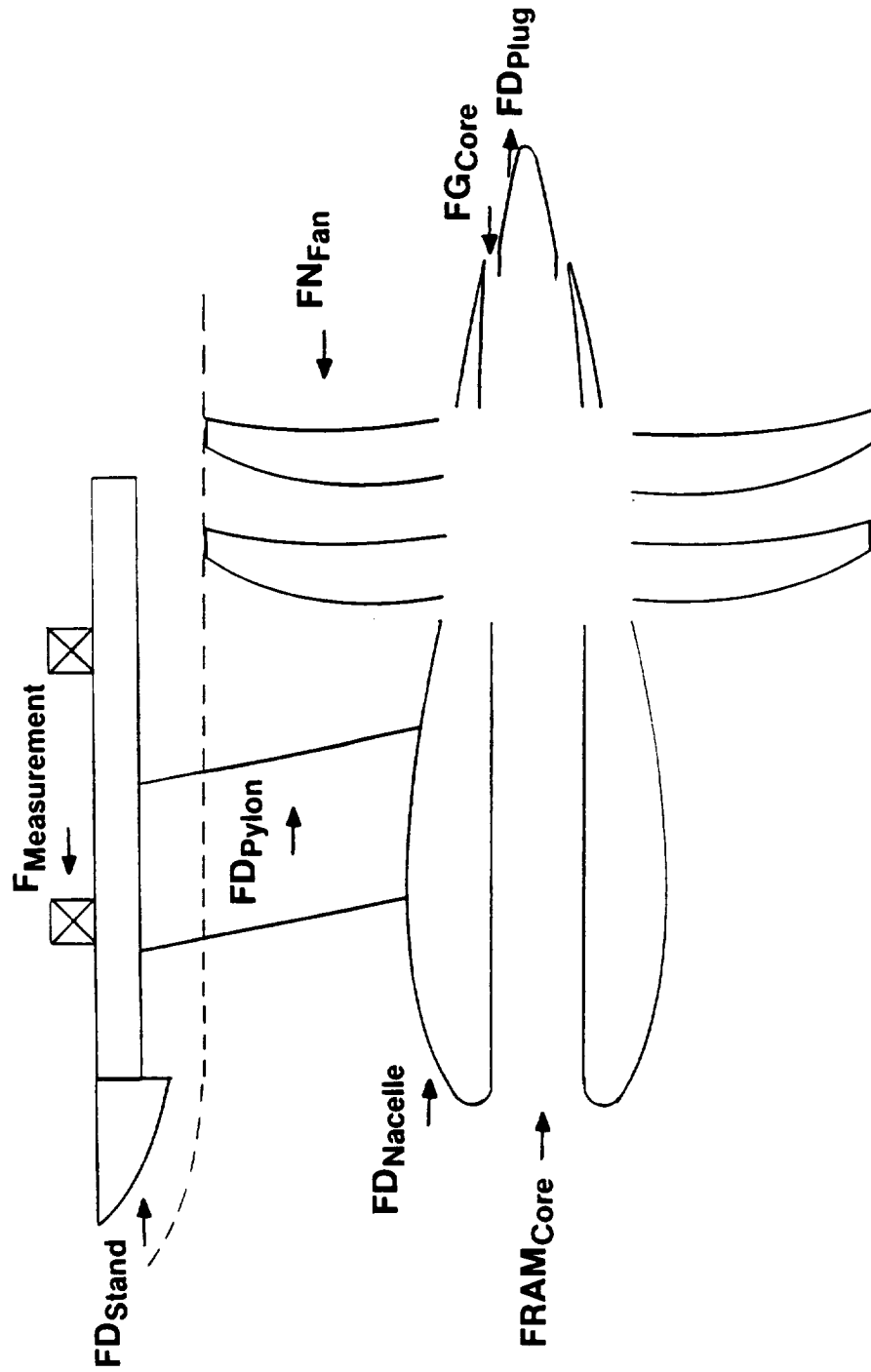
Figure 4-4. Ground Test Thrust Parameters.
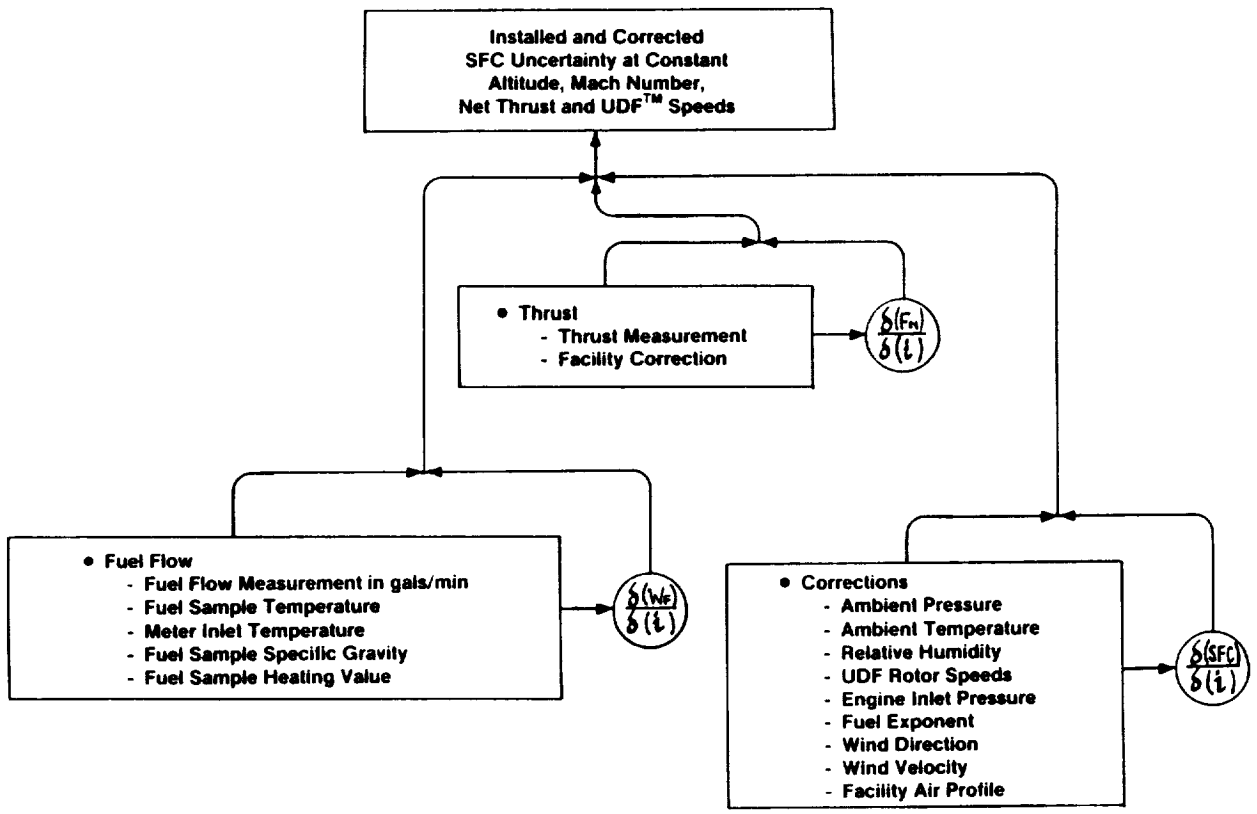
Figure 4-5. Uncertainty Analysis, Model Diagram.

- **Precision Index** $= \sqrt{\Sigma\,(\text{Precision}_i \times \text{Derivative}_i)^2}$

- **Bias** $= \sqrt{\Sigma\,(\text{Bias}_i \times \text{Derivative})^2}$

- **Uncertainty** $\left(\begin{array}{l}\text{Summation Method} \\ \text{99.1\% Confidence}\end{array}\right) = \pm\,(\text{Bias} \pm t \times \text{Precision Index})$

- **Uncertainty** $\left(\begin{array}{l}\text{RSS Method} \\ \text{95.0\% Confidence}\end{array}\right) = \pm\,\sqrt{(\text{Bias})^2 + (t \times \text{Precision Index})^2}$

Figure 4-6.   Uncertainty Analysis, Definitions.

The tests established that the engine health was good, at 3% to 5% better than minimum engine specification, as depicted in Figure 4-7. The effects of variable IPC Stator 1 were as predicted in terms of flow and speed, and the stall line was as expected. The revised IPC variable geometry (VG) schedule, 5.5° closed, gave approximately 4% extra stall margin at constant IPC flow (Figure 4-8); no starting problems or IPC transient problems were encountered.

4.2 PRETEST PREDICTIONS

4.2.1 Definition of Status D5A Cycle

Definition for the GE36/UDF™1 Status D5A cycle has the following upgrades from the GE36/UDF™1 Status D4A cycle:

- F404 performance updated to the status level achieved during the green run tests (Section 4.1.5)

- UDF™ maps based on the model propulsion simulator (MPS) test results were included

- Parasitic flows were revised

- Control schedules were added to the model.

Table 4-1 tabulates the comparison of Status D4A and Status D5A cycles, showing uninstalled thrust (FN), HP turbine rotor inlet temperature (T_{41}) and UDF™ absorbed horsepower (PWSD) at three high power points. Figure 4-9 shows the Status D4A and Status D5A uninstalled sfc and thrust characteristics.

Table 4-1. Pretest Predictions of Cycle
Performance, D5A Cycle.

	FN, lb	T_{41}, ° F	Fan Power, hp
• SLS/+ 27° F			
- D4A	25,000	2,406	15,321
- D5A	25,000	2,369	14,437
• SLS/+ 27° F			
- D4A	27,557	2,520	18,407
- D5A	29,149	2,520	18,406
• SLS/Std			
- D4A	28,981	2,447	20,000
- D5A	31,111	2,472	20,000
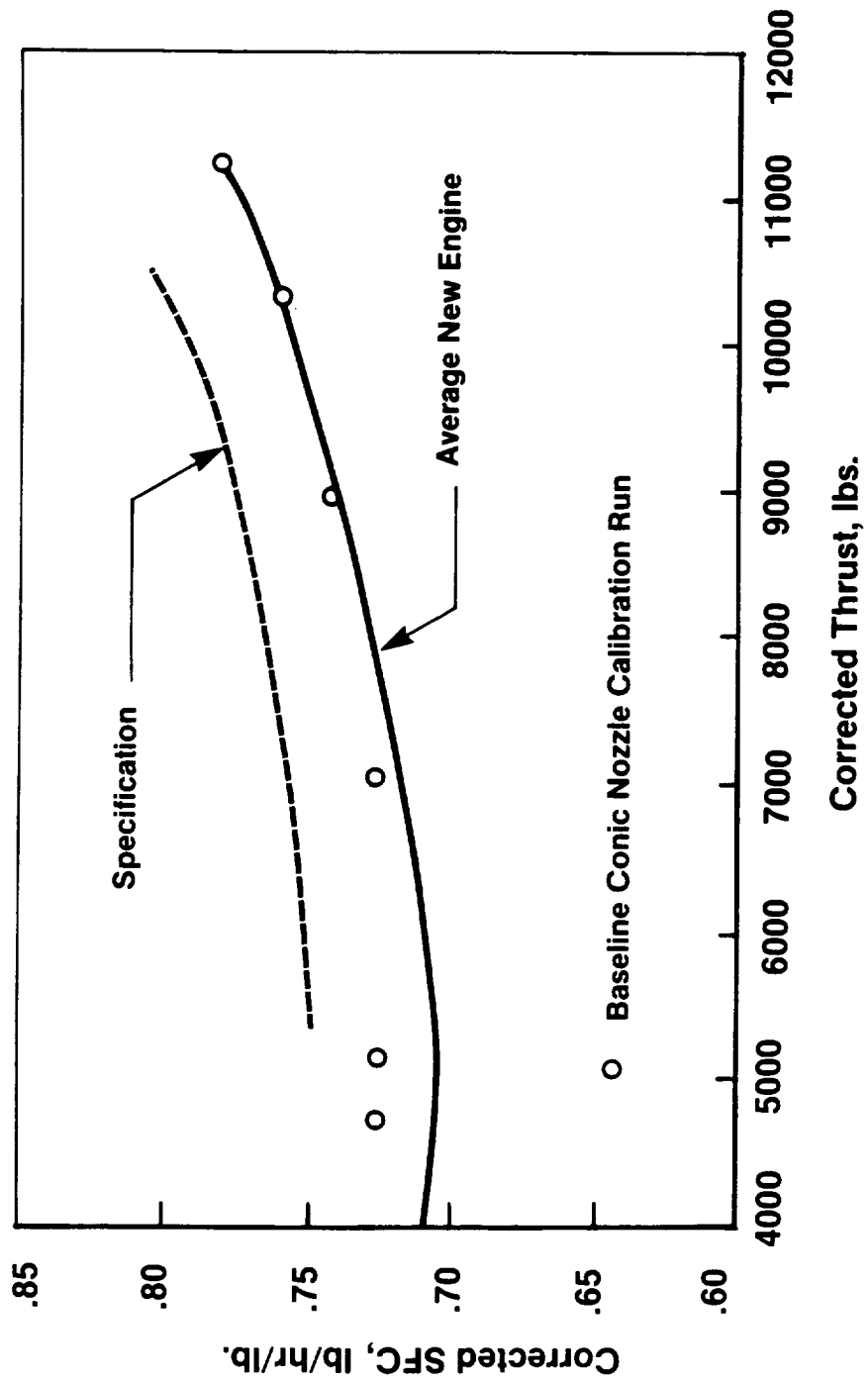
Figure 4-7. Core Engine Test, SFC Versus Thrust.

23
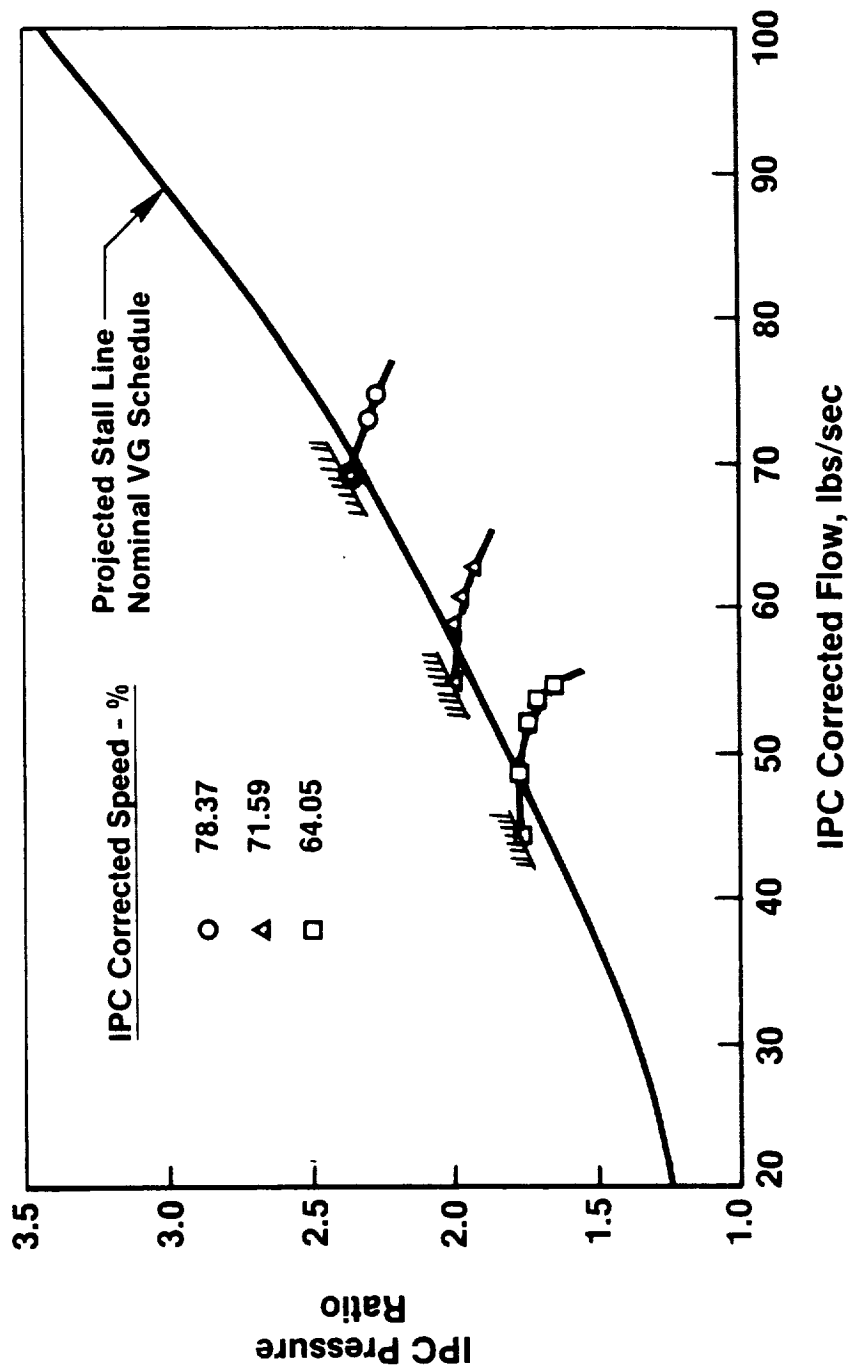
Figure 4-8. Core Engine Test, IPC Stall Line Data (Closed VG Schedule).

24
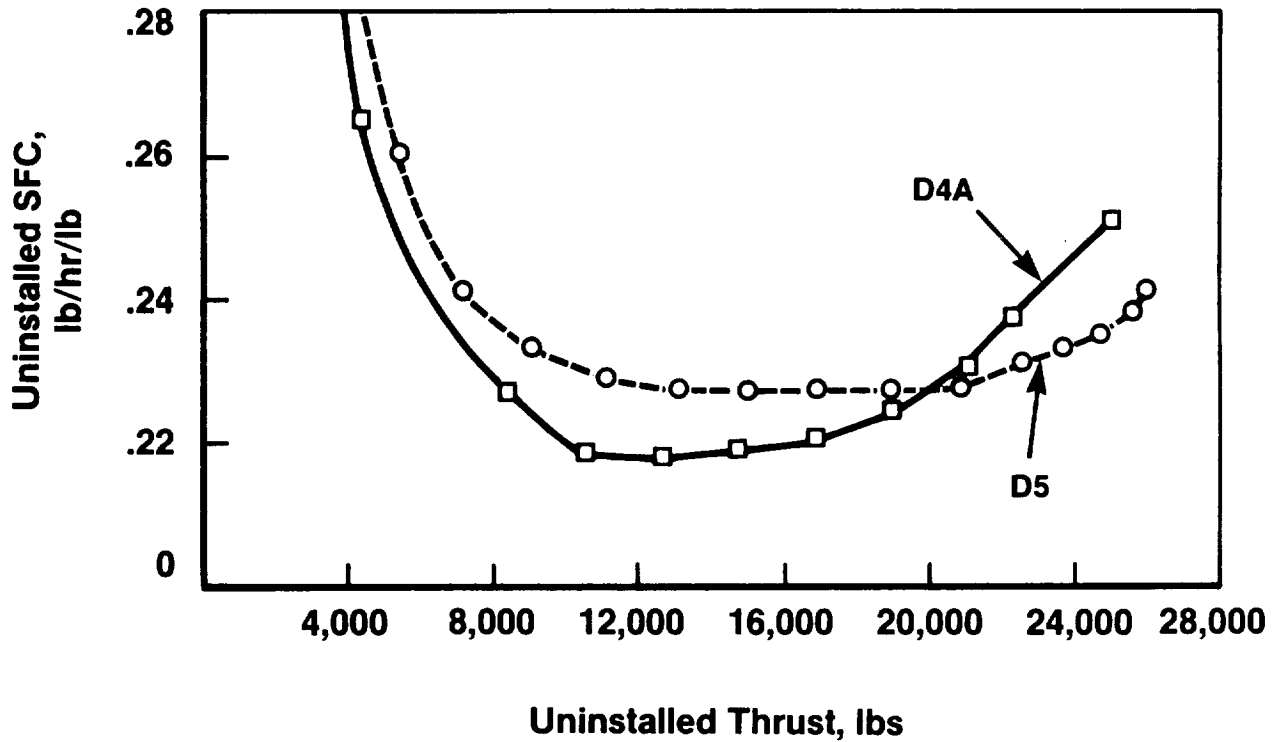
Figure 4-9. Comparison of Status D4A and D5A Uninstalled SFC and Thrust Characteristics.

4.2.2 Posttest LPT Updates for Blade Dampers

The overall effects of the damper pins and open clearances on the LPT performance were -3.24 points in LPT efficiency and -0.63% in LP turbine flow function. The effects of the above items on the cycle, at constant thrust, take-off rating, are presented in Table 4-2.

Table 4-2. Engine Test Modification Effect On Cycle.

	SFC%	IPC Stall Margin
-3.24 Points LPT Efficiency	+ 2.01	- 0.21%
-0.63% LPT Flow Function	+ 0.04	- 0.30%
Total Effect	+ 2.05	- 0.51

4.3 BYPASS BLEED SYSTEM

4.3.1 Bleed System Design

Replacement of the F404 variable area exhaust nozzle with the smaller flow function power turbine reduces the IPC stall margin below its minimum acceptable level. This is illustrated in Figures 4-10 and 4-11. To provide sufficient stall margin relief for unrestricted throttle movement throughout the flight envelope, a bypass bleed system was designed. This system consists of three circumferential ports in the outer bypass duct manifolded into one valve which dumps air through the aft bulkhead at six o'clock. Individual port diameters and locations were selected to reduce circumferential pressure distortion during bleed. The large dump area ensures acceptable back pressurization within the system.

4.3.2 Bleed System Control Logic

The system control logic is contained within the electronic propulsor control, as shown in Figures 4-12 and 4-13. This logic opens the bleed valve in response to any one of the following inputs:

(a) $d(pla)/dt$ (throttle retard rate) > threshold

(b) IPC P/P > scheduled maximum allowable P/P

(c) $d(P)/dt$ (IPC exit pressure decay rate) > threshold.

If Inputs "a" or "c" are satisfied, the control logic is designed to open the valve, hold for 5 seconds, and then ramp closed. This logic guarantees a minimum of 10 seconds prior to closure and avoids transient pressure pulses. If Input "b" is satisfied, the control modulates the bleed valve to maintain the scheduled maximum allowable IPC pressure ratio. If multiple inputs are received, the full open valve response (a or c logic) option is implemented.
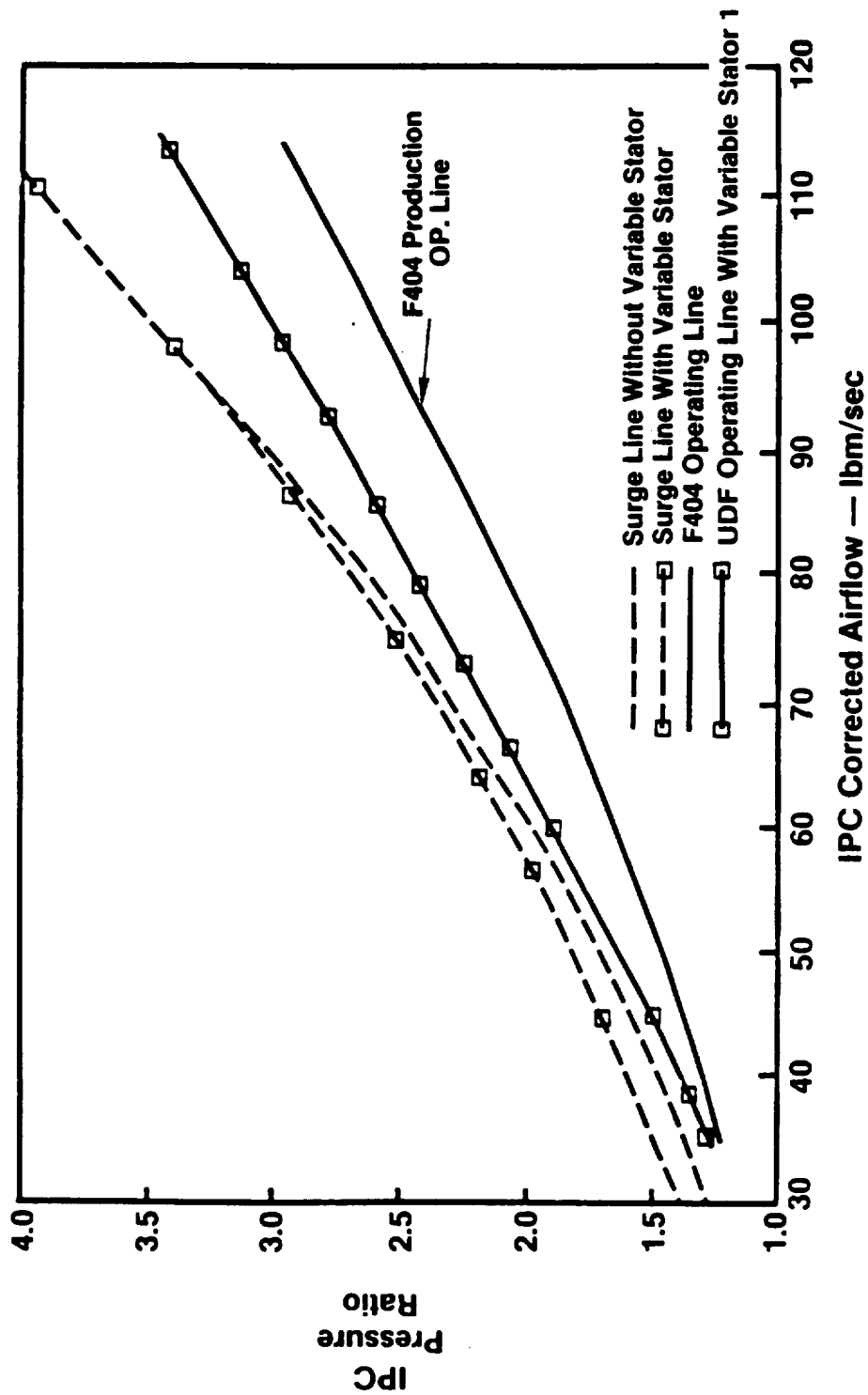
Figure 4-10. IPC Surge Margin Requirements.

Legend (from chart):
- Surge Line Without Variable Stator
- Surge Line With Variable Stator
- F404 Operating Line
- UDF Operating Line With Variable Stator 1

X-axis: IPC Corrected Airflow — lbm/sec

Y-axis: IPC Pressure Ratio

F404 Production OP. Line

27
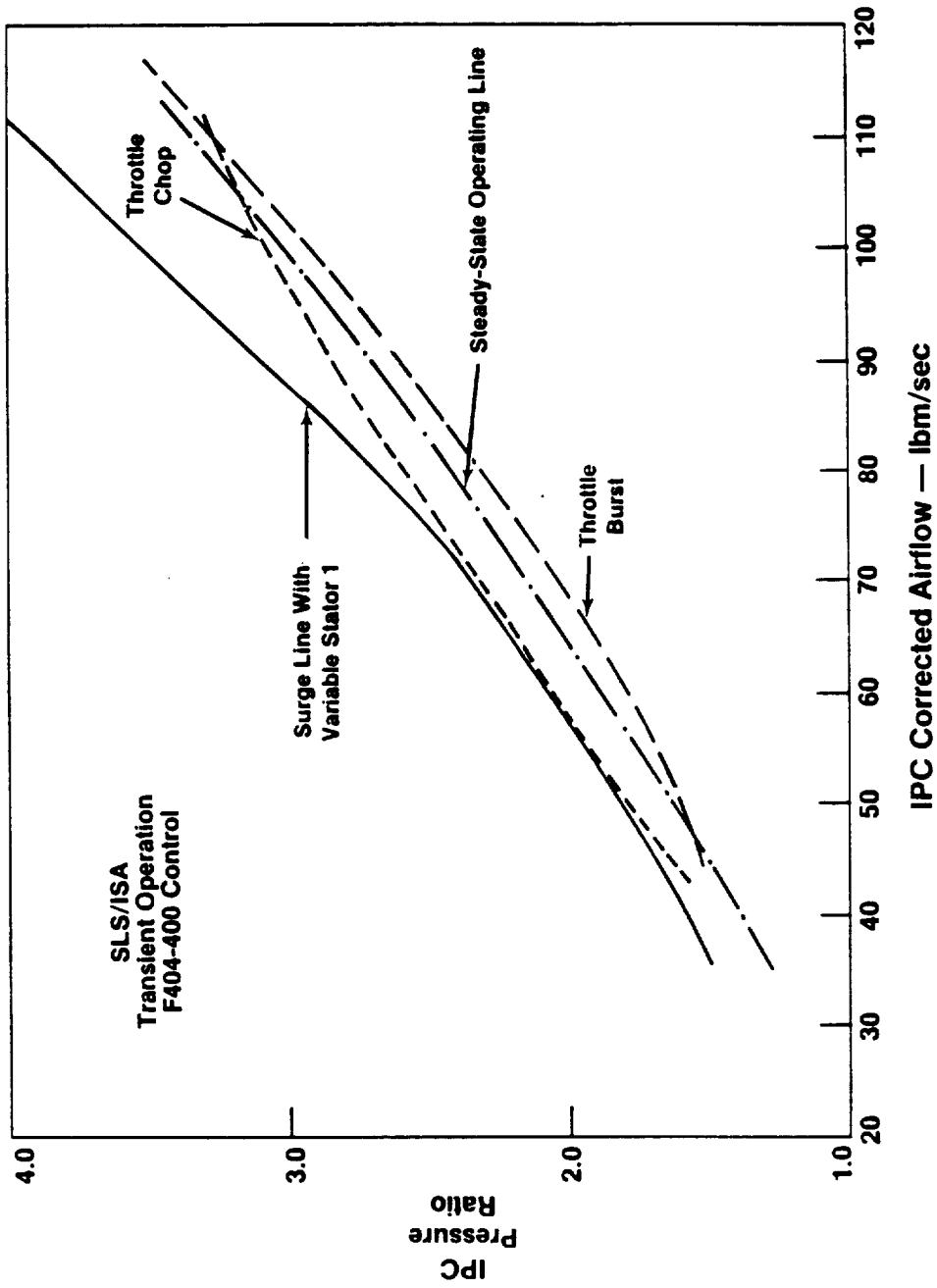
Figure 4-11.   IPC Surge Margin Requirements, Nominal Cycle/Control.

CORRECTED
IP ROTOR SPEED

DUCT PRESSURE
RATIO
DEMAND
SCHEDULE

MEASURED
PRESSURE
RATIO

DUCT BLEED
PRESSURE
RATIO
CONTROLLER

DUCT BLEED
VALVE POSITION
DEMAND

POSITION
CONTROL
LOOP

STROKE
AREA
RELATIONSHIP

DUCT BLEED
FLOW AREA
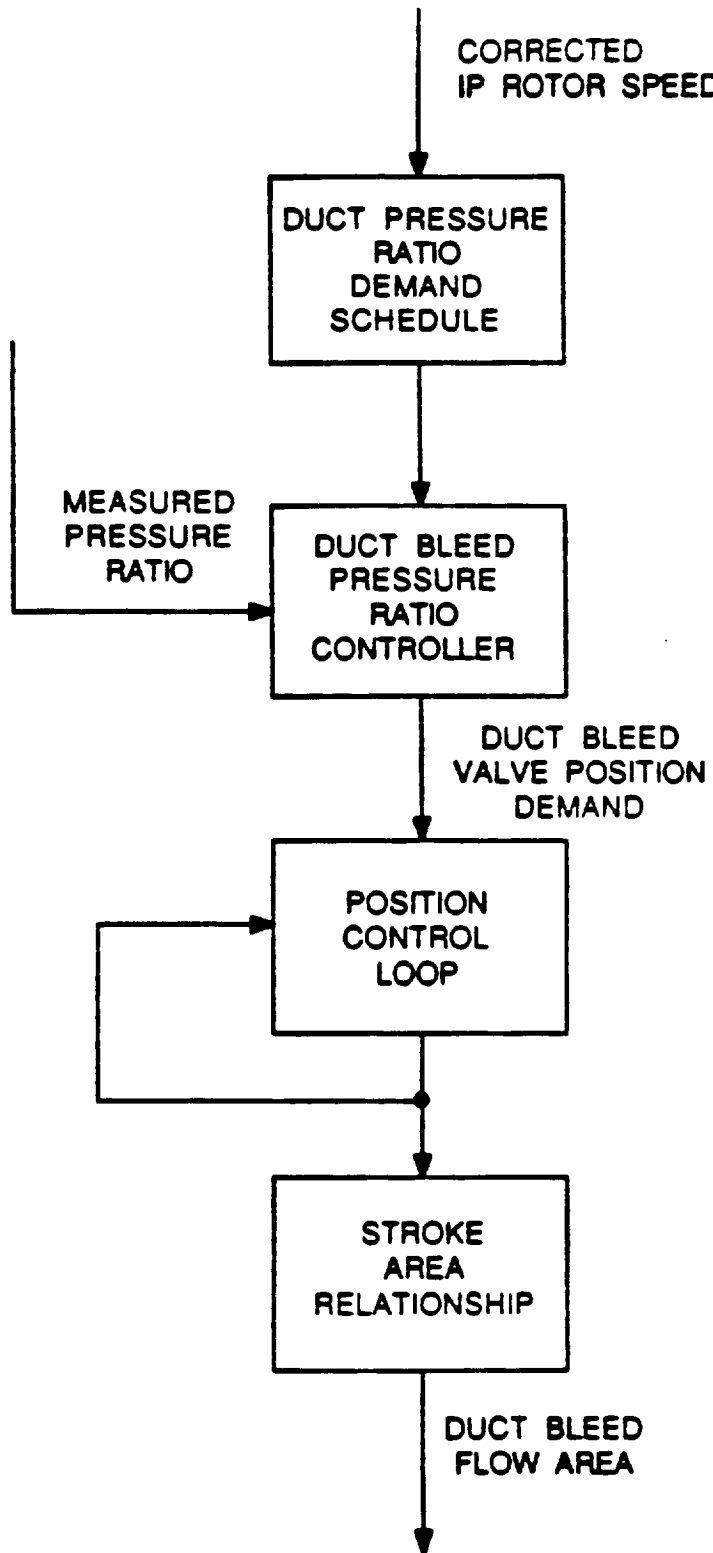
Figure 4-12.   Bypass Bleed System Design, Bleed
Pressure Ratio Controller.
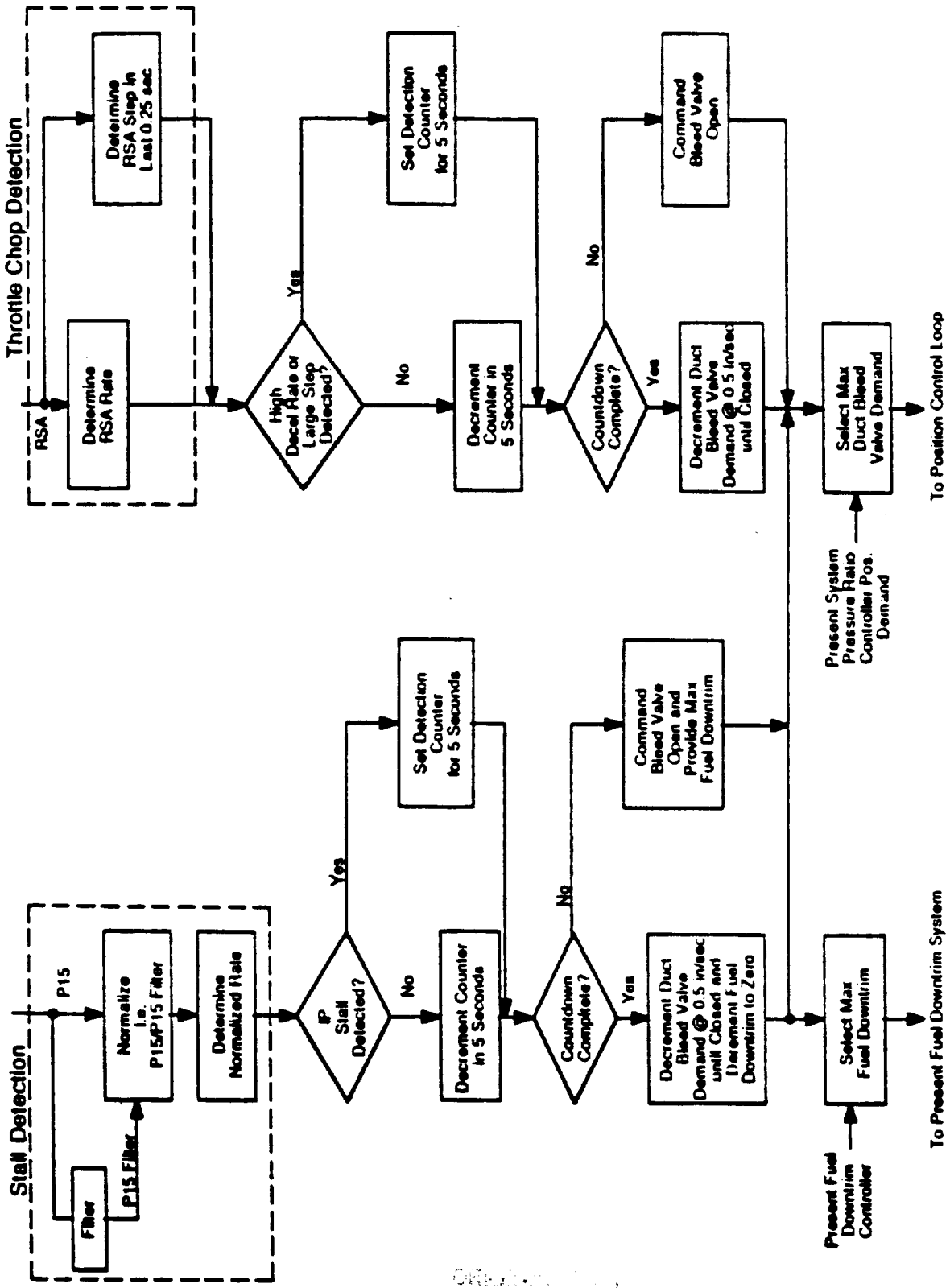
Figure 4-13. Bypass Bleed System Design, Transient IP Stall Avoidance and Recovery Controller.

30

5.0 AERODYNAMIC DESIGN

5.1 NACELLE AERODYNAMIC DESIGN

5.1.1 F404 Inlet Aero Design

The F404 UDF™ inlet was designed as an isolated nacelle with minimal spillage drag down to zero inlet mass-flow-ratio and a cruise drag rise above Mach = 0.8. Avoidance of spillage drag was a top priority consideration to provide the lowest possible flow field distortion to the unducted fan at all engine power settings. Similarly, the inlet lip was designed to operate free of external lip separation at incidence angles well beyond the expected 10° maximum flight test engine incidence angle. A generous internal lip contraction ratio was selected for low core intake total pressure distortion at all anticipated flight conditions.

As depicted in Figure 5-1, the large projected inlet area (D_{max}/D_f) of the core engine was well beyond normal turbofan high speed inlet design experience, a major reason for the unusual appearance of the UDF™ inlet. Airflow demand characteristics of the F404 core permitted much smaller inlet thrust and highlight radii than were selected for the demo UDF™ design. While reducing these dimensions is desirable for a number of reasons, it was found that large increases in forebody length would be required to effectively thin the external forebody and provide the desired high speed drag rise characteristics. The final forebody design provides sufficient length for inlet acoustic treatment requirements while maintaining a balance between high speed and low speed inlet performance characteristics. A longer inlet would have added unnecessary weight, drag, and would have made installation more difficult.

5.1.2 Nozzle Design

A number of factors constrained the UDF™ core nozzle design. In the interest of fan blade performance, the external cowl shape was limited to a very gentle curvature and a low boattail angle. Termination of the nozzle was specified at STA 312 to minimize the rotating hub length but was later trimmed back to STA 311.4 due to vibratory fatigue in the nozzle trailing edge

- Treatment $L_T/D_F = .5$
- No Diffusion ($D_F/D_{TH} = 1.0$)
  - Abundance of Projected Area ($D_{Max}/D_F = 2.458$)
  - High Recovery
- Large Internal Lip Contraction Ratio ($D_{HL} = 1.16$) for Low Distortion at AOA
- Large External Cowl Projected Area ($D_{HL}/D_{Max} = .47$) Necessitated by D_{Max} Requirement → No Spillage Drag
- External Cowl Length ($X/D_{Max} = 1.10$) for M = .80 Design (Isolated Inlet Drag Rise at M > .8)
- Axisymmetric Nacelle Due to Small Cruise Incidence Angles and No Off Design Performance Problems
- Isolated Nacelle Design — Pylon/Fuselage Effects Will be Dealt With by Airframer
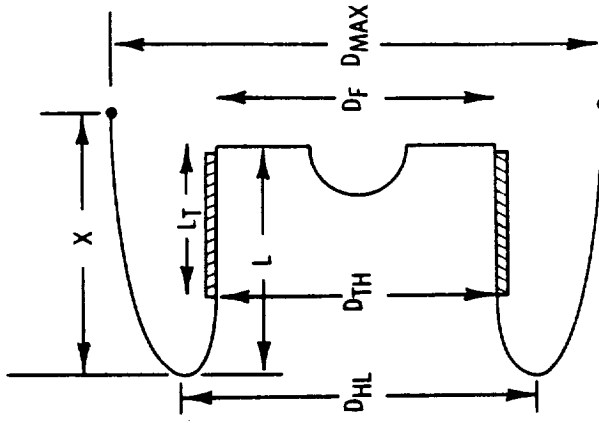
Figure 5-1. Inlet Design Features.

32

structure. A plug angle of 16° (approximately 7° higher than the cowl boat-tail angle) was selected to reduce nozzle suppression, minimize plug length, and provide compatibility with the existing CF6-80. A core nozzle area of 735 in^2 was selected to provide the desired power turbine extraction ratio.

Analysis was used to evaluate the potential for flow separation from the nozzle walls for the nozzle geometry selected. The shortness and considerable offset of the internal nozzle flowpath resulted in a severe plug crown radius of curvature and elevated surface Mach numbers on the plug. Early ground tests of the demonstrator engine indicated that a very high nozzle flow coefficient existed. Expecting nozzle separation at the high altitude, maximum climb power settings, a decision was made to modify the plug for better separation characteristics.

Figure 5-2 reveals the modified plug geometry relative to the original. It is longer with a less severe radius of curvature at the crown. Figure 5-3 illustrates the calculated separation parameter for both plugs at the Mach = 0.72/35K/MxCL (maximum climb) power setting. Analysis has also indicated the new plug will operate separation free at power settings beyond maximum climb, now planned for flight test. Subsequent model tests of both plug designs have verified both the high power separation problem with the original plug and the adequacy of the redesigned plug.

5.1.3 Aircraft Installation Effects

The F404 UDF™ nacelle design was completed prior to an independent design of the flight and ground test support pylon by The Boeing Company, which has claimed responsibility for aerodynamic integration of the F404/UDF™ with the pylon and the B727 aircraft. Boeing transonic wind tunnel (BTWT) testing of the UDF™ flow-through nacelle model on the B727 has been conducted to optimize engine placement, investigate drag trends, and measure wing and pylon wake characteristics.

Installed UDF™ nacelle/pylon drag levels reportedly followed anticipated trends up to Mach = 0.7, beyond which drag divergence was encountered. This is thought to result from body-to-body interference as the pylon and nacelle should produce subcritical flow fields on an isolated basis. For a production

ORIGINAL PLUG

MODIFIED PLUG
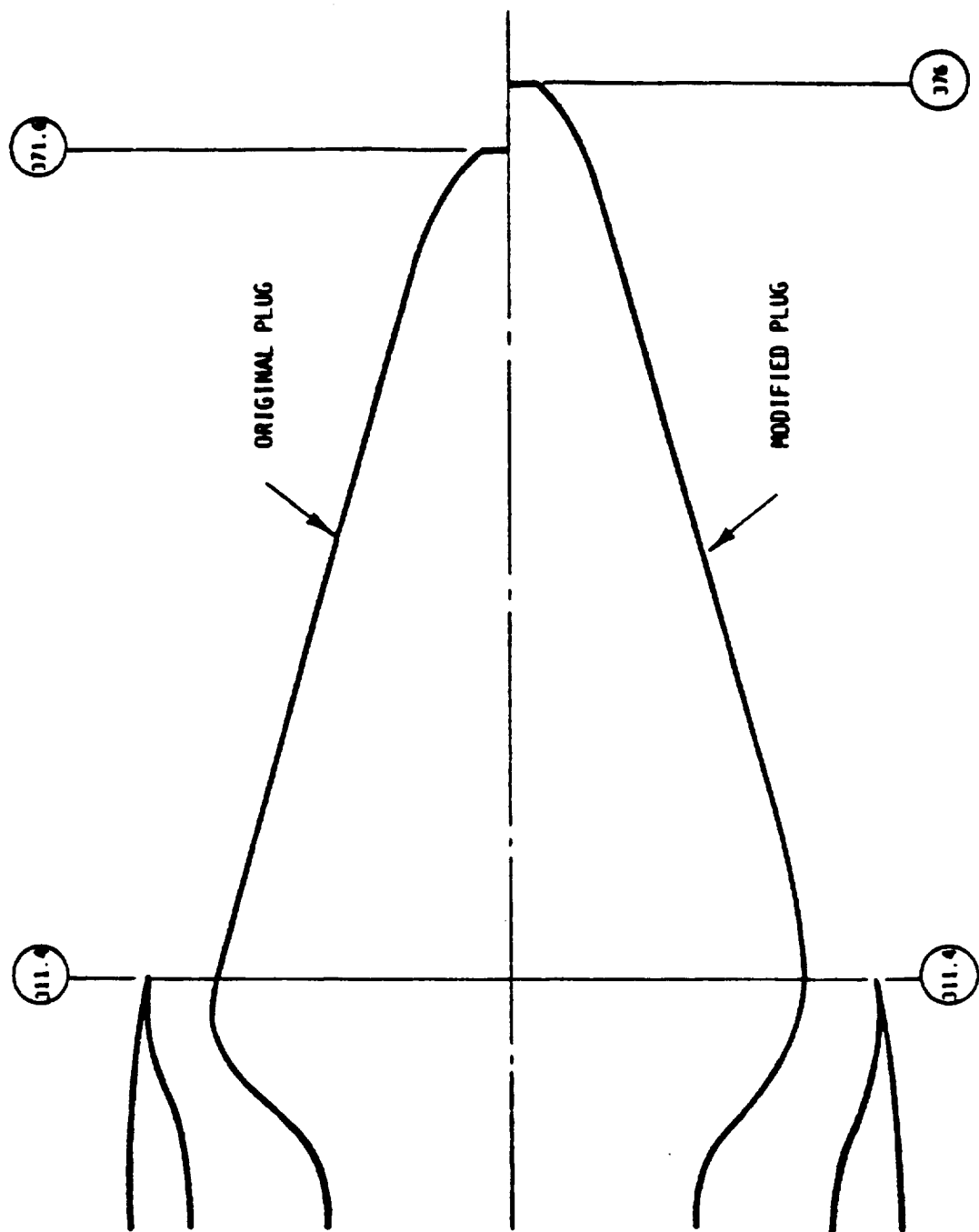
Figure 5-2. Redesigned Nozzle Plug.

34
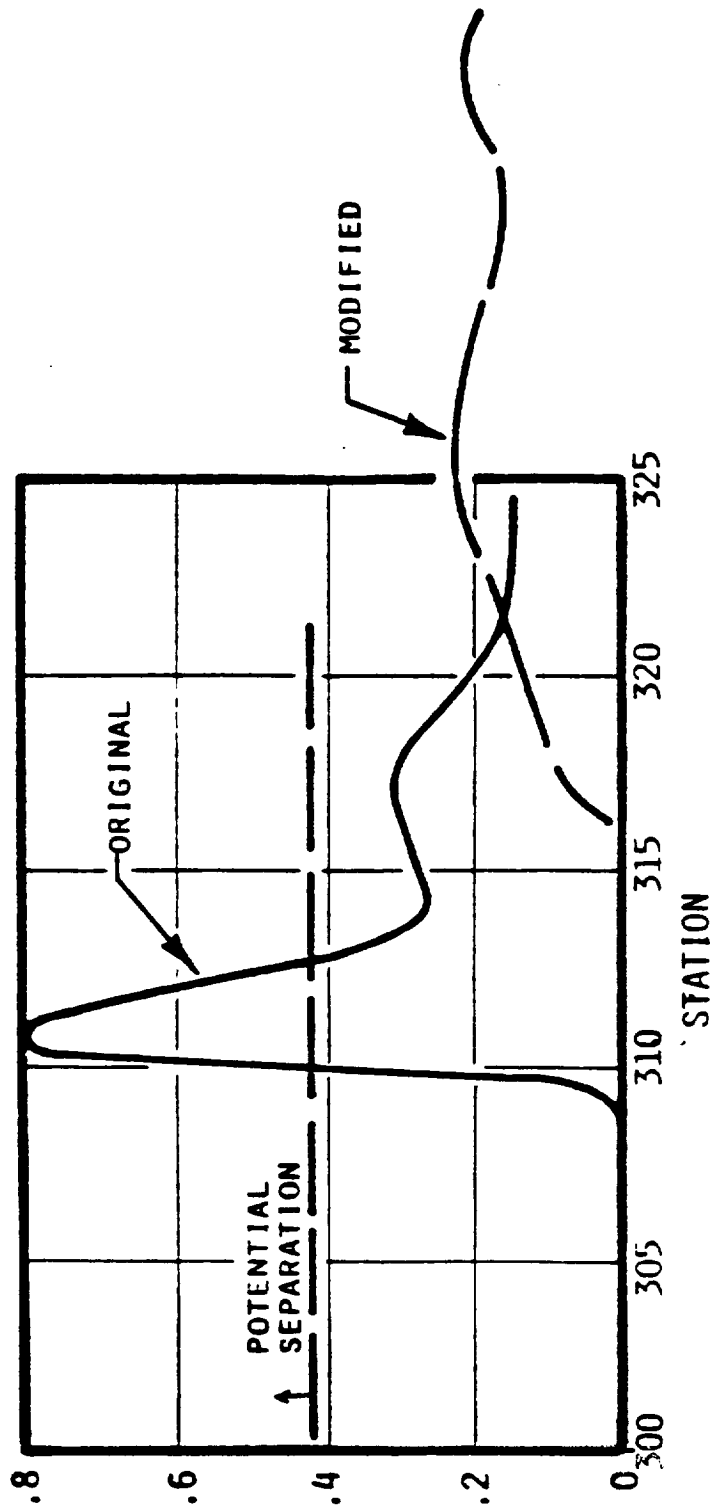
Figure 5-3. Core Plug Separation Parameter, Cruise Condition.

35

engine, this problem would be addressed by nacelle area ruling, recontouring the nacelle, or thinning/lengthening the support pylon. For the demonstrator engine flight test, The Boeing Company indicated no corrective measures would be necessary.

Wind tunnel measurements of the B727 wing wake led to selection of the UDF™ engine centerline at BWL 270; 30 inches above the original location. The movement was made to keep the unducted fan tips out of the wing wake at most flight conditions. Effects of the pylon wake have been determined experimentally in the BTWT 2-foot diameter MPS testing. Both fan blade stresses and performance behind the pylon were within acceptable levels at conditions expected during flight test. No fuselage was simulated in these tests.

5.2 FAN AERODYNAMIC DESIGN

5.2.1 Selection of Fan Flowpath and Configuration

The UDF™ engine configuration consists of eight forward and eight aft counterrotating rotor blades designed for the maximum cruise, 0.72 Mach number, 35,000 feet altitude condition. The blades are designed to run at 780 feet per second tip speed with a high disk loading (SHP/A_{ann}) of 85. The full-scale blade design is identified as F7-A7.

The aerodynamic design of the F7-A7 blades includes the nacelle forebody and the nozzle aftbody flowpaths in the axisymmetric flow calculations. The flow shape with the calculated flow streamlines and calculation stations is shown in Figure 5-4. The forebody is shaped such that its maximum diameter is larger than the blade hub diameter and is located approximately one blade-length upstream of the first rotor. This type of flowpath shape allows the flow to diffuse just upstream of the UDF™ blade rows, thereby lowering the blade inlet Mach numbers. It also provides a gentle concavity to the streamlines through the blades, thus eliminating unnecessary accelerating curvatures and high Mach number regions inside the blade rows. The flowpath through the blades is area-ruled to recognize the flow blockage due to the local blade thickness. Area ruling is accomplished by scalloping the blade platforms from a cylindrical shape to alleviate the high through-flow Mach numbers that occur in the region where the blades are the thickest. The circumferential average radius is then used in the axisymmetric flow analysis.
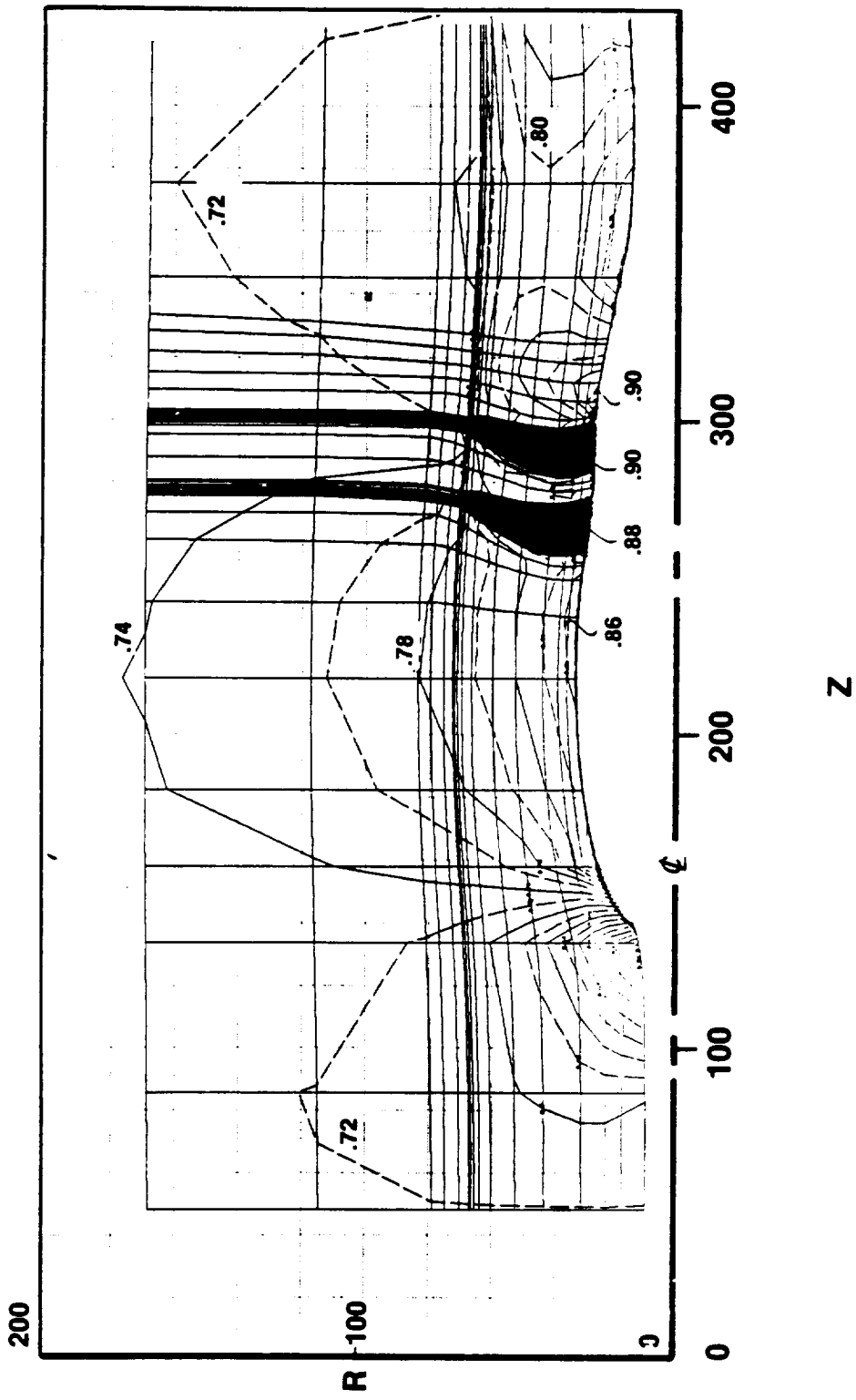
Figure 5-4. Aerodynamic Flow Field.

The blade design configuration was chosen to provide the optimum performance at the maximum cruise 0.72 Mach, 35,000 feet altitude condition. Table 5-1 summarizes the pertinent UDF™ aerodynamic parameters at the design point.

Table 5-1. Aerodynamic Design Point Parameters.

Design Flight Condition (Mach, Altitude)	0.72, 35,000 feet
Advance Ratio (J)	2.80
Total Power Coefficient (PQA)	4.10
Disk Loading (SHP/Aa)	85
Net Thrust (lb)	5,091
Physical Tip Speed (feet per second)	780
Tip Diameter (feet)	11.67
Hub/Tip Radius Ratio	0.425

There are eight forward and eight aft rotor blades closely coupled such that the distance between pitch change axes is 24.13 inches. The blade axes are selected to provide a maximum amount of aero sweep over the blade span while still maintaining aeromechanical blade stability. The F7-A7 blades have 33° and 29° of aerodynamic tip sweep, respectively. The aerodynamic sweep is used to effectively lower the true flow relative Mach number that the blade sees, thereby minimizing the shock losses at high cruise flight speeds. In the inner portion of the blade, the blade is swept forward in order to minimize the amount of blade overhang at the tip. Mach numbers for the forward blade (F7) are kept at just below 1.0; whereas, the Mach numbers entering the rear blade row (A7), enhanced by the forward rotor velocities, are slightly supersonic over the midportion of the blade.

The average blade lift coefficients are 0.425 and 0.400 for the forward and aft blades, respectively. The activity factors are 147 and 152 per blade for the forward and aft rotors, giving a total activity factor of 2392. The hub solidity is less than 1.0, allowing the blades to pass each other through flat pitch for reverse thrust operation.

5.2.2 Aero Design Procedure

The aerodynamic design approach used for the design of the unducted fan blades is the same quasi-three-dimensional approach used for conventional ducted fans. The principal design challenges of the UDF™ are: eliminating the choking of the flow in the blade hub region, and minimizing the passage shock losses due to the high through-flow velocities. Another challenge which is critical to the design is the correct modeling and prediction of the 3D flow field in the open tip region of the blades.

General Electric has previously developed a highly reliable quasi-three-dimensional design procedure that has been utilized to design many successful modern-day transonic fans, such as that used on the NASA/GE Energy Efficient Engine (E^3). This same procedure is incorporated into the design of the UDF™ blades developed under this NASA contract. The circumferential average flow solution is calculated for the UDF™ configuration using the optimum loading distribution developed by Theodorsen for counterrotating propellers (Figure 5-5). The open tip condition is simulated in the calculation by employing a wall boundary far removed from the blade flow field such that 10% of the total flow passes through the blades. A calculation is also made with only 1% of the total flow passing through the blades to further assure that the boundary is not influencing the flow field in the region of the blades. The flow calculation models the nacelle and nozzle flowpaths and the circumferential average flowpath through the blade hub region. The lean and blade blockage terms are incorporated in the radial equilibrium equation, which is solved at each of these stations and streamline grid locations. The resulting vector diagrams, representing the Mach 0.72 aerodynamic design point, are used for setting the blade meanline angles.

The blade platform shape is chosen to give the optimum aeroacoustic sweep distribution while still meeting the aeromechanical stability requirements. Initially, the blade axis is defined for each blade row by radial distributions of sweep and tangential lean. A chord distribution is specified consistent with the spanwise loading distribution. The airfoil sections are then defined along stream surfaces from the blade tip to hub. Radial and chordwise thickness distributions are defined to satisfy the aeromechanical stress and

stability constraints. This, together with the blade meanline angle distribution, specifies an airfoil shape along each streamline. The surface relative Mach numbers are plotted for a streamline of the aft rotor (A7) near the tip of the blade. Airfoil coordinates are defined at the hot running condition (aero design point), and the appropriate deflections calculated from the air loads and centrifugal loads are applied to define the cold manufacturing airfoil shape.
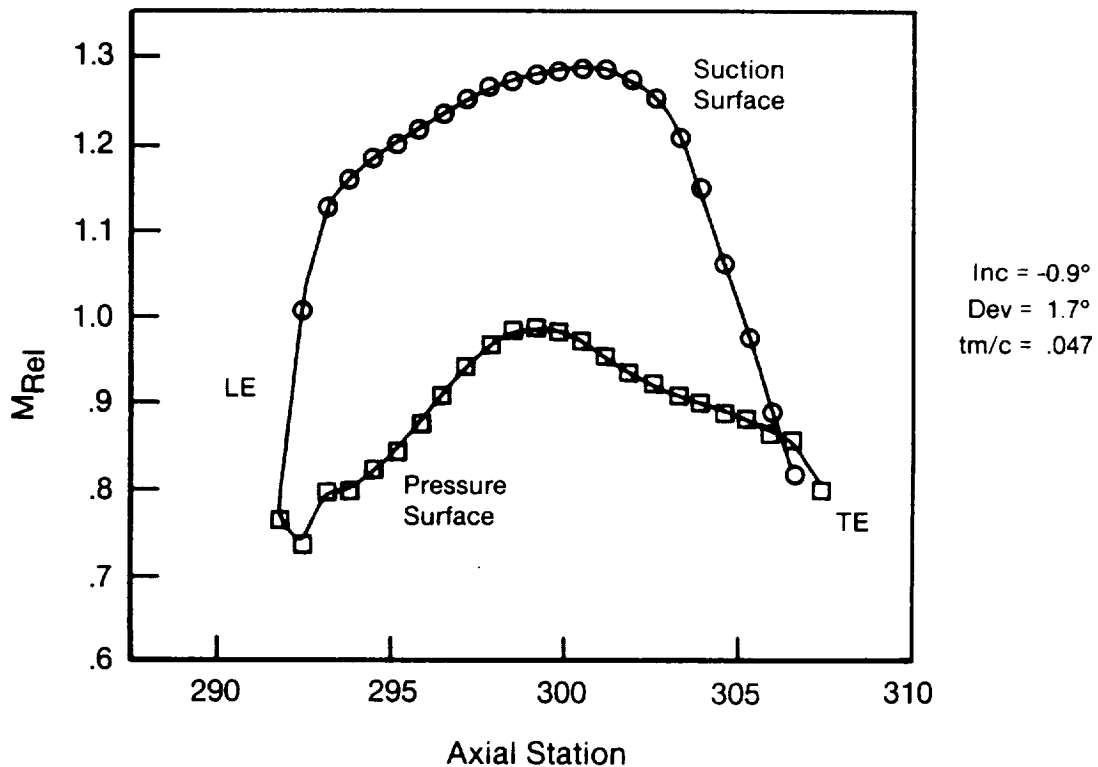
Figure 5-5. GE Euler 3D Airfoil Surface Mach Number Distribution.

5.2.3 Full-Scale Design Verification Through Scale Model Tests

The full-scale design of the F7-A7 blades for the demonstrator engine was completed in July 1984. Scale model blades of the F7-A7 configuration were also designed at this time for testing in the Boeing 8 × 6 ft high speed wind tunnel. The blades were designed to be 24.5-inch diameter (approximately 1/6 demo size) with a 0.425 radius ratio. The model propulsion simulator flowpath

is a direct scale of the demonstrator engine flowpath from the nacelle maximum diameter location to the nozzle trailing edge.

The MPS model was installed in the Boeing transonic wind tunnel, and the F7-A7 scale model blades were tested in November 1984. Testing was performed over a range of Mach numbers from static to 0.83, with a number of pitch angle settings chosen to match the scaled cycle power requirements at each Mach number along the flight path. The pitch angle settings were selected to provide equal torque on each rotor at equal design rotor speeds. The scale model testing included angle-of-attack and pylon effects, as well as rotor-to-rotor axial spacing effects on performance. Test data from the Boeing wind tunnel substantiates cycle power and efficiency requirements for takeoff and maximum cruise conditions.

5.2.4 Performance Map Development

The UDF™ map was generated from BTWT F7-A7 scale model data, adjusted for the Reynolds number difference from model-size to full-size conditions. The map was produced by essentially reversing the data-reduction procedure over a matrix of advance ratios and power coefficients. Any error in the approximation of induced efficiency by ideal efficiency is thereby removed. The virtue of this procedure is that it provides a rational extrapolation of the limited range of test data to cover a much broader range of operating conditions. The resulting map for the demonstrator engine unducted fan at a flight Mach number of 0.25 is shown in Figure 5-6.

5.2.5 SR-3 Design Comparison

Prior to the aerodynamic design of the full-scale F7-A7 counterrotating blades, an analytical study was performed to assess the performance of the single-rotation propfan (SR-3) which was developed by Hamilton-Standard under NASA Contract NAS3-20769. The propfan model has eight blades with 45° aero tip sweep. It was designed in scale model size (24.5-inch diameter) at a cruise flight condition of Mach 0.8; 35,000 feet altitude. A summary of the aerodynamic design point parameters is shown in Table 5-2 and compared to the design parameters of the F7-A7 blades. A comparison of the blade thickness-to-chord ratios is presented in Figure 5-7.
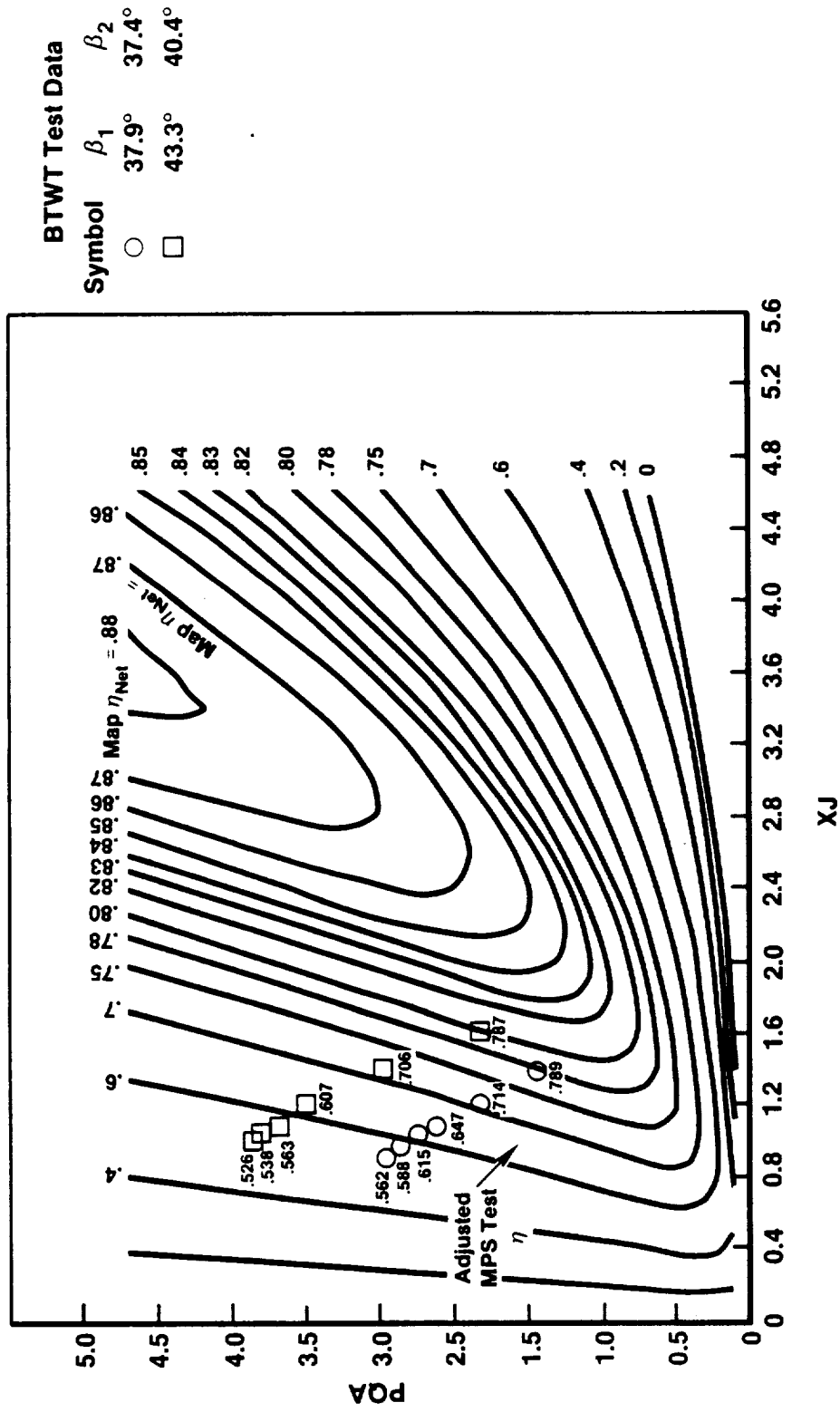
Figure 5-6. Fan Map at Flight Mach No. 0.25.

Table 5-2. Unducted Fan Blade Design Comparison.

	F7-A7 Engine No. 1	SR-3
Flight Mach Number	0.72	0.80
Radius Ratio	0.425	0.24
Number of Blades	8 + 8	8
Advance Ratio, J	2.8	3.1
Power Loading - SHP/D^2	55.5	37.5
Power Loading - SHP/A_a	85.0	50.0
Power Coefficient, C_p	2.66	1.695
Power Coefficient, PQA*	4.20	2.26
Thrust Coefficient, C_T	0.81	0.45
Thrust Coefficient, TQA*	1.27	0.60
Net Efficiency	0.849†	0.812‡
Blade Activity Factor(s)	147/152	235
Aero Tip Sweep Angle, °	33/29	45
Physical Tip Speed, ft/s	780	800
* Based on Annulus Area		
† Full-Scale Goal		
‡ Scale Model Test		
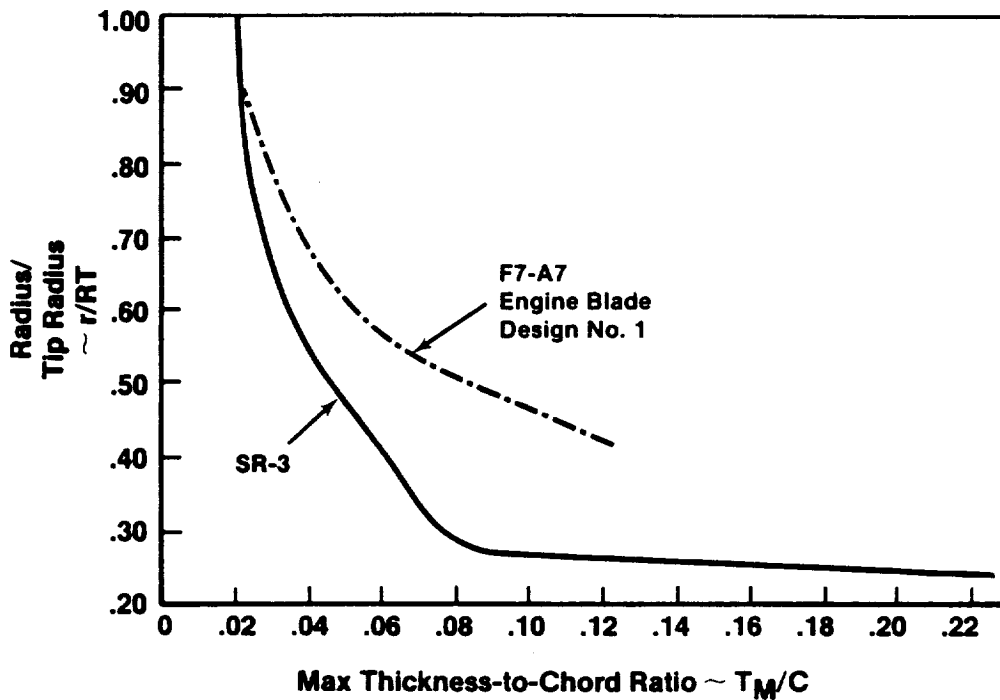
Figure 5-7. Comparison of Blade Thickness-to-Chord Ratio.

A data match analysis of the SR-3 design point test data was performed using the General Electric design calculation procedure. An axisymmetric flow analysis was set up using the SR-3 model flowpath, blade geometry, and design point test data obtained from Reference 1. The results of this analysis are illustrated in Figure 5-8. The flow streamlines and calculation stations are depicted, with contours of meridional Mach numbers superimposed on the plot. Internal to the blade, the Mach numbers peak at 0.99, where the blade root thickness tends to choke the local hub flow. Downstream of the blade trailing edge, the large hub accelerating curvature raises the Mach number greater than 1.0. This analysis compares well with the findings described in Reference 1.

Euler 3D analyses were also performed on the SR-3 blade using the General Electric Euler program. The blade-to-blade 3D flowfield was analyzed at the Mach 0.8 design point, and surface Mach number distributions were obtained. The surface Mach number distributions resulting from this 3D analysis of the SR-3 blade suggests that the thick airfoil sections near the hub plus the lack

$Mo = 0.80$, 35,000 Altitude
$U_r = 800$ fps

SR-3
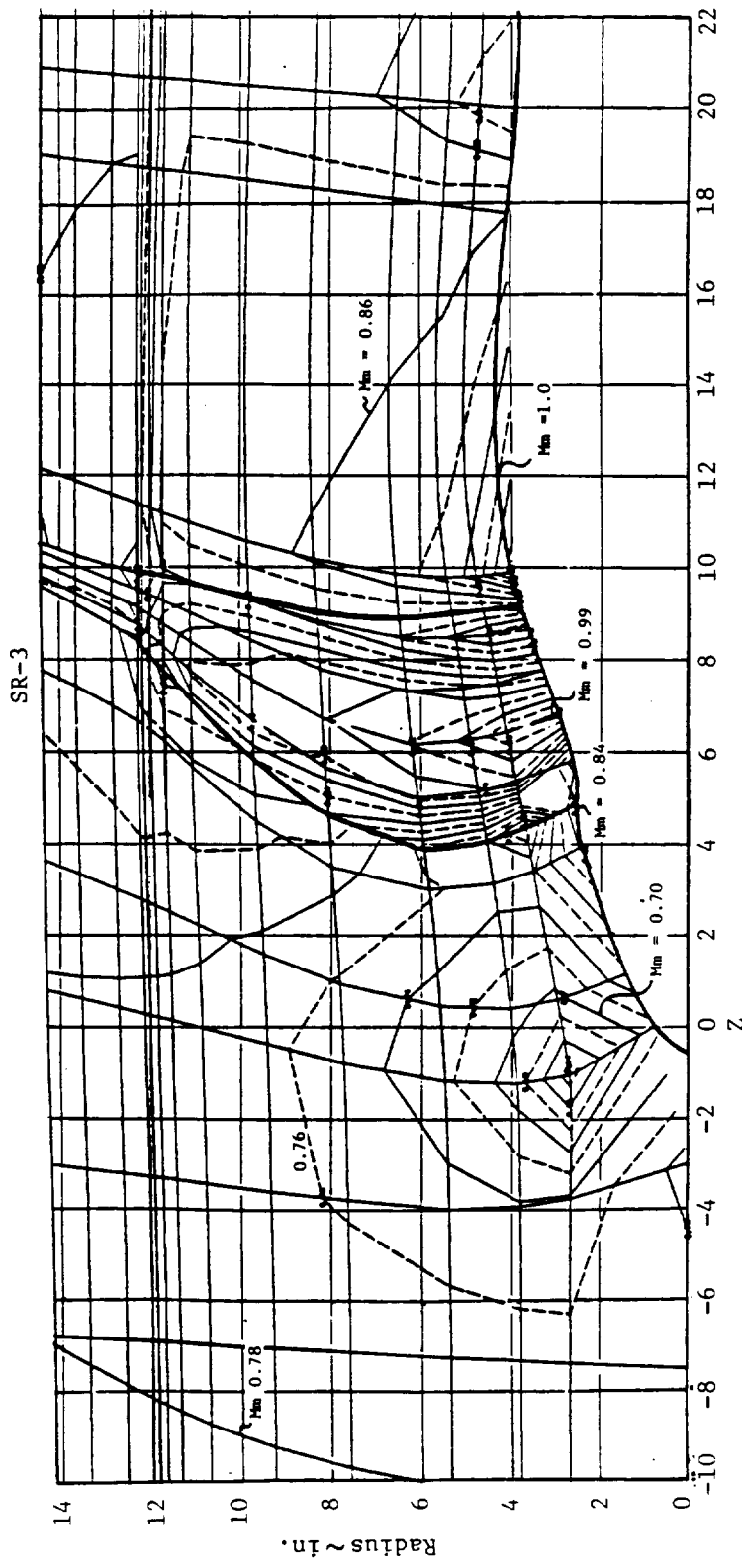
Figure 5-8. SR-3 Axisymmetric Flow Analysis.

of adequate area-ruling in the hub adversely affect the overall aerodynamic performance at Mach 0.80 cruise. Improvements in hub area-ruling and airfoil meanline shaping could lead to better aerodynamic performance.

5.3 POWER TURBINE AERODYNAMIC DESIGN

5.3.1 Counterrotating Turbine Concept

The power turbine for the UDF™ engine is a six-stage turbine plus inlet and outlet guide vanes. The 12 turbine blade rows (excluding the inlet and outlet guide vanes) rotate alternate rows in opposite directions. The average pitchline wheel speed is 218 feet per second, which gives an average stage loading $(h/2U^2)$ of 1.15.

The fundamental concept of the counterrotating, vaneless, multistage turbine is presented in Figure 5-9. Vector diagrams for a conventional stage and a counterrotating stage with symmetric, repeating stages at the same wheel speed (U) are shown. The diagrams for the two blade rows of each stage are identical; therefore, the blade efficiency is the same for each stage. At the same wheel speed, the work per stage for the counterrotating stage is four times the work of the conventional stage. As applied to the UDF™, this theory means that a comparable number of blade rows gives a comparable stage loading at one-half the rpm of a conventional turbine.

The performance characteristics of the GE36 demonstrator power turbine are as follows:

- Two mechanically independent but thermodynamically inter-dependent turbines

- Rotor torques opposite and approximately equal

- Work split and speed ratio variable depending on local characteristics.

5.3.2 Flowpath Aerodynamic Features

The flowpath aerodynamic features are illustrated in Figure 5-10. The six-stage unshrouded turbine incorporates orthogonal blades in the first two stages and cylindrical tip outer diameter blades in the aft stages. The inlet flow is introduced through a high slope transition mixer frame and inlet guide

Conventional Stages

Stator   **Rotor**
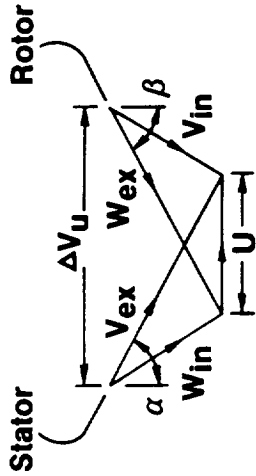
$\Delta V_u = 2U$

$\Delta h = \dfrac{U \Delta V_u}{gJ}$

$\quad = \dfrac{2U^2}{gJ}$

Counter-Rotating Stage (CRT)

Left-Running Rotor   **Right-Running Rotor**
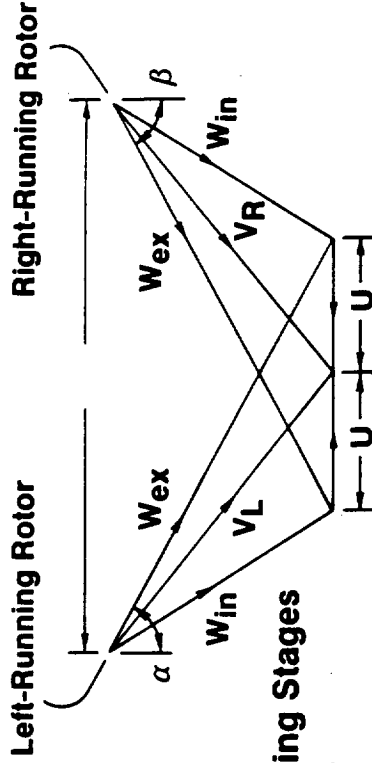
$\Delta V_u = 4U$

$\Delta h = \dfrac{2U \Delta V_u}{gJ}$

$\quad = \dfrac{8U^2}{gJ}$

- **Symmetric, Repeating Stages**
- **V = abs. vel. Vector**
- **W = rel. vel. Vector**

- **Same Vector Diagram — Therefore Same Efficiency**

- **Work Per Stage (2 Rows) for a Counter-Rotating Turbine is Four Times That for a Similar Conventional Stage**

Figure 5-9. Vector Diagram Comparison.

47

Figure 5-10. Flowpath Power Turbine Aerodynamic Features.
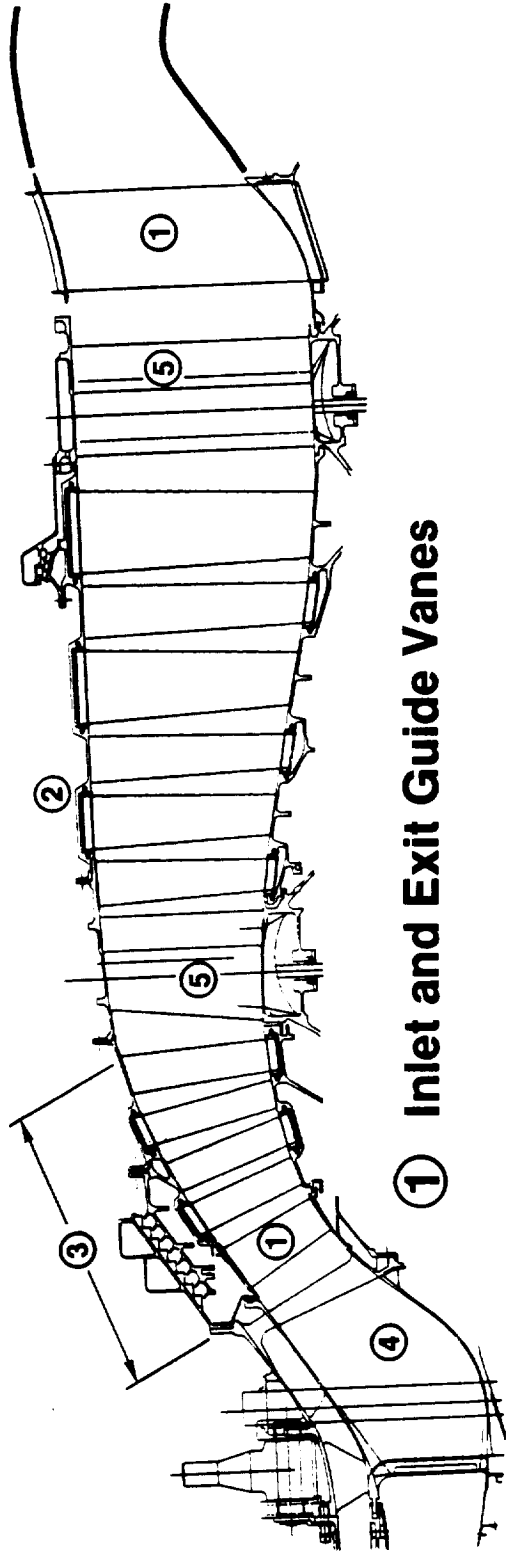
① Inlet and Exit Guide Vanes

② Unshrouded Tip Construction

③ Orthogonal Blading

④ High-Slope Transition Duct/Mixer

⑤ Power Frames

vane assembly, and the exit flow is turned by exit vanes. The transition frame serves as the structural connection and support between the core engine and the propulsor, provides the gas path transition from the low diameter core engine to the higher diameter power turbine, and allows for the addition and mixing of 20% IPC discharge air into the core discharge air. The orthogonal (forward swept) blades are used in the first two stages to avoid high losses, normally the result of high sweep in the high flowpath meridional slope. The power frame aerodynamic design was constrained by strut quantity, thickness, and axial width mechanical design requirements. The resulting hybrid cascade design was chosen to avoid high losses associated with low aspect ratio blade rows.

5.3.3 Design Point Performance Estimate

Table 5-3 lists some of the free vortex, pitchline vector diagram design parameters, indicating the low pressure ratio for each blade row (about 1.12) and the low inlet and exit Mach numbers (about 0.3 and 0.5, respectively). The predicted design point efficiency is given as:

Base Aero Efficiency (at zero tip clearance)	93.13
Tip Clearance	-0.83
Reynolds Number	-1.36
Power Frames	-0.39
Drum Rotor	+0.50
	91.05

The base efficiency, tip clearance, and Reynolds number effects are all predicted with the General Electric Turbine Performance Prediction Program (TP^3) utilizing a highly modified Craig and Cox (Reference 9) loss prediction model. The efficiency effect for the power frames is an estimate of the additional losses caused by the power frames not accounted for by the loss prediction. The drum rotor efficiency credit is obtained from flowpath cavity reductions in the unshrouded design and is based on the results of internal General Electric test data on flowpath overlap/cavity geometries. Figure 5-11 demonstrates an overall turbine map at equal rotor speeds with some selected operating points. The map is essentially the same as a conventional turbine map; however, the operating line is different than that of a conventional

Table 5-3. Power Turbine Vector Diagram Data.

(Free Vortex)

Stage	IGV	1 F[1]	1 R[2]	2 F[1]	2 R[2]	3 F[1]	3 R[2]	4 F[1]	4 R[2]	5 F[1]	5 R[2]	6 F[1]	6 R[2]	OGV
Pitch Radius	17.51	18.47	19.17	19.74	20.22	20.45	20.33	20.10	19.85	19.48	19.21	18.99	18.83	20.51
Δh	- - -	9.19	9.19	9.19	9.19	9.19	9.19	9.19	9.19	9.19	8.55	7.11	5.64	- - -
P_T/P_T	- - -	1.12	1.11	1.11	1.11	1.12	1.12	1.12	1.13	1.13	1.13	1.11	1.08	- - -
M_{in}	0.34	0.35	0.32	0.29	0.28	0.26	0.27	0.28	0.30	0.32	0.34	0.33	0.32	0.40
M_{ex}	0.44	0.50	0.49	0.48	0.48	0.48	0.49	0.51	0.52	0.54	0.51	0.48	0.45	0.36
β_{ex}	47.1	57.4	58.9	60.5	61.5	62.6	61.5	60.5	59.4	58.7	55.1	50.2	45.1	- - -
$\Delta\beta$	37.8	94.4	95.5	97.4	98.4	100.3	98.2	96.4	95.1	94.1	90.6	78.5	64.2	30.4
V_z	547	489	454	421	399	380	399	418	436	454	472	488	505	574
Axial Width	1.83	1.26	1.31	1.27	1.52	1.50[3]	1.64	1.98	1.72	2.68	1.98	3.11	1.97[3]	4.20
TET	0.030	0.030	0.030	0.030	0.030	0.060	0.030	0.030	0.030	0.030	0.030	0.030	0.060	0.030
Clearance	- - -	0.030	0.030	0.030	0.030	- - -	0.030	0.030	0.030	0.030	0.030	0.030	- - -	0.050[4]
Number of Airfoils	60	124	118	120	94	96	90	72	84	54	82	56	80	26

[1] Front Rotor
[2] Rear Rotor
[3] Short Chord Airfoils (4.35 and 4.70 Long Chord)
[4] Shrouded

engine, because the variable fan allows the operating line to be determined for an optimum combination of fan and turbine performance. As a result, there is very little efficiency variation across the operating line.

$$N_F = -N_R$$
(With D.P. Reynolds No. Loss)
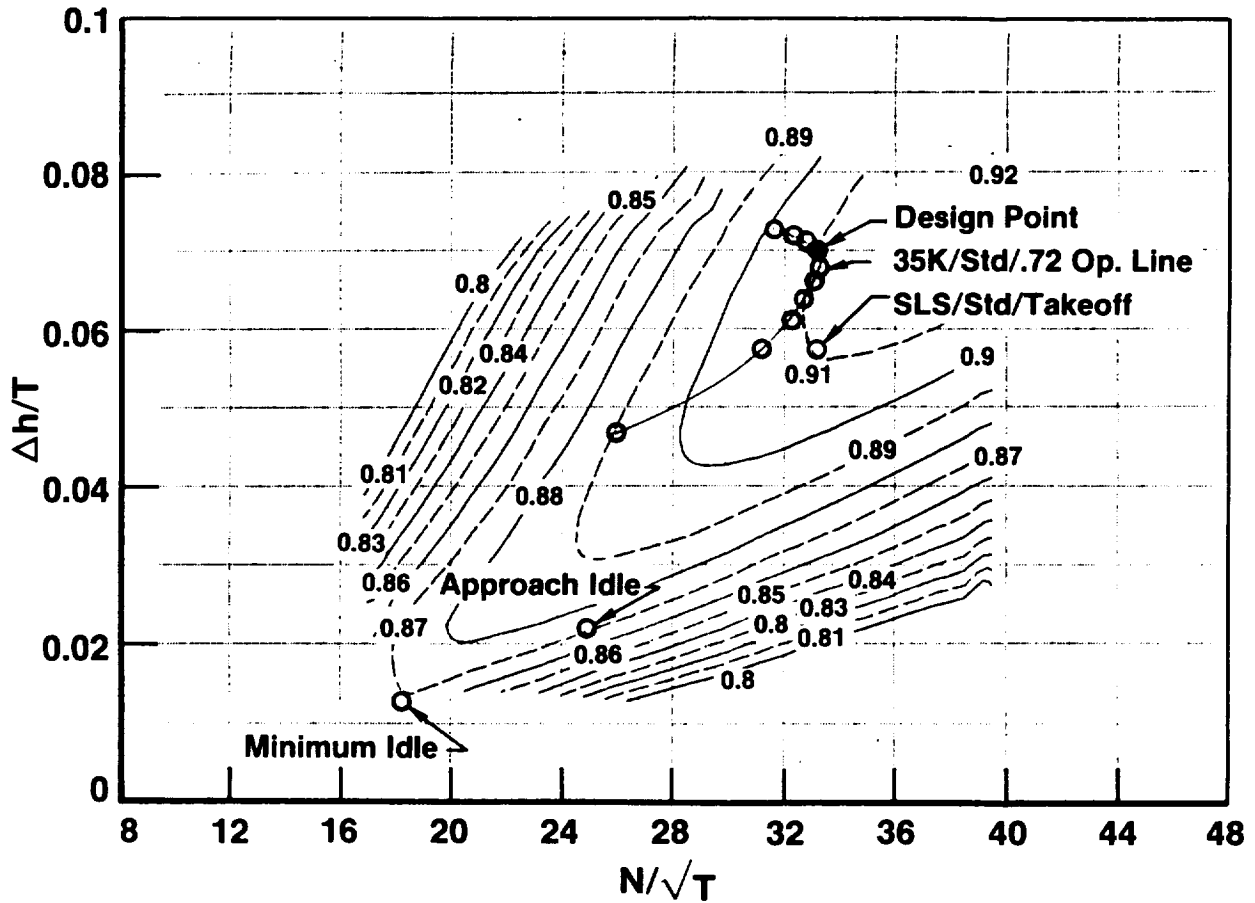
Figure 5-11. Overall Power Turbine Map.

5.3.4 Transition Duct/Mixer Frame Design

The transition duct/mixer frame is a large area ratio annular diffuser with 20 large struts which have a very large number of film cooling holes used to mix IPC discharge air into the core discharge stream. Figure 5-12 depicts

51

IGV
(60)
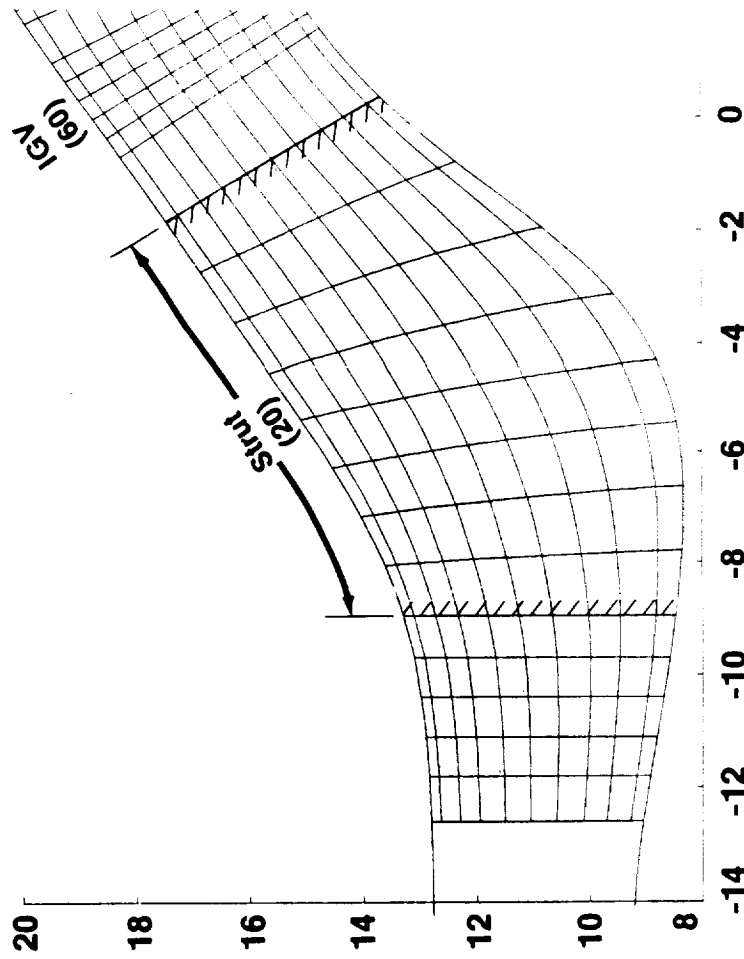
Strut
(20)

$W_{LPT\ Inlet}$ = 38.13 lb/sec
W_{IGV} = 45.72 lb/sec
@ Each of 7 Interior Stations

$W_{Outer\ Wall}$ = 0.69% (35% Penetration)
W_{Strut} = 1.55% (100% Penetration)
$W_{Inner\ Wall}$ = 0.60% (35% Penetration)
W_{Total} = 19.90%

$T_{LPT\ Inlet}$ = 1623.8° R
T_{Bypass} = 740.0° R
T_{IGV} = 1486.3° R

Figure 5-12. Transition Duct/Mixer Frame.

the circumferential averaged flow determination (CAFD) flowpath and the flow addition analysis scheme. Flow is added equally at each of seven stations. Inner and outer cooling is allowed to penetrate into the flowpath 35% from each wall; strut cooling is added across the full annulus height.

5.3.5 Rotor Airfoil Aero Design

Figure 5-13 shows a representative pitchline airfoil and leading edge detail. The Mach number and velocity distributions satisfy all of the General Electric Design Practice requirements with respect to velocity distribution shape, suction side aft diffusion, and pressure side leading edge diffusion.

The power frame design required 8 long chord struts (approximately 4.5 inches) with a maximum thickness of 1.0 inch. As illustrated in Figure 5-14, the hybrid cascade configuration chosen for the rear power frame pitchline satisfies the system requirements; the cascade has nine small airfoils between each of the eight struts. The Airfoils designated 3 through 9 are identical, but Airfoils 2 and 10 are uniquely designed for flow compatibility with the strut airfoils.

5.3.6 Build 2 Turbine Aero Modifications

Because of the turbine blade failure on the first engine build, extensive modifications were made to the power turbine. Damping pins were added to all rotating blade rows except the Rotor 5 power frame. The pin diameters were in the range of 0.110 to 0.150 inch. Also the tip clearance of all odd rotors was increased by 0.050 inch and all even rotors by 0.030 inch. These changes have a major impact on both the turbine efficiency and the flow function. The pins cause a pressure loss, due to drag on the pins, and the opened tip clearance causes an additional leakage loss, both of which decrease the efficiency. The pin drag calculates to be equivalent to an efficiency loss of 2.26 points, and the tip clearance increase causes an efficiency loss of 0.98, for a total efficiency loss of 3.24 points. The pins will cause a flow function decrease due to the pressure loss through the turbine and by causing a throat blockage estimate at one-fourth of a pin diameter with a total effect calculated to be 1.18%. The increased tip clearance will allow the flow function to increase by 0.55% for a net flow function reduction of 0.63%. The net effect on the

Figure 5-13. Rotor 8 Airfoil and Leading Edge Geometry at Pitch Streamline.

power turbine performance caused by the addition of the damper pins is -3.24 points.
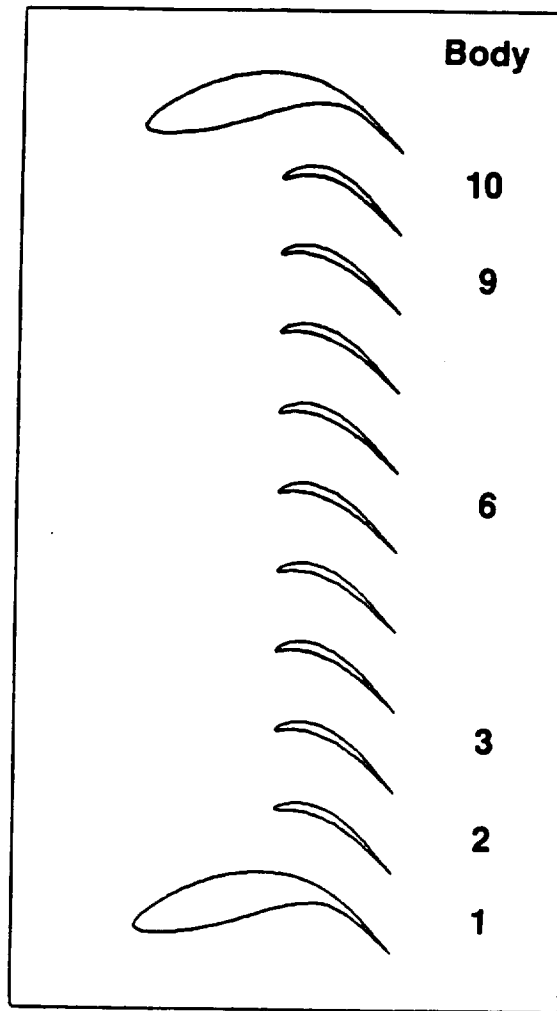
Figure 5-14. Rotor 12 Pitch Streamline.

6.0 F404 REFURBISHMENT AND MODIFICATIONS

6.1 F404 REFURBISHMENT

The UDF™ engine utilizes a modified and refurbished QT F404 gas generator (Figure 6-1), on loan from the U.S. Navy through NASA, as the propulsor power plant. Engine Serial Number 215201 completed 339 hours of service (271 flight hours) through March 1984 with no significant events. The refurbishment incorporated all new product F404 modifications, as well as replacement of worn hardware, including all turbine and compressor airfoils. The fuel manifold system external of the duct enclosure was replaced with the double-walled design common in current F404 engines. Also, in compliance with existing design intent, the Inco 718 rotor structure and related interface hardware were substituted to increase component lives.

6.2 F404 MODIFICATIONS

6.2.1 F404 Fan Module Modifications

Figure 6-2 illustrates the major modifications to the F404 fan module as required to satisfy UDF™ requirements.

The YJ101/YF404 variable IGV and Stage 1 vane system is utilized in the UDF™ system to enhance stall margin lost by flow function reduction at the LPT exit plane. Additional relief is obtained by closing the IGV schedule by approximately six degrees beyond the normal F404 schedule. This design change was confirmed through the F404 Green Run performed at Lynn prior to shipment to Evendale for UDF™ assembly.

Two other modifications have also been incorporated into the standard system. To facilitate the UDF™ inlet, the forward outer flange of the frame was reconfigured as originally designed for the Navy A6 application, and because F404 anti-icing provisions are not required for the UDF™, the six o'clock port on the casing was capped.
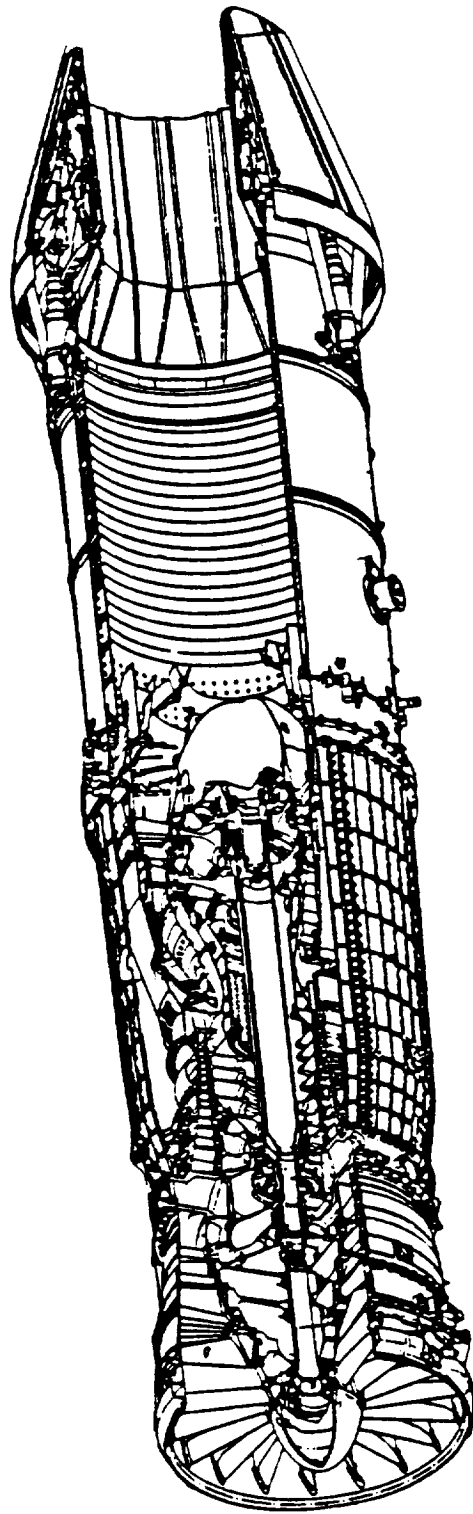
Figure 6-1. F404 Gas Generator.

Inlet

Anti-Ice Manifold

Fwd Flange
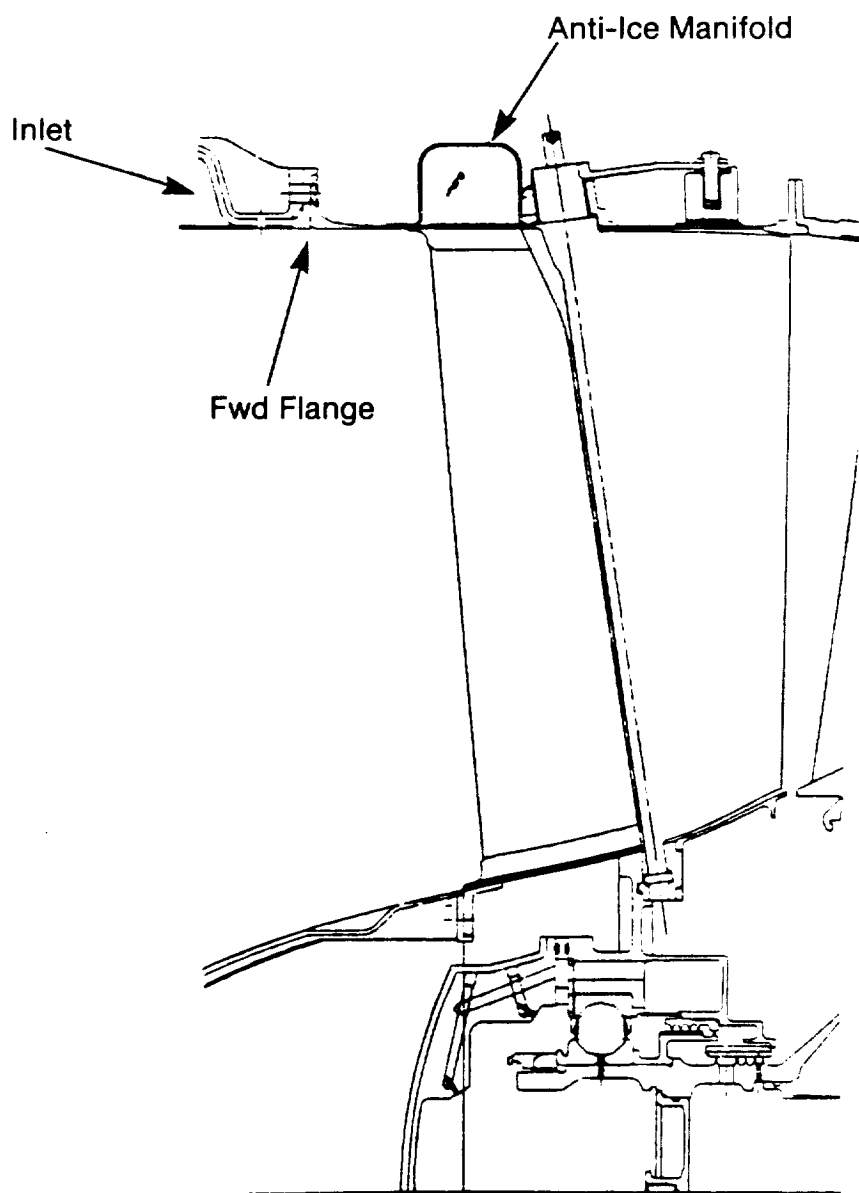
Figure 6-2. F404 Fan Frame Modification.

6.2.2 F404 Compressor Module Modifications

Changes implemented into the compressor module are shown in Figure 6-3.
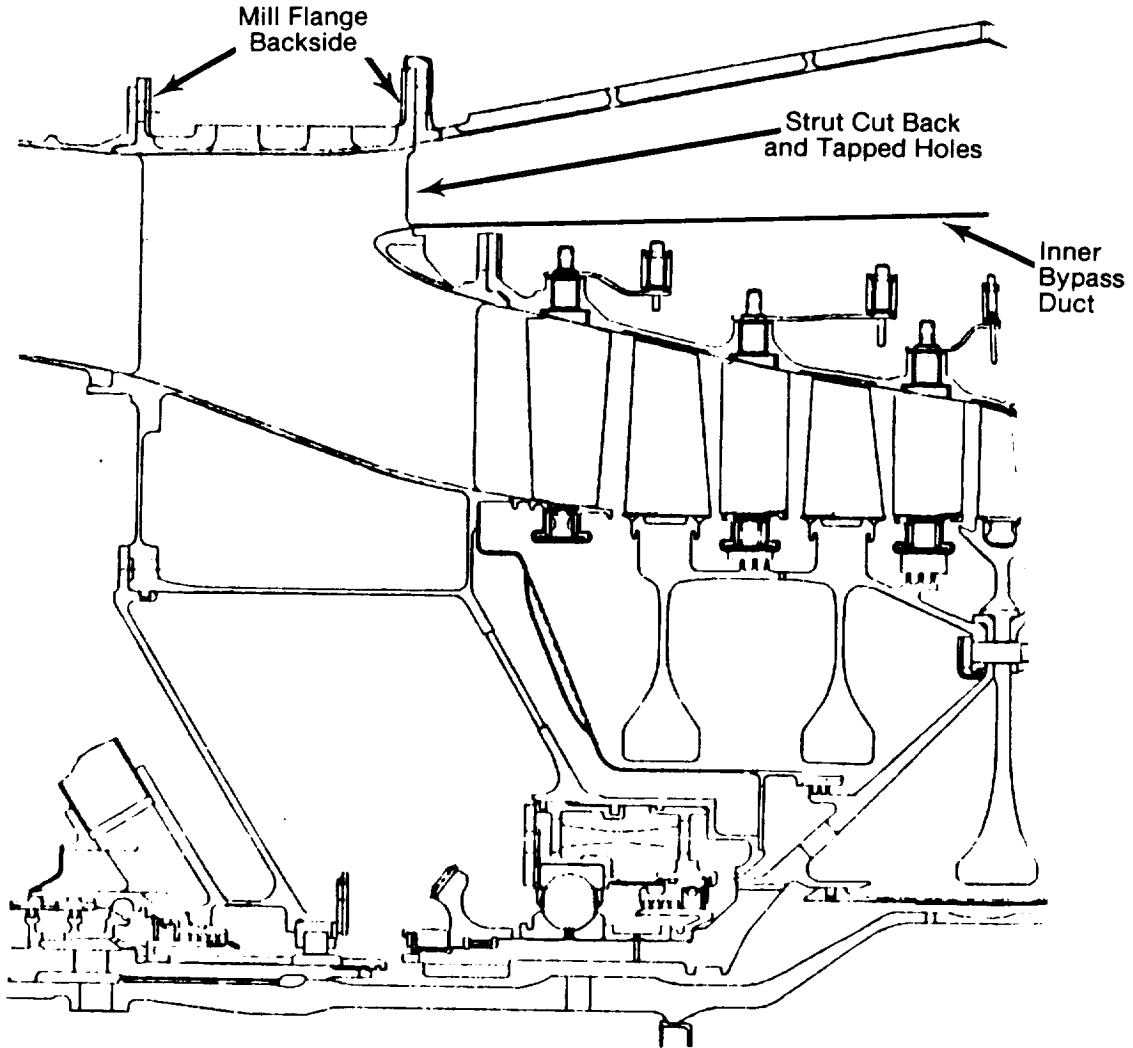
Figure 6-3. F404 Compressor Module Modifications.

By increasing the primary wall and flange thicknesses, structural improvement of the outer bypass duct to meet the UDF™ blade-out criteria of simultaneous blade-out in each propulsor rotor was accomplished. The enhanced design, as illustrated in Figure 6-4, increased the component weight by 90 pounds. Modification for the forward mount on the midframe for both ground and flight test

applications was also completed. To minimize bypass duct aerodynamic losses, the compressor stator rigging lever arms were shielded with an inner duct.
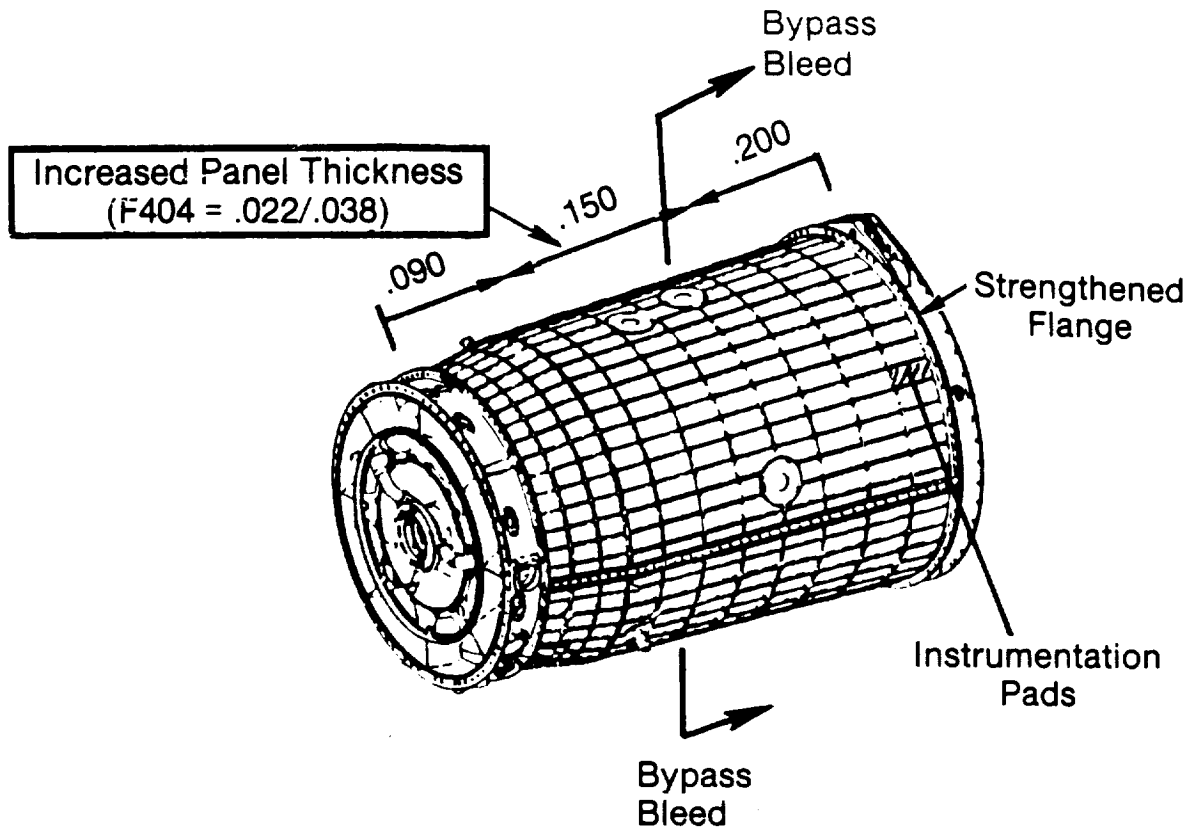
Figure 6-4. Fan Duct.

The duct design was an improvement of previous designs implemented in YJ101 and VABI development testing. Figure 6-5 depicts the duct design and itemizes the features inherent to the hardware.

6.2.3 F404 Combustor and Turbine Module Modifications

Transition of the F404 flowpath and secondary flow systems is achieved through the addition of a new, UDF™ mixer frame. The incorporation of this

hardware, as illustrated in Figure 6-6, requires significant changes to the F404 LP and bypass duct hardware. The new frame replaces the F404 exhaust frame and provides service to the F404 C-sump as well as the UDF™ systems. All services to the sump are functionally identical to the F404 production design which was replaced. A new LPT shroud support, shown in Figure 6-7, rabbets to the frame with a thermal slip joint, thus reducing stress and out-of-round distortions. Concentricity of the shrouds within the new support was maintained by utilizing an assembly grind. Potential backflow of mixer strut cooling flow is avoided by using a bypass duct diffuser. The duct was designed to avoid excitation and potential fatigue problems within the operating range.

Upper Half
Material
(.050 Thick Ti 6Al-4V)

Lower Half
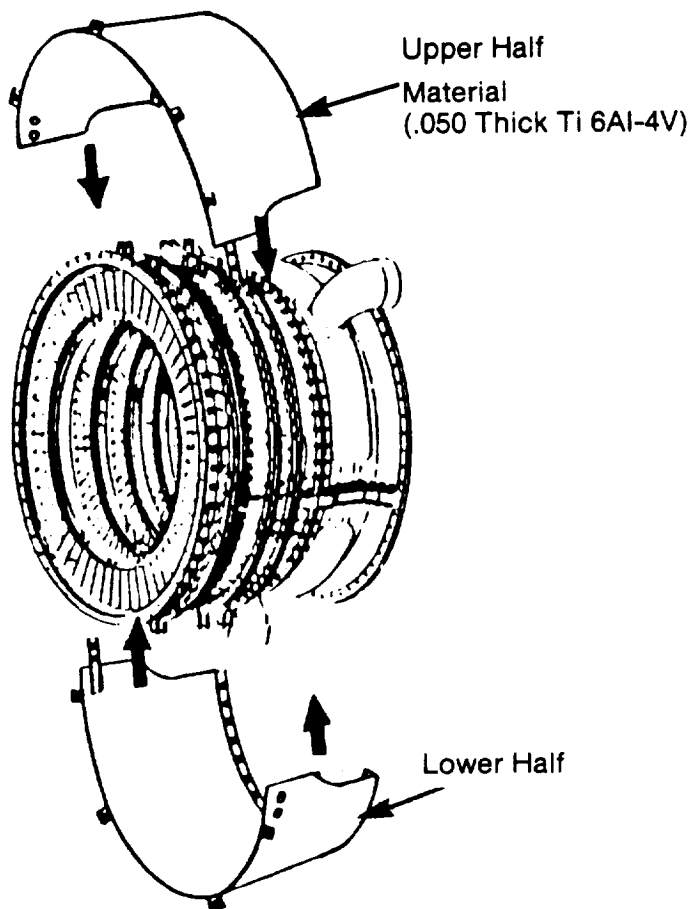
Figure 6-5. Inner Bypass Duct.

61
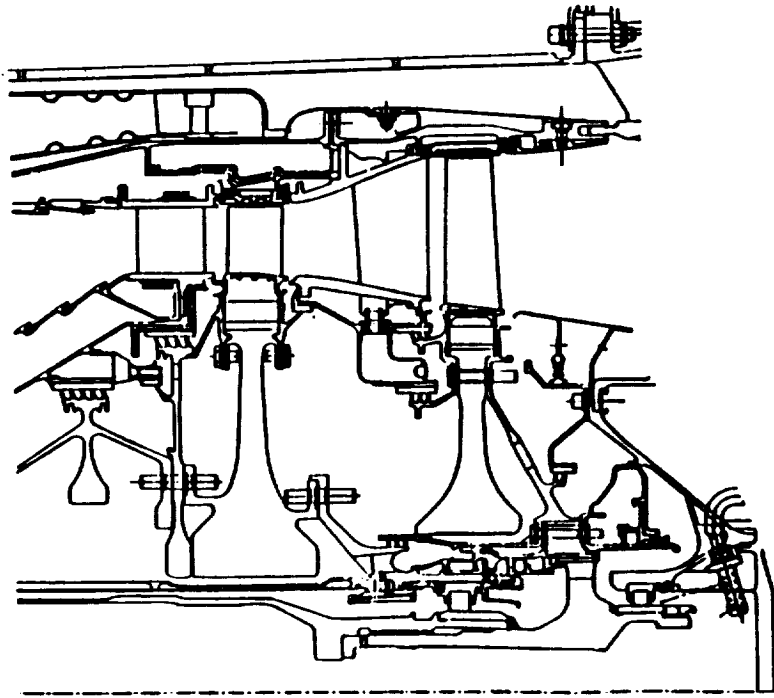
Figure 6-6.   F404 Modifications, Turbine Combustor Modules.
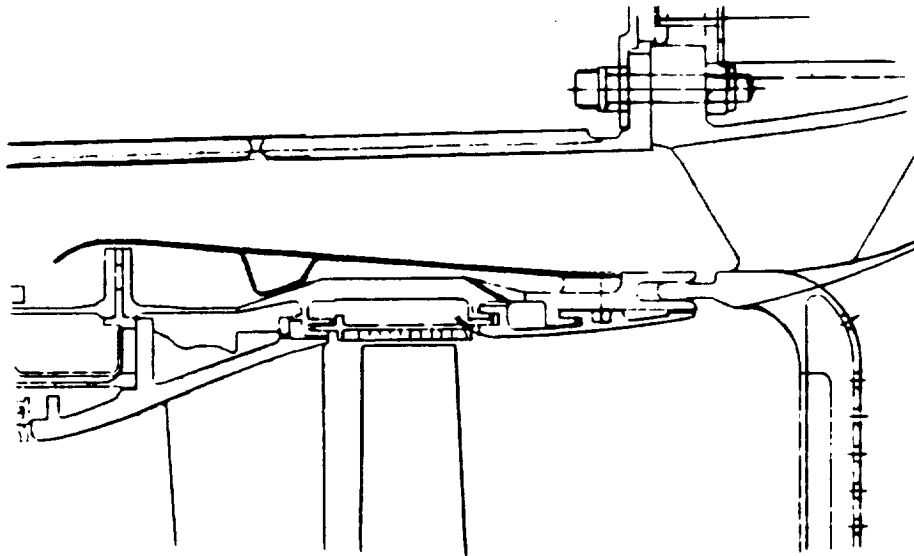
Figure 6-7.   LPT Static Structure.

7.0 HEAT TRANSFER AND SECONDARY FLOW ANALYSIS

7.1 FLOW SYSTEM OVERVIEW

The propulsion system hardware is cooled with F404 bypass air supplied through the transition mixer frame and secondary flow circuit internal to the propulsor. Figures 7-1 and 7-2 illustrate the flow circuits and estimated flows at the rated takeoff (T/O) design point in percent of fan inlet flow (% W_2). The static frame also introduces bypass air into the core stream through a network of laser drilled cooling holes such that the propulsor rotor inlet temperature profile is satisfactory. As illustrated, the secondary flow air is utilized to pack all propulsor sump seals. Additional cooling is supplied to the internal sting tube cavity (which houses the fan blade actuator) and outer nacelle/fan blade retention hardware through scoops in the outer nacelle structure.

7.2 MIXER FRAME HEAT TRANSFER

The mixer frame shown in Figure 7-3 is an Inco 718 cast structure, which is film cooled by approximately 41,000 0.030-inch diameter holes distributed along the outer band, inner band, and struts. An Inco 625, impingement-cooled leading edge with film holes is welded to each strut. The geometry has been designed to minimize flow pressure loss through utilization of an inlet diffuser which recovers a large portion of the velocity head and prevents flow separation.

The frame flowpath static pressure distribution at the minimum backflow margin (BFM) point is depicted in Figure 7-4. Because the strut leading edge flowpath pressure is higher than the strut internal pressure, there are no film holes in the vicinity of the leading edge. The minimum BFM is 0.9% along the inner flowpath fairing just upstream of the strut leading edge.

The frame overall cooling effectiveness is approximately 0.75 at rated takeoff, resulting from a coolant flow of 15% W_2. In addition to a film effectiveness ranging from 0.3 to 0.7, there is a strong film hole effect (ha)$\propto$, due to the great density of the film holes.
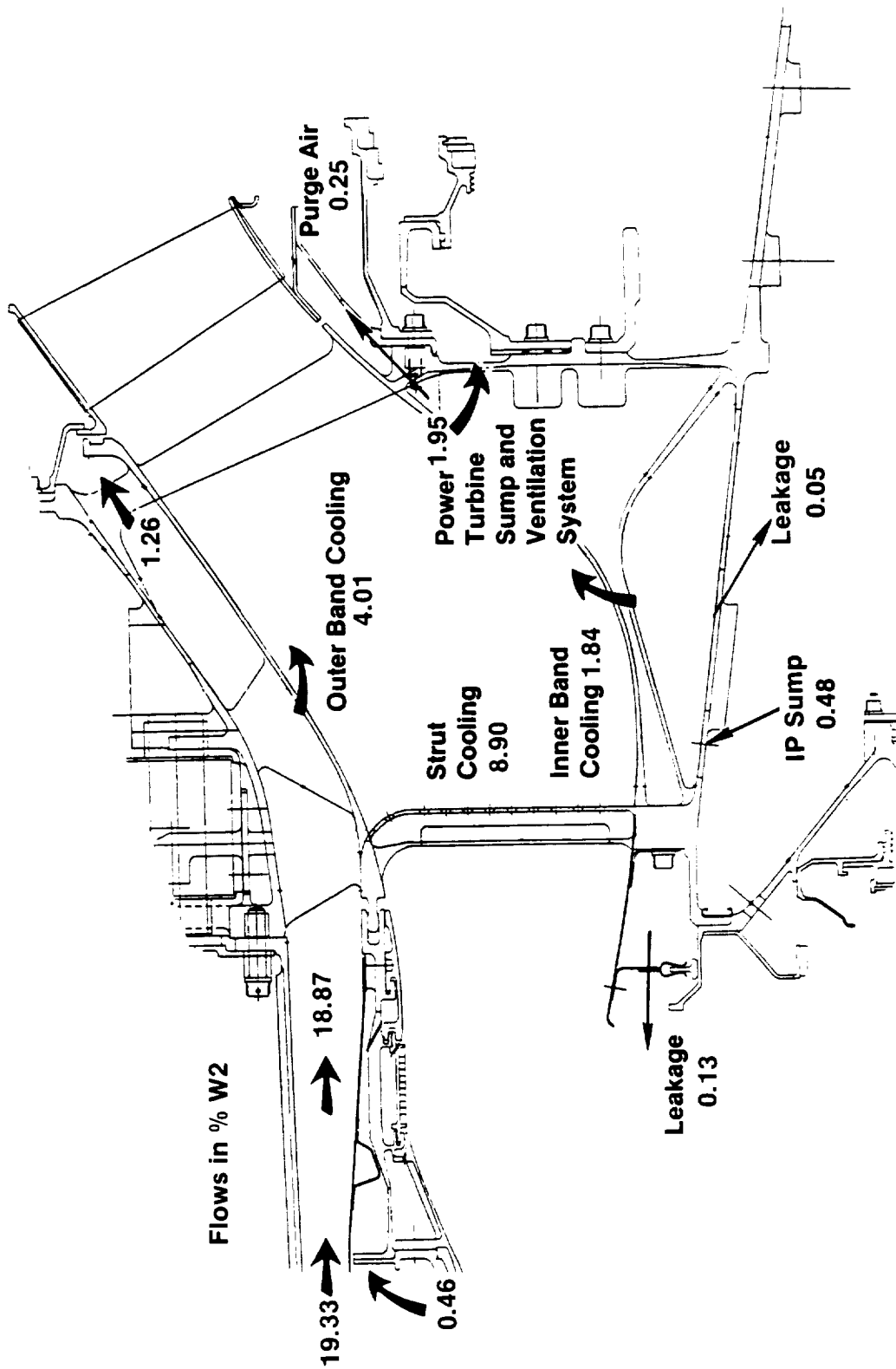
Figure 7-1. Frame Flow System Rated Takeoff.
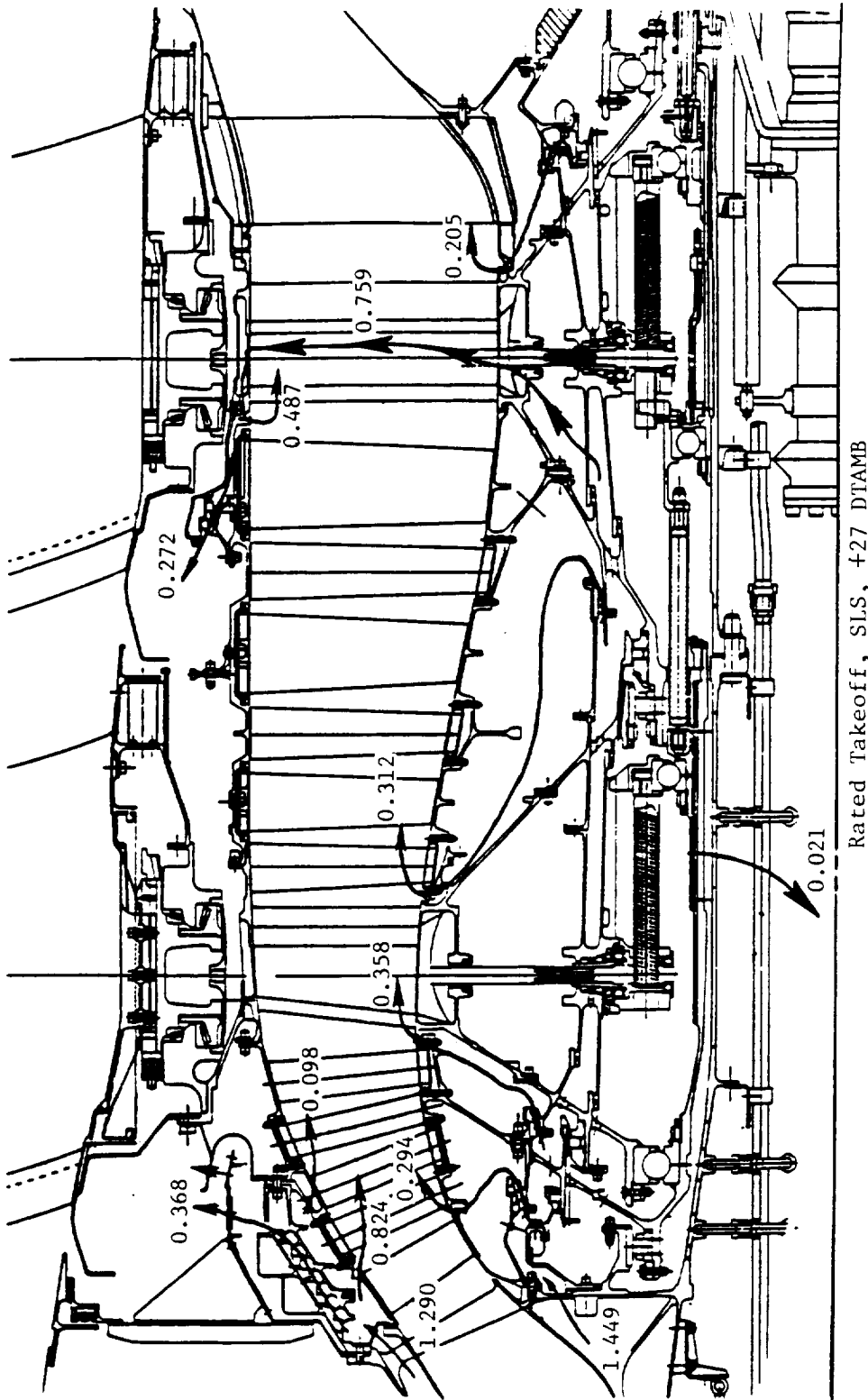
Rated Takeoff, SLS, +27 DTAMB

Figure 7-2. Secondary Flow System Design Point Flows (%W2).

65

Approximately 41,000 Holes Total -
20 Struts

	Strut*	Outer Band	Inner Band
Rows	30	24	32
Holes Per Row	19-29	9-28	7-11
Axial Spacing	6d-10d	10d-13d	9d-10d
Transverse Spacing	6d-9d	6d-10d	6d-12d

1 Row Each Side - 25 Holes Per Row
0.070 Diameter Nominal - Laser Drilled
2.5 L/D
2.9d Spacing

Outer Band
Leading Edge Cooling

Initial Rows to
Cool Inner Band

.030" Diameter Holes Nominal
5.9 L/D
Laser Drilled

25° Nominal

Typical
Hole

.075"

11 Cast Holes
0.120 in. Diameter
3.4d Spacing
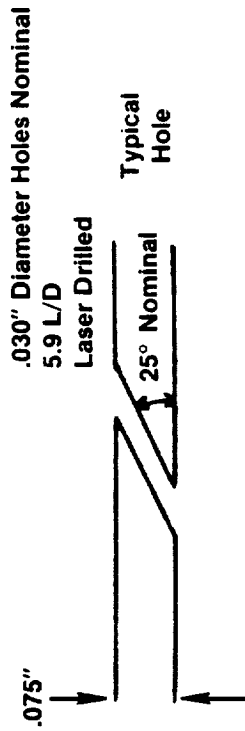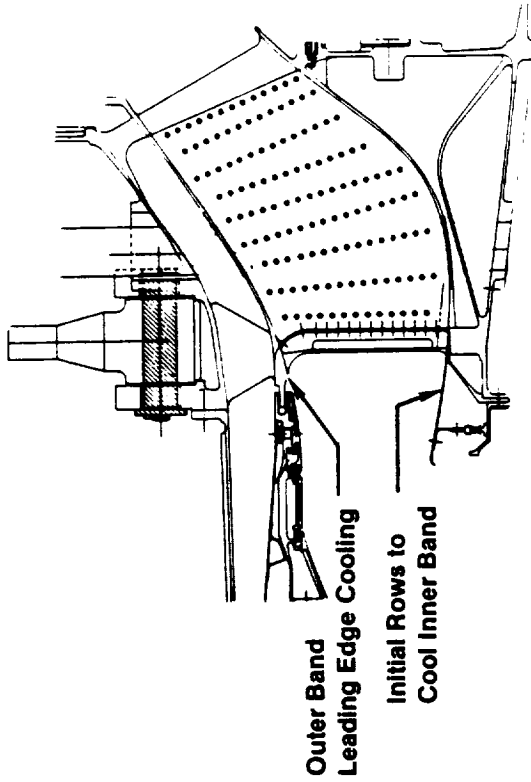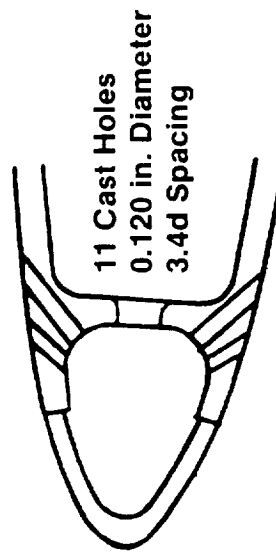
Figure 7-3. Frame Strut Hole Pattern.
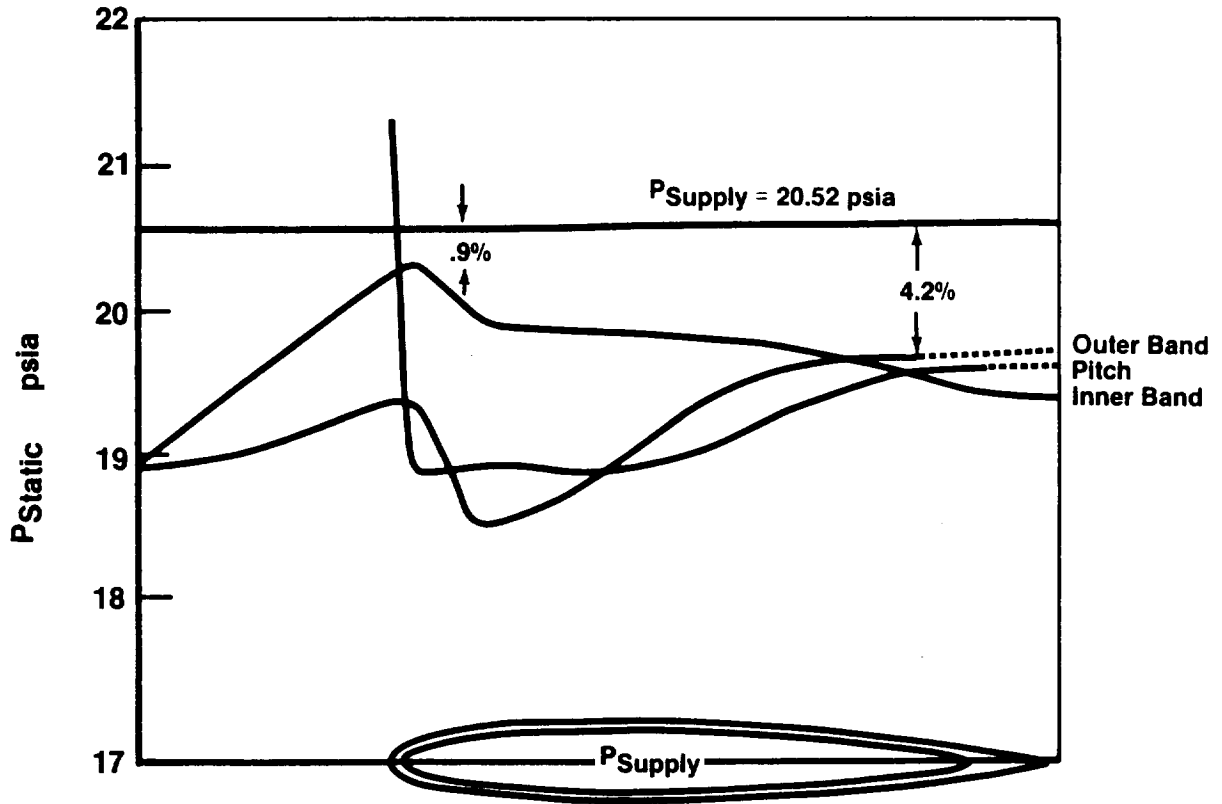
Figure 7-4. Mixer Frame Strut Cooling BFM,
Minimum BFM Case.

The strut leading edge runs hotter than the strut sidewalls and the inner and outer bands. The leading edge hot side heat transfer coefficient of 500 is based on a cylinder in cross flow correlation, while a low cooling impingement heat transfer coefficient of 190 results from a low available pressure drop.

7.3 SECONDARY FLOW SYSTEM

The power turbine secondary flow system provides ventilation, isolates the sump and provides packing air for the outer flowpath labyrinth seals. The

system was designed to provide adequate performance throughout the entire flight envelope for failed, as well as nominal, seal clearances. The flowpath purge flow rates required to prevent hot gas ingestion were determined using rotor cavity momentum balance computer programs matched to engine test data.

Unlike a conventional secondary flow system having one or two flowpath purge locations, this system required five purge locations of varying flowpath pressure. If significant metering was performed by the seals, the purge flow-rates would be very sensitive to varying seal clearance. A failed seal could greatly affect other seal flow rates as well as its own. This flow system is designed such that significant pressure drops are taken across the coolant annulus orifices. The individual seal flow rates then become less sensitive to variations in seal clearance.

Failed lab seal criteria have been applied to all but two of the lab seals. The inner forward and mid-lab seals are set at a nominal clearance of 0.040 inch. This is an unusually large clearance, and the possibility of a seal rub is minimal; thus, it is impractical to apply failed seal criteria to these two seals. Based on analysis, if any one of the three remaining seals is failed, or if all three are failed, positive purge flow is maintained at all locations.

7.4 POWER TURBINE HEAT TRANSFER

Utilizing finite difference modeling, steady-state and transient heat transfer analyses have been performed for the inner and outer spools and the forward and aft power frames. Calculated steady-state temperatures for rated T/O, SLS, +27 DTAMB are also shown on Figure 7-5.

Figure 7-6 illustrates the assumed flowpath temperature profile. Dilution, radial mixing, and energy extraction are considered in determining the stage profiles.

Flowpath heat transfer coefficients were generated from turbulent flat plate data, using spool relative velocity and assuming boundary layer restart at each stage inlet. The inner cavity coolant heat transfer coefficients are based on the GE design practice correlation for rotor cavities. An average tangential velocity is calculated for the cavity air by balancing friction,

drag, and injected and extracted purge air moments. The rotor and stator relative velocities can then be determined and input to the forced convection calculation. The outer spool is cooled through free convection to the nacelle cavity air and radiation to the composite nacelle.
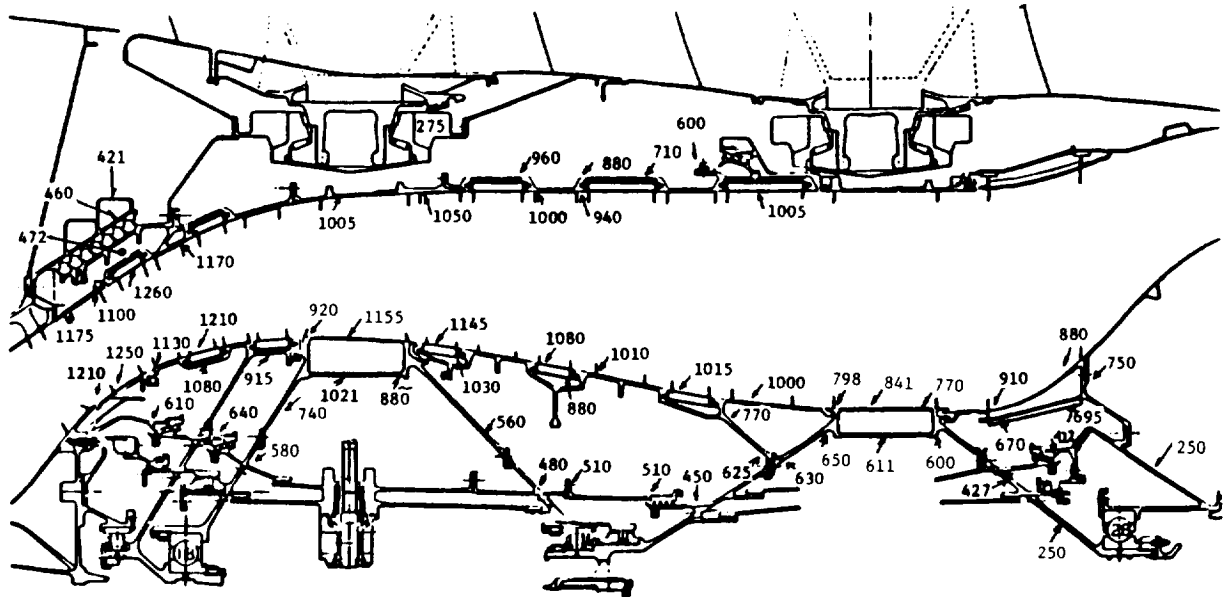
Figure 7-5. Power Turbine Completed Heat Transfer Analyses, Hot Day (+27° F) Rated Takeoff, Steady-State Temperatures.

7.5 CENTER CAVITY VENTILATION SYSTEM

Internal propulsor cavity temperature limits are set by actuation system hardware housed within the cavity. The actuator linear variable differential transformer (LVDT) maximum operating temperature of 360° F is met by venting 180° F (T/O conditions) nacelle air through the mixer and into the aft cavity. Radiation through the aft cover is minimized through utilization of an insulation blanket.

Since the nacelle air pressure is near ambient, it can only be delivered to the center cavity through the use of an ejector. There are two inlet pipes
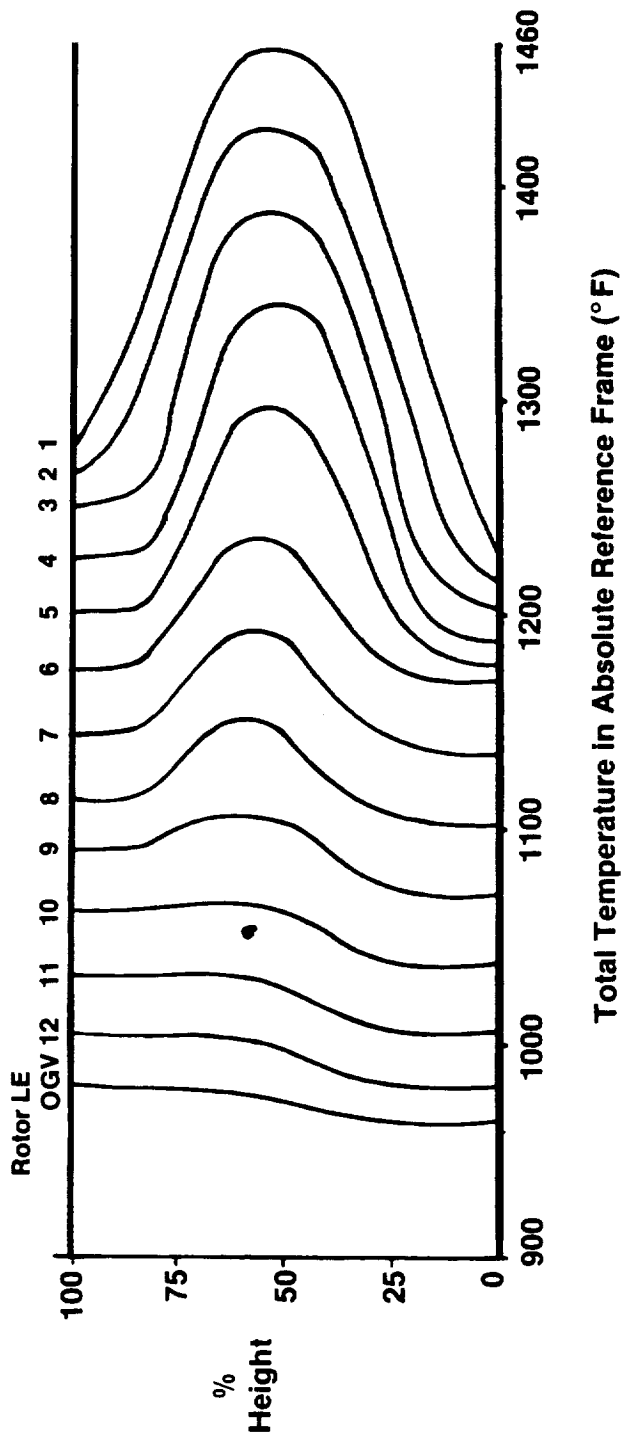
Figure 7-6. Gas Path Profile, Maximum Power Takeoff (+27° F Day).

and one exit pipe. The inlet pipes begin at the mixer frame outer band, configured through the struts, and extend aft inside the support tube all the way to the actuator. The exit pipe travels through a third strut and connects to the ejector, which draws the ventilation air out of the cavity and directs it across the bulkhead into the power turbine nacelle cavity. See Figure 7-7 for routing of vent tube through mixer frame.

7.6 PROPULSOR NACELLE VENTILATION SYSTEM

The nacelle ventilation system is designed to duct ambient air into the nacelle cavity to provide cooling for critical components. The heat source to these components is radiation from the outer rotor structure which ranges in temperature from 800° to 1100° F at rated takeoff, SLS, +27 DTAMB. The composite nacelle, with a conductivity of approximately 0.5 Btu/h ft° F, behaves as an insulator; consequently, heat must be removed by the ventilation air flow circuit.

Air is introduced at three locations: the forward fan blade platform (Figure 7-8), the forward telemetry module (Figure 7-9), and the aft telemetry module (Figure 7-10). The forward fan blade scoops are located on the pressure side of the blade to take advantage of the higher static pressure level. The air dumps into a plenum, and flow is controlled by holes exiting the plenum. Due to the high level of cooling effectiveness required to meet the low telemetry module temperature limit, additional scoops are required within the forward ring. The scoop angle, set to meet the air flow direction, removes heat through free convection and exits between radiation shields. The aft telemetry module scoops, shown in Figure 7-10, are located 3/4 inch above the flowpath and encounter a velocity which is 95% of freestream, with the angle set for takeoff pitch setting.
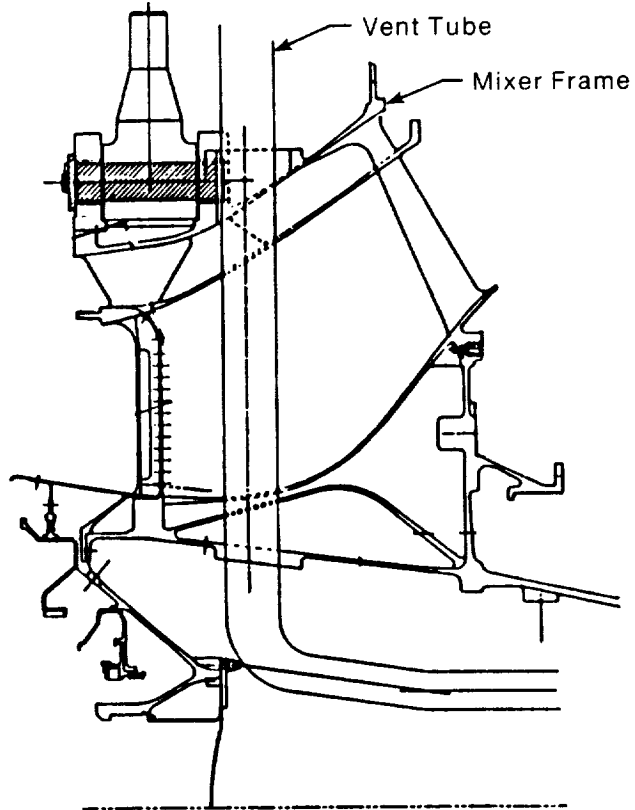
Figure 7-7. Mixer Frame and Vent Tube.
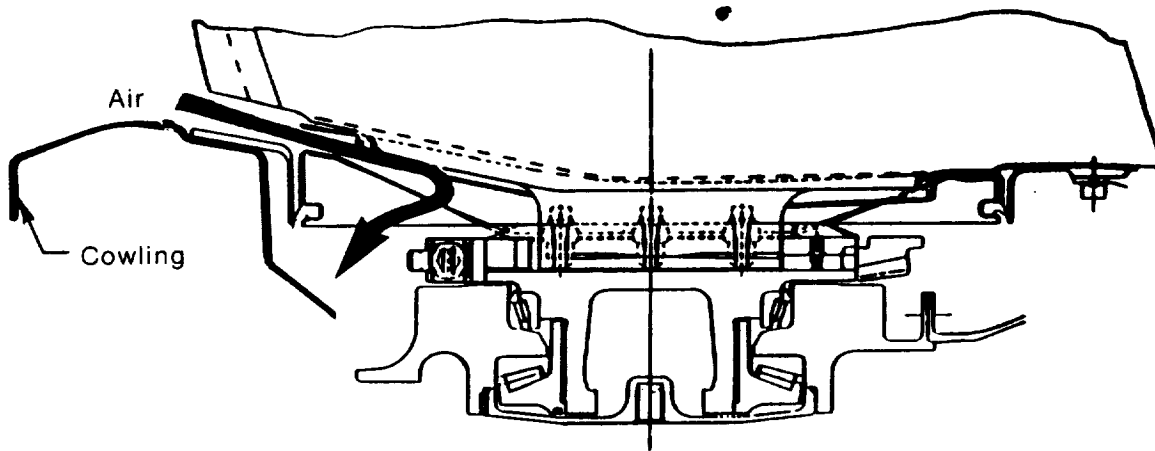
Figure 7-8. Forward Fan Blade Platform Cooling.

Scoops
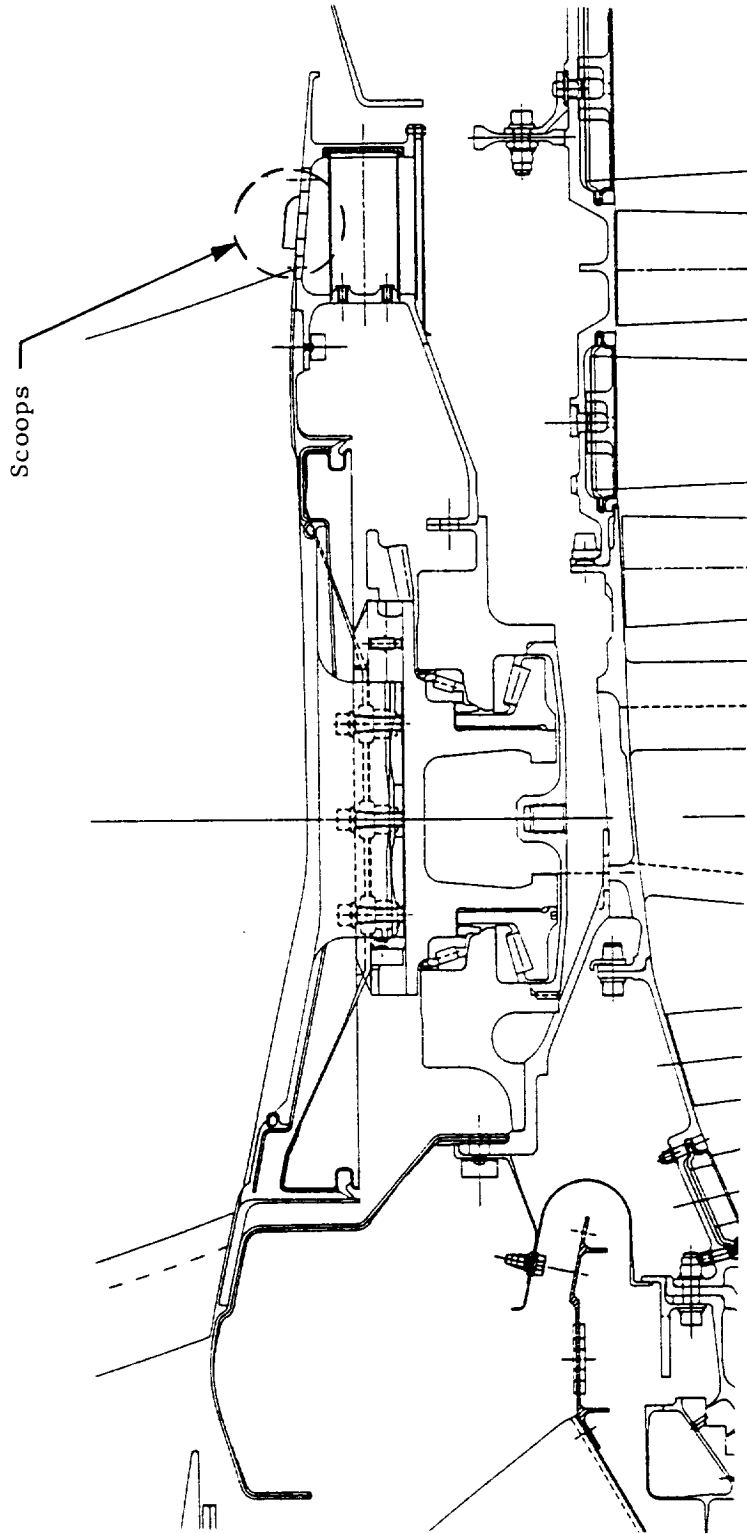
Figure 7-9. Forward Telemetry Ring Cooling.

73

Rotation

37°

30 Scoops

0.5 Inch Diameter Inlet

Scoop Details

Scoops
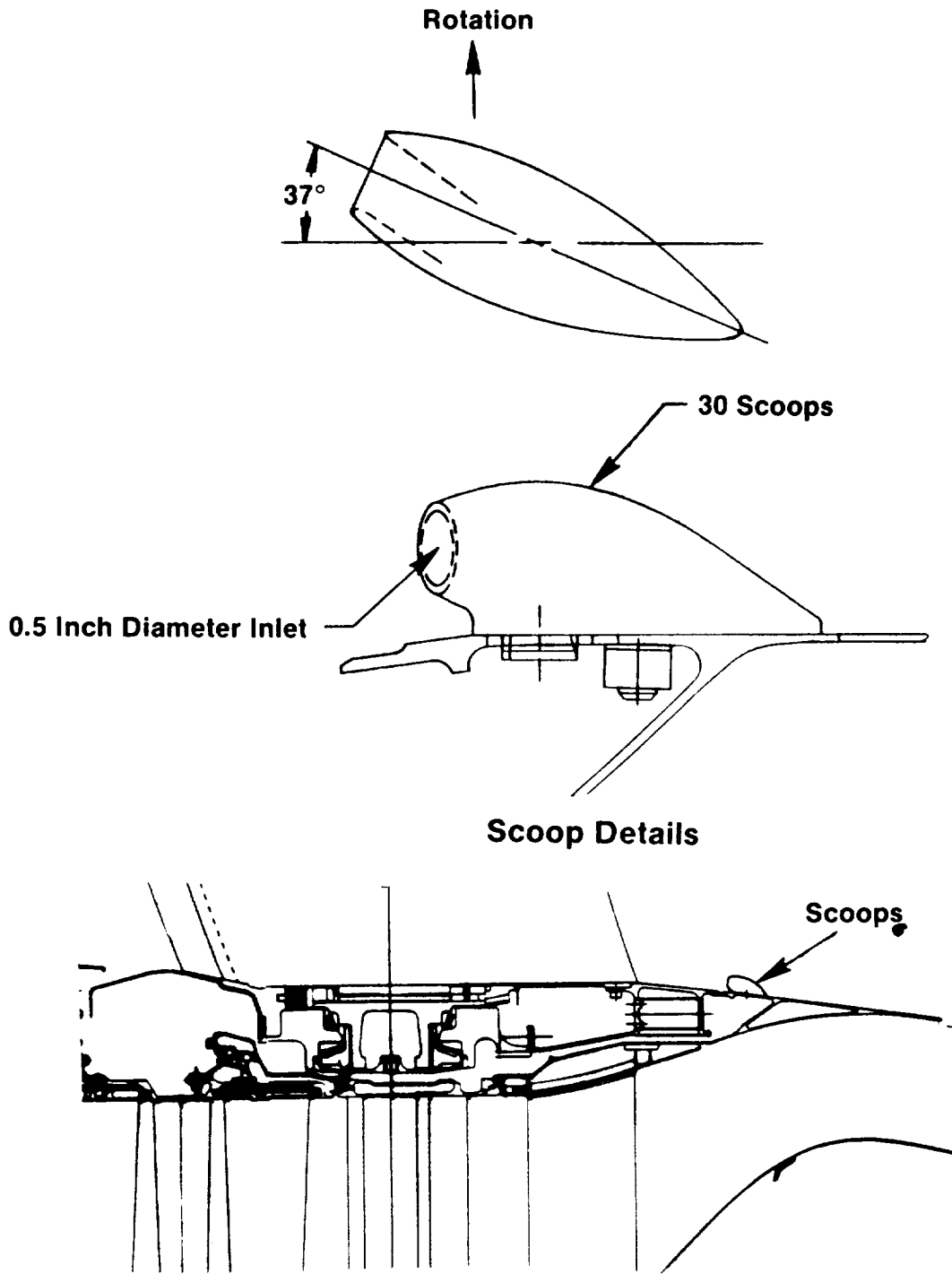
Figure 7-10. Aft Telemetry Ring Cooling.

74

8.0 PROPULSOR MECHANICAL DESIGN

8.1 STATIC STRUCTURE DESIGN

8.1.1 Mixer Frame and Turbine Support

The mixer frame (Figure 8-1) is constructed from a 360° integral Inconel 718 casting with 20 radial struts, twisted slightly from root to tip to match the swirl exiting the F404 LPT. The strut walls and outer and inner flowpaths are protected from the hot gas by about 41,000 laser drilled film cooling holes, and the strut leading edges are protected by a welded sheet metal cover which is impingement-cooled because of the high stagnation pressures. The aft propulsor support cone and flange are forged Inco 718 material and are welded to the casting.

Finite element analyses were employed to determine the normal operating and maximum load stresses of the frame. Results are illustrated in Figures 8-2 and 8-3. These analyses revealed that for normal operation, all areas of the frame have greater than 25,000 cycles low cycle fatigue (LCF) life, except the strut leading edges which have high compressive thermal stresses. Because of the high loading encountered during blade-out, the mixer frame struts have extensions which serve to transition loads into the outer case and hub rings (Figure 8-4).

The power turbine support is an Inco 718 weldment consisting of a casting and forgings. The turbine support has blade-out loading capability, and the normal operating deflections are small. In addition, analysis shows that the support has adequate stiffness to prevent rotor whirl and plug nozzle instability. The mixer frame/turbine support has 32 one-half-inch MP159 bolts, which are torqued to obtain approximately 35,000 pounds clamp per bolt. The bolt and flange stresses are within the appropriate material ultimate strength capability during blade-out loading (Figure 8-5).

The piping that passes through the mixer frame provides all the services required by the propulsor and the core C-sump. These services include: lube supply, scavenge, and drain; sump pressurization and venting; and actuation system oil supply, return, and pitch lock. The tubes are held in place by
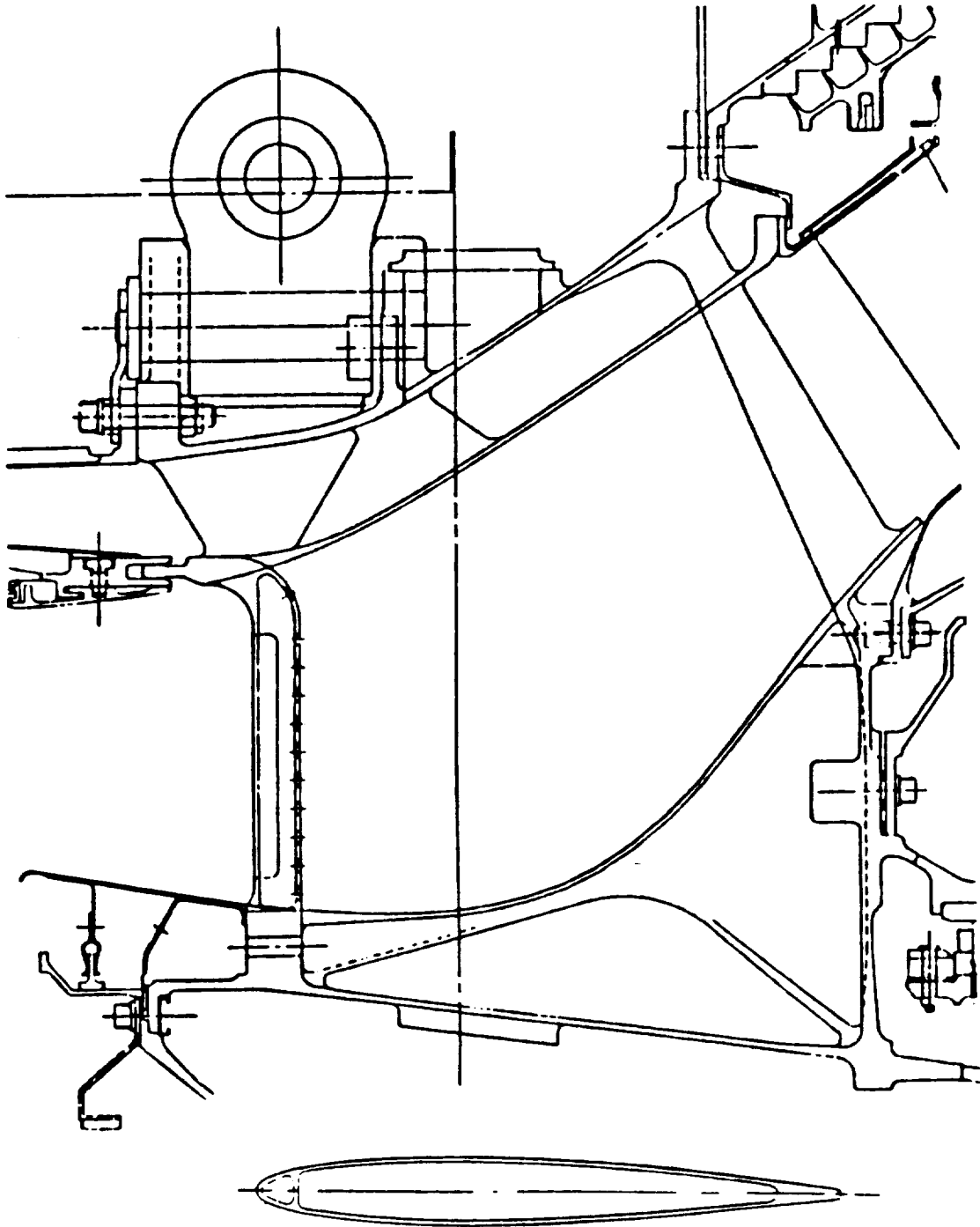
Strut Cross Section

Figure 8-1. Mixer Frame.
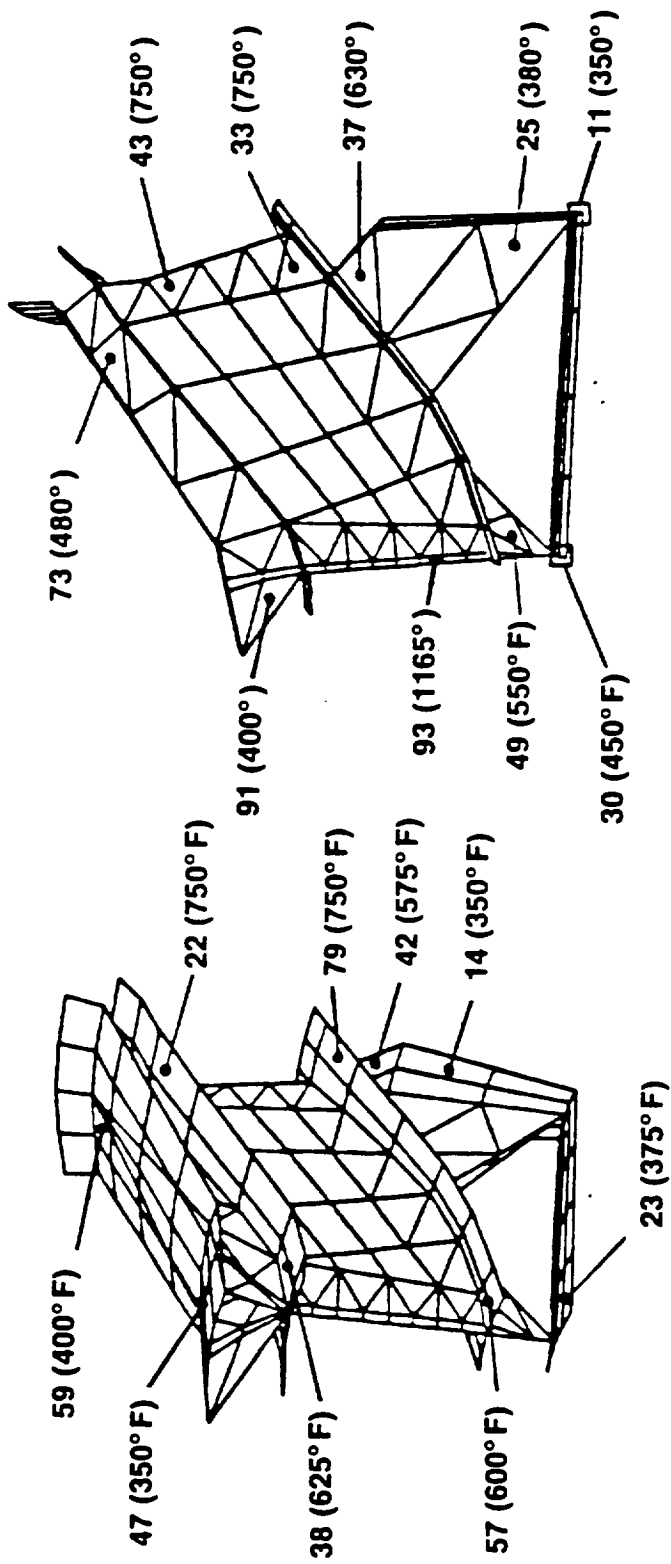
- **Maximum Thermal Stress is 93,000 psi**

  -Strut Leading Edge (3000 Cycles LCF)
  -Strut Leading Edge not Included in Stiffness and Blade Out Calc

- **Other Areas >25,000 Cycles LCF**

Figure 8-2. Mixer Frame - Effective Thermal Stresses.

77
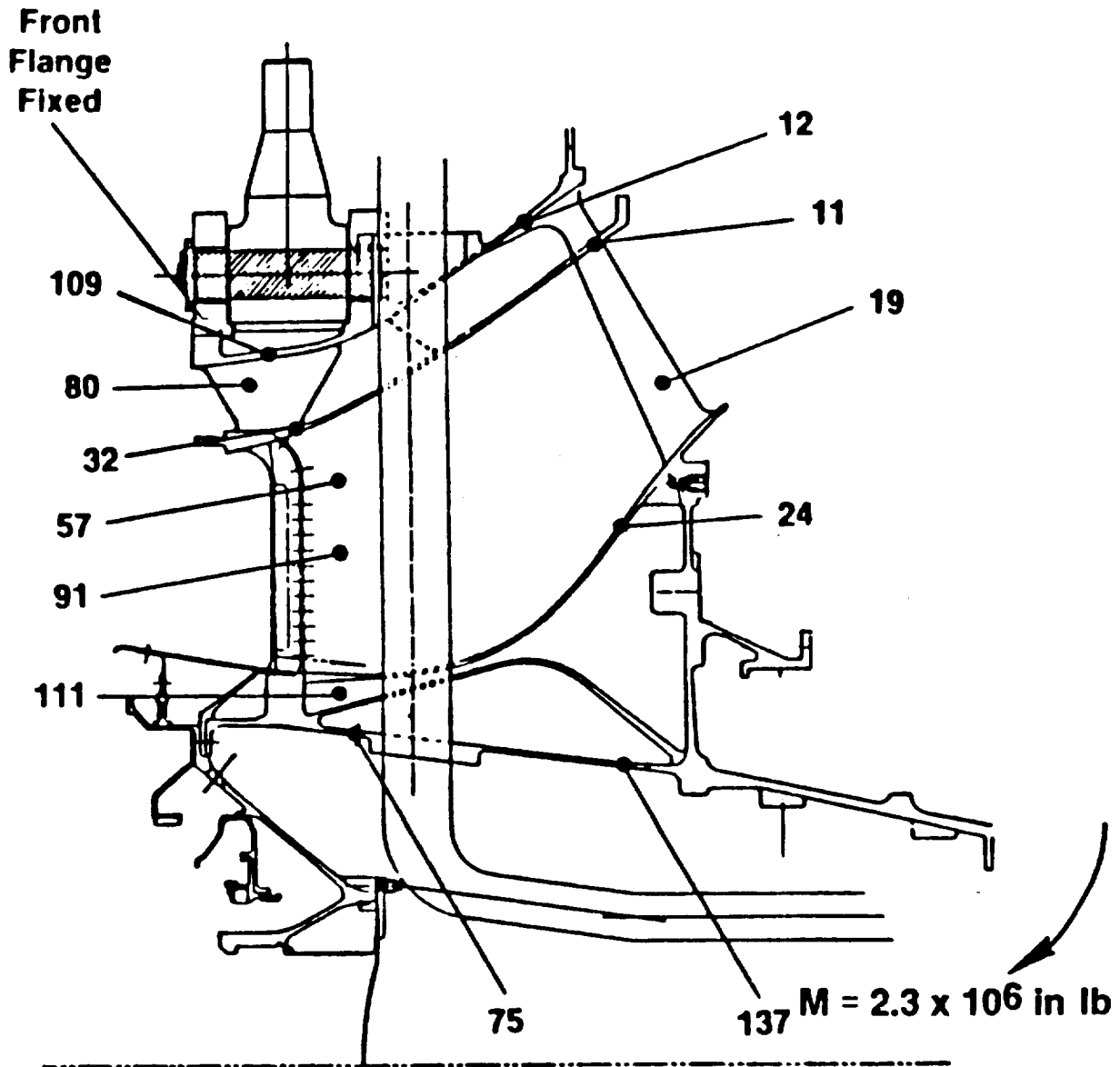
Figure 8-3.   Mixer Frame - Blade-Out Loads (One Fan Blade per Rotor).
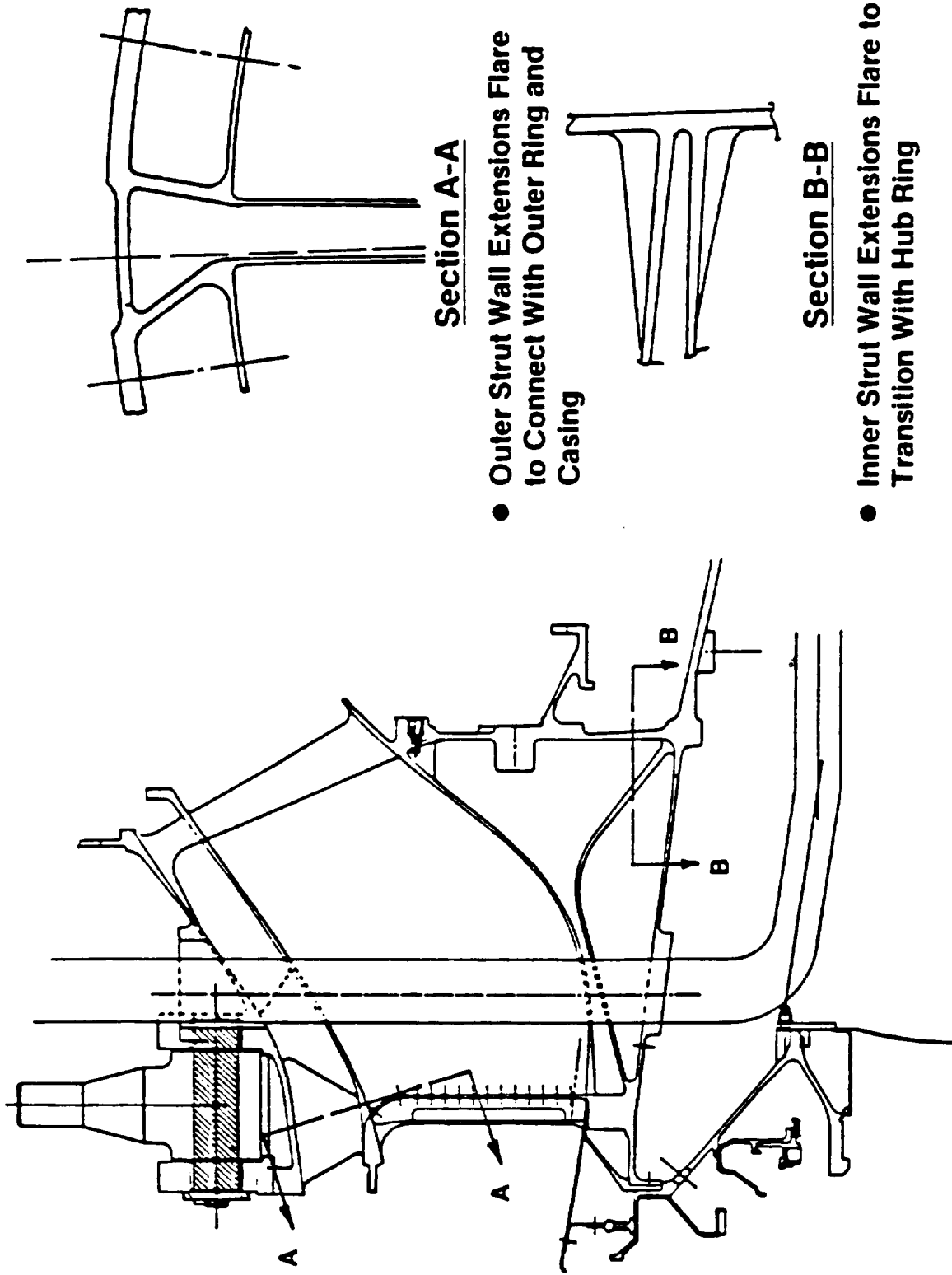
Section A-A

● Outer Strut Wall Extensions Flare to Connect With Outer Ring and Casing

Section B-B

● Inner Strut Wall Extensions Flare to Transition With Hub Ring

Figure 8-4. Mixer Frame Load Transition Features.

79

brazing them to a flange and then bolting the flange to a pad on the outer case of the frame. The tubes have a close tolerance slip fit at the frame hub to account for thermal mismatch between the frame and the tubes. All of the tubes are supported along their length by clamps and brackets; these brackets are supported inside the mixer frame by the forward and aft flanges and are supported inside the turbine support by two independent rings. The tubes and brackets have been analyzed in accordance with GE design practices. The tube and bracket resonant frequencies are outside of the engine operating range, and the bracket stresses are very low.

Bolt Stress = 215 ksi
Flange Bending Stress = 142 ksi
Flange Hub Stress = 120 ksi
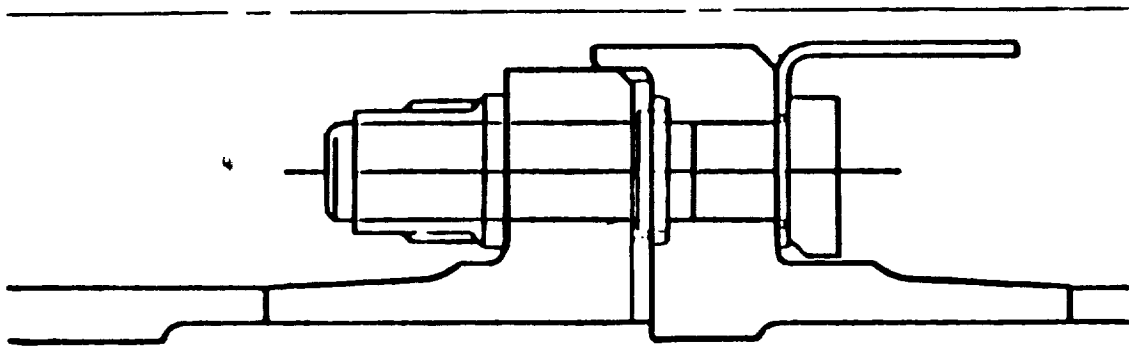
Figure 8-5. Mixer Frame/Support Tube Flange Analysis (Blade-Out).

8.1.2 Power Turbine IGV Assembly

The IGV is a brazed Hastelloy-X sheet metal construction with Hastelloy-X forgings used in the flange areas (Figure 8-6). The airfoils have 0.020-inch-thick sheet metal skins with 0.010-inch corrugated sheet metal stiffeners. This type of construction yielded a lightweight design with critical frequency margin. A detailed, 3D finite element model of the airfoil, inner band, outer band, and overlaps was made for the frequency and stress analysis. The outer band is saw-cut to reduce thermal stress in the vanes. These cuts are first

80

positioned to minimize the effect of circumferential temperature variation caused by the mixer frame strut film cooling and then are covered with sheet metal strips to prevent flowpath gas ingestion into the forward seal cavity (Figure 8-7). Load transition from the airfoils to the inner and outer bands is made through brazed collars at the airfoil tip and root. Figure 8-8 shows the stress levels at steady-state takeoff and 40-seconds transient point.

Mode shapes are illustrated in Figure 8-9, and the Campbell diagram for the final IGV configuration is shown in Figure 8-10. All of the primary modes meet the design intent of missing per revolutions (rev) excitation at engine steady-state operating points, except for a first torsion interaction at idle with a secondary excitation source. The excitation forces are low at this condition, and minimal response levels are expected. Frequencies were verified by component bench tests of the completed IGV assembly.

The inner band flowpath overlap critical frequencies were calculated utilizing a two-dimensional (2D) axisymmetric shell analysis program to insure traveling wave frequency margin. The 2, 3, 4, and 8 nodal frequencies of the overlap exceed the 15% margin over the power turbine maximum speed as specified by General Electric design practice.

Figure 8-6. IGV Overall Design Features.

8.1.3 Outlet Guide Vane (OGV) Assembly

The OGV assembly is a brazed sheet metal construction using Hastelloy-X material. Since the gas temperature profile is uniform, both the inner and outer bands are 360° shells. The entire assembly is supported by a forged

360° Pad

Collar

Cover

Outer Band Detail

Vane Cap

Collar

Flowpath
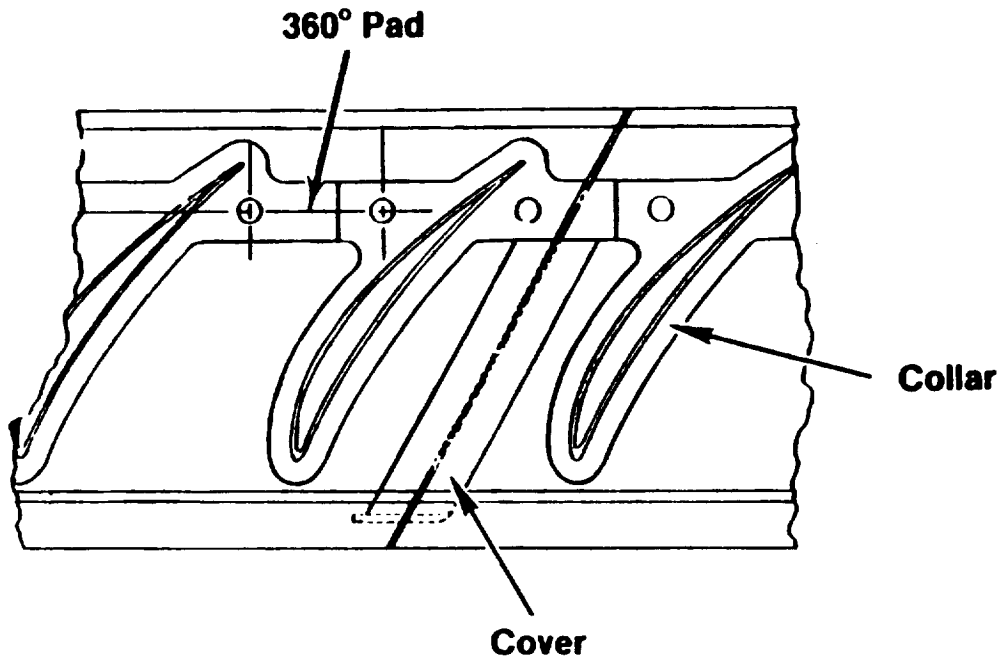
Airfoil
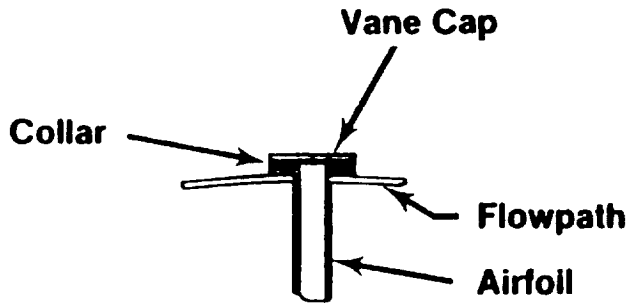
Figure 8-7.   IGV - Outer Band Design Features.

82
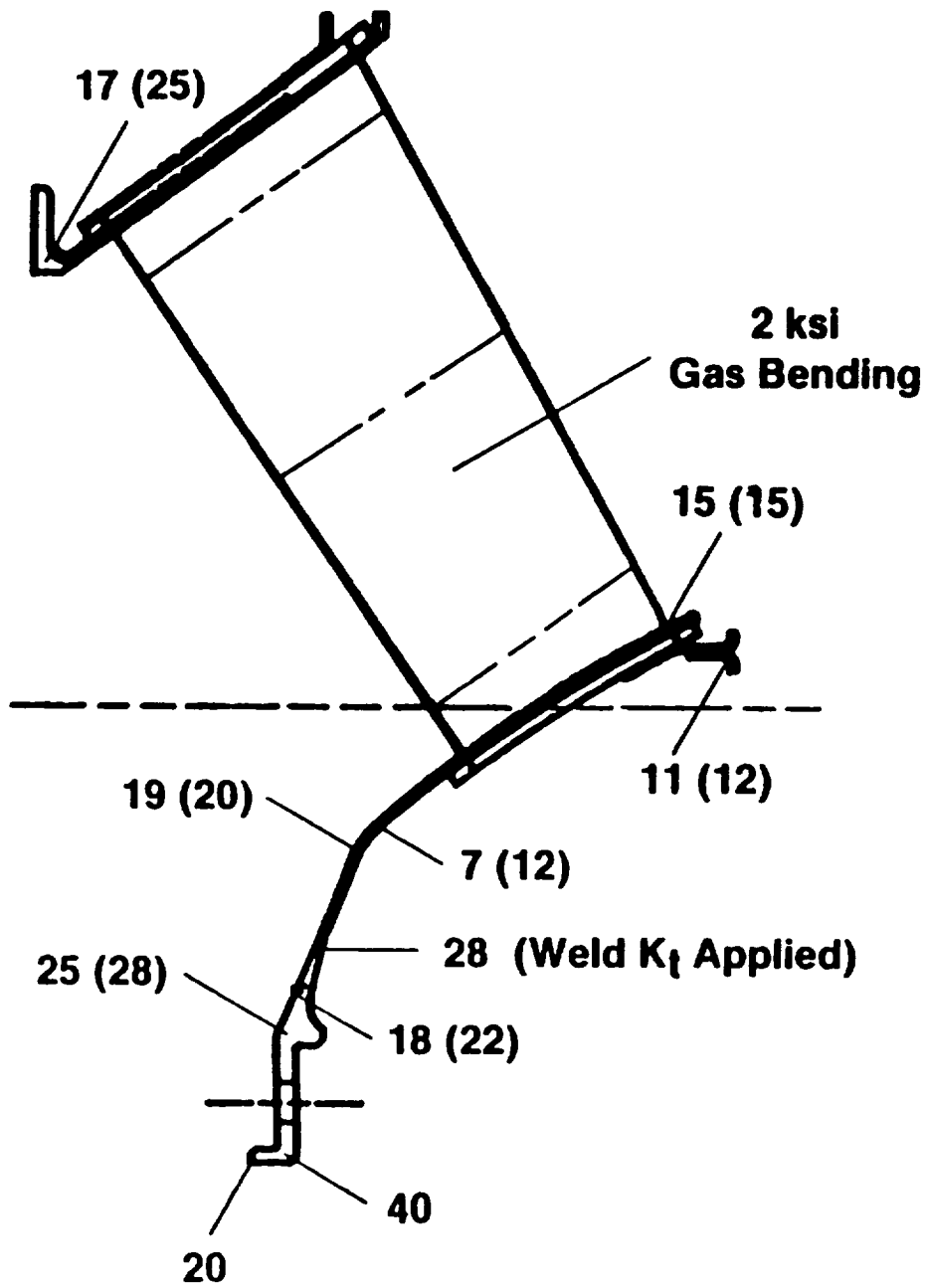
Figure 8-8. IGV Stress Analysis, Steady-State
(Transient – 40 Seconds).
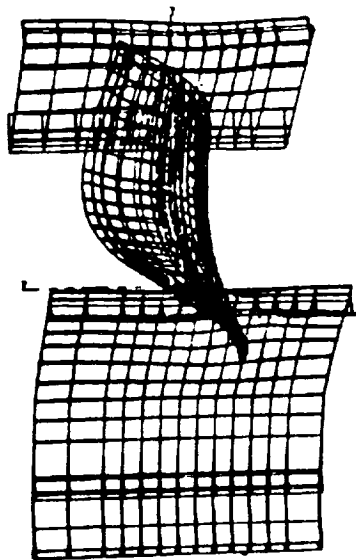
1536 Hz
1st Flex
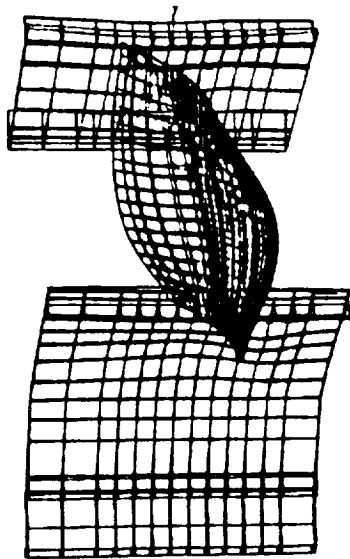
2348 Hz
1st Torsion
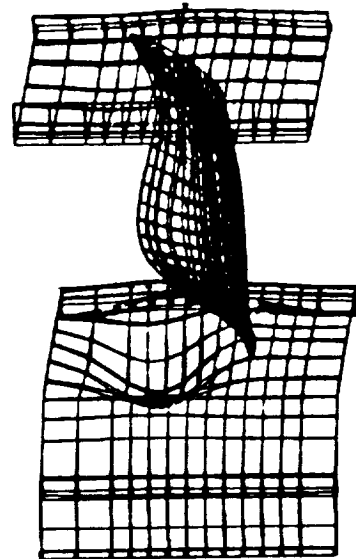
3158 Hz
TE 2F + Bands
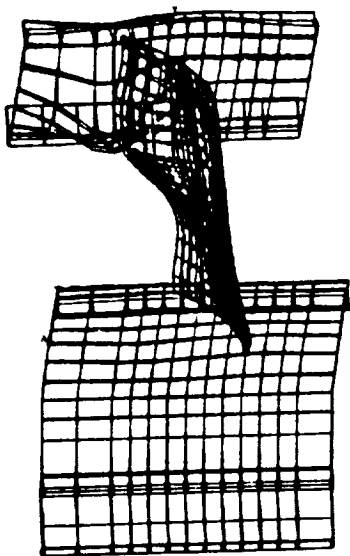
3603 Hz
TE 2F + Bands
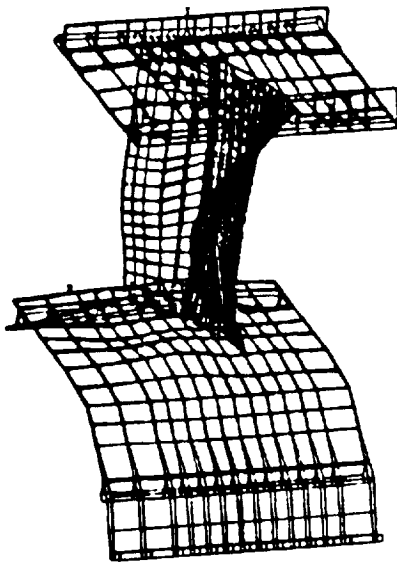
4880 Hz
2 Strip
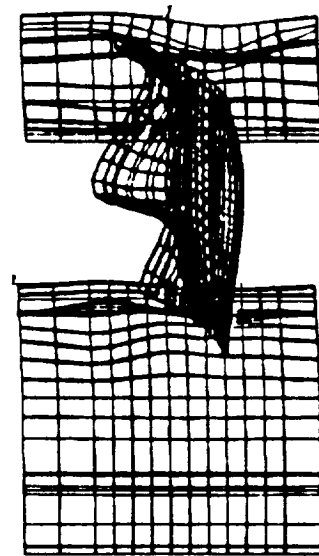
5118 Hz
TE 3F + LE 1F

Figure 8-9. IGV Analysis - Mode Shapes.
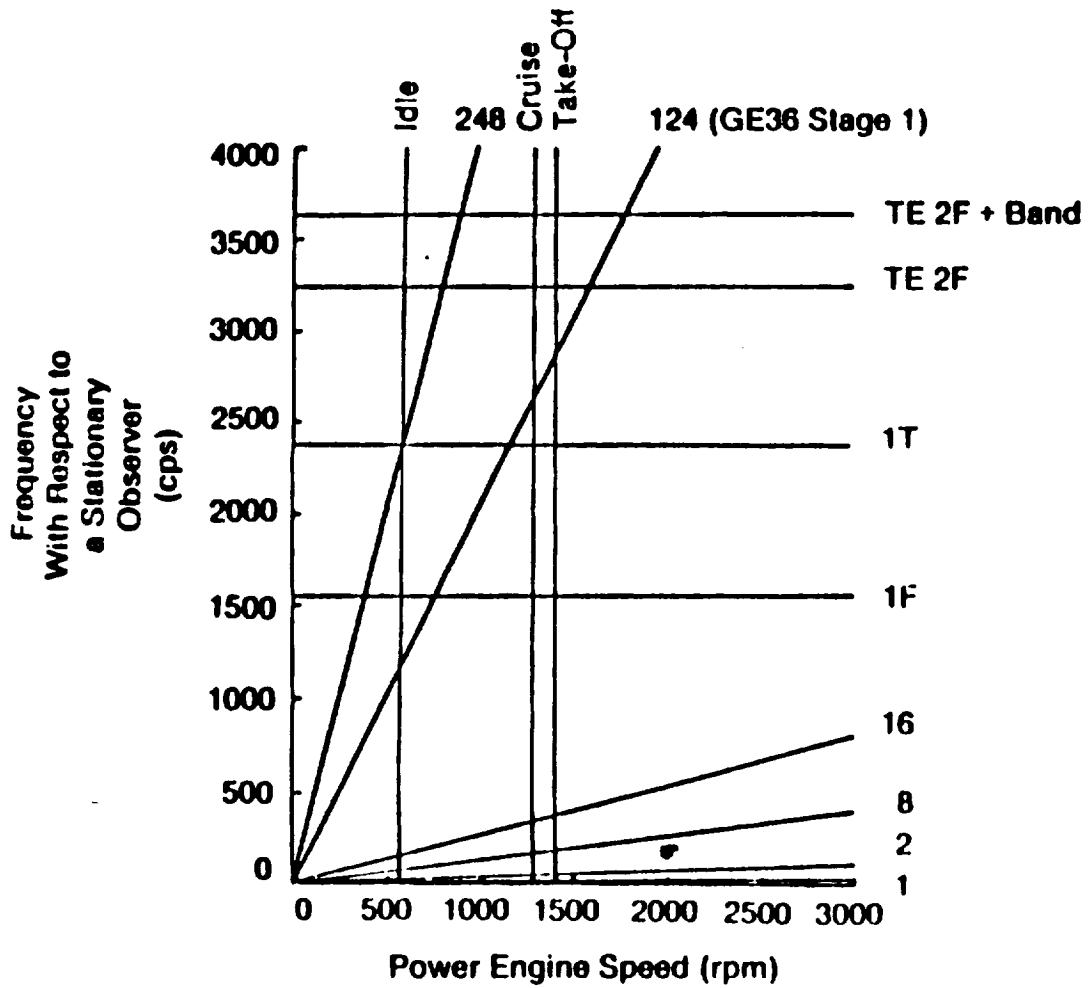
Figure 8-10. IGV - Campbell Diagram.

Hastelloy-X structure and bolts directly to the sump housing. The exhaust nozzle centerbody is also supported by this cone; therefore, the loads from the centerbody are transferred directly to the sump structure and do not pass through the vanes and their supporting structure (Figure 8-11). The vanes are hollow airfoils with corrugated stiffeners and are supported in a box structure at the inner diameter. Brazed collars and clips transition the loads from the vanes to rings on both the inner and outer bands. Since the stress in the inner and outer bands peaks at the vane leading and trailing edges, the bands have keyhole slots at these locations to reduce stress concentrations.

Detailed 3D finite element analyses were used to determine the OGV vane critical frequencies and resulting Campbell Diagram (Figure 8-12). All modes have the required 15% margin from excitations in the engine operating range, except the second-flex mode which, the analysis predicts, could be driven by a blade passing frequency of 80 per rev; however, GE experience has shown that a second-flex mode is not normally driven by a blade passing excitation. Wake energy attenuation calculations also indicated that the 80 per rev pressure pulse would decay to 9% of its original strength by the time it reached the OGV. For these reasons, no dynamic excitation problems were anticipated, and initial engine testing has verified that the response levels are indeed low.

Detailed 2D and 3D finite element analyses were utilized for OGV stress calculations. These analyses predict over 25,000 cycles LCF life for normal operating loads and capability for maximum blade-out loading (Figures 8-13 and 8-14).

8.2   TURBINE AND ROTATING STRUCTURES AND TURBINE BLADE DESIGN

8.2.1   Turbine Blade Design

There are 10 blade rows of power turbine blading similarly designed as shown in Figure 8-15. All are Hastelloy-X sheet metal brazed and welded fabrications, and all utilize circumferential dovetails similar to conventional compressor design practice. Hollow airfoil construction was selected because it allows fundamental frequencies to be met at a weight advantage over solid airfoils. An internal corrugated stiffener is brazed inside the airfoil to control panel modes of vibration and is configured specifically to tune the two-stripe mode.

Braze
Joints

26 Vanes

Centerbody Flange

Internal
Box
Structure
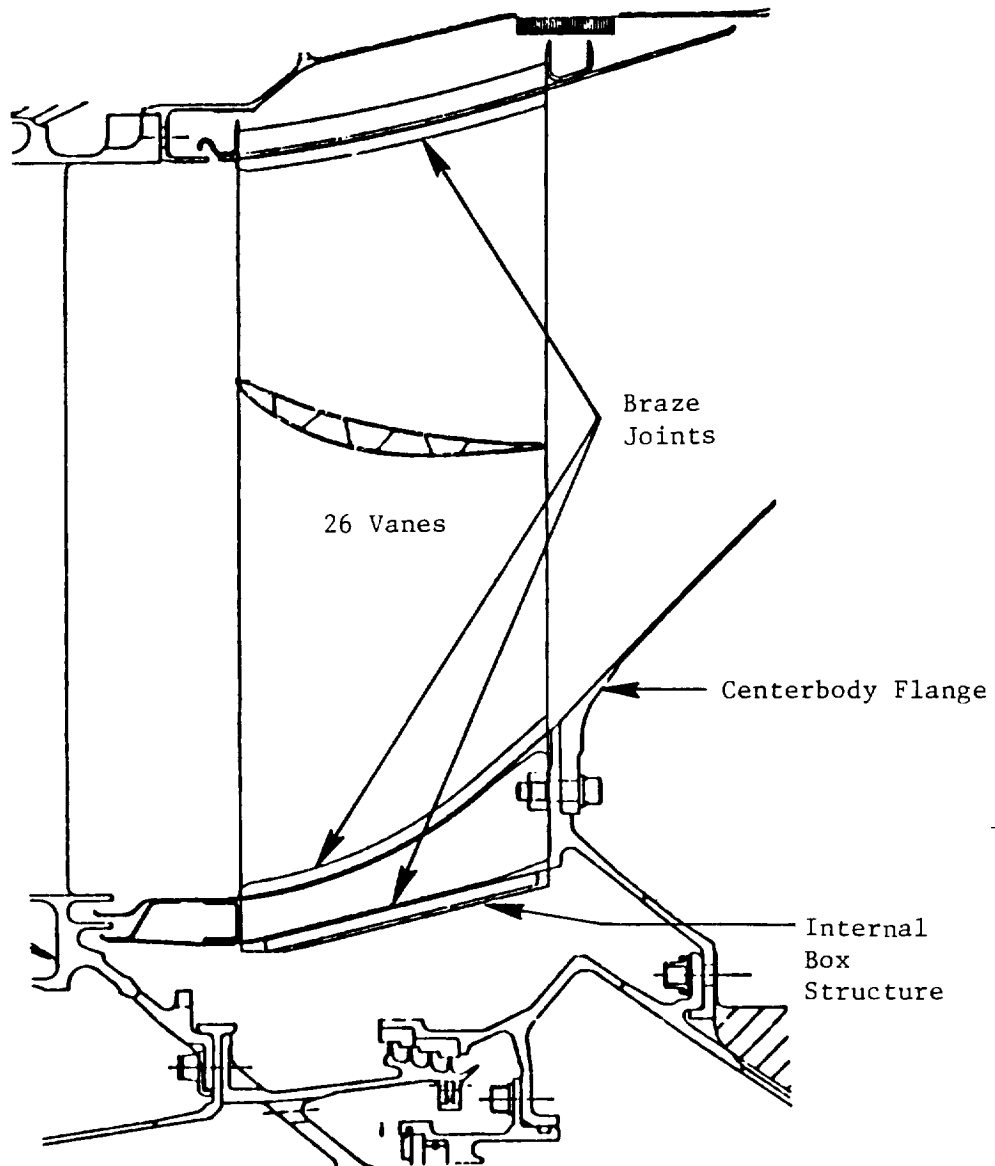
Figure 8-11. OGV - Overall Design.
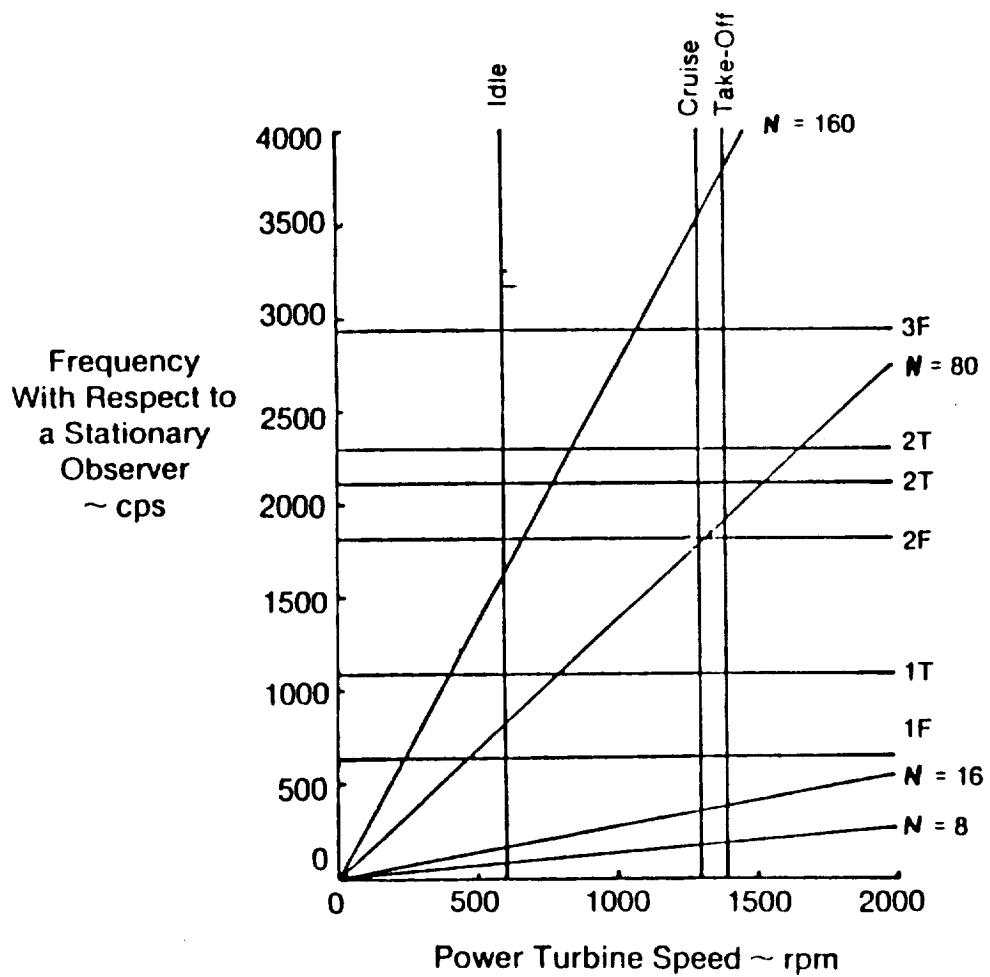
Figure 8-12. OGV - Campbell Diagram.
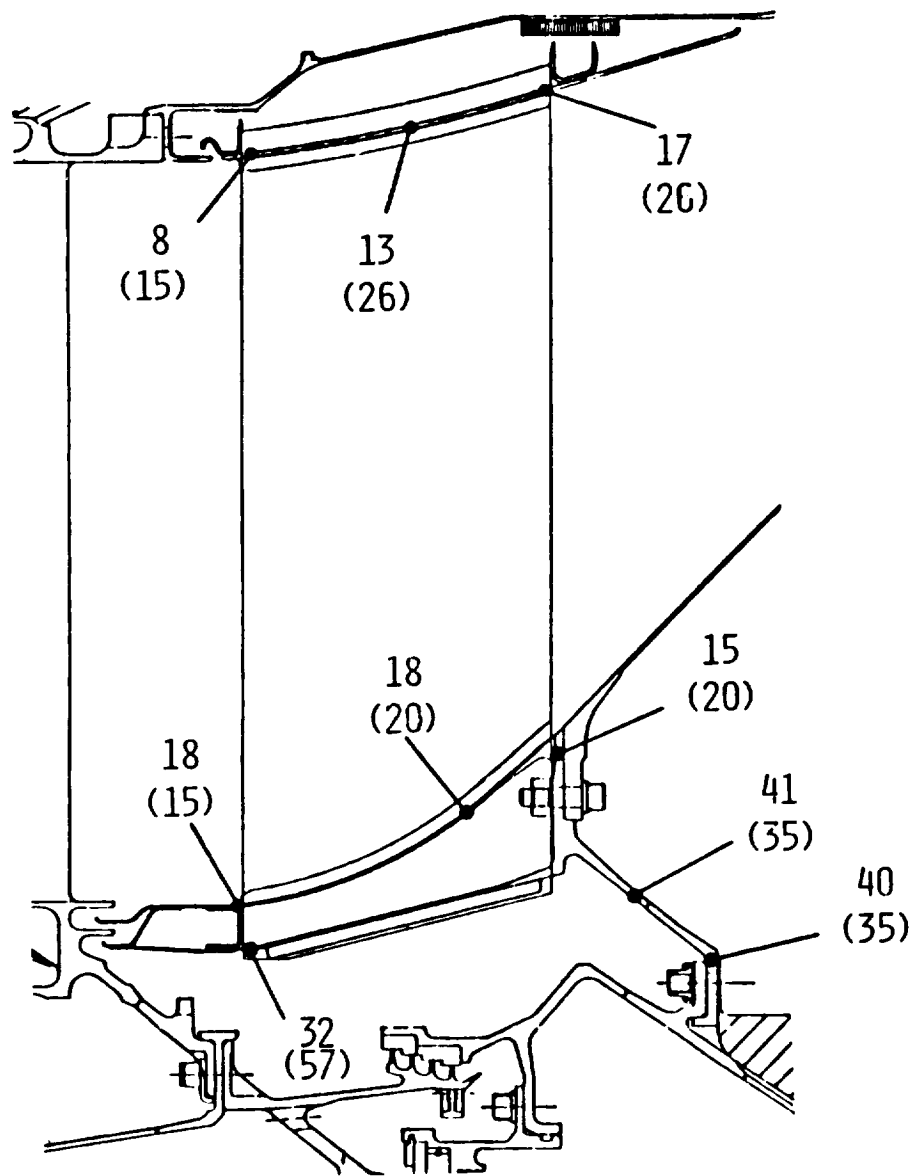
Figure 8-13. OGV - Stress Analysis, Steady-State (Transient) Stress.

Figure 8-14.   OGV - Blade-Out Loading Capability (One Blade per Rotor).

Brazed Tip Cap

0.030 in. Thick
Airfoil With
0.010 in. Stiffiner

Formed Sheet
Metal Base
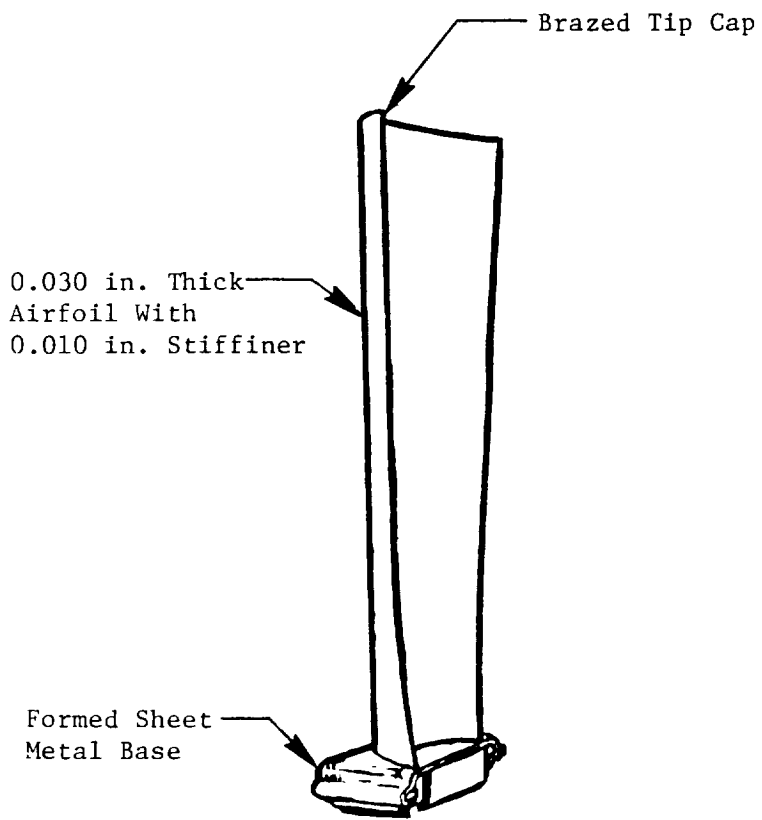
Cross-Section
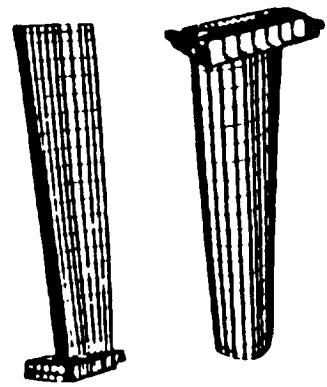
Typical Finite Element Model

Figure 8-15. Power Turbine Blades.

All power turbine blading was designed to meet conventional turbofan dynamics requirements utilizing 3D eight-noded brick finite element analyses. Aeroelastic stability was evaluated by a General Electric reduced velocity parameter. All frequencies were designed to be greater than 4 per rev, and an objective of 15% margin to resonance in the operating range was set for Modes 1F, 2F, 1A, 1T, 2T, and 2S.

All of the blades met accepted limits for aeroelastic stability in the 1F, 1T, and 1A Modes (Figure 8-16). Pretest predictions indicated six potential resonances in the operating range; all but one of which were assessed to have adequate damping or insufficient excitation strength to prevent harmful dynamic response. Table 8-1 summarizes these results; Figures 8-17 through 8-19 depict the pertinent Campbell diagrams. Stage 8 had a predicted 2S resonance with the forward blade passing frequency, and a design modification was initiated to drop the resonance below the operating range (Figure 8-20).

Initial Build 1 testing showed the turbine blades to be highly responsive in first flexural mode due to inadequate damping. This resulted in a fatigue failure of Stage 1 and subsequent gas generator stall. The blade design was modified for Build 2 to incorporate Coulomb damping in the form of pins through holes in the airfoils at approximately 90% span as shown in Figure 8-21.

Blade locks were designed in conjunction with the blading to react torque loads into the spools. Two different configurations were used as a result of blade assembly requirements. Stages 7, 9, and 11 use a bar which spans across the full width of the platform and is attached to the spool by a single bolt. This allows the last blade to be twisted into position, and then the locks are installed to take up the resultant gap. The remainder of the stages utilize separate forward and aft locks with integral threads which pass through cutouts in the blade rails and holes through the spools and which are retained by a selflocking nut. Prior to engine buildup, this latter design was modified to add a spacer to those locations which were clamping across a gap (aft position) to prevent cycling of the threaded joint. All blade locks were designed with 2× load capability to provide a redundancy so that loss of one lock would not result in overload of the next lock. See Figure 8-21a for typical blade lock design.
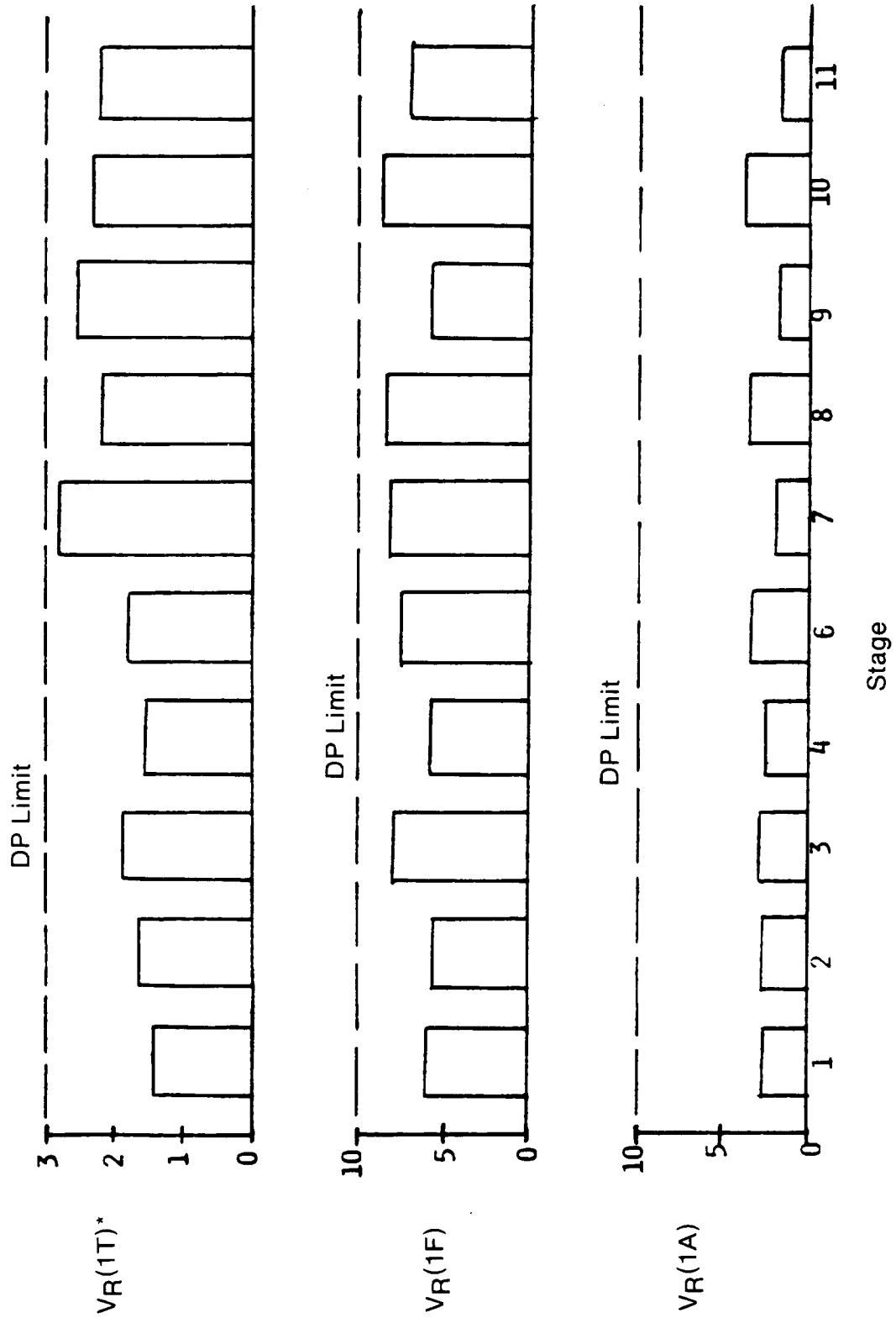
Figure 8-16. Turbine Blade Dynamics, Aeroelastic Stability.

*VR - Reduced Velocity Parameter

93

Table 8-1. Turbine Blade Dynamics Analysis - Results Summary.

- No Resonances - Stages 7 and 11

- Idle Resonances

Stage 3	2F	188/Rev (Stage 4)
	2T	236/Rev (Stage 2)
Stage 6	2T	192/Rev (Stage 5)
Stage 8	2F	108/Rev (Stage 9)
Stage 9	2T	164/Rev (Stage 10)
	2T	168/Rev (Stage 8)
Stage 10	1F	16/Rev (Engine Fundamental)

- Operating Band Resonances - Concern Modes

Stage 10	1A	16/Rev (Engine Fundamental)
Stages 1 and 3	1F	16/Rev (Engine Fundamental)
Stages 2 and 4	1F	16/Rev (Stage 5)
Stage 8	2S	144/Rev (Stage 7)
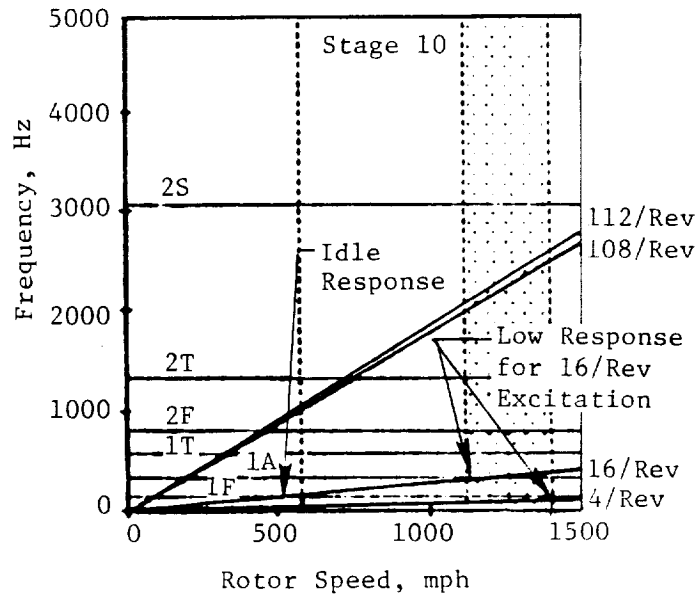
Figure 8-17. Stage 10 Dynamic Results.
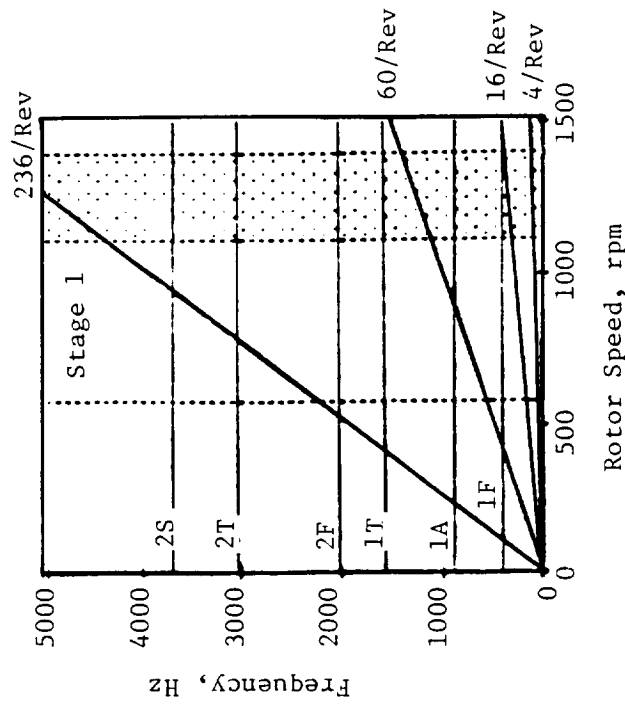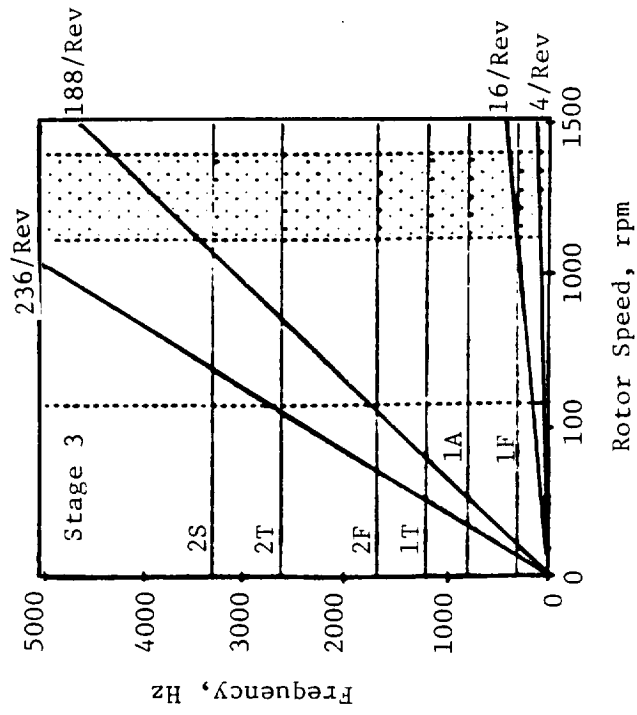
Figure 8-18. Stages 1 and 3 Dynamic Results.
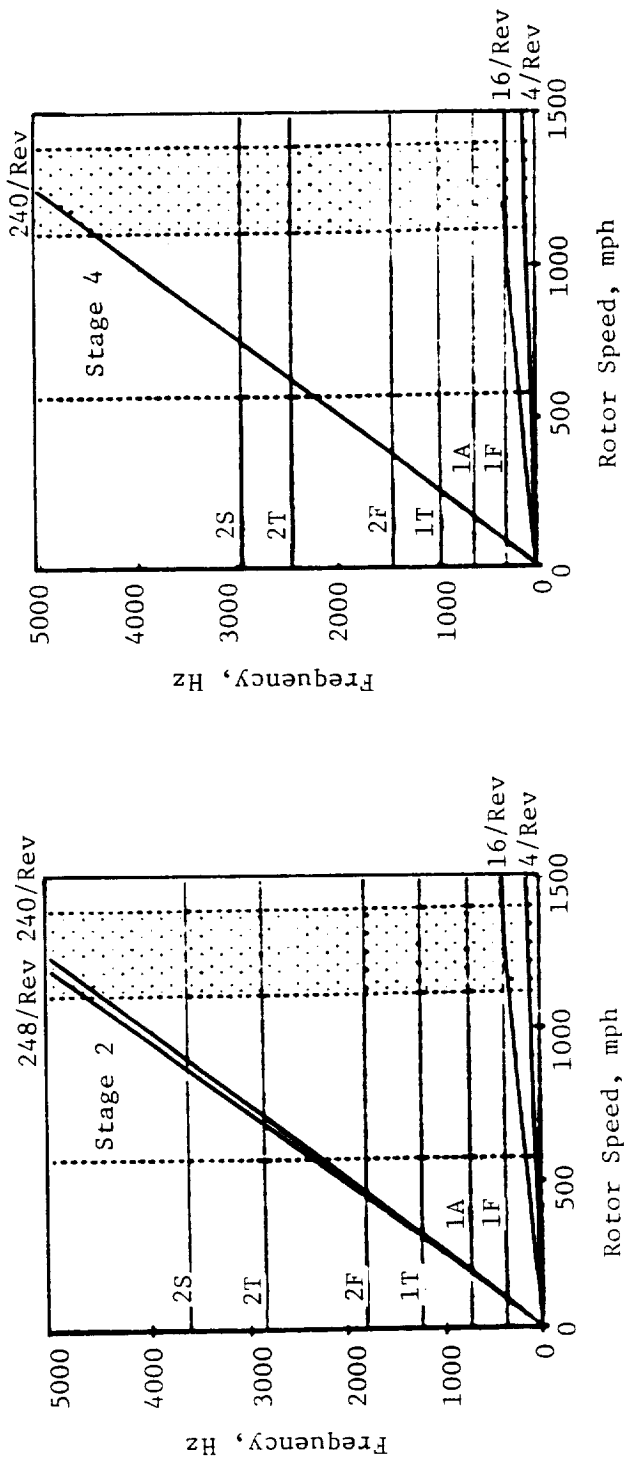
Figure 8-19. Stages 2 and 4 Dynamic Results.
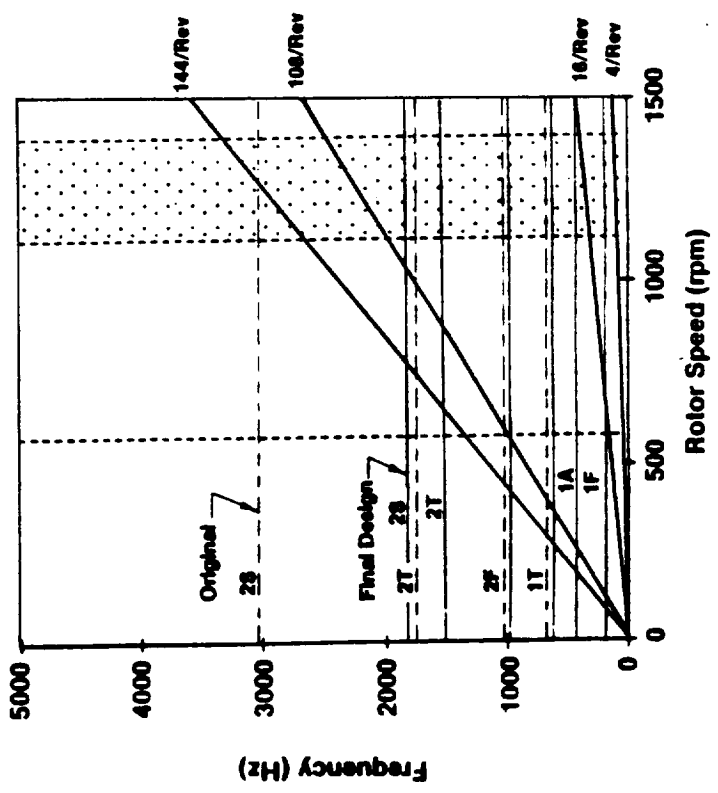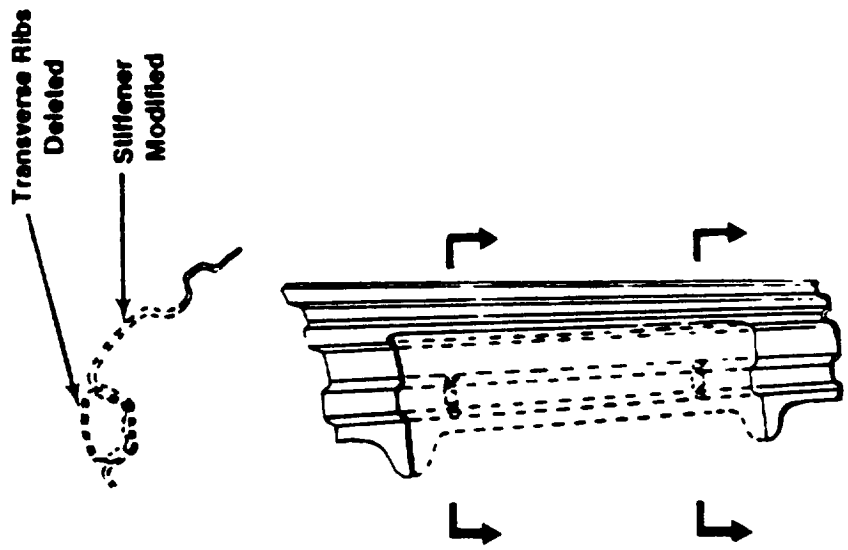
Figure 8-20. Final Stage 8 Blade Design.

**Top View
Looking Down
Stacking Axis
Stage 1**
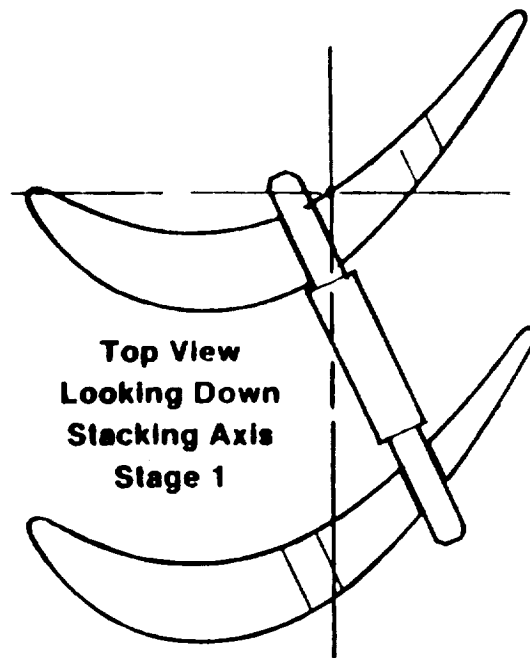
- **Blade-To-Blade Damper Pins**

- **Increased Tip Clearance**
   + 0.050 Inch Stages 1, 3, 7, 9, 11
   + 0.030 Inch Stages 2, 4, 6, 8, 10

- **Reduced Tip Thickness**
   (0.030 → 0.015)

Figure 8-21.   Turbine Blade Fix.
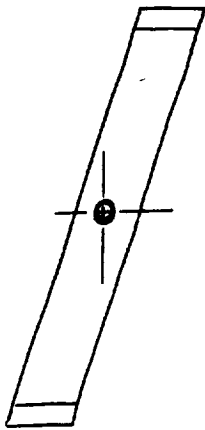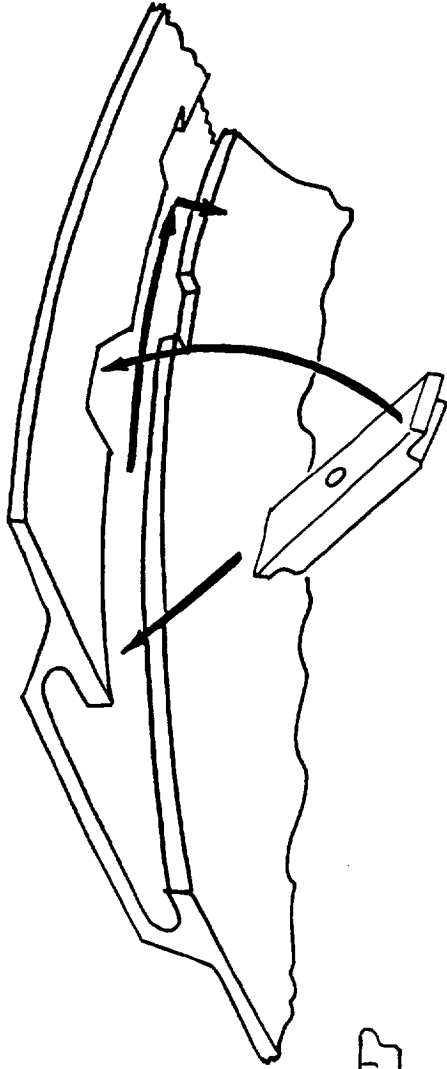
8 Locks per Blade Row

Figure 8-21a. Typical Blade Lock Design.

8.2.2 Propulsor Spools, Shafts, and Seals

All 5 spools are 360°-turned parts (Figure 8-22) made from forged Inconel 718 with abrasive aluminum oxide coating on the blade rub surfaces. Early trade studies showed cost and weight advantages in the power turbine if the number of flanges could be minimized. To accomplish this, the spool dovetail slots were configured to allow blades to be rocked and twisted into position with both inner and outer spools in place (Figure 8-23).

A removable stiffening disk, which allows on-wing hub ring removal and satisfies counterrotation dynamic requirements, was designed as portrayed in Figure 8-24.

All five shafts are turned parts made from forged Inco 718. An electron beam weld (EBW) is implemented to attach the cone wall to the forward shaft, which is then attached, by means of a splined joint (Figure 8-25), to the mid-drive shaft. The male spline length is extended axially to double as a guide for the actuation system. Bearing journals and carbon seal lands are chrome plated and ground surfaces. Integral labyrinth seals, bearing lube holes and sump drainage holes are incorporated in the designs. Aluminum oxide rub coat is applied to the seal teeth.

The two flowpath labyrinth seals are made from A286 material. The inner members are one-piece turned construction with aluminum oxide rub coat applied to the seal teeth. The outer members are welded fabrications with Hastelloy-X honeycomb rub material brazed in place. The remaining four labyrinth seals are Inconel 718 material. As discussed, the inner members are integral with the shafting. The outer member of the aftmost seal is integral with the aft sump housing, while the other three are separate components; all utilize the honeycomb rub material (Hastelloy-X) brazed in place. All six labyrinth seals (Figure 8-26) incorporate split Coulomb dampers of various configurations.

Axisymmetric shell models of the inner and outer rotor structures formed the basis for stress, clearance, and dynamics analyses of the power turbine. The design objective for the power turbine rotor was 25,000 cycles minimum LCF capability, or adequate capability for planned testing with identified means for achieving 25,000 cycles as a product design. The inner rotor structure met or exceeded 25,000 cycles capability. Three locations on the outer rotor

Forward Spools

Weld

Aft Spools

Weld
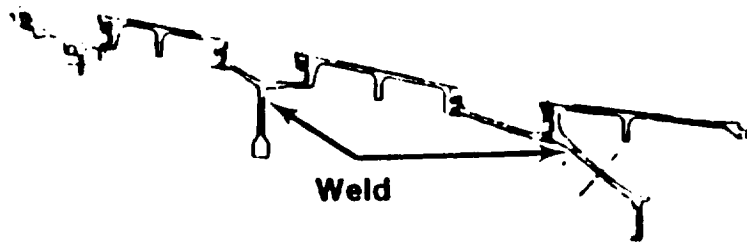
Figure 8-22. Power Turbine Spools.

INNER

OUTER
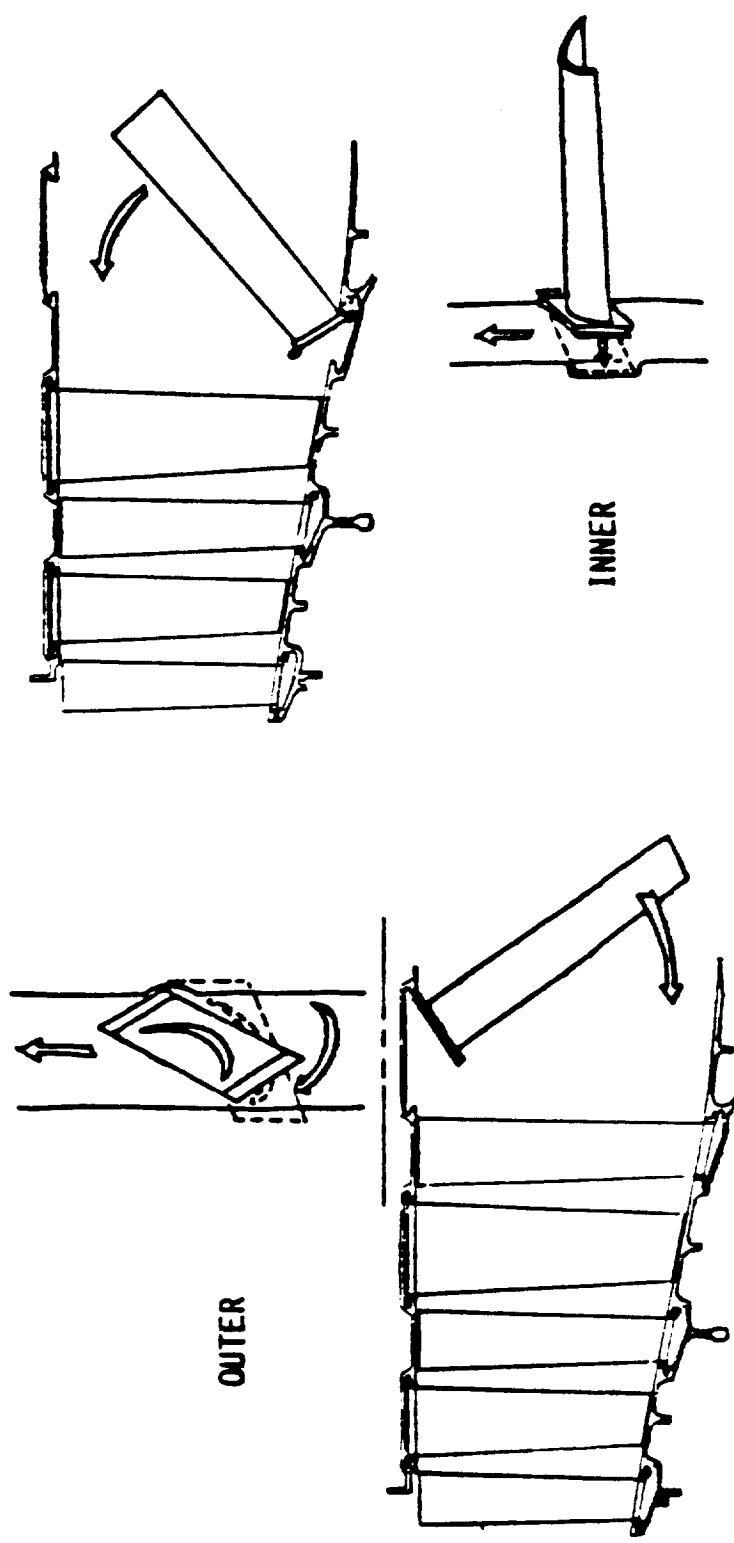
Figure 8-23. Flangeless Spool Assembly.
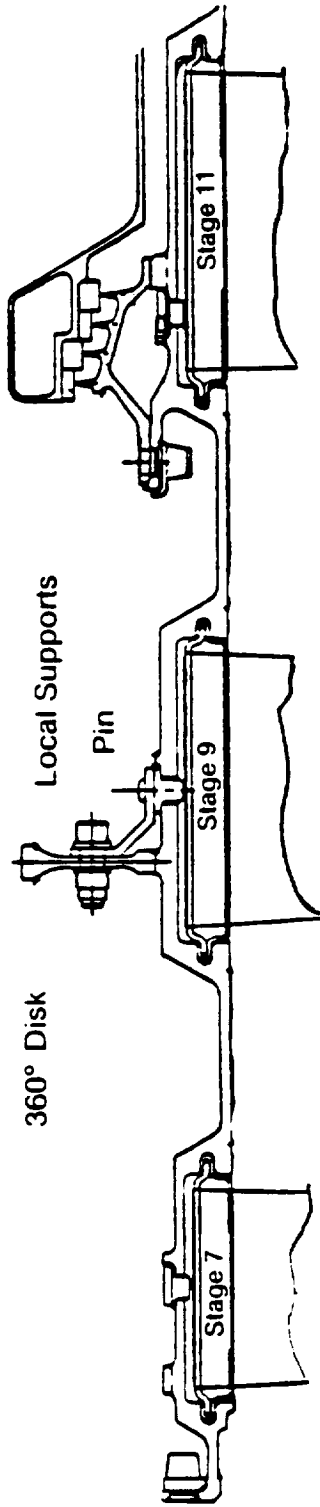
Figure 8-24. Removable Disk Design.

103

Spline

- 68 Teeth, 11.33 Pitch Diameter
- 14½° Pressure Angle
  - Doubles as Actuation Guide
- Lightly Loaded/Infinite Life
  - Capacity > 1,000,000 In-Lb
  - Max Torque = 164,000 In-Lb

Coupling Nut

- 10.88 — 12 Standard Form
- .532 Min Engagement
- High Clamp Capability
  - 21 ksi Thread Stress/25000 Lb
  - 3 ksi Shear Stress/25000 Lb
- Lock Allows 11.23° Indexing
  - 3900 Lb Clamp Variation
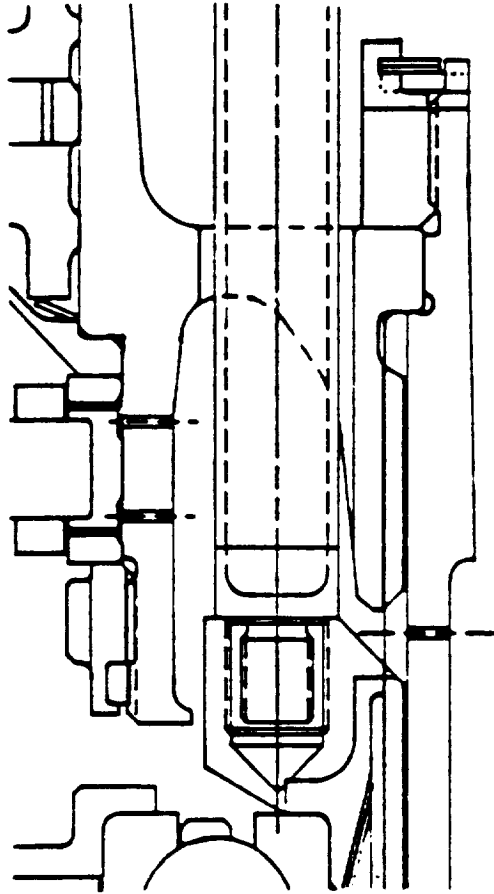
Figure 8-25.   Power Turbine Shafting - Spline and Coupling Nut Design.

104

structure were below the objective life but have adequate capability for planned testing (Figures 8-27 through 8-29). These locations are exposed to high thermal gradients and can achieve the objective life by relocation and reconfiguration of flanges in a product design.
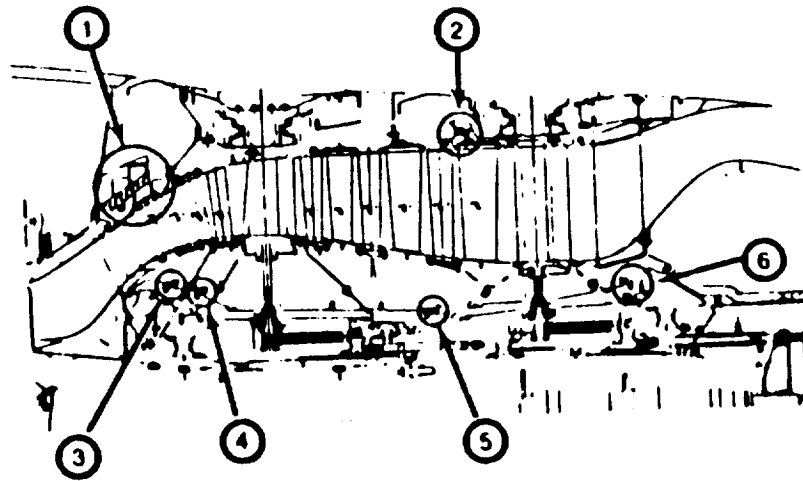
	Critical	Counter-rotating	Material	Damping
1 Forward Flowpath	X		A286	Wire/Sleeve
2 Aft Flowpath	X	X	A286	Wire/Sleeve
3 Forward Sump			IN718	T-Damper
4 Forward Sump		X	IN718	T-Damper/Flange
5 Midsump		X	IN718	Wire/T-Damper
6 Aftsump			IN718	T-Damper

Figure 8-26. Power Turbine Labyrinth Seals.

The conventional turbofan dynamics design requirements were modified for use in the design of the power turbine spools and seals to account for counterrotation. Design criteria are summarized both in Table 8-2 and in Figure 8-30.
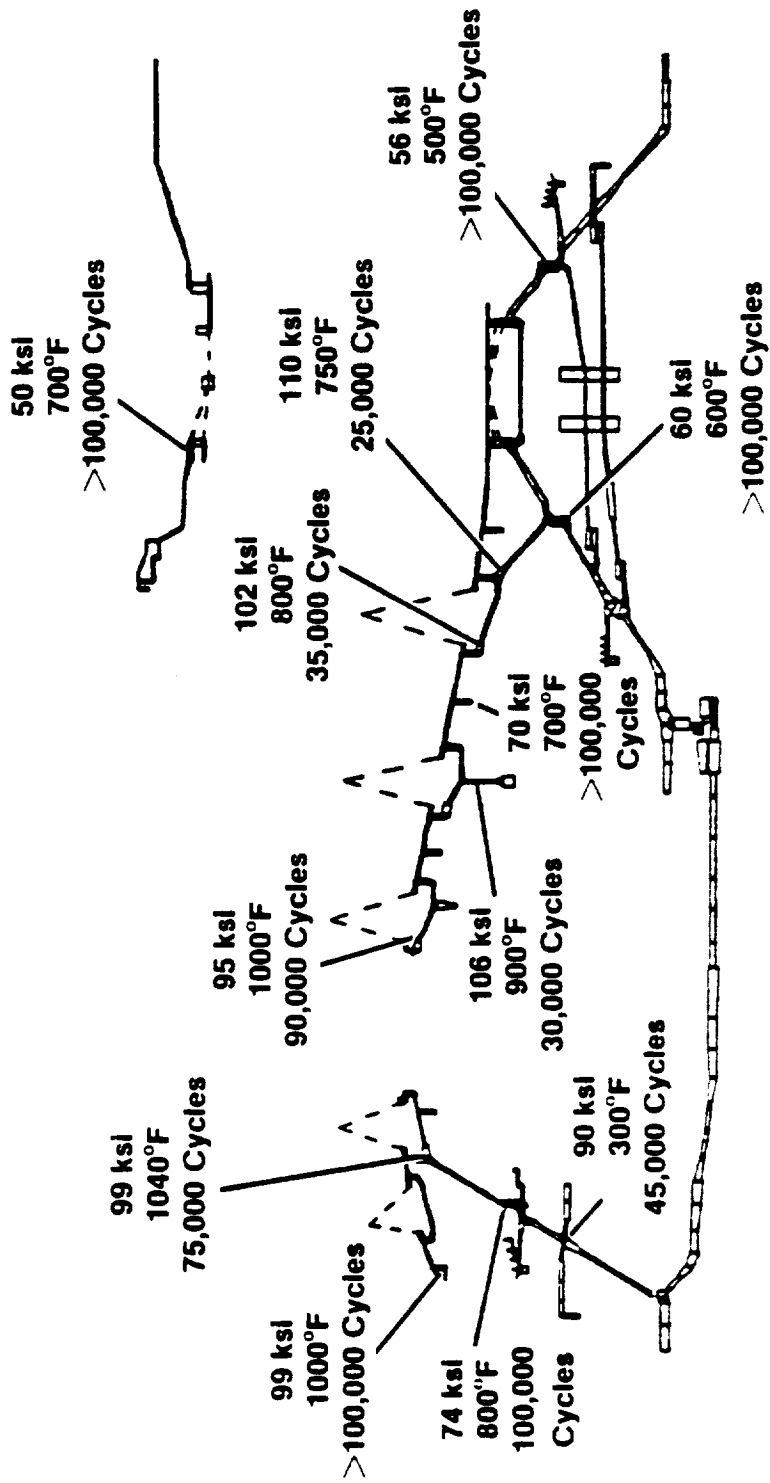
Figure 8-27. Inner Rotor Life Capability Summary.

152 ksl
400°F
>100,000 Cycles

30 ksl
700°F
>100,000 Cycles

65 ksl
300°F
>100,000 Cycles

139 ksl
600°F
12,000 Cycles

30 ksl
350°F
>100,000 Cycles

140 ksl
800°F
10,000 Cycles

184 ksl
400°F
6,000 Cycles

89 ksl
800°F
65,000 Cycles

60 ksl
350°F
>100,000 Cycles
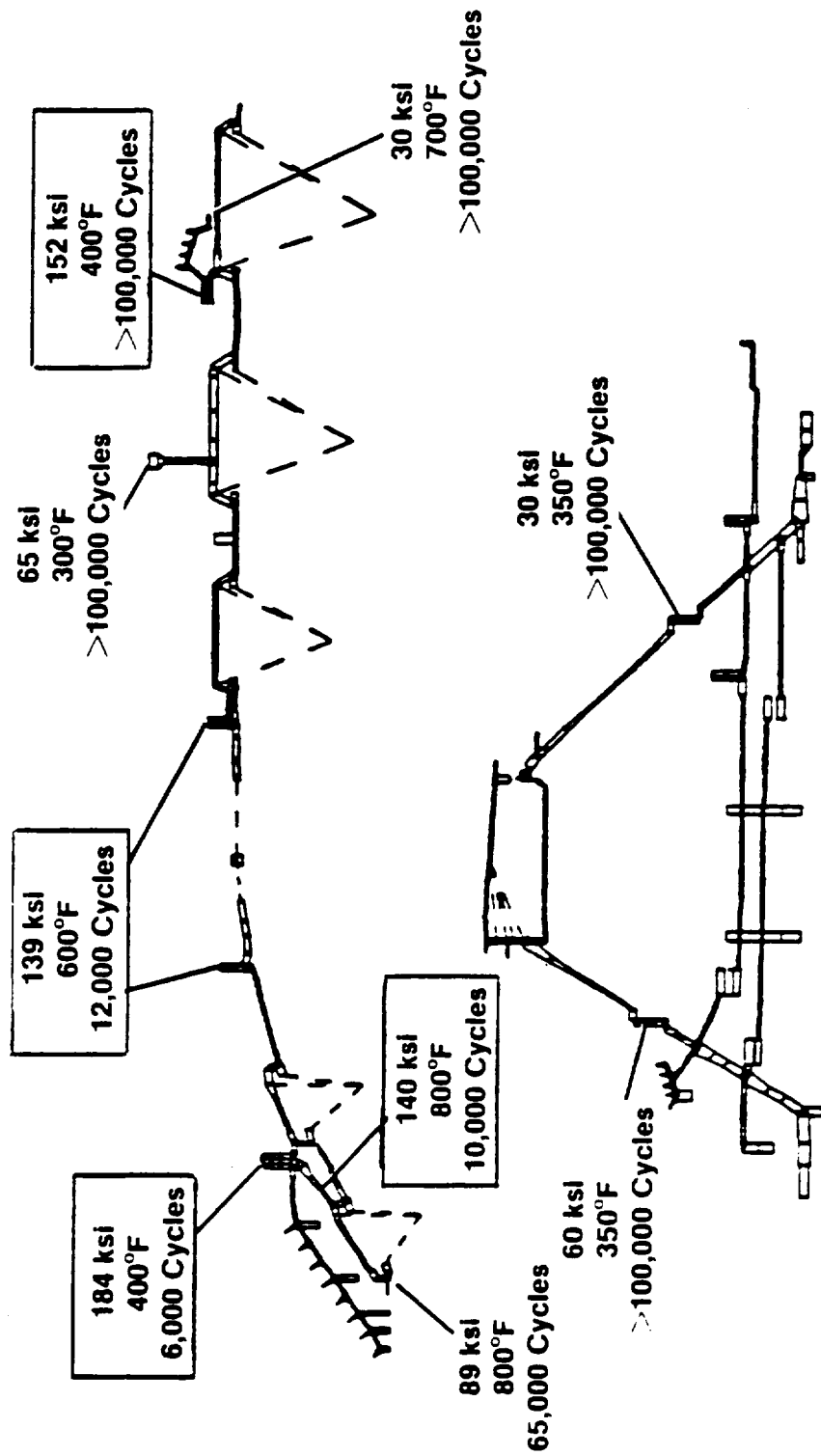
Figure 8-28. Outer Rotor Life Capability Summary.

107

400°F

450°F

1050°F

1075°F

**Original Design
4000 Cycles**

350°F

400°F

800°F

1100°F

**Improved Design
6000 Cycles**
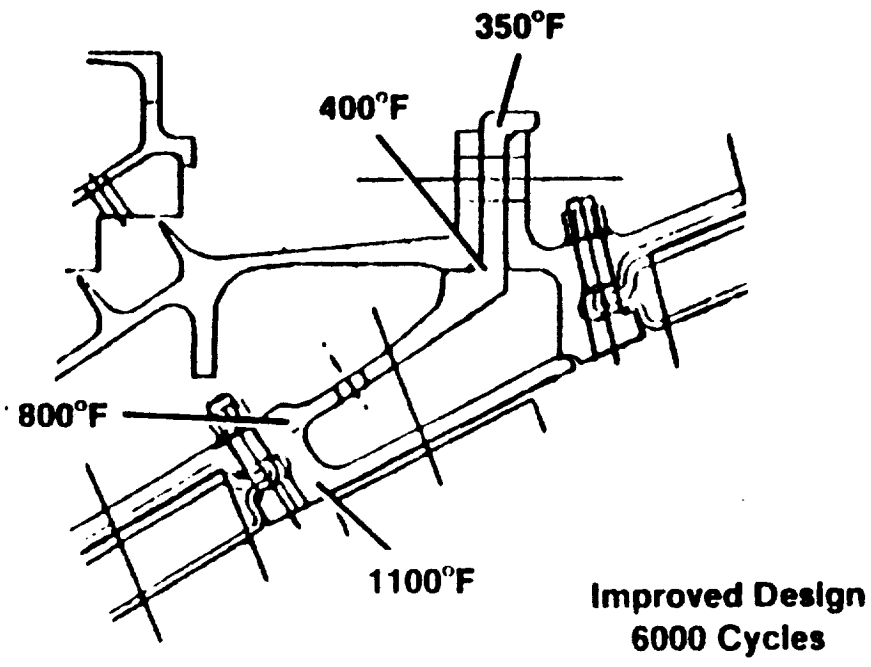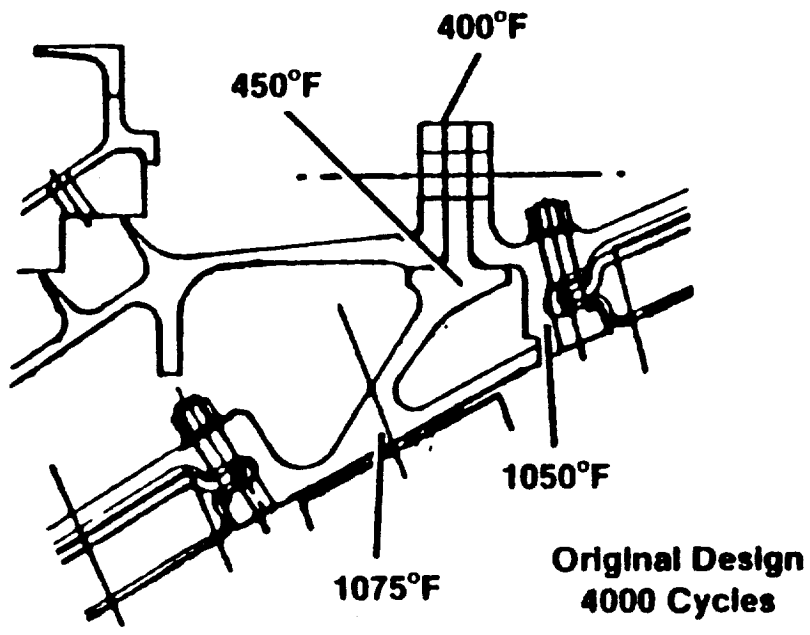
Figure 8-29. Forward Seal/Spool Flanges.
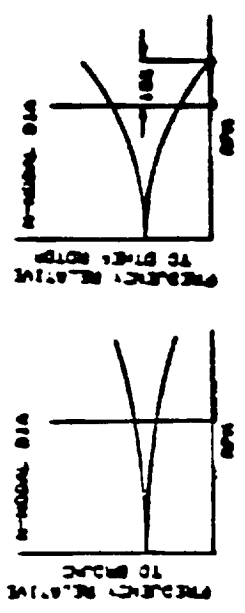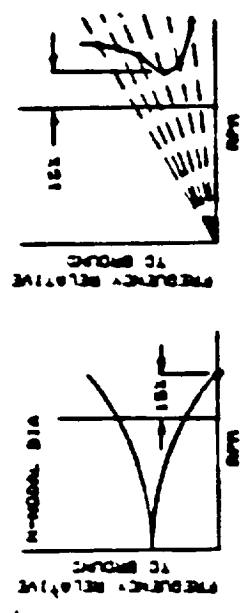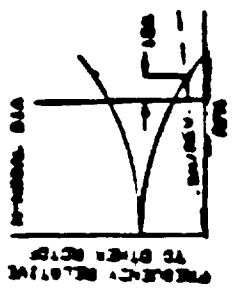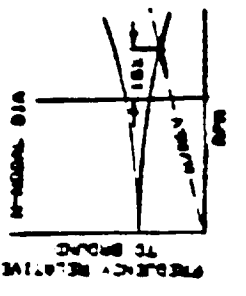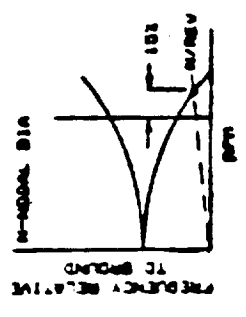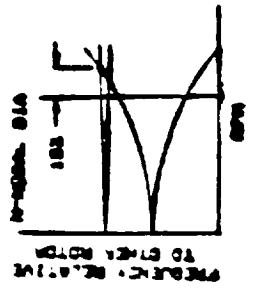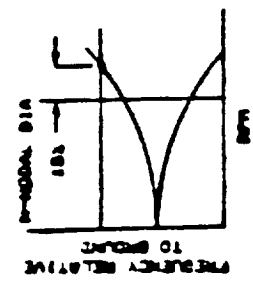
Figure 8-30. Spool and Seal Dynamic Criteria.

Table 8-2. Spool and Seal Dynamics.

Design Criteria

- Aeroelastic Stability
- Standing Wave (Campbell) Margin
- Critical Frequency Per Rev Margin
- Rotor/Stator (Rotor/Rotor) Interaction

Approach

- Modify DP Requirements for Counterrotation
- Class - Mass Analysis of Rotor Systems
- Component Test Verification

Results

- Stability Requirements Met - Seals and Spools Damped
- Campbell Criteria Met
- Potential Per Rev Excitations and Interactions Identified
  - Aft Spools
  - Forward Flowpath Seal
  - Aft Flowpath Seal

All spools met the design criteria. As shown in Figures 8-31 and 8-32, it was predicted that the aft spools would have 3 and 4 nodal rotor/rotor interactions in the operating range; however, damping analyses indicated the centrifugal load of the blades on the spools would provide significant energy dissipation and low response (Figure 8-33).

The labyrinth seals also met the design criteria. The original configuration of the forward flowpath outer seal had inadequate margin to resonant interaction for the 2, 3, and 4 nodal diameter modes (Table 8-3). As detailed in Figures 8-34 and 8-35, changing from solid nonmetallic rub material to honeycomb material provided an increased margin, and dampers were sized to be effective for these low order modes. The aft flowpath and midsump seals also had predicted resonant interactions; dampers for these seals were designed to provide significant energy dissipation for these modes.
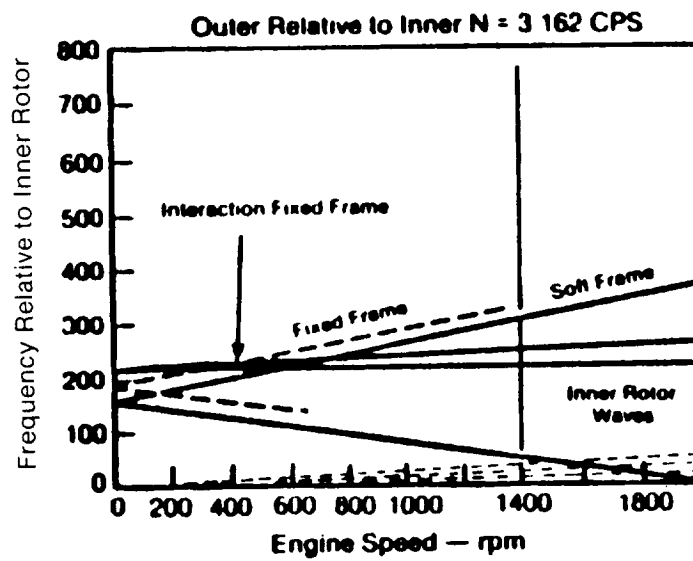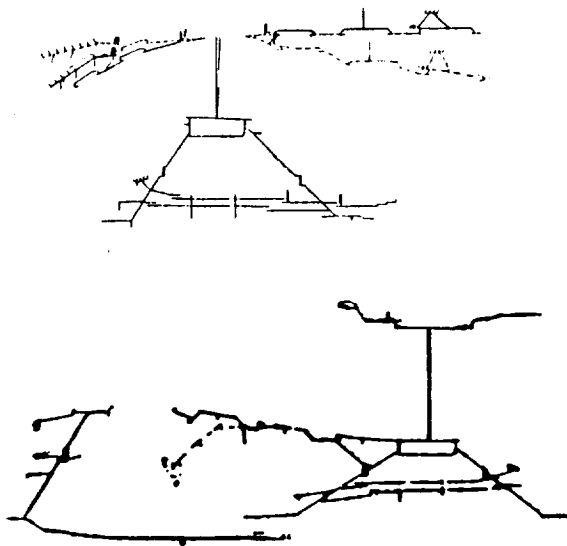
Figure 8-31.   Aft Spools N = 3 Dynamic Analysis.
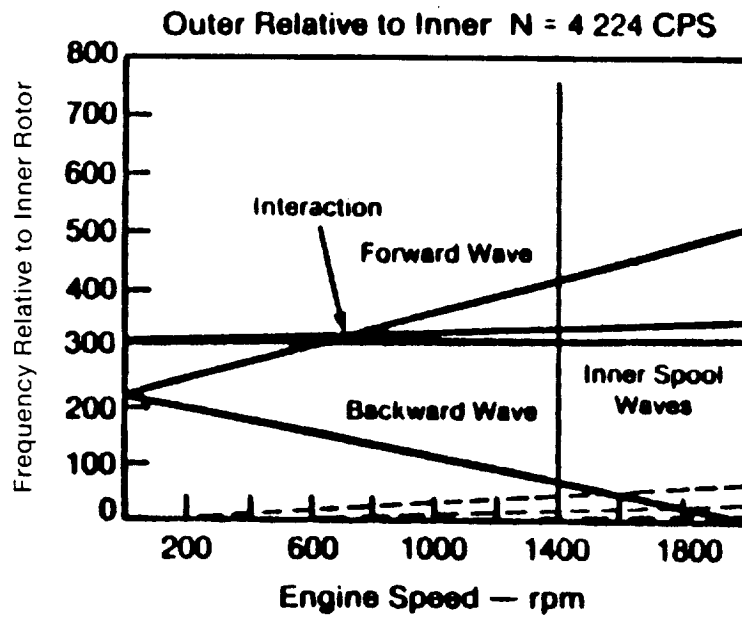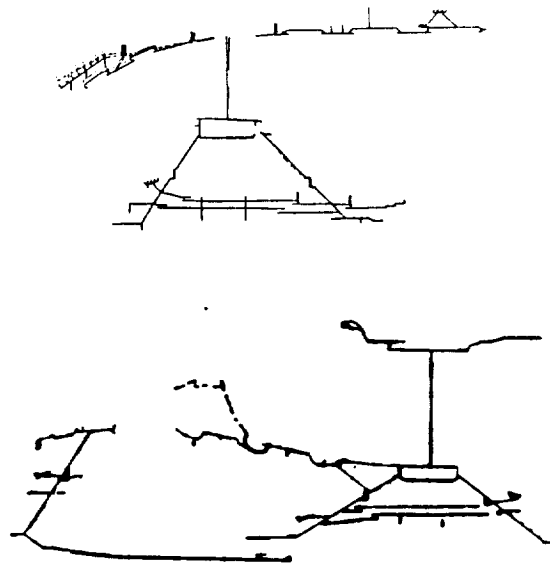
Figure 8-32. Aft Spools N = 4 Dynamic Analysis.
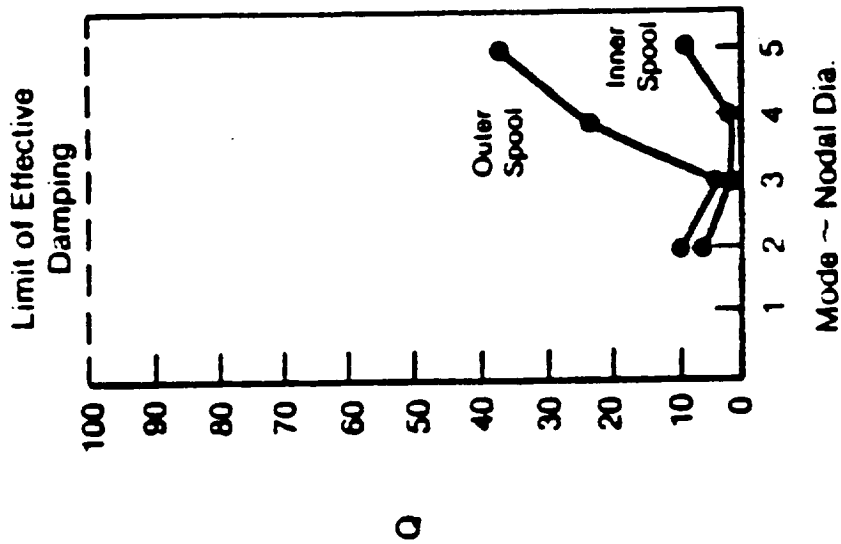
- **Resonant Magnification Factor**

  $Q = \dfrac{\text{Energy in System}}{\text{Energy Dissipated Per Cycle}}$

- **Energy Dissipation (Coulomb Damping) Based on Blade/Spool Relative Axial Motion**

  $\dfrac{1}{Q\,\text{Total}} = \dfrac{1}{Q\text{Stg (N)}} + \dfrac{1}{Q\text{Stg (N+2)}}$

- **Additional Damping Available**
  - Relative Tangential Motion
  - Inner Spool Wire

- **Q < 100 Required for Effective Damping**

Limit of Effective Damping

Q

Mode ~ Nodal Dia.

Outer Spool

Inner Spool

Figure 8-33.   Aft Spools – Damping Analysis.
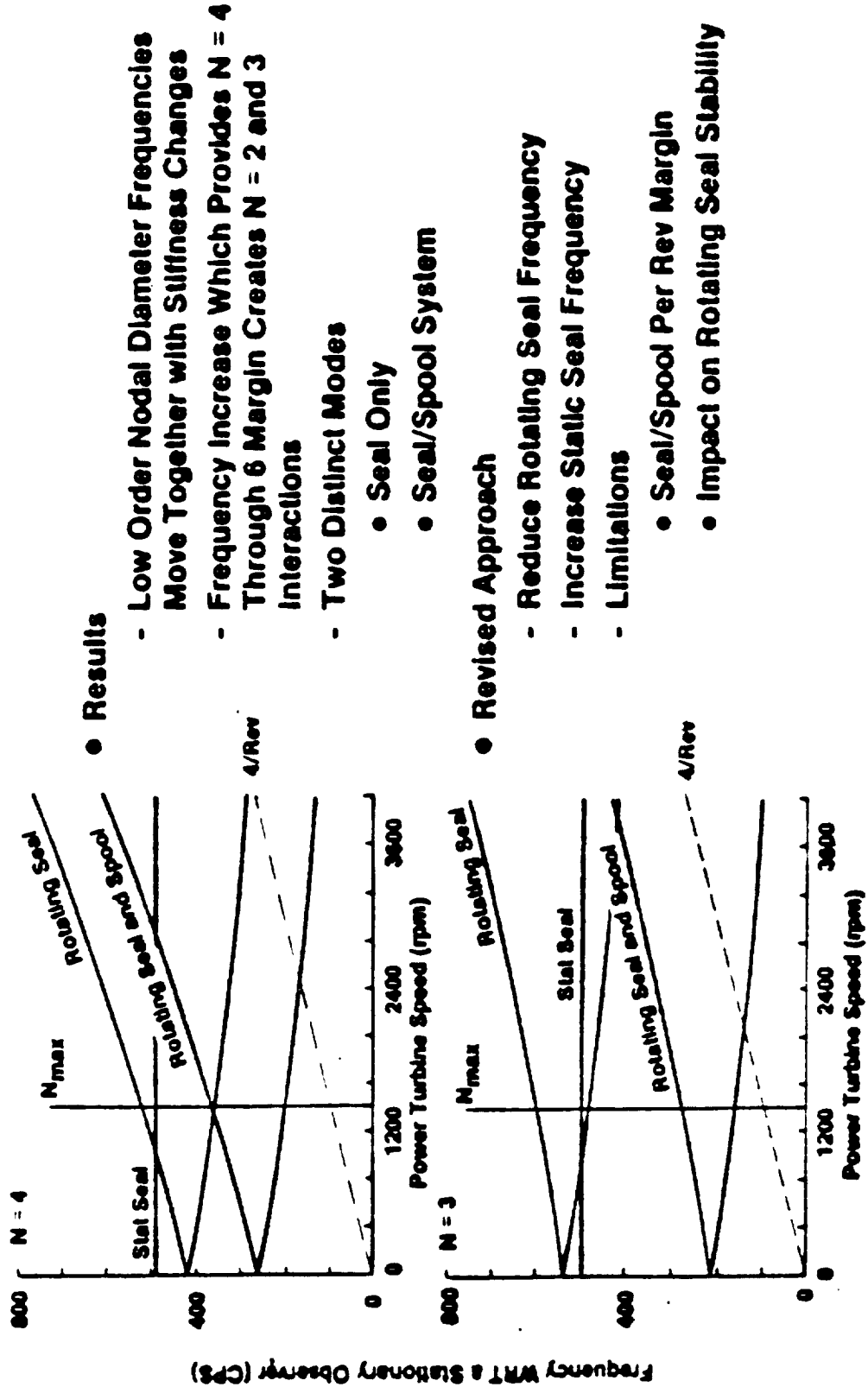
Figure 8-34. Forward Flowpath Seal - Static Seal Redesign Studies.
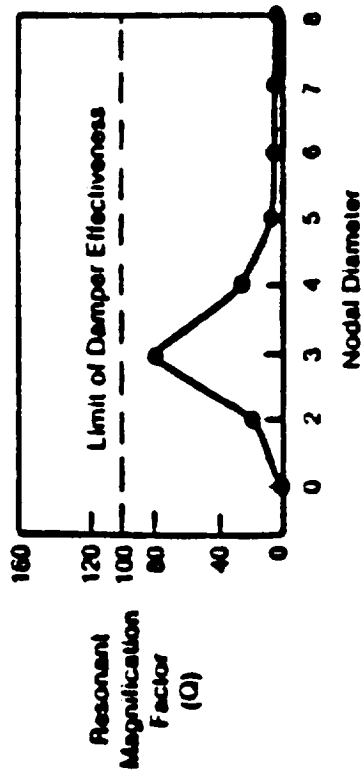
- **Honeycomb Rub Material**
  - **Resonant Interaction Margin**
  - **Weight**
  - **Teflon Requires Process Development**

- **Effective Rotor Damping**

- **W/R Stability Margin**

Resonant Magnification Factor (Q)

Limit of Damper Effectiveness

Nodal Diameter

Nodal Diameter	Seal and Rotor System		Seal	
	Freq (Hz)	W/R (In/In)*	Freq (Hz)	W/R (In/In)*
2	282	0.19 x 10-3	835	0.09 x 10-3
3	213	0.38 x 10-3	519	0.24 x 10-3
4	261	0.26 x 10-3	404	0.43 x 10-3
5	356	0.15 x 10-3	404	0.43 x 10-3
6	436	0.10 x 10-3	499	0.29 x 10-3
8	594	0.05 x 10-3	825	0.11 x 10-3
16	779	0.02 x 10-3	2386	0.01 x 10-3

* W/R > 0.4 x 10-3 In/In Requires Damping

Figure 8-35.   Forward Flowpath Seal Design.

Table 8-3. Forward Flowpath Seal - Resonant Interaction Margin.

Nodal Diameter	Teflon Static Seal		Honeycomb Static Seal	
	Forward Wave, %	Backward Wave, %	Forward Wave, %	Backward Wave, %
2	18	11	18	11
3	2	28	11	38
4	13	72	29	94
5	21	115	33	130
6	19	118	26	117
8	5	77	10	72
16	30	Interaction	31	6
Δ Weight	+ 9 lb		- 9 lb	
Δ Leakage (at Takeoff)	0.0		+ 0.13 lb/s	

8.2.3 Clearance Analysis

Turbine blade design clearance objectives were 0.030 inch at cruise. In addition, clearances had to accommodate maneuver deflections of the rotors and be compatible with the blade assembly techniques. Transient and steady-state rotor growth analyses were utilized to project clearance changes throughout a normal commercial aircraft flight envelope. Design cruise clearances were then set at 0.030 inch, and compatibility with other requirements was checked. Clearances were adjusted as required to meet assembly and maneuver requirements; additional adjustments were made to assure even stages would contact first (in the event of a rub) to prevent a thermal instability. As presented in Table 8-4, the net result was an average cruise clearance of 0.036 versus an objective of 0.030.

A broken carbon seal (assembly damage) during initial testing resulted in oil accumulating in the pockets under Stages 7, 9, and 11. This accumulation slowed the response of the outer spool and resulted in the outer blades rubbing first, creating a thermal instability. To prevent a recurrence, oil drainage holes were added to the spool for Build 2; the even blade clearances were increased 0.030 inch, and the outer blade clearances were increased 0.050 inch.

Table 8-4. Turbine Blade Tip Clearance Analysis.

Stage	Assembly	Pinch Point	Takeoff	Cruise
1	0.054	0.018	0.023	0.033
2	0.058	0.016	0.015	0.034
3	0.036	0.014	0.031	0.033
4	0.030	0.020	0.053	0.040
6	0.044	0.014	0.030	0.029
7	0.044	0.017	0.048	0.042
8	0.036	0.015	0.044	0.033
9	0.060	0.016	0.052	0.046
10	0.046	0.018	0.045	0.033
11	0.041	0.023	0.052	0.040

Radial clearances in the labyrinth seals were analyzed; special emphasis was placed on the large forward flowpath seal. Thermal response of the inner and outer members was matched by purging box sections on the outer member with seal air. Design clearances on all of the labyrinth seals are summarized in Figure 8-36.

All turbine flowpath interfaces were designed to provide double overlap seals to prevent local circumferential recirculation at these locations. As a result of the large number of toleranced dimensions that were involved in assessing these clearances, statistical as well as total arithmetic stackups were performed, with the criteria that a four-sigma stack must provide ample clearance for steady-state, transient, maneuver, and dynamic deflections.

8.2.4 Bolted Joint Analysis

Eight bolted joints were designed for the power turbine rotor. In all cases, 70% of nominal cold clamp was assumed (to account for torque-tension variability); modulus change with temperature and Poisson's effect on flange dimensions were accounted for. Axial loads, moment loads, and the net clamp load required to carry torque in friction were utilized to establish joint separating loads.
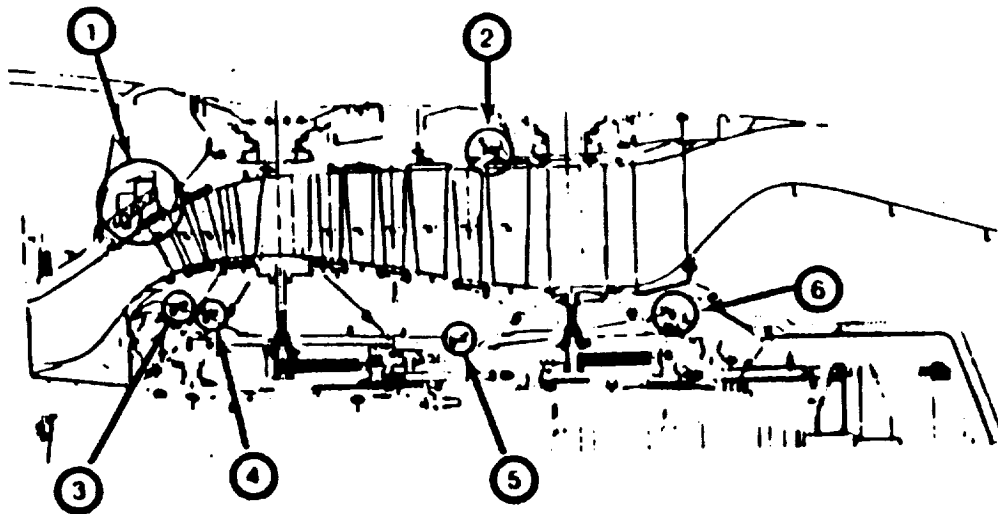
No.	Description	Cold	Takeoff	Cruise
1	Forward Flowpath Seal	0.032	0.015	0.016
2	Aft Flowpath Seal	0.045	0.015	0.033
3	Forward Sump Seal (Stator/Rotor)	0.024	0.024	0.026
4	Forward Sump Seal (Rotor/Rotor)	0.017	0.034	0.031
5	Midsump Seal	0.052	0.054	0.054
6	Aftsump Seal	0.023	0.023	0.024

Figure 8-36. Labyrinth Seals - Radial Clearances.

All flanges except one had more than adequate hot clamp capability using 0.250 inch fasteners (the minimum structural fastener consistent with General Electric design practice). The aft inner spool to Stage 12 power frame joint uses 5/16-inch fasteners because the torque from all of the inner rotor blades must be carried in friction through this joint. Results of the bolted joint analysis are summarized in Figure 8-37.

118

- Use 70% of Nominal Cold Clamp for Minimum Clamp
- Calculate Hot Clamp Based On
    - Modulus Change with Temperature
    - Poisson's Effect on Joint
- Calculate Net Separating Load From
    - Axial Load
    - Moment Load
    - Load Required to Carry Torque (u = 0.15)
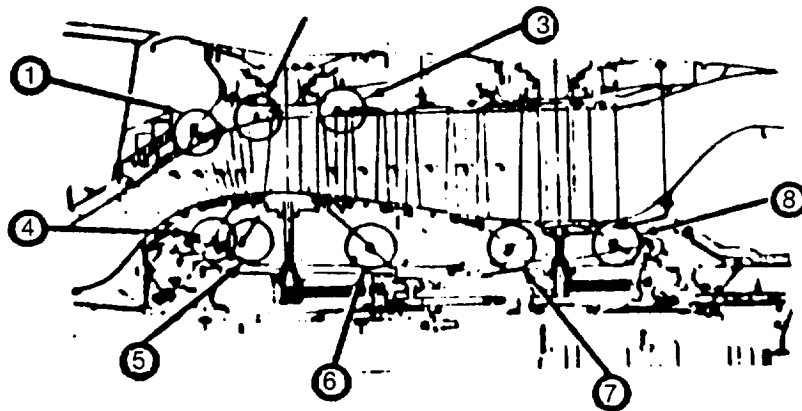
Flange Location	Fastener Size	Quantity	Nominal Cold Clamp Per Bolt	Minimum Hot Clamp Per Bolt	Net Separating Force Per Bolt
1	1/4	120	3550	2171	875
2	1/4	120	3550	2145	552
3	1/4	128	3550	2158	465
4	1/4	100	3550	1985	361
5	1/4	64	3550	2045	626
6	1/4	64	3550	2063	217
7	5/16	72	5800	3678	3564
8	1/4	64	3550	2070	99

Figure 8-37.   Bolted Joint Analysis.

8.2.5 Rotating Frames

Two Inconel 718 rotating power frames provide support for the fan blade polygonal ring assemblies and the turbine structure. The major structural elements of each power frame (Figure 8-38) are the inner box and support cones, large and small airfoil shaped struts and vanes, and a 360° outer flow-path structure. Both components are fabricated from hot isostatic pressed (HIP) Inco 718 castings with electron beam (EB) and tungsten inert gas (TIG) welded cones.

Airfoil geometry for each frame consists of a cascade of eight structural struts and additional small aerodynamic vanes. The hollow struts extend radially into the inner box to provide additional frame stiffness and are sized to provide clearance for the fan blade actuation quill shafts.

Detailed design of the frame structure maximized stiffness while minimizing thermal distortions. Stiffness was requested in order to control flexure vibration of the turbine rotor system, to minimize induced deflections, and consequently, to provide improved blade tip clearance control. Figure 8-39 demonstrates a matrix of frame stiffness studies.

Final steady-state, burst, and transient stresses for the forward power frame are summarized in Figures 8-40 and 8-41 along with calculated LCF lives. The aft inner ring of the forward frame was the life-limiting location with a predicted life of 6000 cycles. This life is satisfactory for the demonstrator engine, but a configuration modification would be required for product engine design. A geometry change and/or revised secondary flow system change in this area would minimize the thermal induced stress in the ring.

8.2.6 Fan Support Ring And Brackets

The dual, counterrotating fan rotors for the UDF™ engine are mounted externally concentric with the power turbine. The primary function of the fan support ring was to support and react to the centrifugal and aerodynamic loads of the fan blades and to provide the required elastic stiffness for coupled system vibration modes. The method by which these loads were transferred to and from the power turbine was also an integral part of this primary function since turbine flowpath distortion control was critical.
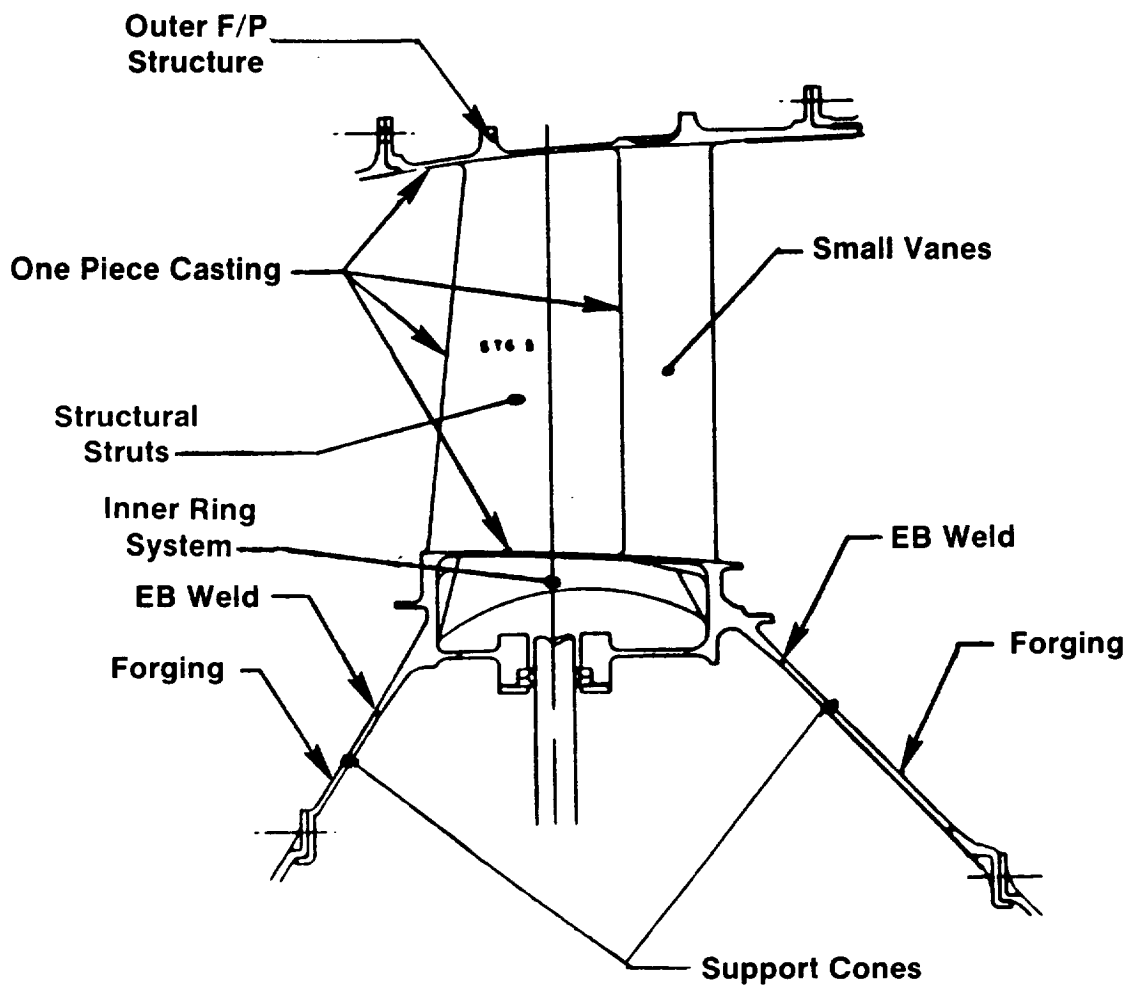
Figure 8-38. Power Frames Construction.
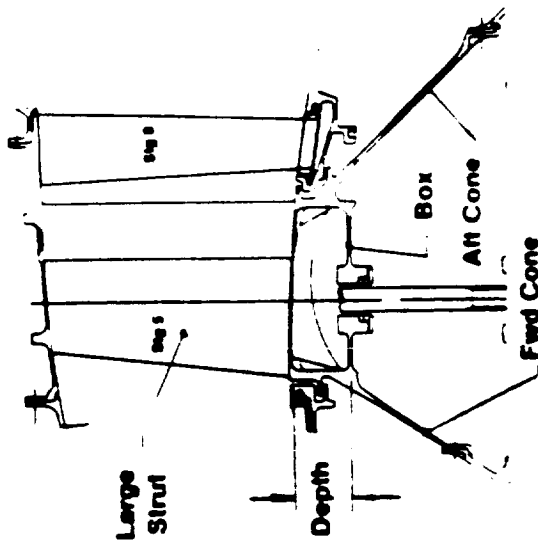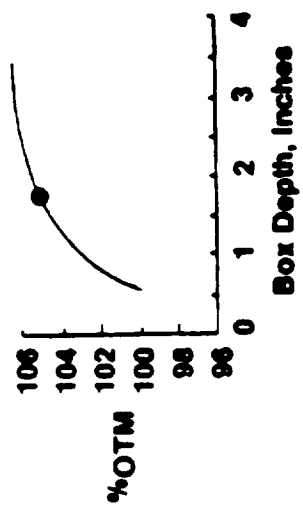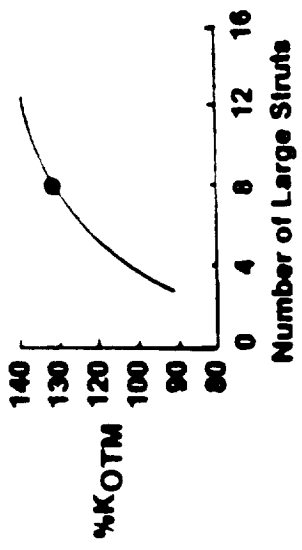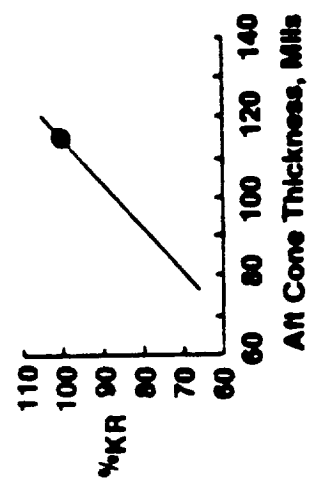
Figure 8-39. Fundamental Power Frames Structural Stiffness.

Location	Temp °F	Kt	Concentrated Effective Stress (ksi)			LCF Cycles
			Mech	Thermal	Combined	
A. Weld	400	1.1	30	75	99	6000
B. Strut-F/P	1015	1.3	14	108	95	15000
C. Boss-F/P	840	1.5	84	39	89	25000
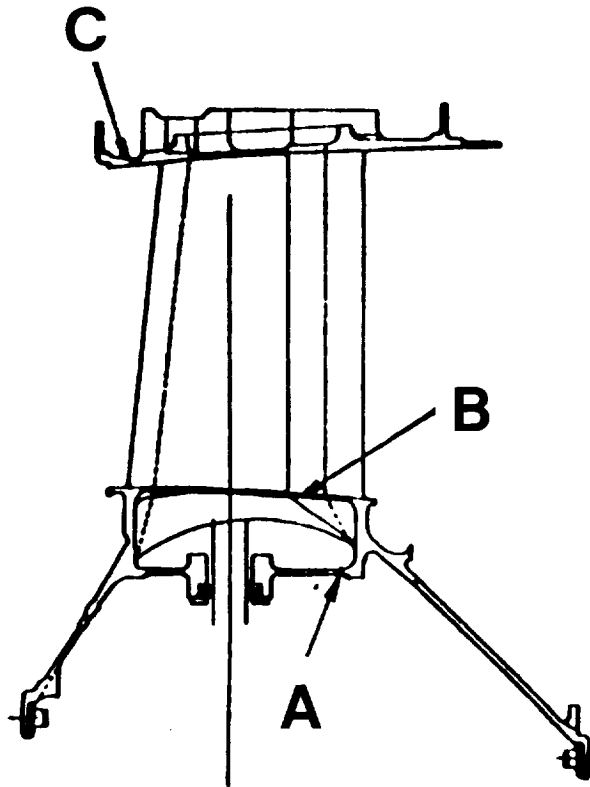
Figure 8-40.   Power Frame Stress and Life Analysis.

A = Below Inner Skin at Large Strut TE

	Location	Local Temp (° F)	Mech Loads	Therm Loads	Combined Loading	Burst Mech Loads	Burst Combined Loading	0.2%YS	Ultimate	HRS 0.2%PC
A.	Shear Web	1010	7.1	72.1	76.9	21.7	93.4	85.0	93.5	3500
B.	Large Strut	1164	8.6	31.8	37.2	13.6	40.8	83.0	90.5	1500
C.	Small Strut	1139	15.1	28.2	42.0	28.4	54.6	83.5	91.0	8500
D.	Inner Ring	762	26.4	42.9	68.7	51.3	93.4	88.0	98.5	$>10^5$
E.	Inner Skin	1108	24.2	69.2	46.8	45.9	29.4	84.0	91.5	6000
F.	Inner Web	675	13.9	32.8	46.4	27.4	59.8	90.0	101.5	$>10^5$
G.	Bearing Cone	770	22.9	32.4	54.7	44.5	76.1	88.0	98.5	$>10^5$
H.	Outer Ring	993	14.6	0.4	14.3	27.9	27.6	85.0	93.5	$>10^5$
I.	Outer Skin	1082	18.4	30.8	13.5	34.4	8.6	84.0	91.5	$>10^5$

Effective Stress (ksi)   Allowable Stress (ksi)

N = 1384 rpm
N_B = 1.41 × 1394 = 1965 rpm

Figure 8-41. Power Frame Stress Analysis - Forward Frame.

After numerous alternate blade support systems were studied, the design concept selected was that of an externally mounted ring structure attached to the frame of each power turbine rotor. The external fan support structure as shown in Figure 8-42 includes the ring structure, eight supporting brackets, and eight hub bulkheads. These structures are mounted in the cavity between the power turbine and the fan flowpath.

- High Strength Titanium Alloy

- Modified Polygonal Construction for Low Stress - Light Weight

- Cross Section Designed for Minimum Distortion and Fan Blade Dynamics

Support Ring Bracket

Bulkhead
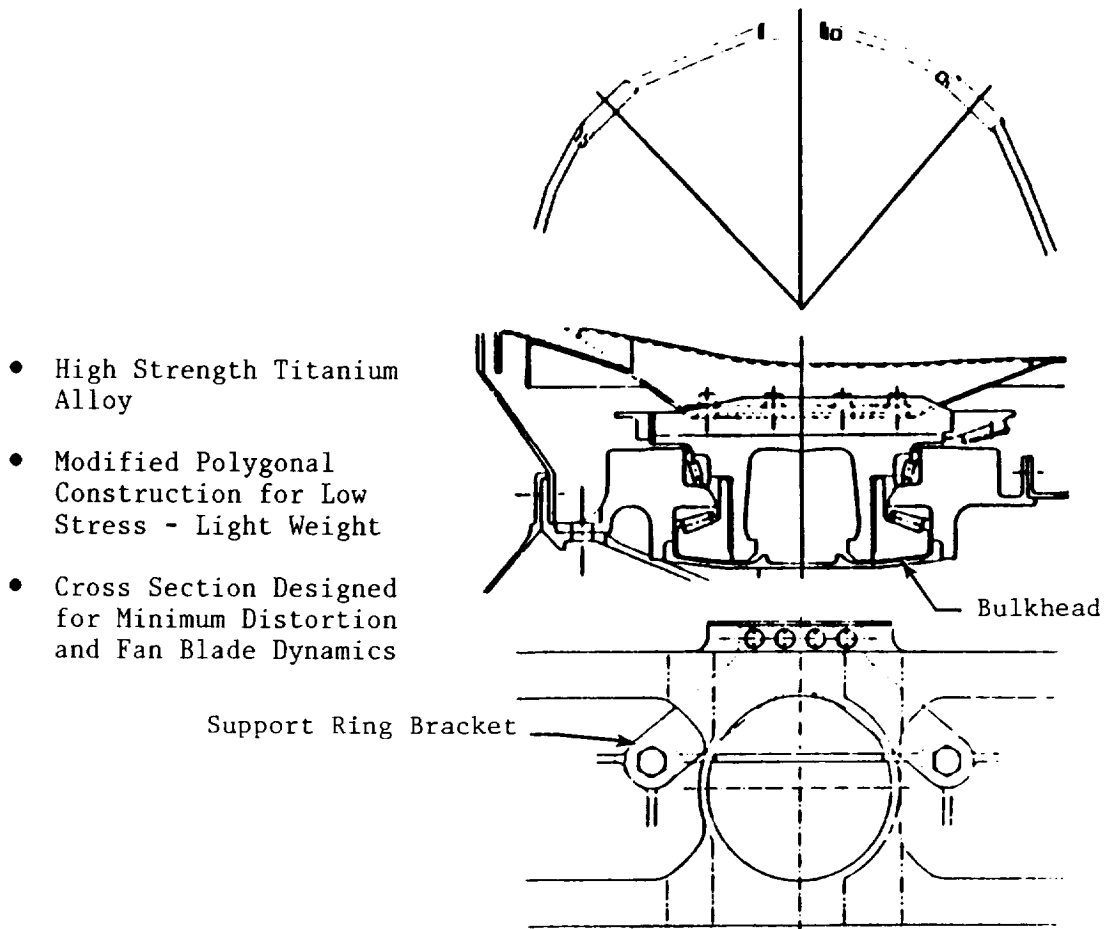
Figure 8-42. Fan Hub Ring Design.

The fan support rings were machined from Ti-6-4 forgings because of its availability and low cost. Other titanium alloys, with their higher ultimate strength capability for this burst-limited structure, could be considered for production applications. The bulkheads and brackets were machined from Inco

718 nickel based alloy as a result of its high temperature fatigue, strength, and modulus properties.

The ring structure depicted in Figure 8-43 consisted of two, eight-sided polygonal shaped rings with eight integral hubs joining the rings together. Mount lugs for attaching the gearbox support brackets were machined integral with the rings midway between alternate blade hubs. This modified polygonal shaped ring geometry provided a uniform stressed (no bending) structure which reacts the centrifugal force (CF) loads of the blades and actuation system hardware in tension with uniform deflections.

The blade hubs of conventional turboprops have support structures with hub depth-to-diameter ratios on the order of 2:1 or greater. However, because of space limitations, the hub depth-to-diameter ratio for this design was only 0.5. This low ratio required an alternate method of stiffening the hubs; this was accomplished by the installation of structural bulkheads (Figure 8-42) in the base of the hubs. Pins pressed into radial holes, match-drilled in the bulkheads and hubs, provided shear compatibility between these parts. Two lock-wired screws per hub provided positive retention of the bulkheads.

Each hub also contained an integral shaft that protruded circumferentially from one side, providing support for the helix gear and bearings of the pitch-change mechanism. Two flanges which protruded axially from both sides of the hub provided attachment points for the mount brackets, cowling support rings, rotating bulkhead, and telemetry rings.

The torque developed by each power turbine rotor is transferred to the blade hubs through eight "V" shaped brackets such as portrayed in Figures 8-42 and 8-44. These brackets also transfer the thrust developed by each rotor, along with maneuver and vibratory-induced loads to the power turbine frames. These brackets were radially bolted to the embossment located on the outside of the frames and also to the flanges on the hubs of the support rings. Providing concentric alignment of the rings to the power turbine, these brackets were designed to be flexible in the radial direction in order to provide for differential thermal growth.

Detail stress, life, and burst analyses for the support rings, brackets, and bulkhead are summarized in Figures 8-44 through 8-49. Results of these

- **Detail Stress and Deflection Analysis Models**

Ring Model
- Beam Elements
  - Flexibilities — Overall

Ring Model
- Tamp 3-D Brick Elements
  - Stresses — Elastic and Plastic
  - Deflections — Local

Spar/Bearing/Ring Model
- Tamp 3-D Brick Elements
  - Deflections — Local
  - Load Distributions
  - Flexibilities — Local

Figure 8-43. Fan Hub Ring Design Analysis.

- **Finite Element Analysis**
    - **SLTO Hot Day**
    - **Max 1P Loads**
- $\sigma_{max} = 91.0$ **ksi**
- **LCF = 40,000 Cycles**
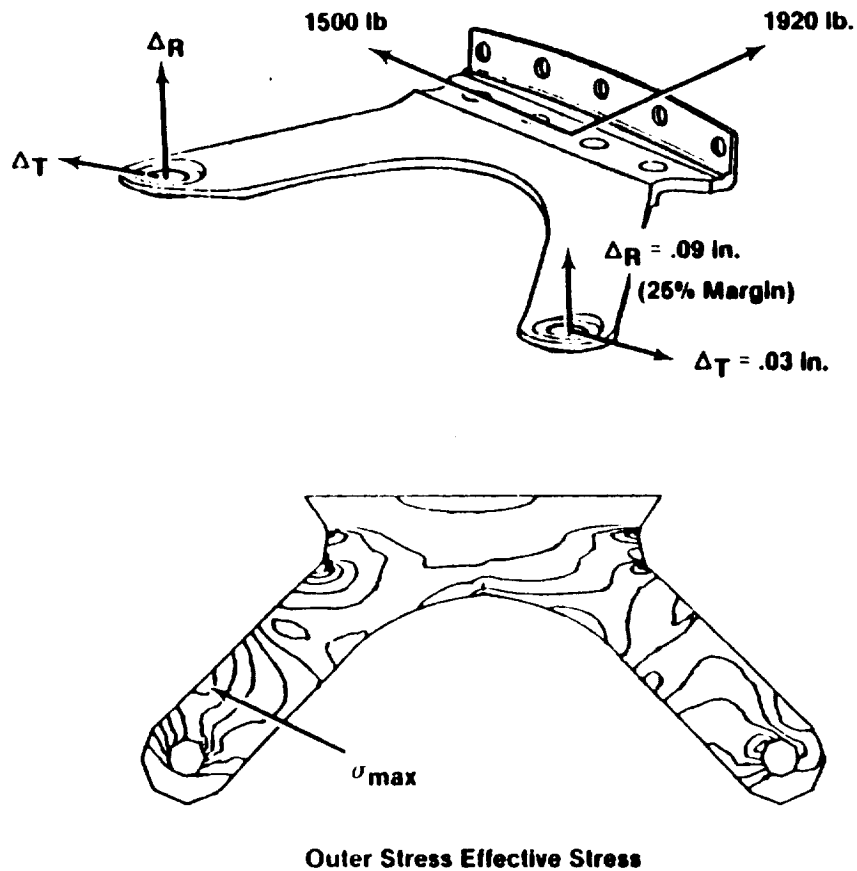
Figure 8-44.   Shear Plate Analysis of Support Ring Bracket.

- **Thrust and Torque Loads Transmitted To Frame**
- **CF and Moment Loads Reacted Internally by Ring**
  - **CF/Tensile**
  - **Moments/Bending**
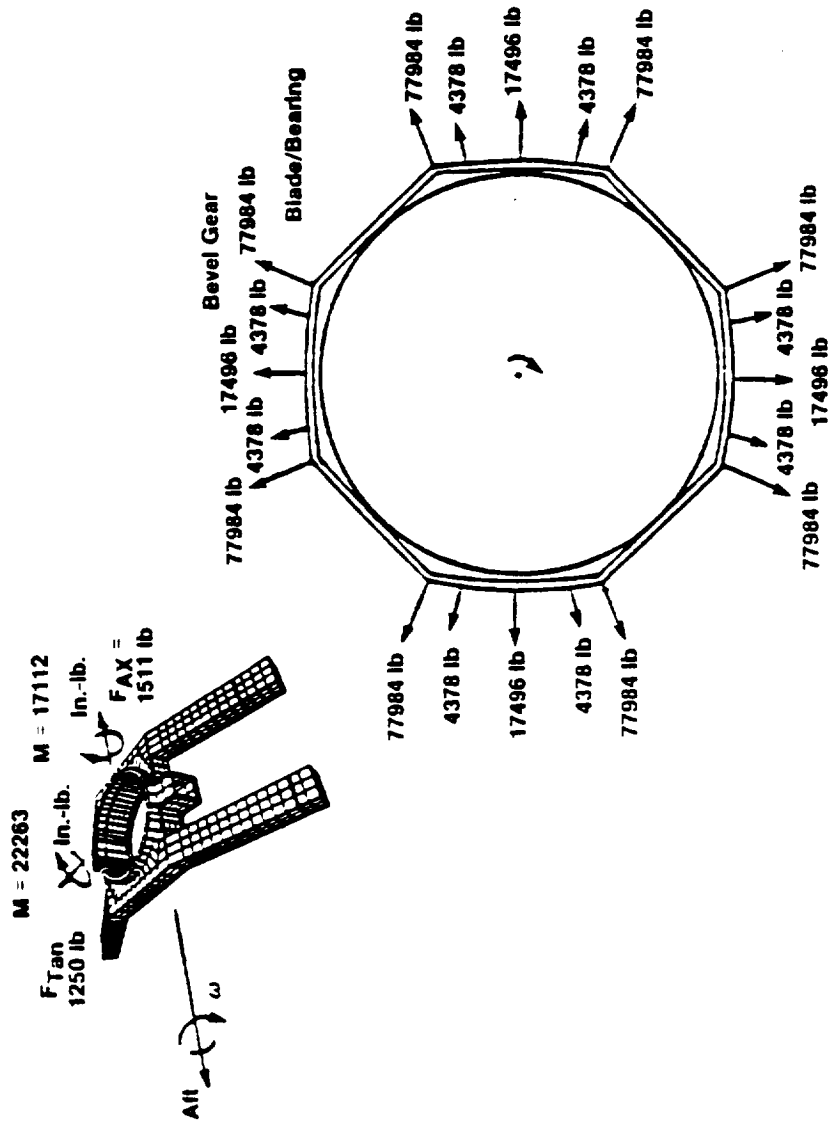
Figure 8-45. Hub Ring Loading at Sea Level Takeoff, Hot Day.

129

- **Analysis of Polygonal Ring**
- **Uniform P/A Stresses**
- **.02% YS = 71.5 Ksi (-3σ) @ 400° F**

36.9 Ksi

36.9 Ksi

35.3 Ksi

36.9 Ksi
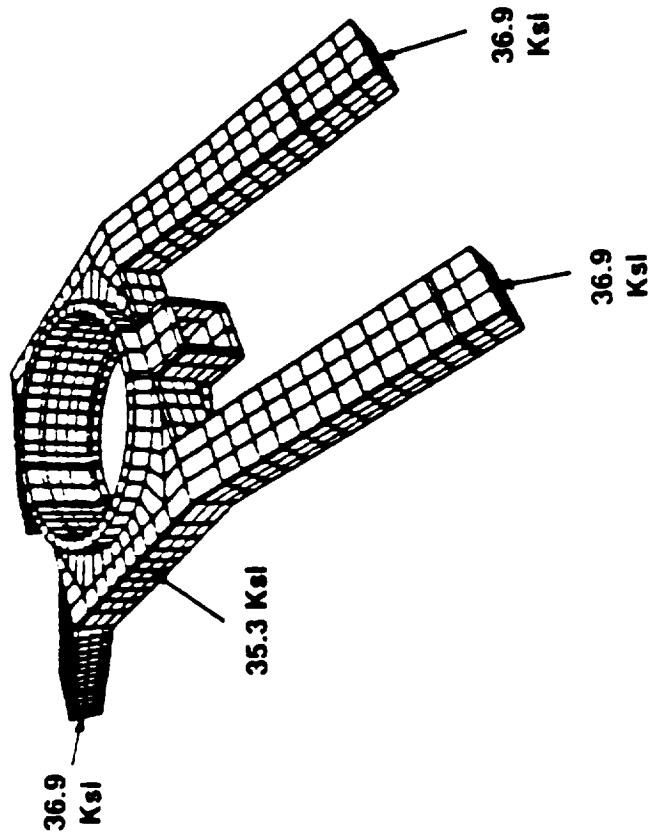
Loading
1. Speed (Take-Off)
2. Blade/Bearing CF Load
3. Acluation System CF Load

Figure 8-46. Fan Hub Ring.

SLTO Hot Day Loads
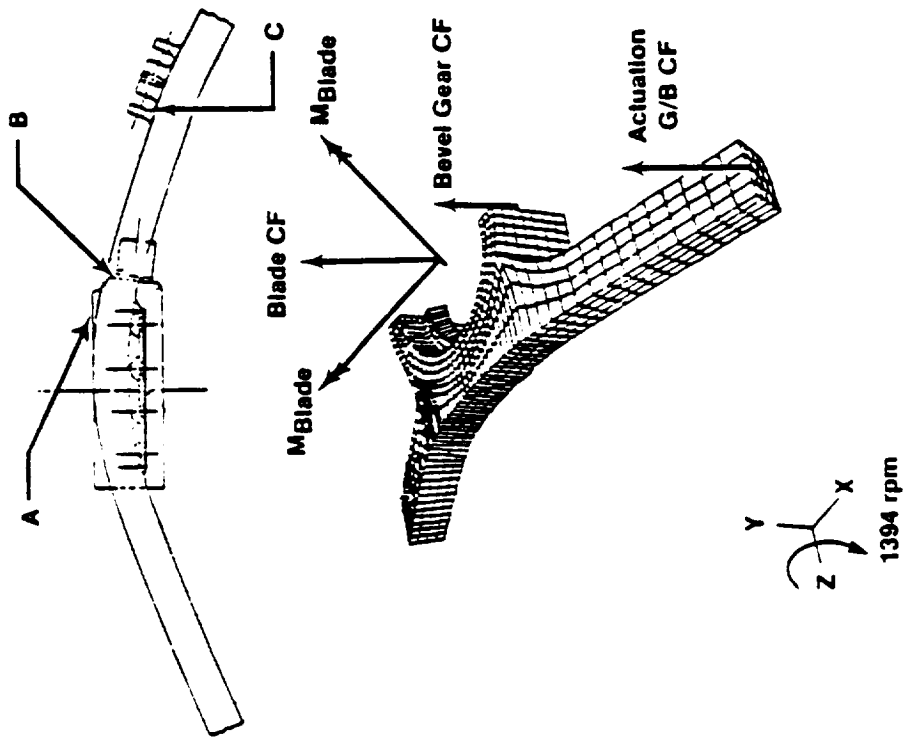
Location	K_T	σ (ksi)	Life (Cycles)
A	1.0	78	25,000
B	1.6	34	63,000
C	1.7	54	26,600

Figure 8-47. Fan Hub Ring Life Analysis.

Nominal Loads @ Cruise
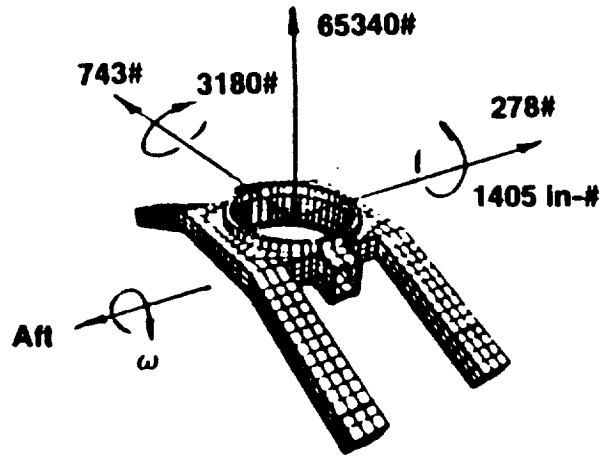
Max 1/P Loads
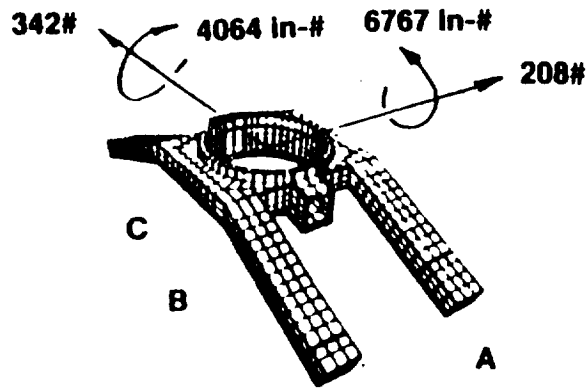
Location	Temp. (°F)	Material	Eff Stress (Ksi) Alt	Mean	Life
A	400	TI 6-4	1.0	31.4	>10^7
B	↓	↓	3.3	32.0	
C			0.5	31.2	

Figure 8-48. Hub Ring I/P Analysis.

132

- **Prime Reliable Structure 41% Overspeed Capability**
- **@ 1966 (2184) rpm**
  - $\sigma_\theta = 84$ ksi
- $\sigma_{ULT} = 101.5$ ksi (-3σ)
- **Meets 2X Requirements with Margin**
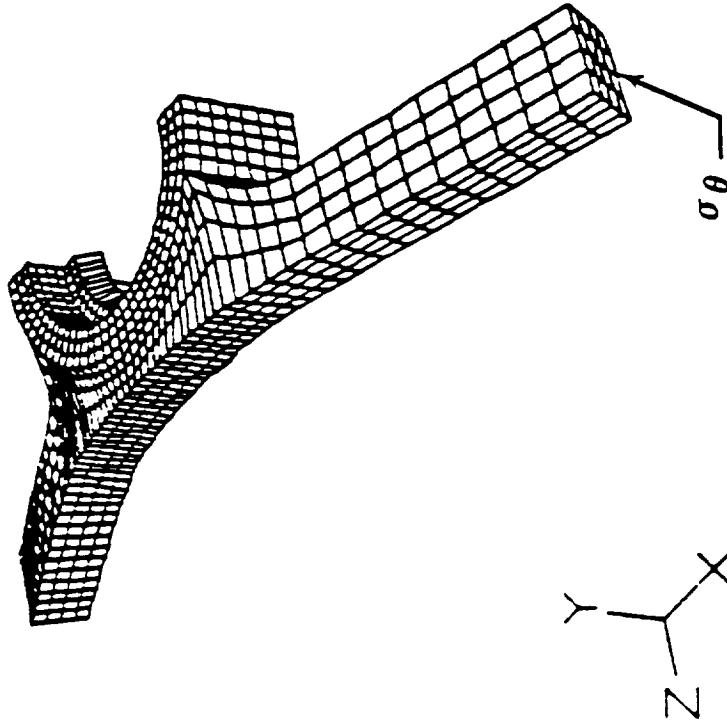
Figure 8-49.   Fan Hub Ring Burst Analysis Results.

133

analyses indicate that these parts meet or exceed the design life goal of 25,000 cycles. The prime reliable support rings also exceed the 2× burst requirements in all locations. The blade-out analysis (Figures 8-50 and 8-51) predicted that the ring can survive the loss of one blade per stage by sharing the unbalanced load with the power frames.

8.2.7 Cowlings, Telemetry, And Exhaust Nozzle

The inner aerodynamic flowpath of the UDF™ is maintained through the use of several rotating cowls, telemetry rings, and a rotating exhaust nozzle. Figure 8-52 details the nomenclature for each part.

As illustrated in Figure 8-53, the rotating cowlings for the UDF™ engine were configured with a shell/panel construction to provide the following key maintenance features for the fan rotors:

- The on-wing removal of the fan blades

- Access to the fan blade pitch-change mechanism for on-wing pitch trimming and maintenance

- Access to the fan blade support ring mounting bracket bolts, thus permitting modular assembly of the rotors.

The shells are fabricated from lightweight, high strength and temperature graphite/PMR15 composite. The inboard surfaces of the shells are configured as radial flanges. These flanges contain bolt clearance holes and rabbets for attaching the shells to the fan blade support rings. The radial ring on the forward end of each shell stiffens the leading edge against aerodynamic-induced vibrations.

Access panels, located circumferentially between the blade hubs, form the midsection of each rotor stage flowpath. These stiffness-limited panels were fabricated from sandwich construction with graphite/PMR15 face sheets and titanium honeycomb core material. The flanges of the panels were configured with tapers that provide gradual section change between the sandwich and flange mount surfaces minimizing stress risers and core crushing. Each flange bolt hole contains a titanium insert that acts as a load spreader and also prevents assembly damage. Both ends of each panel contain semicircular cut-outs that interface with the fan blade platforms. Radial collars, protruding
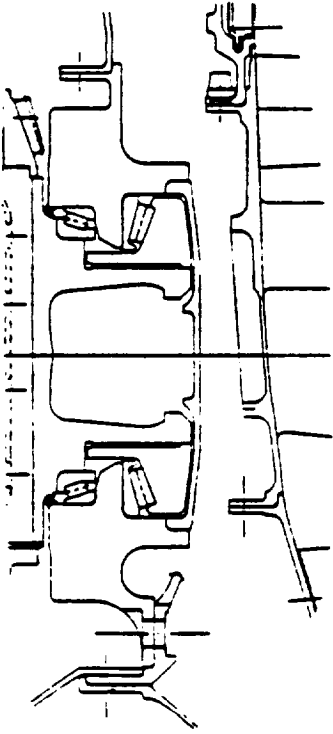
● **Normal Operation**

	Nominal Gap ~ in. Between Ring and Frame
● Cold	.130
● SLTO Hot Day	.060
● Chop From SLTO	.005
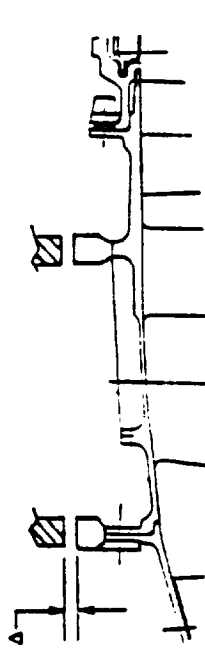
● **During Blade Out**

- Ring Deflects .060 in. Before Impacting Frame
- Frame Shares Unbalance Load With Ring
- Four Pad Locations Distribute Load Into Frame

Pad Locations
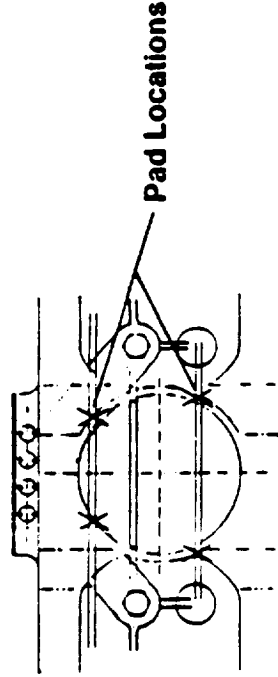
Figure 8-50. Blade-Out Design Features.

135

- **Mass/Spring Analogy**
  - **Determine V_{Impact}**
  - **Energy Balance**
    - **Determine Loads and Deflections**
  - **Finite Element Model**
    - **Determine Static Spring Rates**
  - **Initial Analysis**
    - **$\Delta Total = .310$ in.**
    - **$F_{Total} = 55,200$ lb.**

κ_R

x

κ_F

Deflection

$\xi = 0 - \xi$

$\Delta_{Dynamic}$

Δ_{Static}

Initial Deflection

Instant Prior to Impact
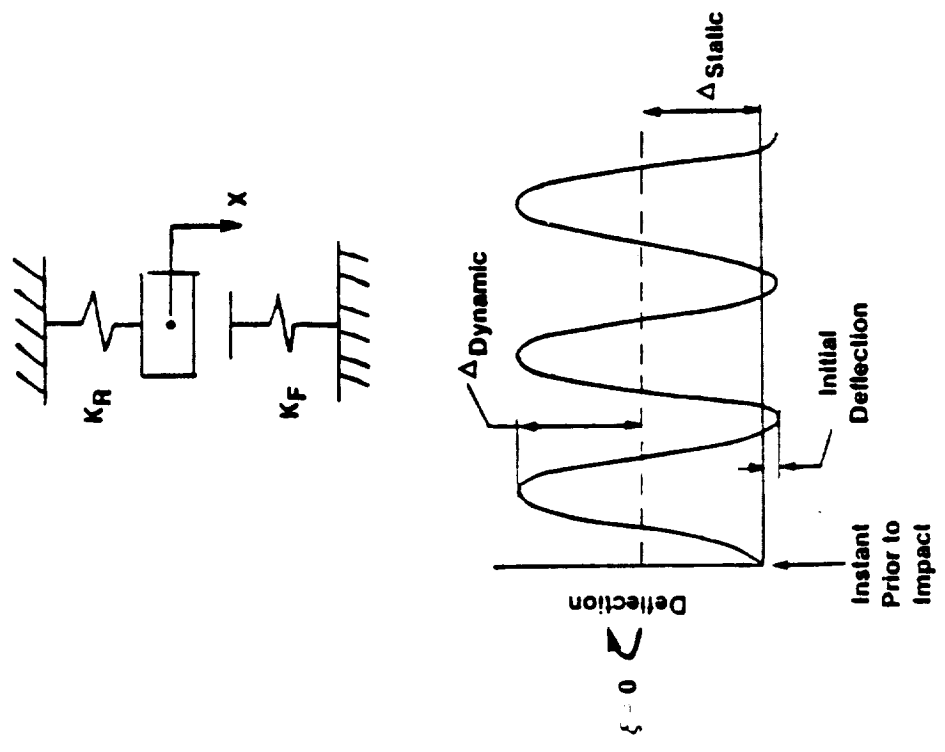
Figure 8-51.   Fan Hub Ring Blade-Out Analysis.
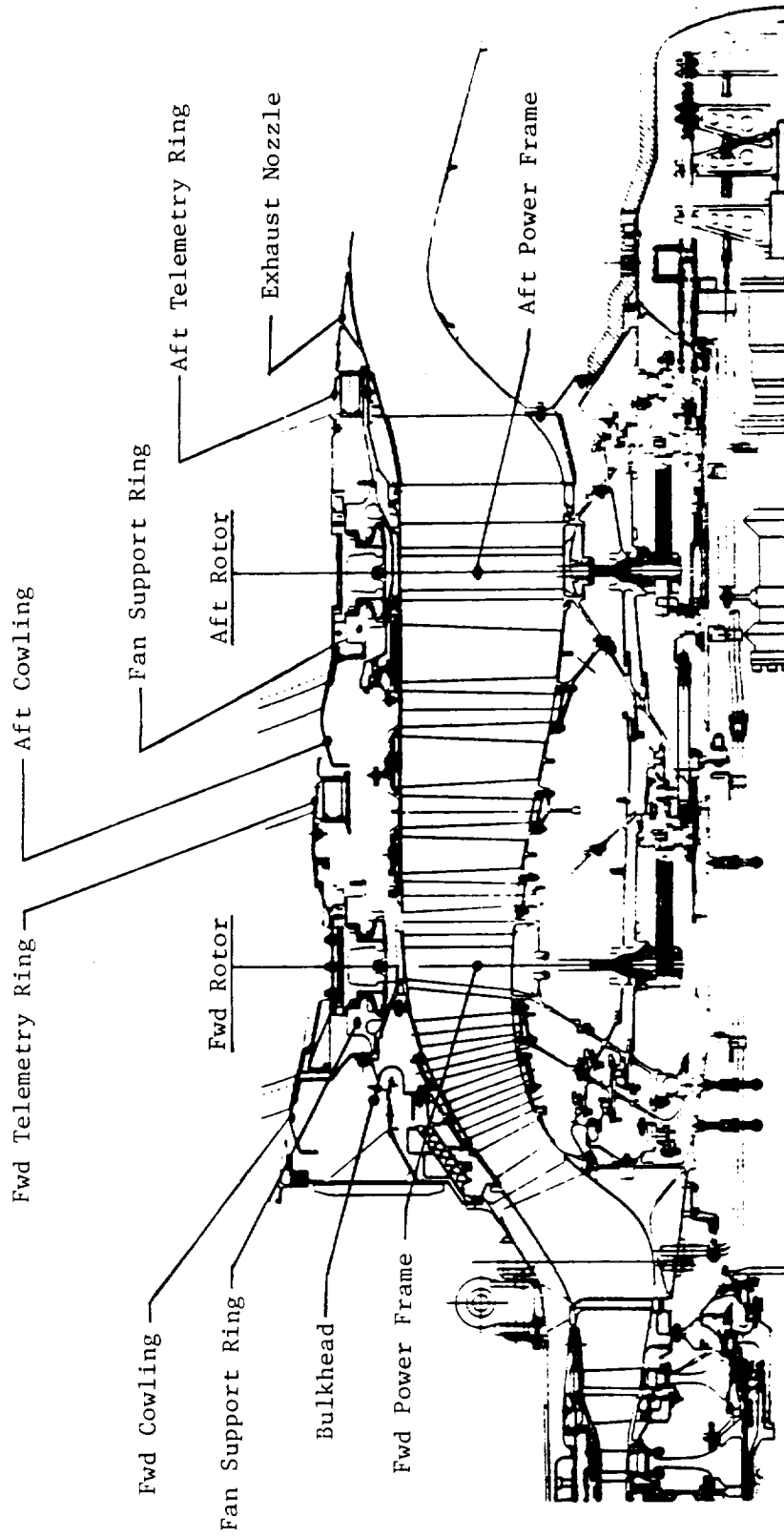
Figure 8-52. Rotating Structures.

Aft Telemetry Ring

Exhaust Nozzle

Aft Power Frame

Fan Support Ring

Aft Rotor

Aft Cowling

Fwd Telemetry Ring

Fwd Rotor

Fwd Cowling

Fan Support Ring

Bulkhead

Fwd Power Frame
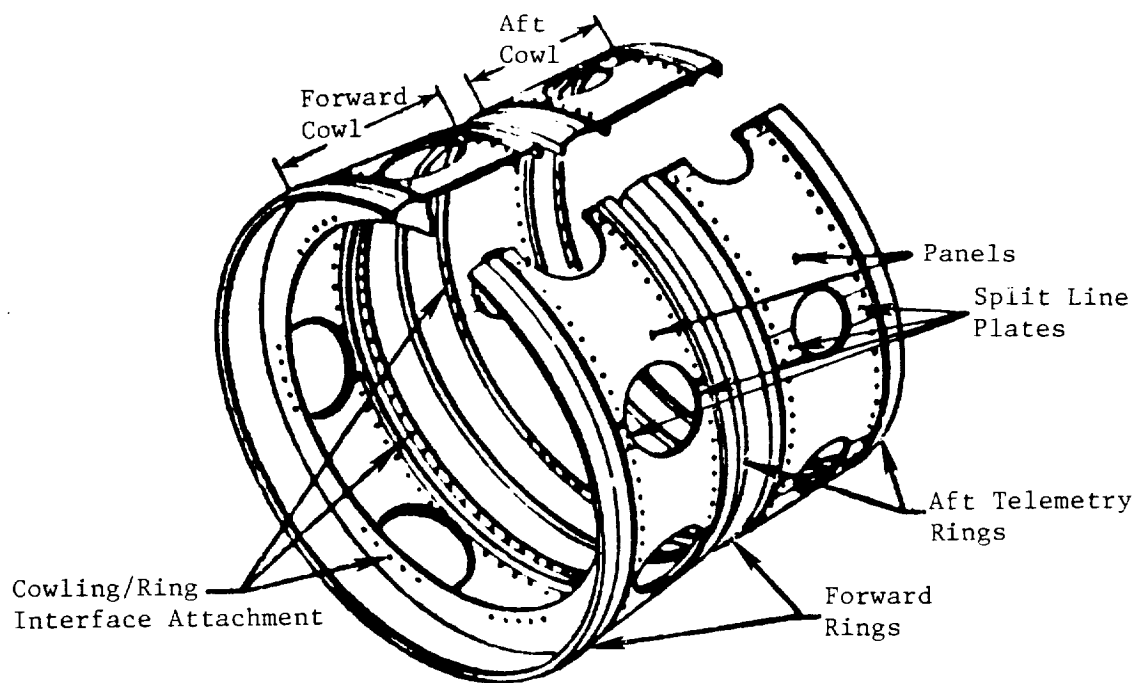
Figure 8-53. Rotating Cowling Design Features.

inboard from these cutouts, serve to stiffen the edge of the panel and also to provide lands for the platform seal.

Battery-powered telemetry modules, located on each UDF™ rotor, transmit engine data, dynamic strains, and temperatures to receiving antennae mounted on engine static components. These rotating modules which include the transmitter, battery, and "G" switch are supported in rotating structures that form the aft end of the fan cowling flowpath of each rotor. The support rings were machined from Ti-6-4 forgings; whereas, the heatshields and support tubes were fabricated from Ti-6-4 sheet stock. Due to its low density and corresponding high fatigue strength at temperatures encountered in the cowl cavity, titanium alloy was utilized for these parts. The air scoops and partitions were fabricated from composite materials.

Maintaining battery temperature limits for adequate operational life was critical to successful operation of the telemetry system. The forward ring incorporates an internal cooling system which supplies fan air to the internal ring cavity by ram air scoops mounted on the flowpath wall of the ring. After convectively cooling the modules, this air flows overboard between two radiation heatshields riveted to the aft rail of the ring. Equally spaced radial partitions were installed in the ring cavity in order to provide off-design flow stability. Ventilation air from under the cowl cavity was used to cool the aft ring modules. Heat is removed from the modules as the air flows forward through holes in both rails of the support rings.

The exhaust nozzle system for the UDF™ proof-of-concept engine contains two structural casings: a rotating outer casing, and a static tailcone. The rotating outer casing combines the functions of the aft cowling and outer core flowpath casing of the conventional turbofan primary (core) exhaust system. The stationary tailcone is identical to conventional system tailcones. The rotating structure was configured with a triangular-shaped, aft section which provides the stiffness required to minimize flexural vibrations. This shape also reduces the thermal-induced stresses caused by the hot core gas and cold fan air. This structure was bolted directly to the aft flange of the rotating power frame of the aft power turbine rotor. The frame reacts the mechanical and aerodynamic loads on the nozzle and provides the load path to the power turbine support structure.

139

The secondary functions of this nozzle include providing support for the rotating telemetry antennae and OGV honeycomb seal on the forward inner shell. Accordingly, 30 aerodynamic shaped air scoops that provide cavity cooling air were bolted to the forward outer shell.

The nozzle is fabricated from Inco 625/718 sheet metal and forgings which are electron beam welded together. This weldment is then solutioned and aged prior to final machining. Inco 718 was used in the aft section of the nozzle structure rather than the standard nozzle material (Inco 625), because of its superior fatigue strength.

Detail stress and life analysis for the rotating nozzle structure is summarized in Figure 8-54.
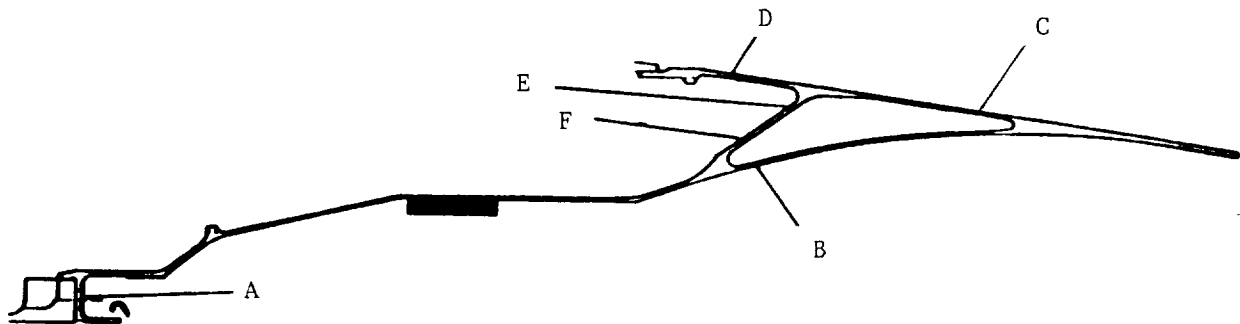
Location	Temp ° F	Concentrated Effective Stress (ksi)				LCF Cycles
		K_t	Mechanical	Thermal	Combined	
A	875	3.0	33	97	122	30000
B	790	2.2	12	111	102	$>10^5$
C	390	1.6	26	115	140	25000
D	190	2.9	40	116	155	20000
E	310	1.0	12	81	89	$>10^5$
F	575	1.1	12	86	78	$>10^5$

Figure 8-54. Rotating Exhaust Nozzle - Stress and Life Analysis.

8.3 FAN BLADE DESIGN

The design objectives for the UDF™ blades are divided into requirements and goals. The requirements are objectives which must be satisfied during the design process; the goals are additional objectives that are desired, but need not be satisfied.

8.3.1 Design Requirements

The design requirements are divided into categories which are explained as follows:

Configuration

•	Number of Stages	2
•	Number of Blades/Stage	8
•	Tip Diameter	3.56m (11.67 ft)
•	Tip Speed at Cruise	238 mps (780 fps)
•	Tip Speed at Takeoff	259 mps (850 fps)
•	Activity Factor per Blade	150
•	Direction of Rotation, Aft Looking Forward (ALF)	

    - Stage 1 - Counterclockwise
    - Stage 2 - Clockwise

Life Requirements - The fan blade assembly shall be designed to provide an infinite high cycle fatigue (HCF) life under the maximum steady-state loads plus one per revolution and any additional vibratory stresses. In addition, the blade assembly LCF life shall be designed to exceed 40,000 flight cycles.

Stability - Under normal operating conditions, the fan blade assembly shall be free of flutter throughout the flight spectrum for a representative aircraft installation.

Frequency Margins - A minimum of 15% frequency margins should be provided for the first flex (1F) mode at the maximum takeoff speed of 1395 rpm. Additionally, 1F and first axial (1A) frequencies shall not be at the same per rev range. Also, the fan blade two-stripe mode frequency shall be clear from the 16/rev line; that is, avoid any 16/rev crossing within the engine operating speed range.

Rotor Overspeeds - The blade shall be capable of withstanding 140% of the maximum operating speed, with some allowable inelastic deformation, but no material separation.

Foreign Object Damage (FOD) - The blade leading edge shall be covered with a metal sheath for protection against erosion. The airfoil surface shall also be protected from erosion by applying a layer of polyurethane film.

The blade does not have to meet the bird ingestion requirement. However, the ability of the blade to withstand the impact will be demonstrated by a static impact test.

Maintainability - On-wing fan blade maintainability shall be provided in the design.

8.3.2 Preliminary Design Development

8.3.2.1 Mechanical Design

The Unducted Fan blades are designed for high disk loadings and for high hub-to-tip blade radius ratios. Two blade configurations have been developed for the program: one for 0.72 Mach, and the other for 0.8 Mach; however, only the 0.72 Mach configuration has been designed and fabricated for the UDF™ engine demonstration program. The 0.8 Mach design has been studied analytically, but no detailed design has been issued.

Prior to contract initiation, it was determined that the UDF™ blades will be of composite construction, consisting of a composite shell, with a titanium spar. The feasibility study predicted that type of design would provide good aerodynamic performance, adequate frequency margin, satisfactory stress margins in all structural components and be aeroelastically stable. Preliminary assessment of the fan blade aeroelastic characteristics was first to establish the correlation between the NASA SR-series test results and the GE in-house General Aeroelasticity Program (GAP). Fan blade stability was then examined at takeoff and cruise conditions.

To achieve fan blade on-wing maintainability requirements, the dovetail design has been incorporated into fan blade configuration. Proper selection of blade airfoil stacking and dovetail position has resulted in a balanced

dovetail loading distribution within the normal engine operating condition. A system optimization was obtained by properly positioning the blade with respect to the pitch-change axis, such that the resultant overturning moment and torque on the blade retention and actuation systems are within acceptable limits.

8.3.2.2 Acoustics

Objectives of the aeroacoustic preliminary design studies were to insure that the Unducted Fan blade design would have a high probability of meeting, or would demonstrate an ability to meet, Federal community noise regulations (FAR36 Stage 3), and that the cabin interior noise levels would be acceptable to passengers. The approach taken for acoustic design studies of the UDF™ was to conduct parametric calculations of the effects of various blade design variables and parameters on both far-field and near-field noise, utilizing a nominal, or baseline, design (designated F1A1) as the starting point. From these parametric calculations, design guidelines for acceptable acoustic characteristics were evolved for factoring into the UDF™ blade design selection. In addition, as design modifications were proposed, in response to mechanical/ aeroelastic/aerodynamic requirements, these specific modifications were evaluated for acoustic impact prior to finalizing blade design changes.

Calculations of the noise characteristics of the SR-3 propfan design were made and compared with published noise test data to verify General Electric's acoustic design evaluation procedures. In addition, the SR-3 propfan design was analytically scaled to the proof-of-concept engine size and operating conditions, to compare projected noise characteristics with the proposed UDF™ fan blade designs. The following paragraphs detail these acoustic design studies.

Parametric Acoustic Studies

Parametric calculations of the effect of sweep, thickness distribution, and loading distribution were conducted using the General Electric frequency-domain, distributed-source, acoustic computer code which evaluates the steady loading and thickness (or volume displacement) noise produced by a propeller rotor. Unsteady loading noise caused by aerodynamic interference between rotors of a counterrotating propeller was not accounted for in these studies,

143

as the theoretical modeling and computer code development for these effects were not completed in time. However, a preliminary assessment of the rotor-to-rotor axial spacing effects on aerodynamic interference between rotors was performed to determine potential spacing effects on noise.

Figure 8-55 shows the effect of rotor blade tip sweep on blade-passing frequency (BPF) tone sound pressure level (SPL) for takeoff power and trends for the 2×BPF tone. As illustrated, the effect of sweep is small over the range of tip sweeps from 0° to 45°. Figure 8-56 demonstrates corresponding results for the cruise condition; at which condition, the effect of sweep is much greater, especially in the forward arc ahead of the plane of rotation. This is due to the more pronounced distributed-source effects (source noncompactness) which occur at supersonic helical tip Mach numbers.

A parametric study of alternative blade maximum thickness distributions relative to the F1A1 baseline distribution was performed. The thickness distributions studied corresponded to 1.25 and 0.75 times the nominal thickness distribution; for example, 25% thicker and 25% thinner. Calculations showed the above thickness changes to have a negligible effect on tone harmonic noise at takeoff. The effect on cruise noise was more significant (Figure 8-57) and suggests that the blade tip region should be as thin as possible. The breakdown between steady loading and thickness noise contributions to the BPF tone level are presented in Figures 8-58 and 8-59 for takeoff conditions and for cruise conditions, respectively. The greater contribution of thickness noise at cruise to the total explains the greater sensitivity of noise to thickness changes at cruise.

Preliminary estimates of the effects of axial spacing were made using fan noise interaction mechanism concepts developed for turbofans. A sketch of the relevant parameters and the mechanisms considered are depicted in Figure 8-60. Initial radial (spanwise) distributions of the spacing/chord ratio for the UDF™ design at takeoff and cruise pitch settings is shown in Figure 8-61. The minimum spacing/chord ratio was found to occur at about 20% span from the hub and to decrease as the pitch angle is increased. Thus, the cruise case has smaller spacing than the takeoff case.
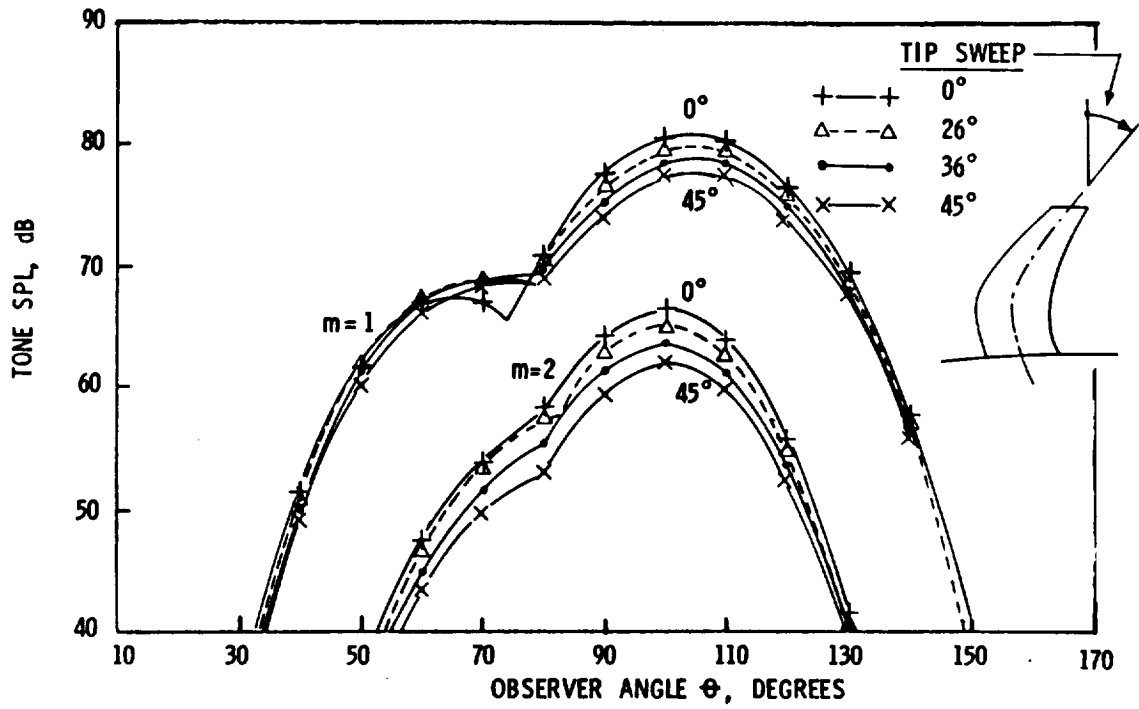
Figure 8-55. Effect of Sweep - Takeoff.
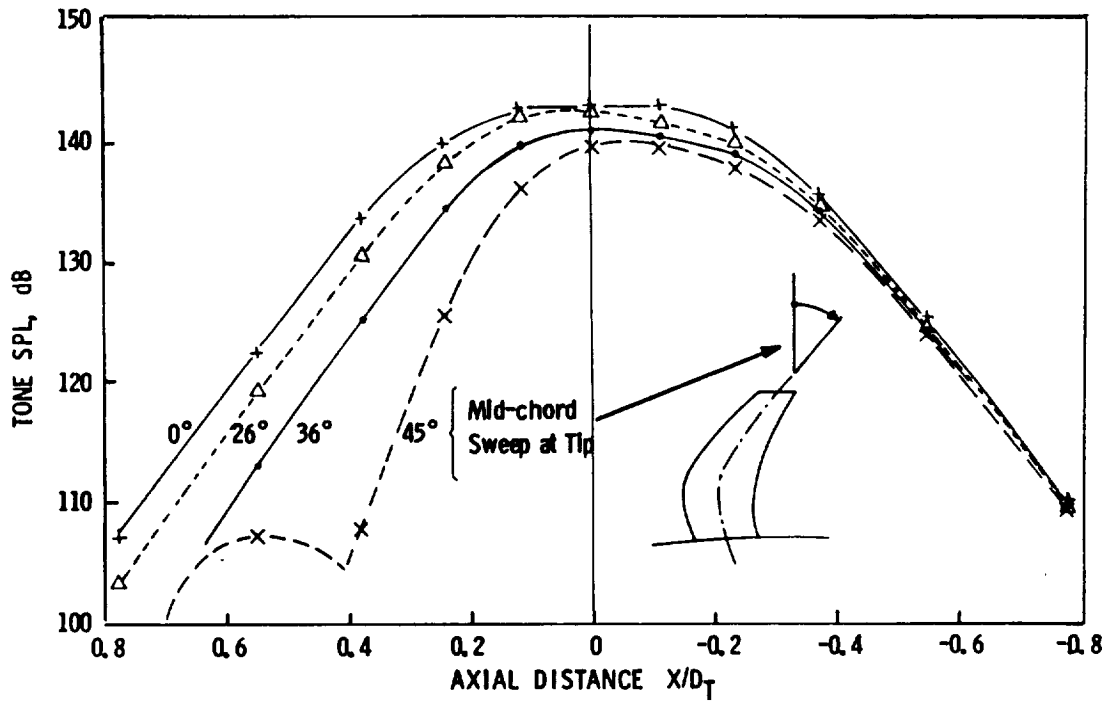
Figure 8-56. Effect of Sweep - Cruise.

145
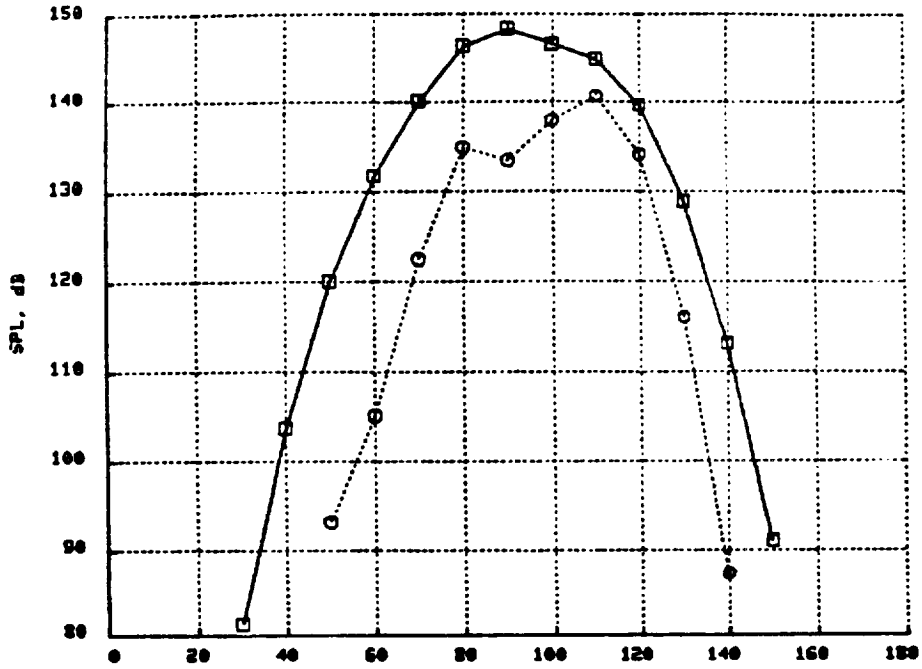
(a) Thickness = 0.75 x Nominal
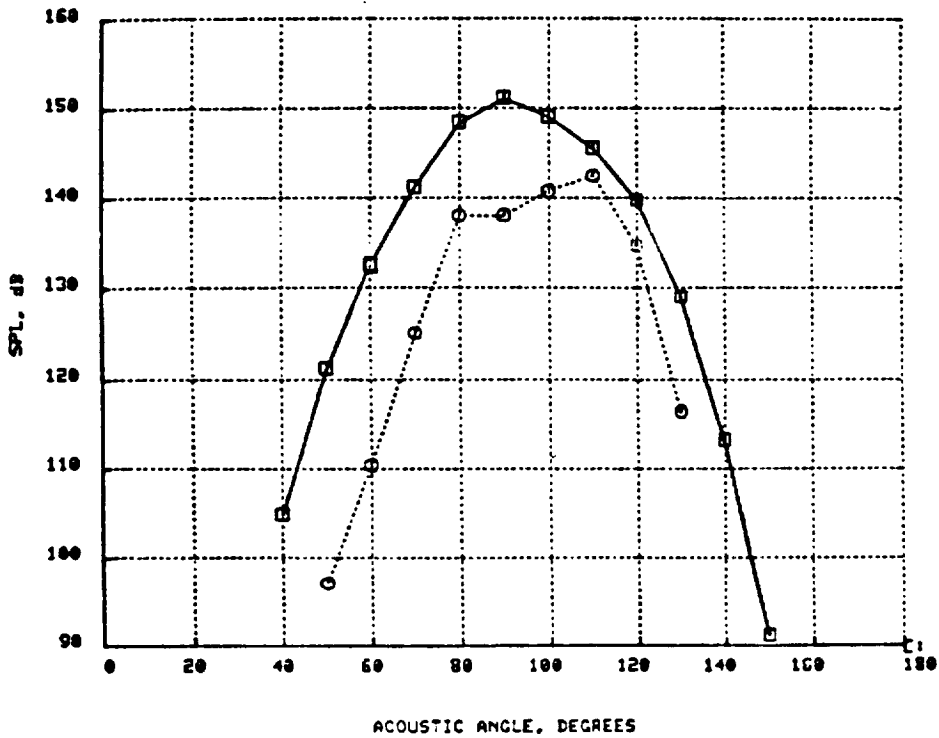
(b) Thickness = 1.25 x Nominal

Figure 8-57.   Effect of Thickness at Cruise.

146
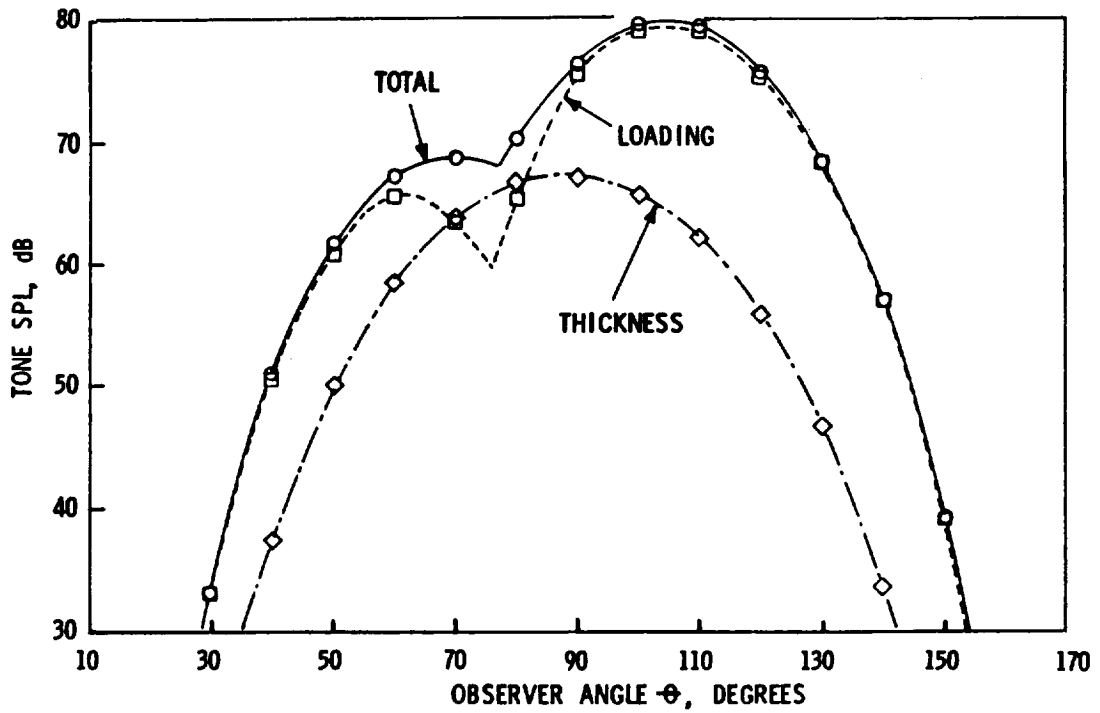
Figure 8-58. Noise Component Breakdown - Far-Field Takeoff.
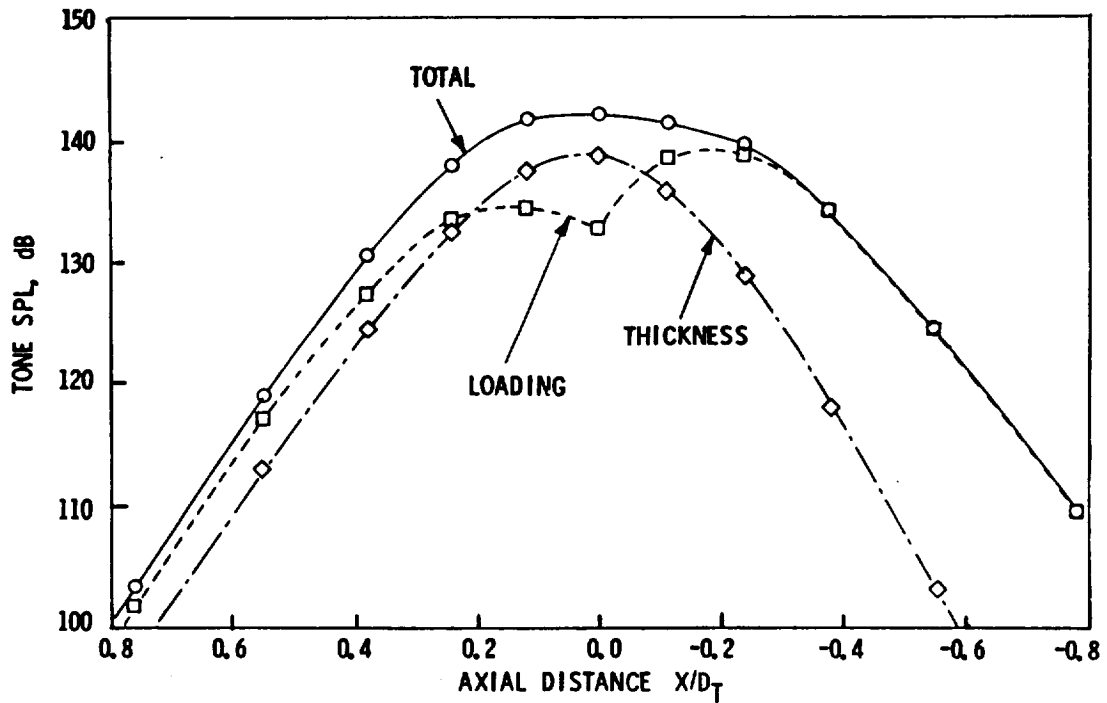
Figure 8-59. Noise Component Breakdown - Near-Field Cruise.

147
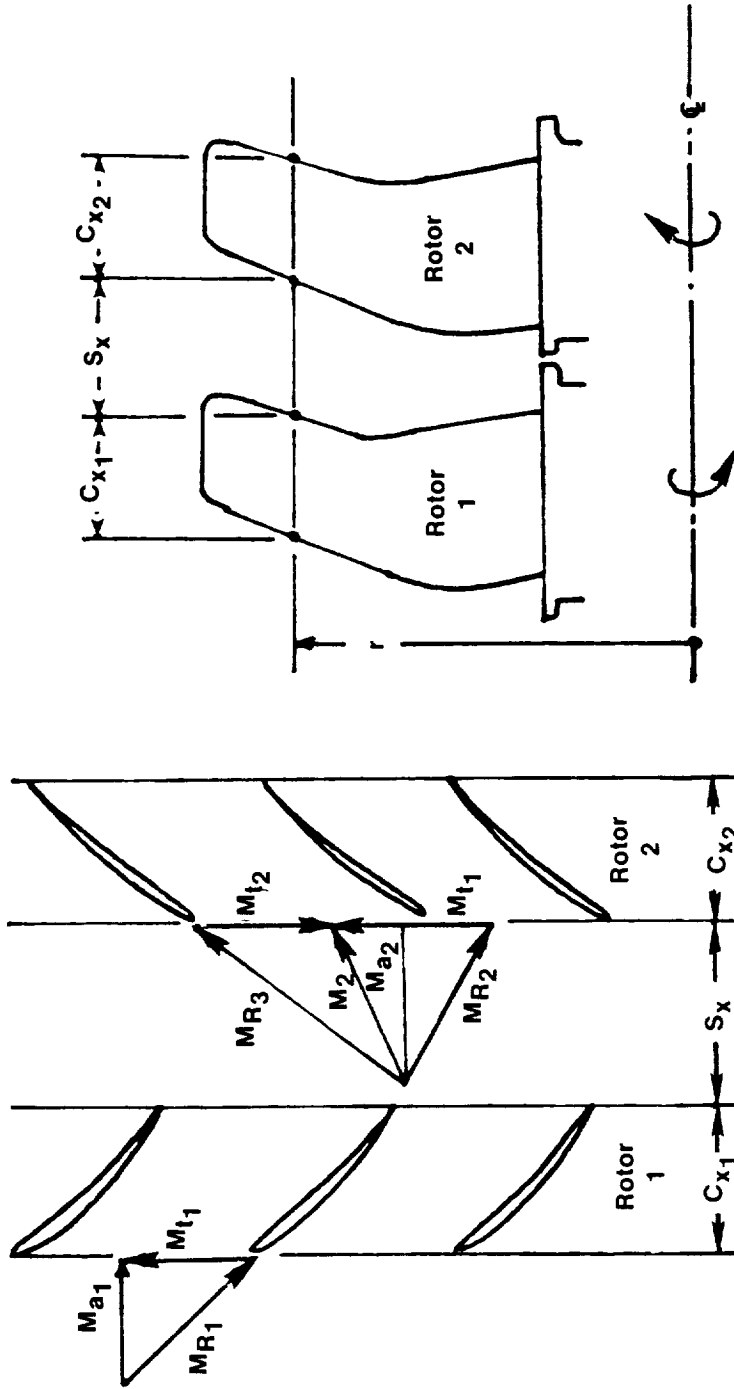
1. Wake From Rotor (1) Interacts With Rotor (2)

2. Pressure Field From Rotor (1) Interacts With Rotor (2)

3. Pressure Field From Rotor (2) Interacts With Rotor (1)

Figure 8-60. Unsteady Loading Rotor-Rotor Interaction Mechanisms.

148
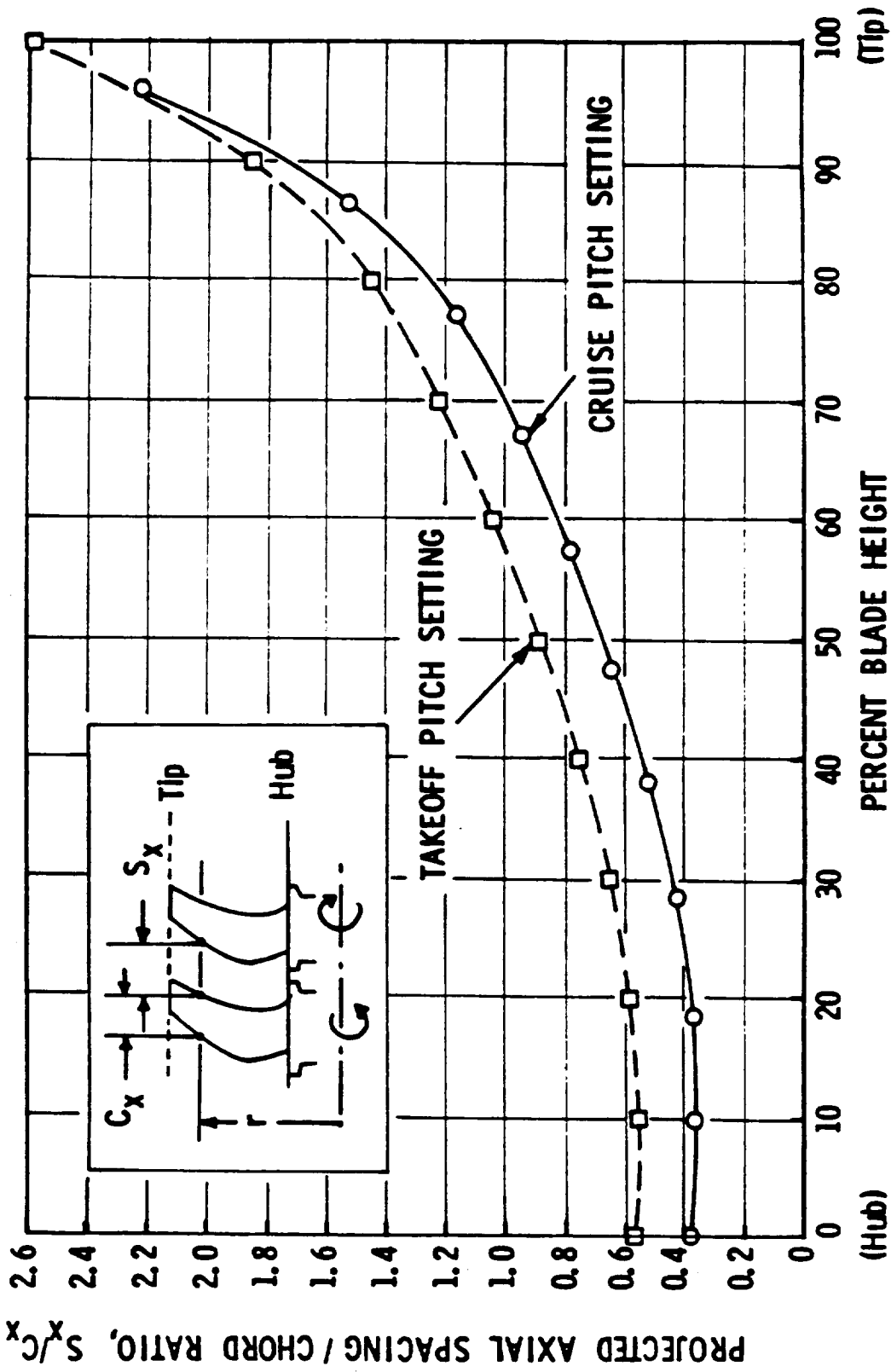
Figure 8-61. Rotor Axial Spacing Variations.

Using fan source noise analytical methods (and a reference level of 20% span at cruise), estimates of peak interaction noise levels were generated as a function of the axial spacing/chord ratio. These estimates are depicted in Figure 8-62. Because potential pressure field interactions (Mechanism 3 of Figure 8-60) were found to dominate the interactions for S_x/C_x 0.3 to 0.4, it was recommended that the minimum cruise S_x/C_x be 0.5 or greater. This would avoid pressure field interactions and make the remaining viscous wake interactions the dominant unsteady interaction noise source, but they would not be a strong function of axial spacing. This recommendation was subsequently incorporated into the design.

Tip Shape Modification Impact

During the design of the full-scale engine blades, it was determined that a mechanical design compromise for blade strength was required in the tip region. Figure 8-63 illustrates the necessary design modifications, involving reduction in tip chord. It was assumed that neither the blade maximum thickness nor the blade section lift coefficients change with tip chord reduction; hence, some reduction in tip loading was implied. Acoustic predictions of the design changes (Figure 8-63) on steady loading and thickness noises at takeoff showed an approximate 0.5 dB reduction in BPF tone level and its harmonics. This slight reduction was attributed to the reduction in tip loading.

At cruise, however, large increases were predicted for those tones which had previously exhibited strong phase cancellation. This effect is shown in Figure 8-64. The resultant change in noise spectrum was not sufficient to appreciably impact A-weighted sound level.

Comparison With SR-3 Blade Design

It was estimated from the studies on axial spacing (Figure 8-62) that the unsteady loading noise was not a significant contributor at cruise; therefore, reasonable cruise noise estimates could be attained using GE's steady loading plus thickness noise analytical model. As a result of the higher disk loading and activity factor per blade, it was speculated that the steady loading plus thickness noise for GE's UDF™ could be greater (at cruise) than for Hamilton-Standard's competitive single-rotation propfan. Comparative calculations were
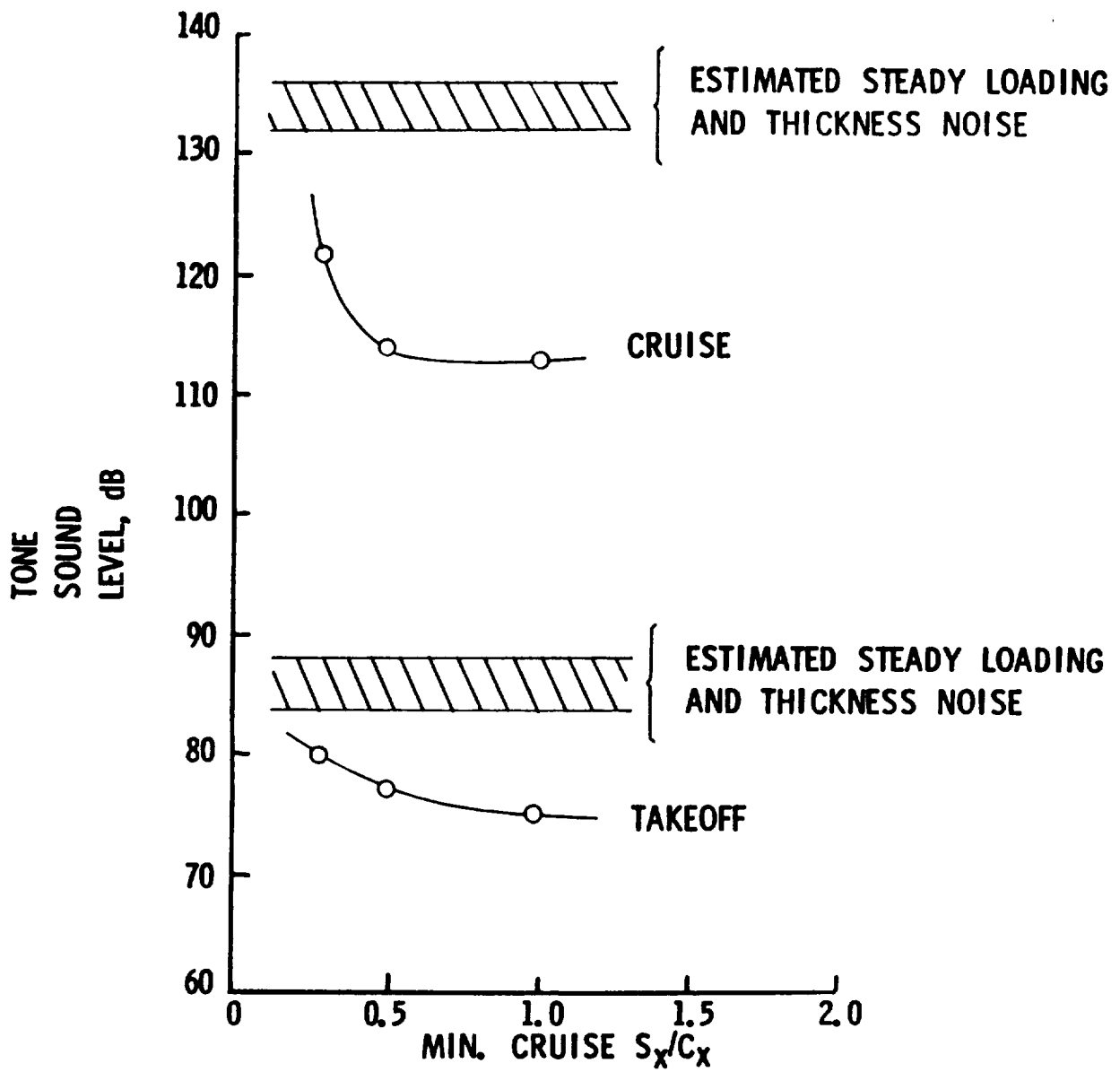
Figure 8-62.   Effect of Rotor-Rotor Spacing on Fundamental Tone Level.

50% Reduction
in Chord at Tip

8%
Span

15%
Span

Thickness T$_{Max}$
Remains the Same

Faired Curve
F1E13 Contour

Original F1E9
Contour
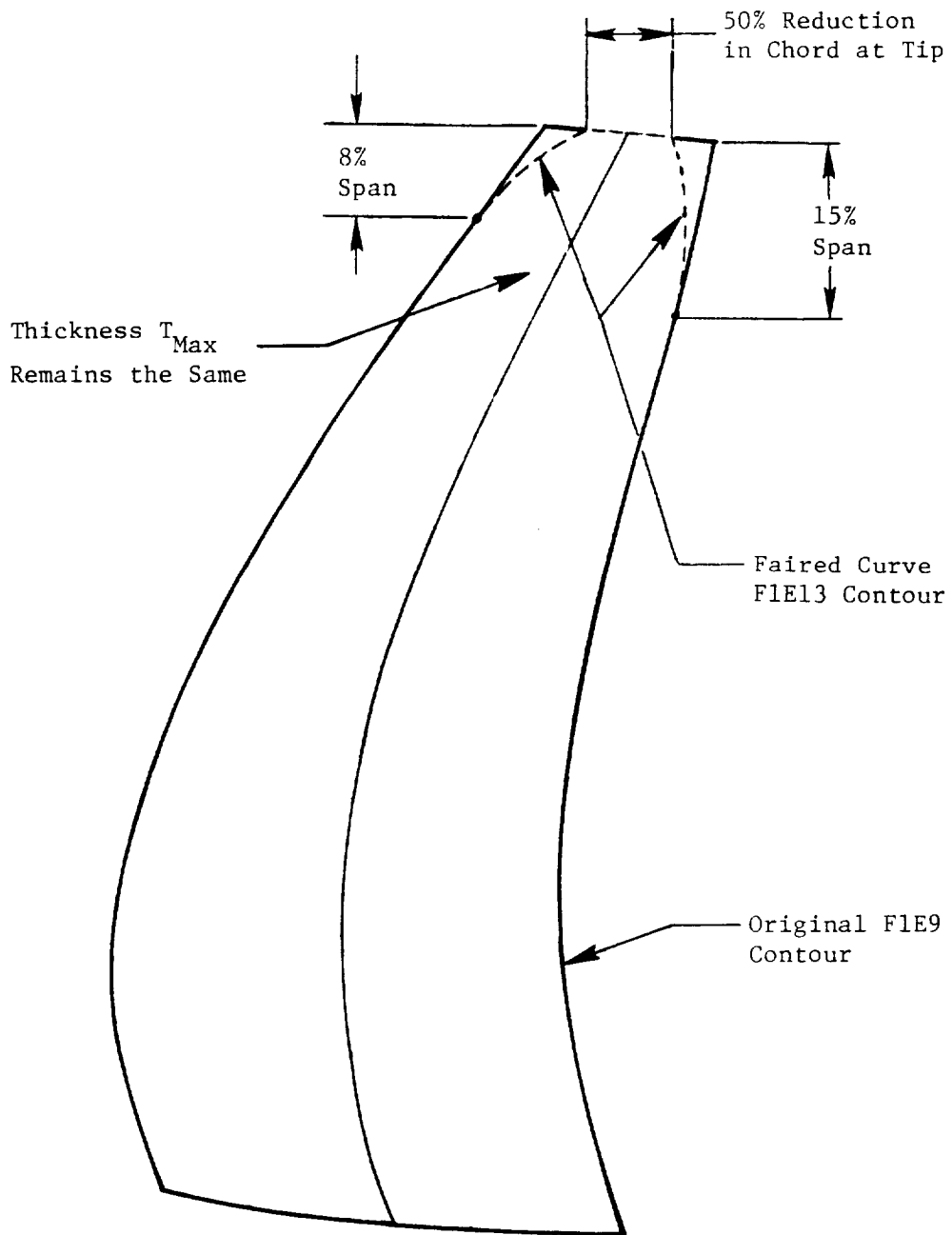
Figure 8-63. UDF™ Blade Design Changes from F1E9 to F1E13.
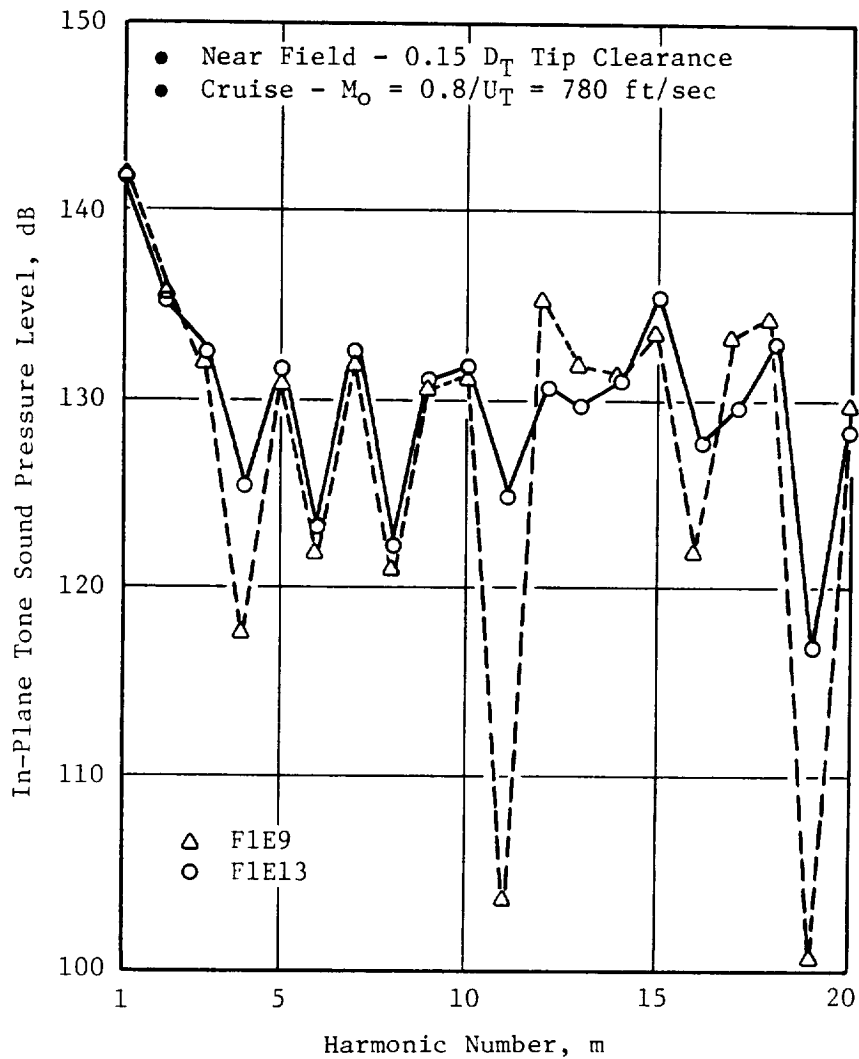
Figure 8-64. Effect of Blade Tip Cutback F1E9 to F1E13
Modification on Cruise Noise Spectrum in
Plane of Rotation.

therefore compiled for the cruise noise characteristics for the GE UDF™ design (F1E13) versus the Hamilton-Standard propfan design (SR-3).

Predictions of the blade design cruise noise for both the UDF™ F1E13 and the propfan SR-3 were made and compared at the same flight Mach number, tip speed Mach number, and horsepower and thrust. The overall level directivity characteristics (OASPL, DBA, dBD) are compared in Figure 8-65. The individual tone level directivities for the first four harmonics are compared in Figure 8-66.

As evidenced (Figures 8-65 and 8-66), the noise peak levels are about the same for the F1E13 and SR-3 blade shapes. The F1E13 peak tends to occur somewhat further forward (80°) than does the SR-3 peak (110°). It was concluded that the blade shape design of the F1E13 does not have any inherent noise disadvantage, relative to the SR-3 propfan blade design.

8.3.3 Final Blade Configuration

The final design is a well-balanced system design which includes the consideration of performance, aeromechanics, stability characteristics, bladed retention, and actuation. The final configurations are designed as F7 and A7 blades, where F7 and A7 refer to the forward and aft rotor blade respectively. The aerodynamics characteristics of the final design are portrayed in Figure 8-67, and the blade stacking data is shown in Figure 8-68. The untwisted planforms of the blades are illustrated in Figure 8-69. The tangential views of the F7A7 blades at takeoff, cruise, and thrust reverse conditions are shown in Figure 8-70.

The mechanical design of the fan blades is detailed in Figure 8-71. A titanium spar (hollow for weight reduction) extends to the blade midspan and serves as the backbone member of the fan blades. The dovetail design provides the blade on-wing maintainability feature. Fabrication of the hollow spar is accomplished by electric discharge machining (EDM) the pocket in the spar and by electronic beam welding (EBW) a cover plate on the spar (Figure 8-72). Two composite half shells of 80% carbon fiber and 20% S-Glass (Prepreg PR288) are bonded on the spar. The shell thickness is 0.25 inch maximum. Two cavities near the airfoil base are filled with foam. An electroformed nickel sheath is

154
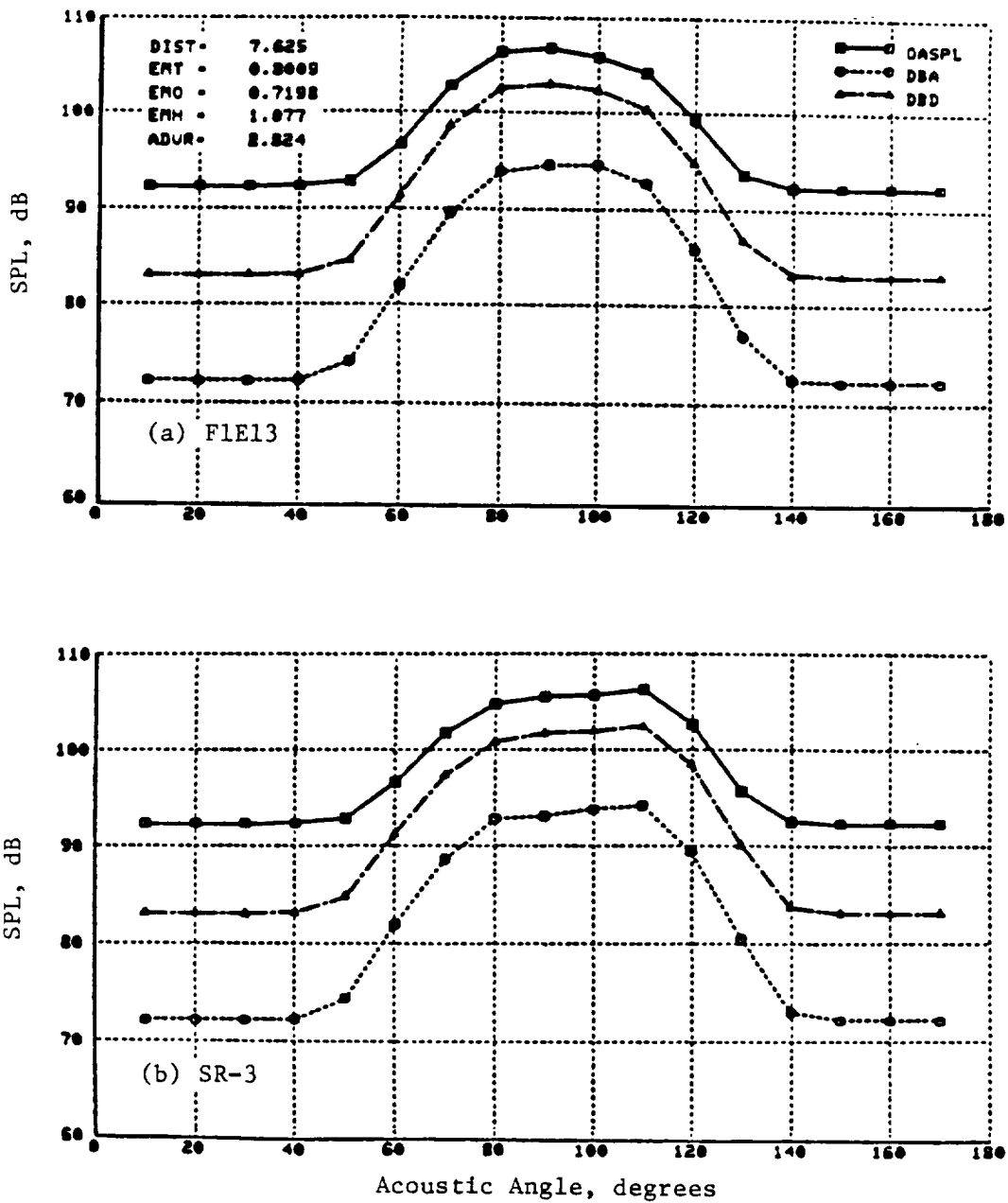
Figure 8-65. F1E13 Versus SR-3 Overall Directivities.
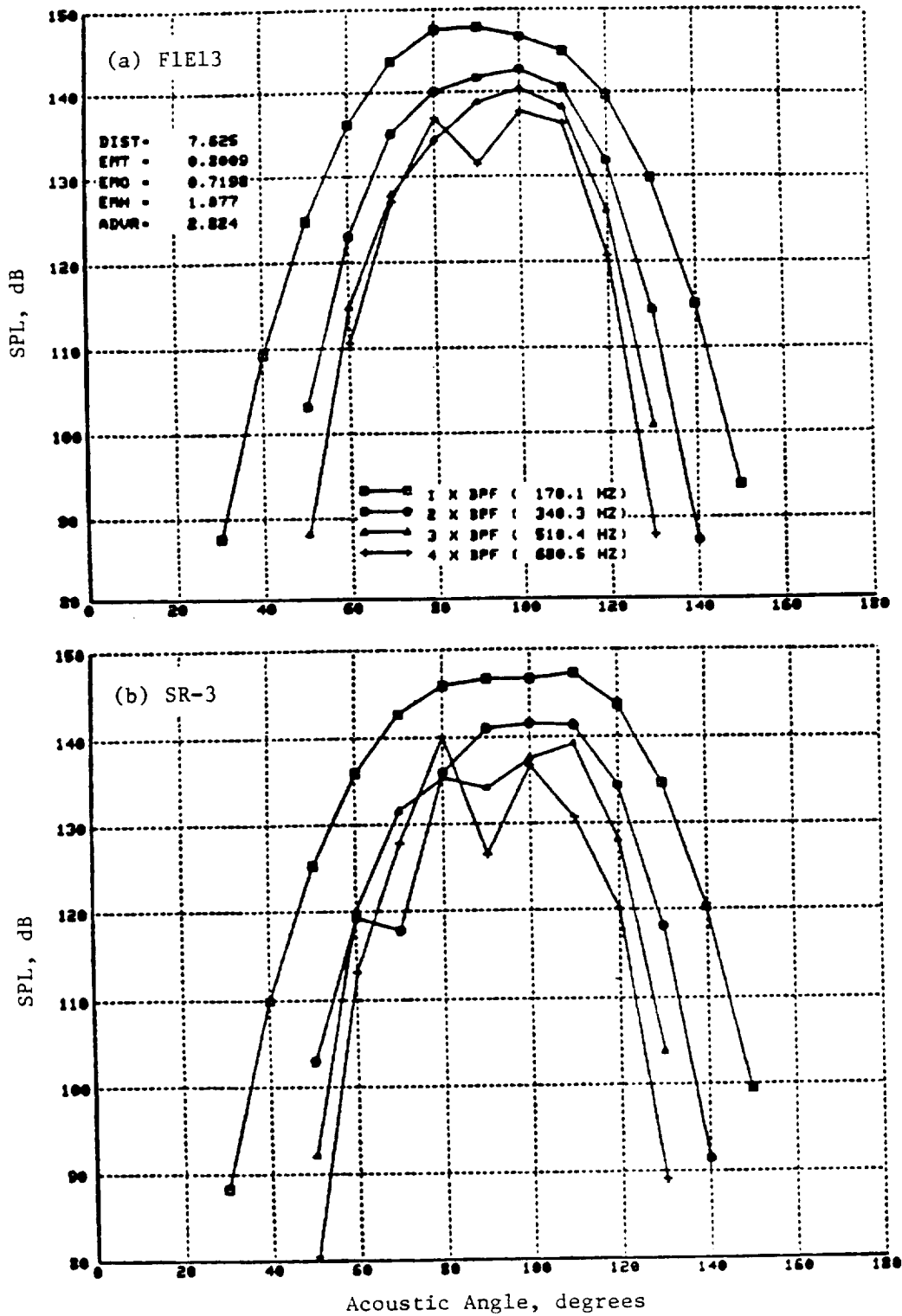
Figure 8-66. F1E13 Versus SR-3 Tone Directivities.

ORIGINAL PAGE IS
OF POOR QUALITY
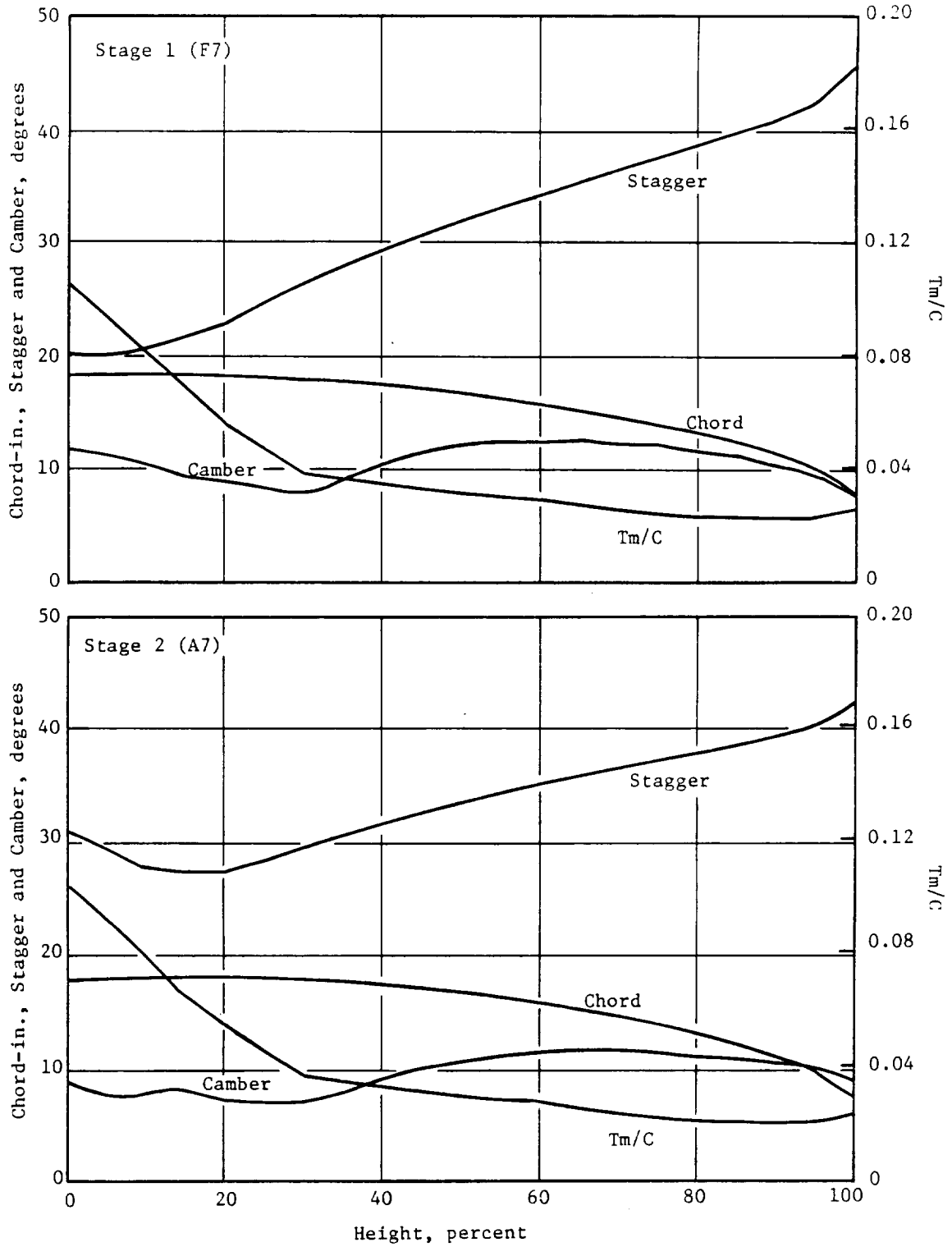
Figure 8-67. Fan Blade Characteristics at Design Cruise.
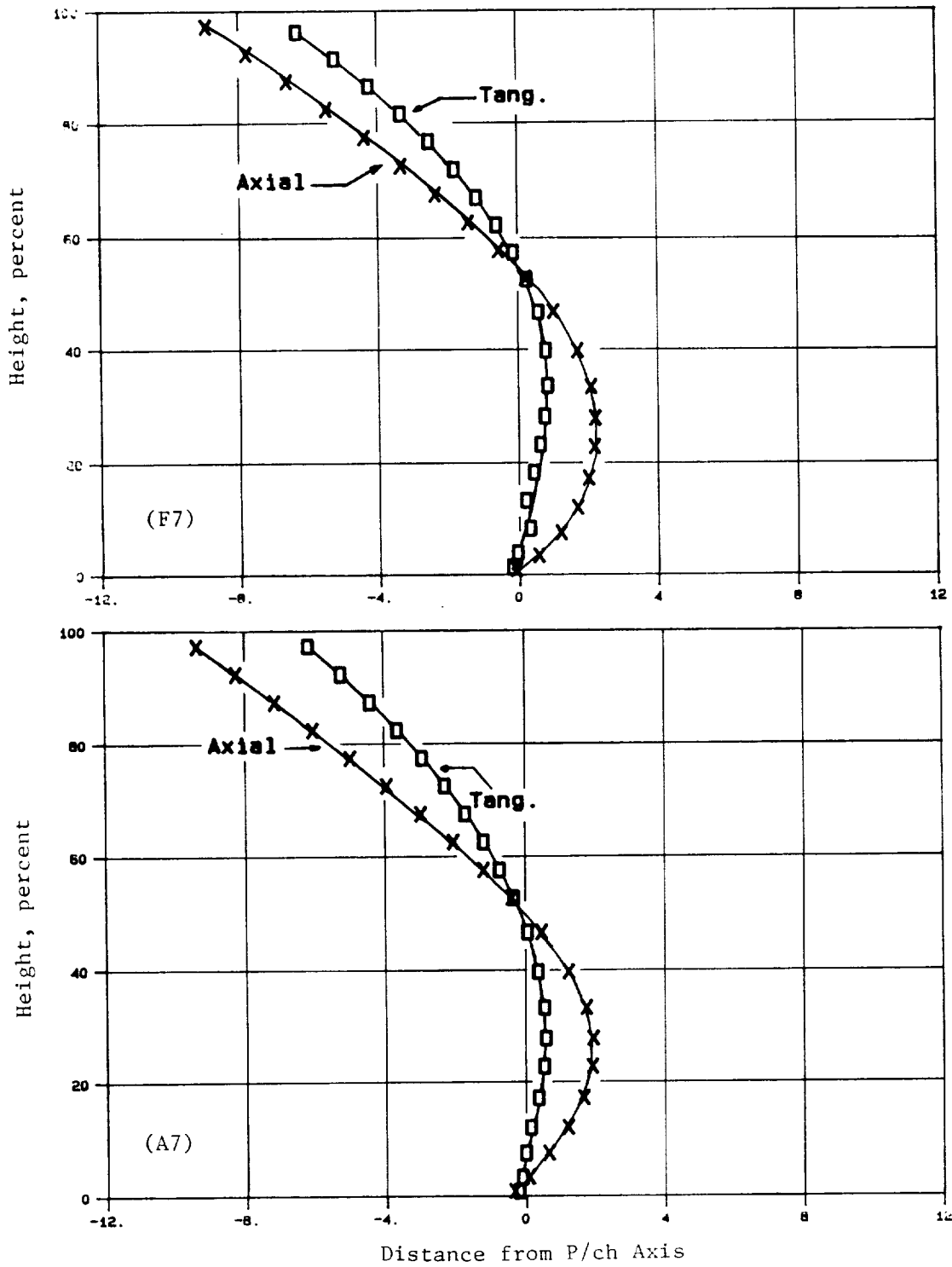
Figure 8-68. Blade Centroid Locations at Design Cruise.

F7

A7
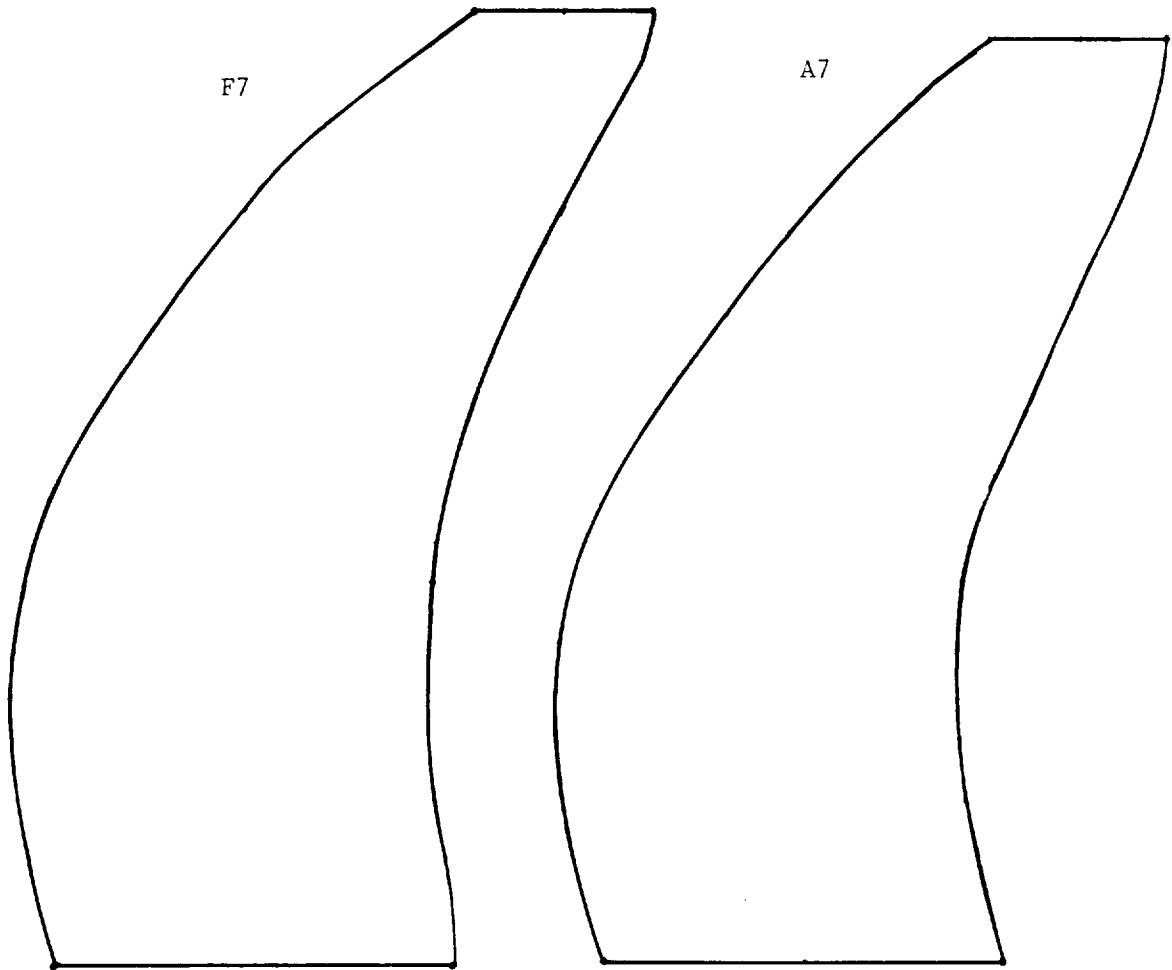
Figure 8-69. Planforms.
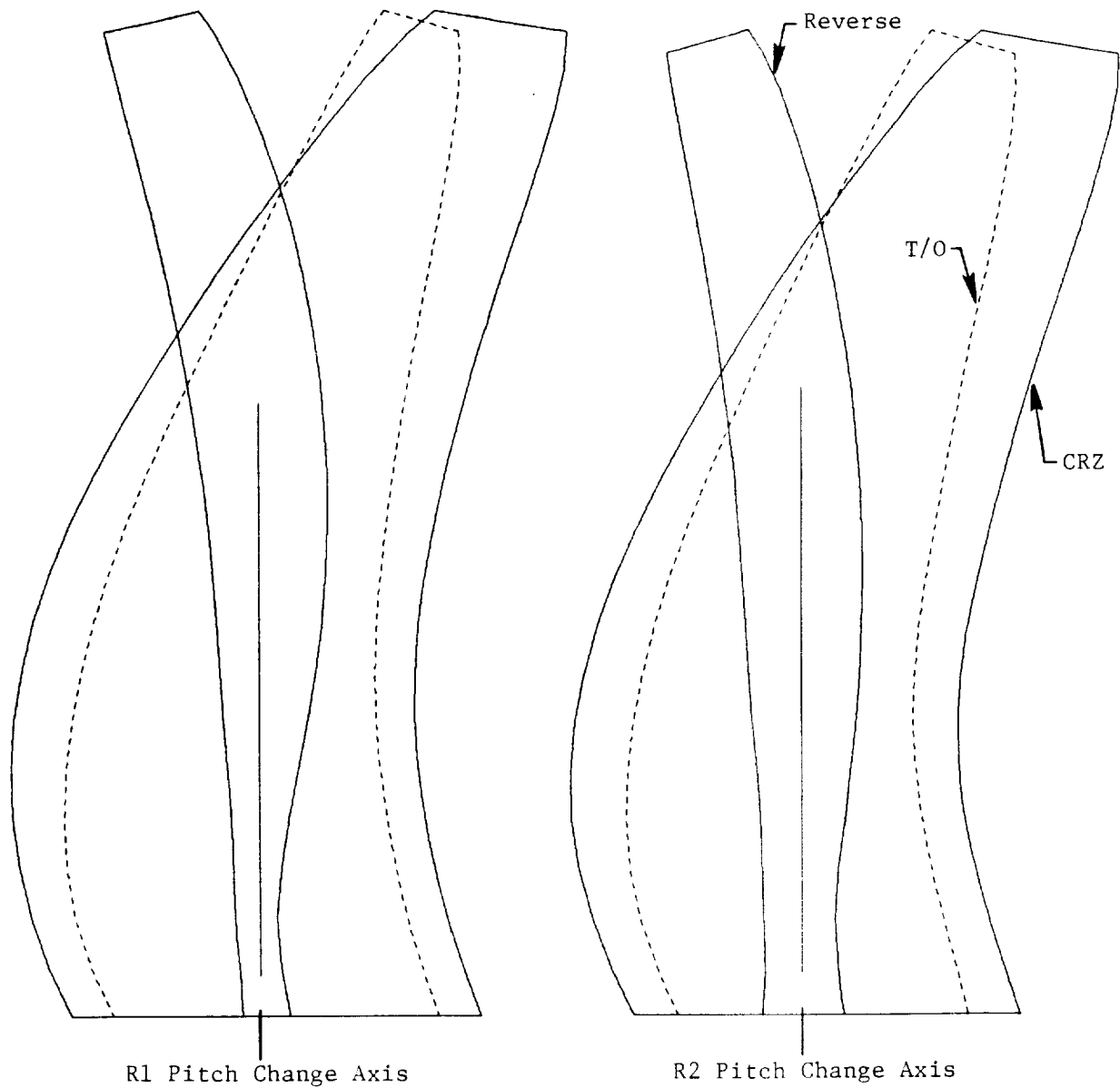
Figure 8-70. Tangential Views of Takeoff, Cruise, and Reverse.

Polyurethane Film

Hybrid
Composite
Shell

Hollow
Titanium
Spar

Foam
Cores

Foam
Cores

Adhesive Film

Balance
Weights
and Potting
Compound

Leading
Edge
Sheath

Polyurethane Film

Figure 8-71.   Blade Basic Construction.

161
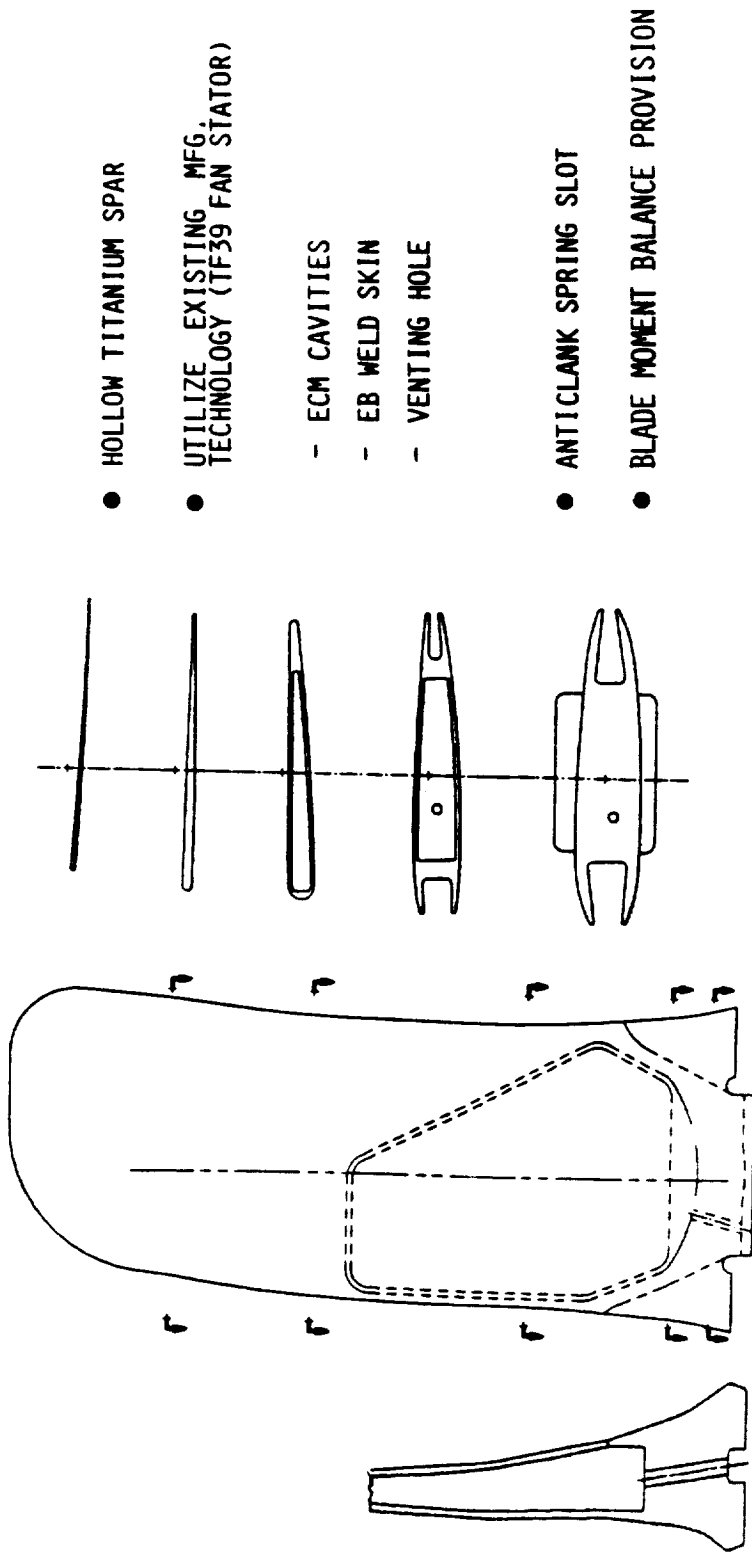
- HOLLOW TITANIUM SPAR

- UTILIZE EXISTING MFG.
  TECHNOLOGY (TF39 FAN STATOR)

  - ECM CAVITIES
  - EB WELD SKIN
  - VENTING HOLE

- ANTICLANK SPRING SLOT

- BLADE MOMENT BALANCE PROVISION

Figure 8-72. Fan Blade Spar Design.

162

installed at the leading edge for erosion and lightning protection. Finally, a thin layer of polyurethane about 10 mils thick is bonded on the airfoil surface for erosion protection.

With this type of blade construction, the blade weight for Stage 1 is 22.5 pounds and 21.5 pounds for Stage 2.

8.3.4 Blade Fabrication and Material Selection

8.3.4.1 Blade Fabrication

The basic construction of the demonstrator engine blades consists of a composite airfoil shell which is molded and bonded around a titanium spar. The basic elements and construction features of the blade are illustrated in Figure 8-71.

Two alternate blade fabrication processes were initially evaluated during the preliminary blade development program. The prime method considered, and finally selected, employed the use of preimpregnated hybrid tape materials for the aerodynamic airfoil shell which was then consolidated, adhesively bonded, and co-cured onto the metallic spar using a compression molding technique. Figure 8-73 diagrams the compression molding method.

The other alternate method which was evaluated was resin transfer molding (RTM). Figure 8-74 demonstrates the basic RTM method of manufacture. This technique involved assembling dry fabric composite shell plies around the metallic spar and placing the complete assembly into a closed mold tool. The resin matrix was injected under pressure to fully impregnate the dry fabric and simultaneously bond the composite shell to the spar.

Although, when compared to the compression molding approach, the resin transfer molding method has many advantages (such as, reduced material costs, low capital investment, low cost tooling, potential for integral molding of metallic inserts, external coatings and protection devices, and improved fiber impregnation - lower void content), the compression molding approach was selected for the demonstrator engine blades as a result of the unavailability of adequate lead-time to fully characterize the resin matrix and dry fabric reinforcements.
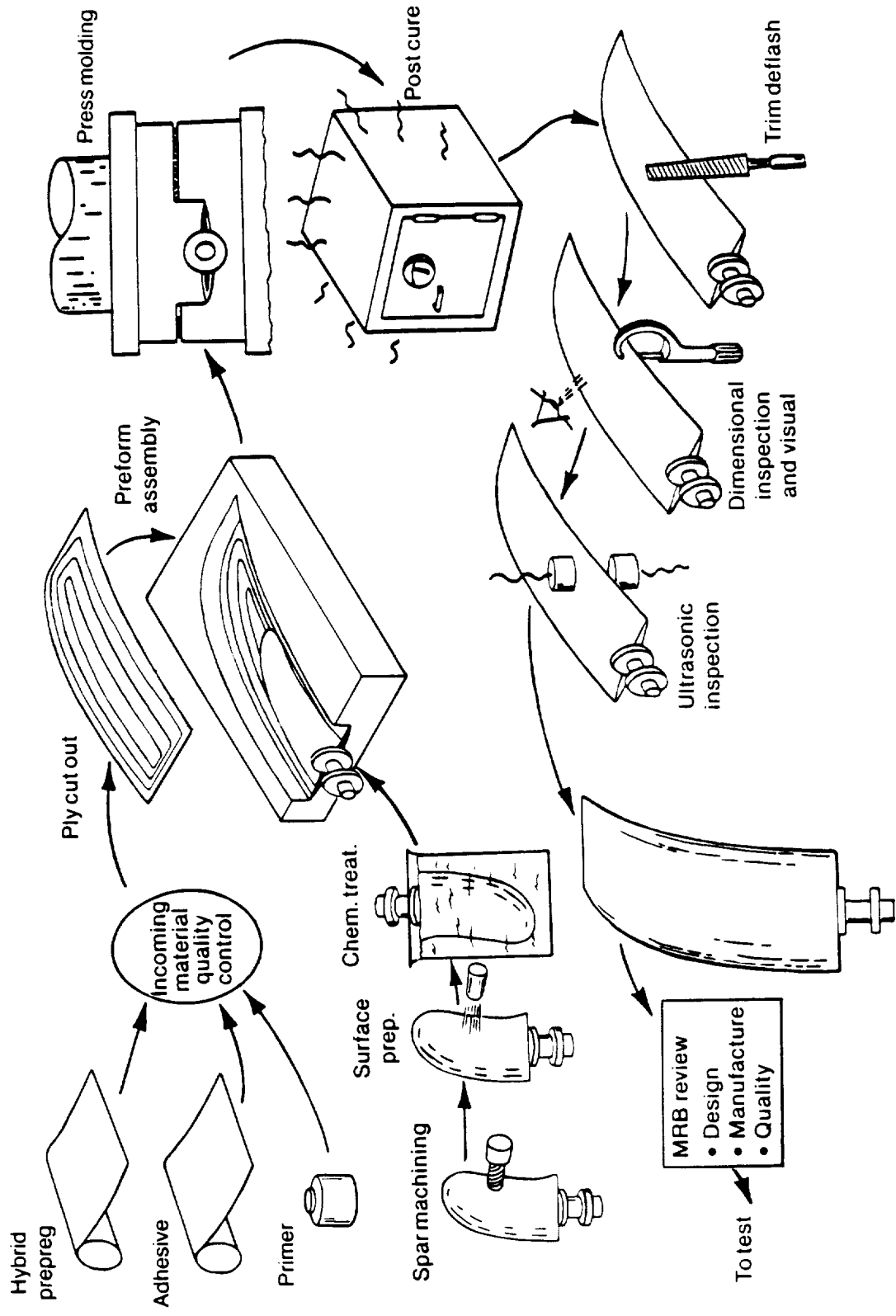
Figure 8-73. Basic Propeller Manufacturing Processes - Compression Molding Process.
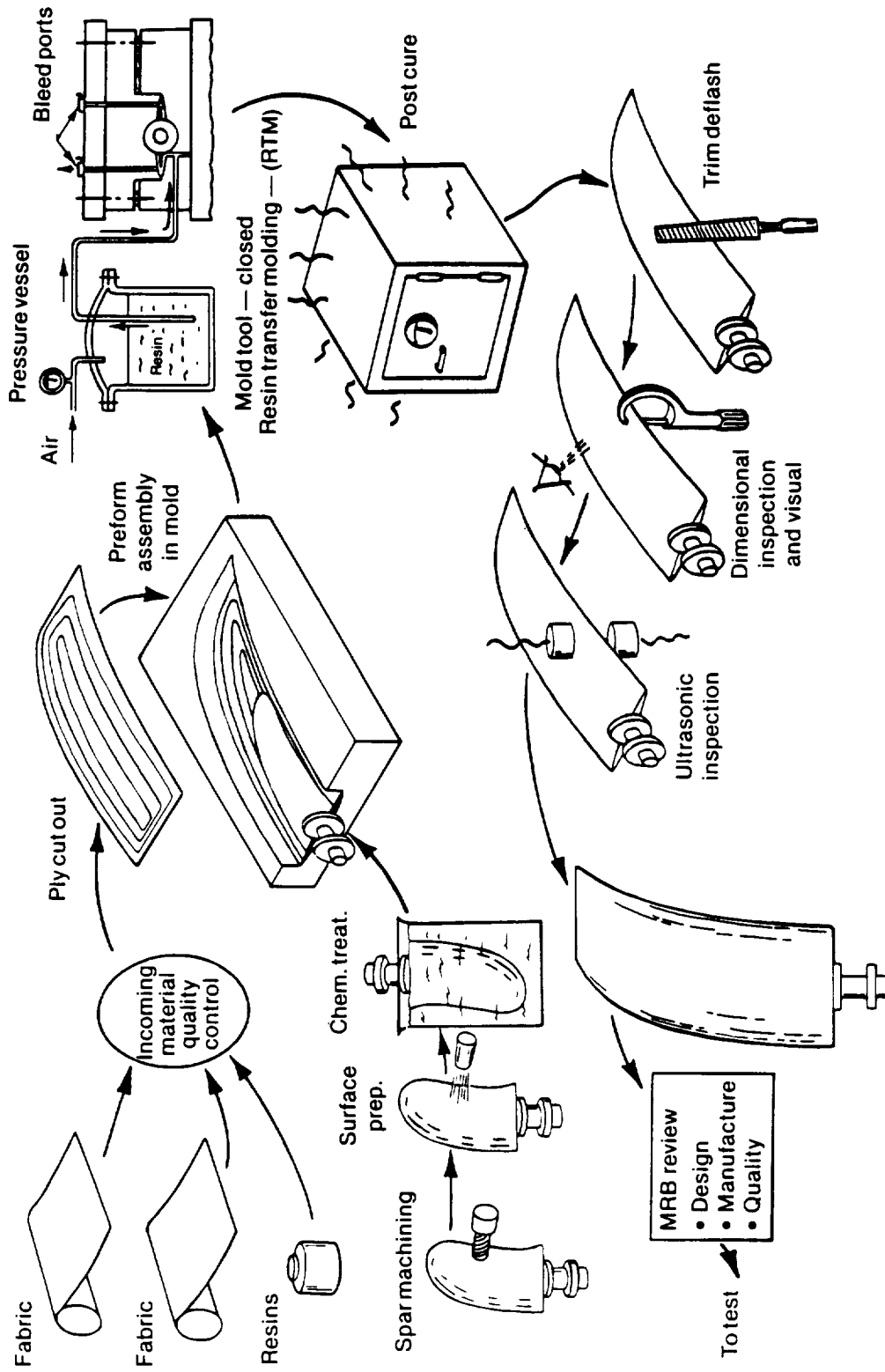
Figure 8-74. Basic Propeller Manufacturing Processes – Resin Transfer Molding Process.

8.3.4.2 Material Selection

Composite Airfoil - The selection of individual composite materials for the airfoil shell was based on high specific strength/modulus and fatigue characteristics, in addition to the requirements for impact damage tolerance from foreign objects.

The airfoils material produced to GE Specification A50TF220 is a unique, hybridized carbon-fiber/glass reinforcement 0.005 inch tape material which is preimpregnated with 3M Company's epoxy resin (designated PR288). The airfoils material, developed by General Electric in the early 1970's, has been used for the fabrication of many composite fan blades and vanes produced as a result of both Government agency and in-house contracts.

Spar to Airfoil Adhesive - Various adhesives for interposing between the titanium spar and composite shell were evaluated in test specimen form. The specimen was designed to simulate the spar/shell joint and consisted of a tapered (10° included angle) wedge of titanium, to which the composite was co-cured and bonded. The results of the tensile shear, HCF, and LCF tests are presented in Figure 8-75. It was found that the basic laminating resin with no additional adhesive interplied yielded the best results.

Leading Edge (LE) and Trailing Edge (TE) Foam Cores - After considerable evaluation testing of polyurethane foam materials, both for foaming into pre-molded blade cavities and as a premolded foam core molded integral with the blade, a sytactic foam (phenolic microballons in epoxy matrix) was finally selected for the demonstrator engine blades. The material could be cast accurately to size and could withstand the nominally 300-psi composite compression molding pressures.

Leading Edge Protection - An electroformed nickel LE sheath was produced to protect the composite airfoil from rain erosion and hard particle impact damage. The sheath also serves as a lightning conductor. The material chosen was a sulfamate nickel electrodeposited onto a model blade which served as the plating mandrel; the adhesive selected for secondary bonding the nickel sheath to the blade was 3M Company's AF3109-U, produced in accordance with General Electric Specification A50TF218.

- **Tested AF3109-2**
  - **AF3185**
  - **AF3185 with Viton**
  - **PR288 (Prepreg)**

- **Selected PR288 Primary**
  - **AF3185 Back-Up**

Test Specimen

Tensile Shear

Low Cycle Fatigue

Run Out (10^7 Cycles) Strain Level 2250 μ for All Three Design Limit <700 μ

High Cycle Fatigue
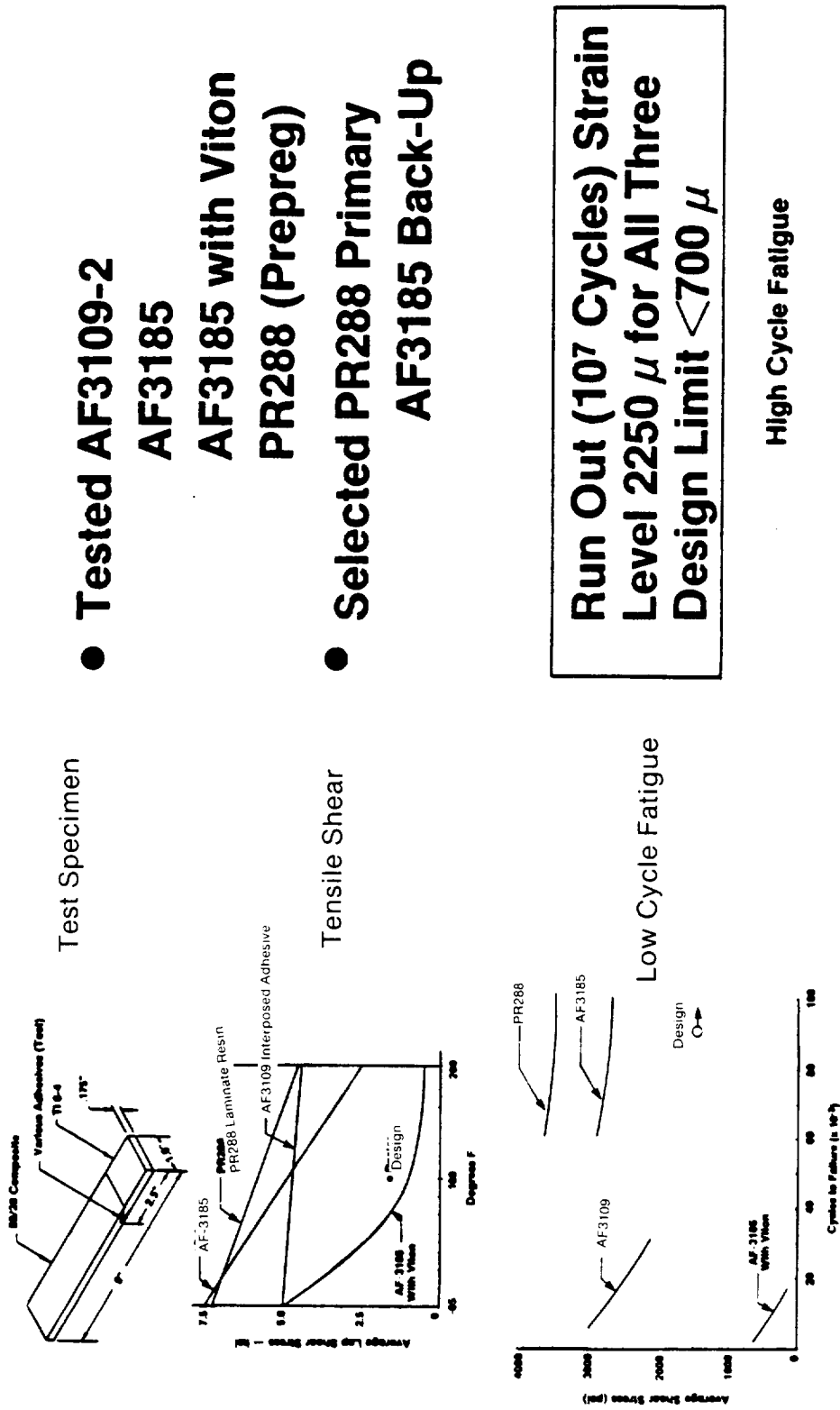
Figure 8-75. Adhesive Strength, LCF and HCF Properties.

167

<u>Erosion Protection</u> - The remainder of the airfoil surface was protected against grit erosion by the application of 0.012-inch-thick polyurethane film which was jointly developed by General Electric and the 3M Company. The film has been demonstrated to be more than 7× more erosion resistant than titanium at a 90° impingement angle. The material is produced in accordance with GE Specification A50TF141.

8.3.4.3 <u>Blade Manufacture</u>

<u>Mold Tools</u> - The mold tools were produced from high temperature filled epoxy tooling compounds using a full-scale aluminum master model to produce the mold cavity. Steel mounting and guide blocks located the titanium spar at the dovetail in order to accurately position it, relative to the airfoil contour. Figure 8-76 shows the Stage 1 blade mold tool mounted in the 300 ton molding press.

<u>Ply Generation</u> - The geometry of the individual layers (or plies) were generated topographically by scribing the master model and titanium spar to assure accurate tailoring and perfectly fill the volume between the spar and the external profile. Individual ply patterns were developed from the topographical map and arranged on a pattern layout to yield minimum wastage of material. The 0.0053- and 0.0106-inch plies were cut out with the appropriate specified fiber orientation. Figure 8-77 shows a typical array of cutout ply patterns which constitute one half-shell preform.

<u>Preform Assembly</u> - Individual plies were assembled into two half-shell preforms using a topographical map to assure accurate relative locations. The titanium spar which had been mechanically and chemically pretreated for adhesion was inserted between the two half-shell preforms. The pretreatment of the spar surface consisted of grit-blast, using 150-grit aluminum oxide. This was followed by an acid etch using Pasajell 107M. The surface was primed with a solution of the PR288 laminating resin produced in accordance with General Electric Specification A50TF181, Class A. Figure 8-78 shows one half preform assembly on a fiberglass-reinforced support tray.

<u>Molding</u> - The composite preform/spar assembly was loaded into the mold tool (preheated to 240° F). The molding press was then closed to a prescribed

168
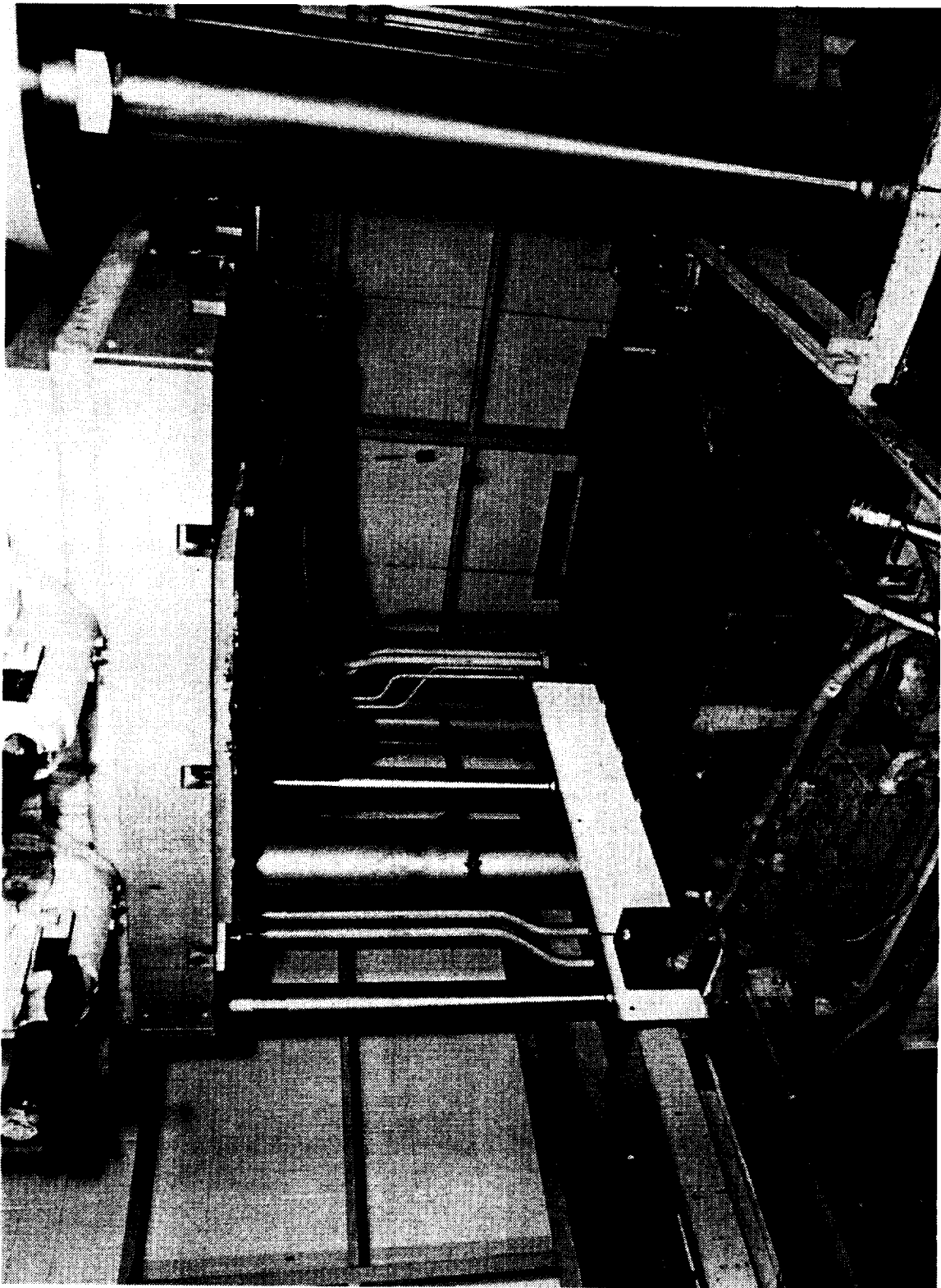
Figure 8-76. Stage 1 Blade Mold.

169

Figure 8-77. Typical Array of Cutout Ply Patterns.

170
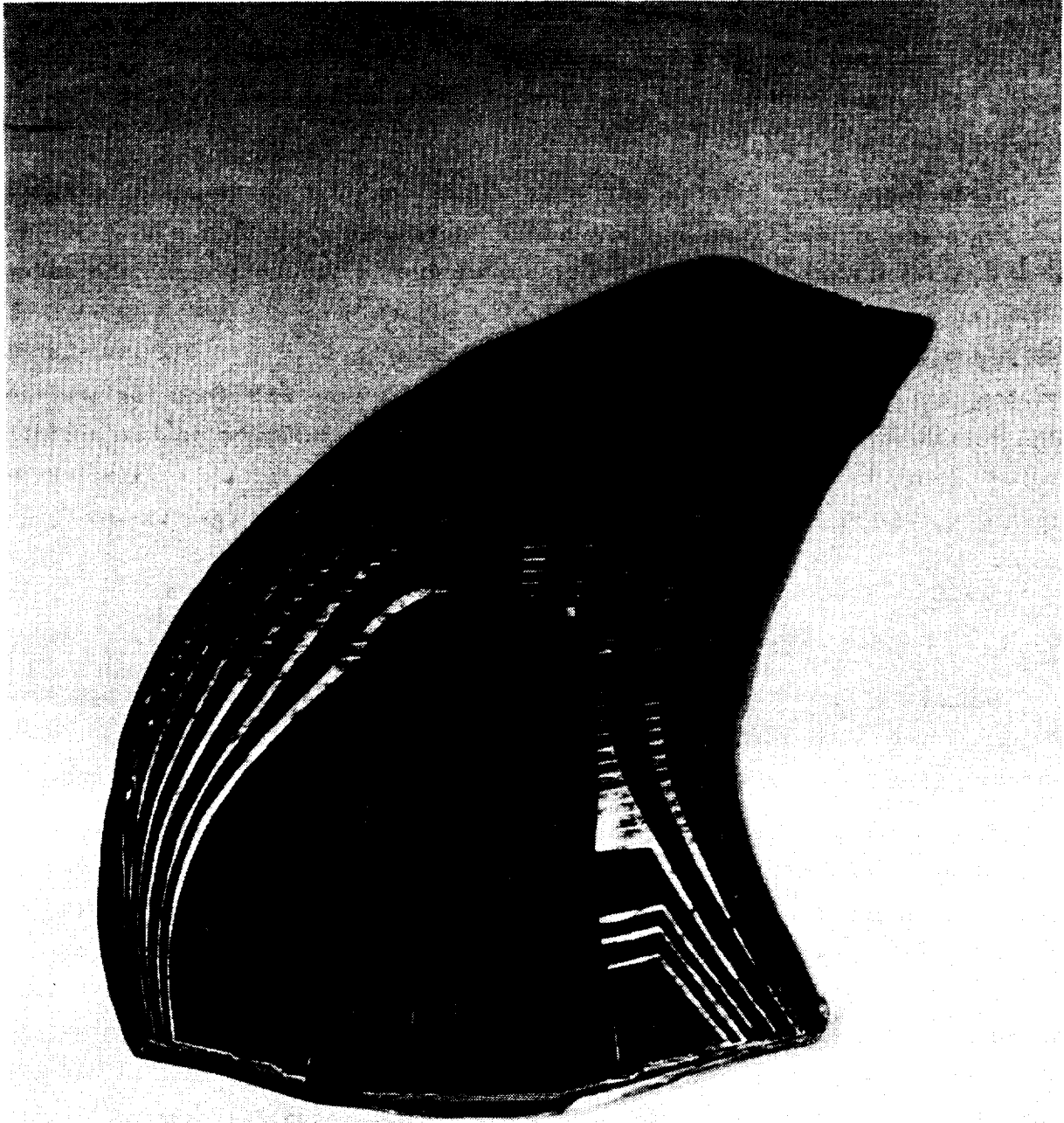
Figure 8-78.   One Half Preform Assembly.

cycle developed to produce optimum properties in the composite airfoil. The part was retained in the mold under 300-psi molding pressure for 2 hours before being extracted hot and transferred into a postcuring oven for 4 hours at 275° F.

Blade Finishing - Various finishing operations were performed to protect the composite airfoil from engine service environmental damage. An electroformed nickel leading edge sheath was bonded into place to protect the sharp composite LE against rain erosion and hard object damage. The remainder of the exposed composite airfoil surface was covered with a 0.012-inch-thick polyurethane film to protect against dust and grit erosion. Both the leading edge sheath and the polyurethane film were adhesively bonded to the airfoil surface using low pressure (50 to 100 psi) autoclave procedures. Figure 8-79 depicts a typical finished Stage 1 blade with the titanium spar in the foreground.

8.3.4.4 Quality Assurance

All of the materials used in the manufacture of the blades were procured in accordance with formal General Electric specifications and the incoming material properties were measured and compared to the vendor-reported data.

All of the manufacturing processes were rigidly controlled through each step of the fabrication cycle in order to verify consistently high quality blades. Typical blade moldings were destructively analyzed for fiber volume fraction void content, in addition to mechanical properties evaluation. A Material Review Board (MRB) committee comprised of representatives from Design Engineering, Manufacturing, and Quality reviewed each individual blade before allocating to engine or component test. A checklist was devised to certify that every aspect of the blade, including documentation, was systematically examined. Each blade was graded for overall quality level, and the MRB checksheet was signed off by all parties. A separate file was maintained for each blade, containing all manufacturing data, route cards, inspection and process records.
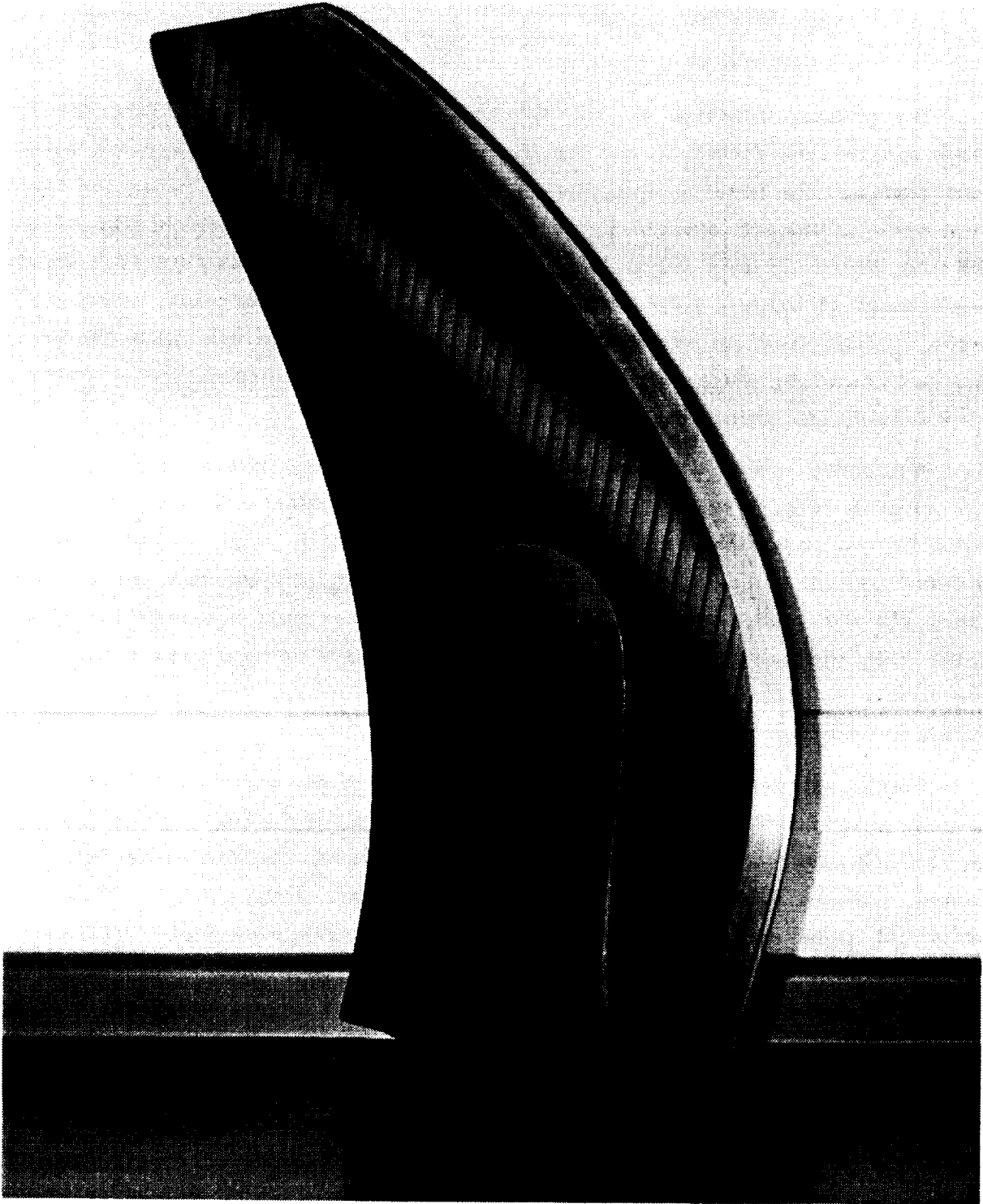
Figure 8-79.   Typical Finished Stage 1 Blade with
Titanium Spar.

8.3.5 Fan Blade Retention

8.3.5.1 Dovetail Trunnion

The primary function of the dovetail trunnion is to integrate the fan blade single-tang dovetail, the fan blade retention bearings, the pitch actuation gearing, the dovetail anticlank device, and the fan blade retention hardware into a compact system that provides for on-wing maintainability of the UDF™ fan blades (Figure 8-80). In addition, the trunnion has to meet a design requirement of being a prime reliable structure (2× load-carrying capability). Trade studies were conducted early in the design phase to determine the optimum configuration which would provide a balance between compactness, ease of maintenance, and structural integrity.

The chosen configuration consists of a one-piece machining of a Marage 250 forging (Figure 8-81) that includes a broached single-tang dovetail slot and a series of machined buttress threads. In addition, the machined features include several closely toleranced diameters which provide the seating surfaces for both the setup row bearing and the sector gear and provide for the pilot with the thrust bearing. In order to minimize weight, lightening holes are machined in noncritical locations. Marage 250 was chosen for its high strength-to-weight ratio in low temperature applications.

Static stresses of the trunnion were evaluated using a detailed 3D finite element model, a 2D photoelastic model, and actual static strain measurements in the trunnion dovetail slot radius acquired during the fan blade whirligig tests. In the life-limiting area of the dovetail slot fillet radius, the estimated peak stress obtained from the 2D photoelastic model corresponded extremely well with the actual measured stress in the radius, apparently due to too coarse of an element mesh. The experimental stress value was used to predict that the trunnion had adequate high cycle and low cycle fatigue life for the demonstrator engine program. Figure 8-82 portrays the Goodman diagram for certain engine operating conditions based on the experimentally determined static stresses and the experimentally determined (during whirligig testing) dynamic response of the trunnion, relative to the fan blade dynamic response.

174
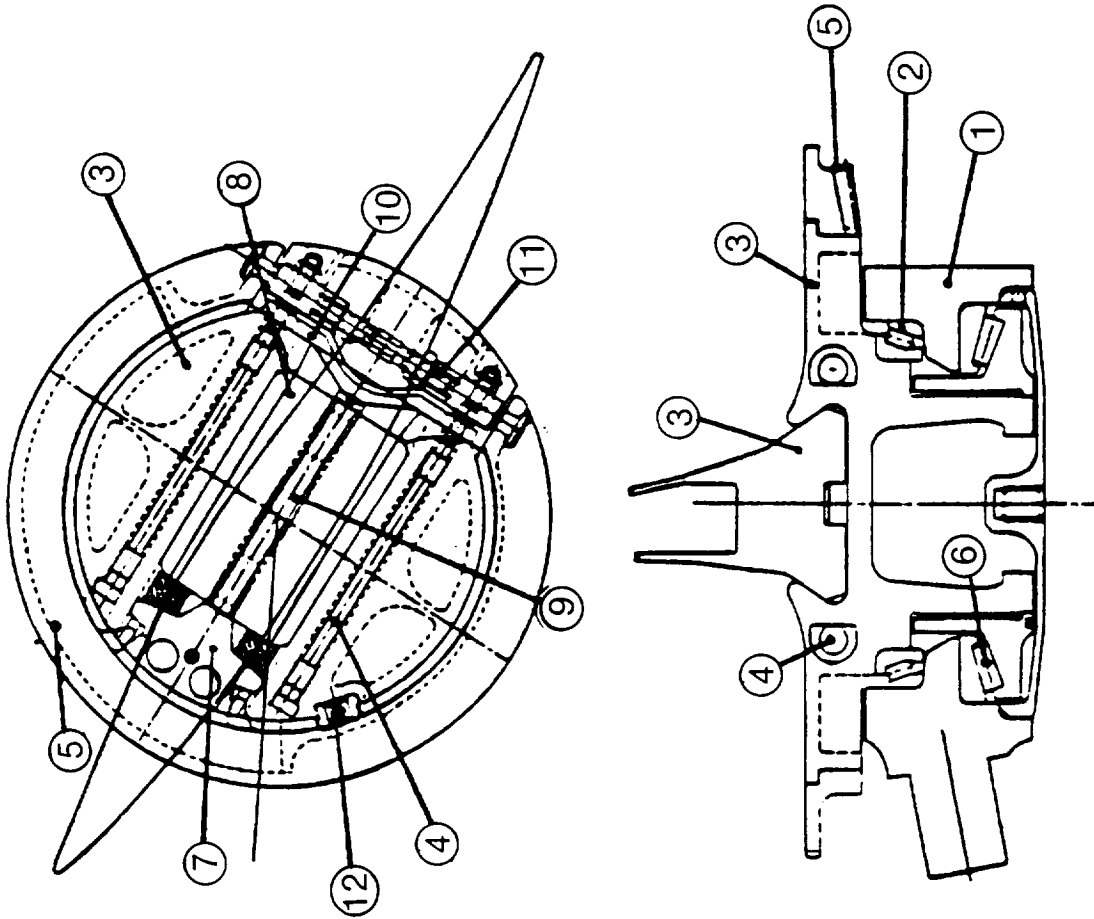
- Components Include
  - (1) Hub Ring
  - (2) Set-Up Roller Bearings
  - (3) Dovetail Trunnion
  - (4) Trunnion Bolts
  - (5) Gear Sector
  - (6) Thrust Roller Bearing
  - (7) Dovetail Spacer
  - (8) Blade Dovetail
  - (9) Anticlank Clamp
  - (10) Dovetail Clamp
  - (11) Gear Sector Clamp
  - (12) Antirotation Key

Figure 8-80. Components of Fan Blade Retention System.

175

- Fan Blade Trunnion
  - Trunnion Material Marage 250
  - Molydag 254 on Blade D/T
  - Dovetail Slot Width
    Increases 0.020 inch During
    2X Loading
  - Meets 2X Pull
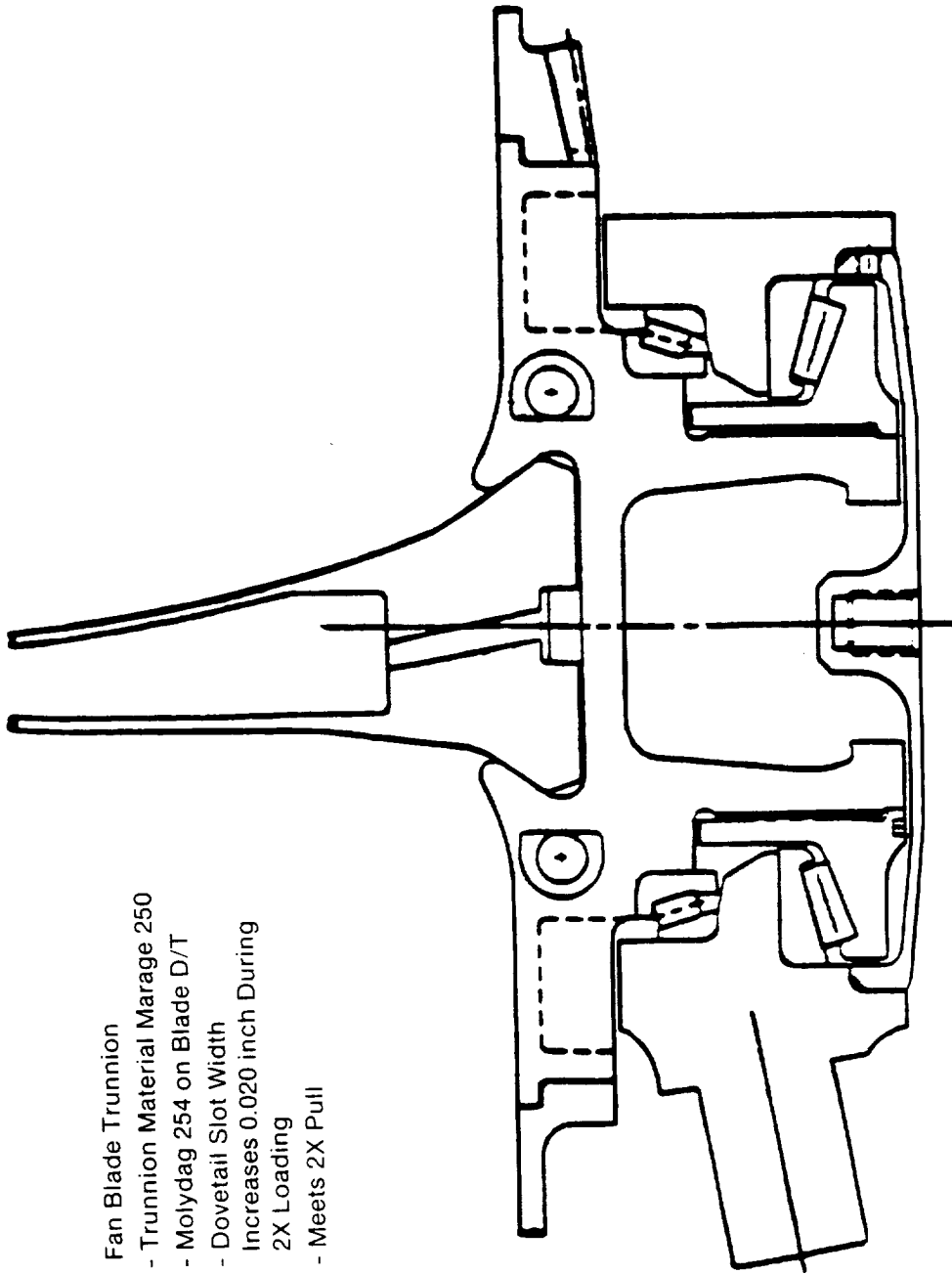
Figure 8-81. Fan Blade Retention System, Trunnion.
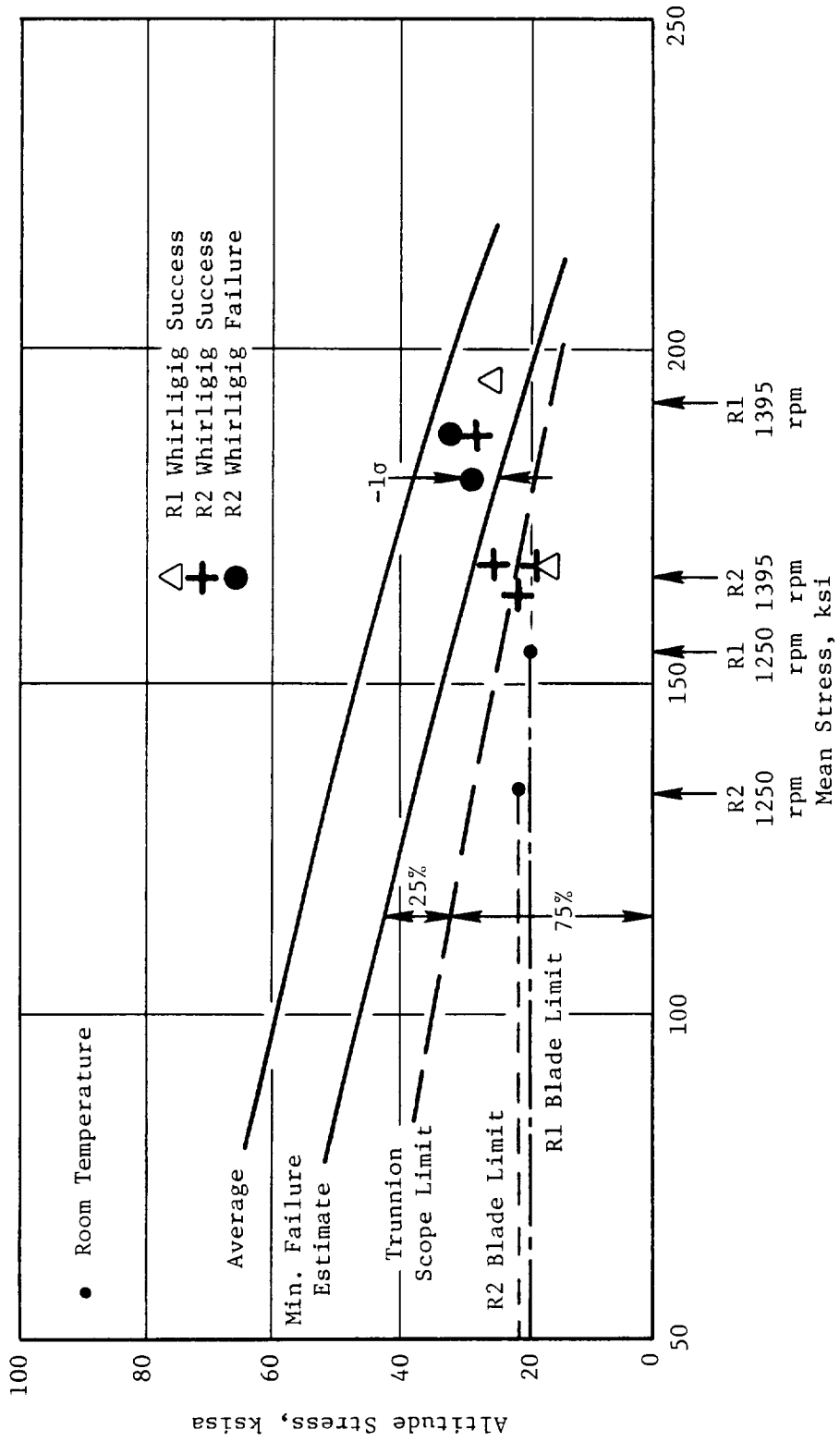
Figure 8-82. Trunnion HCF Limit – Marage 250 10^6 Cycle Stress Range Diagram.

177

8.3.5.2 Fan Blade Retention System

The fan blade retention system (Figure 8-80) consists of numerous small pieces of hardware, each designed to retain the fan blade dovetail in position in the trunnion dovetail slot during all possible flight conditions. All of the retention hardware is designed to survive the cost-limiting load cases of a bird strike, or 2× the normal operating loads, while still retaining the fan blade. In addition, the retention system must be integrated into the overall engine design, such as to also provide the outer flowpath in the vicinity of the fan blades and to provide for on-wing maintainability of the UDF™ fan blades. The retention system consists of the dovetail spacer (Figure 8-83), dovetail clamp (Figure 8-84), anticlank spring, trunnion bolts, gear sector clamp, the Stage 1 platform, and the Stage 2 flowpath cover.

Both the dovetail spacer and the dovetail clamp serve to axially position the fan blade dovetail in the trunnion dovetail slot. The dovetail clamp also serves to load the anticlank spring into position. Both are machined from Ti-6-4 bar stock, which was selected for its high strength/low weight characteristics. The dovetail spacer is seated radially outward into position in the dovetail slot by use of a jacking screw (Figure 8-83), which is reacted against the dovetail slot bottom. A helicoil insert is provided in the dovetail spacer into which the jacking screw is threaded. On Stage 2, where the dovetail spacer and dovetail clamp form part of the flowpath, silicon blade root seals are added.

As illustrated in Figure 8-85, two 0.250-inch-diameter trunnion bolts run lengthwise through the trunnion and attach the dovetail clamp in place against the fan blade dovetail. The bolts are trapped in position by the sector gear with the D-head of the bolts serving as a self-wrenching feature. Inconel 718 bolts were sized to have an optimum length/diameter (L/D) ratio, so as to provide a maximum amount of energy absorption during a bird strike.

The gear sector clamp, illustrated in Figure 8-86, is used to secure the actuation system sector gear in position on the fan blade trunnion. A 0.250-inch-diameter bolt is threaded into each end of the clamp, pulling the sector gear tight around the trunnion. The design insures that the clamp is loaded only in tension, thus eliminating any buckling concern.

178

- **Dovetail Spacer**
  - Ti 6-4
  - Positions Dovetail In Slot
  - Low Deflection
  - Low Contact Stress, Low Wear
  - Withstands Bird Impact

Silicon Blade Root Seals (Stage 2 Only)

Heli-Coil Insert and Jacking Screw
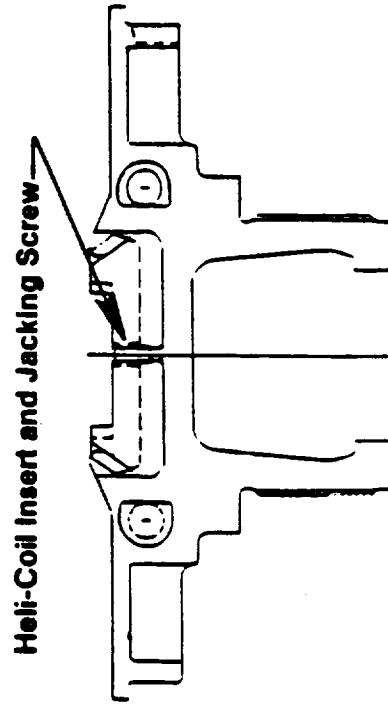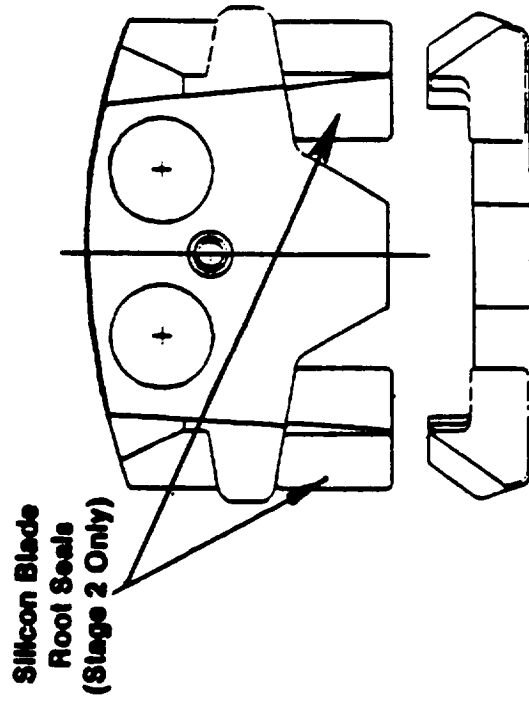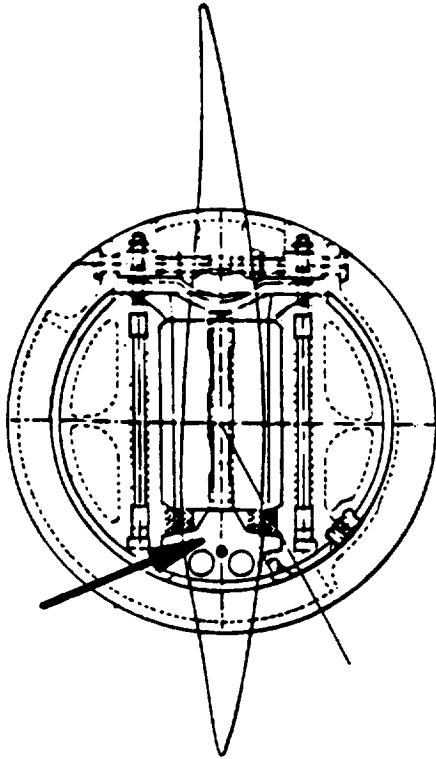
Figure 8-83. Fan Blade Retention System - Dovetail Spacer.

179

- **Dovetail Clamp**
  - Loads Anticlank Spring, and Clamps Dovetail into Place
  - Ti 6-4
  - Low Deflection During Takeoff Load
  - Withstands Bird Impact

10 ksi

6 ksi
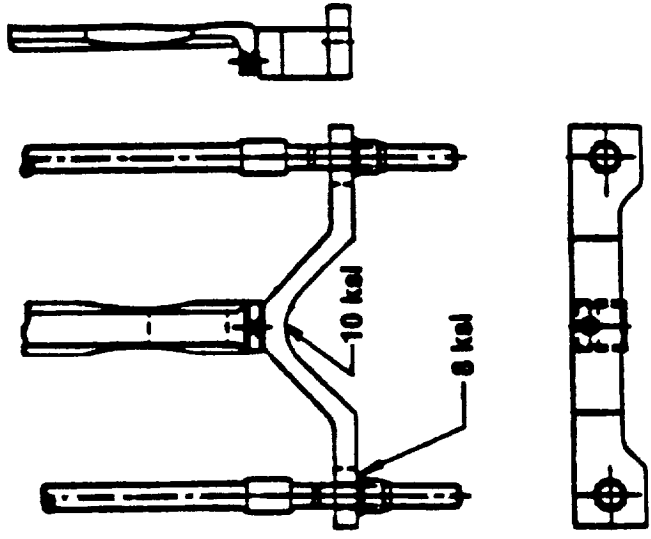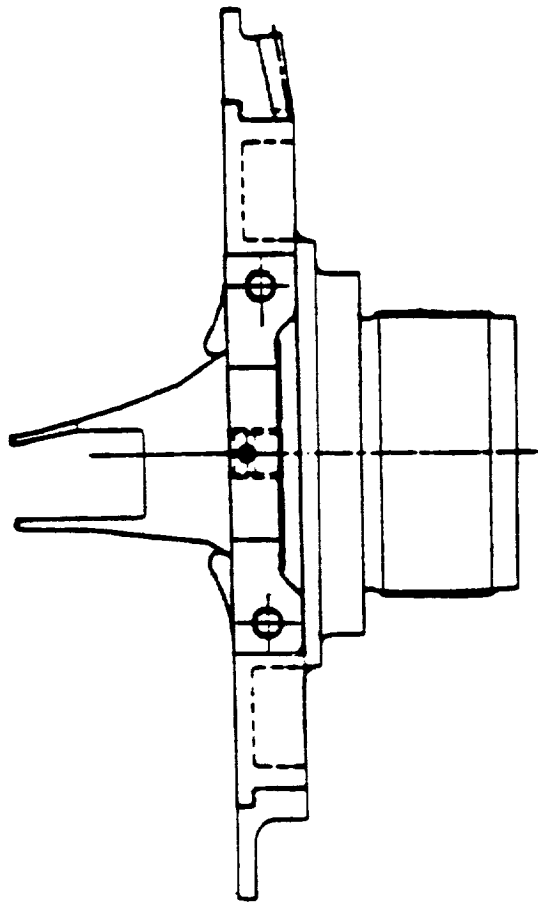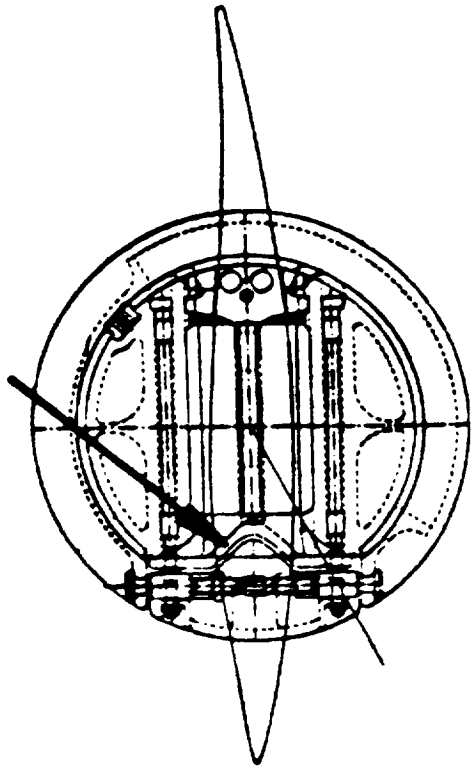
Figure 8-84.   Fan Blade Retention System – Dovetail Clamp.

180
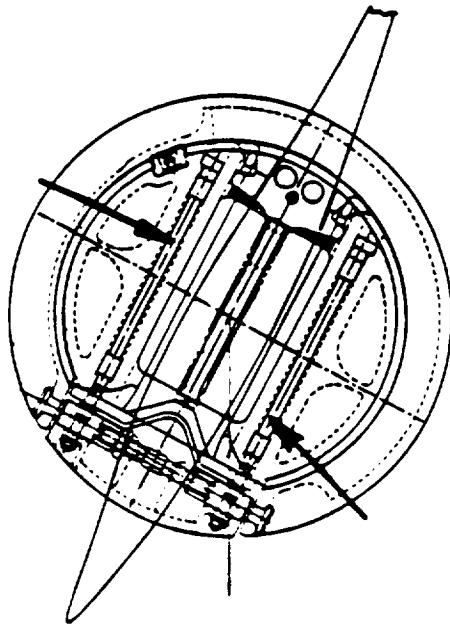
- **Trunnion Bolts**
  - **Draw Dovetail Clamp into Place Against Anticlank Spring**
  - **Inconel 718**
  - **Self Wrenching**
  - **Excess Clamp Margin**
  - **Withstands Bird Impact**

.250-28-UNJF

7.15
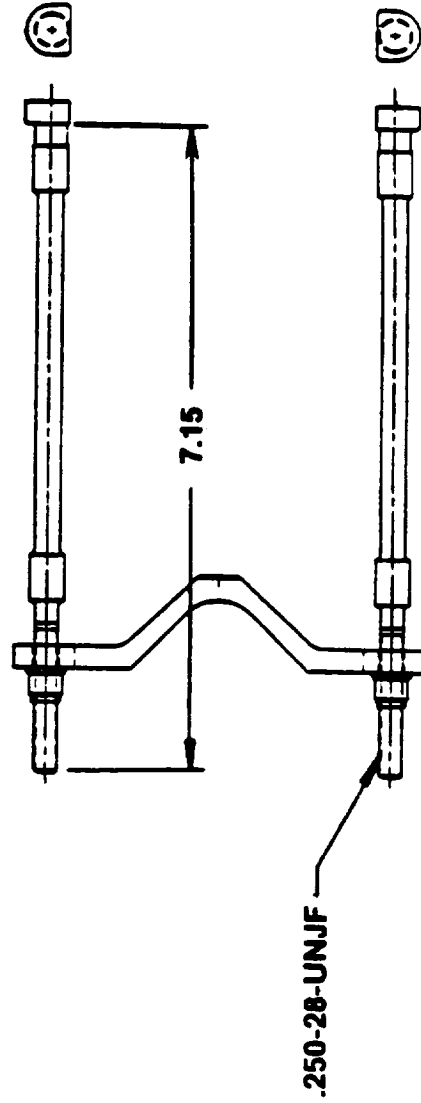
Figure 8-85. Fan Blade Retention System - Trunnion Bolts.

181
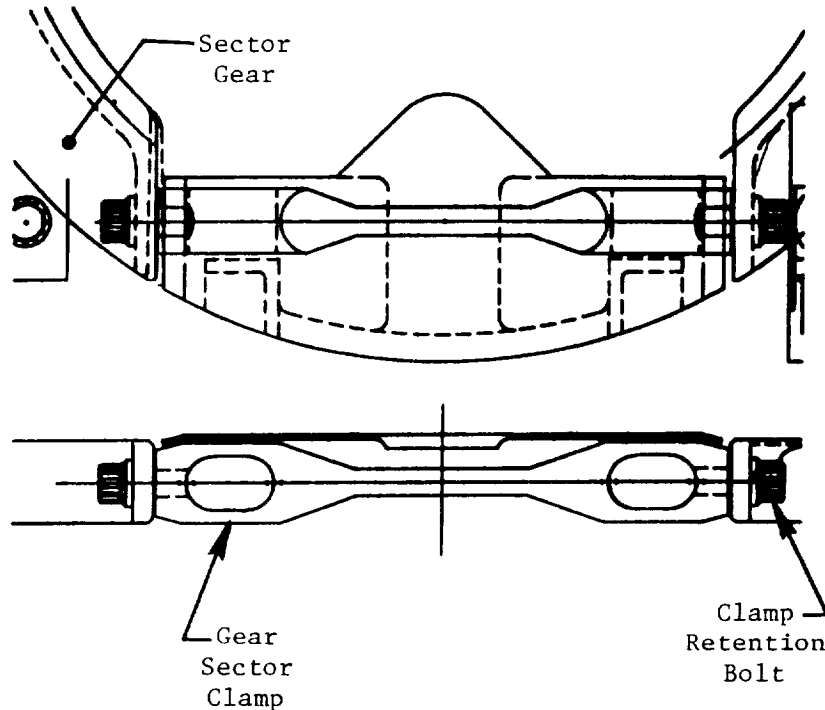
Figure 8-86. Fan Blade Retention System - Gear Sector Clamp.

The fan blade anticlank spring, as detailed in Figure 8-87, is designed to preload the fan blade dovetail in the trunnion dovetail slot to a total load of 450 pounds. The anticlank spring is loaded into position by torquing down the nuts on the trunnion bolts, which draws the dovetail clamp into its assembled position and preloads the spring.

The Stage 1 platform (Figures 8-88 and 8-89) serves not only as the outer flowpath in the vicinity of the Stage 1 fan blade, but also serves as a cooling air scoop at takeoff in order to maintain the temperature of the fan blade retention hardware at an acceptable level. The platform is constructed of a graphite/epoxy, which enables it to meet all the structural requirements, yet to be extremely lightweight. The platform is split into two halves; in each half, a titanium pad (Figure 8-89) is bonded to the graphite/epoxy shell, thus allowing the platform to be mounted to the fan blade trunnion by three 0.250-inch-diameter bolts. These bolts are accessible from outside the engine, thus

● Anticlank Spring
   - ## Inconel 718
   - ## 450 lb. Assembly Preload
   - ## Designed to 0.2% Yield Stress

Tapped Hole for Jacking Screw Removal

450 lbs.
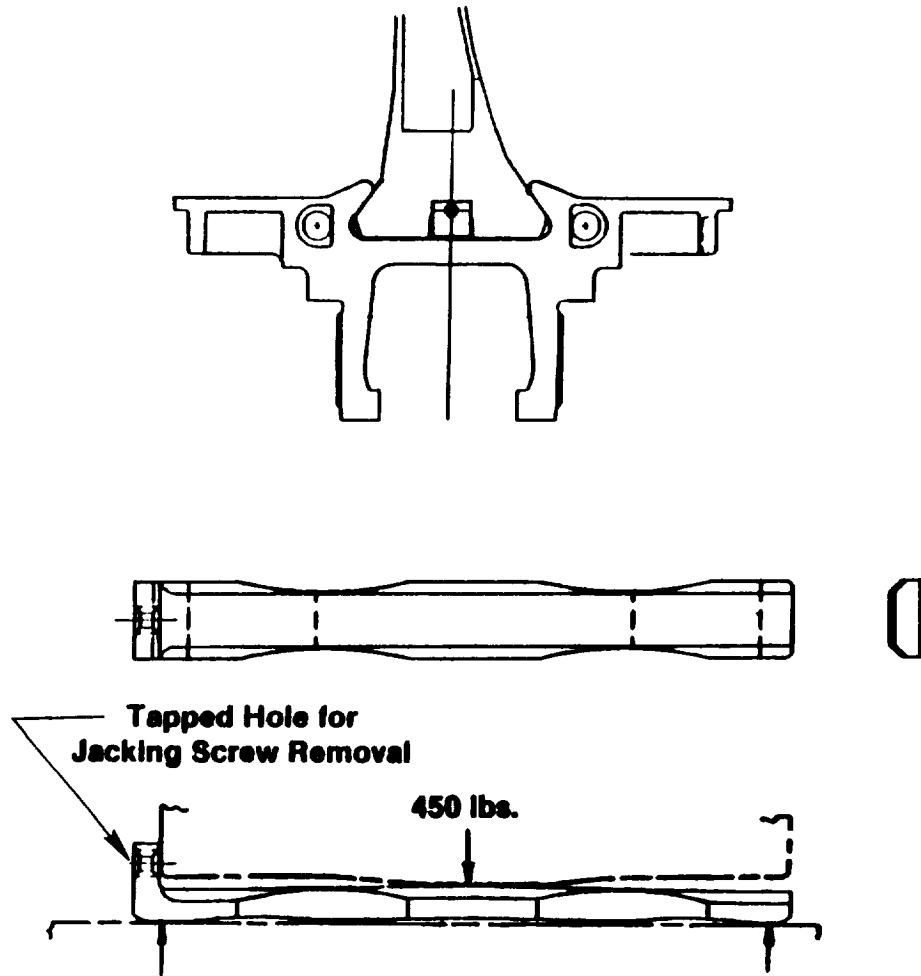
Figure 8-87. Fan Blade Retention System - Anticlank Spring.

- **Stage 1 Platform**
  - Stage 1 Only
  - Provides Flowpath
  - Graphite/Epoxy Construction
  - Cooling Air Scoop (1.2 In² @ Takeoff Pitch)
  - Meets Structural and Maintainability Requirements
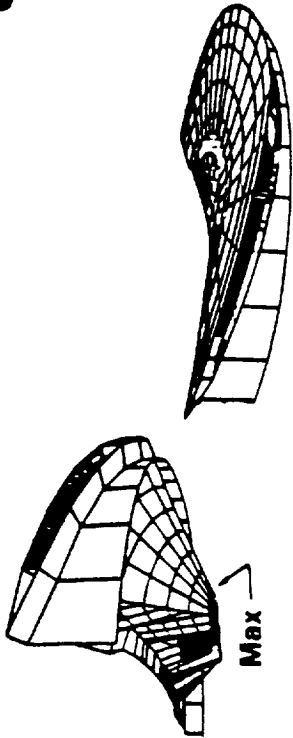
- σ_{max} = 9.1 ksi
- First Mode Natural Frequency Margin 61% Above 16/Rev.

Max

Cowling
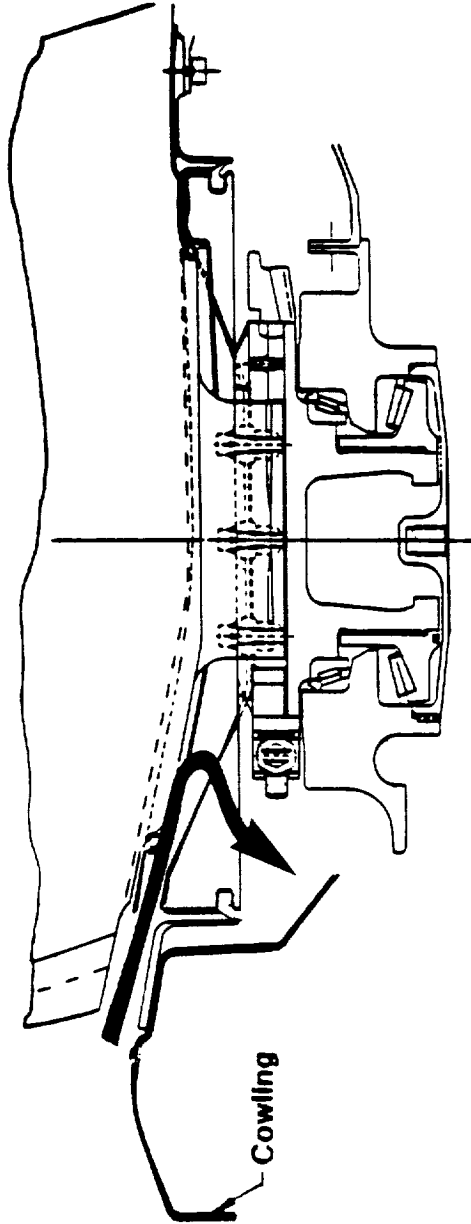
Figure 8-88. Fan Blade Retention System – Stage 1 Platform.

Spiro-Lok
Ring

.250" ∅ Bolt

Bushing

Bolt Access
Covers

Threaded Plug
(Nylon 6-10)

Threaded Insert
In Dovetail Trunnion
(Self Locking)

(Blade Not
Shown)

Blade Seal

Titanium Pad

Section A-A

Air Scoop
(Takeoff Only)

13"OD

A

A
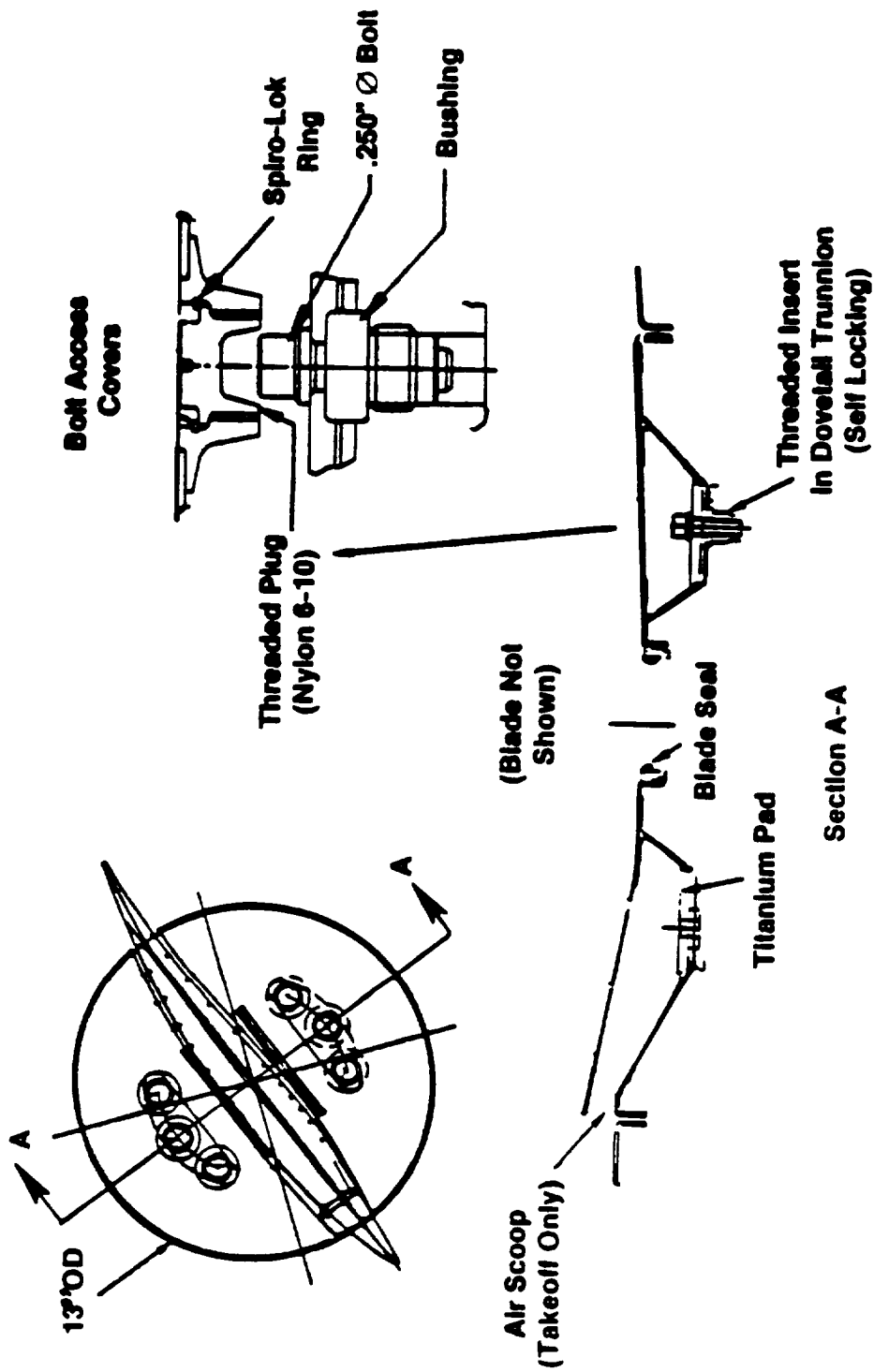
Figure 8-89. Fan Blade Retention System – Detailed Stage 1 Platform.

185

facilitating on-wing maintainability of the UDF™ fan blades. The cooling air scoop in each platform is designed to be open at takeoff to accommodate incoming cool air into the fan rotor cavity but to close off at cruise pitch angles where engine temperatures are lower. The platform was designed such that its first natural frequency has adequate margin above 16/rev throughout the engine operating region.

The Stage 2 flowpath cover, as depicted in Figure 8-90, is a lightweight aerodynamic aluminum fairing which seals the Stage 2 flowpath in the areas of the dovetail and gear sector clamps.

8.3.6 Design Analysis

Finite Element Modeling

Utilizing an in-house finite element analysis code (TAMP/MASS) to represent the 3D blade structure, the blade was modeled as shown in Figure 8-91, with 8 elements chordwise, 20 elements spanwise, and 3 elements through the thickness of the blade. The type of elements used were 3D bricks.

The composite ply lay-up pattern of $(-10°/35°/80°/35°...)_s$ was chosen for the fan blade stability. Bulk properties of this pattern and its basic PR288 fiber undirectional properties are shown in Table 8-5. In the finite element model, the properties and direction of each composite element were calculated based on the number and direction of plies in the element.

The titanium spar was modeled with one layer of 3D brick elements. The elements that modeled the hollow portion of the spar were given the appropriate modulus and density to simulate the flexural rigidity and mass of the hollow titanium.

Two types of boundary conditions at the blade root were used in the blade analysis. One was a fixed-root condition which was primarily for the steady-state and bench frequency analysis. The other was an elastic foundation which simulated the nodal diameter flexibilities of the fan blade supporting structures and actuation torsional stiffness for the fan blade system frequency analysis.

- **Stage 2 Flowpath Cover**
  - **Provides Flowpath at Stage 2 Blade Root**
  - **Provides 'Pie-Plate' Outer Diameter Seal**
  - **6061 Aluminum**
  - **Low Stress and Deflection**
  - **Trapped in Place**

.040 Thick

.130 Thick
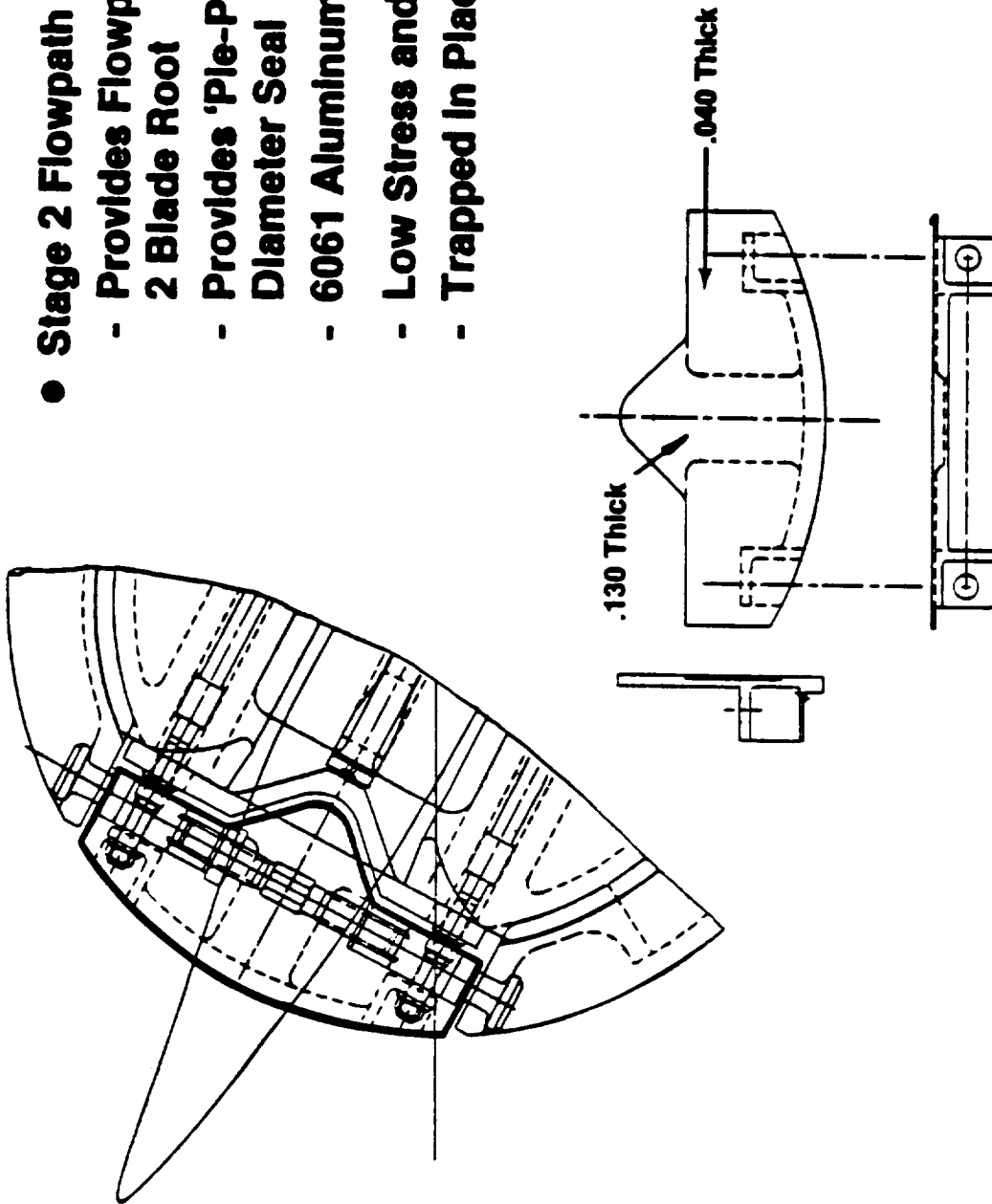
Figure 8-90. Fan Blade Retention System - Stage 2 Flowpath Cover.

187

- Three-Dimensional Finite Element Brick Model

- Fixed and Elastic Foundation

- Three Elements Through-the-Thickness (Skin-Spar-Skin)
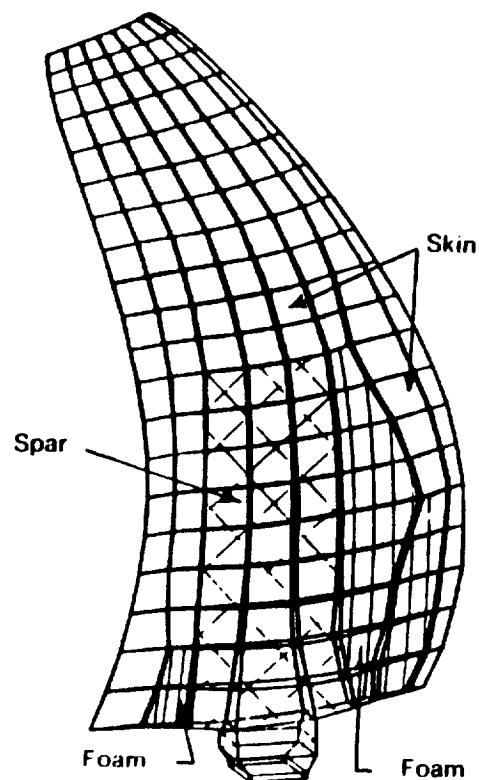
Figure 8-91. Finite Element Model.

Table 8-5. Composite Properties.

- Ply Pattern: $(0/45°/o/45°)_s$
- Density   :   0.056 lb/in^3

	Moduli 10^6 psi	Ultimate, ksi	Allowable, ksi LCF > 10^5	Allowable, ksi HCF > 10^7
Long Tensile	8.6	88.0	44.0	24.7
Chordwise Tensile	2.9	21.0	10.5	5.9
Cross Fiber Shear	2.3	40.0	20.0	11.2

Steady-State Analysis

Fan blade steady-state analysis was performed consisting of the development of a "cold blade" shape which was then analyzed for the following three operating conditions: cruise, takeoff, and reverse thrust. Cold blade is defined as the static, unloaded shape to which the blade will be manufactured. The cold blade, under the design/cruise loadings, will be deflected to closely match aerodynamic cruise/design configuration. Once the cold shape is established, it is used as the basis for determining the deflections and stresses at all operating conditions; consequently, it is imperative that the deflected shape of the blade be established for each condition, because it affects not only the aerodynamics, but also the aeromechanical and aeroelastical characteristics.

Loading Application

Centrifugal and air loads are the two major types of loadings applied onto the fan blades. Centrifugal loads arise from the rotation of the fan blade about the axis of rotation. These loads are generated internally in the TAMP/MASS analysis.

Air loads used in this analysis are based on the results of aerodynamic calculations at selected flight conditions. Spanwise distributed tangential and axial air loads for the steady-state design cruise and takeoff conditions are plotted in Figures 8-92 and 8-93. These distributions are then integrated for each increment of span to obtain the discrete tangential and axial loads at each radial station in TAMP/MASS model.

Tangential and axial loads at each radial station are further decomposed into discrete loads at each grid point along the blade chord. This decomposition is based on chordwise air pressure distribution and the spacing of the grid points. At each flight condition, the chordwise air pressure distribution is assumed to be constant along the blade span, as illustrated in Figure 8-94 for the cruise and takeoff conditions. The discrete loads will preserve the center-of-pressure at each radial station while maintaining the blade thrust and torque reactions at the hub for the specific condition.

189
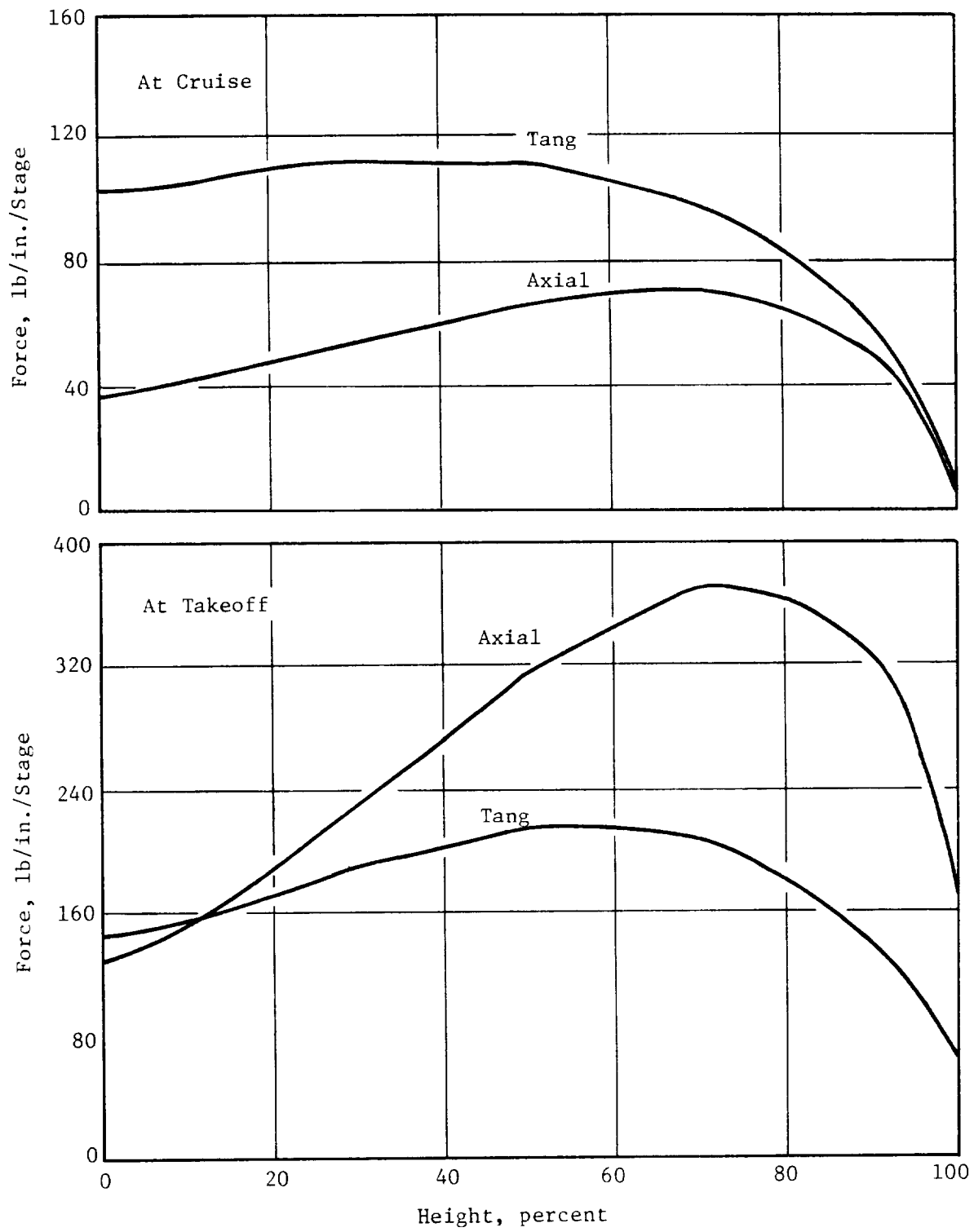
Figure 8-92.   F7 Spanwise Force Distribution.
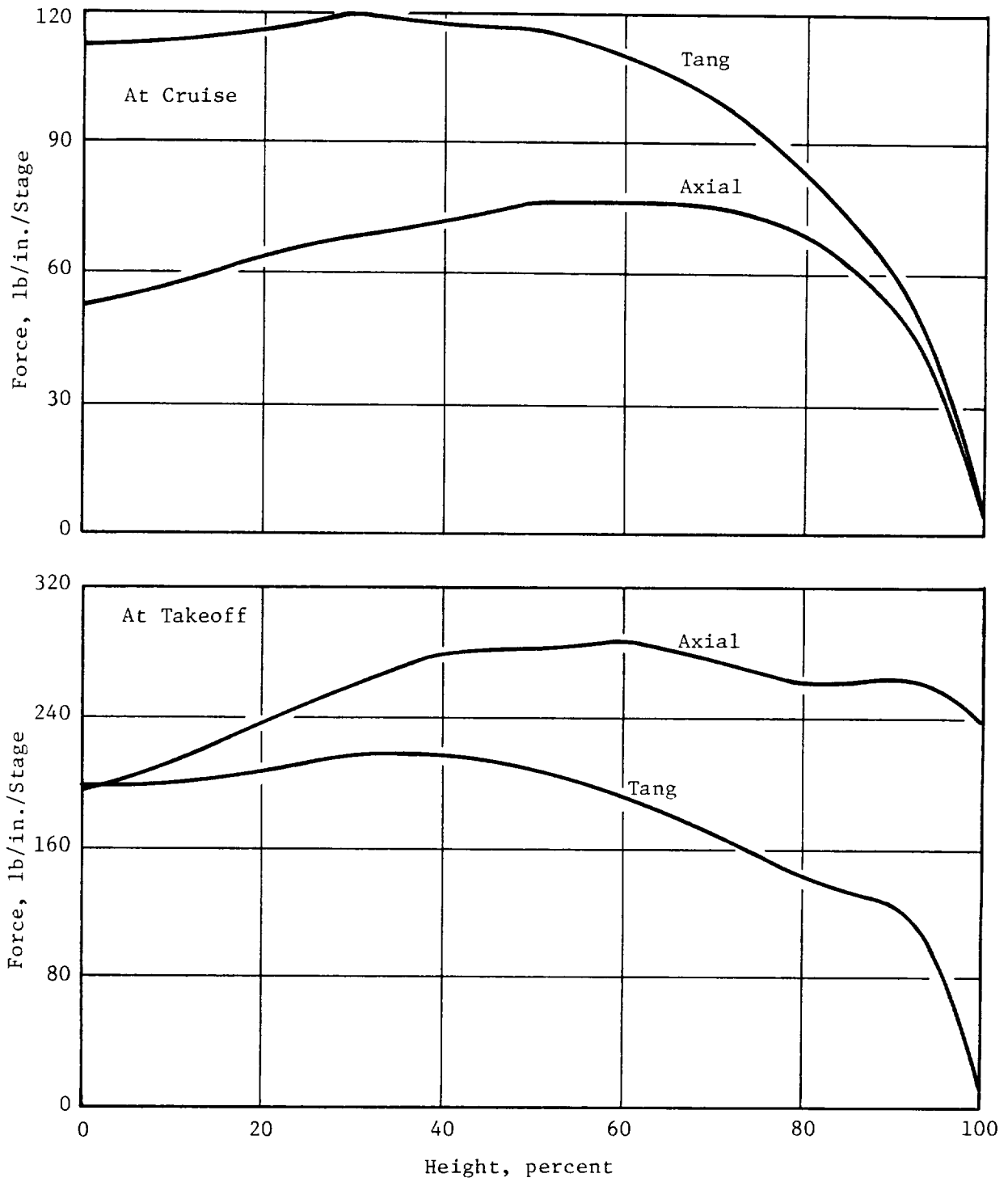
Figure 8-93. A7 Spanwise Force.
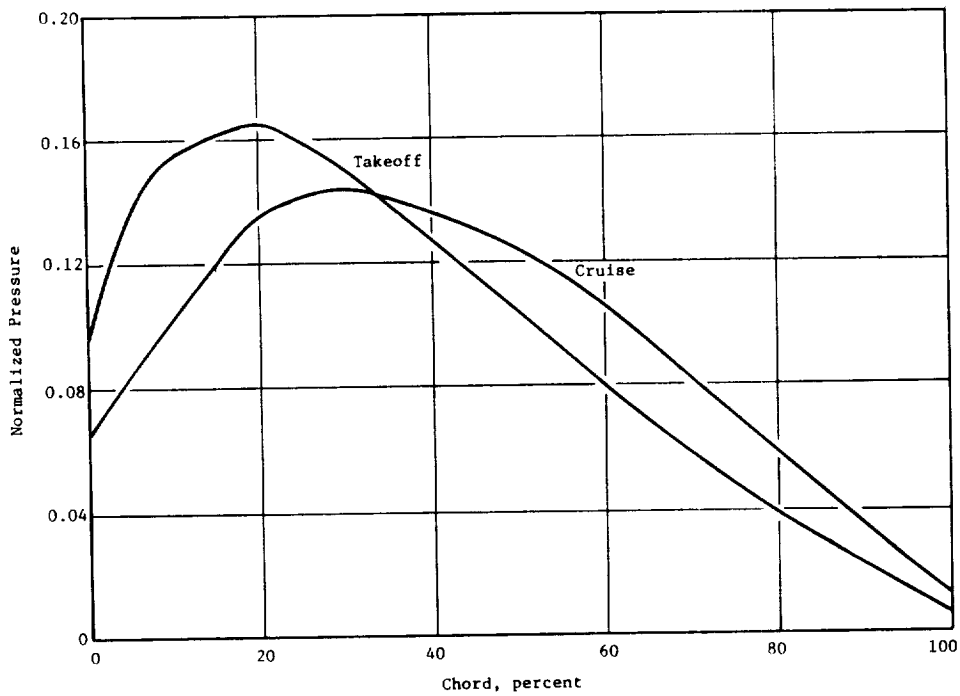
Figure 8-94. The F7/A7 Chordwise Distribution.

Finite Element Solution Technique

An iterative differential stiffening method was used for the cold blade prediction and steady-state stress/deflection analyses of all conditions. Differential stiffening considers the effect of membrane stresses on element bending stiffness, as well as the effect of centrifugal stiffening resulting from the tangential and radial deflections in a centrifugal force field.

Fan blade tip deflections on the order of several inches are common for UDF™ blades. With large deflections, the blades respond nonlinearly; this is due to the presence of nonlinear differential stiffening effects (for example, centrifugal stiffening). To better account for the nonlinear response of the blades, an iteration technique that continuously refines the differential stiffening effect, based on the blade updated deflected shape, was utilized to obtain an accurate approximation of the "large" deflection of UDF™ blades.

192

Cold Blade Shape Iterations

The process of establishing the cold shape of the UDF™ blades, given the desired deflected ("hot") shape such as that defined by the cruise configuration, is summarized as follows:

1. A TAMP/MASS model is created using the hot coordinates and all applicable loadings (centrifugal and air loads)

2. An initial linear solution is performed; calculated deflections are subtracted from the original coordinates; thus, an initial estimate for the cold shape is established

3. A new solution is performed using the estimated cold shape and including any differential stiffening effects

4. The deflections from Step 3 are added to estimated cold shape, determining the calculated hot coordinates, which are then compared to the desired hot coordinates

5. Any variance between the calculated, and the desired, hot coordinates is used to generate a new, estimated cold shape

6. Steps 3 through 6 are repeated until the deflected hot shape closely matches the desired hot shape.

Generally four iterations are required in order to obtain a proper cold shape with a maximum deflection error at the leading edge of the blade tip of less than 0.01 inch.

Final Configuration Analysis

Three conditions were analyzed for steady-state reactions, deflections, and stresses. Based on these reactions, the dovetail stresses were calculated utilizing the in-house dovetail stress-calculation program, CDOVE. The reactions at the blade dovetails are summarized in Table 8-6; whereas, Table 8-7 summarizes dovetail stresses.

Blade deflection, translation, and rotation are plotted in Figures 8-95 and 8-96 for the takeoff/maximum power condition.

Blade isostress plots and spar stress summary are illustrated in Figures 8-97 and 8-98 for the takeoff/maximum power condition. Note that only the takeoff case is demonstrated; this is because takeoff is most severe condition compared to cruise and reverse thrust cases. Based on the blade stress levels

Table 8-6. Blade Root Reactions.

	F7		A7	
	Takeoff	Cruise	Takeoff	Cruise
F_{Tang}	1085.0	727.4	1253.0	853.3
F_{ax}	1399.0	281.7	1321.0	331.7
CF	45940.0	38690.0	42790.0	36050.0
M_{Tang}	861.7	11970.0	6086.0	129.4
M_{ax}	20790.0	5768.0	12730.0	2747.0
Torque	11490.0	7146.0	9817.0	7875.0

Force - lb
Moment - in/lb

Air

Table 8-7. Dovetail Stress (ksi).

	F7			A7		
Location	Takeoff	Cruise	Rev	Takeoff	Cruise	Rev
1	24.0	5.5	36.9	31.3	19.5	39.5
2	40.9	16.0	8.0	17.4	13.9	3.1
3	21.6	32.1	5.5	10.7	15.5	1.0
4	1.4	18.2	35.4	24.6	17.4	35.8
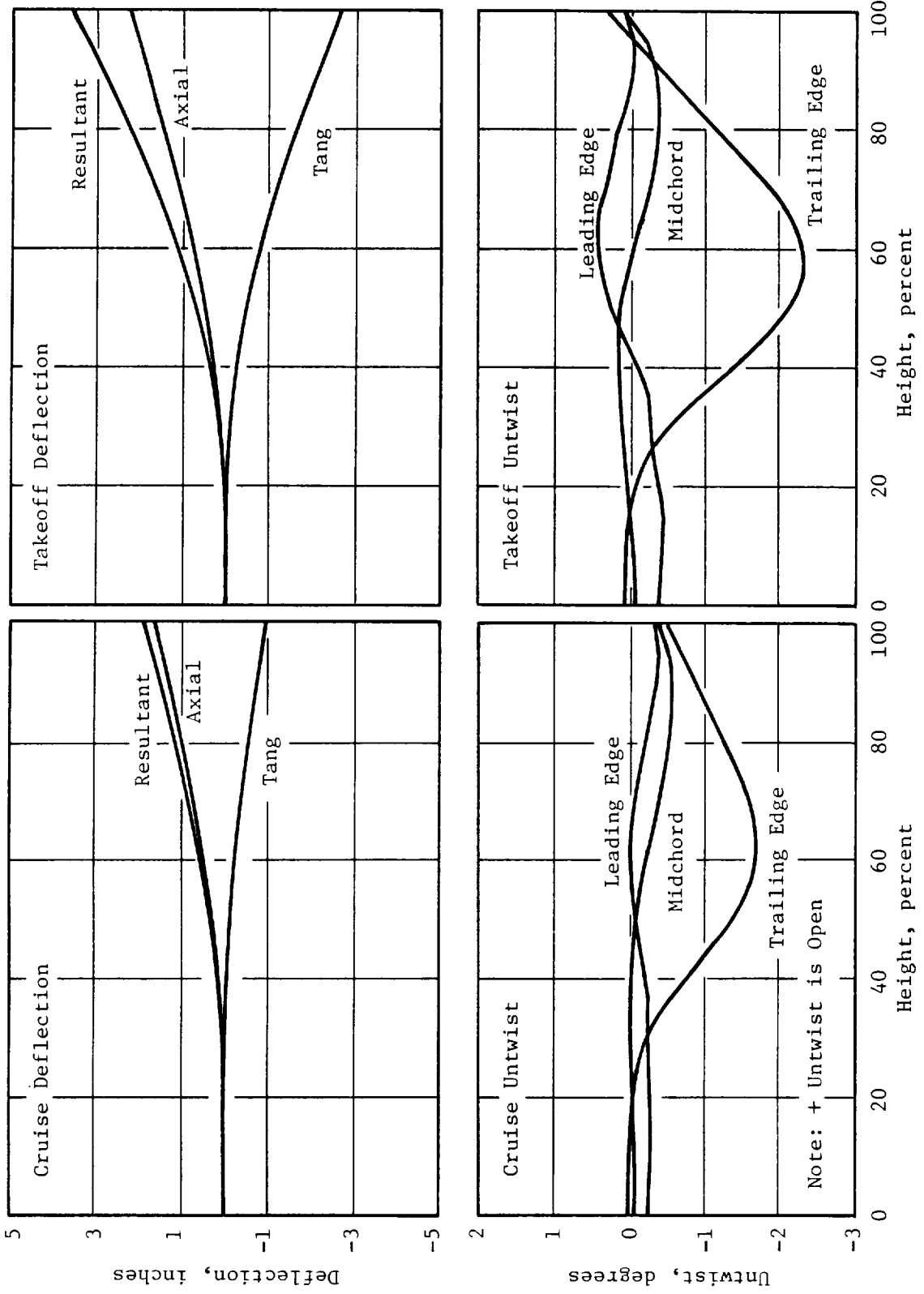
Figure 8-95. F7 Blade Steady-State Deflections.
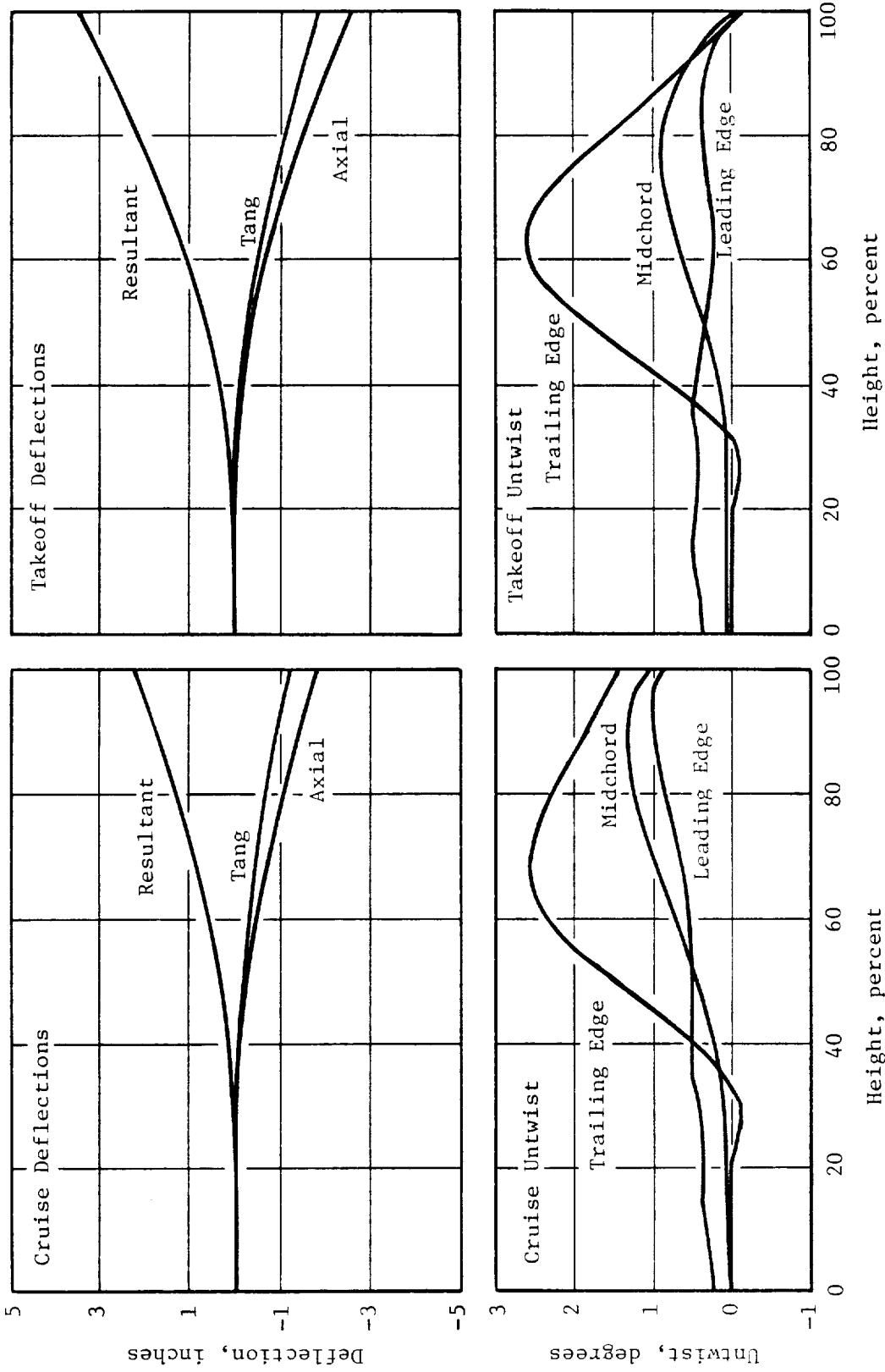
Figure 8-96. A7 Blade Steady-State Deflections.

Tensile

Spanwise	15,400
Chordwise	3,200
Weld	8,100

Surface Shear

Spanwise	2,100
Chordwise	900
Average Cap	92

Spar Stress, psi

Spanwise Stress, ksi

F7 Convex Surface

F7 Concave Surface
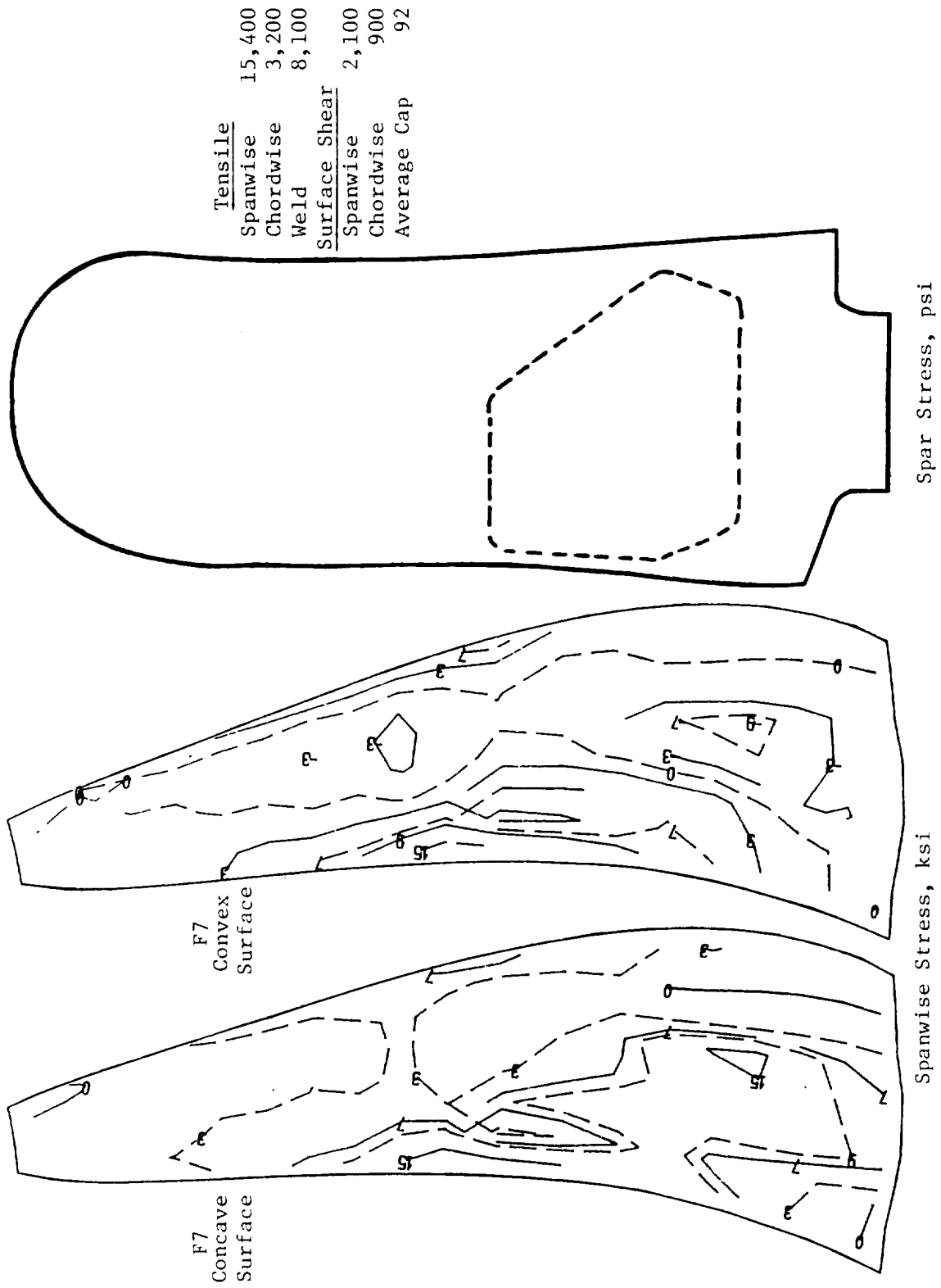
Figure 3-97. F7 Blade Steady-State Stress at Takeoff.

Tensile	
Spanwise	16,900
Chordwise	3,500
Weld	11,700
Surface Shear	
Spanwise	1,830
Chordwise	790
Average Cap	90

Spar Stress, psi

Spanwise Stress, ksi

A7
Left
Convex
Surface

A7
Right
Concave
Surface
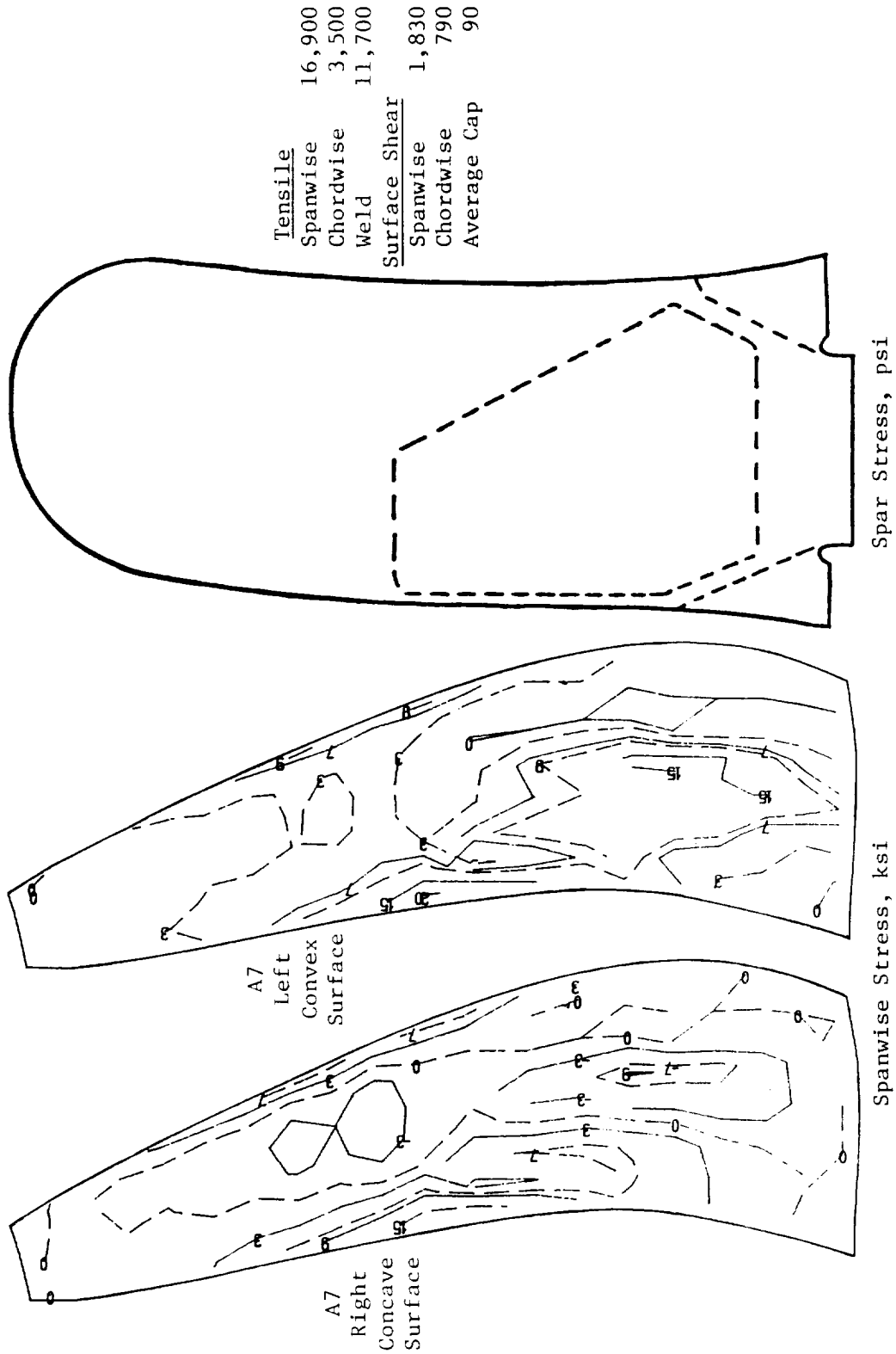
Figure 8-98.   A7 Blade Steady-State Stress at Takeoff.

presented, the designed UDF™ blades will have low cycle fatigue life exceeding 10^5 zero-takeoff/maximum power-zero cycles.

Vibration Analysis

The UDF™ blade frequency/mode shape analysis was conducted for stationary and operating conditions. Because the accuracy of the fan blade stability prediction is highly dependent upon the accuracy of frequency/mode shape calculation, it is imperative to validate the calculation. This validation was performed by comparing the analytical result with bench test results. The frequency/mode shape comparisons are presented in Table 8-8 and Figure 8-99, and show excellent agreement for the first five modes; however, the mode shape agreement for the higher modes is less desirable, although the agreement in frequencies is good. Aeromechanically and aeroelastically, these higher modes are not as important as the lower modes, particularly the first three modes.

Table 8-8. Frequency Comparison Analysis
Versus Bench Test.

Mode	Analytic	Bench Test
1st Flex (1F)	23.5	24
2st Flex (2F)	73.6	73
1st Torsion (1T)	108.6	106
3rd Flex (3F)	154.0	148
2nd Torsion (2T)	176.0	175
3rd Torsion (3T)	291.0	251
4th Flex (4F)	263.0	261
4th Torsion (4T)	384.0	339
5th Flex (5F)	395.0	363
2nd Strip (2S)	408.0	415

Another important parameter in the fan blade vibrations analysis is the influence of the flexibility of the fan blade supporting structures. As shown in Figure 8-100, a finite element model of these supporting structures was
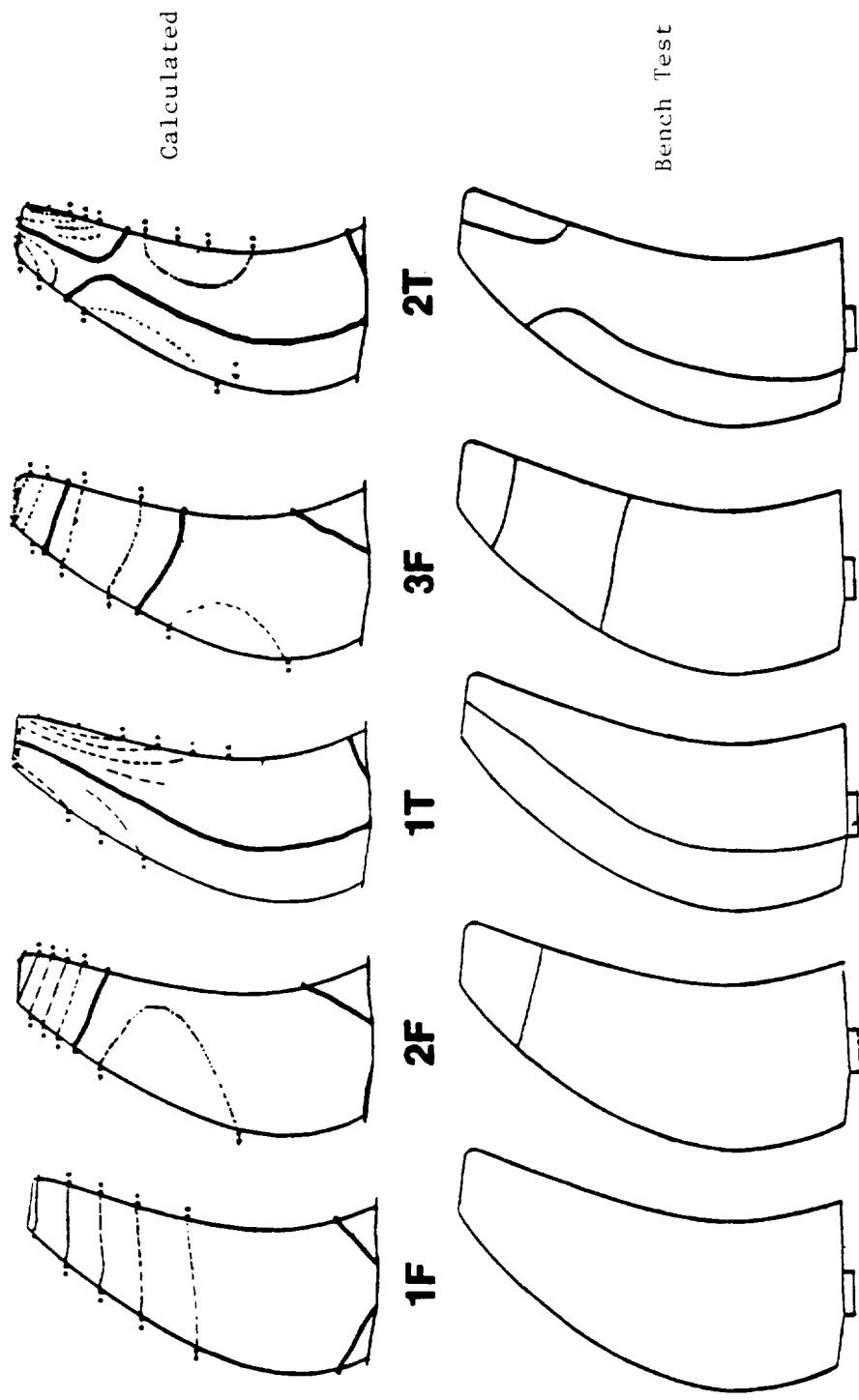
Figure 8-99. F7 Mode Shape Comparison.
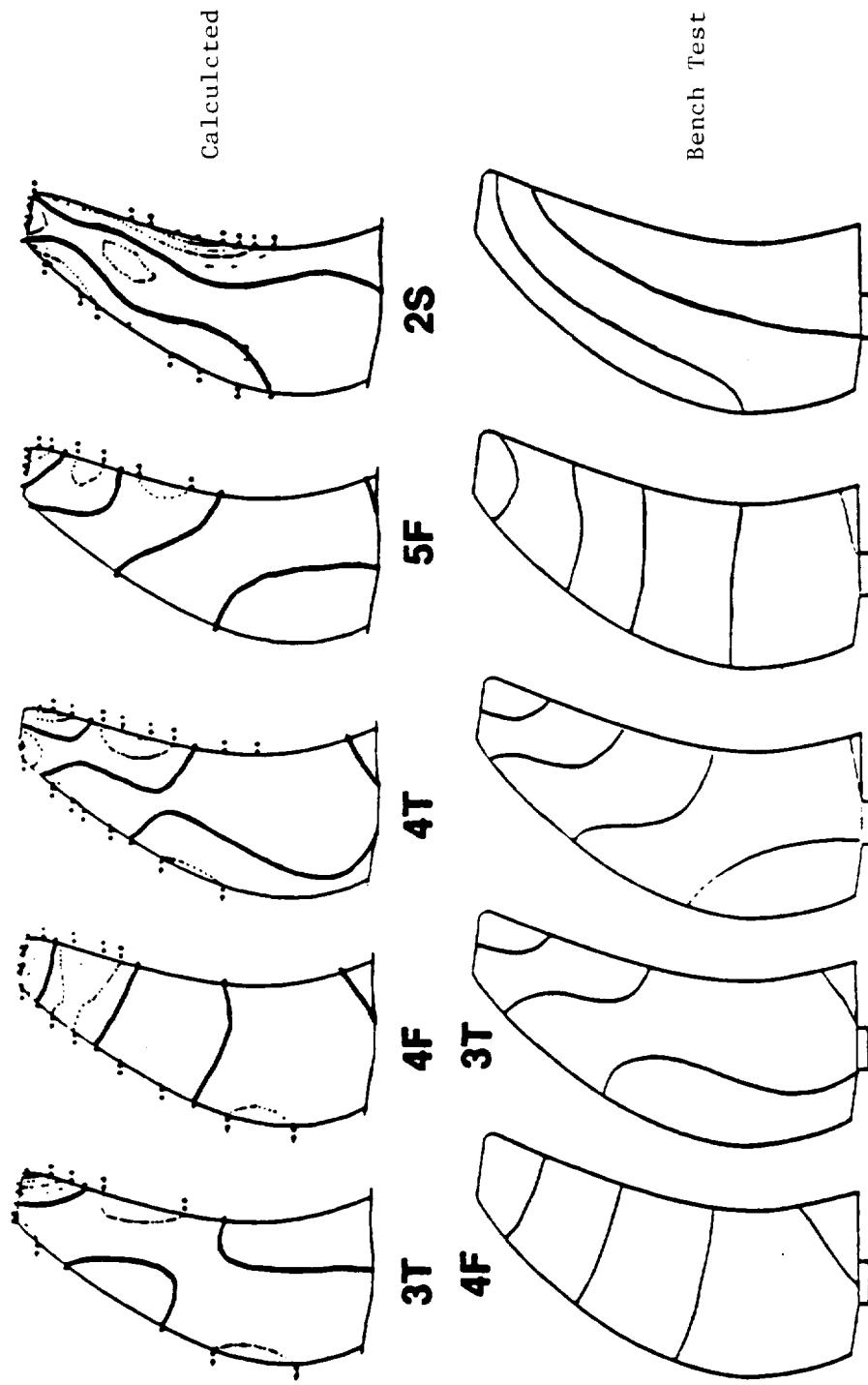
Figure 8-99. F7 Mode Shape Comparison (Concluded).

201

created for evaluating the flexibility. Note that the blade root torsional flexibility resulting from the blade pitch change actuation system was calculated separately from this model. The combined flexibilities arising from the supporting structures and actuation system were then attached to the blade root of the finite element model to calculate fan blade system modes, particularly 2- and 3- nodal diameter (nd) modes. To assess the accuracy in obtaining the blade root flexibilities, ping testing was conducted on the Stage 2 fan rotor assembly, with fan blades installed. Figure 8-101 depicts a sample of the ping test results. The ping test and analytical frequency results are listed in Table 8-9. Good agreement is apparent; this correlation establishes the validity of the blade root flexibility calculation.

Direct Method
(Blade/Hub Ring/Power Turbine
By Beam Model)

Indirect Method
(F E. Blade Model With
Attachment Flexibility Evaluated
From the Model Above)
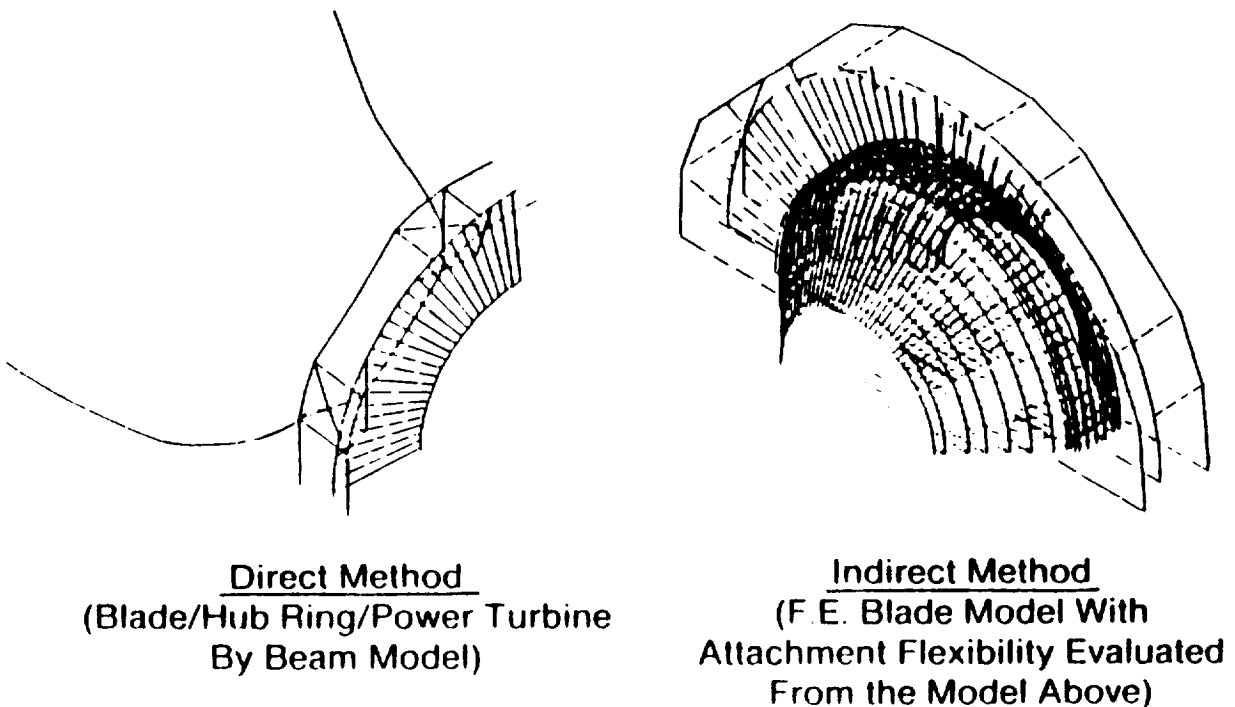
Figure 8-100. System Mode Analysis.

The finite element model for vibration analysis at operating conditions was created from the deflected blade shape at the point; first, a steady-state linear elastic analysis was performed to obtain the blade stiffness matrix, which included the differential stiffening effect arising from the element
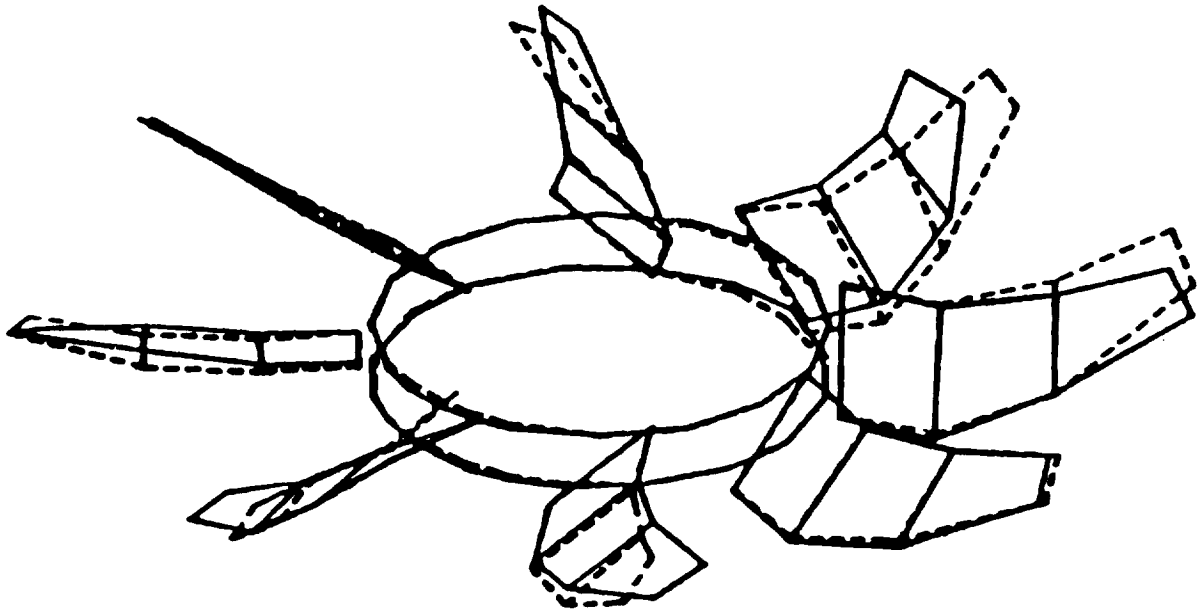
Stage 2 Fan Rotor Assembly

Figure 8-101. The 3-Nodal Axial Mode.

Table 8-9. Ping Test Frequency.

Mode	2-Nodal		3-Nodal		Fixed	
	Analysis	Test	Analysis	Test	Analysis	Test
1F	25.0	26.25	26.0	27.50	29.3	29.8
1A	50.8	49.06	61.4	58.44	---	---
2F	77.0	74.38	74.6	75.94	83.4	83.0
Tests Utilized A7 Blades with no Polyurethane Coat and no Leading Edge Protection						

membrane stresses. The mass matrix, including the vibratory and centrifugal inertia terms, was then combined with this stiffness matrix to form an eigenfunction for frequency and mode shape calculation.

Campbell diagrams of the UDF™ blades are presented in Figures 8-102 and 8-103; these diagrams were constructed based on the calculated frequencies at takeoff and bench test conditions. In these diagrams, the 2-n.d. and 3-n.d. system frequencies were used for the first three lower modes; whereas, other higher mode frequencies were calculated using the rigidly fixed blade root condition. This approach recognized that the higher modes are insensitive to root flexibilities; moreover, for a synchronized system vibration, the root flexibilities rapidly decrease inversely to nodal diameter number.

The diagrams indicate that the frequency margins on the first flex modes are about 10% at takeoff speed, which is less than the design objective of 15% margin. However, it appears to be well tuned for the 16/rev rotor-to-rotor interacting frequency.

It is noted that the root flexibilities of low order nodal patterns will introduce one first axial mode which does not exist in the fixed root condition. Further, the root flexibilities will alter the mode shapes somewhat, as illustrated in Figure 8-104.

Blade-Out Trajectory

The fan blade-out trajectory was analyzed assuming blade root failure; as demonstrated in Figure 8-105, the results indicate that the released blade would barely contact the following blade at the tip region, 90% span, or above. There also would be no contact with the blades of the other stage.

8.3.7 Stability

The objective of the aeromechanical analyses of the UDF™ counterrotating fan blades was to evaluate their stability characteristics in the operating envelope, obtain experimental correlations, recommend corrective actions (if appropriate), and to define a stable, final design. GE's General Aeroelastic Program (GAP), described in Figure 8-106, was used to predict the stability characteristics of the UDF™ blade system. Figure 8-106 represents the general
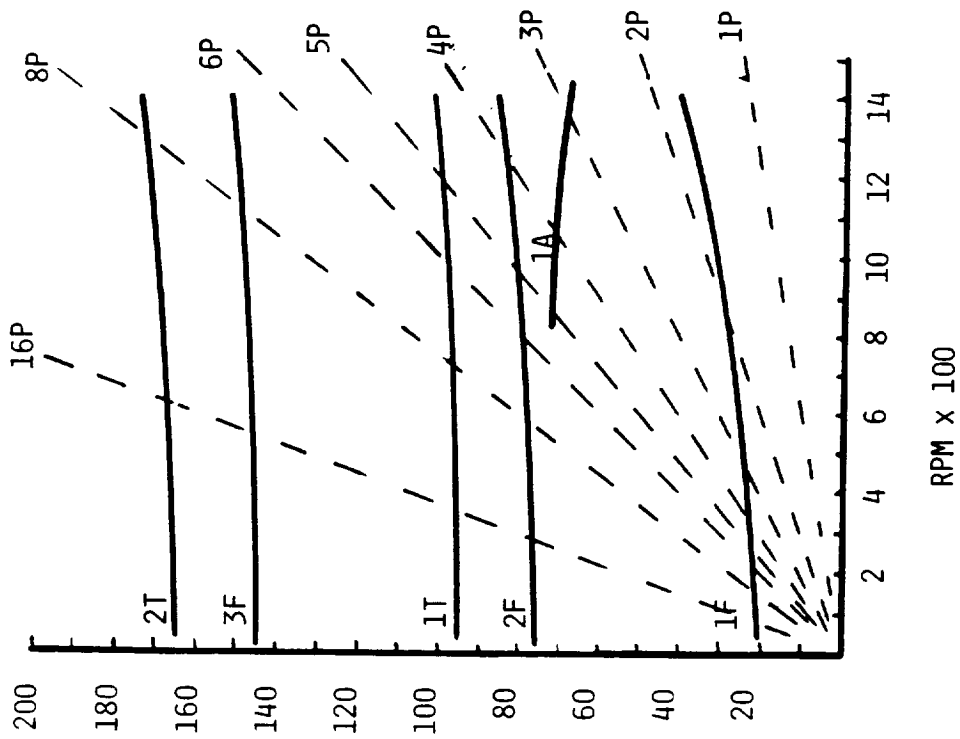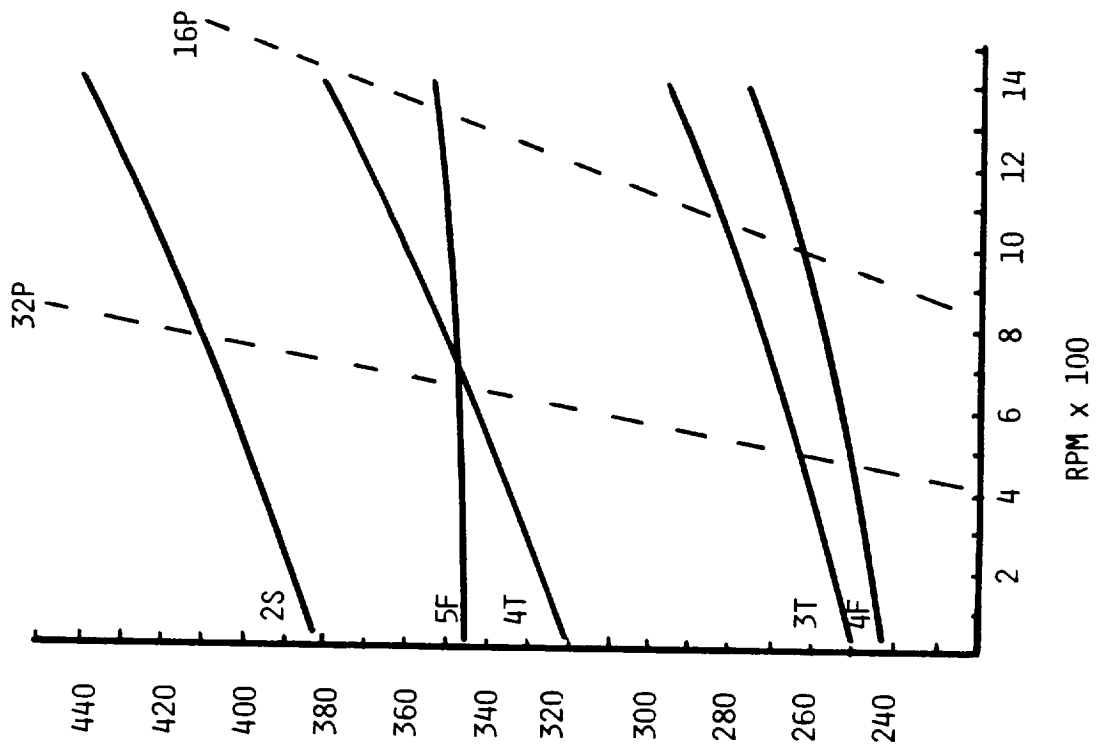
Figure 8-102. Stage 1 F7 Campbell Diagram.
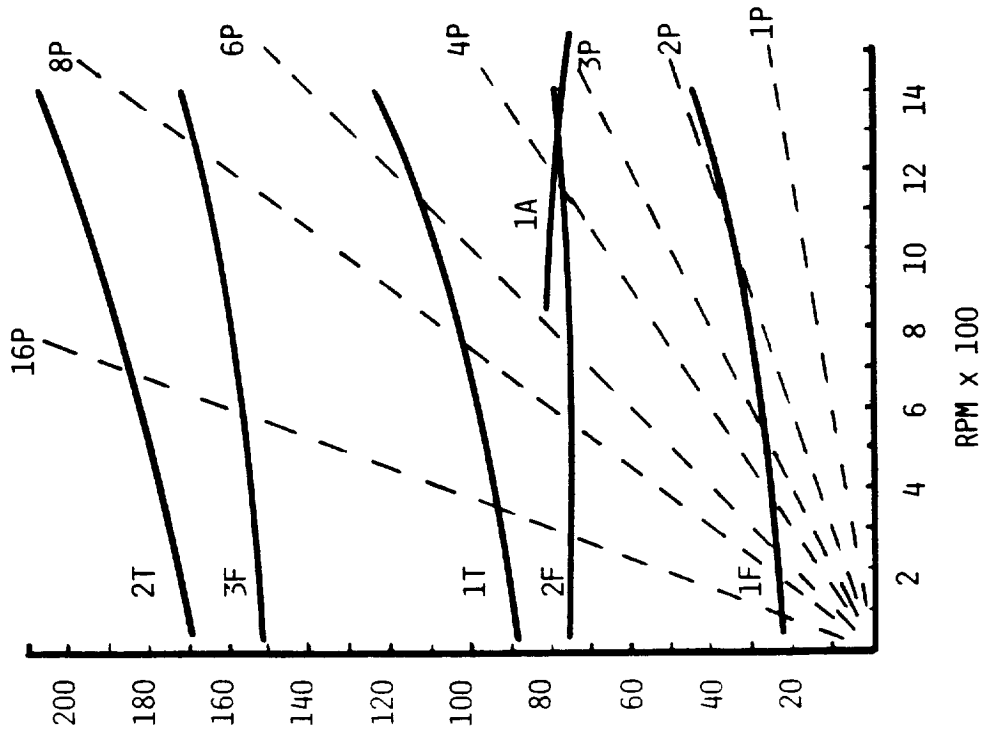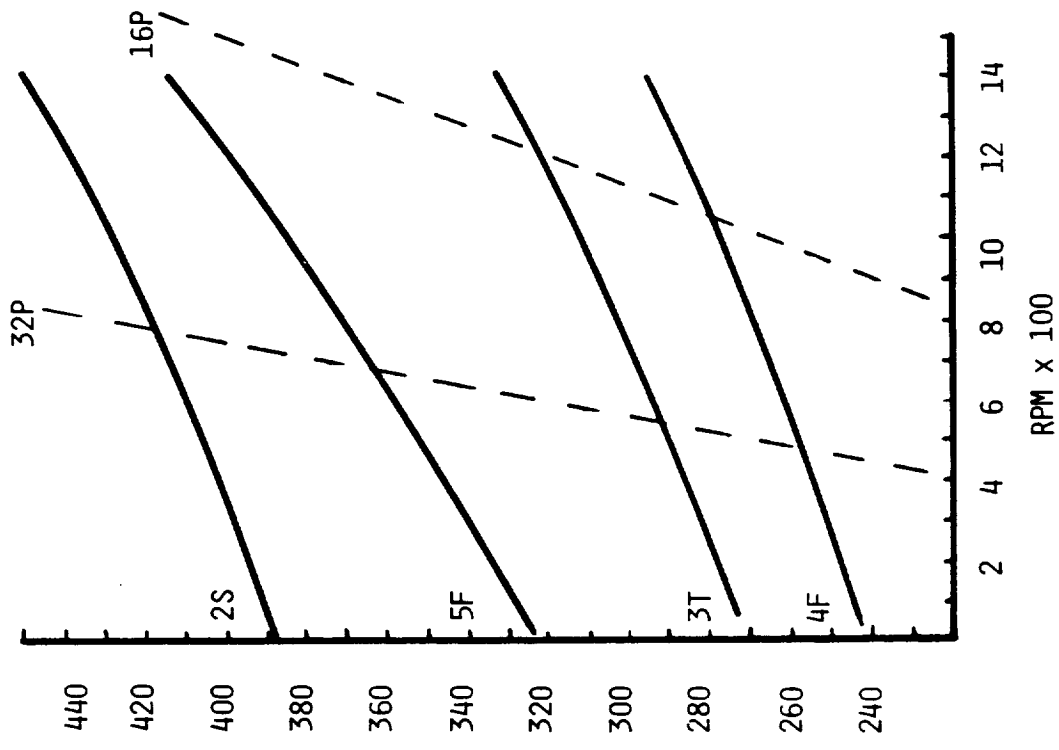
Figure 8-103. Stage 2 A7 Campbell Diagram.

Fixed Hub

| 39.1 Hz | 83.8 Hz | 129.1 Hz | 173.1 Hz |

2-N.D. Spring
Flexibility

| 37.3 Hz | 76.2 Hz | 122.7 Hz | 129.6 Hz |
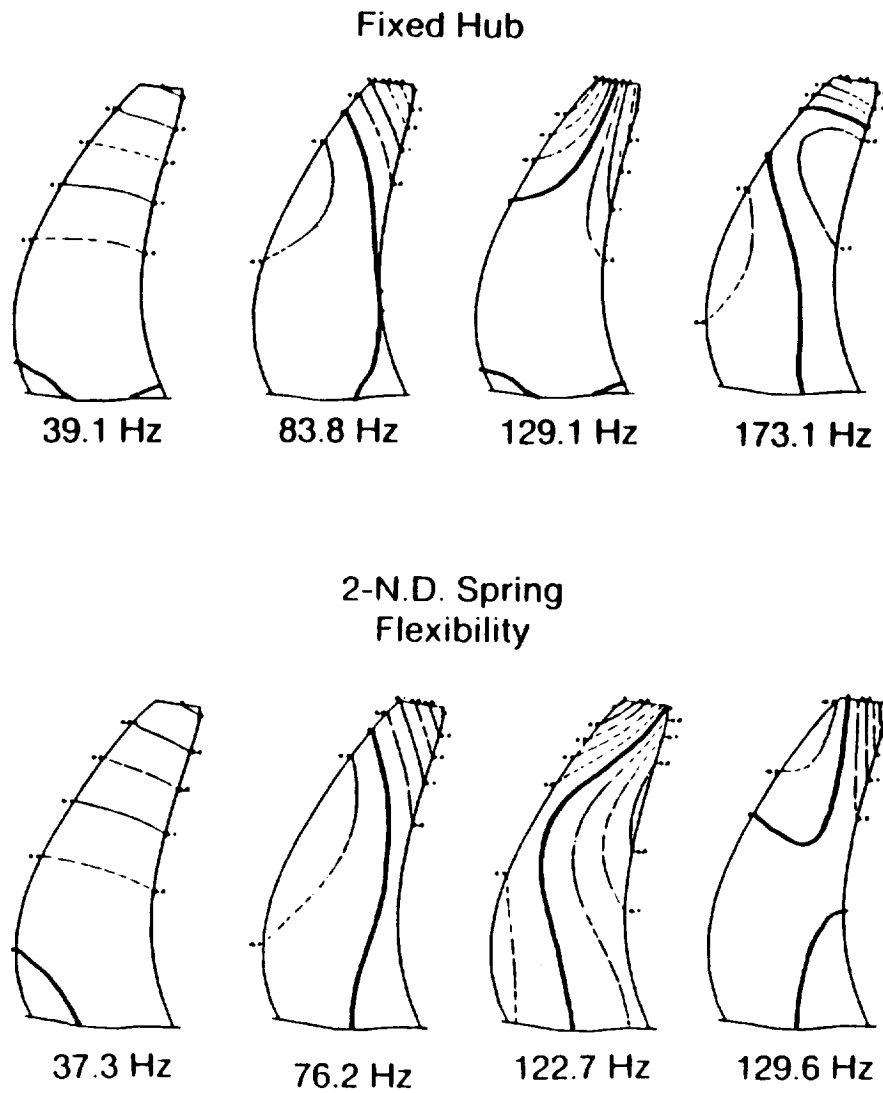
Figure 8-104. Effect of Blade Attachment Flexibilities (F7 Blade).
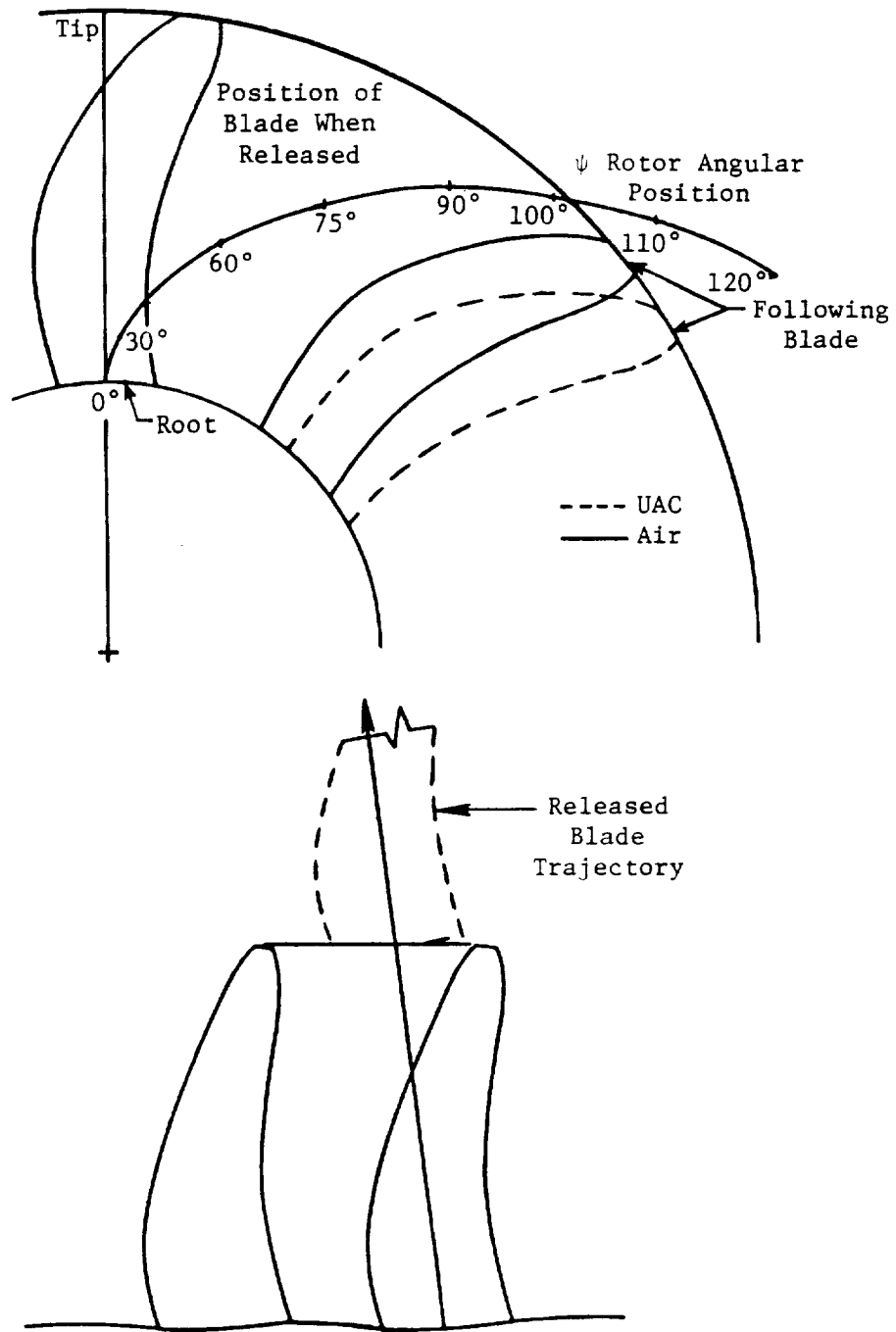
Figure 8-105. Fan Blade-Out Trajectory.
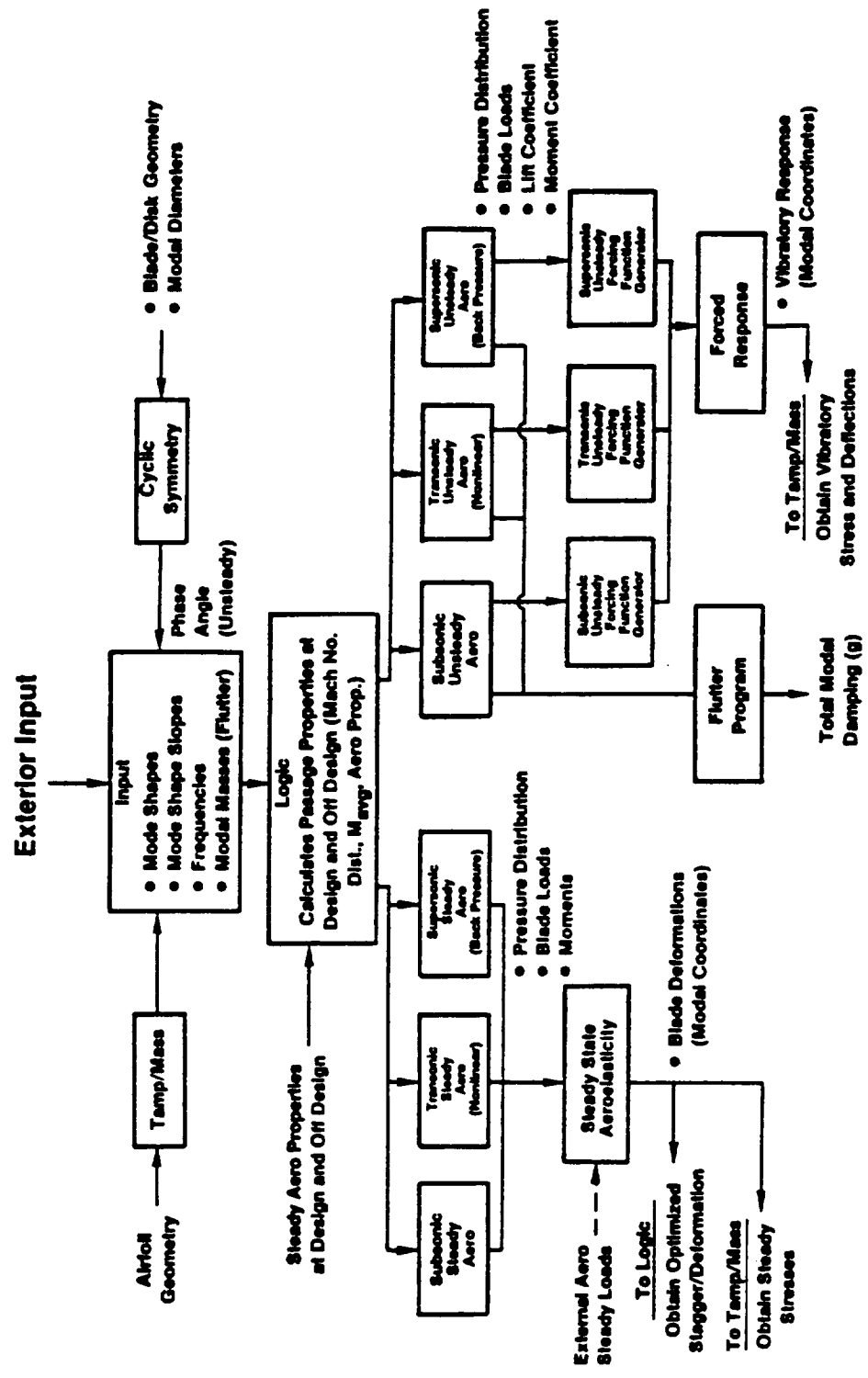
Figure 8-106. General Aeroelastic Program.

network of aeroelastic computer codes which provide flutter solutions, steady-state aeroelastic deformations, and forced-response evaluations. These codes are integrated into a unified system and are fully operational.

The analysis is conducted such that: steady and unsteady aerodynamic programs describe the characteristics of the airflow and its effects in inducing steady and unsteady loads on the airfoil, including frequencies, mode shapes, modal stress distributions, and modal masses. Centrifugal stiffening and aerodynamic stiffening or unstiffening effects are also included. The combined solution techniques utilize results obtained from the aerodynamics and mechanical system programs, in an iterative feedback approach, to predict the required combination of aerodynamic environment and mechanical, geometric, and dynamic properties to be used in the forced-response and flutter prediction calculations.

Utilized throughout this analysis, the modal method is an approximation to the full 3D finite element matrix system of equations, retaining all of the essential characteristics of the blade system. The primary advantage of the modal method is that all parameters required in the stability and forced vibration system of equations can be readily generated without the inversion of large global matrices. In addition, a modal analysis reduces the flutter and vibratory response solutions by orders of magnitude in complexity, while retaining all of its basic features.

The network is basically a linear system, in that linear aerodynamic theories are applied for steady and unsteady modal subsonic, transonic, and supersonic aerodynamic load calculations. Because these are linear programs, semiempirical adjustments have been incorporated through the logic module in Figure 8-106 to account for realistic nonlinear cascade flow field effects, such as thickness, camber, separation at high positive incidence near stall, choke (high negative incidence), and others. This logic module, essentially, accounts for cascade channel passage flow on a semiempirical basis and provides effective Mach numbers and solidities (due to flow separation); it then implements these modified parameters in the steady and unsteady aerodynamics programs for greater accuracy in stability and forced-response evaluation.

There is no smooth transition from subsonic to transonic flow, nor from transonic to supersonic flow in linearized theory, since these three regions are represented by three different assumptions and sets of equations within the linear theory. Consequently, adjustments in the steady and unsteady aerodynamic codes have been made to account for these discrepancies and to provide a smoother transition between these regions.

For unducted, highly swept blades, the effect of leading edge sweep is accounted for by including the factor $\cos \Omega$, where Ω is the local leading edge sweep angle, in the unsteady moment and lift coefficients at each spanwise location. This approach, though equivalent to the more commonly used "normal to the elastic axis" approach, is selected for the following three reasons:

- It does a better job of representing aerodynamic conditions at the root and at the airfoil tip

- It does not arbitrarily impose a Kutta condition at the airfoil trailing edge for flow at low supersonic freestream Mach number

- It is consistent with aerodynamic representations used in fan and compressor airfoils.

To account for the unducted flow at the airfoil tip, the pressure distribution is rolled off by using a $\sqrt{(1-\eta^2)}$ factor where $\eta = 1$ represents the tip.

Table 8-10 shows a correlation between experimental observations from SR3 and SR5 stability tests and the corresponding analytical predictions using the GAP. Analytical predictions, which assumed no structural damping, agree well with the test data.

In addition to correlations with the above NASA blades, GAP was further verified with data from the Scale Model Program (NAS3-24080) as shown in Table 8-11. Here, rather than the previously described single mode instabilities which were encountered in the SR blades, "mixed mode" instabilities occurred in what is usually referred to as "limit amplitude" flutter. That is, the instability occurred in one blade mode shape, at another mode shape frequency, and the stress amplitude did not continue to increase once some limit had been attained.

For example, the first case in Table 8-11 shows that the MPS (A7 - 13° ply) blades, on the aeromechanical hub, experienced an instability in the

Table 8-10. GAP Stability Predictions Versus
Test for SR3 and SR5 Blades.

Configuration	Prediction	Test Results
SR-3 C-X2 22.5° Ply C-3 45° Ply Ti	 Unstable 1F Stable Stable	 Unstable 1F Stable Stable
SR-5 Ti	 Unstable 1F	 Unstable 1F

Table 8-11. MPS Test/Prediction Correlation.

	Prediction	Test Data
A7 - 13° Ply (A/M Hub)	2F Mode at 1A fn = 351 Hz	2F Mode at 1A fn = 380 Hz (Cell 41, Mach 0.25)
A7 - 35° Ply (A/M Hub)	2F Mode at 1A fn = 351 Hz	2F Mode at 1A fn = 380 Hz (Cell 41, Mach 0.25)
A7 - 13° Ply (Fixed)	1T Mode at 2F fn = 336 Hz	1T Mode at 2F fn = 354 Hz (Boeing, Mach 0.6)
F11 (Fixed)	1T Mode at 2F fn = 530 Hz (2n) = 510 Hz (1n)	1T Mode at 2F fn = 540 Hz (NASA, Mach 0.8)
F21 (Fixed)	1T Mode at 1F fn = 523 Hz	1T Mode at 2F fn = 480 Hz (NASA, Mach 0.8)

2F Mode responding at the 1A Frequency of 380 Hz. The corresponding GAP prediction agrees well, indicating the same response at 351 Hz. Therefore, these examples bear out the fact that the GAP has correlated very well in predicting the stability characteristics of unducted highly swept blade systems.

8.3.7.1 Operating Envelope Stability Evaluation

Figure 8-107 identifies the 727/UDF™ demonstrator flight test envelope and the cases where stability analyses were preformed utilizing the GAP; Table 8-12 lists, for each case, the Mach number and altitudes analyzed. The analysis of Case 121, at sea level, is of particular interest, since it corresponds to the conditions tested at the Peebles, Ohio test facility. The GAP analyses proved the third system mode stability estimate to be critical. (The first five modes were included in the analysis.) The analysis further indicates the forward rotor to be more flutter-prone. Figure 8-108 plots the third system mode stability estimate for F7 demonstrator blades for Case 121 at sea level; that is, at takeoff. This figure reveals that the third system mode will be unstable, responding at the first system mode (1S) frequency, if there is no structural damping. Also shown is that if there is 6% structural damping in the system, the blades will be stable. Because these blades were fully tested during the Peebles ground tests and were found to be completely stable, then, by inference, it can be argued that the system has at least 6% structural damping. Consequently, assuming this value for structural damping in the GAP analysis, all cases shown in Figure 8-107 were predicted to be stable, except Case 362 - M_∞ = 0.60 at sea level, further demonstrated in Figure 8-109.

Table 8-12. Demo Flight Mapping (F7/A7).

Case 121	M_∞	=	0.0	H =	0, 5, 10, 15 KFT
Case 307	M_∞	=	0.20	H =	0, 10, 20 KFT
Case 263	M_∞	=	0.40	H =	25, 35, 42 KFT
Case 362	M_∞	=	0.60	H =	0, 10, 15 KFT
Case 318	M_∞	=	0.85	H =	15, 20, 25 KFT
Case 274	M_∞	=	0.85	H =	25, 35, 42 KFT
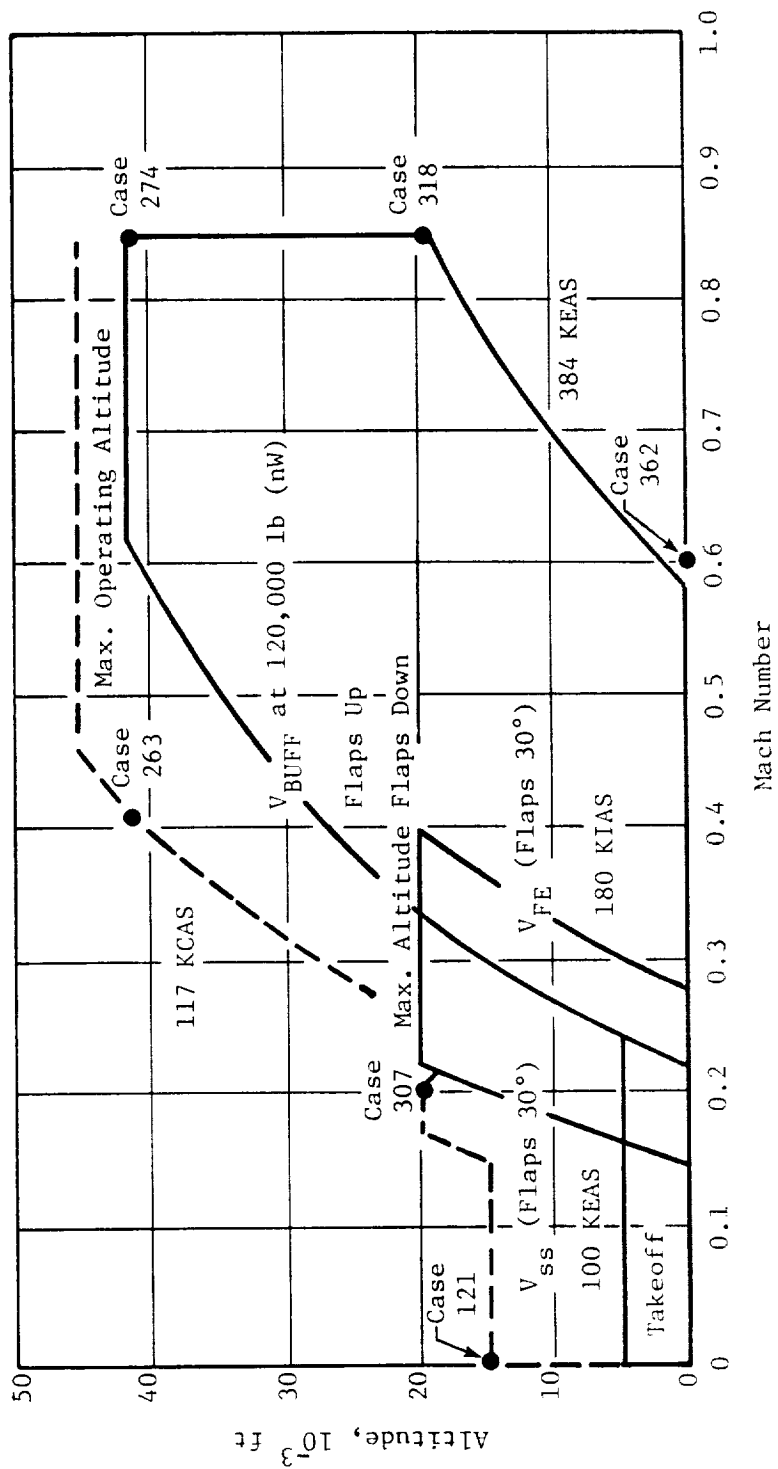
Figure 8-107. 727 Flight Envelope for GE UDF™ Flight Test.
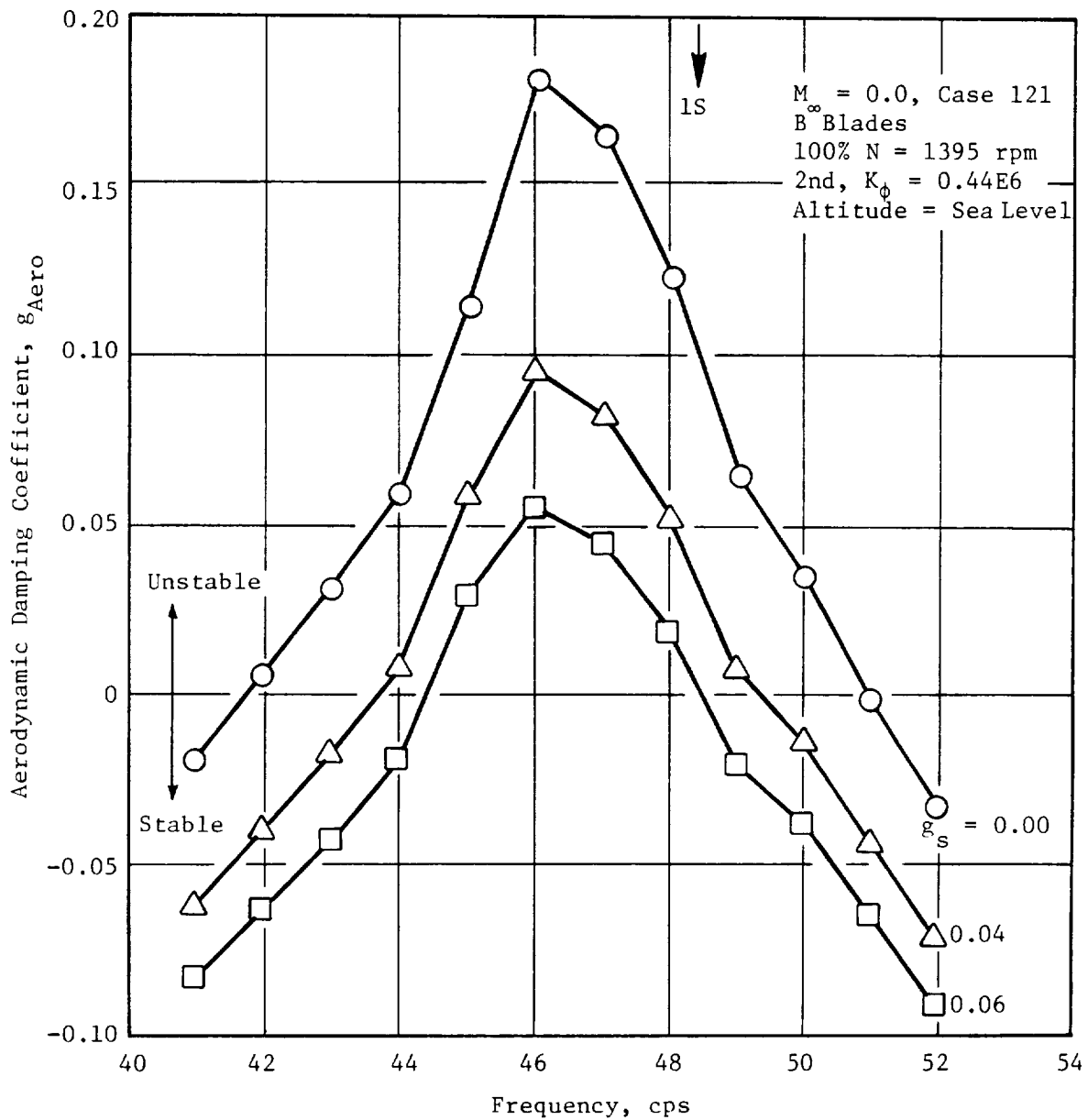
Figure 8-108. Third System Mode Stability Estimate for GE36 Demo F7 Blades, Case 121.
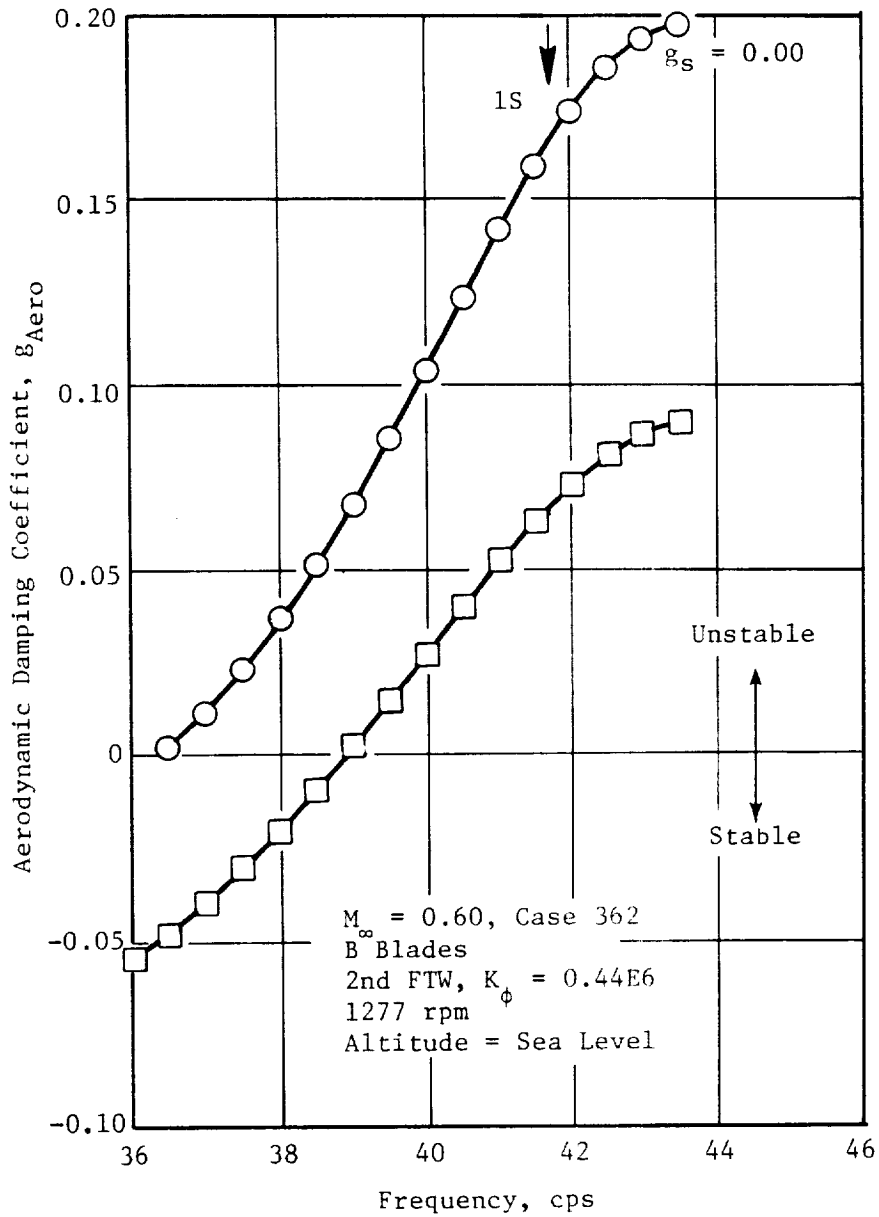
Figure 8-109. Third System Mode Stability Estimate for GE36 Demo F7 Blades, Case 362.

This means there is a region around Case 362 where the UDF™ blades have been predicted to be unstable. (Analyses have shown that the stability of the blading can be improved by either increasing altitude or decreasing Mach number.) As yet, the extent of the predicted unstable region is undetermined. On the other hand, the unstable region around Case 362 tends to be of academic interest only, since flight testing is not planned in this region.

8.3.8 Operational Limits

Scope limits corresponding to fan blade operational strain gage stress limits were defined by lowest allowable vibratory levels among fiber longitudinal, in-plane shear, and spar/shell lap shear. A General Electric in-house computer program (SCOPELMT) was utilized to perform a layer-by-layer analysis to identify the lowest allowable stress levels for each fan blade mode of vibration.

The Goodman diagrams developed from the composite material test program were used for the fiber, matrix, and in-plane shear directions. Minus three sigma values were used in all three cases.

As mentioned, shell debonding must be prevented, in order to prevent spar weldline failures. The static HCF test results indicated that when the No. 4 airfoil gage stress was 23 ksi, the average lap shear stress at the blade root was 805 psi. The Goodman diagram for spar/shell lap shear strength was developed, based on the static vibratory stress of 805 psi and an ultimate stress of 5500 psi, as illustrated in Figure 8-110. Scope limits for the lap shear strength were set at 75% of the endurance limits.

Based on the aforementioned procedures, the engine gage scope limits at takeoff/maximum power conditions were defined as shown in Table 8-13. Among all of the vibrational modes, only the first flex mode would have the limits set by the spar/shell debonding criterion.
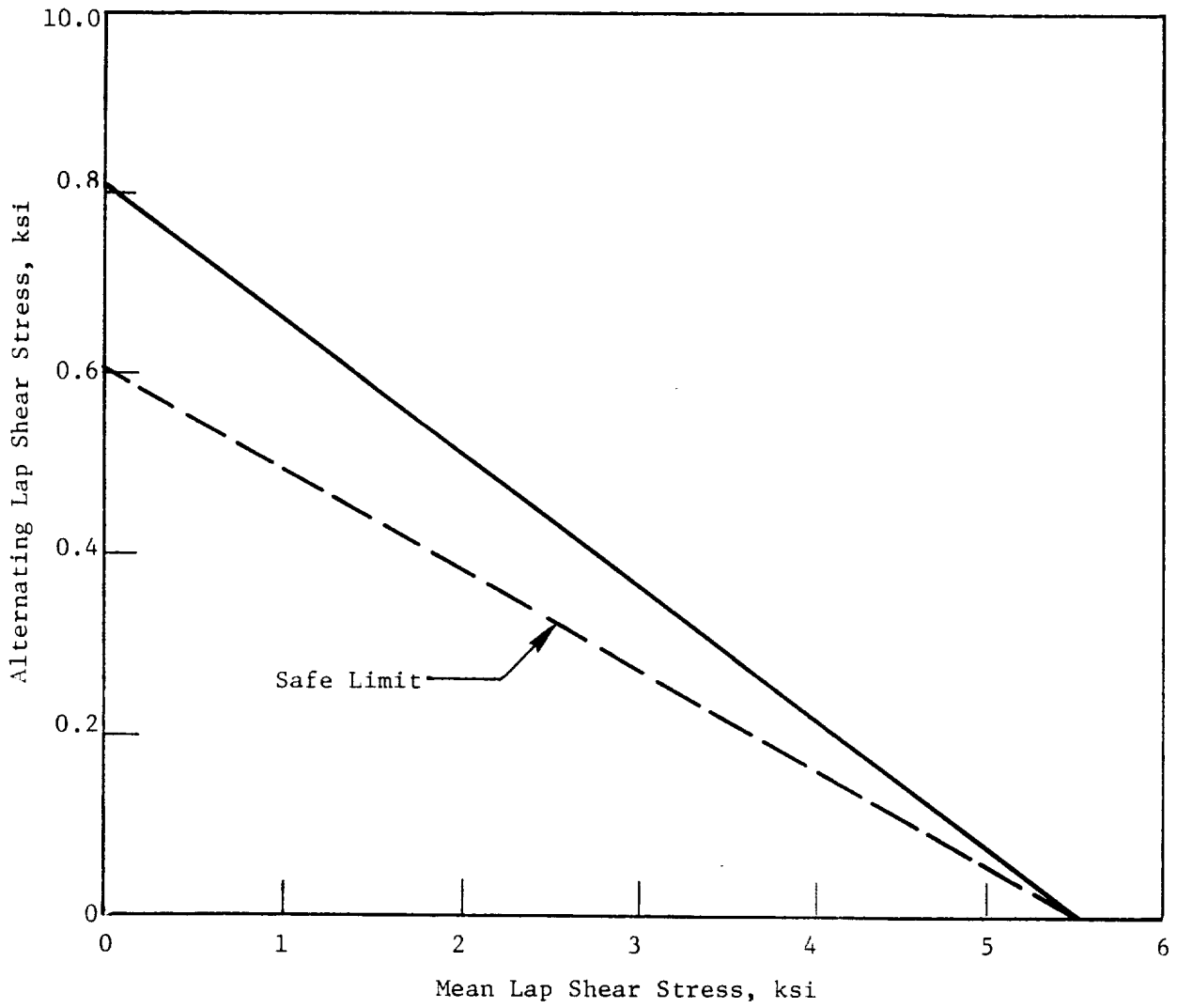
Figure 8-110. Adhesive Goodman Diagram.

Table 8-13. Fan Blade Scope Limits - Results, ksida.

Mode	Gage Location	F7				A7			
		1	2	3	4	1	2	3	4
1		1.4	7.9	8.8	15.0	1.4	4.4	7.7	15.0
2		5.0	25	24	23	5.1	14.6	26.9	19.0
3		3.4	16	8.9	12.7	6.4	19	23	18
4		3.6	6.2	6.8	16	5.6	5.9	4.5	6.0
*		1.8	10	5.3	6.5	4.3	3.3	3.1	1.5

* Higher Mode Near 16/R

8.4 SUMP AND CARBON SUMP SEAL DESIGN

8.4.1 Sump Design

8.4.1.1 Description

The UDF™ propulsor lube system (Figure 8-111) is completely separate from the F404 gas generator lube system. The additional lube system supplies oil to the propulsor, the starter adaptor gearbox, and the lube pump adaptor gearbox. The main components of the lube system are proven accessories "borrowed" from more mature engine programs. The components were modified in size and in flow, as necessary, to function in the propulsor lube system.

The lube system is a dry sump, pressure supply design vented to ambient pressure. The primary lubricant is MIL-L-23699; but, the system is also compatible with 7808 oil used by some military operators. The system is unique in the fact that the sump walls are rotating. The walls have been carefully designed to eliminate oil storage pockets and to direct the oil to the ends of the sump where it is scavenged. Two scavenge lines service the forward end of the sump, and a single large element is used in the aft end of the sump. The oil will reach 1 G at about 57 rpm, where it will begin to cling to the rotating sump walls. The large diameter of the oil seals also serves to make the sump unique. The large diameter is necessary to accommodate the actuation system. Carbon seals are utilized to control the leakage flows to reasonable levels at these large diameters.

Figure 8-111. GE36 Lubrication System.

The lube system components were selected from the F25, CF6-50, (F6-8D, and LM2500 engines. All of the components have a long history of successful operation on the parent engines. Some modifications were made to mount the components and, in some cases, the flows, pressures, and temperatures were not in the same range as the parent design.

The oil tank which was selected was an F25 unit modified to fit under the UDF™ nacelle. The modifications included shortening the unit by changing the end dome to a smaller sphere; the volume capability was reduced approximately 1 quart. The unit was designed to operate at 9.5 gallons per minute (gpm). On the UDF™, the maximum flow rate was 8 gpm, but the air entrainment was higher than F25 design due to the large scavenge elements used on the UDF™. A remote fill unit was designed to pressure fill the tank during long test runs.

The lube pump selected was a Lear Siegler unit used on basically all of GE Evendale's large commercial jet engines. The pump is rated at 16 gpm on the supply side and a total of 34 gpm from the five elements on the scavenge side. A bypass orifice was incorporated in the lube supply line to bypass one half of the supply oil back to the pump inlet. Eight gpm was all the oil that was required for the UDF™ lube system. The pump was driven at design speed (6000 rpm) by a reduction gearbox which replaced the afterburner (AB) fuel pump and control on the F404 gearbox. About 5 horsepower is required to drive the pump.

During subidle operation and on starts, there is insufficient secondary air pressure to seal the aft carbon seal. In addition, the rotating gravity field is not established to pump the scavenge oil to the ends of the sump. For these reasons, a system was designed to bypass oil around the propulsor to the scavenge line during starts and subidle operation. Energized by a digital electronic control (DEC), the system is a failsafe design that cannot prevent oil from reaching the propulsor during high power operation. During normal operation, the supply system is completely normal except for a 3-psid check valve used to bias the oil toward scavenge when the bypass valve is open.

Oil is supplied to the propulsor bearings using controlled orifices to achieve the desired flow rate. Both jet and under-race lubrication are used. The bearings are of every variety: inner-race static, outer-race static,

counterrotating, and some even move axially with the actuation system. All bearings receive a positive supply of lubrication. The supply system is also designed to provide the necessary cooling flow to the bore rubbing circumferential carbon seals at each end of the sump. Splines and actuation gearboxes are mist lubricated in the sump. Outer actuation gearboxes and bearings are grease packed.

Both ends of the propulsor sump are scavenged. Three elements are used, with a total capacity of 22 gpm. The starter gearbox and sump adaptor gearbox are also pump scavenged. Pump scavenge elements are equipped with screens and magnetic chip detectors to monitor for oil contamination. After the scavenge pump, the oil is filtered with a CF6-50 scavenge filter using 15 µm filter elements; the filter normally operates at 16 gpm on the CF6 and is operating at about half the flow on the UDF™. It is equipped with a 2 pressure alarm to indicate clogging.

Scavenge oil is then air-cooled using a CF6-80 integrated drive generator (IDG) air cooler which mounts on the bulkhead between the gas generator and propulsor, and the air flow is powered by the pressure drop between the core compartment and the fan inlet. On the CF6-80, the unit operates at 12 gpm and removes about 1000 Btu per minute. The UDF™ oil flow is 8-gpm maximum, giving an oil-side pressure drop of 2 psid. Analysis has shown that the UDF™ sump transfers heat to the secondary at ground idle (GIDL) and low power. At high power, sufficient fuel flow is available to keep the UDF™ oil-cooled in the fuel oil cooler alone. As soon as tubing is available, the air/oil cooler will be removed, and the engine tested to confirm the analysis.

The majority of oil cooling is accomplished in a CF6-50 fuel oil cooler. The fuel has already passed through the hydraulic oil cooler where its temperature has increased about 100°. The fuel picks up an additional 20° to 30° across the fuel oil cooler. In fact at low power, the fuel is cooled with oil from the UDF™. The cooler was designed for 16 gpm; with the UDF™ flow (about half), the scavenge line pressure drop is about 10 psid. The scavenge oil then returns to the tank through a swirling air/oil separator. The de-aerator uses the scavenge pressure to swirl the scavenge oil, and the air is removed from the center of the vortex. The vent air is routed through another separator in the pump adaptor gearbox and then through a static separator under the

nacelle. The vent is ducted to the pylon and exits outboard of the fan at the pylon trailing edge. Engine test reveals that the vent air is ingested by the fan, and streams through at about fan pitch line for sea level static (SLS) operation.

8.4.1.2 Function

The primary function of the lube system is to cool and lubricate the main engine and actuation bearings in the propulsor. The propulsor sump contains four main bearings and three large actuation bearings; the oil supply is sized for minimum heat generation; too much or too little oil will increase the heat generation and the oil temperature rise across the sump. The oil also cools the sump walls and removes the heat generated by the bore rubbing carbon seals at either end of the sump. No dedicated oil is supplied for the sump walls; instead, only oil that already has been used to lubricate the bearings is used for sump wall cooling. However, actuation gearboxes and splines are splash lubricated.

The No. 2 roller (2R), although associated with the Stage 2 fan, but the forward roller in the sump, is under-race lubricated through the shaft. The inner race rotates; the outer race is mounted on the mixer frame. The other main roller bearing, the No. 1 roller (1R), is the same part. In this case, it is used as an intershaft bearing, so the DN is double. The 1R bearing is lubricated in a similar manner, using under-race lubrication which must cross the shaft twice due to the shaft configuration (Figure 8-112).

The No. 1 ball bearing (1B) is an intershaft counterrotating bearing. Oil supplied from a jet in the sting tube to the inner shaft for under-race cooling. Chamfers and slots feed oil through the inner race to the rolling elements. The No. 2 ball bearing (2B) is also under-race lubricated, with oil supplied by a dedicated jet in the aft sump wall. These features are depicted in Figure 8-113.

The outer race is static. Oil travels through the inner race in the same manner as 1B. Each ball bearing receives about 2 gpm of oil; whereas, rollers receive approximately 1 gpm at maximum speed. Each bearing receives oil from at least two orifices to insure the flow in case one of the orifices becomes contaminated.
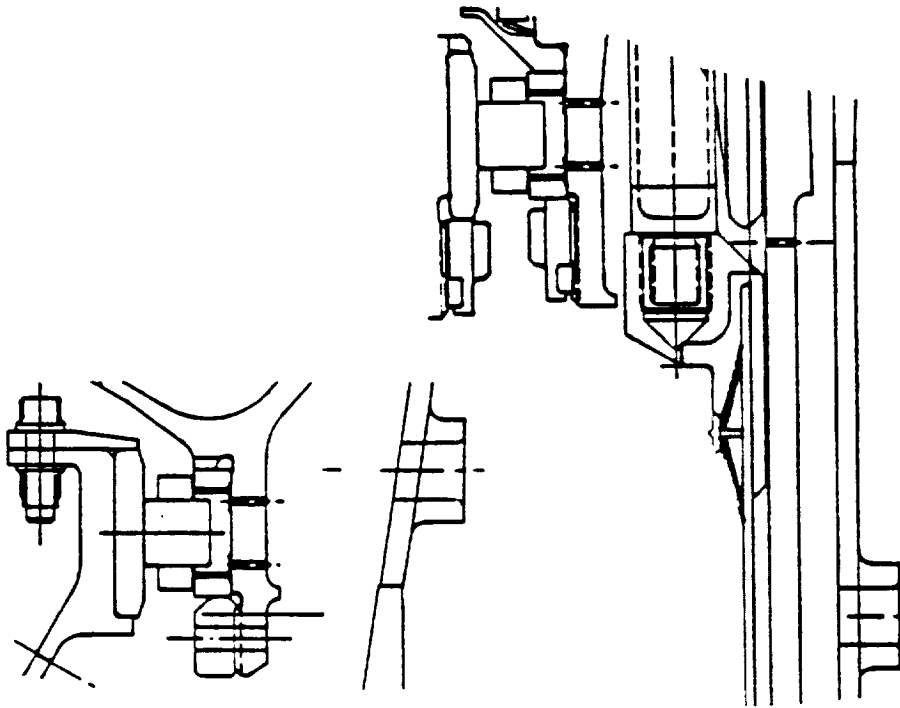
- Inner Race Riding Cage
- Under Race Cooled
- No Dedicated Cage Land Cooling
- No 2R
  - Dedicated Lub Jets (2)
  - Shaft Manifold and 2 Sets 48 x .062 ϕ Holes
  - Inner Race Manifold and 2 Sets 20 x .040 ϕ Holes
- No 1R
  - Dedicated Lube Jets (2)
  - Shaft Manifold and 34 x 062 ϕ Holes
  - Inner Race Manifold and 2 Sets 20 x .040 ϕ Holes

Figure 8-112. Main Shaft Roller Bearing.
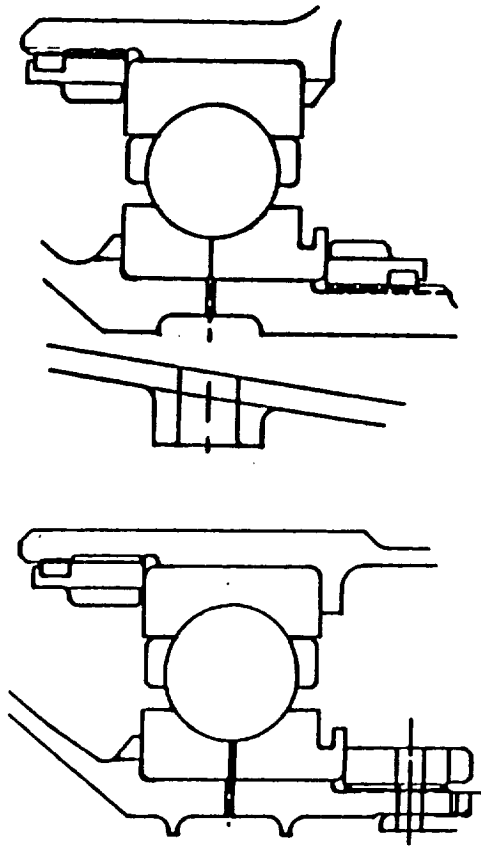
- Under Race Cooling
- Dedicated Lube Jet (2) Both Locations
- No 1 B
    - Shaft Manifold and 40 x .062 ϕ Holes
    - Inner Race Chamfer and 40 Slots
- No 2 B
    - Shaft Manifold and 46 x .062 ϕ Holes
    - Inner Race Chamfer and 40 Slots

Figure 8-113. Main Shaft Thrust Bearing Lubrication.

Lubricated through the push rods that move the actuation system, the 2A and 3A actuation ball bearings move with the actuation system. Two lube jets are provided for each bearing; in these cases, the inner rates are static, and the rage and balls distribute the oil. The 1A actuation bearing is an inner shaft bearing, and the oil is supplied under race and through the inner shaft. Since this bearing also moves with the actuation system, the moving actuation spline is utilized to deliver the oil axially to the 1A bearing as illustrated in Figure 8-114.

Most of the oil delivered to the sump is directed toward the forward end of the sump by the configuration and the rotating walls of the sump. All of the wails are tapered to deliver oil to the ends of the sump when the rotors are turning. This scavenge oil cools the bore-rubbing carbon seals. The sump is provided deflectors to prevent the oil from reaching the inner-shaft carbon seals, which are designed to run dry on air films only (thus, no rubbing or heat generation). All bearings have vent areas around the outer race so that no scavenge oil can contaminate the bearing from the loss of another bearing in the sump.

8.4.2 Carbon Sump Seal Design

The primary seals of the propulsor sump are carbon seals which are used to seal between the two rotors at two locations, and at eight locations around the radial fan blade actuation rods. The types of carbon seals employed are: air-bearing piston ring intershaft seals, circumferential bore-rubbing seals, and magnetic face seals. Unique features of the seals are the large diameter, of the intershaft and circumferential seals, and the high gravity field of the magnetic seal. A description of the seal features is presented, together with the methodology and results of the design analyses.

8 4.2.1 Design Procedure

Despite the detailed steps, a straightforward design approach is utilized for the seals. Unfortunately, a tradeoff of several parameters must be made, and the design methodology becomes an iterative process to find the optimum combination of parameters. For each of the seals, the basic goal was to minimize seal airflow while meeting the life, weight, and stability criteria.

226
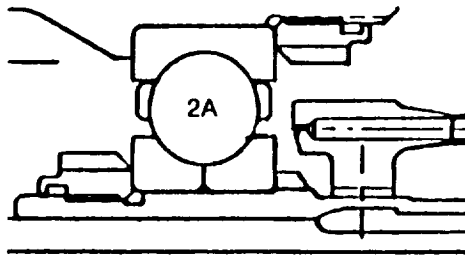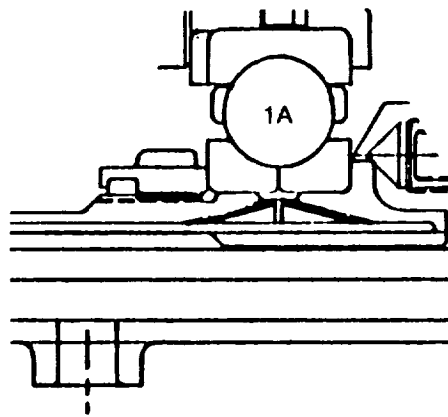
- No 1A Under Race Lubricated
  - Oil Path
  - 2 Lub Jets in Stingtube, Manifold,
    Manifold in Actuation HSG, Holes,
    Holes in Shaft and Slots in Bearings

- No 2A and 3A Jet Lubricated
  - Targeted Between Inner Race (Stator)
    and Cage
  - Two Lube Jets (3 O'Clock and
    9 O'Clock)
  - Supplied Through Actuation Rods
  - Supply Moves With Bearing

Figure 8-114. Actuation Bearing Lubrication.

Intershaft Seal

Studies conducted and implemented in the tradeoff to met these design criteria were as follows:

- Distortion of the carbon element, races, shafts, and retention system due to the centrifugal, thermal, pressure, and friction forces

- Sensitivity of the carbon element force balance to insure minimal wear

- Airflow sensitivity to obtain performance prediction

- Hydrodynamic lift pad geometry optimization for low power force balance

- Mechanical stability sensitivity to operational and geometric parameters

- Acoustic stability to assure no selfexcited vibration problems.

The starter gearbox shown in Figure 8-115, and the pump adaptor gearbox, depicted in Figure 8-116, are lubricated from the propulsor lube system. The starter gearbox (not pressurized) contains a jet-lubricated ball/roller combination. It is vented to the air/oil de-mister, and the same vent line is used to reclaim oil separated from the vent system.

The pump adaptor gearbox contains four bearings and one gear mesh, all of which are jet lubricated. The carbon seals are pressurized with fan discharge air; the input shaft is used as an air/oil separator for vent air from the lube tank. The separator spins at 26,000 rpm and is sized to handle approximately 30 scfm efficiently. The gear ratio of the adaptor gearbox is sized to obtain 6,000 rpm at the pump at a core speed of 16,810 rpm. This is the design point of the CF6 lube pump.

During initial testing the UDF™ was run at subidle speeds for extended periods of time. The pressure available to seal the aft carbon seals was too low to adequately contain the oil. The scavenge pumps require a minute or two to establish a steady scavenge flow, and the oil puddle in the bottom of the sumps at startup and shutdown requires a minimum speed to distribute uniformly around the rotating sump walls. These off-design conditions resulted in the

3.750 ϕ

O-Ring
J221P132

O-Ring
J221P126
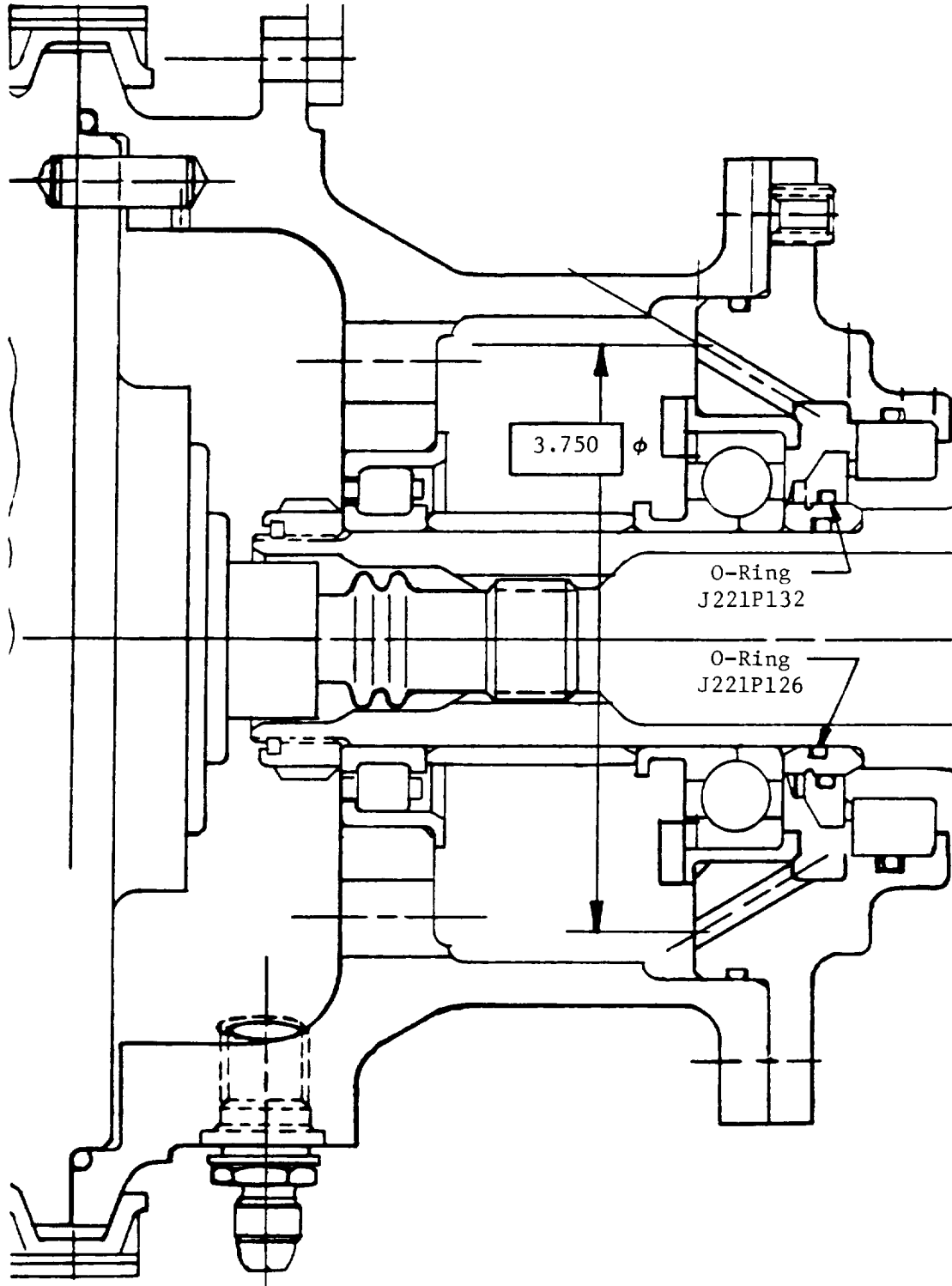
Figure 8-115.   Starter Gearbox.

From Mixer
Frame ➤

RPM – 26753
OD – 225
ID – 0.9
Holes – 24 at 0.87

To
Pylon
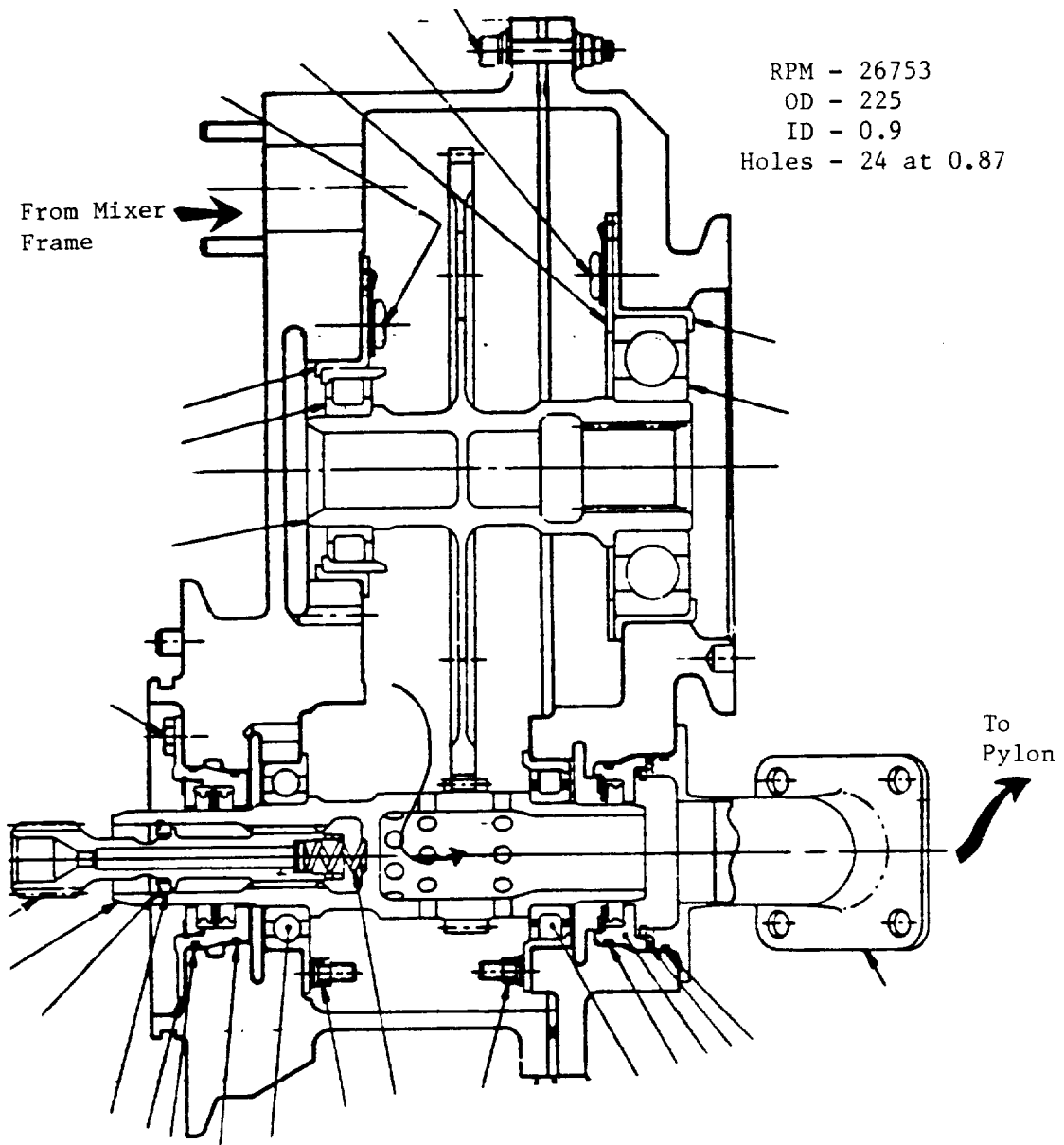
Figure 8-116. Pump Gearbox, Air/Oil Separator.

loss of oil into the turbine rotors and smoke on hot shutdowns. Testing at 700 rpm idle speeds corrects the steady-state problems.

To improve the transient startup and shutdown oil loss, an oil bypass system was designed that utilizes a solenoid valve that is controlled by the DEC. The valve is normally closed; however, when the DEC is powered up, the valve is opened, and the supply oil is bypassed directly to the oil scavenge circuit. As soon as the DEC detects ignition and core speed, the valve is closed, and oil flows to the propulsor. On shutdown the valve is opened as soon as ignition is lost, and the valve stays open until the DEC is shut down. A 3-psid check valve was added to the supply line to bias the oil flow toward the scavenge side when the valve is open (bypassing). Not all of the oil is bypassed, however, and a failed valve cannot destroy the bearings before a low oil-pressure alarm shuts down the engine test.

Stationary Circumferential Seals

Studies conducted and used in the tradeoff are described as:

- Distortion of the seal housing, carbon elements, shafts, and housing supports due to operational loads

- Force balance and heat generation of the carbon element

- The stability of the carbon/springs and housing/shaft to rotor vibrations

- Wind-back performance.

Magnetic Sump Wall Seals

Little analysis was conducted on the magnetic sump wall carbon seals. Engine testing will provide insights as to leakage and wear characteristics. Due to the operating conditions and the similarity to seals used in gearboxes, no significant wear or leakage is expected.

8.4.2.2 Detailed Description

Intershaft Seals

Sealing between the rotors is accomplished by the air-bearing piston ring intershaft seals which consist of a single carbon piston ring that operates

between two AMS 6322 races. The outside diameter (od) of the two seals is: 21.4 inches and 16.5 inches, large for aircraft carbon seal applications. The intershaft seal configuration is detailed in Figure 8-117. In operation, the carbon ring rotates in the direction with the od shaft, while the two races and carbon spacer rotate in the opposite direction with the id shaft. A coil spring in the carbon ring sawcut provides a radial preload to assure that the carbon rotates with the od shaft. The axial load on the seal components is controlled by a Belleville spring that maintains adequate clamp, while allowing the parts to slide, thus minimizing distortion due to friction. The carbon element is pressure balanced with hydrostatic pockets and hydrodynamic lift pads. This pressure balance permits the carbon ring to float between the two seal races when the carbon and races rotate in opposite directions. In theory, the carbon element should never rub on either face, and the only wear should be on the outer diameter as the seal adjusts to relative axial growth between the rotors. Figure 8-118 identifies the forces acting on the carbon element and provides a typical force balance diagram. Force balance diagrams were generated for several operating conditions.

The frictionless equilibrium point is the point on Figure 8-118 where the closing total force equals the opening closing force. The actual seal operating clearances will vary slightly from this point, due to friction, wear, and geometry effects.

Distortions of the carbon element, races, and shafts due to centrifugal, thermal, pressure, and friction forces w determined and evaluated to be within the seal operating clearance. The distortion analysis, the results of which are summarized in Figure 8-119, determined the overall size of the seal cross section and provided the hydrostatic pocket size envelope.

Figure 8-120 illustrates a typical airflow characteristic for the seal. The curve indicates that the total airflow through the seal, for a given total seal clearance, is fairly insensitive to small variations in the equilibrium point. The airflow characteristic curve was generated for several operating points.

Rayleigh hydrodynamic lift pads are used for force balance at low power operation when the seal pressure differential is low. The tapered/sloped pads

232

Forward Seal

Chrome Plated
Inco 718

USG 67

410SS

B5F5

8740

Aft Seal

Oil Side Race

OD Shaft

Carbon Ring

Spacer

17-7PH

Belleville Spring

17-22PH

Air Side Race
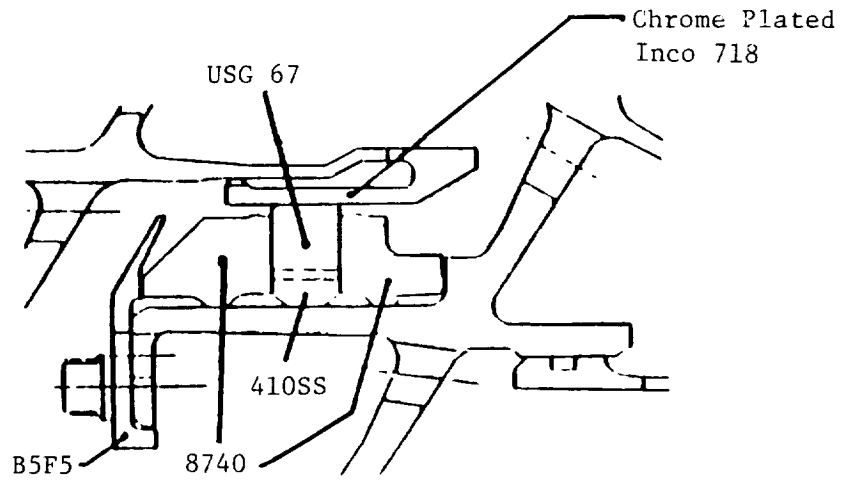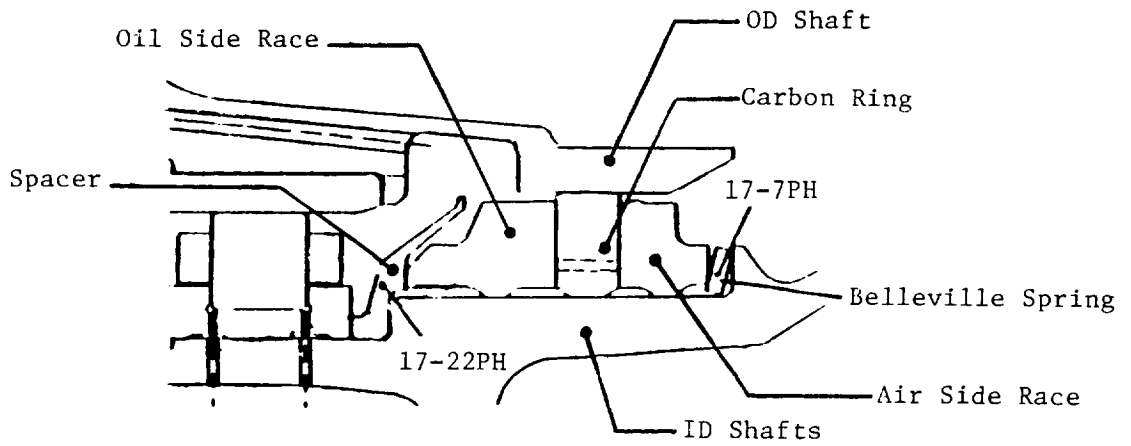
ID Shafts

Figure 8-117. Intershaft Seal Configuration.

Carbon Forces
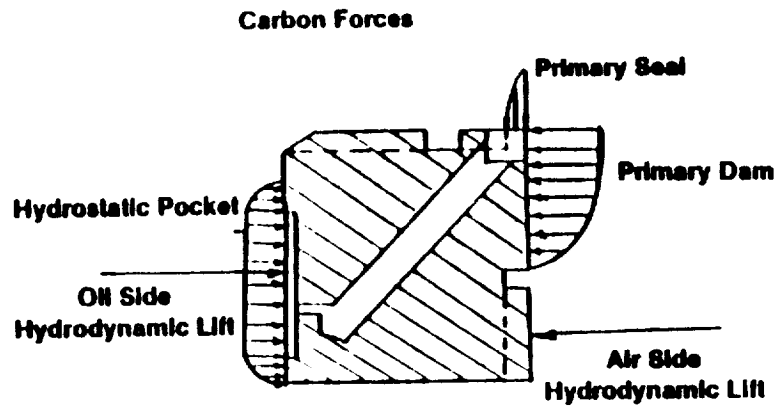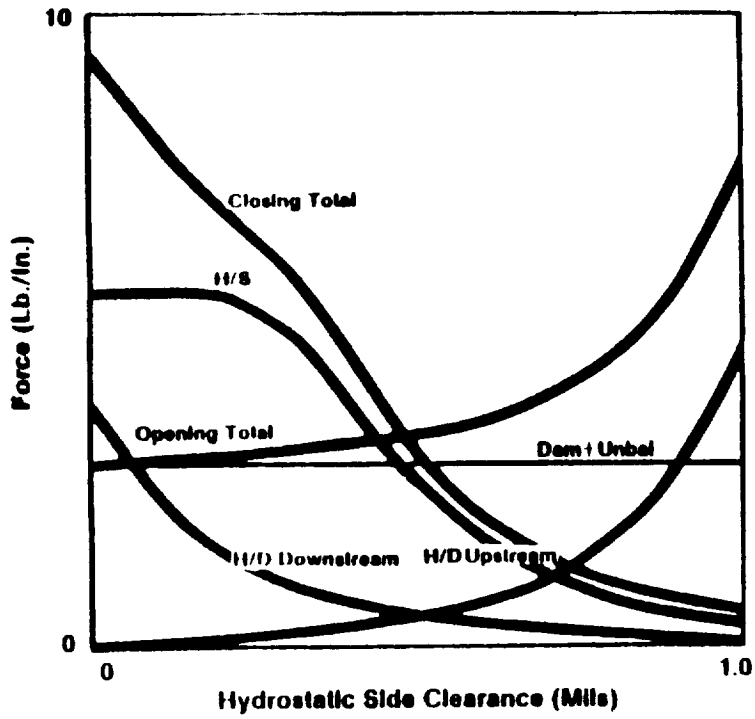
Figure 8-118. Intershaft Seal Force Balance/Wear.

234

Forward Seal
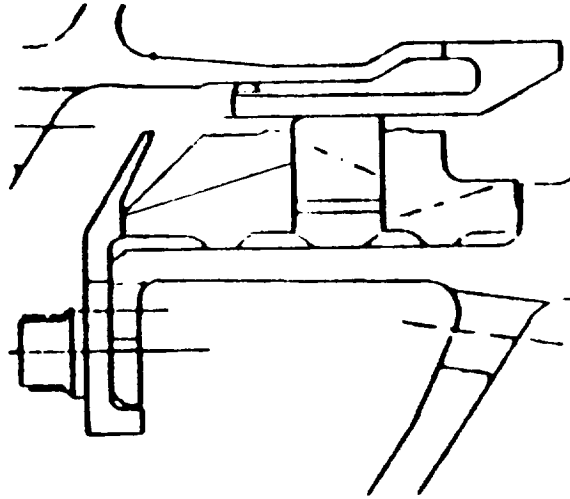
- **Parallelism Between Rings and Carbon Required to Prevent Binding/Wear**

- **Maximum Ring Face Slopes Due to Centrifugal, Thermal, and Pressure Effects**

  - **Oil Side Ring: 0.1 mil**
  - **Air Side Ring 0.04 mil**
  - **Carbon Ring: 0.2 mil**

- **Clearance Reduction Due to Friction 0.25 mil**

- **Total Side Clearance - No Distortion**
  - **Cold: 0.6 to 1.4 mil**
  - **Hot: 1.0 to 1.8 mil**

Aft Seal
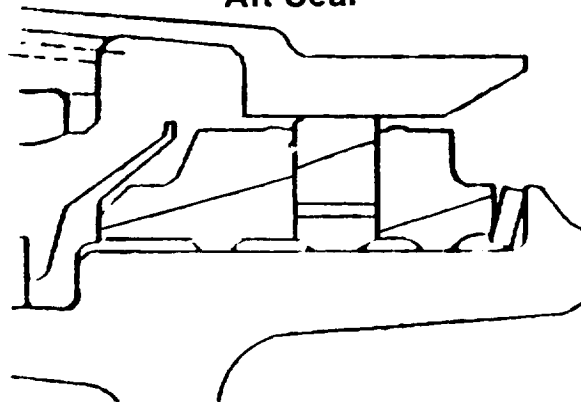
Figure 8-119.   Intershaft Seal Distortion.

were designed to provide a large force versus clearance slope at idle operating conditions. The large slope will provide a large restoring force when the carbon element deviates from the equilibrium point. Figure 8-121 demonstrates the final configuration of the lift pads; Figure 8-118 portrays a typical lift force versus clearance characteristics.
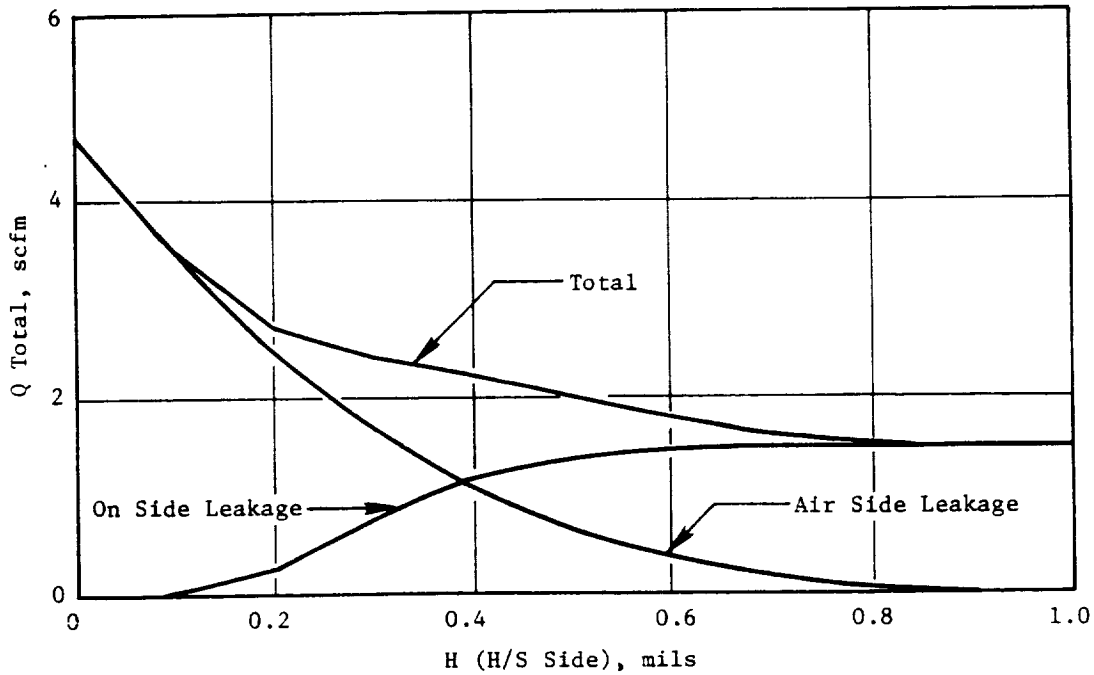
Figure 8-120. Intershaft Seal Airflow.

Mechanical stability of the system was analyzed using classical control theory. The system is described by two differential equations, based on the equation of motion and the conservation of mass which result in time-dependent variables for clearance and hydrostatic pocket pressure. The output of the analysis consists of transient plots of seal clearance and pocket pressure. The study was conducted for various initial conditions as well as operating conditions. In addition, sensitivity studies were performed to evaluate the friction level, carbon mass variation, flow coefficients, seal clearance variations, geometry variations due to face wear, and tracking response to various

236

4X
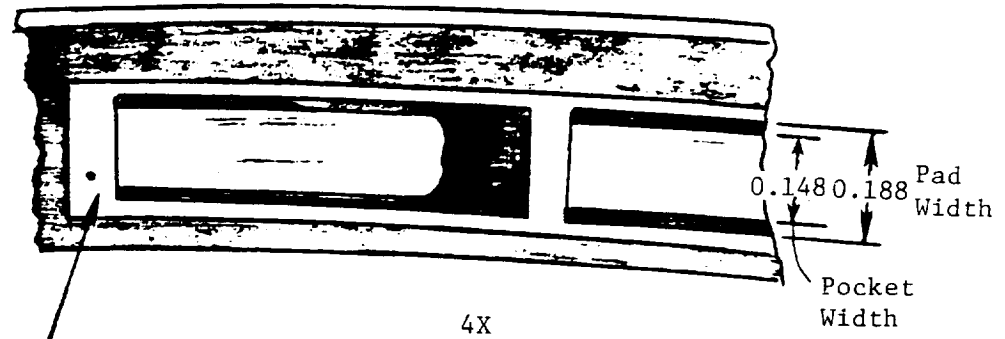
3 Pads per Hydrostatic Pocket
78 Pads/Side for 21.4 Dia Seal
60 Pads/Side for 16.5 Dia Seal

All Dimensions
in Inches
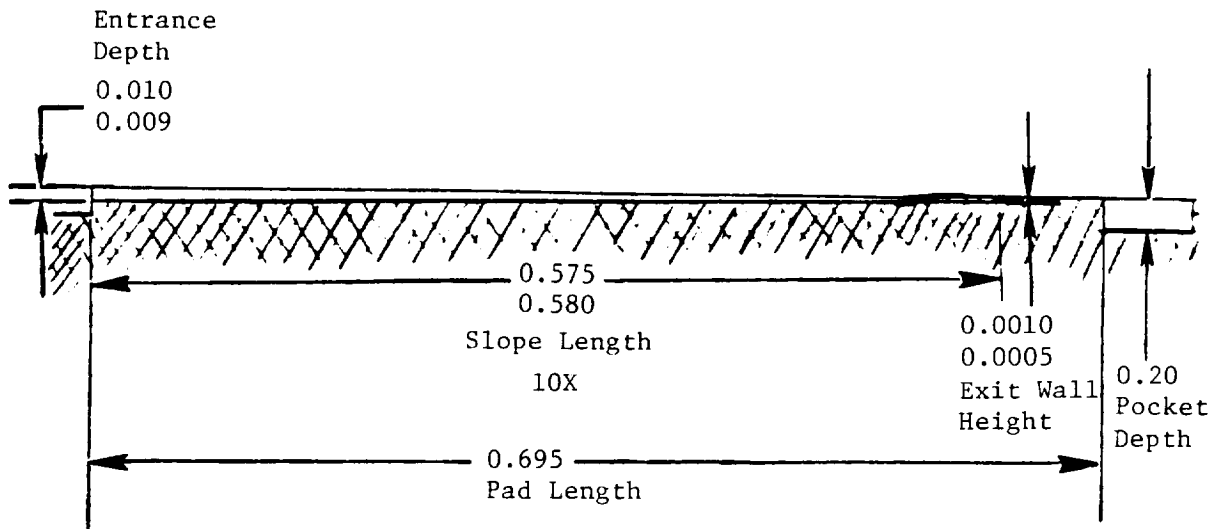
Figure 8-121.   Hydrodynamic Lift Pad Configuration.

sinusoidal motion (frequency and amplitude) of the races. for each analysis, a stable result was one that decayed with time to a steady-state position. A sample output of the study is illustrated in Figure 8-122. The study predicts stable operation for all expected operating conditions, including chops and bursts. Unstable characteristics are predicted if the friction level is less than 50% of the minimum expected level or if the oil-side hydrodynamic lift pads wear away, and the total seal clearance increases significantly.
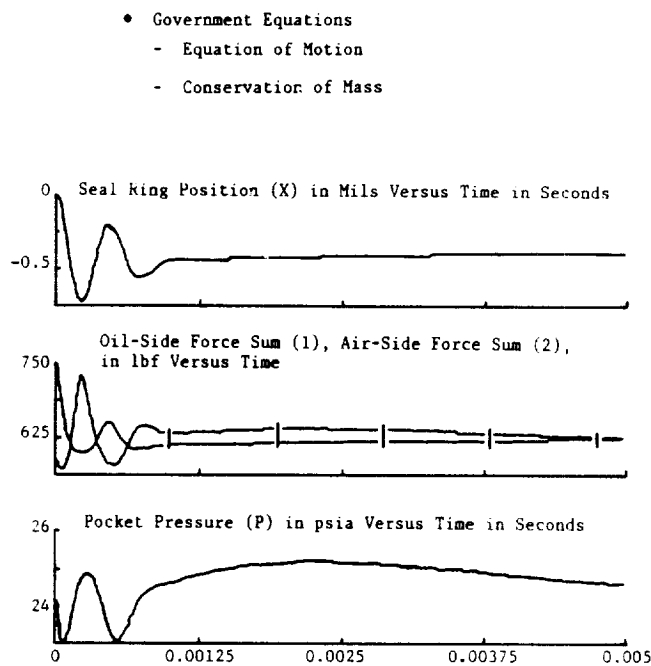
Figure 8-122. Mechanical Stability.

The acoustic stability of the hydrostatic pocket was studied. Helmholtz resonator and quarter-wave-length frequencies were calculated and determined to be outside of the operating range. For verification, a component test of a single pocket was conducted. No acoustic problems are anticipated.

Stationary Circumferential Seals

These circumferential seals are quite similar to conventional, single, undercooled, bore-rubbing carbon seals utilized in several aircraft engine applications. The only differences are the relatively large diameter (22.1 inches and 20.0 inches) and the use of a large number (10) of segments to make up the carbon ring. Figure 8-123 depicts the configuration of the seals and summarizes the basic results. Surface velocity, pressure, and temperature are all within GE experience ranges. Analysis indicates that these seals should function properly.

Magnetic Sump Wall Seals

Standard parts in aircraft engine gearboxes are the magnetic carbon face seals which, for the propulsor, are used to seal between the fan blade radial actuation rods and the sump walls. These seals consist of a carbon ring sandwiched between a magnet and a steel case as illustrated in Figure 8-124. The only motion of the seal occurs during a fan blade pitch change, which is limited to three revolutions per maximum blade excursion. The magnetic loading on the carbon element is 10 to 20 psi, while centrifugal loading is a maximum of 103 psi. The unique feature of this application is the addition of the centrifugal loading on the seal.

- Oil Wind-Back Incorporated

- Chopper on Aft Seal

- Life (0.20 Inch Dry Wear)

  - 9,000 Hours Forward Seal
  - 16,000 Hours Aft Seal
  - 2,000 Hours Required

- Force Balance Analysis Indicates Both Seals
  Will Track Radial and Axial Vibrations

- Heat Generation

  - Forward Seal - 7° Cooling Oil Rise
  - Aft Seal - 9° Cooling Oil Rise
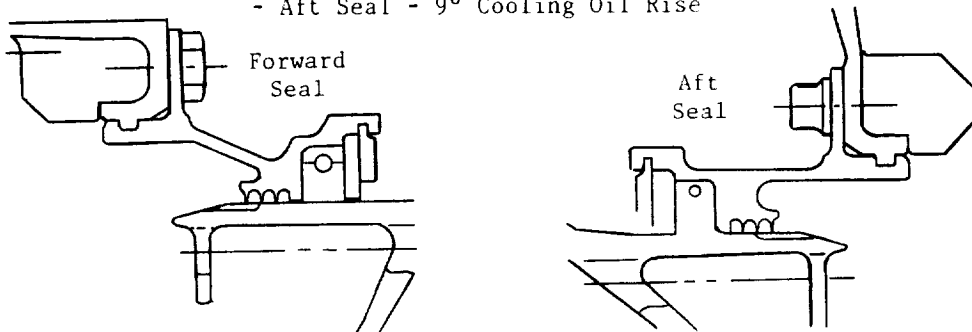
Figure 8-123. Circumferential Seal.

- Magnetic Carbon Face Seal

①Magnet (ALNICO-5)
②Carbon Ring (Carbon Graphite - GS-100)
③Steel Case (416 Stainless)
④O-Ring (Fluorocarbon)
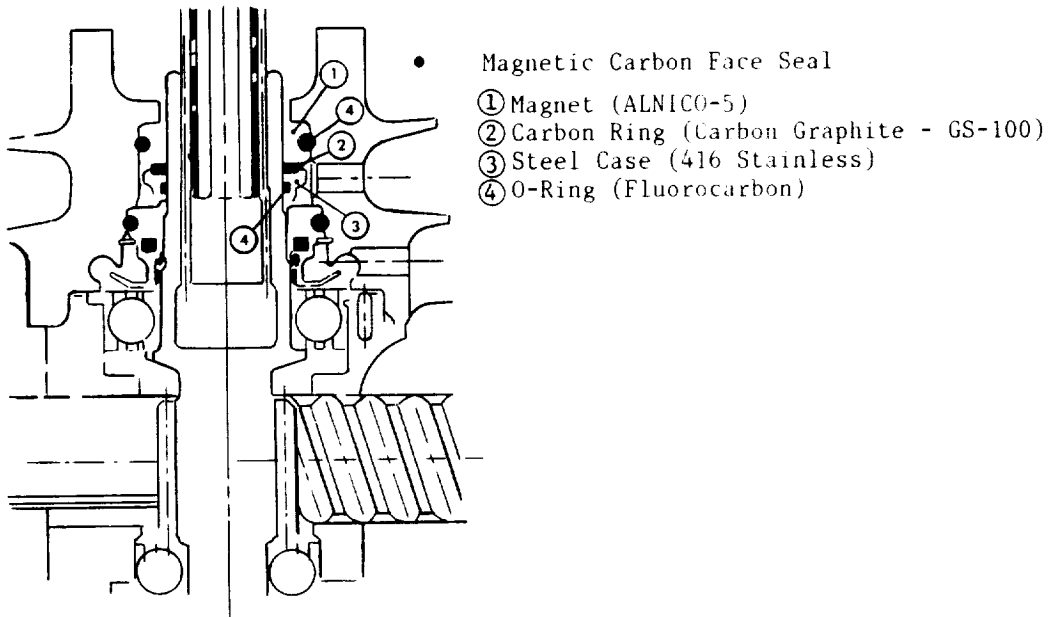
Figure 8-124. Sump Wall Seals.

240

9.0 ENGINE DYNAMICS

9.1 INTRODUCTION

An engine dynamics analysis was conducted to predict the dynamic behavior of the UDF™ engine. A model of the UDF™ engine was built for this analysis utilizing VAST (an in-house engine dynamics program). The flexibilities used to develop this mount-system model were based on predictions from the NASTRAN finite element (3D) model of the pylon/aircraft structure.

Four separate analyses are presented in this report:

- Nominal unbalance (1000 gm-in) in the forward and aft UDF™ P/T rotors
- Single blade-out in each of the P/T rotors simultaneously
- Nominal unbalance (20 gm-in) in various stages of the gas generator
- Maneuver loads and deflections.

Vertical and horizontal models referred to in this report are relative to the aircraft coordinate system.

9.2 ASSUMPTIONS

The following assumptions have been made in conjunction with analyses.

- Hooke's Law Applies
- Linear Damping.

9.3 CRITICAL SPEED ANALYSIS

9.3.1 Analysis Details

The analysis performed using this VAST model (Figure 9-1) is basically a two-dimensional planar analysis, with both gyroscopic and mount-flexibility effects incorporated. The critical speed analysis was conducted with nominal unbalance of 1000 gm-inch in the forward and aft UDF™ P/T rotors. The following damping values (Q = Cc/2C) were used in the analysis:

- Static Structure   10
- Rotors   100

Figure 9-1. GE36 Demonstration Engine Model.

15

242
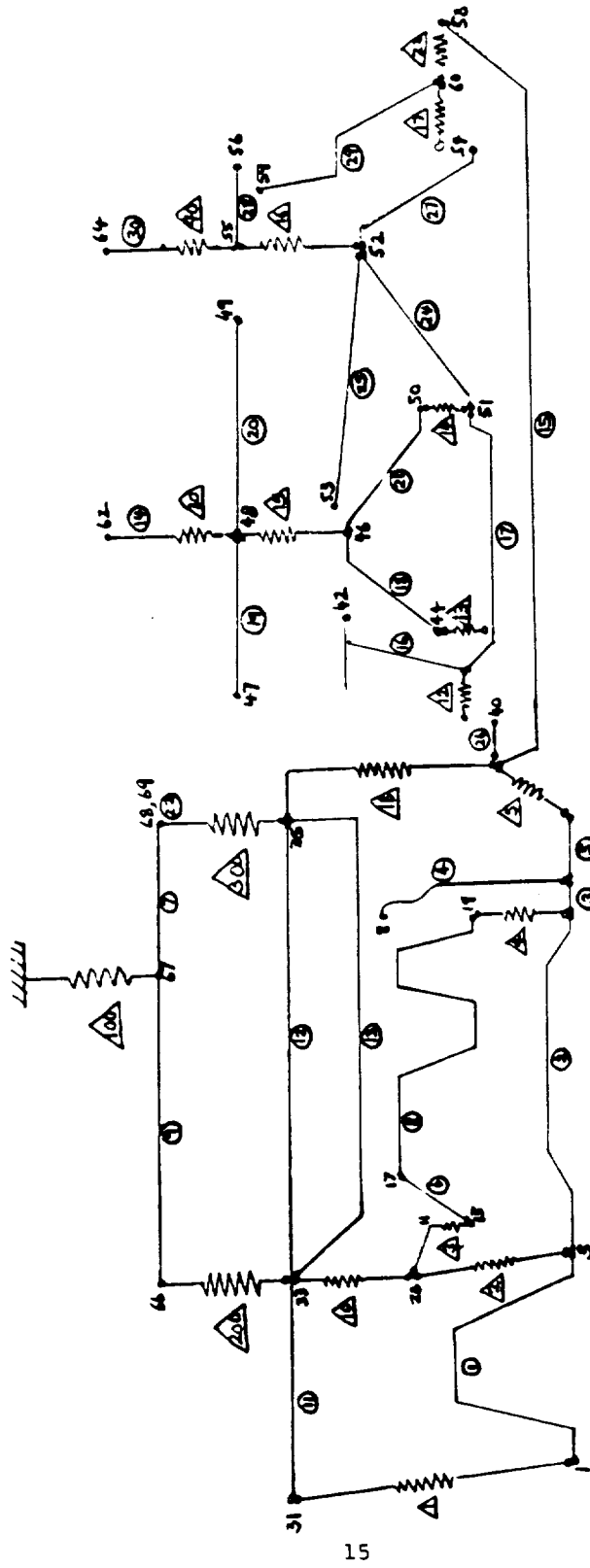
SPAN AND SPRING IDENTIFICATION

Span No.	Identification
1	Fan Rotor
2	LPS
3	LP Conebase
4	LP Torque Cone
5	LP Cone Aft
6	Compressor Forward Shaft & Forward Spool
7	Dummy Span
8	Compressor and Turbine
9	Dummy Span
10	No. 3 Bearing Support
11	Bellmouth/Fancase/AGB
12	Bypass Duct
13	Compressor/Combustor/Turbine Cases
14	Fan Blades
15	Support Tube
16	Stage 2/4 Spool & Cone
17	Shaft
18	Forward Cone,Forward Sump
19	Outer Spool - Forward
20	Outer Spool - Aft
21	Aft Cone,Forward Sump
22	Dummy Span
23	Shaft Forward of Bearing
24	Forward Cone,Aft Sump
25	Inner Spool - Aft
26	Forward Bearing Support
27	Aft Cone,Aft Sump
28	FAN - R14
29	OGV Assembly & No 2 Bearing Support
30	FAN BLADES - R14

Spring No.	Identification
1	No 1 Bearing and Forward Fan Frame
2	No 2 Bearing
3	No 3 Bearing (Damper)
4	No 4 Bearing
5	No 5 Bearing
10	Compressor Mid Frame
12	Forward Roller Bearing Support
13	Forward Thrust Bearing
14	Aft Roller Bearing
15	Forward Power Frame for UDF
16	Aft Power Frame for UDF
17	Aft Thrust Bearing
18	Mixer Frame
22	Aft Thrust Bearing Support Structure
100	Pylon
200	Forward Isolator
300	Aft Isolator

Figure 9-1.   GE36 Demonstration Engine Model (Concluded).

- Isolators   4
- Pylon   25.

The following isolator stiffnesses (pounds per inch) were used in this analysis:

- Front Mount Horizontal   300,000
- Front Mount Vertical   257,000
- Rear Mount/Radial/Lower   122,000
- Rear Mount/Radial/Upper   122,000
- Rear Mount/Axial/Lower   238,000
- Rear Mount/Axial/Upper   238,000.

9.3.2 Results

Table 9-1 defines the critical speeds and response factors with a nominal unbalance of 1000 gm-inch in the forward and aft UDF™ P/T rotors; the response factors are modal displacements in mils SA.

Table 9-1. Critical Speeds and Response Factors.

Vertical Model				Horizontal Model			
		Modal Response Fac, mils SA				Modal Response Fac, mils SA	
RPM	Description	S-5	S-12	RPM	Description	S-5	S-12
206	Rigid Body	8.2	10.7	355	Rigid Body	3.7	5.9
608	Rigid Body	1.5	2.5	1071	Support Tube Bending	4.0	0.2
1171	Support Tube Bending	3.3	0.1	1462	Pod Rocking and Support Tube Bending	0.6	0.4
1937	LP Shaft	0.04	---				
2090	Support Tube and Rotor Bending	4.0	8.5	1939	LP Shaft	0.07	---
				2120	Support Tube and Rotor Bending	5.3	7.0

The preceding list of criticals is for the engine/aircraft configuration. Critical speeds are slightly higher than those predicted and measured for the ground test Peebles installation. The major difference from the previous VAST model exists in the vertical model, where the second rigid body mode moves up in critical speed from 312 to 608 rpm. As expected, response factors for the vertical and horizontal models differ from previous analyses, but the underlying trend is the same. Since the current model has a more accurate definition of the mount system, and because the weight distribution is more in line with the measured values, it can be concluded that the dynamic characteristics are better predicted by this model.

Table 9-2 indicates the loads and deflections in the operating range at various locations on the engine with the nominal unbalance.

Table 9-2. Loads and Deflections.

Location	Loads, lb		Deflections, mils DA	
	S-5	S-12	S-5	S-12
Front Mount	178	70	2.9	3.8
Aft Mount	135	31	4.3	2.3
F404 No. 1 Bearing	17	1	5.8	4.8
F404 No. 2 Bearing	8	3	2.9	3.9
F404 No. 3 Bearing	12	1	2.9	3.7
F404 No. 4 Bearing	14	3	4.5	2.5
F404 No. 5 Bearing	21	4	4.6	2.3
P/T Forward Radial Bearing (1R)	199	18	4.5	1.8
P/T Forward Thrust Bearing (1B)	11	48	4.5	1.6
P/T Aft Radial Bearing (2R)	88	53	2.5	1.4
P/T Aft Thrust Bearing (2B)	83	22	2.2	2.5

Figures 9-2 through 9-17 show the variation in loads and deflections at the mount system and at the bearings due to the 1000 gm-inch unbalance in the P/T rotors as a function of rotor speed.

245
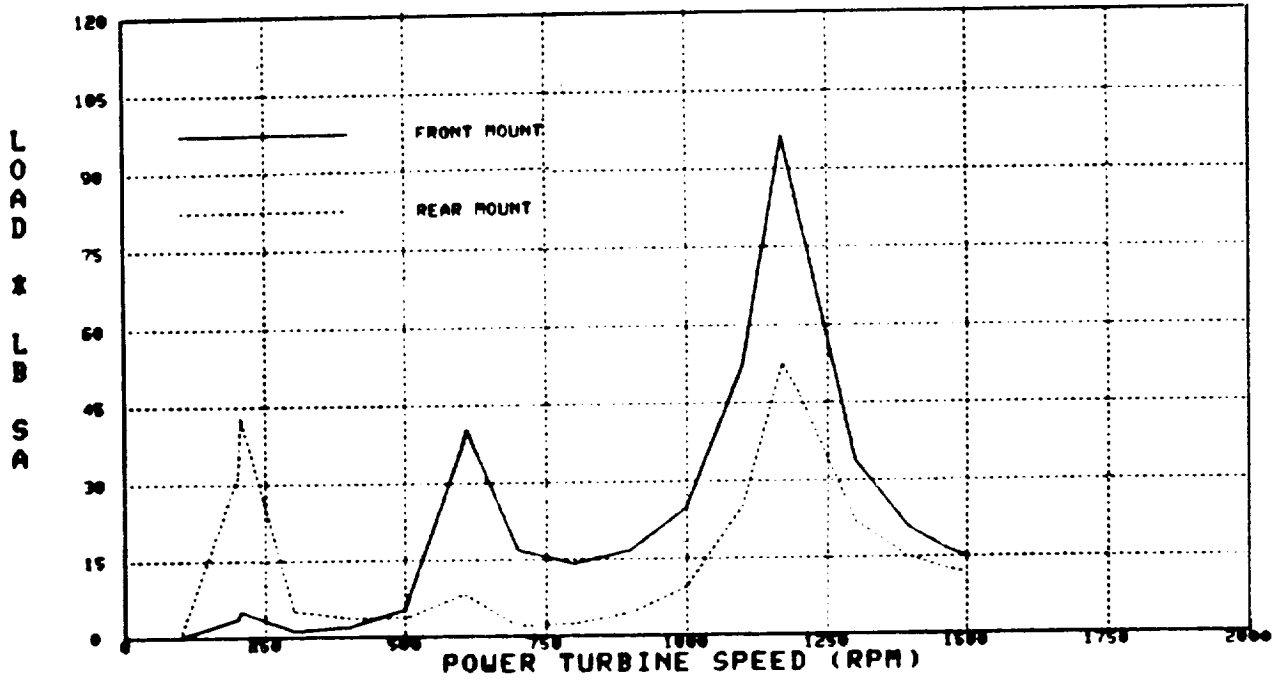
Figure 9-2. GE36 P/T Stage 5 Imbalance - Vertical Model.
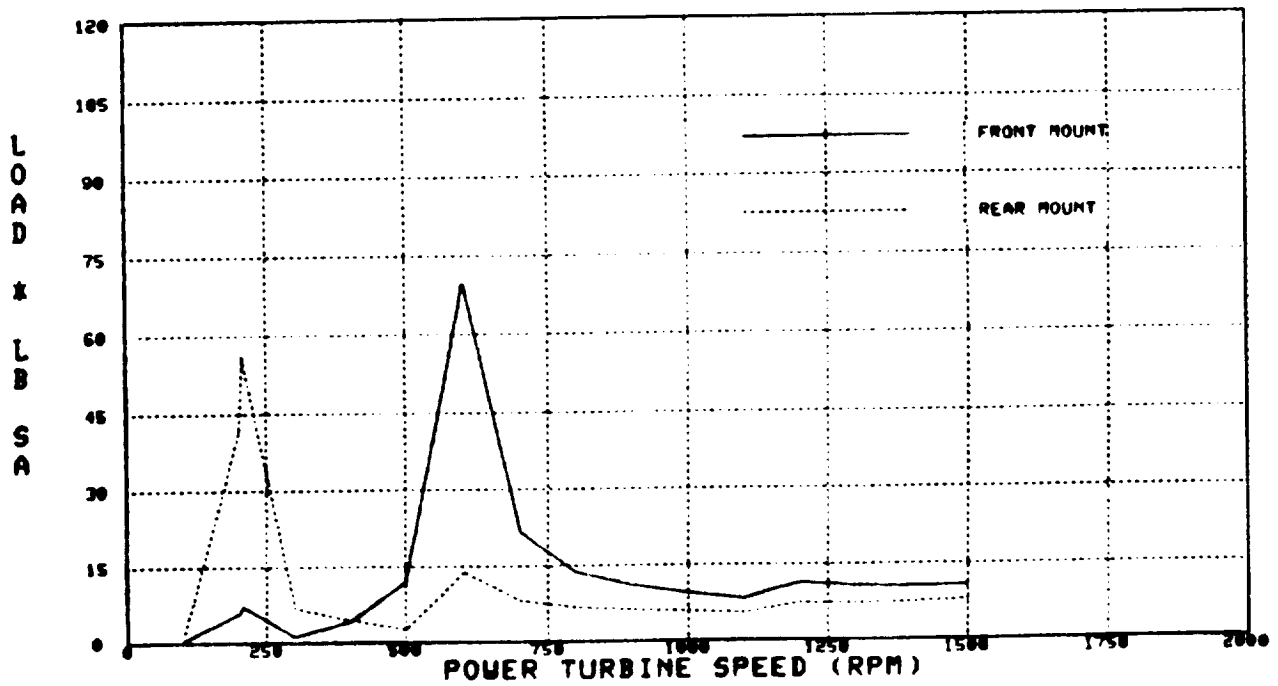
Figure 9-3. GE36 P/T Stage 12 Imbalance - Vertical Model.
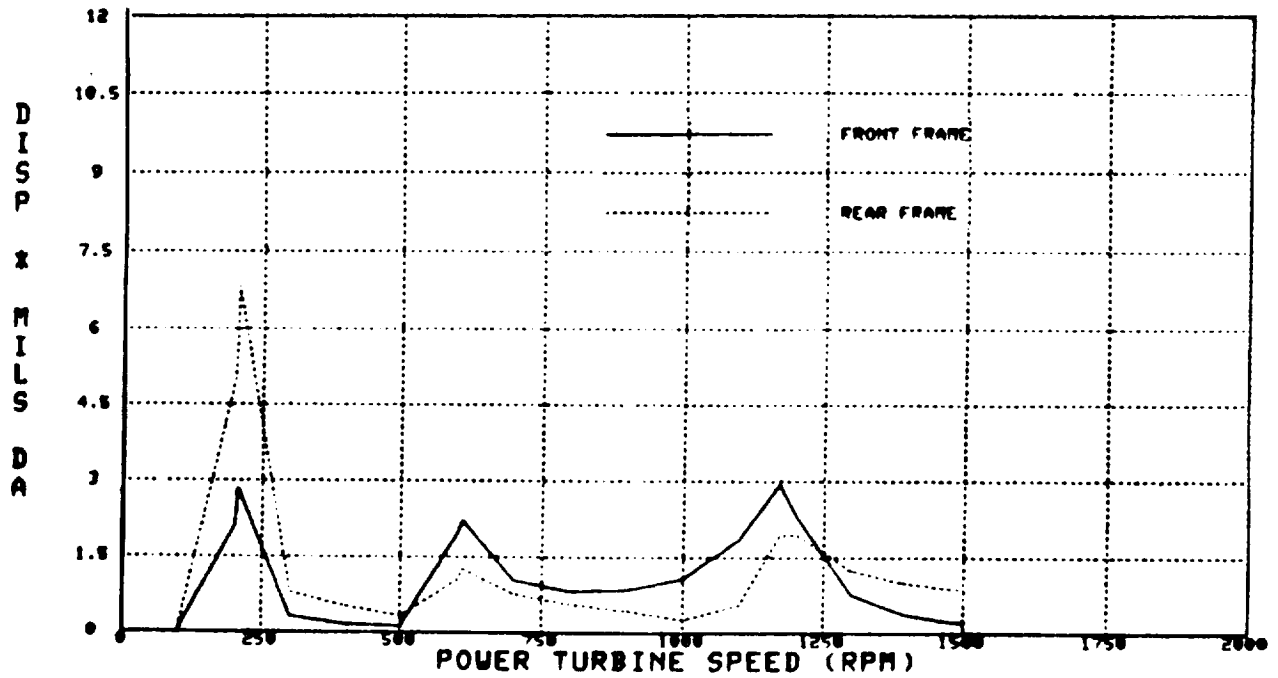
Figure 9-4. GE36 P/T Stage 5 Imbalance - Vertical Model.
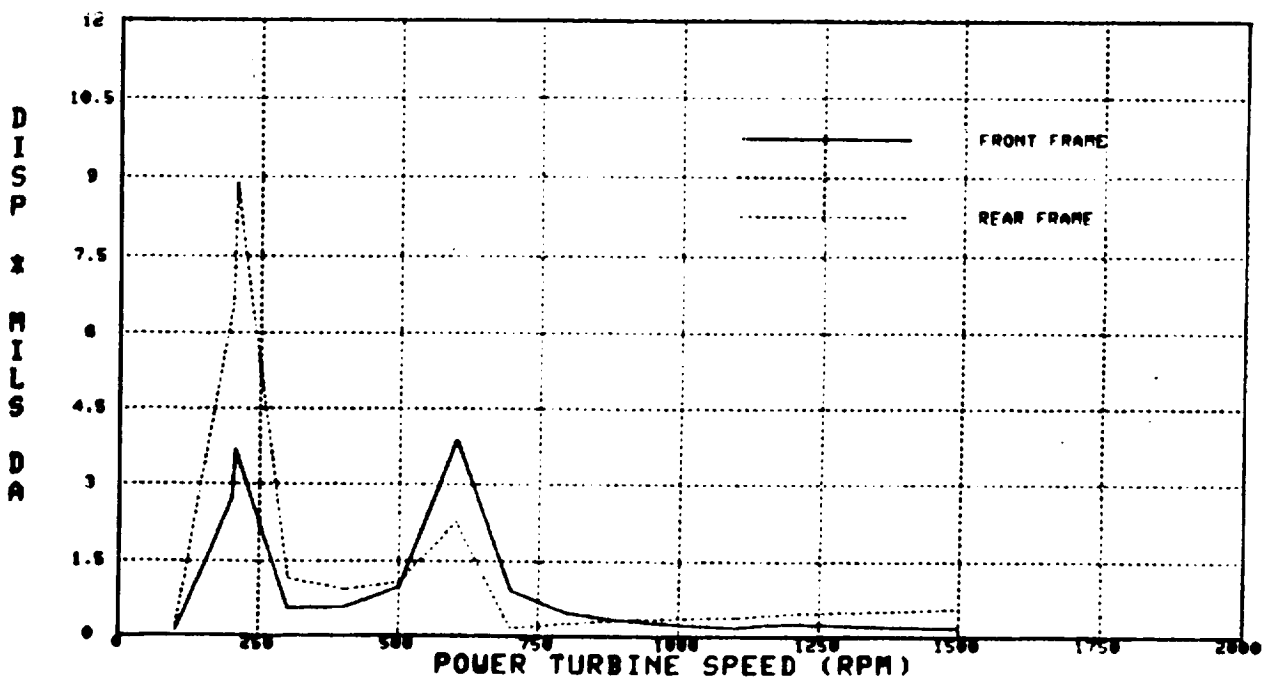
Figure 9-5. GE36 P/T Stage 12 Imbalance - Vertical Model.
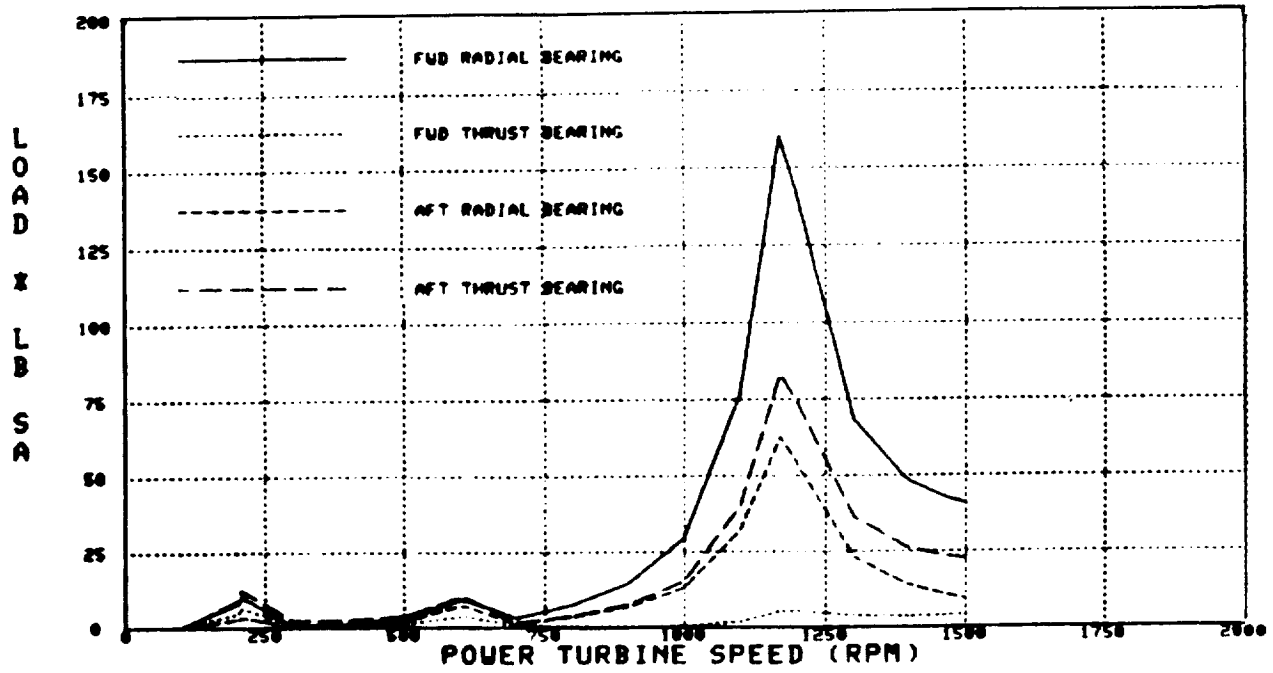
Figure 9-6. GE36 P/T Stage 5 Imbalance - Vertical Model.
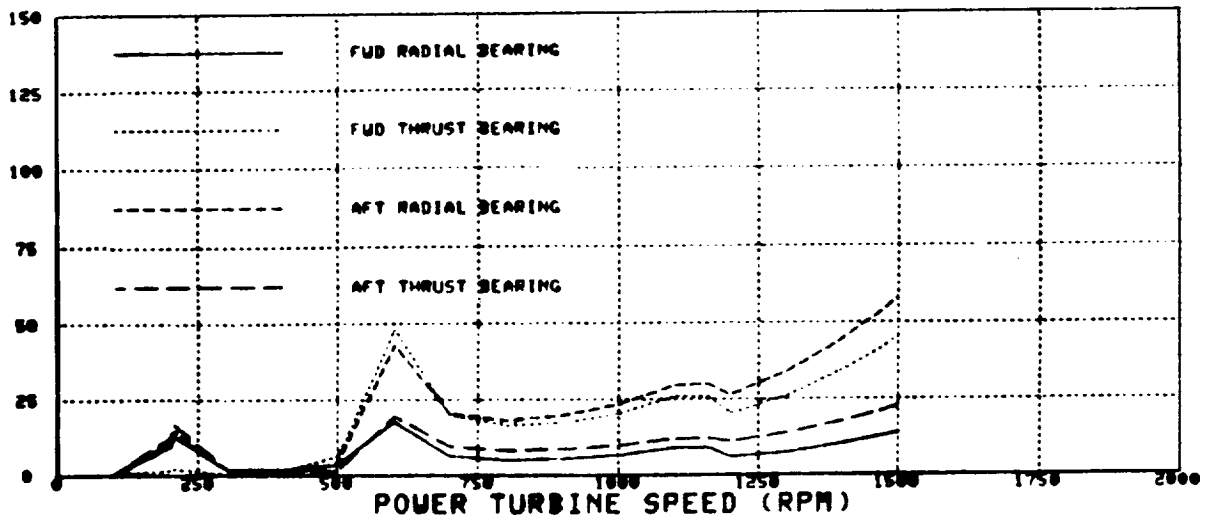
Figure 9-7. GE36 P/T Stage 12 Imbalance - Vertical Model.
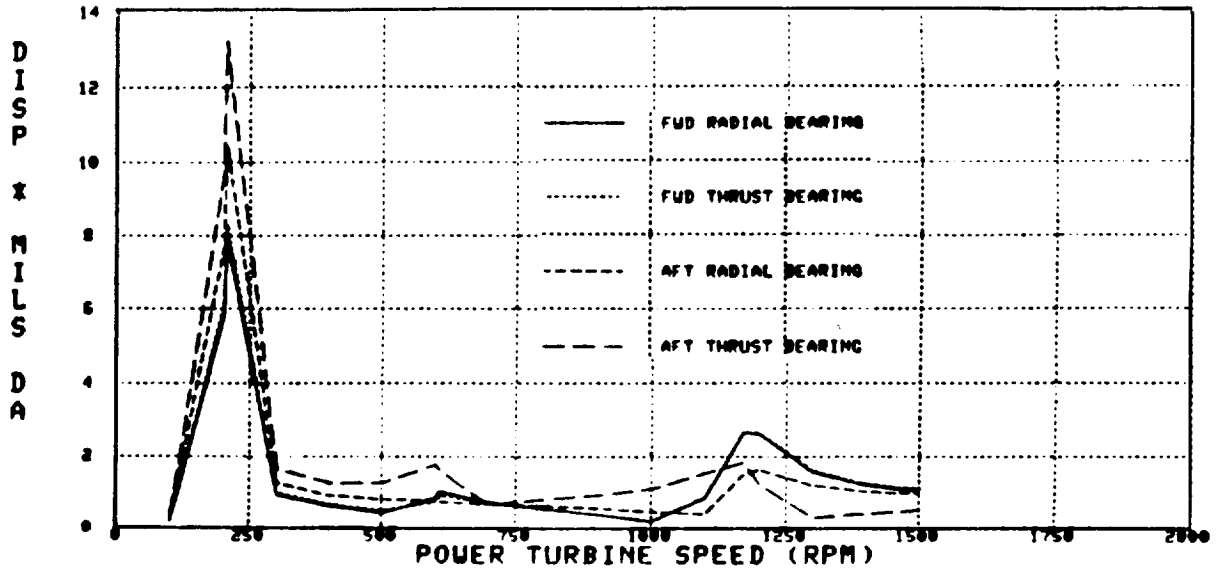
Figure 9-8. GE36 P/T Stage 5 Imbalance - Vertical Model.
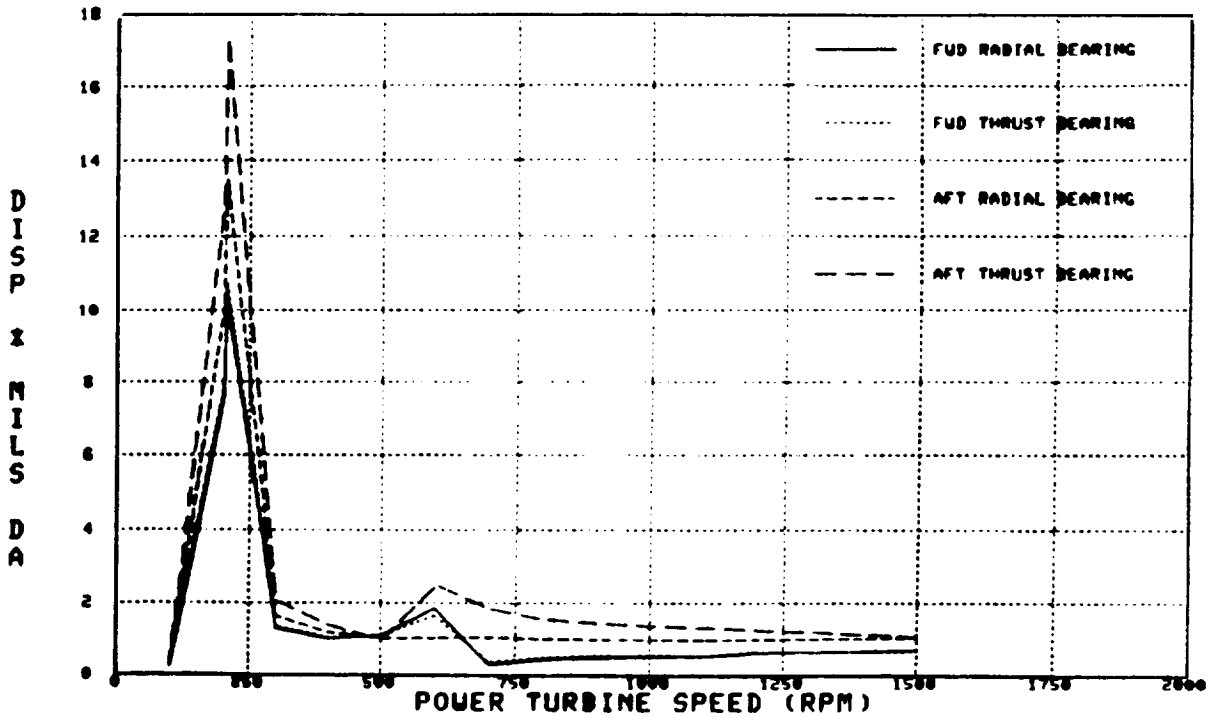
Figure 9-9. GE36 P/T Stage 12 Imbalance - Vertical Model.
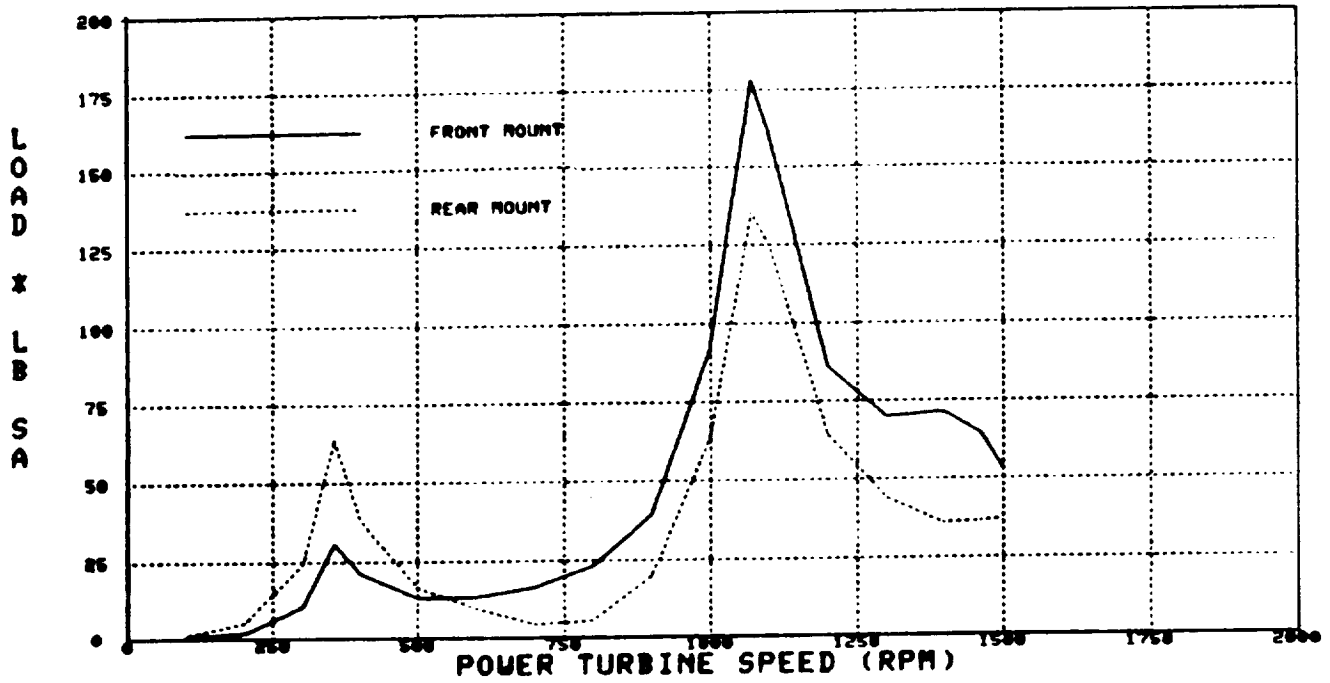
Figure 9-10. GE36 P/T Stage 5 Imbalance - Horizontal Model.
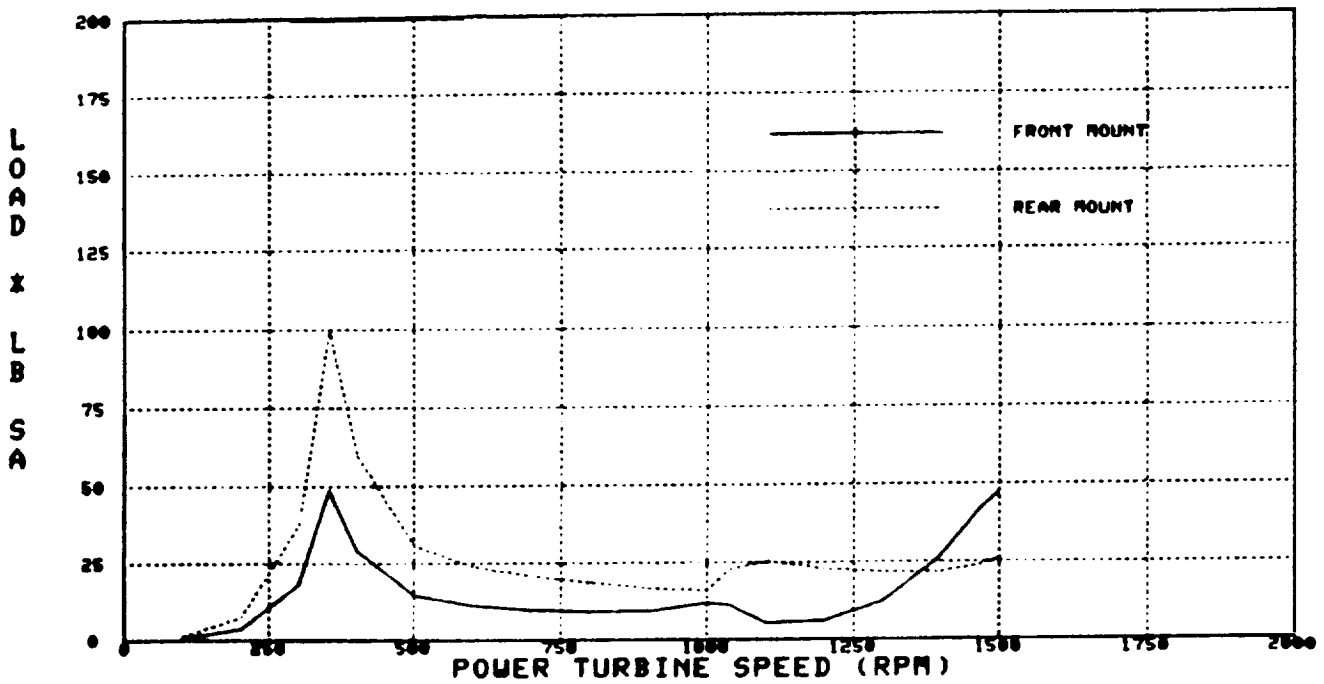
Figure 9-11. GE36 P/T Stage 12 Imbalance - Horizontal Model.

250
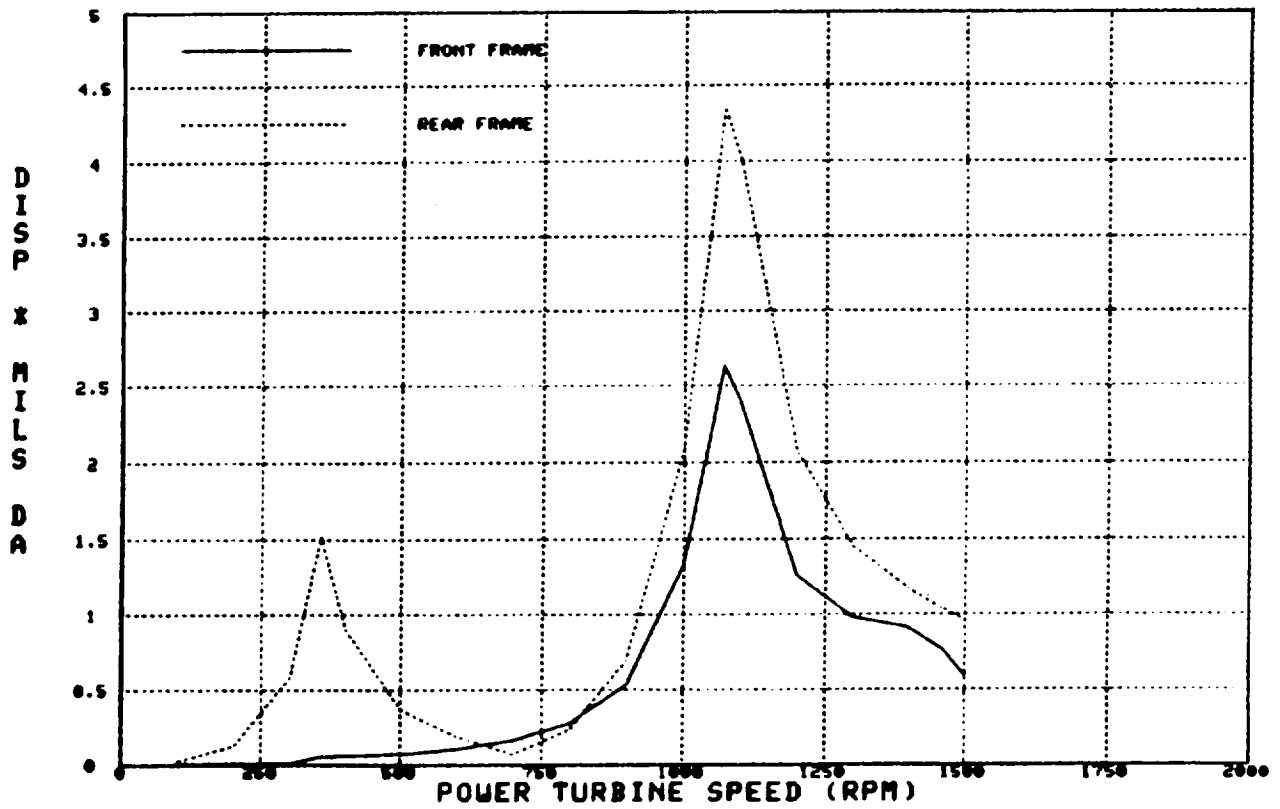
Figure 9-12. GE36 P/T Stage 5 Imbalance - Horizontal Model.
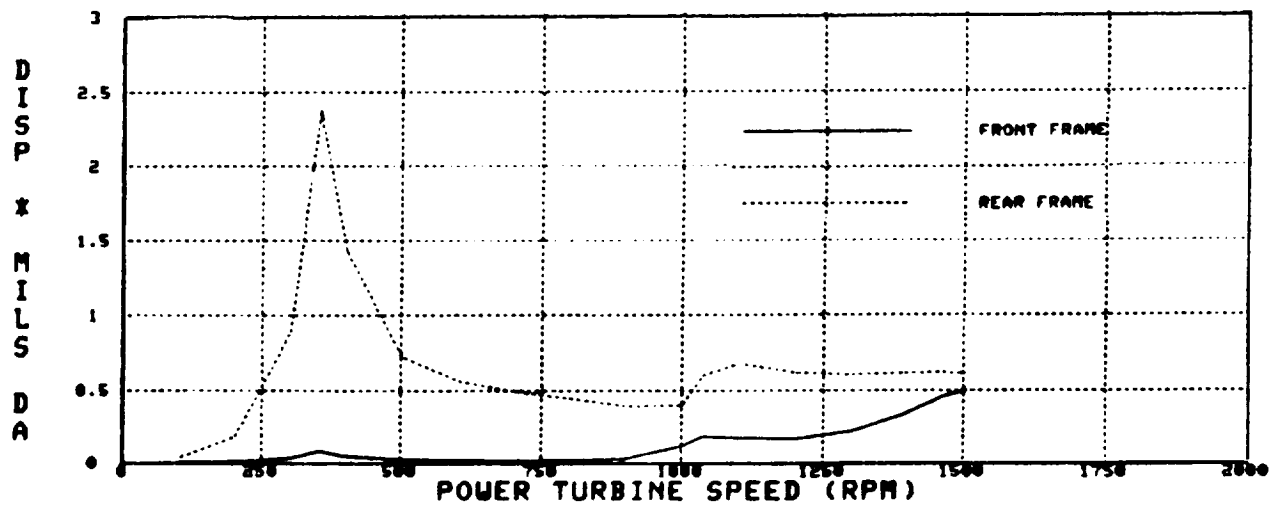
Figure 9-13. GE36 P/T Stage 12 Imbalance - Horizontal Model.

251
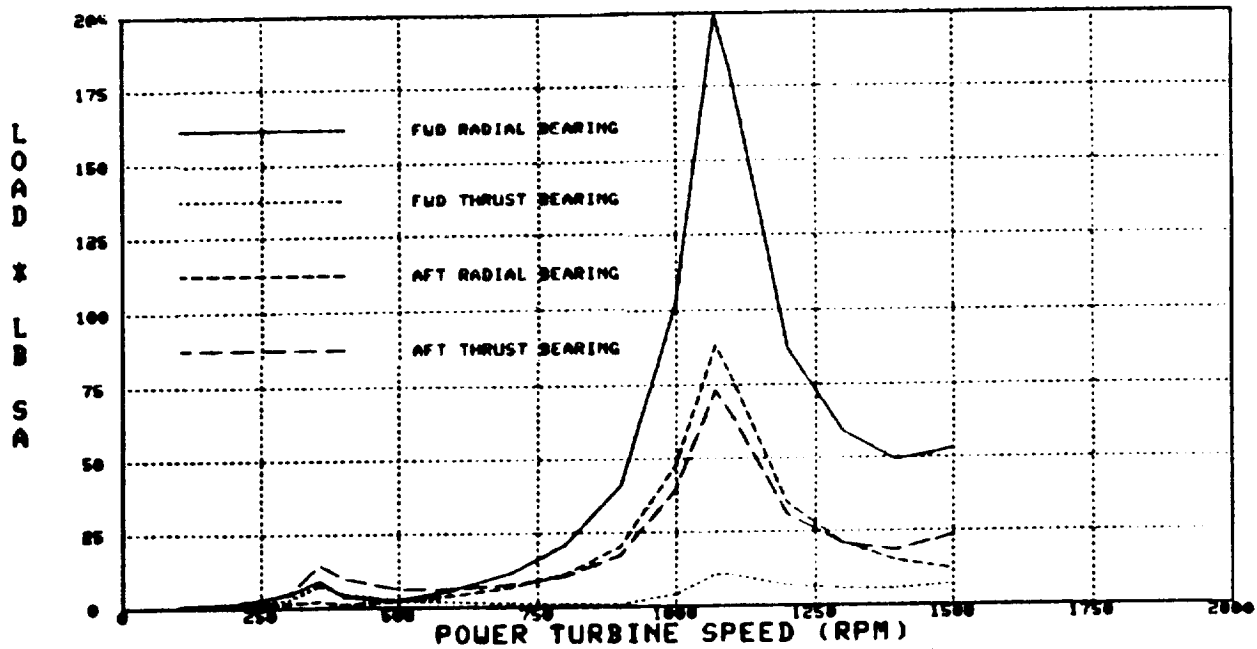
Figure 9-14. GE36 P/T Stage 5 Imbalance - Horizontal Model.
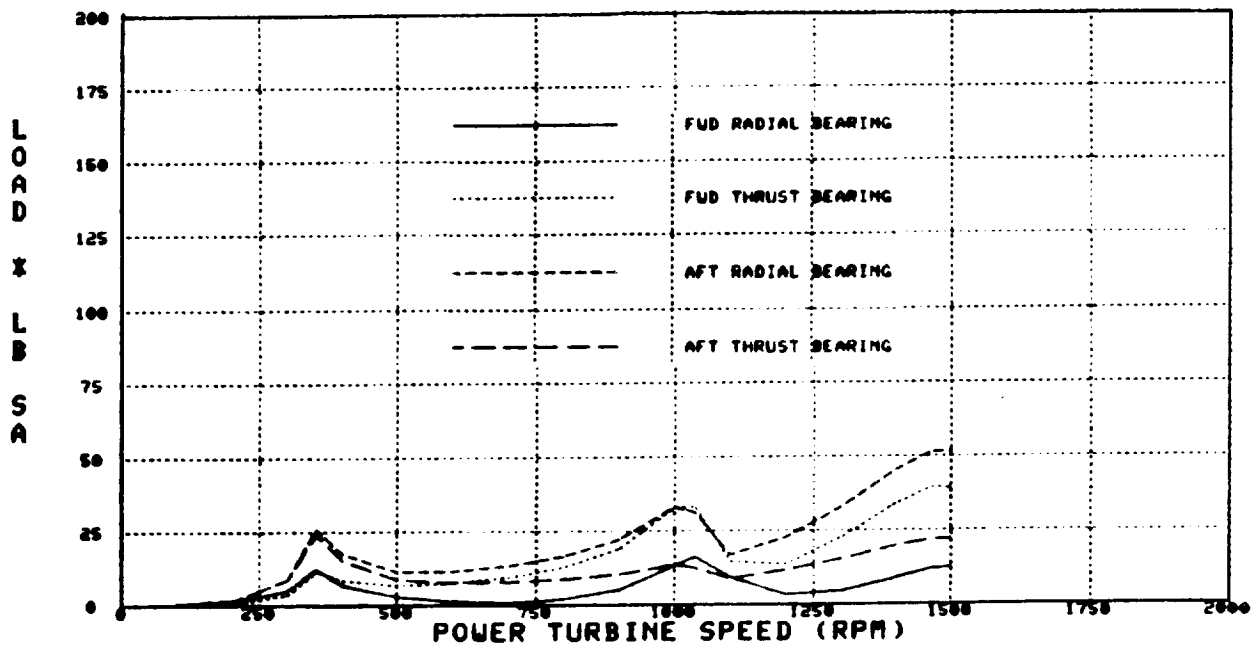
Figure 9-15. GE36 P/T Stage 12 Imbalance - Horizontal Model.

252
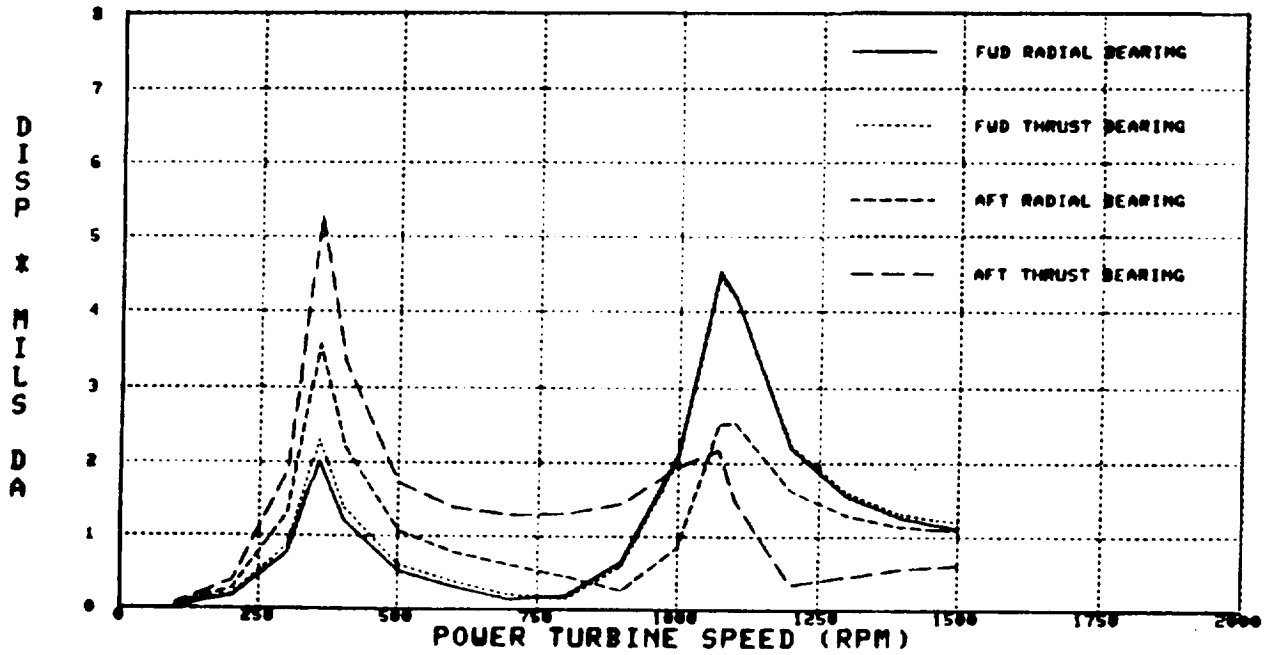
Figure 9-16.   GE36 P/T Stage 5 Imbalance - Horizontal Model.
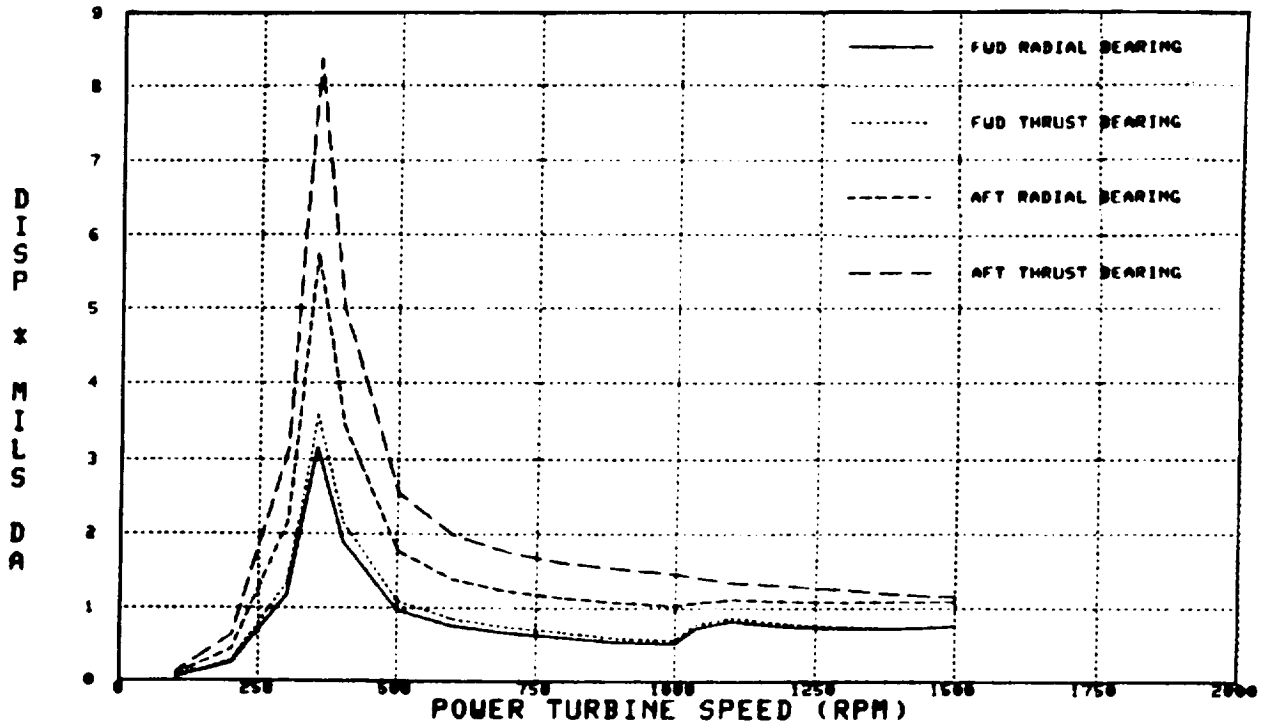
Figure 9-17.   GE36 P/T Stage 12 Imbalance - Horizontal Model.

9.4 BLADE-OUT ANALYSIS

9.4.1 Analysis Details

Separate VAST analyses were conducted for the blade-out event in each of the UDF™ P/T rotors. The calculated unbalance due to a blade loss in the forward rotor is 395,000 gm-inch and in the aft rotor 398,000 gm-inch; therefore, the combined effect of losing a single blade in each of the two rotors is 793,000 gm-inch.

The following damping values (Q) were used in the analysis:

- Static Structure   6
- Rotors   100
- Isolators   4
- Pylon   25

The damping in the static structure was increased from that utilized in the nominal unbalance analysis based on the results of the turbofan blade-out tests which reveal an increase in damping with high unbalance.

The following isolator stiffnesses (pounds per inch) were used for this analysis:

- Front Mount Horizontal   150,000
- Front Mount Vertical   125,000
- Rear Mount/Radial/Lower   60,000
- Rear Mount/Radial/Upper   60,000
- Rear Mount/Axial/Lower   125,000
- Rear Mount/Axial/Upper   125,000

9.4.2 Results

Table 9-3 identifies the maximum loads in the mount system in the event of a simultaneous blade-out in each of the P/T rotors. The rear mount radial component is derived from the predicted maximum loads for the vertical and horizontal models. Broadly speaking, these loads are slightly higher than those predicted by the previous model, but this is to be expected due to the new pylon system and the increase in the mass of the engine.

Table 9-4 lists the predicted maximum loads at various locations in the engine.

254

Table 9-3. Maximum Loads in the Event of Simultaneous Blade-Out.

Mount	Direction	Predicted Load, lb	RPM	Isolator Design Loads, lb
Forward	Vertical	26,510	564	80,000
Forward	Horizontal	50,360	1000	60,000
Aft	Vertical	26,800	196	
Aft	Horizontal	34,600	289	
Aft	Axial	19,090	196	60,000
Aft	Radial	34,800	289	50,000

Table 9-4. Predicted Maximum Loads.

Location	Maximum Load, Pounds × 1000
No. 1 Bearing	4.0
No. 2 Bearing	1.8
No. 3 Bearing	2.8
No. 4 Bearing	2.6
No. 5 Bearing	4.1
P/T Forward Radial Bearing	41.9
P/T Forward Thrust Bearing	20.9
P/T Aft Radial Bearing	27.7
P/T Aft Thrust Bearing	25.5

9.5 GAS GENERATOR UNBALANCE

Two separate VAST analyses were carried out with the following nominal unbalance. These analyses are described as follows:

- **LP Run**

  - 20 gm-inch low pressure compressor (LPC) Stage 1
  - 20 gm-inch low pressure turbine (LPT)

- **HP Run**

  - 20 gm-inch high pressure compressor (HPC) Stage 1
  - 20 gm-inch HPC Stage 3
  - 20 gm-inch HPC Stage 5
  - 20 gm-inch HPC Stage 7
  - 20 gm-inch high pressure turbine (HPT).

The LP run was made between 4,956 and 18,000 rpm. The HP run was made between 5,000 and 22,000 rpm.

9.5.1 Results

LP Run - The variation in response factors (due to 20 gm-inch unbalance in the LPC Stage 1 and in the LPT) is listed in Table 9-5.

Table 9-5. Variation in Response Factors, LP Run.

Speed, rpm	Modal Response Factors, mils SA		Description
	LPC-S1	LPT	
5,668	0.00	0.14	Fan Case, Bypass Duct
6,099	0.15	0.98	No. 3 Bearing, HP Rotor Rocking
7,343	0.14	0.25	Center Body, Aft Prop and Aft Sump
8,705	1.85	1.91	No. 3 Bearing, HP Rotor, IPC Rotor
9,861	2.50	1.00	No. 1 Bearing, IPC Rotor
10,096	0.22	0.39	Aft Rotor
10,174	0.02	0.18	Bypass Duct, Case Bending
11,830	0.22	0.01	Case Bending, Intake
12,733	0.04	0.04	Mixer Frame, Forward Spool
13,783	0.01	0.00	Stage 5 Mount Ring
14,752	0.01	0.06	Stage 5 Mount Ring
15,376	0.01	0.03	Stage 14 Mount Ring
15,988	0.64	0.04	Case Bending, Intake
16,687	0.06	0.10	Stage 5 Mount Ring, Aft Cone, Aft Sump
17,800	0.11	0.37	Forward Thrust Bearing, Aft Cone, Forward Sump

The modes involving the gas generator are similar to the modes for the proven F404 engine; those involving the propulsor have low response.

Table 9-6 demonstrates the peak dynamic response in the operating range due to 20 gm-inch unbalance in the LP rotor.

Table 9-6. Peak Dynamic Response.

Location	Loads, lb		Deflections, mils DA	
	Fan S-1	LPT	Fan S-1	LPT
Front Mount	24	26	0.2	0.3
Rear Mount	10	11	0.2	0.3
No. 1 Bearing	642	243	4.0	1.6
No. 2 Bearing	501	192	2.0	0.8
No. 3 Bearing	259	210	3.4	3.5
No. 4 Bearing	186	148	1.3	2.3
No. 5 Bearing	431	383	1.1	0.9
P/T Forward Radial Bearing	49	74	0.2	0.2
P/T Forward Thrust Bearing	89	109	0.1	0.1
P/T Aft Radial Bearing	56	94	0.1	0.1
P/T Aft Thrust Bearing	72	131	0.1	0.2

HP Run - Table 9-7 shows the HP excited critical speeds and the response factors due to 20 gm-inch nominal unbalance in the HPC Stages 1, 3, 5, 7, and the HPT.

The modes involving the gas generator are similar to the modes for the proven F404 engine; those involving the propulsor have low response.

The maximum loads due to unbalance in the HP rotor in the operating range are presented in Table 9-8.

9.6 MANEUVER LOADS AND DEFLECTIONS

Table 9-9 reflects the bearing loads for the gas generator under various maneuver conditions. The maximum angular velocity maneuver experienced on the commercial transport is 0.25 radian per second, which is based on input from airframe manufacturers, and includes gust loading due to turbulence, etc.

Power turbine bearing loads for the unit maneuver conditions are listed in Table 9-10.

Table 9-7. HP Critical Speeds and Response Factors.

Speed, rpm	Modal Response Factors, mils SA					Description
	S1	S3	S5	S7	HPT	
5,651	0.26	0.20	0.16	0.13	0.10	Fan Case, Bypass Duct
6,010	2.02	2.31	2.35	2.37	1.73	No. 3 Bearing, HPC, and HPT
7,333	0.62	0.54	0.44	0.37	0.18	Aft Cone, Aft Sump, HPC, HPT, and Aft Thrust Bearing
8,410	3.90	3.26	2.50	1.93	1.84	No. 3 Bearing, HPC, and HPT
9,759	1.45	1.26	0.96	0.78	0.72	No. 1 Bearing, Fan, HPC, and HPT
10,023	0.31	0.25	0.18	0.14	0.13	Aft Inner Spool, Fan
10,139	0.12	0.10	0.07	0.06	0.06	Bypass Duct, Case Bending
11,823	0.01	0.01	0.02	0.02	0.01	Intake, Case Bending
12,634	0.14	0.10	0.06	0.04	0.11	Mixer Frame, Forward Spool
13,940	0.03	0.02	0.01	0.01	0.02	Stage 5 Mount Ring
14,723	0.21	0.16	0.10	0.05	0.17	Stage 5 Mount Ring
15,329	0.04	0.06	0.05	0.04	0.02	Stage 14 Mount Ring
15,664	0.03	0.46	0.59	0.65	0.20	Intake, Fan Case
16,813	0.15	0.07	0.00	0.04	0.14	Stage 5 Rotor
17,811	0.33	0.15	0.00	0.09	0.29	Casing, Aft Cone, Aft Sump
18,632	2.00	0.56	0.38	0.93	1.61	Compressor Midframe, Bypass Duct
19,364	0.15	0.06	0.01	0.05	0.11	Bypass Duct, Case Bending
19,945	0.54	0.38	0.15	0.00	0.45	Intake, Bypass Duct
20,216	0.10	0.07	0.02	0.01	0.08	Stage 14 Mount Ring
21,072	2.01	1.03	0.08	0.50	1.49	No. 4 Bearing, LP and HP Rotors
21,584	0.38	0.37	0.19	0.08	0.35	Support Tube, No. 1 Bearing
21,820	0.41	0.04	0.17	0.28	0.22	Support Tube, No. 1 Bearing

Table 9-8. Maximum Loads Due to Unbalance in HP Rotor.

Location	Loads, lb				
	S-1	S-3	S-5	S-7	HPT
Front Mount	41	38	39	40	38
Rear Mount	24	21	20	19	11
No. 1 Bearing	345	299	229	183	174
No. 2 Bearing	269	235	181	146	135
No. 3 Bearing	420	353	271	260	198
No. 4 Bearing	428	302	307	308	311
No. 5 Bearing	668	560	431	394	317
P/T Forward Radial Bearing	148	129	121	116	115
P/T Forward Thrust Bearing	192	161	124	115	140
P/T Aft Radial Bearing	232	201	163	140	203
P/T Aft Thrust Bearing	315	273	222	189	94

Table 9-9. Gas Generator Bearing Loads.

Condition	Bearing Loads, lb				
	No. 1	No. 2	No. 3	No. 4	No. 5
1000 lbf	0.3	-0.4	0.0	0.0	0.1
1 G	89	126	127	171	255
0.25 Rad/Sec Angle of Velocity	247	-185	330	-330	-390
1 Rad/Sec/Sec Acceleration	16	16	12	8	8

Table 9-10. Power Turbine Bearing Loads.

Condition	Bearing Loads, lb			
	Forward Radial	Forward Thrust	Aft Radial	Aft Thrust
1000 lbf	---	---	---	---
1 G	-2040	880	874	1660
0.25 Rad/Sec Angular Velocity	185	-5075	5075	185
1 Rad/Sec/Sec Acceleration	54	41	-125	-203

Table 9-11 defines the gas generator clearances for various maneuver conditions.

Table 9-11. Gas Generator Clearances.

Location	Thrust, 1000 lb	1 G	Closure, mils	
			0.25 Rad/Sec Angle/Velocity	1 Rad/Sec/Sec Angle/Acceleration
Fan Stage 1	0.003	0.47	0.46	0.07
Fan Stage 3	0.005	0.59	-0.66	0.09
Compressor Stage 1	-0.005	1.30	2.70	0.14
Compressor Stage 4	-0.024	1.12	2.46	0.17
Compressor Stage 7	-0.032	1.04	2.32	0.19
HP Turbine Rotor	-0.032	0.63	1.02	0.17
LP Turbine Rotor	-0.030	0.39	1.47	0.16

For the four maneuver conditions listed, a maximum clearance of 2.7 mils is predicted at the compressor Stage 1. These results confirm that the maneuver loads and deflections are low.

Table 9-12 details the power turbine clearance closures for the various maneuver conditions.

260

Table 9-12. Power Turbine Clearances.

Location	Thrust, 1000 lb	1 G	Closure, mils	
			0.25 Rad/Sec Angle/Velocity	1 Rad/Sec/Sec Angle/Acceleration
P/T - Stage 1	0.2	3.49	9.5	-0.65
P/T - Stage 4	0.1	3.36	-3.5	-0.28
P/T - Stage 6	-0.2	-3.43	2.8	0.45
P/T - Stage 8	-0.2	-4.47	-5.3	0.59
P/T - Stage 11	-0.2	-8.62	-19.6	1.13

9.7 CONCLUSIONS

Analysis predicts no propulsor bending criticals in the engine operating range. All modes in the operating range are well damped and, therefore, have low response. Gas generator-excited criticals involving significant energy in the F404 gas generator are similar to those observed on the proven F404 engine. Those IP and HP criticals involving propulsor activity are predicted to be very low in response.

The predicted blade-out loads for one blade in each rotor are reasonable and within the design values. The maneuver loads and deflections are also reasonable.

10.0 POWER CONTROL AND CONFIGURATION DESIGN

10.1 POWER CONTROL SYSTEM

10.1.1 Introduction

The power control system for the UDF™ (Figure 10-1) controls the engine's forward and reverse thrust by means of mechanical linkages and cabling. The system includes a pylon-mounted throttle converter assembly, a push/pull cable arrangement to actuate the engine hydromechanical control power lever, an electric power circuit to actuate the engine mounted shut-off solenoid valve, and instrumentation to indicate throttle lever position.

The engine portion of the control system interfaces with the aircraft mechanical throttle control system on the pylon's forward mount beam structure. Electrical interfaces are achieved through Cable W100, Connector P103 for the resolver and P104 for the potentiometer which connect to the aircraft core electrical junction box. The electrical interfacing is schematically illustrated in Figure 10-2.

10.1.2 Function

The function of the aircraft/engine throttle control system is to provide mechanical remote control of the engine power through aircraft cockpit control levers, cables, and linkages. Two subfunctions of the control system are: to provide fuel supply shut-off capabilities and fan blade pitch positioning.

Engine power is controlled by moving the engine main fuel control lever from 18.5° to 102°, which correspond to an idle power setting and full power, respectively. Reverse thrust power settings are within this range; therefore, a throttle converter "switching" mechanism is required to convert the rotary unidirectional aircraft input into an oscillatory motion at the main fuel control.

Fuel flow is controlled by a pilot-operated switch which powers an engine mounted solenoid actuated four-way valve. When this solenoid is energized, fuel from the engine control unit is directed to the combustor fuel manifold. When the solenoid is deenergized, the fuel is bypassed to the main fuel pump

Figure 10-1. UDF™ Power Control System Schematic.

Figure 10-2. On-Engine Electrical Interconnection Schematic.

booster discharge manifold. This valve also connects the combustor manifold to the drain collector tank. Figure 10-3 is a schematic of this fuel shut-off bypass.

Fan blade pitch positioning is determined by a resolver coupled to the main fuel control power lever shaft; the power lever angle is, therefore, an indication of the engine thrust level. The resolver provides a signal to the DEC of the power lever angle. Excitation and signal conditioning is, in turn, provided by the DEC, which determines the required fan blade pitch angle and fuel flow at a particular power lever angle and also commands reverse thrust deployment by means of a reverse stop solenoid.

As a backup to the resolver on the fuel control power lever, a rotary potentiometer was added to the throttle control system. The potentiometer emits a signal to the DEC of impending reverse thrust actuation by inputting throttle position. At a preselected angle, the DEC sends an electrical signal to a reverse/stop solenoid which, upon being energized, retracts a latch lever that allows the pilot to proceed into the reverse thrust power regime.

10.1.3 Geometry

The aircraft power lever control consists of a cable-driven pulley system which extends from the aircraft cockpit pedestal through the nacelle strut to the mount beam interface. The aircraft system inputs an 180° shaft rotation to command thrust from full power (106°), to idle (0), to full reverse (-74°).

The engine portion of the throttle system connects to a spline shaft interface at the mount beam inside the nacelle and adjacent to the engine; the mechanism which attaches to the spline shaft is a four-bar linkage assembly, referred to as a throttle converter (Figure 10-4). This converter must change the angular motion of the aircraft input drum to the oscillatory motion needed at the main fuel control. The main fuel control then moves from full thrust (102°), to idle (18.5°), to full reverse (74°).

The throttle converter provides the necessary output motion, generated by the rotation of the spline shaft, to rotate the engine power lever within the operating range of the main fuel control. The converter can be characterized as a "rocker" mechanism. That is, neither the crank (later referred to as the
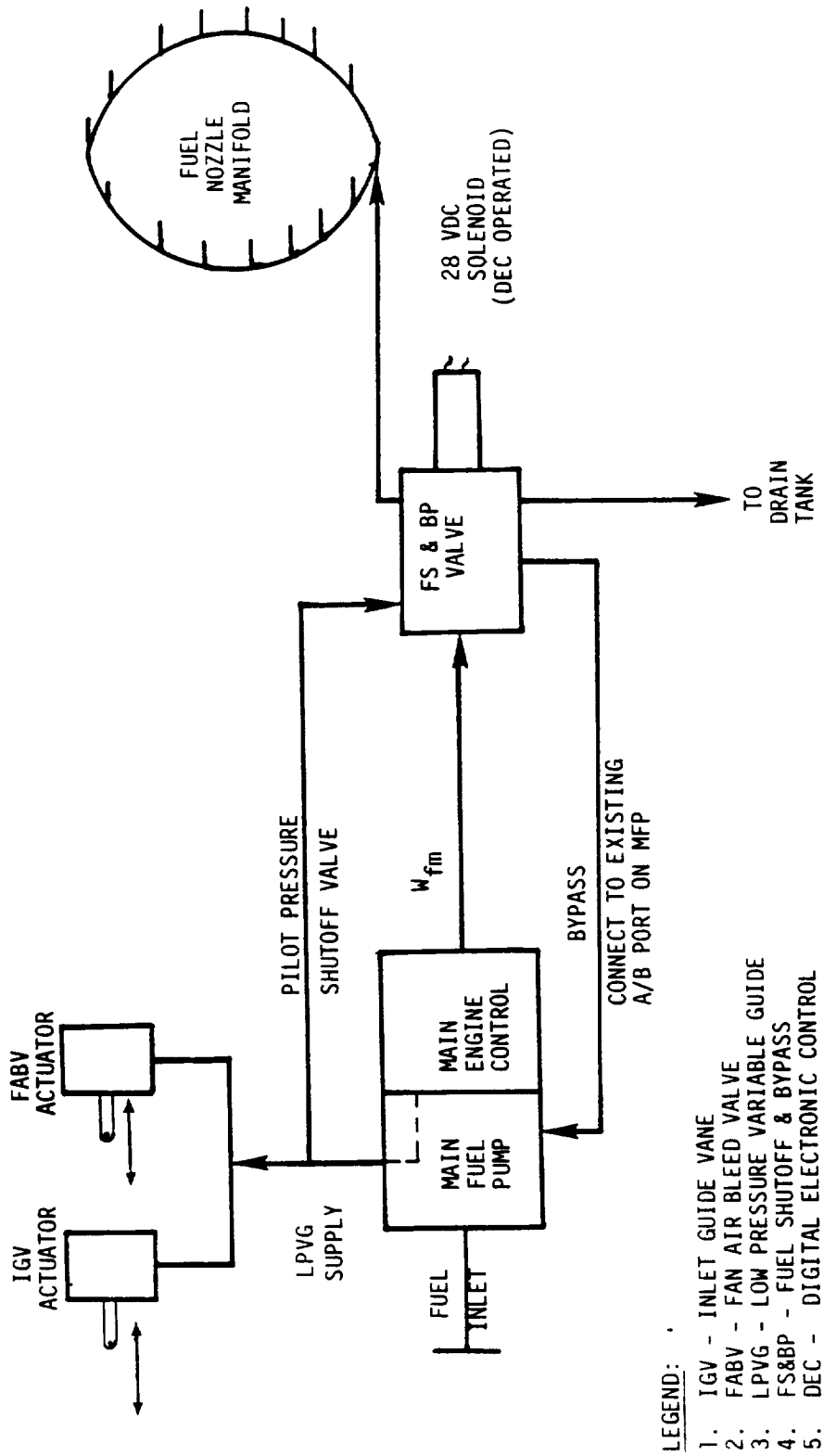
Figure 10-3. Fuel Shutoff/Bypass and Manifold Drain Valve.

LEGEND:

1. IGV - INLET GUIDE VANE
2. FABV - FAN AIR BLEED VALVE
3. LPVG - LOW PRESSURE VARIABLE GUIDE
4. FS&BP - FUEL SHUTOFF & BYPASS
5. DEC - DIGITAL ELECTRONIC CONTROL

"drive lever") nor the beam ("idler lever") can fully rotate about their axes; however, as the crank rotates through its maximum position, the beam oscillates through one cycle.

THROTTLE
DRIVE LEVER

LATCH
LEVER

RETRACT SOLENOID
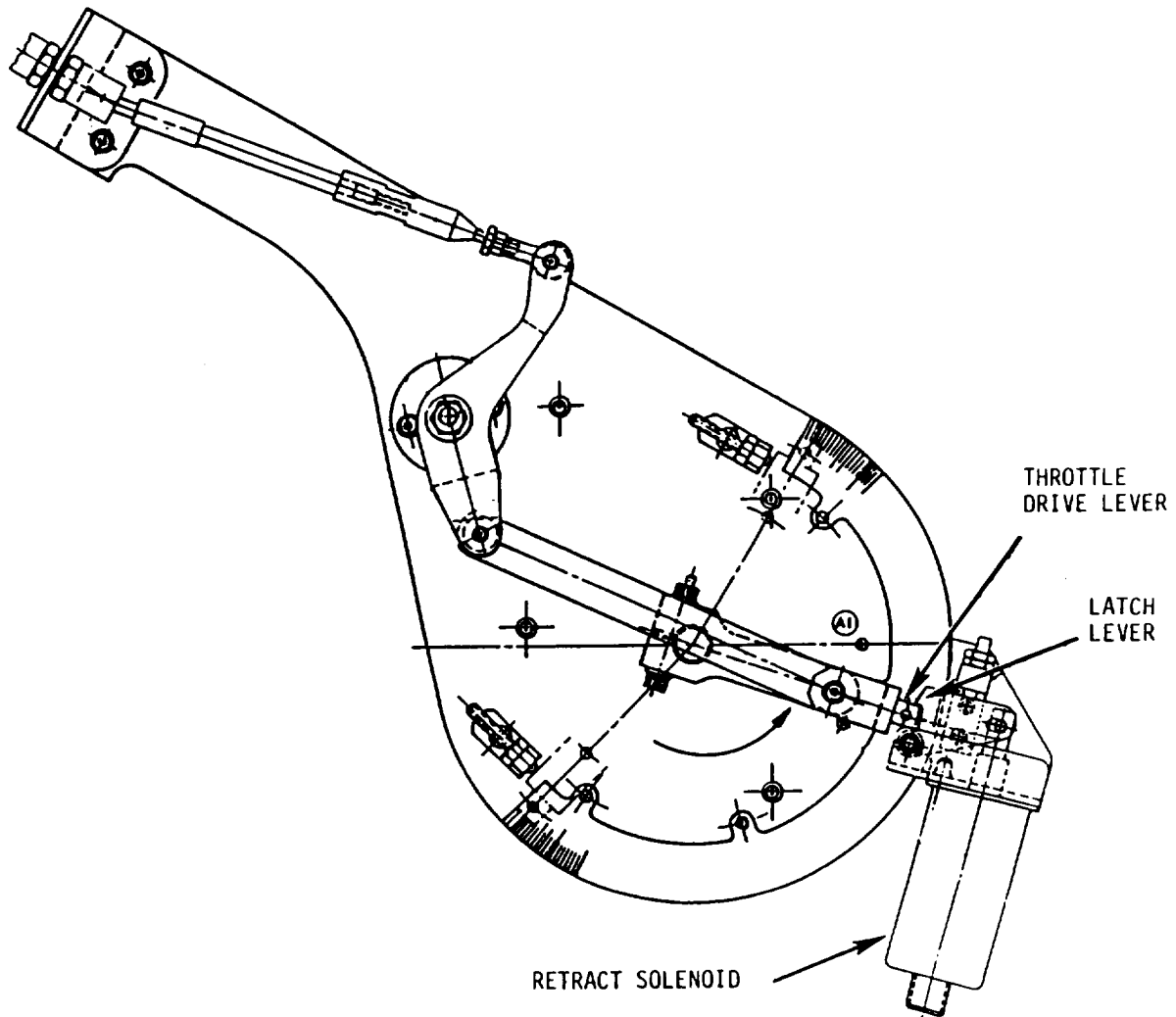
Figure 10-4. Throttle Converter and Reverse/Stop Installation.

Attached to the mounting plate of the throttle converter is a reverse/stop mechanism; the function of which mechanism is to prevent a reverse thrust power selection until the fan blade reverse pitch angle has been deployed. The reverse/stop mechanism consists of a latch-lever, pivot, retract solenoid, and a support bracket. It is positioned such that the latch lever will engage

and prevent the rotation of the drive lever in the reverse idle flat region, corresponding to 0° to -6°. Accordingly, the drive lever will remain engaged until an electrical signal from the DEC energizes the retract solenoid. The DEC provides the electrical signal only after the fan blade reverse pitch has been deployed.

The angular motion of the idler lever is translated to the engine power lever angle through a flexible push-pull cable. Brackets support and attach the cable sheath at either end. Routing and positioning of the throttle cable is controlled by engine mounted brackets and clamps in several locations.

Attached to the power lever is an extension spring serving two purposes:

- To reduce the throttle cable hysteresis effects by placing the cable in constant tension throughout its operating regime

- To pull the power lever to an idle engine power setting in the event of an engine throttle control system component failure (separation).

As shown in Figure 10-5, the resolver is mounted to a bracket attached to the main fuel control housing and positioned directly above the power lever input shaft. A threaded shaft with a flexible coupling connection provides "positive" attachment and centering of the resolver to the power lever input spline.

Located inside the mount beam, the potentiometer is coupled to the input shaft of the throttle converter; a support bracket positions the potentiometer with respect to the input shaft centerline. The potentiometer rotates with respect to the throttle converter.

Rigging provisions are provided on the throttle converter and the main fuel control drum corresponding to a maximum power angle of 106° and 102°, respectively. The throttle converter rig position will simultaneously set the aircraft shaft cable drum position for rigging the aircraft throttle levers. Adjustable mechanical stops at the maximum forward and reverse angles are provided on the throttle converter assembly to prevent exceeding predetermined power settings at the power lever. The power lever is not equipped for these stops since these settings are normally interim power settings on the engine control.
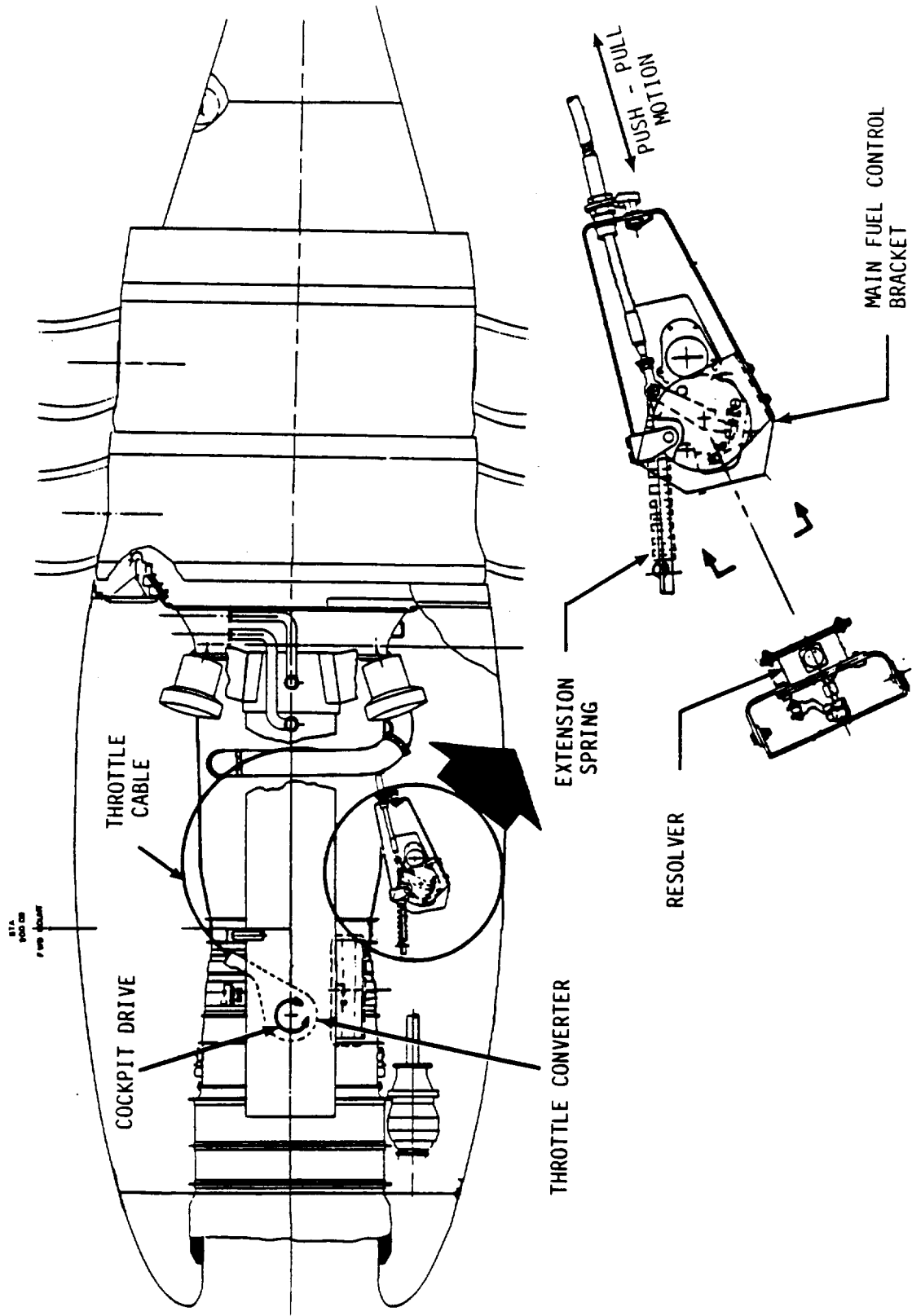
Figure 10-5. UDF™ Resolver Installation.

COCKPIT DRIVE

THROTTLE CABLE

THROTTLE CONVERTER

EXTENSION SPRING

RESOLVER

PUSH - PULL MOTION

MAIN FUEL CONTROL BRACKET

Angular relationships between the aircraft throttle lever angular input and cable travel, from the minimum power idle datum to the maximum forward and reverse power settings, to the corresponding angles on the throttle converter and main fuel control power lever are presented in Figures 10-6 and 10-7.

The throttle converter transmission assembly is designed to withstand an applied torque of 800 inch-lb at the mount beam shaft connection without failure.

The reverse/stop mechanism is designed to withstand an applied torque of 230 inch-lb at the mount beam shaft connection without permanent deformation to the latch lever. The torque required to back drive the reverse/stop latch lever is 45 inch-lb maximum, applied at the mount beam shaft connection.

The torque required to rotate the power lever through its range of travel does not exceed 25 inch-lb. Unless an external torque is applied, the power lever does not move with the engine operating.

The maximum allowable loads on the power lever are as follows:

- Axial   50 lb
- Shear (transverse)   50 lb
- Bending   100 inch-lb
- Torque (against stops)   300 inch-lb.

The extension spring provides a maximum force of 12.5 lb in the maximum power lever angle position.

Currents and voltages in the electrical components of the system are:

Resolver	Rotary Potentiometer	Retract Solenoid
Input: 5V at 2600 Hz	Input: 20 VDC	Input: 28 VDC
Maximum: 2.3 mA	Maximum: 10 KOHMS	Maximum: 1.5A

10.2 CONFIGURATIONS DESIGN

10.2.1 Design

Configurations is the provision of pipes and hoses which transfer fluids between the engine and the controls and accessory hardware. The major design objectives are: sufficient fluid flow, proper routing, and adequate support.
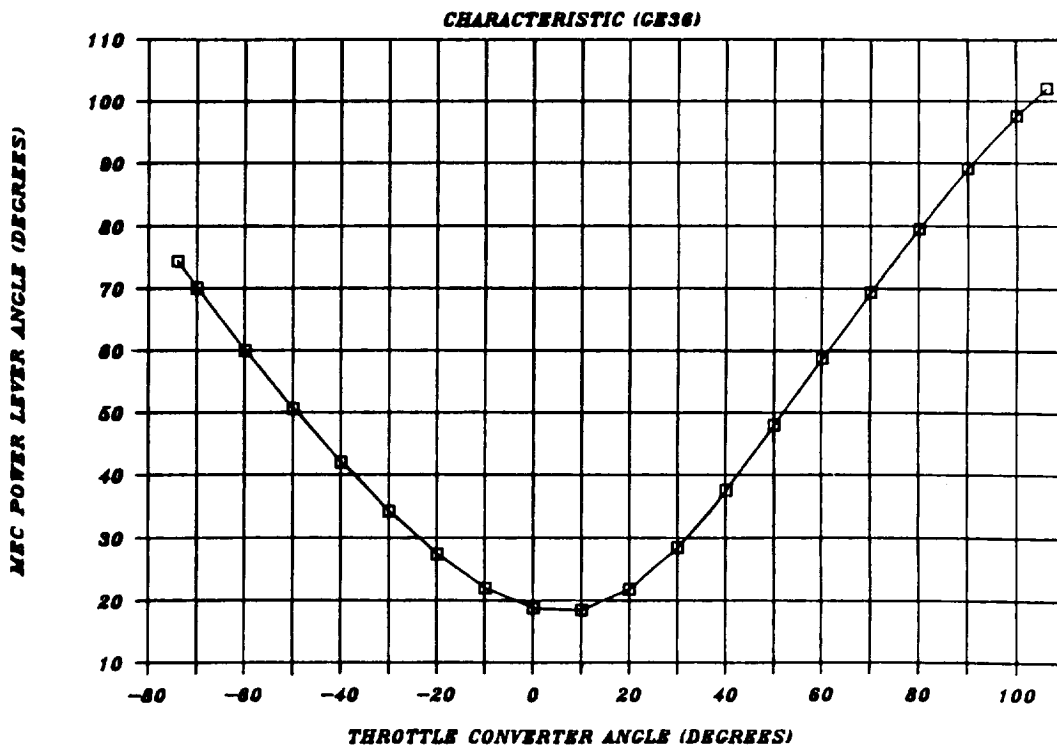
Figure 10-6. Throttle Linkage Converter - Characteristic (GE36).
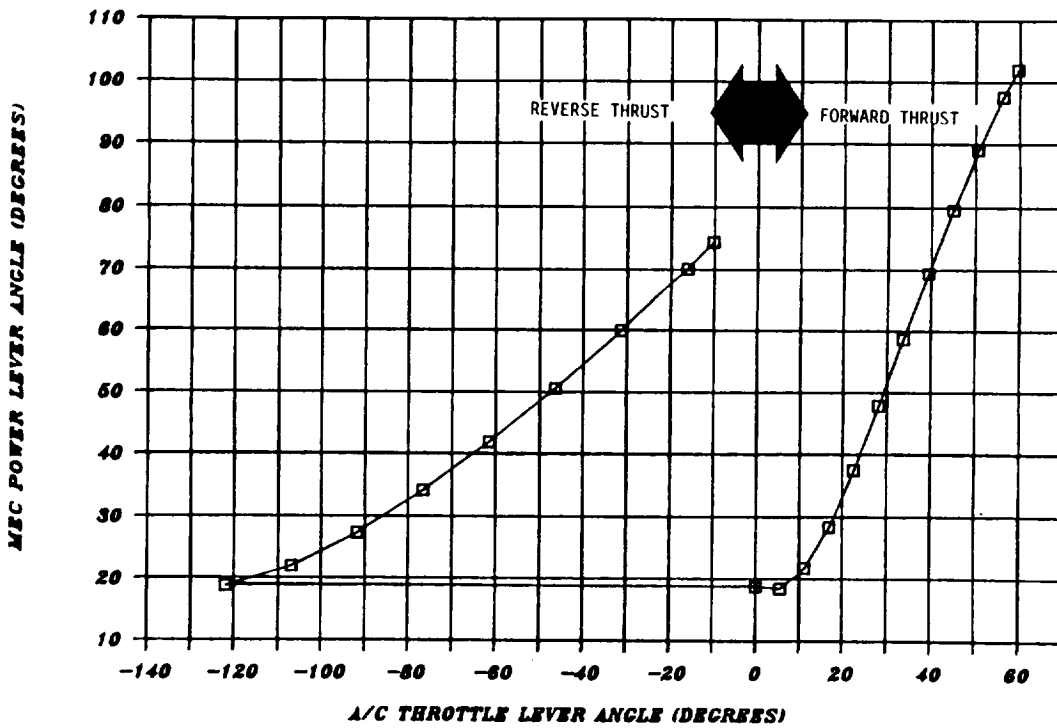
Figure 10-7. MEC PLA Versus A/C Throttle Lever.

To achieve this, a new and unique method was developed for the configurations design for the UDF™ engine. Use of drafted layouts and parts detail drawings results in a lot of hardware interference. To avoid this, a configuration was designed using an actual F404 engine casing and its controls and accessories components as a tool. A wire running between ports was utilized to define the routing from one component port to another; after the routing was established, a tube definition was derived. This was accomplished by taking the bent wire to a vectoring machine to determine its coordinates which were then programmed into a numerically controlled tube bending machine. A tube bent by the numerically controlled machine was then trial-fit on the design tool. If the tube fit properly, it then was sent to the manufacturing shop where three identical tubes were manufactured. A drawing of the part was then generated defining the fittings and overall length. The tube shape was defined with coordinates derived from the vectoring machine. This data was then recorded as the engineering definition on the drawing.

If the tube (after forming) did not fit properly, it was tweaked slightly by hand until it fit. After the proper fit was established, it was returned to the vector machine to redefine its coordinates and then sent to the manufacturing cycle. Figures 10-8 and 10-9 depict the design tool used to design the GE36 tubing.

This innovative design method achieved normal design goals of low stress, natural frequencies outside of the engine operating range, and no leaks. Its major improvement, however, was the lack of tubing which did not fit. Former configuration designs produced a large percentage of tubing which did not fit the first time assembled. However, this new method virtually eliminated the problem of hardware which could not be assembled due to interference problems. Accordingly, this design process reduced the cost by 40% and the cycle time, from design start through hardware completion, by 50%.

The configuration hardware was designed conforming to General Electric's Design Practice (DP6001). This assured a design which would meet all life and safety requirements of the ground demo program.

Tube material and wall thickness was selected with an adequate margin for internal pressure stress. Routing was performed to minimize thermal stress

272
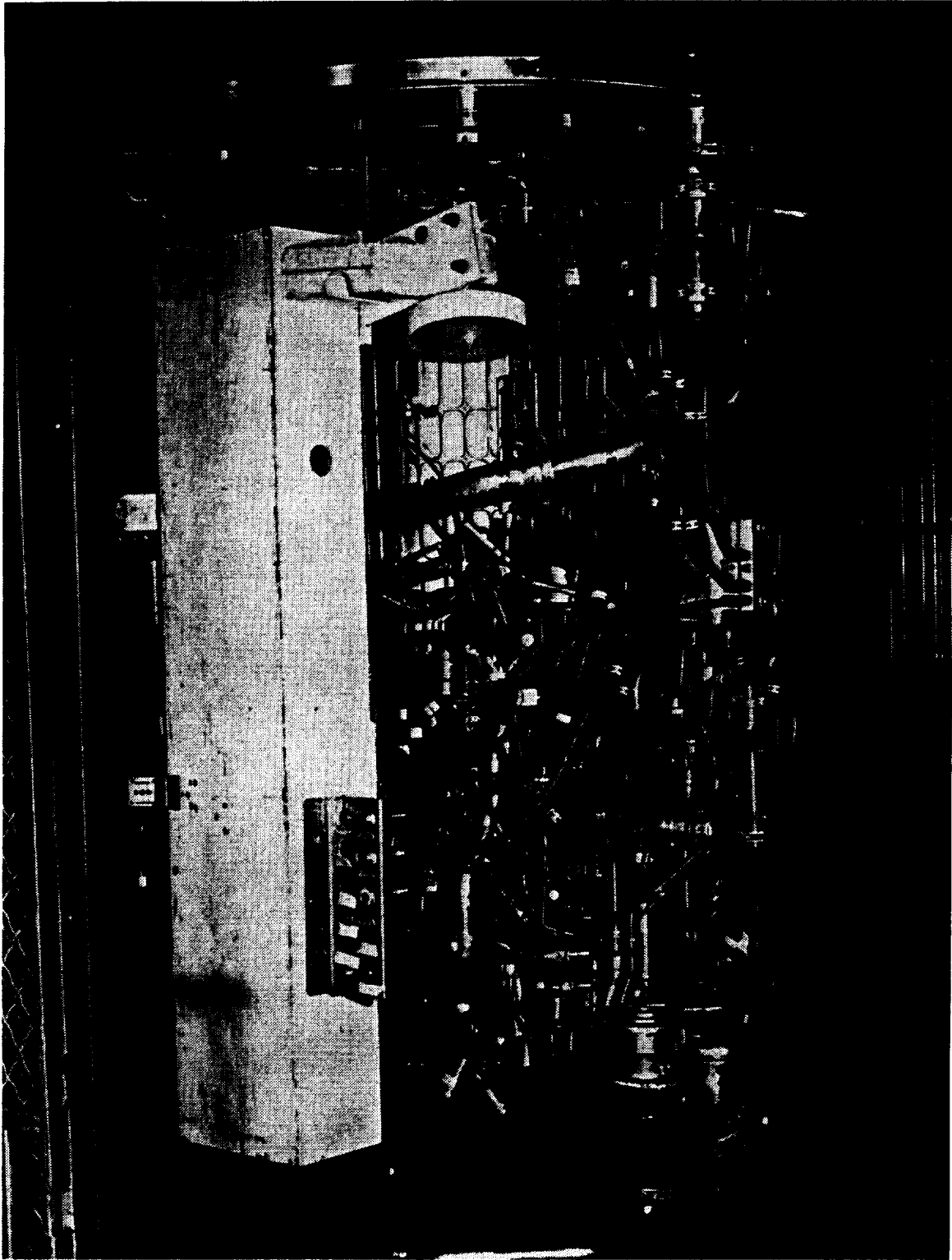
Figure 10-8. Design Tool Implemented to Design 6936 Tubing.

273
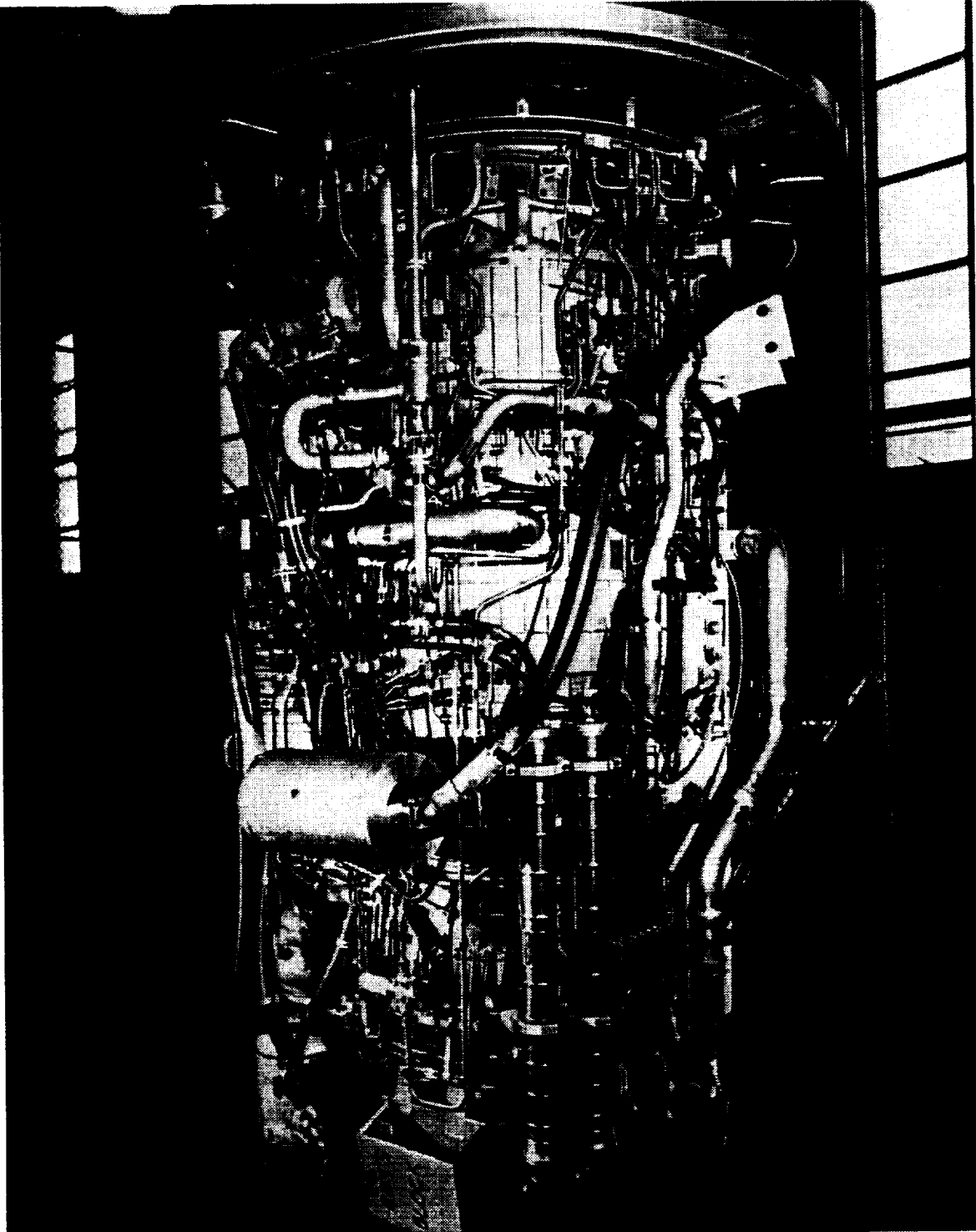
Figure 10-9.   F404 Engine Casing and C&A Components Utilized as a Design
Tool.

274

C-4

while providing ample support points to keep the piping natural frequencies above the engine operating range.

Line forward fittings were chosen to minimize the chance for leakage, as has been established by past experience with this type of end fittings.

10.2.2 Piping Natural Frequency Testing

A major consideration with configuration piping is that the natural frequencies be kept outside of the engine operating range. To accomplish this, measurements were made of the natural frequencies of all pipes mounted on the design tool or engine. If these frequencies were low, brackets were added to drive them out of the engine frequency range (280 Hz). Figure 10-10 and Table 10-1 demonstrate a frequency scan for a typical configurations tube. This assures that no tubes will fail due to high cycle fatigue.

10.2.3 Piping Internal Pressure Testing

All the tube wall thicknesses were sized using standard stress formulas. After the tubes were manufactured, they were subjected to a pressure test of 1.25× to 2× their maximum operating levels, to assure that each had adequate burst margin.
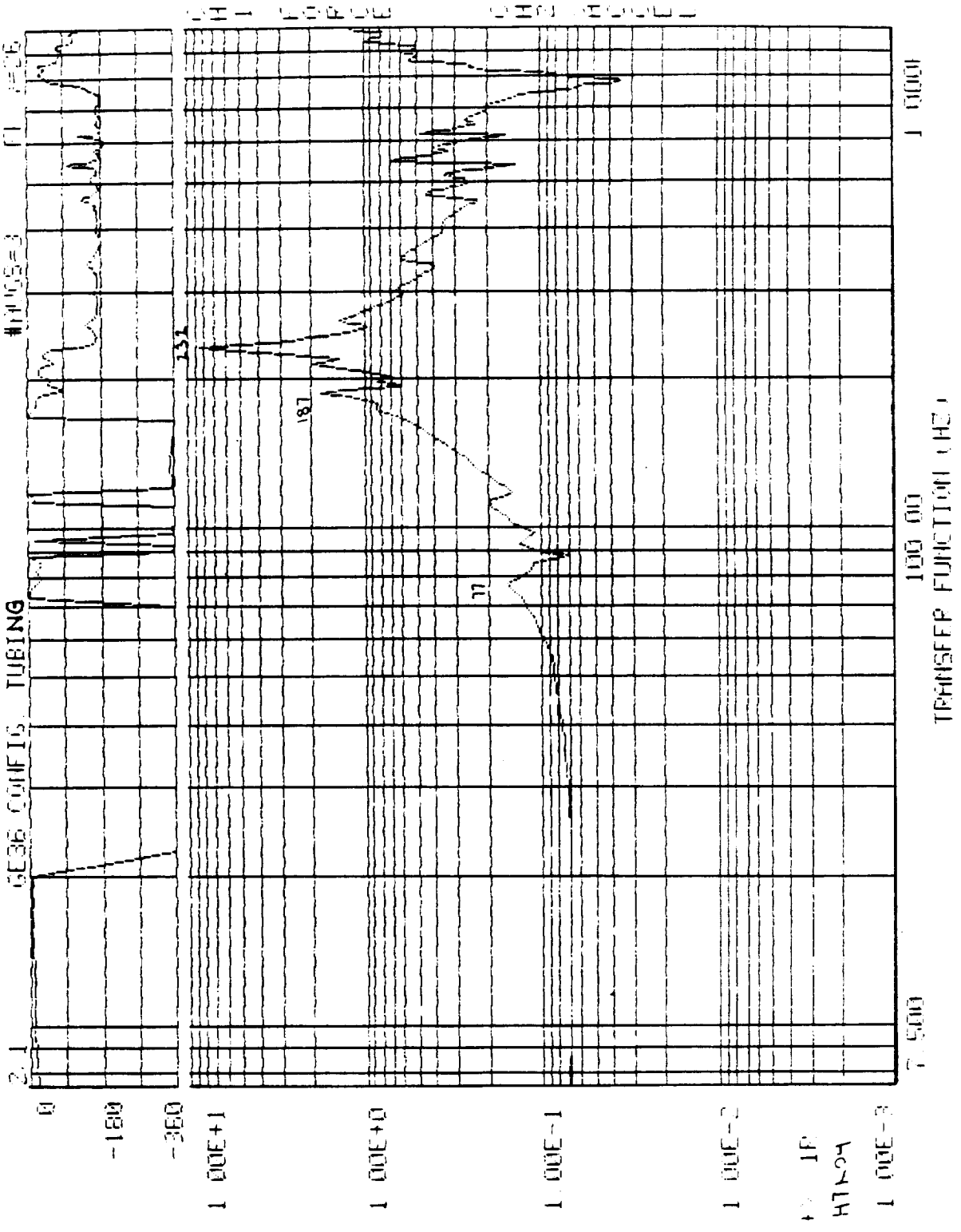
Figure 10-10. Frequency Scan for a Typical Configuration Tube.

276

Table 10-1. Frequency Scan Values (Sample Rate: 2.560 KHz)
for a Typical Configurations Tube.

Rank	Bin	Frequency	F1(N)	F2(N)
1	93	232.50	8.39E+0	-1.17E+2
2	86	215.00	1.97E+0	-4.97E+1
3	75	187.50	1.75E+0	-4.60E+1
4	105	262.50	1.38E+0	-1.52E-2
5	70	175.00	8.44E-1	-1.59E+1
6	79	197.50	8.36E-1	-4.58E+1
7	121	302.50	6.44E-1	-1.67E+2
8	140	350.00	6.01E-1	-1.59E+2
9	188	470.00	4.37E-1	-1.54E+2
10	166	415.00	3.52E-1	-1.71E+2
11	161	402.50	3.51E-1	-1.71E+2
12	45	112.50	1.97E-1	-1.11E+1
13	31	77.500	1.58E-1	-1.39E+1
14	37	92.500	1.32E-1	-3.59E+2
15	3	7.500	7.21E-2	-1.50E+1

Rank	Bin	Frequency	F1(N)	F2(N)
1	399	997.50	1.19E+0	-1.25E+2
2	377	942.50	9.77E-1	-9.75E+1
3	220	550.00	6.89E-1	-1.39E+2
4	358	895.00	6.00E-1	-8.35E+1
5	345	862.50	5.48E-1	-6.17E+1
6	249	622.50	4.70E-1	-1.62E+2
7	232	580.00	4.07E-1	-1.71E+2
8	206	515.00	3.37E-1	-1.62E+2
9	265	662.50	2.61E-1	-1.72E+2
10	334	835.00	2.53E-1	-4.11E+1
11	280	700.00	1.95E-1	-1.70E+2
12	312	780.00	3.61E-2	-1.05E+2

11.0 CONTROL SYSTEM DESIGN

11.1 CONTROL SYSTEM DESCRIPTION

The control system for the GE36 demonstrator engine provides control of the following:

- Fuel Flow
- Gas Generator HP Compressor Variable Geometry
- Gas Generator IP Compressor Variable Geometry
- Bypass Duct Bleed
- Fan Pitch.

By controlling each of these functions, the system provides steady-state and transient control of engine thrust in response to power lever demand and does not exceed any operating limits or require any special crew attention.

The control system incorporates the following features:

- Integrates unducted fan blade pitch and gas generator schedules

- Provides thrust/power level management

- Provides the capability to synchronize and synchrophase counterrotating blade rows to minimize noise

- Provides the capability to run in both off-design and alternate modes for investigation of performance and noise sensitivities

- Controls fan speeds through adjustment of blade pitch angle to secure maximum fan operating efficiency

- Controls fan speed and/or blade pitch angle and gas generator power level to set reverse thrust.

11.2 SCHEMATICS

The total engine control system is depicted in Figures 11-1 through 11-4.

11.3 HYDROMECHANICAL CONTROL SUBSYSTEM

The hydromechanical control is an unmodified F404 fuel-operated electro-hydromechanical component as described in the following paragraphs.

Figure 11-1. On-Engine Electrical Interconnection Diagram.

279
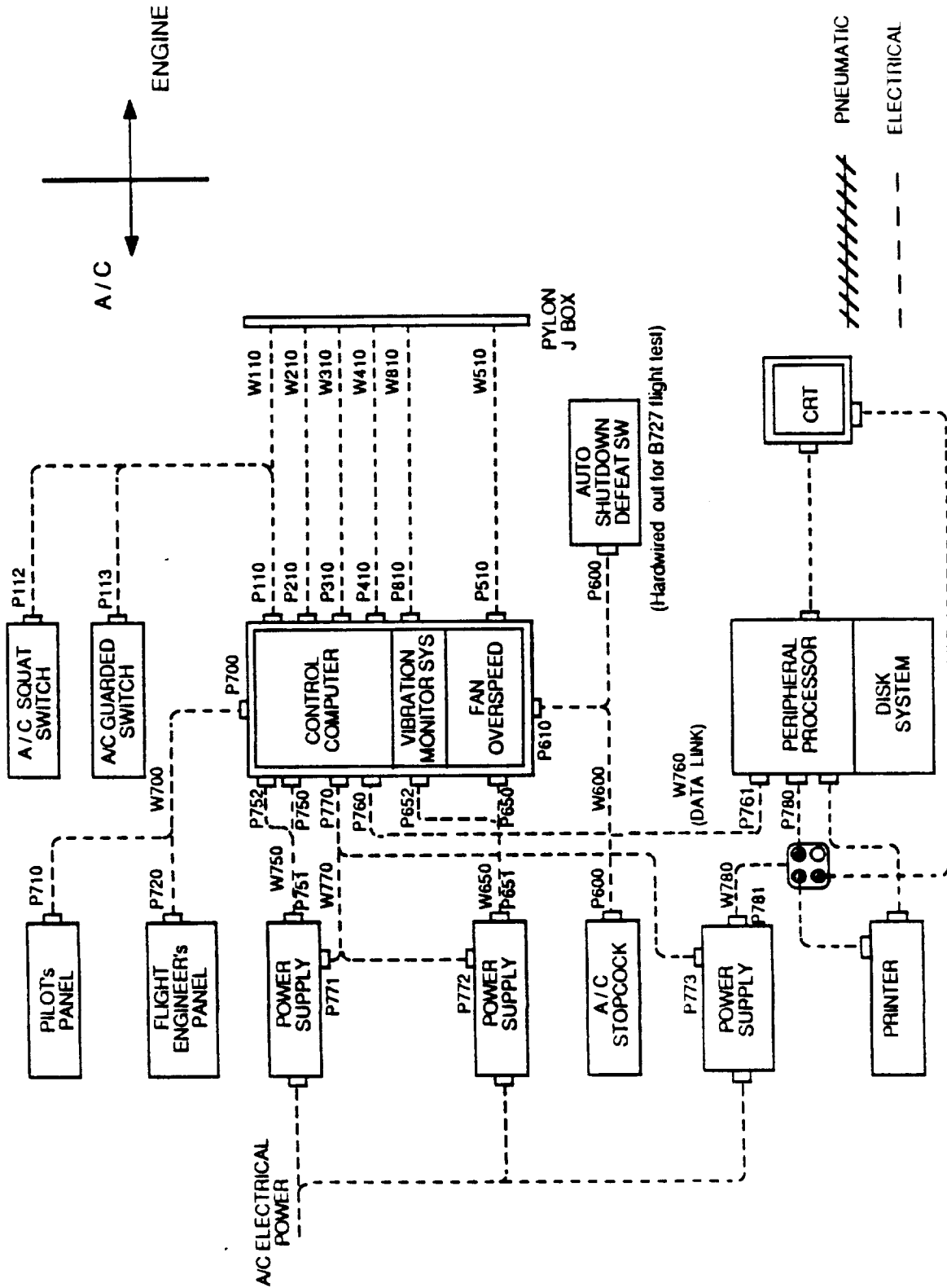
Figure 11-2. Off-Engine Electrical Interconnection Diagram.
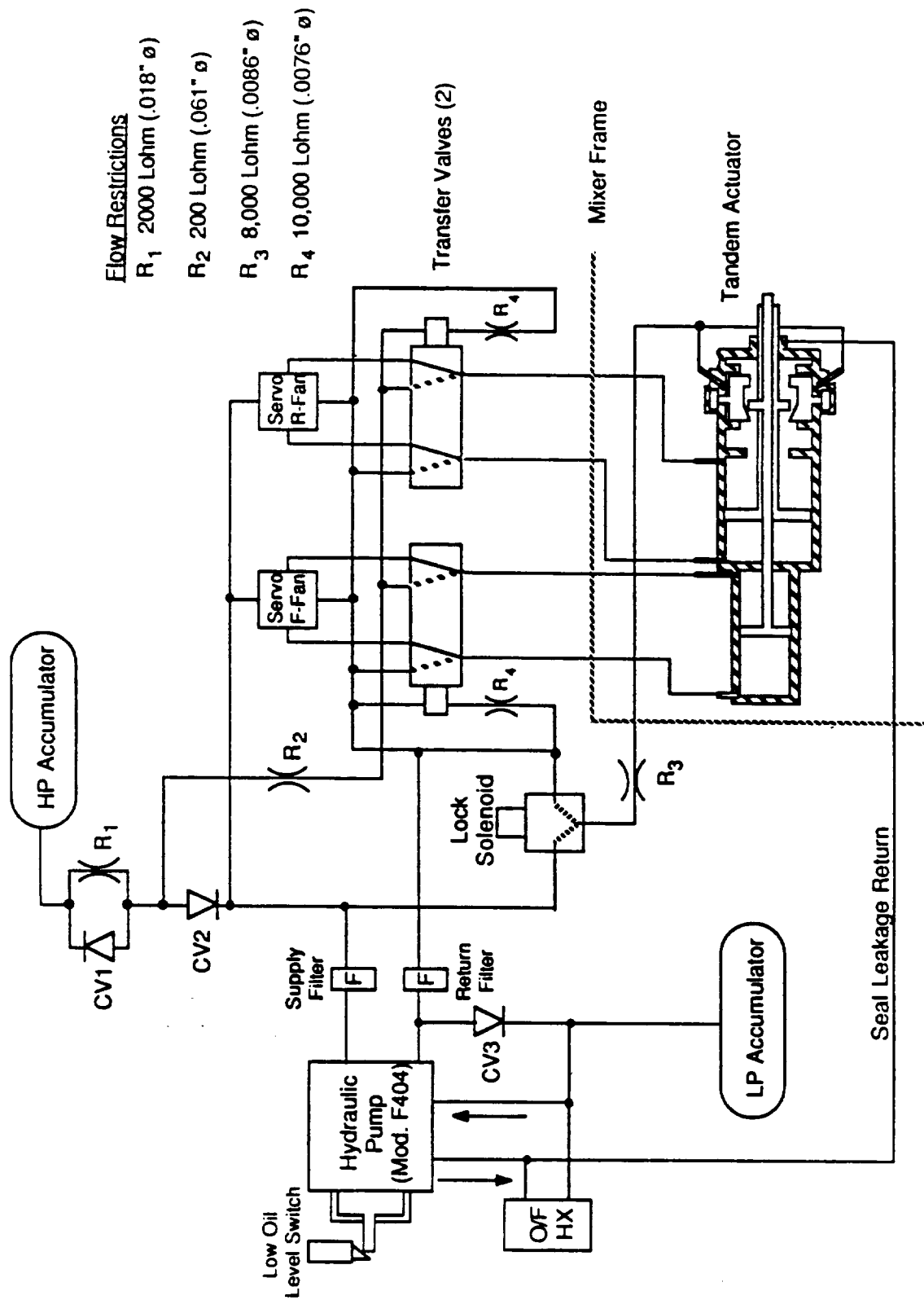
Figure 11-3. Fan Pitch Hydraulic System Schematic.
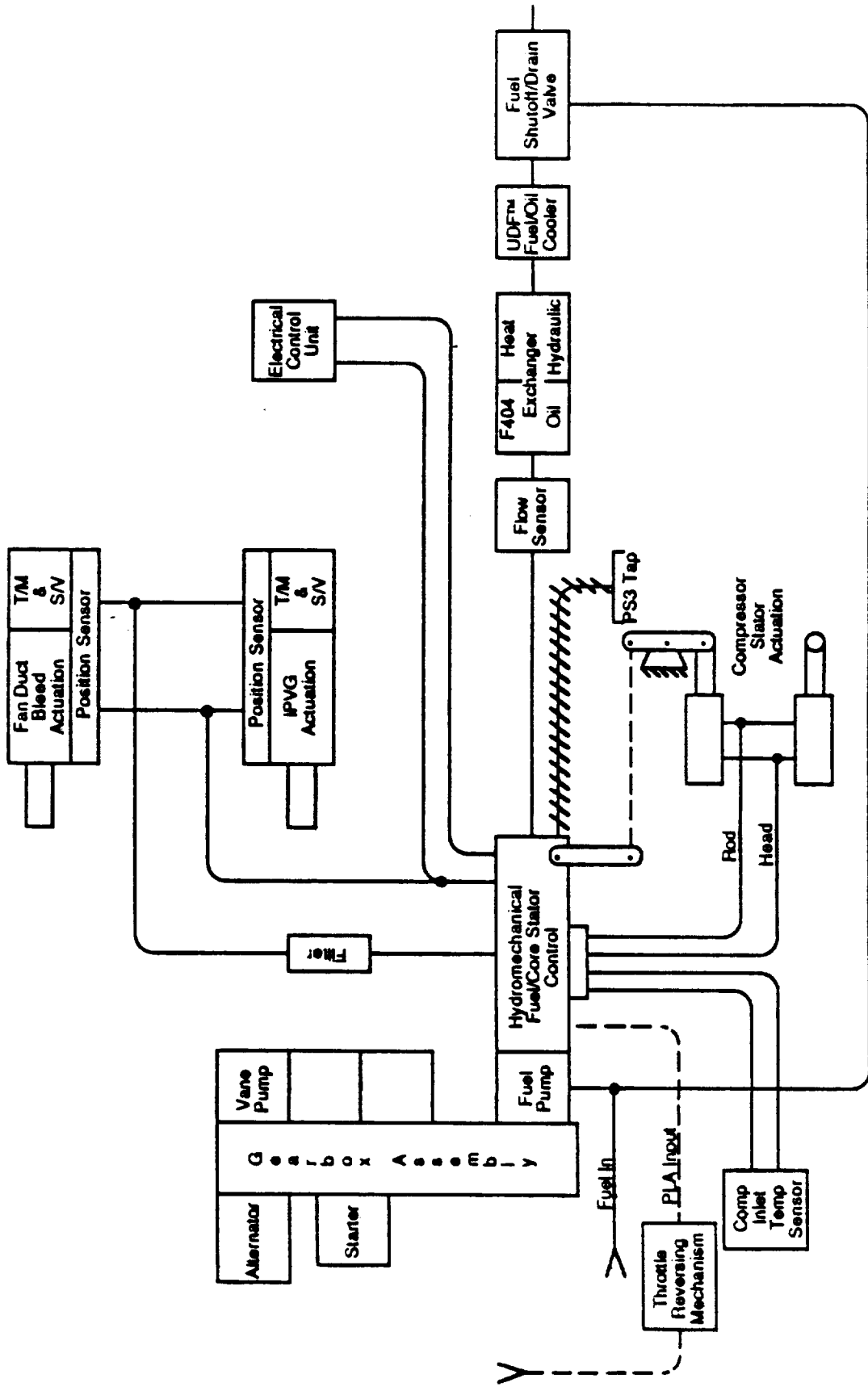
Figure 11-4. Fuel System Schematic.

282

Fuel Flow Override - The hydromechanical unit (HMU) accepts an externally generated electrical signal to reduce the metered fuel flow with a designated authority range and to incorporate a linear variable differential transducer (LVDT) which produces an electrical signal proportional to metered fuel flow. A LVDT, contained in the HMU, provides a metering valve feedback signal to the control computer (CC) by means of the electrical control unit (ECU). The electrohydraulic servovalve contained in the HMU operates in response to electrical input signals from the CC to port hydraulic pressure to the metering valve actuator.

HP Shaft Overspeed Limit - The primary HP shaft overspeed protection is provided by fuel scheduling. In addition, the HMU is mechanized such that the fuel flow is reduced from 12,000 pounds per hour to less than 1,000 pounds per hour in 0.05 seconds (maximum) after the overspeed (XN25) set point speed plus 0.5% is achieved. The XN25 overspeed setting is 105.5% Crpm.

IP Shaft Overspeed Protection - The HMU provides IP shaft overspeed protection by accepting an electrical overspeed signal from the ECU; upon receipt of this overspeed signal, metered flow is reduced to approximately 200 pounds per hour by porting control case pressure to the spring side of the proportional bypass valve.

HPC Variable Geometry (VG) Stator Control - The HMU incorporates provisions for controlling HPC variable stators. By means of hydraulic (fuel) flow from two ports, the HMU causes HPVG actuators to extend (or retract). Accordingly, HPVG feedback is retracted (or extended) relative to the HPVG servo-reference. The schedule of variable geometry feedback position is a function of corrected HP rotor speed.

11.4 GAS GENERATOR ECU AND ASSOCIATED COMPONENTS

11.4.1 Electrical Control Unit

The ECU is a modular solid-state component, mounted on the engine, that is supplied with power from the engine alternator and cooled by fuel from the fuel pump. It provides signal excitation and signal conditioning as follows.

HP Shaft Speed (XN25) - The signal for HP shaft speed (XN25) is obtained from the ECU winding of the alternator. The frequency of the XN25 signal is

proportional to HP shaft speed. A conditioned, direct current (dc) signal which is proportional to HP shaft speed is transmitted to the CC.

IP Shaft Speed (XN2) - The signal for IP shaft speed comes from two eddy-current sensors. The frequency of the XN2 signals is proportional to IP shaft speed, and 100% XN2 is 9,289 Hz (13,270 rpm). A conditioned DC signal proportional to IP shaft speed is transmitted to the control computer.

IP Shaft Speed Protection Features - The ECU supplies twenty ± 2 VDC at a maximum of 200 mA to an overspeed solenoid in the HMU whenever the XN2 signal is greater than 15,127.8 rpm. The solenoid voltage is latched "ON" until XN25 is less than 7,564.5 rpm. Enerizing the fan overspeed solenoid results in the fuel flow being reduced to approximately 200 pounds per hour.

Interturbine Temperature (T46) - The ECU accepts individual mV signals from four thermocouple probes and interconnects them for averaging in the ECU. The T46 mV signal conforms to the chromel-alumel (Type K) characteristic of NBS Nomograph 125. A conditioned signal proportional to interturbine temperature is transmitted to the control computer.

Inlet Temperature (T2) - The electric control unit converts the resistance of a T2 resistance thermal device (RTD) to a suitable electrical signal and provides a regulated direct current of 52 mA, maximum, to the T2 sensor. The ECU shall be designed so that any possible failure does not subject the T2 sensor to a current greater than 100 mA. The ECU conditions a direct current signal proportional to inlet temperature prior to transmission to the control computer.

Fuel Metering Valve LVDT (XWF36) - The ECU provides regulated, alternating current (ac) excitation voltage to the primary of the HMU metering valve LVDT and accepts its ac output. The output of the HMU metering valve LVDT is a function of metering valve position, and the ECU conditions a dc signal that is proportionate to the fuel metering valve position prior to transmission to the control computer.

IP Compressor Stator Actuator LVDT (XLPVG) - The ECU provides a regulated ac excitation voltage to the primary of the IP compressor stator actuator LVDT and accepts its secondary output. The output of the LVDT is a function of IP compressor stator actuator position, and the ECU conditions a dc signal which

is proportionate to the IP compressor stator actuator position prior to trans-mission to the control computer.

11.4.2 Alternator

The alternator consists of a rotor and a stator, which are assembled to the gearbox. The stator has three separate windings which provide electrical power to the ignition exciter and ECU and a HP shaft speed (XN25) signal to the cockpit.

11.4.3 IP Compressor Stator Actuation

A fuel-powered actuator and bellcrank system is mounted on the IP stator case and front frame at the eight o'clock position. The bellcrank has two arms; one of which is connected directly to the actuator; the other is link-connected to the front frame inlet and Stage 1 guide vane actuating rings. In operation, when the fuel-powered actuator moves the bellcrank, the actuating rings also move, opening or closing the inlet and Stage 1 guide vanes. The IP compressor stator schedule is computed in the control computer. Closed-loop IP stator control is accomplished by operation of the servovalve and the LVDT position feedback.

Actuator - The fuel-powered actuator contains the electrohydraulic servo-valve and the electrical position feedback.

Position Sensor - A linear variable differential transformer, contained in the IP stator actuator, provides the IP stator position feedback signal to the CC, through the ECU.

Servovalve - The electrohydraulic servovalve (contained in the IP stator actuator) operates in response to electrical input signals from the CC to port hydraulic pressure to the IP stator actuator.

11.4.4 Engine Interface Unit (EIU)

The control computer provides excitation for, and receives signals from, three pressure transducers that are contained in the engine-mounted EIU. The inlet total (P2), duct total (P15), and interturbine total (P46) pressures are

measured. Each transducer receives an air pressure input and, with excitation voltage applied, provides an output signal proportionate to input pressure.

11.4.5 Ignition System

The engine ignition system is activated and terminated from an external source and is, thus, electrically self-sufficient requiring no external power. Ignition switch connections are provided for external wiring, and one ignitor and a separate exciter output circuit are provided.

11.5 CC, INTERFACE CIRCUITRY, AND OVERSPEED PROTECTION SYSTEM

The control computer, interface circuitry, and the overspeed protection system are mounted on standard cards incorporated into rack-mounted boxes and are compatible with the input/output (I/O) features of the system. The CC, interface circuitry, and overspeed protection system will meet these needs:

- Excite, then condition, signals from engine sensors and input these signals to the control computer.

- Execute the control alogrithms and provide output drivers for these control outputs.

- Communicate with a peripheral computer system (PCS).

- Provide independent circuits for fan overspeed protection.

- Use separate I/O equipment compatible with the control computer I/O for the engine sensors and control outputs. Communication with the PCS will be through a general purpose interface bus (GPIB), as covered in IEEE-488 Specification, 1978 Issue, and as modified in 1980. Reference: IEEE Standard 488-1978 and IEEE Standard-A-1980; Institute of Electrical and Electronics Engineers, Inc., 345 East 47th Street, New York, NY 10017.

11.5.1 Inputs

This section defines pertinent characteristics and requirements of the sensors which provide signals to the control computer (Figure 11-1).

Fan Speed Sensors - Fan speed will be sensed by means of electromagnetic pickups which provide electrical pulses in response to the teeth on a multi-toothed rotating wheel. One coil from each of the four dual-coil fan speed

286

sensors will be used by the CC for fan speed and phase measurement. The CC will contain zero-crossing detectors (ZCD) and interface circuitry necessary to detect and decode each sensor signal.

Pressure Sensors - Three pressure transducers are housed in the engine-mounted EIU. The CC shall provide excitation for, and receive signals from, three remote pressure transducers. Each transducer receives an air pressure input and, with excitation voltage applied, provides an output signal, which is proportional to the input pressure.

Power Lever Angle Sensing - Power lever angle is sensed by two devices:

- A resolver mounted directly on the hydromechanical fuel lever (RSA)

- A rotary potentiometer mounted on the throttle converter link-age unit (AAQA).

Fan Pitch, Duct Bleed, and Fan Pitch Limit LVDT - The control computer provides the fan pitch, duct bleed, and fan pitch limit LVDT with excitation voltages having a sine waveshape and a fundamental frequency of 2600 ± 200 Hz. The voltage has an amplitude of 5.00 volts RMS ± 5% and a linearity of 0.05% of peak. When excited with the voltage above, the LVDT require a maximum of 0.5 volt-amperes each, when the LVDT secondary is loaded to 10,000 ohms mini-mum resistance. These signals are converted into digits directly through the use of an Analog Devices 2950 series converter. The digital outputs are input into the control computer memory as described in the VMEbus input section.

Vibration Amplifiers - The control computer accepts inputs from each of the four vibration amplifiers. Digital conversion and input of these signals into the control computer memory is described in the I/O bus input section. Software is used for blade-out detection and automatic shutdown.

Discrete Input Data Word (Logic Signal) - Circuits are included to create a 16-bit data word, where each bit is set or cleared by separate input sig-nals. The data word is input into the control computer memory as described in the VMEbus input section.

Control Computer Input Interface

I/O Bus Input - The CC input/output channel interface provides an 8-bit asynchronous data communications path between the microprocessor unit (MPU) and the analog-to-digital (A/D) converter output. The I/O channel interface also provides the housekeeping functions and control signals necessary for this data communication between the MPU and A/D converter output. All analog signals are multiplexed through a single analog-to-digital converter. The CC requests input/output data transmission of a particular A/D channel, and this request is decoded by the A/D circuitry causing that signal to be transmitted separately. The A/D output is a 12-bit digital word that interfaces with the I/O bus.

VMEbus Data Transfer - The VMEbus contains a high speed, asynchronous, parallel data transfer bus (DTB), which is used to transfer the digital data to or from the control computer memory. The address and data are placed on address and data buses, and the address and data strobes are generated. The MPU waits until the data transfer acknowledge signal is given before continuing with the current instruction cycle.

Control Computer Output Interface

I/O Bus Output - The control computer input/output channel interface provides an 8-bit asynchronous data communications path between the MPU and the digital-to-analog (D/A) converter input and also provides the housekeeping functions and control signals necessary for this data communication between the MPU and D/A converter input. The digital signals required to drive the torque motors are obtained from the I/O bus through a D/A converter, which converts digital data into analog voltage. A 12-bit digital word is converted into an equivalent current, then an amplifier converts this current into an equivalent voltage.

VMEbus Output - The VMEbus contains a high speed asynchronous parallel data transfer bus, which is used to transfer the digital data to and from the control computer memory.

Torque Motor Driver Outputs - Interface circuitry delivers dc currents to five torque motors in response to signals from the control computer I/O bus.

288

<u>Solenoid Driver Characteristics</u> - Circuits are provided to power the following solenoid systems:

- Pitch Actuator Limit - This is mechanized such that energizing the solenoid retracts the limit

- LP Lube Oil Bypass - This is mechanized such that energizing the solenoid limits the LP lube oil supply

- Thrust Reverse Limit - This is mechanized such that energizing the solenoid permits high power reverse operation.

11.5.2 <u>Control Computer/Peripheral Computer Data Interface</u>

Both the control computer and the peripheral computer are equipped with a Motorola MVME300 GPIB controller with direct memory access (DMA) which provides a complete IEEE-488 bus/listener/talker/controller interface for use with a VMEbus system. Data is sent to and from the processor in single transmissions using DMA.

11.5.3 <u>Fan Overspeed Protection</u>

The fan overspeed system is powered from an independent, noninterruptable power supply. Independent circuitry is provided for sensing each of the two fan speeds, comparing each fan speed with an overspeed limit, signaling an overspeed condition (defined as either speed sensor indicating an overspeed), and initiating an overspeed emergency shutdown. This system accepts an emergency shutdown signal from the CC and provides for automatic self-testing. An overspeed occurrence or an emergency shutdown signal from the control computer will activate the following:

- Shuts off main fuel flow (by deenergizing the fuel shutoff solenoid valve)

- Provides positive actuation to the fan stage feather position (by deenergizing the solenoid valve, which controls the pitch actuation transfer valve).

<u>Fan Speed Sensing</u> - Dedicated inputs from two fan speed sensors are used (that is, one fan speed sensor from each rotor is used). Digital read-outs for each sensed fan speed are provided on the overspeed unit.

Overspeed Trip - The overspeed trip is set to activate at 99% ± 0.25% rpm of either fan rotor and is externally adjustable from 95% to 125% rpm. This overspeed trip is mechanized using an up/down counter, such that the overspeed condition is in effect for one complete revolution (eight successive overspeed indications) before the overspeed trip is activated. This trip and associated functions are in effect within 0.050 seconds after the overspeed has occurred.

Overspeed Fuel Shutoff - This function is achieved by deenergizing the fuel shutoff solenoid, thus cutting off fuel flow.

Overspeed Fan Stage Feathering - When the overspeed trip occurs, the two transfer valve solenoids are deenergized, thus porting supply pressure to the rod end and return pressure to the head end of each actuator, providing positive means of positioning the fan pitch mechanism to the feather position.

Solenoid Test - A circuit is provided that deenergizes both the fuel shutoff and fan stage feathering solenoid valves, and sets the fan overspeed circuitry status flag each time the A/C shutoff switch is turned off. This occurs, under normal conditions, each time the engine is shutdown.

Overspeed Logic Self-Test - A circuit is provided that performs a self-test of the overspeed logic. The circuitry provides two sets of thumbwheel switches - one for normal operation, and the other for an overspeed test mode. Self-test is accomplished as the control computer, under software control, selects the overspeed test mode thumbwheel switch. If fan speed is above the overspeed test mode thumbwheel switch setting, the overspeed circuitry latches the overspeed trip and sets the fan overspeed circuitry status flag to indicate that the circuit has been tripped. Upon receipt of an overspeed trip indication signal, the control computer rearms the circuit.

Aircraft Shutoff Switch

The aircraft shutoff is a double pole double throw (DPDT) switch, break-before-make, powered from the aircraft, functioning as follows:

● Shutoff "open-to-close" trips circuit

● Shutoff "close-to-open" arms circuit

● Circuit powers up tripped

• Circuit holds overspeed circuit in present state if DPDT switch indicates failure.

Hardware/Software Integrity (Watchdog Timer) - Circuits are included to incorporate a resettable timer, such that if the timer times out, engine shutdown is initiated, and a fault is indicated. The timer is reset by software control during an 11.95 ms to 12.15 ms time window. Elapsed timing before the window is open is under software control. The system is designed to power up in the failed mode; a start pulse that is followed by a punch in the window, clears this fault. However, an attempt to reset the timer at any time outside the window causes an immediate fault indication, initiating engine shutdown.

11.5.4 Peripheral Computer System

The peripheral computer system (PCS) is a Motorola VME/10 microcomputer system (Figure 11-5), which consists of a chassis, a keyboard, a display unit, and a Texas Instrument (TI) Model 855 printer.

The PCS software monitors the variables in the control computer system by means of the IEEE-488 data link between the two systems. It provides a real-time data display to the operator and records data for posttest analysis. The PCS provides the operator with the capability to adjust gains, time constants, control modes, etc., in the control computer.
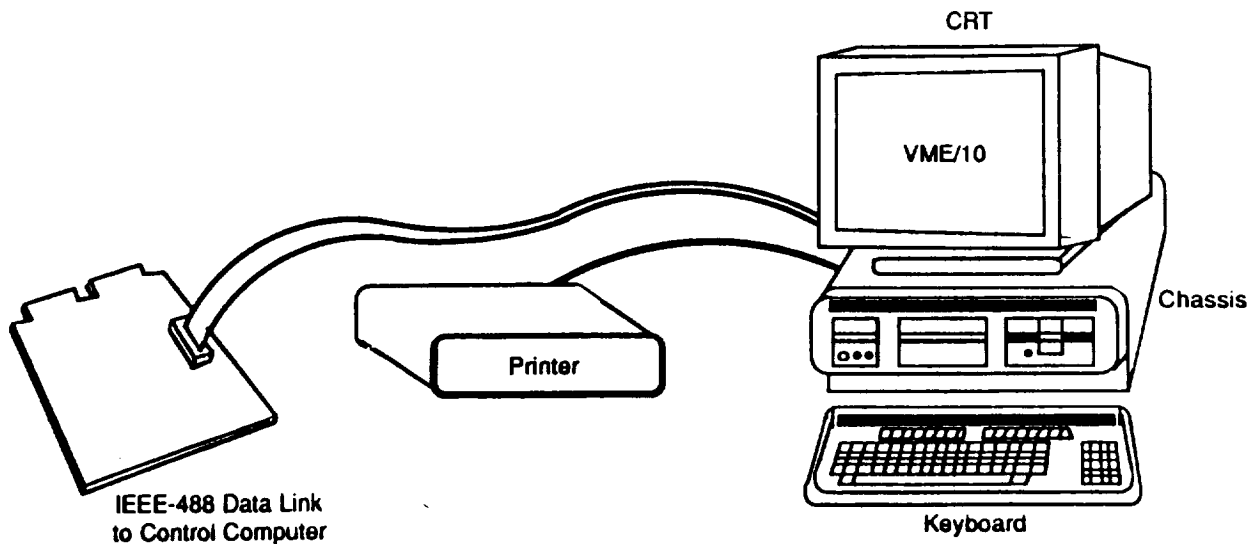
Figure 11-5. Peripheral Processor System.

11.6 FUEL DELIVERY SYSTEM

The fuel delivery system of the UDF™, as illustrated in Figure 11-4, is further described in the following subsections.

11.6.1 Fuel Pump

The fuel pump, mounted on the aft side of the gearbox, is gear-driven and provides a mounting pad for the fuel control. The pump has an inlet and three pumping elements on the same shaft. These pumping elements are described as:

- A low pressure, inducer element which minimizes fuel cavitation under loss of aircraft boost

- An intermediate pressure, centrifugal element accepting return flows from:

  - IP Compressor Variable Vane Actuator
  - ECU Cooling Flow
  - HMU Servo Return
  - Bypass Duct Bleed Actuator

- A high pressure, positive-displacement vane element supplying flow to the HMU.

Capable of providing up to 12,000 lb/hr for engine flow, the pump also provides fuel flow for cooling the ECU and contains the fuel filter. The fuel filter, which is mounted inside the fuel pump, is a 10-μm absolute, disposable type filter which incorporates both an impending bypass indicator and a bypass indicator. The impending bypass indicator is a yellow button that extends at a filter differential pressure of 13 ± 1.3 psid. The bypass indicator is a red button that extends when the bypass valve opens (at 15.0 psid minimum). Once activated, indicators remain extended until manually reset (internally) after filter element removal.

11.6.2 Fuel Control

Mounted on the aft end of the fuel pump, the fuel control is a hydro-mechanical type control. In addition to supplying metered fuel flow to the combustor, the HMU provides the filtered servo supply fuel for the bypass duct bleed system and the IPC and HPC variable geometry actuation systems. The gas generator speed is a function of RSA, PS3, and T25. Engine pressure ratio has

been chosen for power management and is controlled by a signal from the CC as a function of RSA, T2, and P2. In addition, the HP rotor speed is limited by maximum T46, XN2, and PS3. The following functions are also provided by fuel control:

- Schedules HP compressor variable stator angle based on HP rotor speed and T25

- Provides acceleration and deceleration fuel flow limits for transients

- Provides minimum/maximum compressor discharge pressure limits

- Provides HP rotor overspeed protection; when the HP rotor speed reaches 105%, fuel flow will shut off. After speed decreases, by approximately 2%, fuel flow will start again. If fuel flow restarts, the engine will cycle between 103% and 105%. This cycling will continue until the throttle is retarded enough to stop the cycling, or until the cause of the overspeed has been eliminated.

HP Compressor Inlet Temperature Transmitter (T25) - The HP compressor inlet temperature sensing system consists of a gas-filled tube coil mounted on the midframe. The gas pressure is transmitted through an armored capillary to a hydromechanical receiving servo, which is mounted on the HMU. The receiving servo converts the gas pressure signal to a position output which is used for schedule computation in the HMU.

11.6.3 Heat Exchangers

Gas Generator and Fan Pitch Control (FPC) Hydraulic Unit Oil Cooler - The oil cooler, located on the outer bypass duct, consists of an aluminum shell and tube, cross-counterflow fuel-to-oil heat exchanger, incorporated in the oil system. The cooler is a full flow type with no provisions for temperature regulation. Engine fuel is warmed as it passes through the tubes, cooling the lubricating oil which flows around the tubes. The fan pitch control (FPC) oil cooler is an integral part, mechanically, although lubrication and FPC oil are separated functionally. The fuel flows in series, first through the lube oil cooler, then through the FPC oil cooler.

Power Turbine Oil Cooler - A CF6-50 fuel/oil heat exchanger, located on the outer bypass duct, is used to remove excess heat from the power turbine lube system.

11.6.4 Fuel Shutoff Valve

Fuel shutoff is controlled by a solenoid-operated, pilot-actuated, 4-way valve that is mounted to the engine fuel manifold connection on the bypass duct. When the solenoid is energized, fuel from the HMU is directed to the combustor fuel manifold; however when the solenoid is deenergized, engine fuel is bypassed to the main fuel pump booster discharge manifold. This connects the combustor manifold to the drain collector tank (Figure 11-4). With inlet pressure at 400 psia, engine fuel flow at 30 gpm, and servo pressure at 1000 psi, the fuel shutoff valve will automatically:

- Open $\leq$ 0.25 seconds

- Close $\leq$ 0.10 seconds

Approximately 30 in^3 of fuel drains into the ecology tank each shutdown. Volumetric capacity of the ecology tank is 280 in^3.

11.6.5 Fuel Nozzles

The 18 dual-cone type fuel nozzles contain a fixed primary orifice and a secondary orifice which opens at above 125 to 150 psig for higher flow rates.

11.7 FAN PITCH HYDRAULIC SYSTEM

The fan pitch hydraulic system provides two independently controlled rod outputs operating in response to signals provided from the control computer. The hydraulic fluid used is Mil-L-23699. Upon loss of the 3000 psig hydraulic supply, the system has sufficient stored energy to drive both pistons from full-extend to full-retract and hold for 30 seconds. The actuation system is designed such that a linear relationship is maintained between the stroke of each piston and the angular rotation of a row of fan blades. The outer rod (forward spider) rotates the rear blade row, and the inner rod (rear spider) rotates the forward blade row. The actuation system is rigged to produce the following.

Pistons	Stroke, inch	Pitch Angle, °	Condition
Retracted	0.0	86.0	Feather
Extended	6.0	-19.97	Maximum Reverse

11.7.1 Schematic/Description

The fan pitch hydraulic system schematic is presented in Figure 11-3.

11.7.2 Fan Pitch Actuator

The fan pitch actuator, mounted along the P/T centerline, features tandem pistons and coaxial rods. The position of each piston is independently controlled by separate servo loops; the fully retracted position of each rod is designed as maximum coarse pitch, or feather position. Operational requirements for the fan pitch actuator are set forth as follows:

- The actuator has two independently controlled outputs which act along a common centerline and are capable of stroking 6 inches

- The actuator minimum piston area is 4.95 in^2

- Retractable stops with internal LVDT for position feedback are provided on each rod to prevent fine pitch on fan blades during flight operation

- Retractable locks are provided to retain each rod at the full-retract (feather) position; it is possible to engage this lock even if the locks are commanded to be engaged (hydraulic signal less than 250 psig)

- Rod relative travel is limited to ± 0.5 inch

- Dual-position feedback to the control computer is provided for each rod position

- Load capabilities are ± 15,000 lb/piston, with the direction of load not always the same for both pistons

- Pressure capabilities are 3,000 psig maximum operating for rod or head pressure and for the seal drain 150 psig maximum.

11.7.3 Hydraulic Pump (Modified Variable Exhaust Nozzle Power Unit)

The hydraulic pump is a modified variable exhaust nozzle (VEN) power unit which is mounted on and driven through the lube and scavenge oil pump. Having a self-contained reservoir, the pump is a pressure-compensated, variable displacement pump. The reservoir is pressure-filled and isolated from the engine oil systems. The pump supplies 6.0 gpm (at rated speed) at 2800 psig supply pressure. Flow is proportional to HP rotor speed at part power conditions for

discharge pressures less than 2800 psig. Pump destroking is controlled by the pressure compensator, such that displacement is zero for discharge pressures greater than 3000 psig. The pump discharge relief valve is set at 3150 psid above inlet pressure.

11.7.4 Servovalves (Two Required)

The electrohydraulic servovalves (mounted on the bypass duct case) operate in response to electrical input signals from the control computer to port hydraulic pressure to the fan pitch actuator. Torque motor drivers for these servovalves are part of the control computer.

11.7.5 Transfer Valves (Two Required)

The electrohydraulic transfer valves, mounted on the bypass duct case, operate in response to electrical input signals from the CC. The transfer valve solenoid is energized from the fan overspeed circuitry. When these transfer valve solenoids are energized (+ 28 vdc) the system is in the normal (run) condition and ports flow from the servovalves to the head and rod ends of each fan pitch actuator piston.

When the transfer valve solenoids are deenergized, the system is in the shutdown condition and:

- Ports flow from the high pressure accumulator to the rod end of each fan pitch actuator piston

- Ports flow from the head end of each fan pitch actuator piston to pump return.

11.7.6 Three-Way (Lock) Solenoid Valve

Mounted on the bypass duct case, the solenoid valve is powered by a signal from the control computer and controls the hydraulic pressure signal to the fan pitch actuator lock mechanism, operating as follows.

Solenoid Valve	Hydraulic Pressure Signal	Pitch Lock (Reference)
Deenergized	Hydraulic Pump Return	Engaged
Energized	Hydraulic Pump Discharge	Retracted

11.7.7 Flow Control Orifices and Check Valves

The following flow control orifices and check valves, installed in system tubing fittings, control the hydraulic fluid flow rates for HP accumulator charging, fan blade feathering, lock actuation, and pilot valve purging:

- Orifice R_1 regulates the charging rate of the HP accumulator from pump discharge pressure. Check valve CV1, paralleling R_1, allows rapid discharge flow for blade feathering.

- Orifice R_2 regulates HP accumulator flow to the rod sides of both pistons when the transfer valves are deenergized.

- Orifice R_3 regulates flow to and from the actuator stop positioning pistons.

- The two orifices, R_4, permit a small purging flow through the transfer valve pilot stages, thereby preventing contamination accumulation.

- Check valve CV2 prevents loss of the HP accumulator oil charge in the case of a hydraulic pump failure.

- Check valve CV3 allows the LP accumulator oil charge to provide makeup flow for the hydraulic pump during startup.

11.7.8 High Pressure Accumulator

The high pressure accumulator, mounted on the bypass duct case, supplies hydraulic fluid under pressure to drive both fan pitch actuator pistons to the full-retract position. With a nitrogen charge of 1250 psig at 70° F, the high pressure accumulator stores a minimum of 115 in^3 of fluid at 3000 psig and 70° F as the supply to flow control orifice R_2.

11.7.9 Low Pressure Accumulator

The low pressure accumulator is mounted on the bypass duct case parallel with the reservoir built into the hydraulic pump. The pump reservoir provides approximately 115 in^3 of hydraulic fluid. With a nitrogen charge of 40 psig at 70° F, the LP accumulator stores an additional 60 in^3 of hydraulic fluid when the system static pressure is charged to 66 psig at 70° F.

11.7.10 Filter Assemblies

The UDF™ supply filter assembly is mounted on the bypass duct case and provides 3-μm absolute filtration of the supply flow to the hydraulic system components. The filter assembly also provides element bypass, high differential pressure indication, and thermal lockout. A similar 3-μm absolute filter assembly protects the hydraulic pump return.

11.8 DUCT BLEED SYSTEM

Figure 11-6 depicts the duct bleed control system. The duct bleed air is delivered into the air exit cavity by a single 5-inch pipe which has air manifolded to it from three circumferential locations. The duct bleed system also includes the electrohydraulic servovalve, one linear actuator, one butterfly valve, and the electrical position feedback. The bleed schedule is computed in the CC, and closed-loop duct bleed valve control is accomplished by operation of the servovalve and LVDT position feedback.

Actuator - One fuel-powered actuator is used to operate the duct bleed system.

Position Sensor - A linear variable differential transformer contained in the duct bleed actuator provides the duct bleed valve position feedback signal to the control computer.

Servovalve - The electrohydraulic servovalve, contained in the duct bleed actuator, operates in response to electrical input signals from the control computer to port hydraulic pressure to the duct bleed actuator. The torque motor driver for the servovalve is provided by the control computer.

11.9 VIBRATION MONITORING SYSTEM

Figure 11-7 portrays the vibration monitoring system. The four differential output accelerometers are mounted on the outside structure of the engine. The cable assembly is low noise, twisted pairs, shielded two-conductor, teflon dielectric, and jacked. The vibration amplifier provides velocity output in analog format that is conditioned for input into an A/D converter. Control software is utilized to process the signals and set the threshold level for automatic shutdown.

298

STA 255

Servo Fuel

Digital
Electronic
Control

STA 225

Servo
Valve

Actuator   Pos

Manifold
Junction

Aft Nacelle
Bulkhead

Butterfly Valve

2 ports 2.85" I.D.
1 port 3.60" I.D.

Mount Beam

45   45

Bleed Manifold

Fuel

Electrical

Air
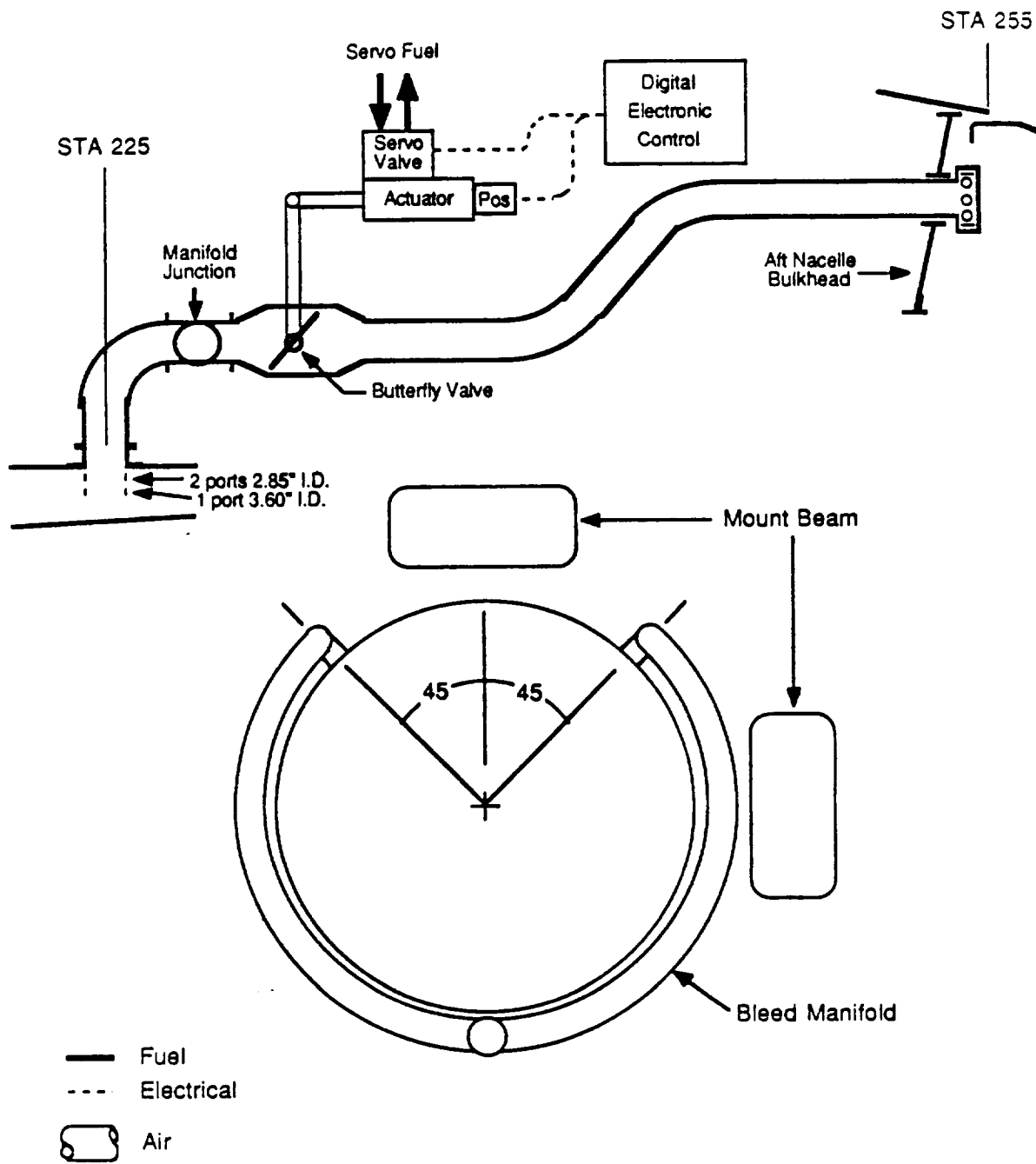
Figure 11-6. Duct Bleed System.
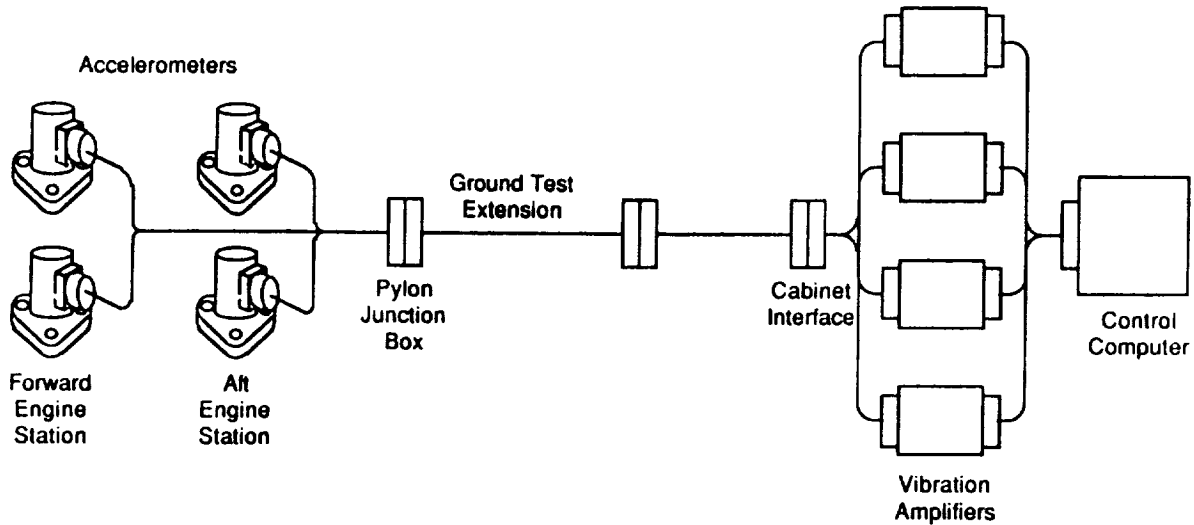
Figure 11-7. Vibration Monitoring System.

11.10 CONTROL STRATEGY

The design goal was to provide a safe control which would enable the gas generator and propulsor to be set (to both the design schedules and a range of off-design points) in order to evaluate the sensitivity of the propulsion system in noise as well as performance aspects. The F404 engine comes with a sophisticated hybrid electronic/mechanical control, capable of providing the required performance, flexibility, and protection. A new digital electronic control is linked to the existing F404 control system through ECU outputs, and a common throttle input was chosen as the most cost-effective means of integrating the gas generator and propulsor to provide single-lever thrust/power level management. A separate computer (PCS) processor was linked to the CC through a high speed data link to provide control system data gathering and operator interface facilitating the investigation of off-design points.

11.10.1 Gas Generator Control Functions

The gas generator speed is a function of the power lever angle, HPC discharge pressure (PS3) and compressor inlet temperature (T25). Engine pressure ratio (P46Q2) has been chosen for power management, and the control computer

provides the thrust rating schedules. P46Q2 is scheduled as a function of the inlet pressure (P2) below the corner point and as a function of inlet temperature (T2) above the corner point. These rating schedules are modified by the power lever angle for part power conditions to provide linear thrust as a percent of maximum climb. An HP rotor speed override signal is transmitted from the control computer to the fuel control which, in turn, reduces fuel flow to maintain the appropriate power setting for the gas generator.

In addition, the HP rotor speed is limited by the maximum interturbine exit temperature (T46), the maximum IP rotor speed (XN2), and the maximum HP compressor (PS3). Engine starting, HPC stator operation, and minimum/maximum PS3 are completely hydromechanical functions, as are accelerated and decelerated fuel scheduling, but the HP rotor speed acceleration rate is controlled by downtrimming fuel flow by the control computer. The HP variable geometry is scheduled from HP rotor speed (XN25) and T25; the IP variable geometry is a function of XN2 and T2 and is controlled by a signal from the CC. Duct bleed, which is required to preserve IP stall margin, maintains duct pressure ratio (P15Q2) and is scheduled as a function of corrected IP rotor speed. The decel throttle rate is used to preopen duct bleed as a stall avoidance feature and rate of change of duct pressure.

11.10.2 Propulsor

The control computer schedules corrected propulsor speed as a function of P46Q2 and provides direct pitch control for subidle and reverse thrust conditions. Fan pitch is modulated to provide synchronization; capability for synchrophasing is provided. Maximum corrected and physical limits are imposed on propulsor speed, and both rotors are nominally set to the same base speed.

12.0 NACELLE STRUCTURES DESIGN

12.1 INTRODUCTION

The nacelle structures hardware consists of the cowling assemblies, strut (pylon), mount beam, strut fairings, vibration isolators, and the fuse pin assembly. The cowling assemblies consist of the inlet, core cowling, apron cowling, and aft bulkhead. These structures provide an aerodynamic flowpath, nacelle ventilation, and fire protection. The centerbody is the structure, together with the rotating exhaust nozzle, that provides the power turbine aerodynamic exit flowpath. The strut attaches to the aircraft or test stand and acts as the load path between the aircraft and the engine mount beam. The mount beam provides the load path between the isolators and the strut. The strut fairings provide an aerodynamic flowpath around the strut. Isolators provide the structural link between the engine and the mount beam and provide controlled flexibility and damping to the connection. The fuse pin assembly provides a known failure point in the mount system to allow a clean break between the engine and the mount beam in the event of a catastrophic engine failure; such as, the loss of more than one fan blade per rotor. This provision protects the aircraft from any damage.

Figures 12-1 and 12-2 illustrates the nacelle systems.

12.2 COWLING

The cowling consists of four primary elements: the inlet assembly, core cowl, aft bulkhead, and apron assembly. Together they provide an aerodynamic flowpath, nacelle ventilation, and fire protection for the engine.

12.2.1 Inlet Assembly

The inlet assembly (Figure 12-3) is bolted to the forward flange of the engine. It has an acoustic inner barrel for reduced noise level, a nose lip that directs air into the engine, and an inlet/forward bulkhead that provides stiffness to the nose lip and a land for the cowl leading edge. Its aerodynamic shape permits favorable flow for both the engine and nacelle. Figure 12-3 diagrams the inlet and provides additional design features.

302
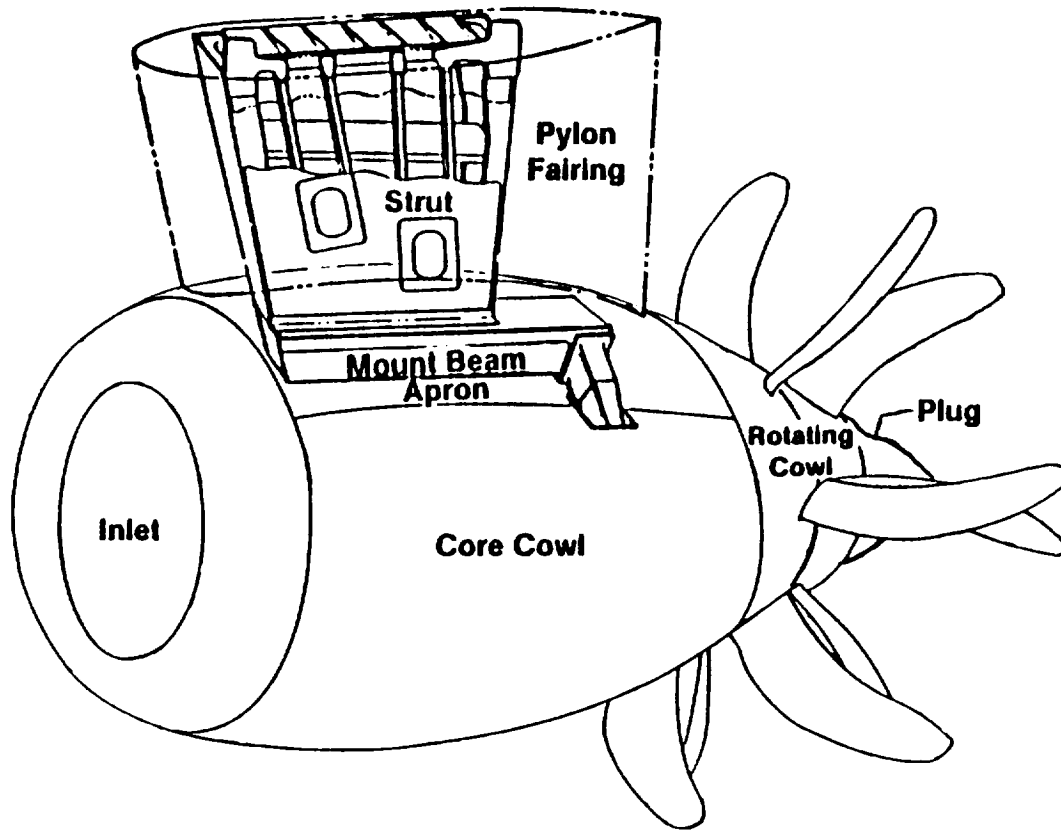
Figure 12-1.   UDF™ Nacelle Systems.

Cowl Door (Upper)
Assembly

Aft Bulkhead
Assembly

Centerbody
Assembly

Cowl Door (Lower)
Assembly

Core Engine

Strut
Assembly

Apron
Assembly
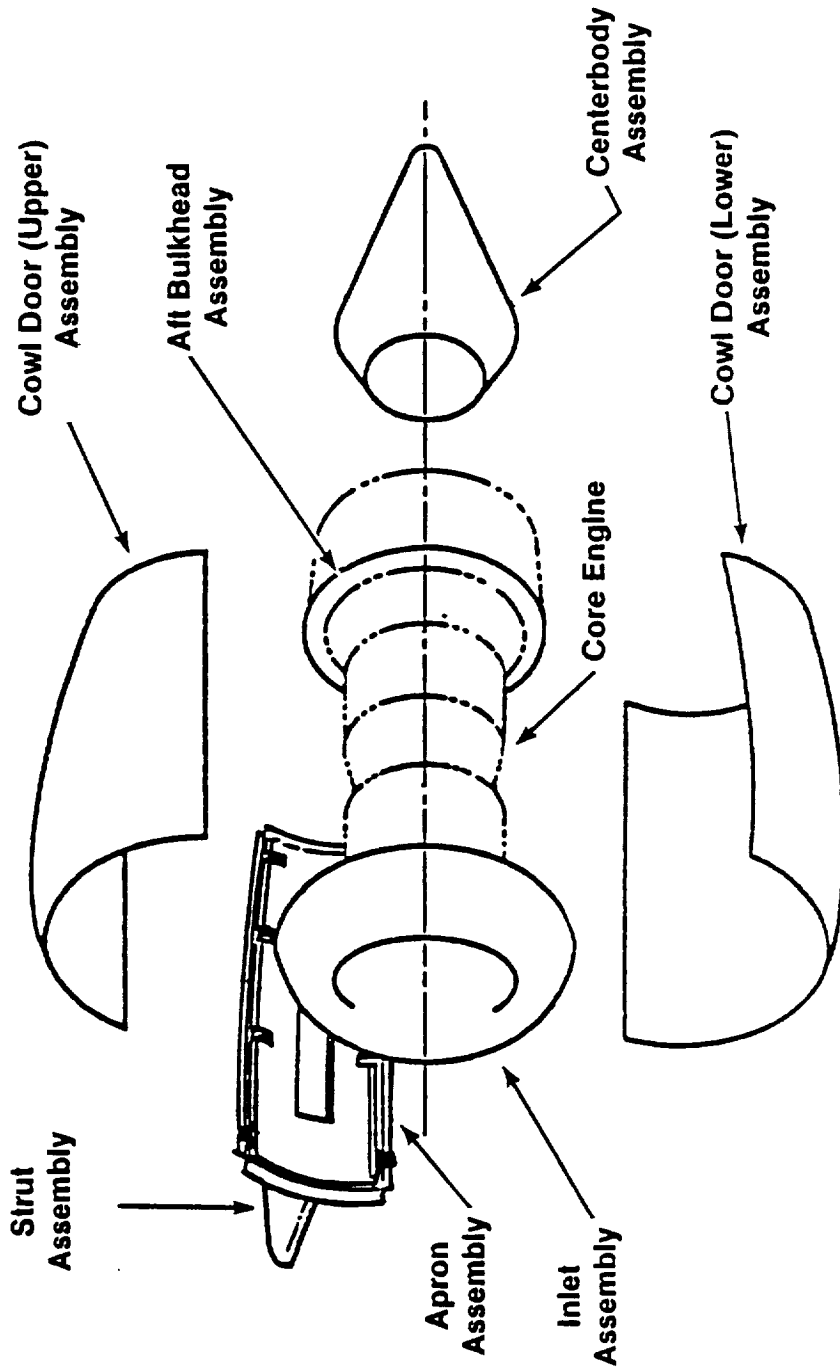
Inlet
Assembly

Figure 12-2. Exploded View of GE36/UDF™ Nacelle.

- **Metal Inlet for Future Anti-Ice Consideration**

- **Acoustic Treatment**
  - **2" Treatment for 2000-3000 Hz**
  - **1" Treatment for Higher Tones**
  - **Insures UDF™ Noise Not Masked by F404 Compressor Noise In Flight**
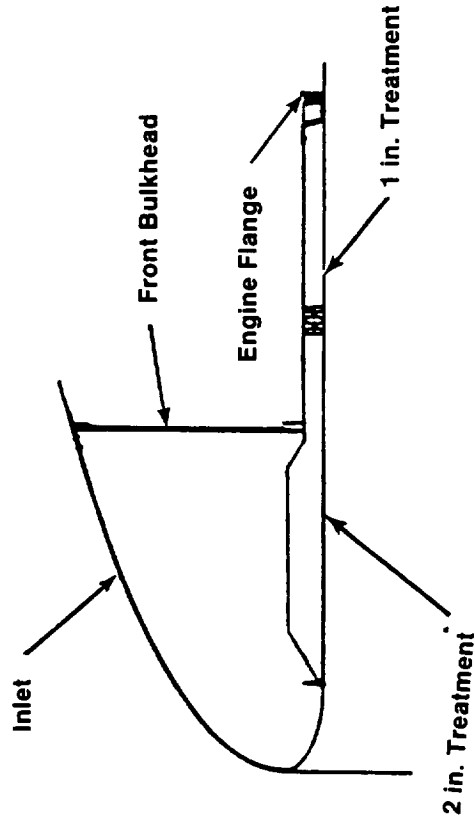
- **Inlet Length Established for 0.8 Mach Cruise**

- **Provides Cowl Axial and Radial Support**

Figure 12-3. UDF™ Inlet.

12.2.2 Core Cowl

The core cowl (Figure 12-4) provides an aerodynamic fairing that extends from the inlet cowl to the rotating cowl (propulsor assembly), thus enclosing the engine. It is manufactured in two sections: left- and right-hand units (doors) during ground testing, or upper and lower units during flight testing. They are constructed from bonded composite honeycomb sheet with an inner fire barrier lining (MA25) and provide access for engine maintenance. There are four latches and four hinges on each door. Hinge fittings are attached to the apron, which floats around the pylon. Cowl doors are installed by connecting the cowl hinges to the apron hinge fittings.

The core cowl also has a forward-facing air inlet scoop flush with the nacelle for ventilation and an aft-facing exhaust vent at its trailing edge. Inflatable seals are located between the strut and cowl apron to reduce air leakage. Finally, there are two telescoping hold-open rods; each supports a cowl door in up to 65-mph surface winds. They hold the doors open to a maximum angle of 90°.

12.2.3 Apron

The apron cowling (Figure 12-5) is located between the two core cowl doors and fits around the strut. The apron consists of two sections to permit assembly around the strut. After assembling the apron around the strut, the leading edge of the apron is bolted to the inlet "V-groove", and the trailing edge of the apron fits on the aft bulkhead land. Two pins that are attached to the rear portion of the apron fit into two slots on the aft bulkhead. This provides axial freedom of motion for thermal expansion. The apron is a skin stringer stainless steel construction and provides a land for the hinges which attach the cowling to the strut. Inflatable seals are placed between the apron cowling and strut to reduce air leakage. The apron is 27-inches wide and 98-inches long with thick skins.

12.2.4 Aft Bulkhead

The aft bulkhead (Figure 12-6) is a sheet metal structure which provides radial support to the trailing edge of the cowl and serves as the aft boundary

- **Forward Lip Provides Axial Fixity**
- **Aft End Free to Expand (Thermal Growth)**
- **Cowl Doors Hinged to Apron**
- **2 Positive Hinges**
- **2 Link Hinges (Not on Hinge ₵)**
- **Seals at All Nacelle Joints (Circumferential and Axial)**
- **Nacelle Can Take Hoop Loads When Latched (Load Path Through Hinges and Latches)**

Seals

Pressurizing Line

Seal (Typical)

Expanded Position
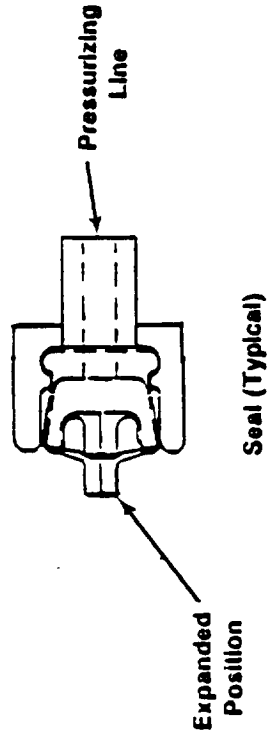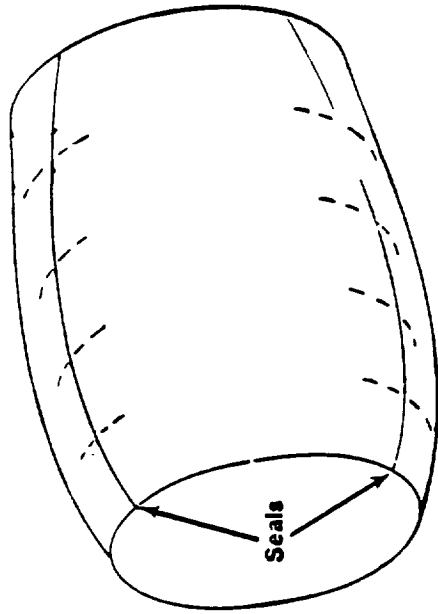
Figure 12-4. UDF™ Nacelle Cowl System Design Features.
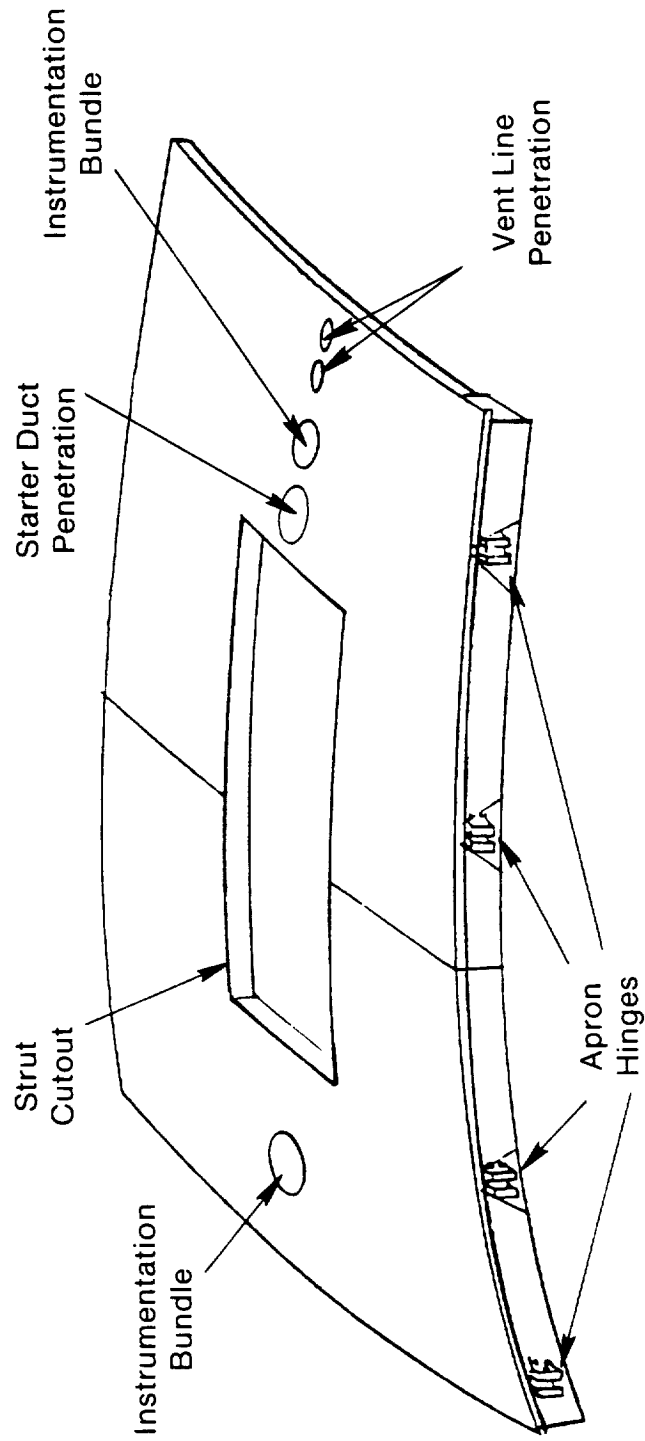
Figure 12-5. Apron.
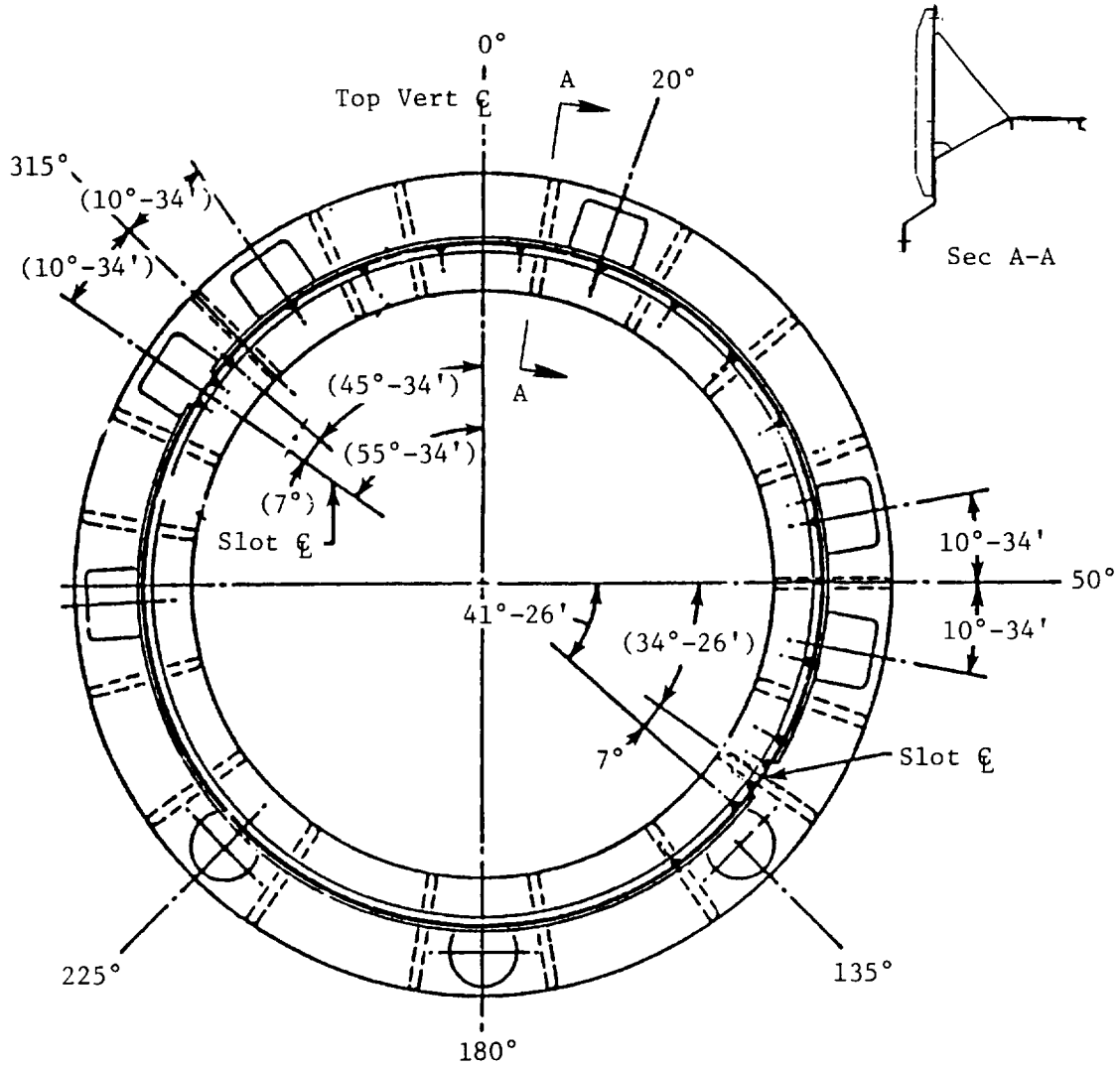
Orientation View
Aft Looking Fwd
Scale: None

Figure 12-6. Aft Bulkhead.

309

of the core fire zone. It has provisions for mounting and penetration of stationary telemetry speed sensors, and nacelle ventilation and piping.

12.2.5 Fire Detection and Extinguishing

The nacelle cowling and engine mount beam provide attachment points for the engine fire detection and extinguishing system. The fire detection system (Figures 12-7 and 12-8) is a Systron Donner temperature sensitive wire loop which activates the release of the extinguishing agent.

12.2.6 Nacelle Ventilation

A moderated environment is required in the undercowl cavity to prevent overheating of components and to remove the threat of fire. To accomplish these objectives, core compartment cooling and ventilation air are provided by an induced airflow from an inlet in the core cowl. The cooling flow enters the nacelle cavity through a scoop placed at the stagnation point on the external flowpath. To regain dynamic pressure, a ramp was built at the scoop inlet. The aft lip of the air inlet was rounded to cause smooth flow for ground operation, yet still enabling it to recover 11% of the dynamic pressure under flight conditions. The air flows through the nacelle cavity, exits through ports in the aft bulkhead, and then escapes to the atmosphere in between the bulkhead and forward rotor (Figure 12-9). The inlet location yields a higher static pressure than exists aft of the bulkhead; thus, facilitating airflow through the nacelle cavity (Note: the pressure drop through the cavity is on the order of 0.2 psig). Air residency inside the compartment was designed to be less than 10 seconds (6 air changes/minute minimum) at full speed ground testing and at flight speeds.

12.3 CENTERBODY ASSEMBLY

As illustrated in Figure 12-10, the centerbody assembly is the structure (along with the rotating exhaust nozzle) that provides the power turbine aerodynamic exit flowpath. Unlike the exhaust nozzle, however, the centerbody is stationary. It consists of two parts, the forward and aft centerbodies. Both are of sheet metal construction with structural stringers.

310
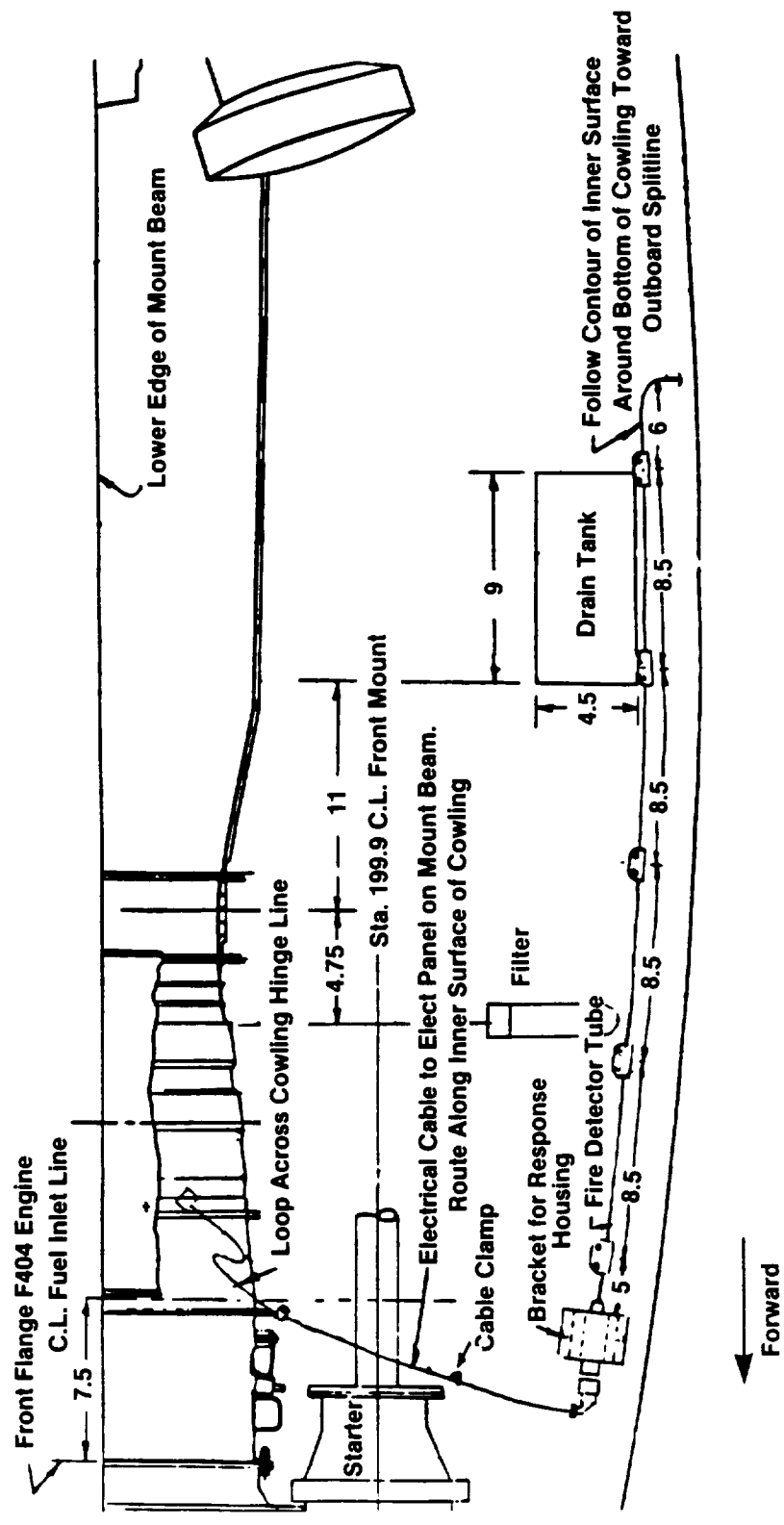
Figure 12-7. Fire Detection and Extinguishing System.

311
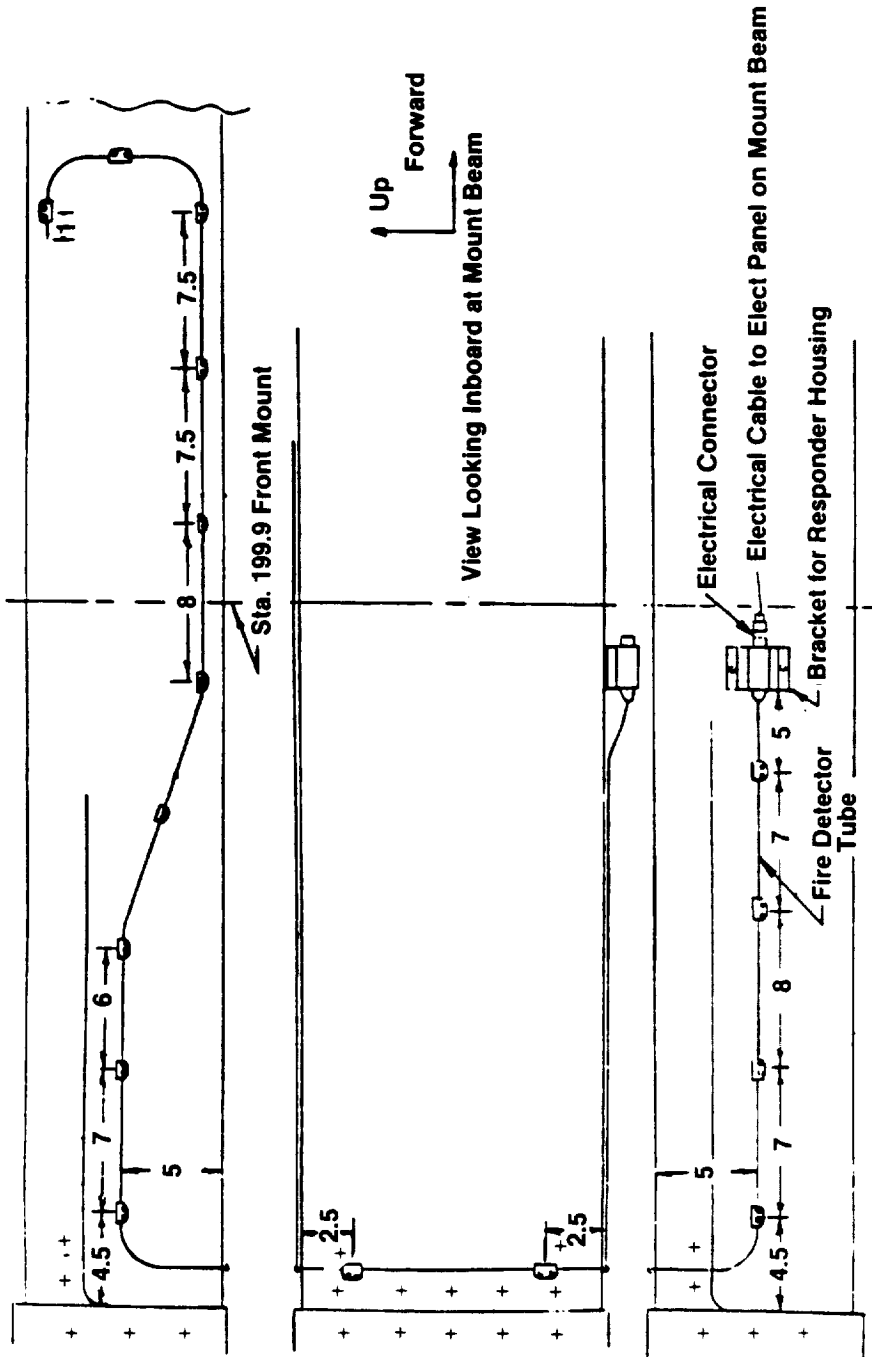
Figure 12-8. Fire Detection Sensors.
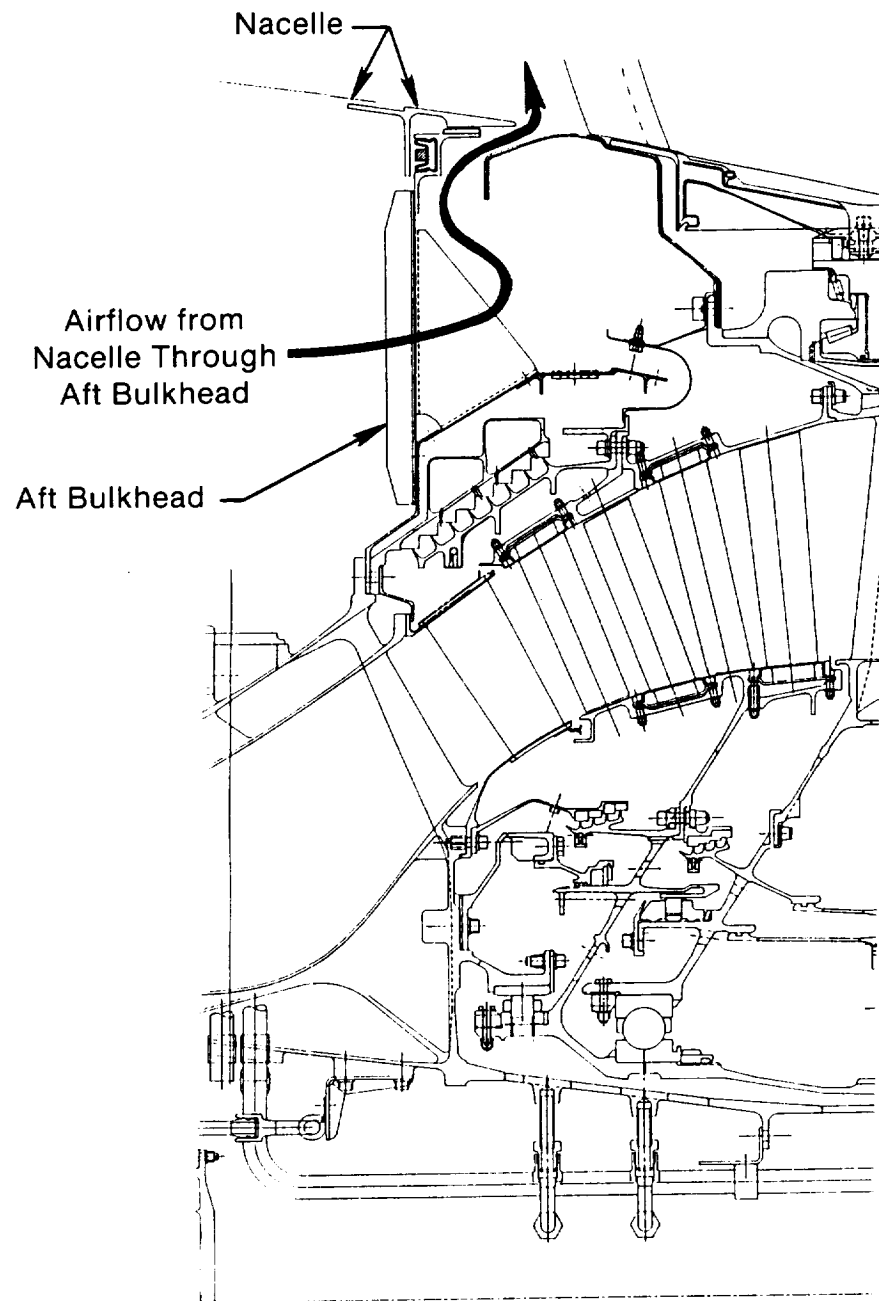
Figure 12-9.   Nacelle Ventilation; Airflow from Nacelle
Through Aft Bulkhead.
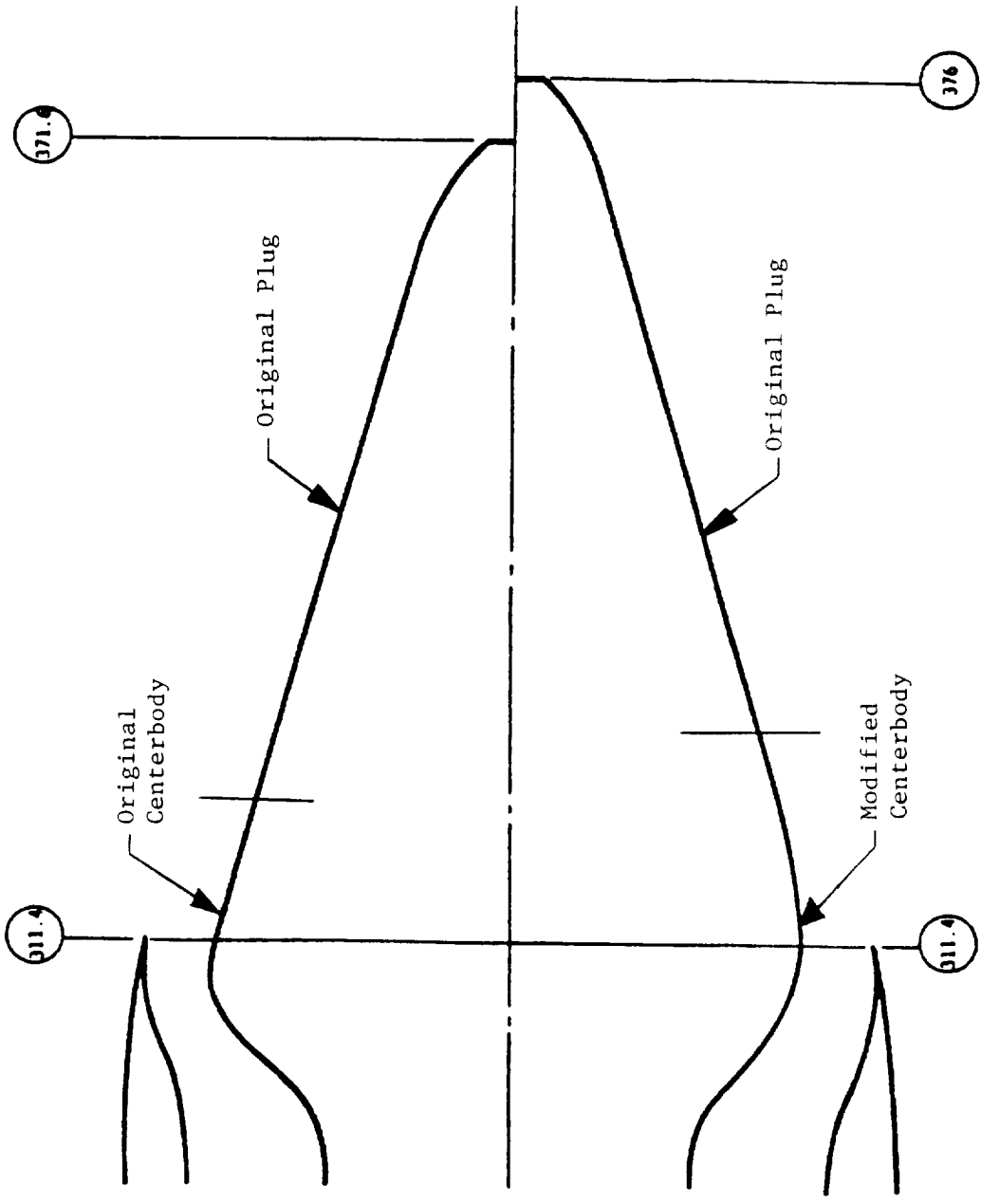
Figure 12-10. Redesigned Centerbody.

314

The new forward centerbody was designed strictly for the UDF™ engine. Analysis and wind tunnel testing of the original design revealed an undesirable flow separation in some regions of the flight envelope. It was redesigned to remove the possibility of flow separation. The shape was changed;however, it utilized the same assembly techniques and attachment points as the original design. Figure 12-10 shows the change in the centerbody flowpath.

The aft centerbody attaches to the aft flange of the forward centerbody to form the entire centerbody assembly. Unlike the forward centerbody, the aft centerbody is the application of a present commercial production engine part. When the forward section was redesigned, it was not necessary to change the aft design.

12.3 STRUT, MOUNT BEAM, AND FAIRINGS

12.3.1 Strut and Mount Beam

The strut, shown in Figure 12-11, supports the engine and acts as a link to the aircraft. It attaches to the mount beam which supports the isolators. Its two spars and three ribs provide a structural path between the mount beam and side of the fuselage. The strut, designed with steel skin and stringer construction, also provides support for the fiberglass aerodynamic fairings.

The mount beam (Figure 12-12) along with struts and fairings, is a steel torque box structural fabrication which acts as the load path between the isolators and the strut. The three isolators are attached to the mount beam with bolts, as illustrated in Figure 12-12. The mount beam is 72-inches long with a cross section of 9 inches by 14 inches.

The strut and mounted beam together provide the structural load path for installation of the engine onto the aircraft or test stand. They are based on a Boeing-supplied design, and both consist of a steel structure using bolts and screws rather than rivets.

12.3.2 Strut Fairings

The strut fairings, mid (upper and lower), leading edge, and trailing edge are depicted in Figures 12-12 and 12-13. They are shaped for aerodynamic efficiency and are constructed from fiberglass and aluminum. Figure 12-13

Intermediate Rib — Upper Skin

Gusset Plate

Front Spar

Rear Spar

Gusset Plate

Side of Body Rib

Body Fitting (Ref)

Body Fitting (Ref)

Lower Skin

Stringer 4 Place Each Skin

Access Hole 3 Places Each Skin
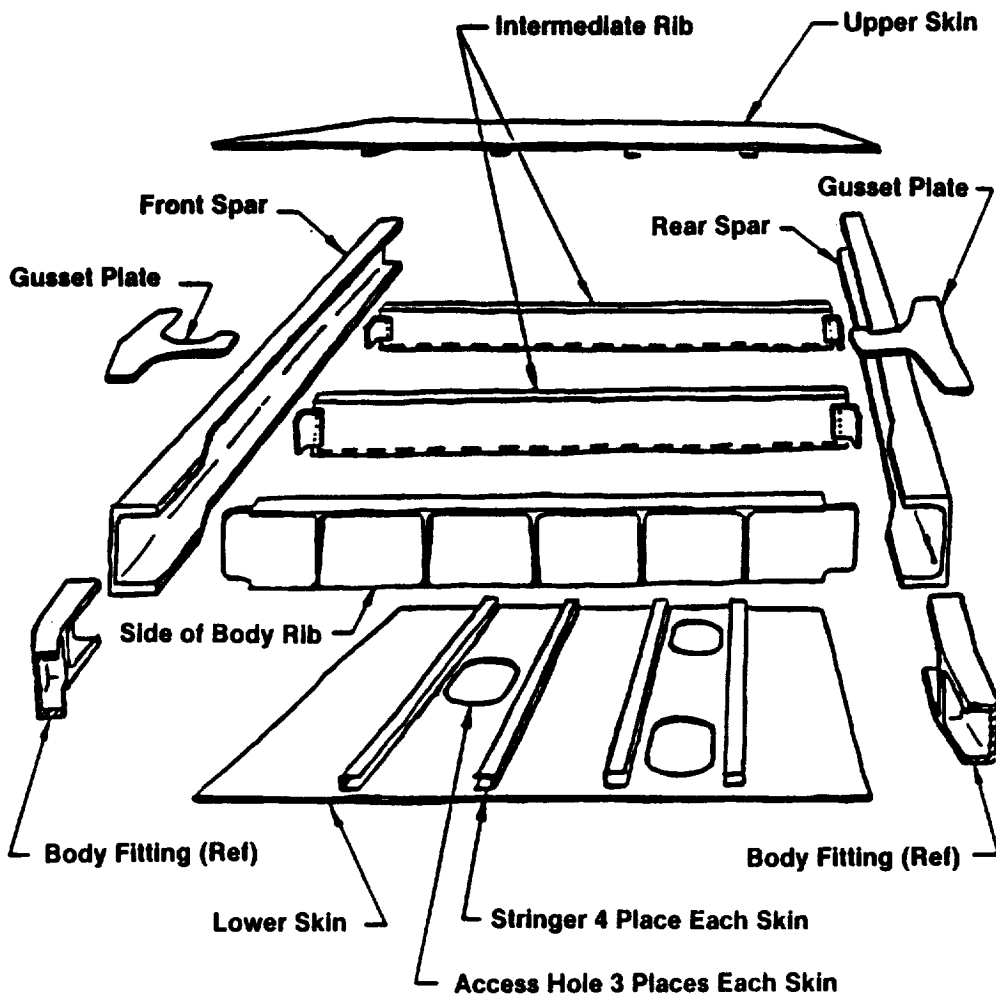
Figure 12-11. Strut Construction.

Strut Upper Fairing (Lower Fairing Omitted)

Leading Edge Fairing

Forward

Front Engine Mount and Isolator

Engine Mount Beam

Rear Engine Mounts and Isolators

Side of Body Rib

Body Fitting

Side of Body Joint

Strut Box

Trailing Edge Fairing
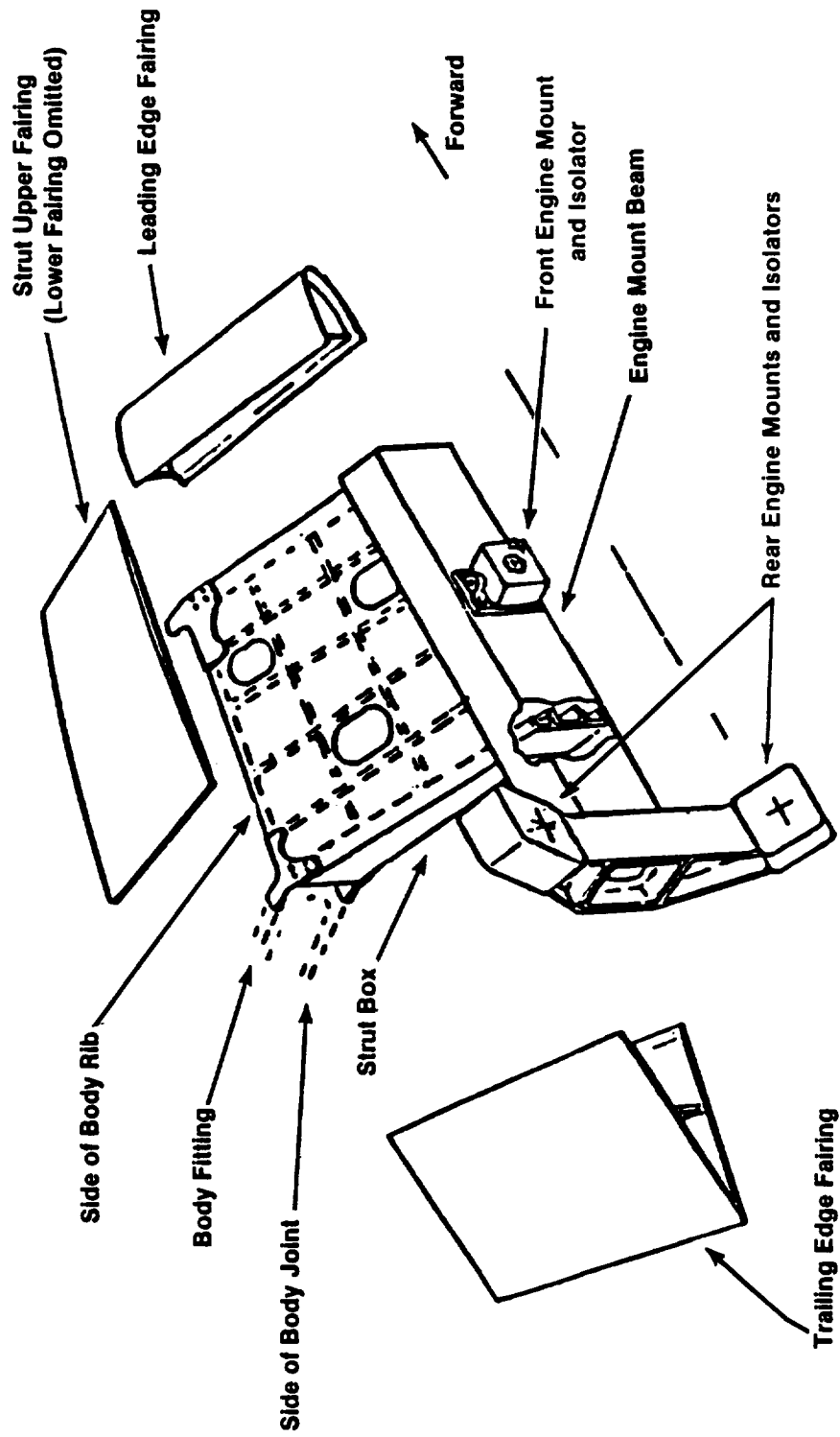
Figure 12-12. Strut Assembly.

317

Part	Type	Material
Leading Edge Fairing	Sandwich Structure	0.50 in. Thick Aluminum Flexcore Fiberglass/Epoxy Laminated Skins
Upper Fairing Lower Fairing	Fiberglass Epoxy Laminate	0.46 in. Min Thickness
Trailing Edge Fairing	Sandwich Structure	0.50 in. Thick Aluminum Flexcore
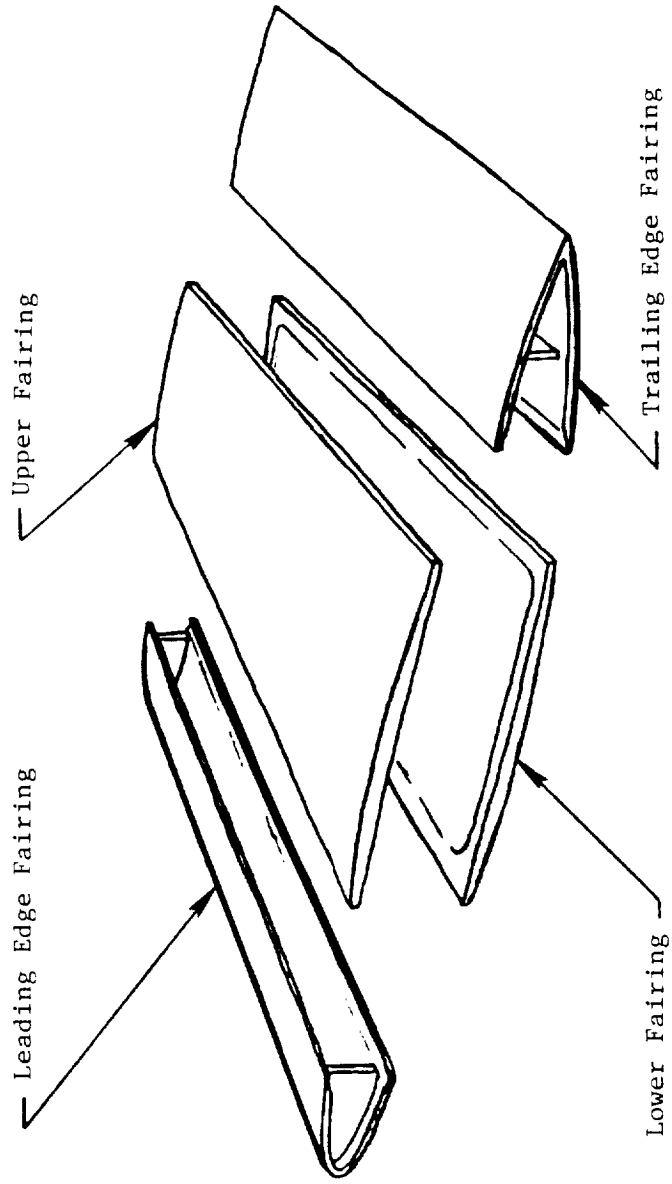
Figure 12-13. Strut Fairings.

also gives construction types and materials. The four fairings are attached to the strut with screw-type fasteners.

12.3.3 Structural Design Criteria

Ultimate Strength

The ultimate strength criteria of the structural components are based on:

- Engine inertia, thrust, and gyroscopic load factors

- An 1.25 times maximum engine/strut fuse strength combined with 1.0 G loads, with or without a 1.0 factor normal cabin pressure

  - Maximum engine/strut fuse strength = 1.10 times minimum
  - Minimum engine/strut fuse strength based on:
    - Dynamic analysis with one blade out each rotor
    - Engine inertia, thrust, and gyroscopic load factors.

Fatigue

The structural components fatigue design criteria are based on:

- 500 hours minimum of normal operating loads

- 1000 cycles minimum of blade-out loads during spool down.

Load and Safety Margin Summary

Table 12-1 is a summary of load factors and design criteria for the strut and mount beam. Table 12-2 presents a summary of structural component margins of safety, based on load conditions.

12.4 MOUNT ISOLATORS AND FUSE PINS

Three isolators, one forward and two aft (Figures 12-14 through 12-16), provide structural support between the engine and the mount beam. Consisting of steel housings, flexible metal mesh core elements, and cone bolts (engine fittings), they also provide controlled flexibility and damping to the connection. The cone bolts are connected to the engine mounts with fuse pins. The fuse pins (Figure 12-17) provide a known failure point (fuse point) to protect

Table 12-1. Strut and Mount Beam - Loads.

Load	Factors	Design Criteria
• Weight		8000 lb
• Vertical	Down	+8.0 +8.0 G + 1.5 T_c
• Lateral	Left/Right	±5.0 G
• Axial	Forward/Aft	+12 with 1.33 FF, -6
• Thrust	Forward	3 T_{Max} 3 T_{Max} + 3 G Down
	Aft	3 T_{Rev} 3 T_{Rev} + 3 G Down
• Gyroscopic	Yaw	±3.0 Rad/Sec With/Without 1.5 T_c and 1.5 G Down
	Pitch	±2.25 Rad/Sec With/Without 1.5 T_c and 3.75 G Down
• Blade Out Dynamic Loads	-	-
• Seizure Torque	-	350 kip/in
• T_{Max}	-	27,787 SLS
• T_c (Cruise)	-	21,000 at Cruise
• T_{Rev} (Reverse)	-	-6113 SLS

320

Table 12-2. Strut and Mount Beam - Margins of Safety (Minimum).

Component	Load Condition	MS
• Front Spar 5/8" Bolts	- Fuse Failure × 1.25 Factor	0.06
• Lower Spar Chord 3/4" Bolts	- Fuse Failure × 1.25 Factor	0.015
• Box Beam at Mount	- Blade Out	0.09
• Front Spar Bulkhead	- 8 G Down	0.05
• Front Spar Mount Attach Bolt	- 8 G Down	0.08
• Rear Spar Bulkhead - 1/2" Bolt	- Blade Out	0.05
• Rear Spar Mid Section Stability	- 8 G Down	0.22
• Skin Panel Fastener (Upper)	- 8 G Down	0.13
• Skin Panel Fastener (Lower)	- Blade Out	0.06
• Fiberglass (E_{181}) Fairing	- 10 psi Internal Pressure	1.3
• Gusset Plate (321 Cres)	- 10 psi Internal Pressure	0.3
• L/E Rib Bolt	- 10 psi Internal Pressure	0.26

322
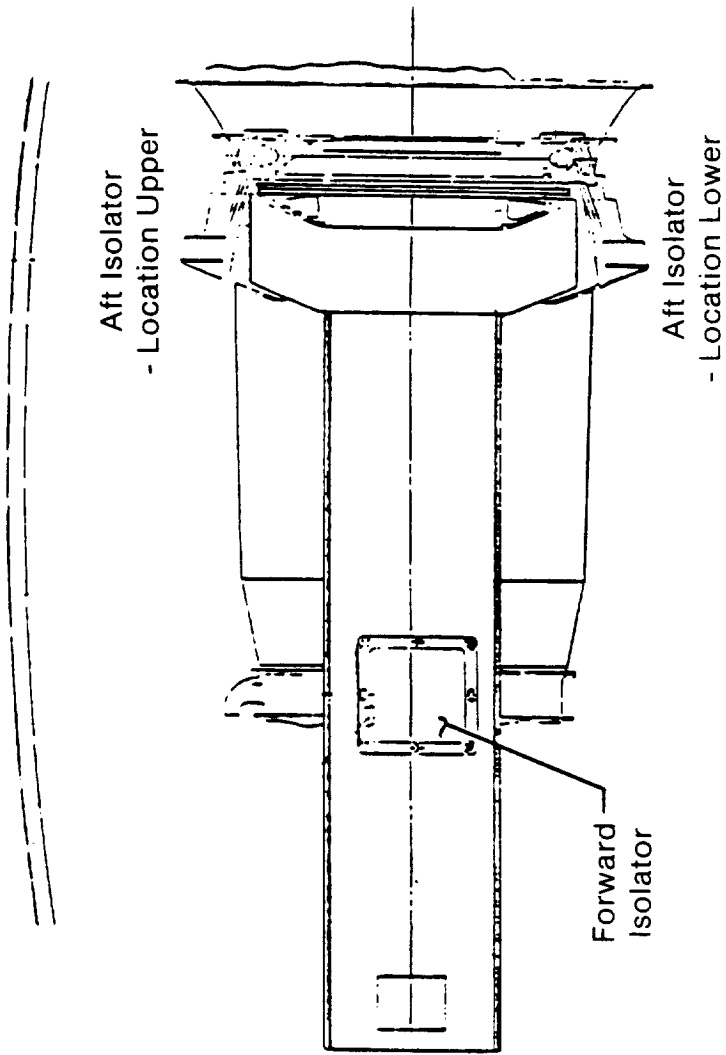
- Forward Isolator Located in Mount Plane
- Aft Isolators Located Forward of Mount Plane
  - Leaves Area Over Strut Ends Clear for Piping
  - Meets Damping and Stiffness Requirements

Aft Isolator
- Location Upper

Aft Isolator
- Location Lower

Forward
Isolator

Figure 12-14. Mount Beam.
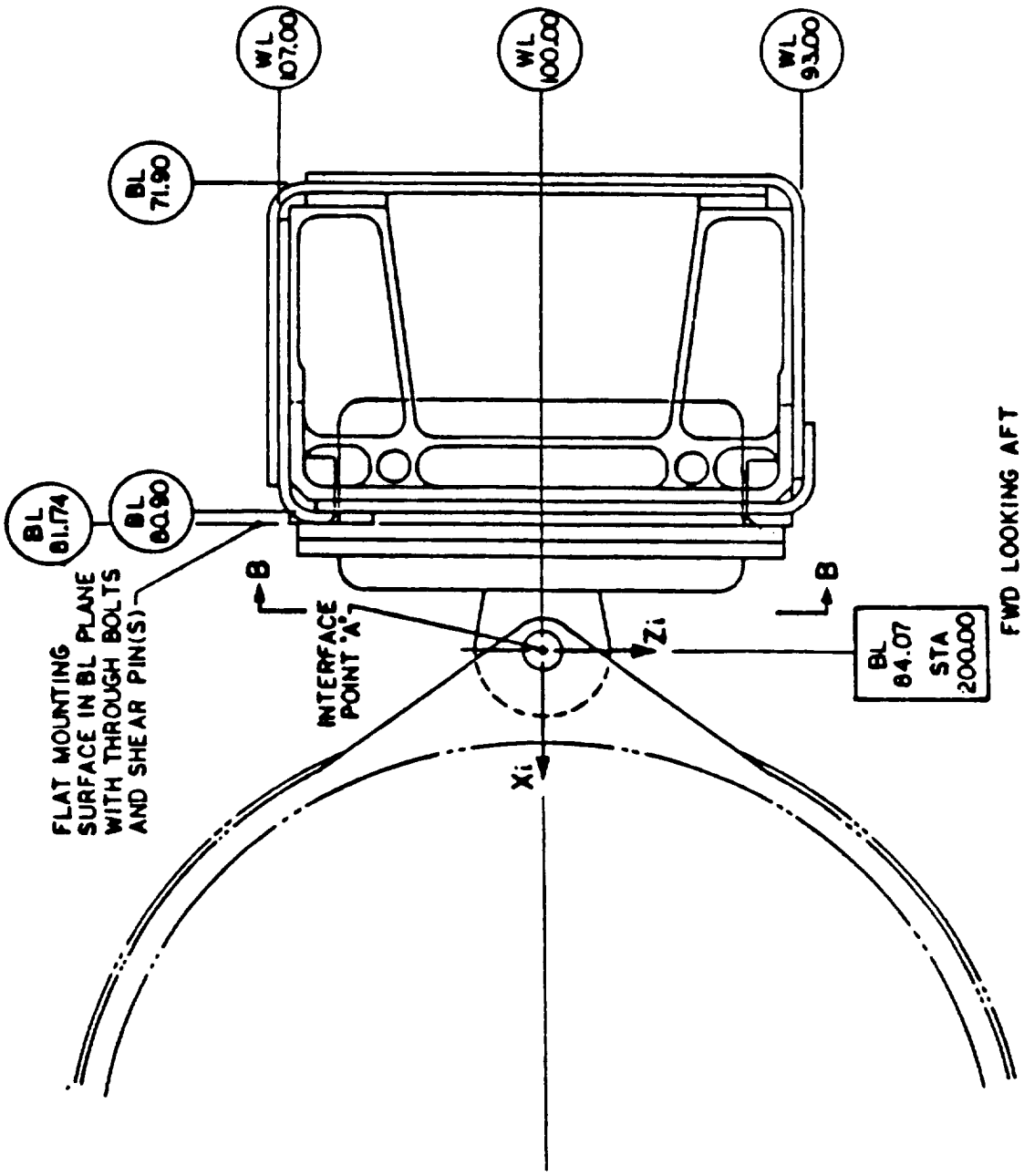
Figure 12-15. GE36 Forward Mount Isolator.

323
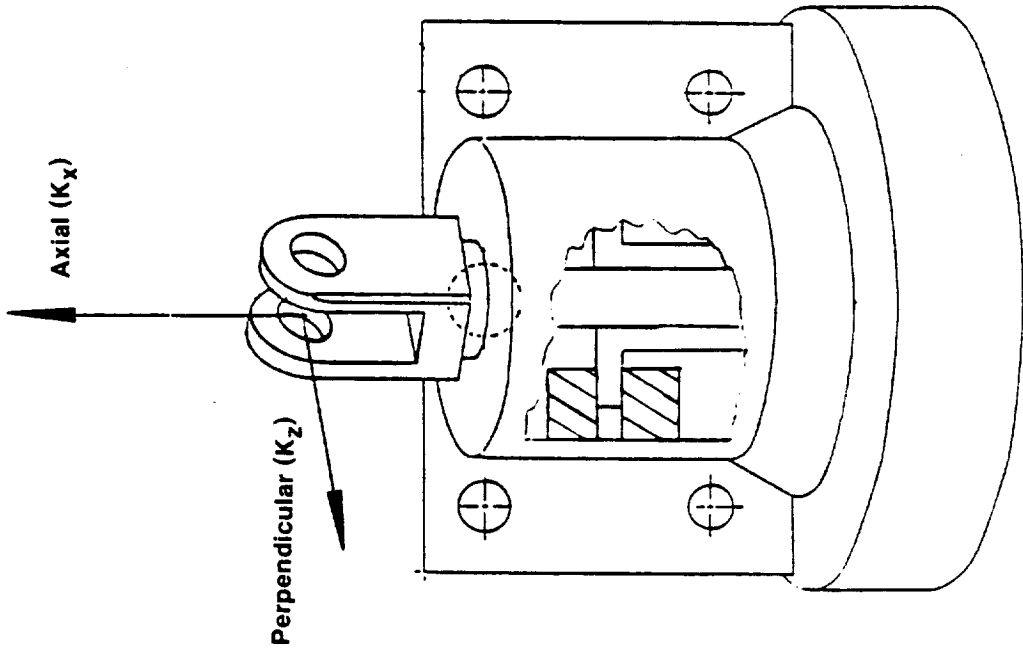
- **Provide Primary Load Connection Between The Engine and Pylon**

- **Metal Flex Cushions Provide**

  - **Stiffness Control**
  - **Damping of Vibratory Loads**
  - **Attenuation of Load Input to Aircraft**

  Spring Rates

  Axial   125 Kips/in
  Perpendicular 60 Kips/in

Axial (K_x)

Perpendicular (K_z)

Figure 12-16. UDF™ Mount Isolator (Aft).
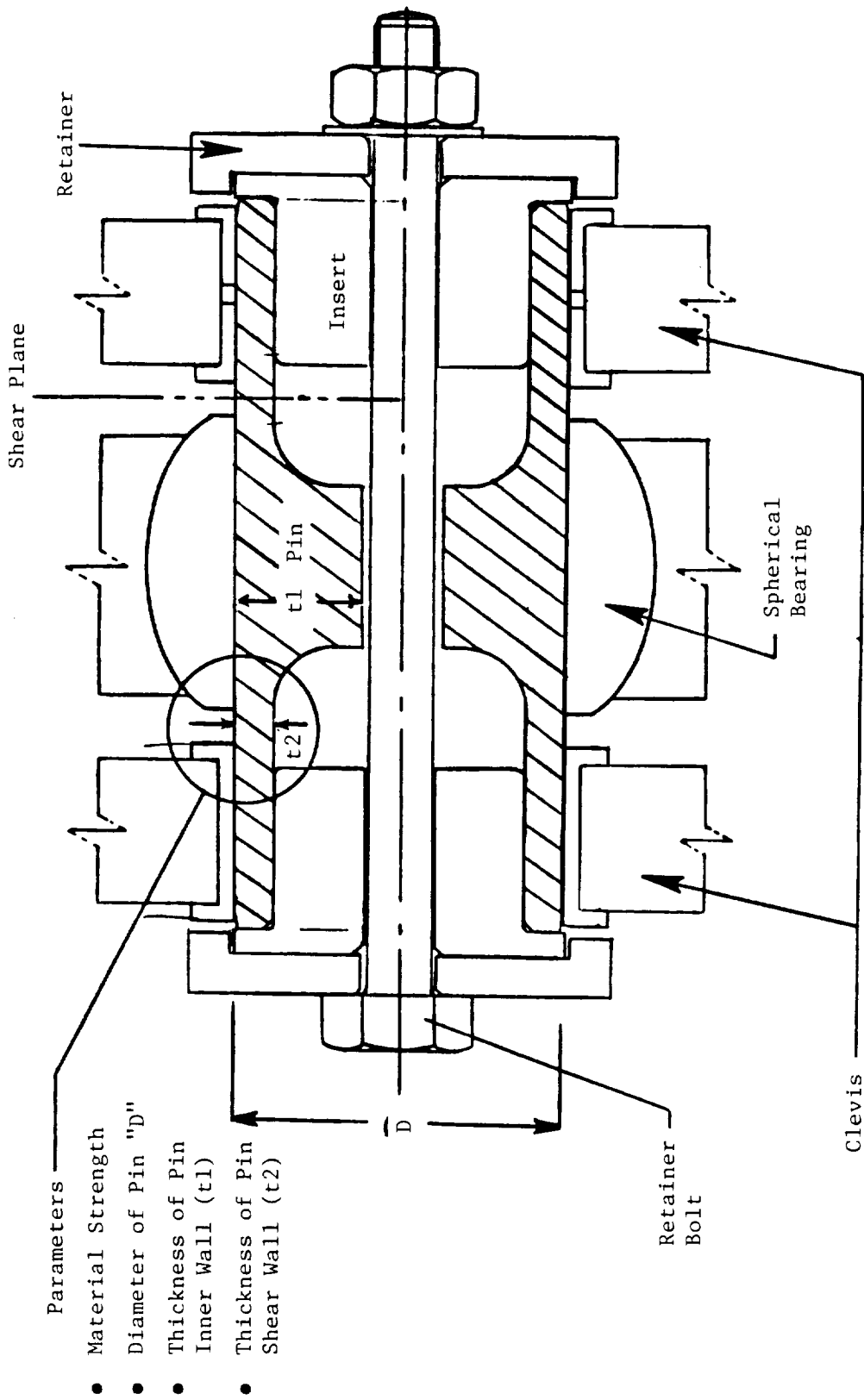
Figure 12-17. Critical Parameters of Fuse Pin Design.

Retainer

Shear Plane

Insert

t1 Pin

t2

Spherical
Bearing

Parameters

● Material Strength
● Diameter of Pin "D"
● Thickness of Pin
  Inner Wall (t1)
● Thickness of Pin
  Shear Wall (t2)

D

Retainer
Bolt

Clevis

the aircraft in the case of massive engine unbalance or excessive shock load. The steel housings are bolted to the mount beam.

Utilizing proven technology, this engine mount system had to meet the following requirements:

- Structurally attach the engine to the strut.

- Provide isolation of dynamic loads for blade-out criteria to protect the aircraft (Figure 12-18). The mount must withstand at least one fan blade out per row.

- Provide structural fuses to protect the aircraft in case of a massive failure (such as loss of more than one fan blade per rotor) and to provide a means to ensure clean departure of the engine from the aircraft. The fuse design is based on Boeing Company criteria.

- Mount, along with strut and mount beam, required to elevate engine 10° above horizontal to avoid any wing wake.

- To withstand torque loads resulting from a combined F404 rotor and propulsor rotor seizure, which is a conservative design approach. The combined F404 and propulsor-torque generated during a combined rotor failure is 222,500 in-lb.

  - 225,00 x 1.5 (safety factor) = 337,500 in-lb.
  - 350,000 in-lb used for design analysis.

12.4.1 Isolator Design Requirements

Isolators, which must absorb the dynamic force during blade-out conditions, contain a load-absorbing wire mesh. This is the material that provides the isolators with their dynamic load-isolating capability. Design requirements for the isolators are as follows:

Stiffness Requirements

	Forward Isolator	Aft Isolators
K_X	150,000 lb/in	125,000 lb/in
K_Y	No Requirement	No Requirement
K_Z	125,000 lb/in	60,000 lb/in

Criteria

- One Blade Out From Each Row
- 15 Seconds at Full Speed (Pilot Reaction)
- 15 Seconds to Shut Down and Feather to Zero P/T rpm
- OK to Lose Engine Above 1 Blade Out Per Row

Engine Limitations
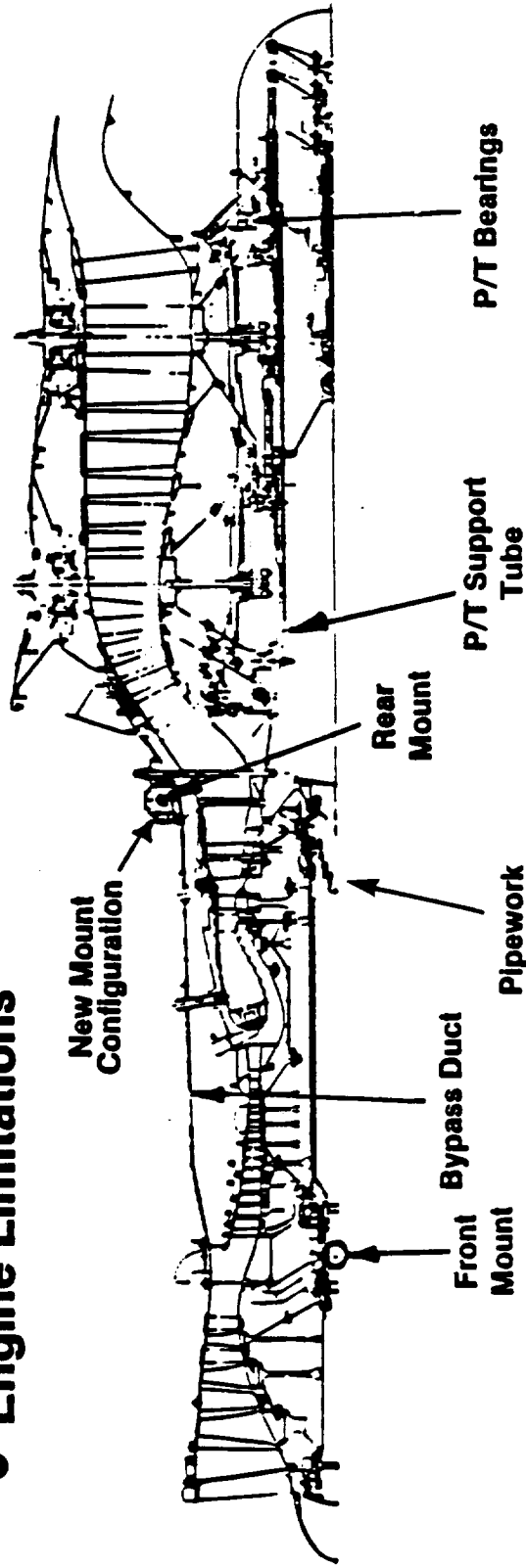
Figure 12-18. UDF™ Engine Mounting Blade-Out Criteria.

<u>Damping Requirements</u>

Minimum of 12% Damping

$(C/C_c = 0.12 \text{ minimum})$

12.4.2 <u>Fuse Pin Design</u>

The following flight maneuver conditions were used as design criteria for the mount loads:

- 8 G Down
- 7 G Up
- 8 G Down + 1.5 × Cruise Thrust
- 9 G Forward with a 1.33 Fitting Factor = 12 G
- 3 × Maximum Thrust + 3 G Down
- 3 × Maximum Thrust
- Seizure
- Maximum Blade-Out Conditions

where Maximum Thrust = 28 kips (actual max thrust = 25 kips)

   Cruise Thrust = 6.1 kips.

The maximum allowable design pin loads, without the required 1.25 factor of safety, were 96.25 kips for the forward fuse pin and 65 kips for each of the two aft fuse pins. It was further required that the fuse pins have a D/T ratio less than, or equal to, 6 if the flat length is greater than 0.3 inches (Figures 12-17 and 12-19).

The following criteria were used to determine the minimum and maximum fuse pin sizes:

$$FF_{max} = 0.8 \times FF_A$$

$$FF_{min} = 0.91 \times FF_{max}$$

where: FF_{max} = Maximum fuse load for the pin

   FF_A = Maximum allowed fuse pin load

   FF_{min} = Minimum fuse load for the pin.
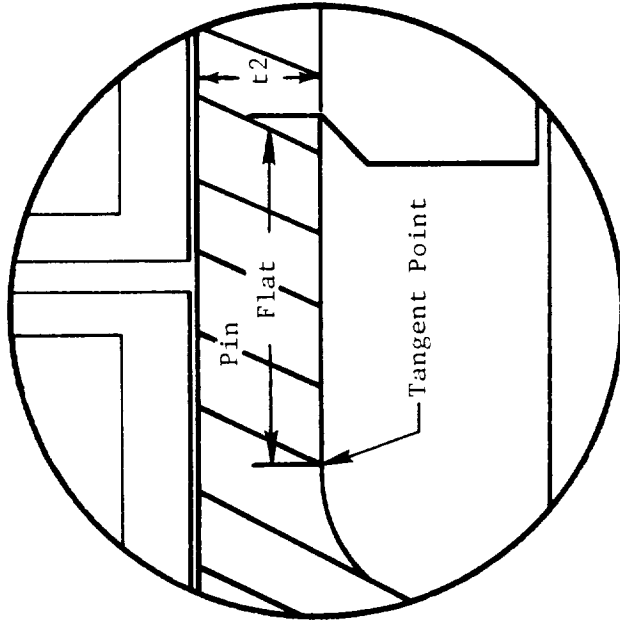
- Pin Must Be Designed with a Minimum Flat to Assure Shear Plane is in Flat for All Possible Shear Planes Using Max Assembly Tolerance.

- Max Flat = Min Flat + 0.03

- $D/t_1 \leq 4.0$

- $D/t_2 \leq 6.0$ if Flat > 0.3 in.

- Heat Treat to Specified Strength with Ultimate Tensile $\geq$ 150 ksi and $\leq$ 210 ksi

- Boeing Approve D/t Values if "Flat" is Less than 0.3 in.

Fuse Pin Geometry

Figure 12-19. Boeing Design Practice.

Thus, it was determined that the forward fuse pin capacity should be 70.1 to 77 kips, and the aft fuse pin capacity should be 47.2 to 52.0 kips. The minimum load capacities were then compared to the original design criteria as shown in Table 12-3. The pin designs chosen (Table 12-4) both exceed the D/T ratio limit prescribed (D/T $\leq$ 6), but were approved since the flat length is less than 0.3 inch. Table 12-5 compares the fuse pin maximum allowable loads to the maximum allowable loads, side of body (S.O.B.), in the aircraft.

Figures 12-20 and 12-21 demonstrate the maximum allowable loads and the maximum and minimum design loads for the fuse pins. These loads are then compared to the combined static and dynamic loads at blade-out conditions (Table 12-6) varying from one to four blades per rotor. Figures 12-20 and 12-21 show that the forward pin can withstand between 1.13 and 1.29 blades lost per rotor before shearing, and the aft pins can withstand between 1.05 and 1.23 blades lost.

Table 12-3. Design Mount Loads (Kips).

Design Condition	Upper Aft	Lower Aft	Forward
• 8 G's Down	40.7	58.9	1.2
• 7 G's Up + 1.5 T_{Max} Con	35.5	52.6	3.8
• 8 G's Down + 1.5 T_{Max} Con	41.4	58.2	1.4
• 9 G's Forward (with 1.33 Fitting Factor) = 12 G	56.7	56.7	30.7
• 3 T_{Max} + 3 G's Down	49.7	47.3	24.4
• 7 G's Down (Reference Maximum Load)	---	(47.2)	---
• 3 T_{Max}	46.0	46.0	24.9
• Seizure (FS = 1.0)(350 kip in)	42.3	42.3	22.9
• Maximum Blade-Out	30.5	32.8	54.5
• Fuse Size (Minimum)	47.3	47.3	70.1

Note: Original Design Capability of 8 G's was Compromised to 7 G's with Boeing Approval Due to Engine Weight Increase of 30%.

(Updated to Latest Weight (8635 lbs) and Inertia Characteristics as of 7/14/86.

Table 12-4. Fuse Pin Design Values

Boeing Criteria	Drawing Criteria		
	GE Loads	567J125614-1	56J1125614-3
---	70-77 kips	70-77 kips	---
---	47.3-52 kips	---	48-52 kips
D/t ≤ 6	---	6.83	10.55
Flat Length > 0.3"	---	0.27"	0.24"
HT 150-210 ksi	---	150-170 ksi	150-170 ksi

Table 12-5. Summary of Fuse Pin Maximum Load for S.O.B. Allowables.

(Kips)						
			S.O.B. (Equivalent Elements Allowable)			
			Forward		Aft	
Forward	Aft Upper	Aft Lower	Upper	Lower	Upper	Lower
96.25	65	65	203	203	341	341.
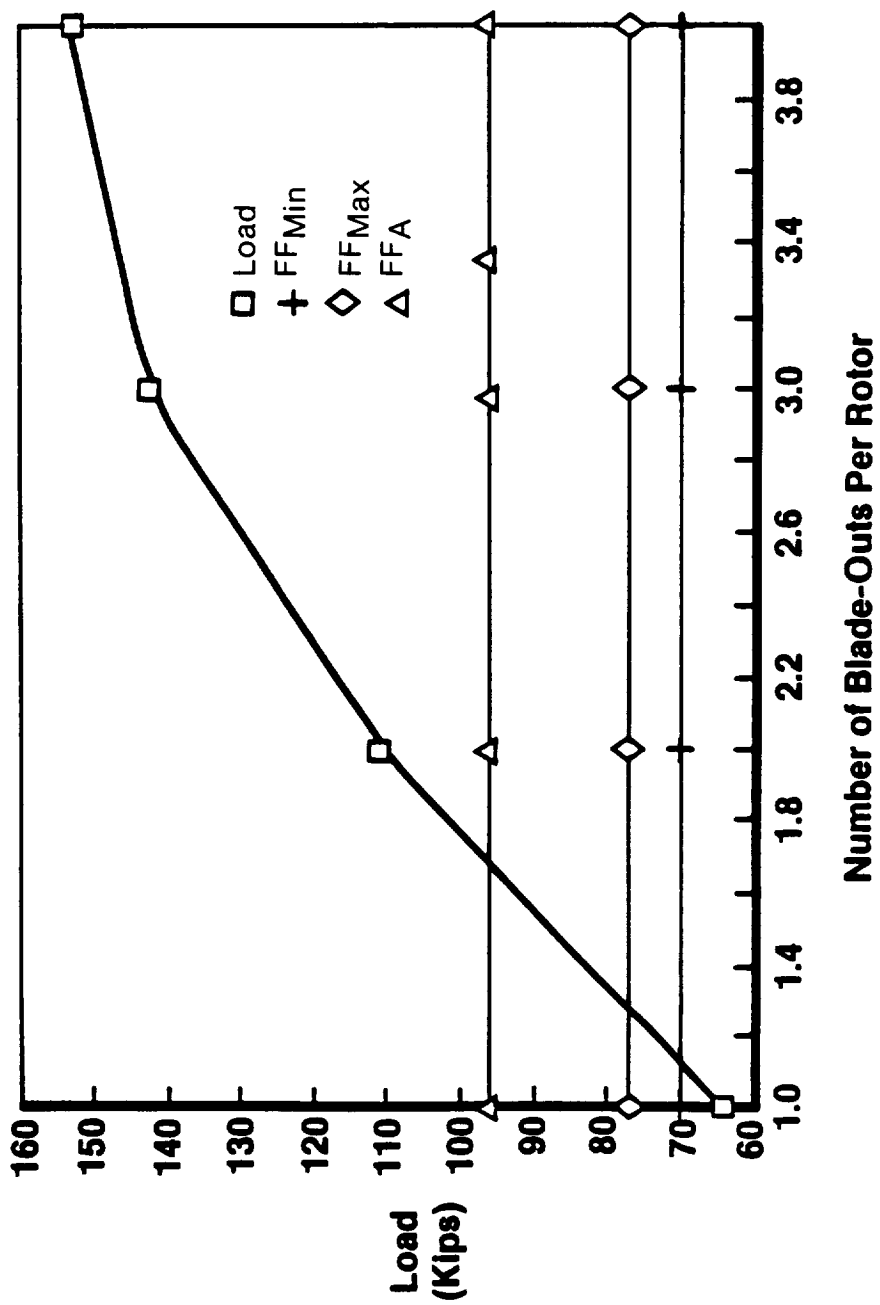
Figure 12-20. Front Pin Load for Blade-Out Conditions.
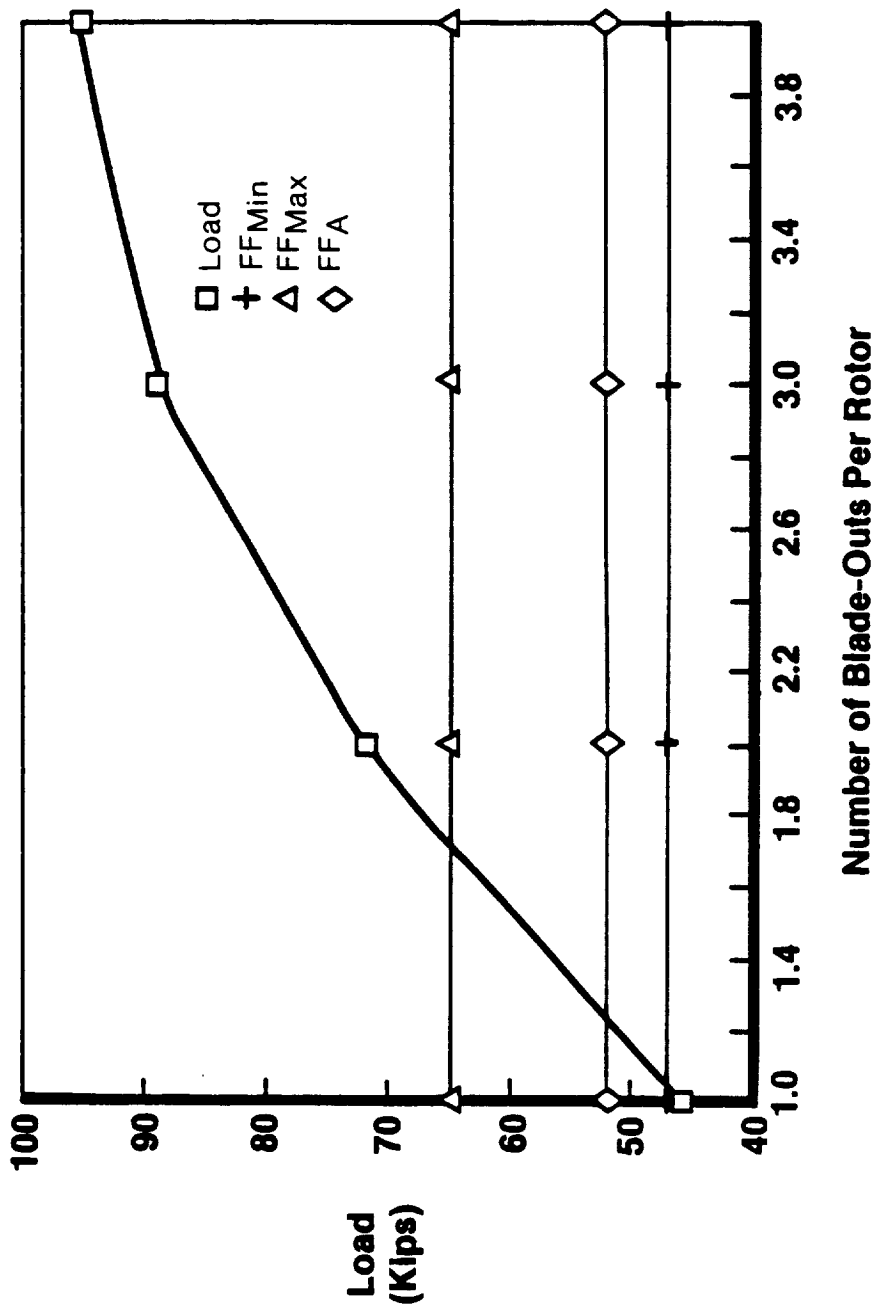
Figure 12-21.   Rear Pin Load for Blade-Out Conditions.

Table 12-6. Fuse Pin Resultants for Blade-Out Capability.

(Kips)				
Pin	Description of Blade Out Load	Latest Design Loads	Fuse Strength	FS
Forward	● Blade Out and Static Simultaneous	63.5	70.1-77.0	1.10
Aft Upper	● Same	43.2	47.2-52.0	1.09
Aft Upper	● Same	46.0	47.2-52.0	1.03

● Maximum Dynamic = Blade-Out Load (2 Blade-Out, 1 Each Rotor) with Phasing

● Static Loads

- 1 G Down
- T/O F_N = 28K Max Less 20% Damage = 22.4K
- Seizure Load = 60 Kip-in
- Aero-Inlet Up @ T/O = 1500 lbs

13.0 CONCLUSIONS

A valid attempt has been made to meet the design requirements and objectives for this engine as detailed below.

- Unducted ultra high bypass turbofan for high efficiency

- Counterrotating fans - to recover exit swirl between blades and convert this to thrust, thus increasing efficiency

- Ungeared fan rotors - less weight, more reliability

- High fuel efficiency

- 25,000 pound static thrust

- Application to subsonic commercial and military transport aircraft

- Ability to operate in flight at 0.8 Mach or higher

- Minimum life requirements of 6000 cycles and 42,000 hours

- Use of 95/99 material properties for all life calculations unless same part data was available

- Ultimate load capability for a complete simultaneous airfoil loss for both stages in conjunction with a 1 G maneuver load

- Enhancements to the F404 gas generator structure to meet UDF™ blade out requirements.

The validity of the engine design concepts are to be established by component testing and actual engine test. This validation testing is covered in the Component Test and Engine Test Reports required by NASA Contract No. NAS3-21210.

14.0 SYMBOLS/ABBREVIATIONS

A/B	Afterburner
A/D	Analog to Digital
A_{Ann}	Annular Area (in^2)
Ax	Axial
BPF	Blade Passing Frequency
BFM	Back-Flow Margin (%)
BTWT	Boeing Transonic Wind Tunnel
β_1	Rotor 1 Pitch Angle (degree)
β_2	Rotor 2 Pitch Angle (degree)
C	Damping
CAFD	Circumferentially Averaged Flow Determination
CC	Control Computer
C_c	Critical Damping
CF	Centrifugal Force (lbs)
DEC	Digital Electronic Control
EB	Electron-Beam
ECU	Electrical Control Unit
EIU	Engine Interface Unit
ex	Exit
FD	Drag Thrust (lb)
FG	Gas Generator Thrust (lb)
FN	Uninstalled Net Thrust (lb)
FOD	Foreign-Object Damage
FPC	Fan Pitch Control
FRAM	Gas Generator Drag (lb)
g_{aero}	Aerodynamic Damping Coefficient
GAP	General Aeroelasticity Program
HIP	Hot Isostatic Pressed
HP	High Pressure
HMU	Hydromechanical Unit
HPC	High-Pressure Compressor
HPT	High-Pressure Turbine

HPVG	High Pressure Compressor Variable Stator
ID	Inner Diameter
IGV	Inlet Guide Vanes
in	Inlet
I/O	Input/Output
IPC	Intermediate-Pressure Compressor
IPT	Intermediate-Pressure Turbine
J	Advance Ratio
KCAS	Calibrated Air Speed (Kts)
KEAS	Equivalent Air Speed (Kts)
KIAS	Indicated Air Speed (Kts)
K_{otm}	Overturning Moment Stiffness
K_R	Radial Stiffness
K_t	Stress Concentration Factor
LCF	Low Cycle Fatigue
L/D	Length/Diameter Ratio
LP	Low Pressure
LPT	Low Pressure Turbine
LVDT	Linear Variable Differential Transducer
M	Mach Number
m	Beat Frequency Multiple
MPU	Microprocessor Unit
MPS	Model Propulsion Simulator
MRB	Material Review Board
M_{Rel}	Relative Mach Number
nd	Nodal-diameter
OD	Outer Diameter
OGV	Outlet Guide Vanes
0.2% PC	0.2% Plastic Creep
PCS	Peripheral Control Computer
PQA	Total Power Coefficient
PS3	HP Compressor Discharge Angle
P/T	Power Turbine (Propulsor)
PLA	Power Lever Angle
PWSD	UDF™ Absorbed Horsepower (hp)

P15Q2	Duct Pressure Ratio
P46Q2	Engine Pressure Ratio
RSA	Power Lever Angle
RSS	Root Sum Square
SA	Single Amplitude
SFC	Specific Fuel Consumption (lb/hr)
SLS	Sea-Level Static
SLTO	Sea-Level Takeoff
SPL	Sound Pressure Level (dB)
Sx/Cx	Spacing - Chord Ratio
Tan	Tangential
TE	Trailing Edge
TIG	Tungsten Inert Gas
U	Wheel (Turbine Rotor) Speed
UAC	Vacuum
UDF™	GE36 Unducted Fan Engine
V_{buff}	Velocity for Onset of Buffeting (KTS)
VEN	Variable Exhaust Nozzle
V_{FE}	Minimum Velocity with Flaps Extended
VG	Variable Geometry
V_L	Absolute Velocity Vector of Left Running Rotor
V_R	Absolute Velocity Vector of Right Running Rotor
V_R	Reduced Velocity Parameter
V_{SS}	Onset of Stick Shake Velocity
V_U	Absolute Velocity Vector in U Direction
W_f	Fuel Flow
$\dfrac{W}{R}$	Dimensionless Criterion for Self Excited Vibration
W2AR	IPC Corrected Airflow (lb/sec)
XN2	IP Shaft Speed (rpm)
XN25	HP Shaft Rotational Speed (rpm)
YS	Yield Strength
2A	Second Axial Frequency (cps)
ZCD	Zero-Crossing Detectors
ZF	Second Flexural Frequency (cps)

ZT	Second Torsional Frequency (cps)
1A	No. 1 Acutation Bearing, etc.
1B	No. 1 Ball Bearing, etc.
1R	No. 1 Roller Bearing, etc.
$\dfrac{\delta(W_f)}{(i)}$	Partial of Fuel Flow with Respect to Any Variable i

15.0 References

1. "Full-Scale Technology Demonstration of a Modern Counterrotating, Unducted Fan Engine Concept - Component Test," GE, NASA Contract No. NAS3-24210, CR-180868, December 1987.

2. "Full-Scale Technology Demonstration of a Modern Counterrotating, Unducted Fan Engine Concept - Engine Test," GE, NASA Contract No. NAS3-24210, CR-180869, December 1987.

3. "UDF^{TM} Airworthiness Executive Review," GE, NASA Contract No. NAS3-24210, July 1986.

4. "The Unducted Fan Engine - Quarterly Review Number 8," GE, NASA Contract No. NAS3-24210, May 13, 1986.

5. "The Unducted Fan Engine - Quarterly Review Number 7," GE, NASA Contract No. 24210, November 18, 1986.

6. "The Unducted Fan Engine - Quarterly Review Number 6," GE, NASA Contract No. NAS3-24210, August 16, 1985.

7. Theodorsen, T., Theory of Propellers, McGraw-Hill, New York, 1948.

8. Rohrbach, C., Metzer, F.B., Black, D.M., and Ladden, R.M., "Evaluation of Wind Tunnel Performance Testings of an Advanced 45° Swept Eight-Bladed Propeller at Mach Numbers from 0.45 to 0.85," Hamilton-Standard, Windsor Locks, Connecticut, NASA Contractor Report 3505, NAS3-20769, March 1982.

9. Craig, H.R.M. and Cox, H.J.A., "Performance Estimation of Axial Flow Turbines," Inst. Mech. Engrs. Proc., Vol. 185, No. 32/71, London, UK, 1971.

10. Abernathy, C.L., Item of Interest: "GE36 UDF^{TM}-1 Core Plug Model Tests At Fluidyne," 1986.

11. Bender, S., "Vibration Isolators; Engine Mounts," Aircraft Engine Group Specification M50IE3221, Issue No. 52; FSCM 07482, August 9, 1985.

12. Military Standardization Handbook: Metallic Materials and Elements for Aerospace Vehicle Structures, MIL-HDBK-5D, United States Department of Defense and Federal Aviation Administration, January 1, 1984.

13. GE36 (UDF Model Demonstrator) Propulsion System Functional Interface Control Document (FICD), GE, Evendale, OH, 1984.

14. "Low Temporary Curing Epoxy Resin Impregnated Glass Fabric," GE (Temporary Specification), Spec. No. A50TF191-1(T), Code I.D. No. 07482, January 18, 1977.

DISTRIBUTION

Government Agencies

NASA Headquarters
600 Independence Avenue, SW
Washington, DC 20546
    Attn: R/R.S. Colladay
          RJ/C.C. Rosen
          RP/G.M. Reck
          RP/J.R. Facey

NASA Lewis Research Center
21000 Brookpark Road
Cleveland, Ohio 44135

Attn:		
J.A. Ziemianski	MS 86-1	
R.J. Shaw	MS 86-1	
P.G. Batterton	MS 86-1	
G.K. Sievers	MS 100-5	
M.J. Hartmann	MS 3-7	
R.E. Kielb	MS 23-3	
L.J. Kiraly	MS 23-3	
J.F. Groeneweg	MS 86-7	
J.C. Williams	MS 500-211	
R.W. Niedzwiecki	MS 77-6	(2 copies)
D.W. Drier	MS 86-2	
B.A. Miller	MS 5-3	
J.J. Reinmann	MS 77-10	
L.J. Bober	MS 86-7	
A.G. Powers	MS 86-4	
J.J. Coy	MS 86-4	
R.E. Coltrin	MS 77-10	
C.L. Ball	MS 77-6	
E.A. Willis	MS 86-1	
L. Reid	MS 77-10	
E.T. Meleason	MS 77-10	
R.D. Hager	MS 86-7	(3 copies)
Library	MS 60-3	(2 copies)
Report Control Office	MS 60-1	
Tech. Utilization Office	MS 7-3	
D.C. Mikkelson	MS 6-12	(2 copies)
AFSC Liaison Office	MS 501-3	
Army R & T Propulsion Lab	MS 77-12	

NASA Ames Research Center
Moffett Field, CA 94035

Attn:	
R.P. Bencze	MS 227-6
R.C. Smith	MS 227-6

NASA Langley Research Center
Hampton, VA 23665
    Attn: D.G. Stephens   MS 462
    Research Information Center   MS 151A

NASA Scientific and Technical Information Facility
P.O. Box 8757
B.W.I. Airport, MDE 21240
    Attn: Accession Dept. (20 copies)

NASA Dryden Flight Research Center
P.O. Box 273
Edwards, CA 93523
    Attn: D-OP/R.S. Baron (2 copies)

Department of Defense
Washington, DC 20301
    Attn: R. Standahar, 3D1089 Pentagon

Wright-Patterson Air Force Base
Dayton, OH 45433
    Attn: AFWAL/PO/Col. J. Radloff
           AFWAL/POTA/M.F. Schmidt
           AFWAL/POT/H.I. Bush
           ASD/EN/Col. L.G. vanPelt
           ADS/SR/K.I. Collier

Eustis Directorate
U.S. Army Air Mobility
R & D Laboratory
Fort Eustis, VA 23604
    Attn: J. White
           J. Gomez, Jr.

Navy Department
Naval Air Systems Command
Arlington, VA 20360
    Attn: G. Derderian, AIR-310-E

Naval Air Propulsion Test Center
Trenton, NJ 08628
    Attn: P.J. Mangione, MSPE-32
          R. Valeri, MSPE-34

U.S. Naval Air Test Center
Code SY-53
Patuxent River, MD 20670
    Attn: E.A. Lynch

USAVRAD Command
P.O. Box 209
St. Louis, MO 63166
      Attn: R.M. Titus

Department of Transportation
NASA/DOT Joint Office of Noise Abatement
Washington, DC 20590
      Attn: C. Foster

Federal Aviation Administration
New England Region
12 New England Executive Park
Burlington, MA 01803
      Attn: D.P. Salvano

Engine Manufacturers

AVCO Lycoming
550 S. Main Street
Stratford, CT 06497
      Attn: H. Moellmann

Detroit Diesel/Allison Division
P.O. Box 894
Indianapolis, IN 46206
      Attn: B. Wallace

Garrett Turbine Engine Company
111 South 34th Street
P.O. Box 5217
Phoenix, AZ 85010
      Attn: R. Heldenbrand

Garrett Turbine Engine Company
Torrance, CA 90509
      Attn: F.E. Faulkner

General Electric Company/AEG
1 Neumann Way
Evendale, Ohio 45215
      Attn: T.F. Donohue

General Electric Company/AEG
1000 Western Avenue
Lynn, MA 01910
      Attn: B. Weinstein

General Electric Company
P.O. Box 88186
Cleveland, OH 44181
    Attn: M.H. Rudasill

Pratt & Whitney Aircraft Group
United Technologies Corporation
Engineering Division
400 Main Street
East Hartford, CT 06108
    Attn: R.W. Hines   161-04
          G.L. Brines   162-25
          G.L. Bywaters   162-23

Pratt & Whitney Aircraft Group
United Technologies Corporation
Military Products Division
P.O. Box 2691
West Palm Beach, FL 33402
    Attn: R.E. Davis   713-11
          T.R. Hampton   713-07

Pratt & Whitney Aircraft Group
United Technologies Corporation
24500 Center Ridge Road
Suite 280
Westlake, OH 44145
    Attn: A. Leiser

Teledyne CAE, Turbine Engines
1330 Laskey Road
Toledo, OH 43612
    Attn: R.H. Gaylord

Williams International
2280 West Maple Road
Walled Lake, MI 48088
    Attn: R. vanNimwegen
          R. Horn

Airframe Manufacturers

Boeing Commercial Airplane Company
P.O. Box 3707
Seattle, WA 98124
    Attn: Dr. C.G. Hodge
          F. Davenport
          J. Farrell

Boeing Company
Wichita Division
P.O. Box 7730
Wichita, KS 67277
    Attn: D. Tarkelson
            C.T. Havey

Cessna Aircraft Company
P.O. Box 154
Wichita, KS 67201
    Attn: D. Ellis Dept 178

Douglas Aircraft Company
McDonnell Douglas Corporation
3855 Lakewood Boulevard
Long Beach, CA 90846
    Attn: M. Klotzsche
            W. Orlowski

Gates Learjet Corporation
P.O. Box 7707
Wichita, KS 67277
    Attn: E. Schiller

General Dynamics Convair
P.O. Box 80844
San Diego, CA 92138
    Attn: S. Campbell

Grumman Aerospace Corporation
South Oyster Bay Road
Bethpage, NY 11714
    Attn: N.F. Dannenhoffer

Gulfstream Aerospace Corporation
P.O. Box 2206
Savannah, GA 31402-2206
    Attn: R. Wodkowski

Lockheed-California Company
Burbank, CA 91502
    Attn: J.F. Stroud   D/75-42
            R. Tullis   D/75-21

Lockheed-Georgia Company
86 S. Cobb Drive
Marietta, GA 30063
    Attn: W.E. Arndt   D/71-01, Zone 13

McDonnell Aircraft Company
McDonnell Douglas Corporation
P.O. Box 516
St. Louis, MO 63166
        Attn: G. Phariss

Rockwell International
International Airport
Los Angeles Division
Los Angeles, CA 90009
        Attn: A.W. Martin

Airlines

American Airlines
Maintenance and Engineering Center
Tulsa, OK 74151
        Attn: C. Wellmershauser

Continental Airlines, Inc.
2929 Allen Parkway
Houston, TX 77019
        Attn: J. Arpey

Delta Airlines, Inc.
Hartsfield-Atlanta International Airport
Atlanta, GA 30320
        Attn: J.T. Davis

Eastern Airlines
International Airport
Miami, FL 33148
        Attn: E. Upton

Federal Express Corporation
Box 727
Memphis, TN 38194
        Attn: J. Riedmeyer

Pan American World Airways, Inc.
JFK International Airport
Jamaica, NY 11430
        Attn: R. Valeika

Trans World Airlines
605 Third Avenue
New York, NY 10016
        Attn: K. Johnson

United Airlines
Maintenance Operations Center
San Francisco International Airport
San Francisco, CA 94128
        Attn: J. Goodwine

Others

Hamilton Standard
United Aircraft Corporation
Windsor Locks, CT 06096
        Attn: B. Gatzen   MS 1-2-11
               S. Ludemann   MS 1-2-11

Massachusetts Institute of Technology
Department of Astronautics and Aeronautics
Cambridge, MA 02139
        Attn: Library

Penn State University
Department of Aerospace Engineering
233 Hammond Building
University Park, PA 16802
        Attn: Dr. B. Lakshminarayana

Rohr Corporation
P.O. Box 878
Foot and H Street
Chula Vista, CA 92012
        Attn: Library

TRW, Inc.
TRW Equipment Group
23555 Euclid Avenue
Cleveland, OH 44117
        Attn: I. Toth

University of Michigan
Gas Dynamics Laboratories
Aerospace Engineering Building
Ann Arbor, MI 48109
        Attn: Dr. C.W. Kaufmann

University of Tennessee Space Institute
Tullahoma, TN 37388
        Attn: Dr. V. Smith

Cessna Aircraft Company
McCauley Accessory Division
3535 McCauley Drive
Vandalia, OH 45377
     Attn: H.G. Starnes

Hartzell Propeller Products
P.O. Box 1458
1800 Covington Avenue
Piqua, OH 45356
     Attn: D. Edinger

University of Washington
Seattle, WA 98195
     Attn: Dr. R. Decher

1. Report No.	2. Government Accession No.	3. Recipient's Catalog No.
CR-180867		

4. Title and Subtitle	5. Report Date
Full-Scale Technology Demonstration of a Modern Counterrotating Unducted Fan Engine Concept - Design Report	December 1987
	6. Performing Organization Code
	535-03-01

7. Author(s)	8. Performing Organization Report No.
GE36 Design and Systems Engineering	
	10. Work Unit No.

9. Performing Organization Name and Address	11. Contract or Grant No.
GE Aircraft Engines	NAS3-24210
1 Neumann Way	
Evendale, Ohio 45215	13. Type of Report and Period Covered

12. Sponsoring Agency Name and Address	Topical
NASA Lewis Research Center	14. Sponsoring Agency Code
21000 Brookpark Road	
Cleveland, Ohio 44135	

15. Supplementary Notes

16. Abstract

The UDF™ engine is a new aircraft engine concept that is based on an ungeared, counterrotating, unducted, ultra high bypass turbofan configuration. This engine is being developed by GE to provide a high thrust-to-weight ratio power plant with exceptional fuel efficiency for subsonic aircraft application. This report covers the design methodology and details for the major components of this engine. The design intent of the engine is to efficiently produce 25,000 pounds of static thrust while meeting life and stress requirements. The engine is required to operate at Mach = 0.8 levels or above.

17. Key Words (Suggested by Author(s))	18. Distribution Statement
Unducted Fan Counterrotation Ultra High Bypass Engine Design Propfan	

19. Security Classif. (of this report)	20. Security Classif. (of this page)	21. No. of Pages	22. Price
Unclassified	Unclassified	366	